

# **Effects of the Environment in Hydrogen-Bonded Polymers**

## **Dissertation**

zur Erlangung des Doktorgrades der Naturwissenschaften  
(Dr. rer. nat.)

der

Naturwissenschaftlichen Fakultät II  
Chemie, Physik und Mathematik

der Martin-Luther-Universität  
Halle-Wittenberg

vorgelegt von

Herrn Chenming Li  
geb. in Henan, P.R. China

Gutachter:

1. Prof. Dr. Wolfgang H. Binder (Martin-Luther-Universität Halle-Wittenberg)
2. Prof. Dr. Johannes C. Brendel (Universität Bayreuth)

Date of Defense: 07.10.2025

Place: Halle (Saale)

## Acknowledgment

I would like to express my deepest gratitude to all those who have supported me throughout my PhD journey. This work would not have been possible without the guidance, encouragement, and assistance of many individuals, to whom I am sincerely indebted.

First and foremost, my heartfelt thank goes to Prof. Dr. Wolfgang H. Binder for providing me with the invaluable opportunity to work under his supervision. His profound knowledge, insightful guidance, and continuous support have been instrumental in shaping my research. I am truly grateful for the opportunity to learn under his mentorship.

I would also like to express my sincere appreciation to Ms. Anke Hassi, whose readiness to answer my questions and assist with organizational matters significantly eased the bureaucratic aspects of my work. Her support has been invaluable. I am equally grateful to Ms. Susanne Tanner and Ms. Julia Grossert for their assistance in providing the necessary chemicals and laboratory equipment, as well as for conducting numerous measurements that contributed to my research.

I am deeply thankful to all my former colleagues and the current members of our research group. In particular, I would like to acknowledge Dr. Xiaozhuang Zhou, Dr. Newton Sen, Dr. Zviadi Katcharava, Farahnaz Navazandeh Tirkalaei, Marah Mohd Abdelmajed Alqaisi, and many others. The friendly and supportive atmosphere made overcoming challenges not only manageable but also enjoyable. Your camaraderie and encouragement have been truly invaluable.

Finally, my deepest gratitude goes to my wife, Dr. Yue Cai, for her unwavering mental and physical support, her insightful scientific suggestions, and her constant inspiration in both my personal and professional life. I am also profoundly grateful to my family and friends, whose unwavering belief in me and constant emotional support have been my greatest source of strength. Their encouragement has been the foundation upon which I have built my perseverance and determination.

To all those who have contributed in various ways to this journey—thank you.

## Kurzdarstellung

Wasserstoffbrückenbindungen (H-Brücken) sind zentrale nicht-kovalente Wechselwirkungen, die die Struktur und Funktion natürlicher und synthetischer Materialien bestimmen. Ihre Stabilität ist temperaturempfindlich, und polare Spezies wie Wasser schwächen sie zusätzlich durch kompetitive Bindung. Trotz ihrer weit verbreiteten Anwendung in Biopolymeren und synthetischen Materialien bleibt das H-Brückenverhalten in Polymeren weitgehend unerforscht. In fortschrittlichen Materialien wie polymeren ionischen Flüssigkeiten (POILs) und Polymergelen wird das H-Brückenverhalten zudem noch komplexer.

Diese Dissertation untersucht drei H-Brücken-Systeme, Barbiturat/Thiobarbiturat (Ba/TBa)-Selbstassoziation, Ureido-Pyrimidinon (UPy)-Dimere und Hamilton-Wedge-Barbiturat-Komplexe (HW-Ba-Komplexe), in verschiedenen molekularen Umgebungen. Im ersten Teil bestätigten NMR-, FT-IR- und DSC-Analysen, dass TBa schwächere, weniger geordnete und langsamer sich bildende H-Brücken als sein sauerstoffhaltiges Gegenstück Ba ausbildet, während rheologische Untersuchungen nur geringe Einflüsse der unpolaren Polyisobutylen-Matrix (PIB) zeigten. Im zweiten Teil erwiesen sich die in POILs eingebetteten UPy-H-Brücken als stabil bis  $\sim 70^{\circ}\text{C}$ , bestätigt durch Festkörper-MAS-NMR und FT-IR. Rheologische Untersuchungen zeigten, dass die Zugabe ionischer Flüssigkeiten (ILs) die Relaxation der POILs beschleunigte, ohne die Festigkeit im glasartigen Zustand zu beeinträchtigen, was auf intakte UPy-H-Brücken in der ionischen Umgebung hinweist. Im dritten Teil wurde das H-Brückenverhalten von alkenmodifizierten HW-Ba-Komplexen mittels UV-Vis-Titration untersucht, um die Auswirkungen von Lösungsmittelpolarität, zusätzlichen Bindungsstellen und thermodynamischen Faktoren zu analysieren. Eine zweistufige Strategie, kovalente Fixierung durch Alken-Cross-Metathese, gefolgt von ESI-MS-Analyse, wurde entwickelt und erfolgreich auf HW-Ba-Aggregate in einer lösungsmittelfreien PIB-Matrix angewendet.

Diese Arbeit zeigt, wie molekulare Nähe, einschließlich polymerer Gerüste und niedermolekularer Spezies, die Stabilität von H-Brücken beeinflusst. Die Ergebnisse liefern wertvolle Erkenntnisse für das gezielte Design von H-Brückenbasierten Polymersystemen mit optimierten funktionellen und mechanischen Eigenschaften.

## Abstract

Hydrogen bonds (H-bonds) are key noncovalent interactions shaping the structure and function of natural and synthetic materials. In solutions, the stability of H-bonds is temperature-sensitive, and polar species like water further weaken them through competitive binding. Despite their broad use in biopolymers and synthetic materials, H-bond behavior in bulk polymers remains largely underexplored. The H-bond behavior also complicates more in advanced materials such as polymeric ionic liquids (POILs), and polymer gels.

This thesis investigates three distinct H-bonding systems, barbiturate/thiobarbiturate (Ba/TBa) self-association, ureido-pyrimidinone (UPy) dimers, and Hamilton wedge-barbiturate (HW-Ba) complexes, across various molecular environments, including solvents, ionic media, and bulk polymer matrices. In the first part, NMR, FT-IR, and DSC studies confirmed that TBa exhibits weaker, less-ordered, and slower H-bonds than its oxy-counterpart Ba, while rheology revealed minimal influence from the nonpolar and non-H-bonding polyisobutylene (PIB) matrix. In the second part, the UPy H-bonds incorporated in POILs were confirmed stable till  $\sim 70^{\circ}\text{C}$  via solid-state MAS NMR and FT-IR spectroscopy. Rheology studies showed that mixing with low-molecular-weight ionic liquids accelerated POILs relaxation without compromising material strength in the glassy state, indicative of intact UPy H-bonds in the ionic environment. The third study examined alkene-modified HW-Ba complexes through UV-Vis titration, revealing the effects of solvent polarity, extra H-bonding sites, and entropy-enthalpy contributions. A two-step aggregate study, i.e., covalent fixation via alkene cross-metathesis followed by ESI MS analysis, was established and successfully extended to study HW-Ba aggregates in a solvent-free PIB matrix.

Overall, this work highlights the influences of molecular proximity on H-bond stability. The findings offer key insights into the rational design of H-bonded polymer systems with optimized functionalities and mechanical properties.



# Table of Content

<b>1. Introduction</b>	<b>1</b>
1.1. Hydrogen-Bonds and the Bonded Polymers	1
1.1.1. Hydrogen-Bonds and the Motifs	1
1.1.2. Synthesis of Hydrogen-Bonded Polymers	4
1.1.3. Hydrogen-Bonded Macromolecular-Assembly and the Formation of Aggregates	6
1.2. Impact of Polymers on the Dynamic Equilibria of Hydrogen-Bonds in Various Surroundings	9
1.2.1. Assembly of H-bonded Supramolecular Polymers in Solution	9
1.2.2. In the Solid State of a Single Polymer	14
1.2.3. In Other Novel Surroundings	21
1.3. Probing Hydrogen-Bonding Strength in Polymers	24
1.3.1. Quantitative Analysis of Hydrogen-Bonding Strength in Solutions	24
1.3.2. Probe Hydrogen-Bonding Strength in the Solid State	29
<b>2. Scope of the Thesis</b>	<b>35</b>
2.1. Aim of Thesis	35
2.2. Scientific Approach	37
<b>3. List of Publications</b>	<b>40</b>
[P1] Comparing C2=O and C2=S Barbiturates: Different Hydrogen-Bonding Patterns of Thiobarbiturates in Solution and the Solid State	
[P2] Synthesis and Characterization of Quadrupolar-Hydrogen-Bonded Polymeric Ionic Liquids for Potential Self-Healing Electrolytes	
[P3] Stability of Quadruple Hydrogen Bonds in an Ionic Liquid Environment	
[P4] Proximity Effects and Aggregation of Hamilton-Receptor Barbiturate Host-Guest Complexes Probed by Cross-Metathesis and ESI MS Analysis	
<b>4. Conclusion</b>	<b>88</b>
<b>5. Reference</b>	<b>95</b>

<b>Appendix .....</b>	<b>130</b>
-----------------------	------------

**Curriculum Vitae**

**Eigenständigkeitserklärung**

## List of Abbreviation

DQ	Double-Quantum
DSC	Differential Scanning Calorimetry
EG	Ethylene Glycol
ESI	Electrospray Ionization
FT-IR	Fourier-Transform Infrared Spectroscopy
G	Guest
H	Host
H-bond	Hydrogen-Bond
HBP	Hydrogen-Bonded Polymer
HFiP	Hexafluoroisopropanol
HG	Host-Guest Complex
HW	Hamilton Wedge
IL	Ionic Liquid
iPA	Isopropanol
ITC	Isothermal Titration Calorimetry
K <sub>a</sub>	Association Constant
LAP	Living Anionic Polymerization
LCCP	Living Carbocation Polymerization
MALDI	Matrix-Assisted Laser Desorption/Ionization
MeCN	Acetonitrile
MeOH	Methanol
M <sub>n</sub>	Molecular Weight
MS	Mass Spectrometry
NMP	Nitroxide-Mediated Radical Polymerization
NMR	Nuclear Magnetic Resonance Spectroscopy
OAC <sup>-</sup>	Acetate
PA6	Polyamide6
PAA	Poly(acrylic acid)
PCL	Polycaprolactone
PDI	Polydispersity
PDMS	Polydimethylsiloxane
PEK	Poly(ether ketone)
PEO	Poly(ethylene oxide)

PhOH	Phenol
PI	Polyisoprene
PIB	Polyisobutylene
PiC	Polyisocyanate
PLA	Poly(lactic acid)
PMAc	Polymethacrylamide
PMMA	Poly(methyl methacrylate)
PnBA	Poly(n-butyl acrylate)
POIL	Polymeric Ionic Liquid
PPO	Poly(propylene oxide)
PS	Polystyrene
PU	Polyurethane
PVA	Poly(vinyl alcohol)
PVAc	Poly(vinyl acetate)
PVP	Polyvinylpyrrolidone
Pyr	Pyridine
RAFT	Reversible Addition-Fragmentation Chain-Transfer Polymerization
SANS	Small-Angle Neutron Scattering
ss NMR	Solid-State Nuclear Magnetic Resonance Spectroscopy
TBa	2-Thiobarbiturate
TEM	Transmission Electron Microscopy
TFT	$\alpha,\alpha,\alpha$ -Trifluorotoluene
T <sub>g</sub>	Glass Transition Temperature
THF	Tetrahydrofuran
Thy	Thymine
ToF	Time of Flight
UPy	Ureido-Pyrimidinone
UV Vis	Ultraviolet-Visible Spectrophotometry
VT	Variable Temperature

# 1. Introduction

## 1.1. Hydrogen-Bonds and the Bonded Polymers

### 1.1.1. Hydrogen-Bonds and the Motifs

Hydrogen bonds (H-bonds), a fundamental supramolecular interaction characterized by their dynamic and reversible nature, have been extensively studied and widely applied in soft materials. Although more than a century has passed since their initial definition,<sup>1,2</sup> research on H-bonds continues to be a forefront topic in modern science. While the definition of H-bonds has been a subject of historical debate,<sup>3-7</sup> the International Union of Pure and Applied Chemistry (IUPAC) provided a standardized definition in 2011, stating:

*“The hydrogen bond is an attractive interaction between a hydrogen atom from a molecule or a molecular fragment X–H in which X is more electronegative than H, and an atom or a group of atoms in the same or a different molecule, in which there is evidence of bond formation.”<sup>8</sup>*

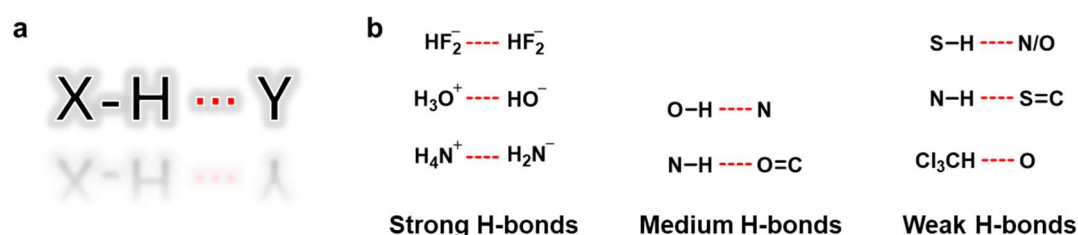


**Figure 1.1** a) Generalized H-bonding structure between a proton connected with an electronegative atom X as the H-bonding donor and an electronegative atom Y as the H-bonding acceptor; b) Examples of strong H-bonds, medium H-bonds, and weak H-bonds.

In H-bonds an electron-rich atom X, typically nitrogen (N), oxygen (O), or fluorine (F), acts as a proton acceptor (H-bonding acceptor, A), donating electron density to attract electron-deficient protons (H-bonding donor, D) linked to another electronegative X atom (**Figure 1.1a**). While strong H-bonds with an ionic nature exist with a bonding energy of  $\sim 15\text{--}40 \text{ kcal}\cdot\text{mol}^{-1}$ , medium H-bonds usually are formed between noncharged elements with a bonding energy of  $5\text{--}15 \text{ kcal}\cdot\text{mol}^{-1}$ , whereas weak H-bonds are characterized by a bonding energy of  $\sim 0.5\text{--}5 \text{ kcal}\cdot\text{mol}^{-1}$ .<sup>9</sup> H-bonds can be further engineered for various functional

groups to enable diverse H-bonding motifs, ranging from single H-bond pairs like pyridine-phenol to self-complementary multiple H-bonding synthons such as acid-acid, amide-amide, urea-urea, and ureidopyrimidinone (UPy)-UPy dimers (**Figure 1.2a**).

H-bonding motifs can vary in their molecular design to tune their specific bonding strengths, as described by the association constant ( $K_a$ ), strongly dependent on factors like the molecular geometry,<sup>10-12</sup> substituent polarity,<sup>13</sup> and secondary interactions<sup>14-16</sup> from adjacent dipoles, which exert attractive or repulsive forces. Especially secondary forces can enhance or weaken H-bonding strength, highlighting the critical role of molecular design in optimizing H-bonding interactions by reducing secondary expulsions.<sup>14-16</sup> As a prominent example, the UPy-motif, introduced by Meijer et al.,<sup>17-19</sup> has attracted significant research interest due to its facile synthesis and strong dimerization-ability, driven by a distinct quadruple donor-donor-acceptor-acceptor (DDAA) H-bonding array. This array incorporates two secondary attractive forces, one repulsive force (**Figure 1.2b**), and an optimal spatial design, resulting in a high association constant ( $K_a \approx 10^7 \text{ M}^{-1}$ ). In comparison, if the secondary forces are all attractive, such as those in the H-bonding complex X-Y<sup>20</sup> in Figure 1.1b) with the similar quadruple DDDD-AAAA H-bonding array, the association constant of an X-Y complex can further reach values up to  $K_a \approx 10^{12} \text{ M}^{-1}$ .

Beyond self-associating H-bonding motifs, hetero-complementary complexes comprising two distinct H-bonding partners play a crucial role, such as H-bonding systems derived from thymine-diaminopyridine (Thy-DAP), thymine-diaminotriazine (Thy-DAT), and the Hamilton-wedge-barbiturate (HW-Ba) as shown in **Figure 1.2**, with binding constants as indicated, ranging from  $10^2$  to  $10^6 \text{ M}^{-1}$ . Due to their complementary binding sites, these motifs enable selective molecular recognition in the sense of a key/lock-system. Additionally, they offer greater flexibility for modifying donor/acceptor locations, molecular configurations, and substituents for further functionalization. In the early 1990s, Hamilton et al.<sup>21-23</sup> introduced the Hamilton wedge (HW) as a molecular receptor for barbiturates (Ba) (**Figure 1.2c**), embedding two diaminopyridine moieties bound to a m-substituted aromatic-unit, able to selectively bind barbiturate Ba via sextuple H-bonds, yielding a  $K_a$  of  $\sim 10^4 \text{ M}^{-1}$ . When preorganized into a closed cyclic structure (cHW1), the binding affinity increases to  $\sim 10^6 \text{ M}^{-1}$ . However, excessive rigidity, such as in cHW2 reduces

the binding constant to  $\sim 10^5 \text{ M}^{-1}$ , highlighting the critical role of structural preorganization in optimizing H-bonding strength.

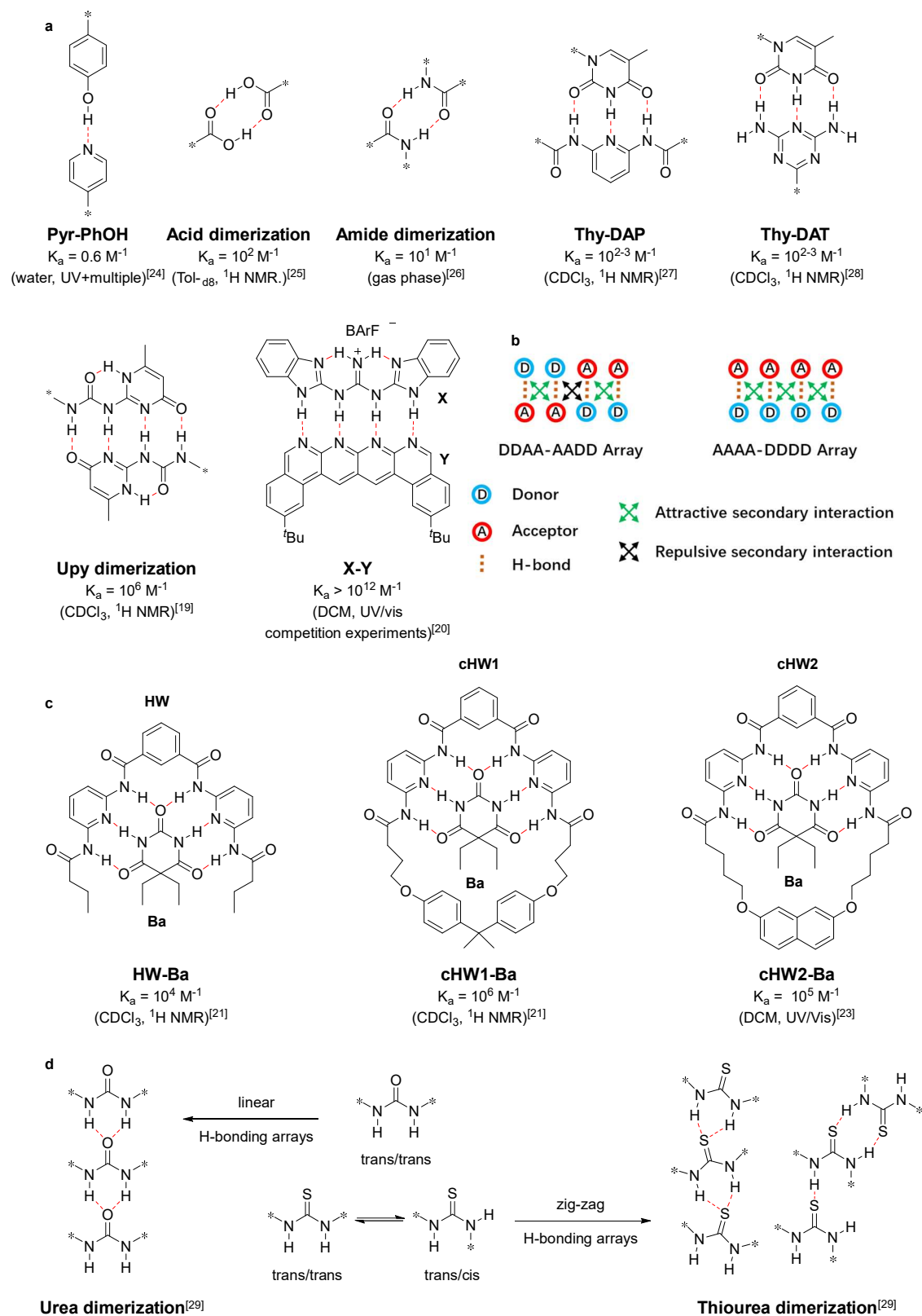


**Figure 1.2** a) H-bonding motifs with association constants: phenol-pyridine (PhOH-Pyr)

with single H-bond,<sup>24</sup> acid-acid dimer with double H-bonds,<sup>25</sup> amide-amide dimer with double H-bonds,<sup>26</sup> thymine-diaminopyridine (Thy-DAP) with triple H-bonds,<sup>27</sup> thymine-diaminotriazine (Thy-DAT) with triple H-bonds,<sup>28</sup> ureido-pyrimidinone (UPy)-UPy dimer with quadruple H-bonds,<sup>19</sup> and X-Y with quadruple H-bonds<sup>20</sup>; b) the schematic illustration of secondary force in quadruple DDAA H-bonding array; c) prototypes of Hamilton wedges-barbiturate (HW-Ba) complex, with the Hamilton wedge bearing linear (HW1<sup>21</sup>) and cyclic (cHW1<sup>21</sup> and cHW2<sup>23</sup>) outer rim; d) the illustration of linear H-bonds in urea and zig-zag H-bonds thiourea.<sup>29</sup>

Typical H-bonding motifs involve receptor atoms such as oxygen (O) and nitrogen (N), while sulfur (S) from the sixth group can also function as an H-bond acceptor. Due to its larger atomic size, S displays a lower electronegativity and more diffused electron density than O, leading to the widely held belief that sulfur-centered H-bonds are generally weaker than oxygen-centered H-bonds.<sup>30-32</sup> Additionally, sulfur-centered H-bonds exhibit longer bond lengths and more distorted angles than their oxygen-centered counterparts, as observed in studies on urea and thiourea (**Figure 1.2d**).<sup>29,33</sup> While urea adopts only a trans/trans conformation, thiourea allows both trans/trans and trans/cis conformers.<sup>29</sup> When embedded into polymers, despite their weaker association in comparison to urea, thiourea's flexible conformations contribute to unique material properties, such as enhanced mechanical strength and faster self-healing.<sup>34-37</sup> Moreover, sulfur's higher polarizability enables it to act as a potential H-bond acceptor.<sup>38</sup> Sulfur-centered H-bonds play crucial roles in biological systems, influencing biomacromolecular functions,<sup>39</sup> regulating redox potential in iron-sulfur proteins,<sup>40</sup> and shaping the 3D structures of membrane proteins for functional specificity.<sup>41</sup> In polymer science, thio-based H-bonding motifs, including thiourea, thioamide, and thiobarbiturate (TBa), have recently been widely explored for applications in electronics,<sup>42-44</sup> super elastomers,<sup>35,45,46</sup> and dielectric gating materials,<sup>47-49</sup> underscoring the comparable significance of sulfur/oxygen-centered H-bonds.

### 1.1.2. Synthesis of Hydrogen-Bonded Polymers

To synthesize H-bonded polymers (HBPs), H-bonding motifs must be covalently incorporated into the polymer structure, either at the termini, on side chains, or along the main chain of the backbone. These polymers can be synthesized through various approaches, including de novo synthesis from monomeric building blocks<sup>50-52</sup> and post-polymerization modification.<sup>53-55</sup>



In the de novo synthesis of HBPs, H-bonding motifs are covalently attached to reactive monomers to produce side-chain HBPs. These monomers typically are based on acrylate,<sup>56-58</sup> styrene,<sup>59</sup> and acrylamide<sup>60,61</sup> monomers for chain-growth polymerization or modified multifunctional monomers<sup>36,51</sup> for step-growth polymerization with for instance isocyanate-alcohol/amine chemistry, alcohol/amine-acid condensation (**Figure 1.3**). For H-bonding motifs at polymer termini, polymerization reagents are first modified with the desired motifs. These reagents include modified chain transfer agents (CTA) in reversible addition-fragmentation chain-transfer polymerization (RAFT),<sup>62-65</sup> radical initiators in atom transfer radical polymerization (ATRP),<sup>66-68</sup> nitroxide-mediated radical polymerization (NMP),<sup>69</sup> and modified chain stoppers with H-bonding motifs in step-growth polymerization<sup>70</sup>.

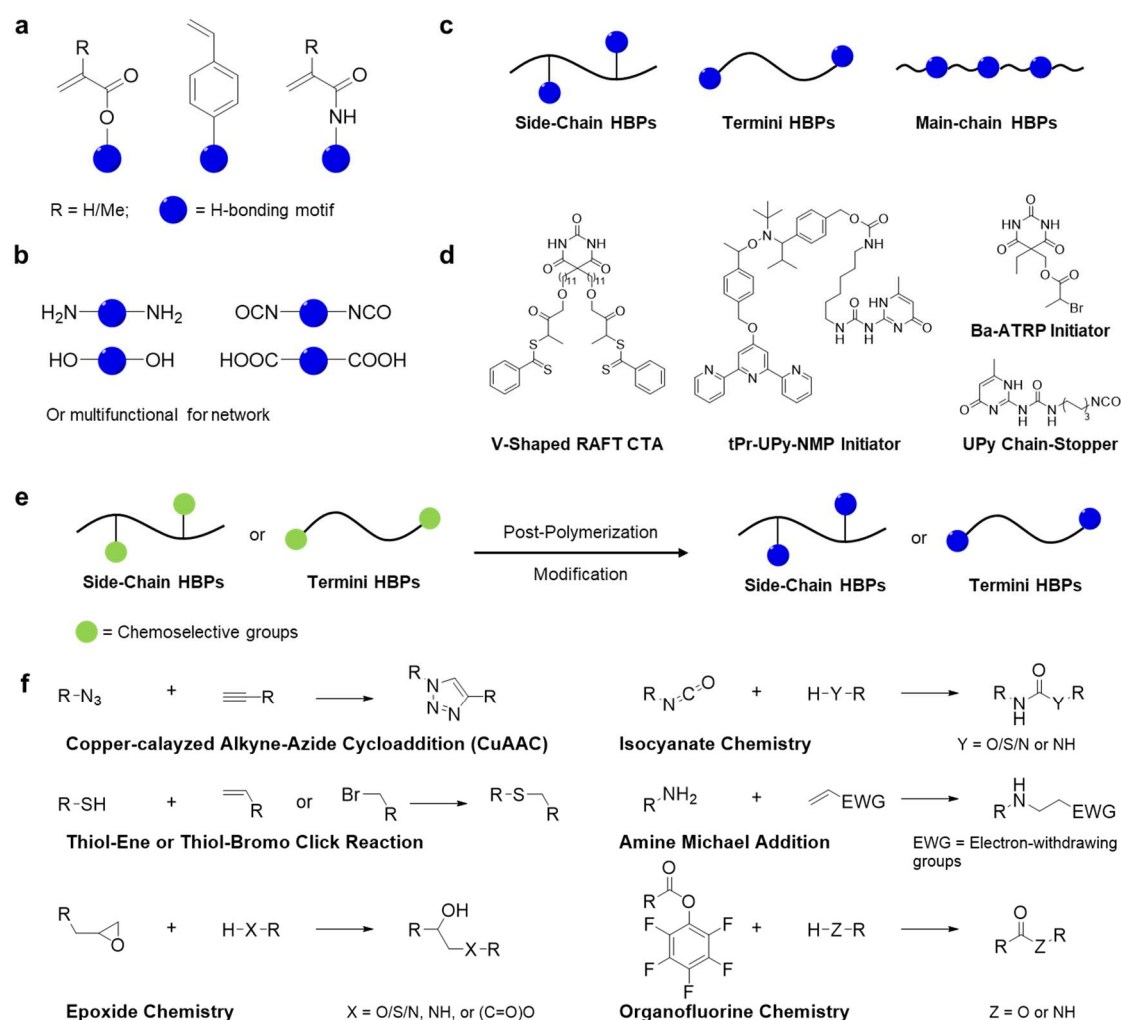


**Figure 1.3** H-bonding monomers for a) chain-addition and b) step-addition polymerization; c) schematic illustration of side-chain, termini-, and main-chain HBPs; d) examples of the V-shaped CTA for RAFT polymerization,<sup>52</sup> the initiator with terpyridine(tPy) and UPy motif

for NMP,<sup>69</sup> the Ba-modified initiator for ATRP,<sup>67</sup> and the chain-stopper with UPy motifs used in PU synthesis;<sup>71</sup> schematic illustration showing the post-polymerization to embed H-bonding motifs on polymer chains with defined functional groups; f) the chemoselective groups for post-polymerization modification.<sup>54,55,72-74</sup>

Incorporating H-bonding motifs into the main chain is more challenging and typically achieved via step-growth polymerization, as often seen in polyurethane.<sup>51,75,76</sup> Here, H-bonding motifs with bivalent reactive groups, such as amine, alcohol, or isocyanate, react with other multivalent monomers or macromonomers to form main-chain HBPs. Additionally, acyclic diene metathesis polymerization (ADMET)<sup>77</sup> offers alternative routes, resembling polycondensation or polyaddition processes for main-chain polymer synthesis.

An alternative approach to synthesizing HBPs is via post-polymerization modification.<sup>54,55,72,73</sup> This method requires chemoselective functional groups to be strategically incorporated into the polymer backbone or side chains (**Figure 1.3d&e**). Given that post-modification involves macromolecules with multiple reactive sites along a single chain, reactions must proceed under mild conditions while ensuring high conversion efficiency and fidelity of the functional groups. Commonly employed post-polymerization reactions include copper-catalyzed alkyne-azide cycloaddition (CuAAC),<sup>67,78,79</sup> thiol-ene<sup>80-82</sup> or thiol-bromo click reaction,<sup>83-85</sup> epoxide chemistry,<sup>74,86</sup> isocyanate reactions,<sup>87-89</sup> Michael addition,<sup>90-92</sup> and organofluorine chemistry.<sup>54</sup> In ATRP<sup>55</sup> and RAFT<sup>55,72</sup> polymerization, the presence of a bromide initiator or chain transfer agent (CTA) generates reactive  $\omega$ -chain ends, facilitating terminal modification for terminifunctionalized HBP. Similarly, living anionic polymerization (LAP)<sup>93,94</sup> and living carbocation polymerization (LCCP)<sup>95,96</sup> exploit their active ionic growing centers to introduce tailored terminal groups, further enabling terminifunctionalized HBP synthesis. Overall, post-polymerization modification provides a versatile route for functional polymer synthesis while maintaining the same parent polymer structure which enables systematic studies of HBPs, minimizing structural variations such as molecular weight ( $M_n$ ) and polydispersity (PDI), thereby ensuring consistency in comparative analyses.

### 1.1.3. Hydrogen-Bonded Macromolecular-Assembly and the Formation of Aggregates

Low-molecular-weight H-bonding motifs, due to their directional and selective

nature, can self-assemble into diverse structures, including linear oligomers, polymers, and networks.<sup>97</sup> Motifs with rational topologies can be further organized into higher-order structures.<sup>98,99</sup> When tethered on polymeric backbones, these motifs similarly drive synthetic polymers toward macromolecular assembly in solutions, resembling their low-molecular-weight counterparts while also integrating backbone interactions.<sup>100-102</sup> In biological systems, H-bond-mediated macromolecular assemblies play a crucial role in the formation of the DNA double helix,<sup>103-105</sup> protein secondary structures,<sup>106-108</sup> and enzyme-substrate recognition.<sup>109-111</sup> These H-bonding processes cope cooperatively with other interactions, including hydrophobic<sup>112,113</sup> and electrostatic forces,<sup>114,115</sup> further stabilizing complex biological architectures.

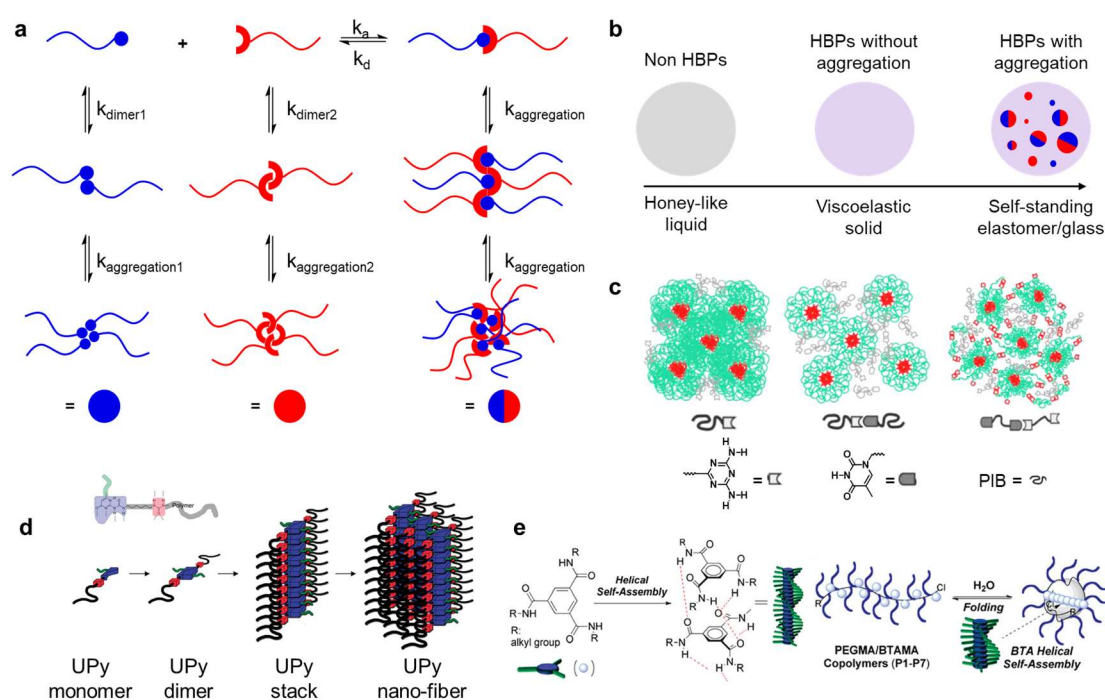


**Figure 1.4** a) Possible H-bonding association in a polymer matrix, including self-association, hetero-complementary association, and further high-order aggregation; b). schematic illustration: non-HPBs are generally honey-like liquids, when equipped with H-bonds, they could be reinforced into viscoelastic solid, and further into a self-standing elastomer or glass if H-bonded aggregation presents; c) DAT/Thy functionalized polyisobutylene (PIB) forming different micellar aggregates in the bulk polymer (adapted with permission from reference,<sup>116</sup> Copyright 2014 American Chemical Society); d) UPy motif modified with a nonpolar polyolefin backbone first dimerize then aggregate into stacks, and further into nano-fiber (adapted with permission from reference,<sup>117</sup> Copyright 2011 American Chemical Society); e) the hydrophobic benzene-1,3,5-tricarboxamide (BTA) motifs drive the hydrophilic PEG segments into stacks in an aqueous medium (adapted with permission from reference,<sup>118</sup> Copyright 2011 American Chemical Society).

Beyond driving macromolecular assembly, associative H-bonding motifs in neat polymers can form H-bonded aggregates, significantly influencing matrix properties.<sup>119</sup> As depicted in **Figure 1.4a**, H-bond motifs in the bulk polymer can form multiple aggregates, depending on the molecular environment. They can form the complementary complex, while they could also self-associate, owing to the limited available counterparts in adjacent, which is constrained by the anisotropic nature of polymer bulk and diffusion limitations.<sup>120-122</sup> However, these unique aggregates via associative H-bonding motifs in neat polymers significantly influence matrix properties.<sup>119</sup> Compared to, e.g., low-molecular-weight non-HBPs which are typically honey-like liquids, when equipped with H-bonds, their viscoelasticity is altered, transitioning into viscoelastic solids.<sup>67,123</sup> Further, if there were H-bonded aggregates or even separated microphases, the mechanical strength of the matrix polymers would be significantly enhanced.<sup>50,89,124</sup> Thy-DAT complex is widely explored for such ability to alter polymer mechanical strength. For instance, the Thy-DAT complex, when embedded in a PIB backbone, can generate micellar aggregates in the bulk polymer, consequent for the altered viscoelasticity of the PIB matrix.<sup>116</sup> When only Thy motif was embedded into a poly(propylene oxide) (PPO) matrix, the weak self-association of Thy in the bulk PPO leads to the crystallization of Thy motifs, enhancing the PPO matrix into a self-standing solid. However, when the Thy-DAT complex was embedded into the same PPO matrix, such a stronger hetero-complementary H-bonding complex lead to a counterintuitive weaker mechanical strengthening, changing the matrix into a viscous liquid, which is due to disruption of the Thy crystalline assembly via its self-association.<sup>125,126</sup> Besides hetero-complementary H-bonding motifs, self-complementary motifs such as UPy for its strong quadruple H-bonds are also widely incorporated into various polymer systems. Owing to the strong dimerization of UPy motifs, high-order structures such as nano-fiber<sup>117</sup> or needle-like stacks<sup>127</sup> are often observed in polymers modified with UPy motifs. Such high-order structures of UPy aggregates can even form in an aqueous environment,<sup>128,129</sup> by shielding via hydrophobic functional groups. Alternatively, the hydrophobic benzene-1,3,5-tricarboxamide (BTA) motif achieves a cooperative effect between  $\pi$ - $\pi$  stacking and H-bonding, resulting in molecular stacking in aqueous medium (**Figure 1.4e**), utilized to create single-chain folding of BTA-modified polymers for catalytic systems.<sup>118</sup> Thus, H-bond-mediated aggregation substantially alters polymer properties, conferring changes in mechanical strength,<sup>70,78,130</sup> morphology,<sup>59,101,131</sup> and stimuli responsiveness,<sup>132-134</sup> making these materials

highly relevant for biomedicine,<sup>113,135,136</sup> 3D printing,<sup>71,137</sup> and reversible adhesive.<sup>57,83,138</sup>

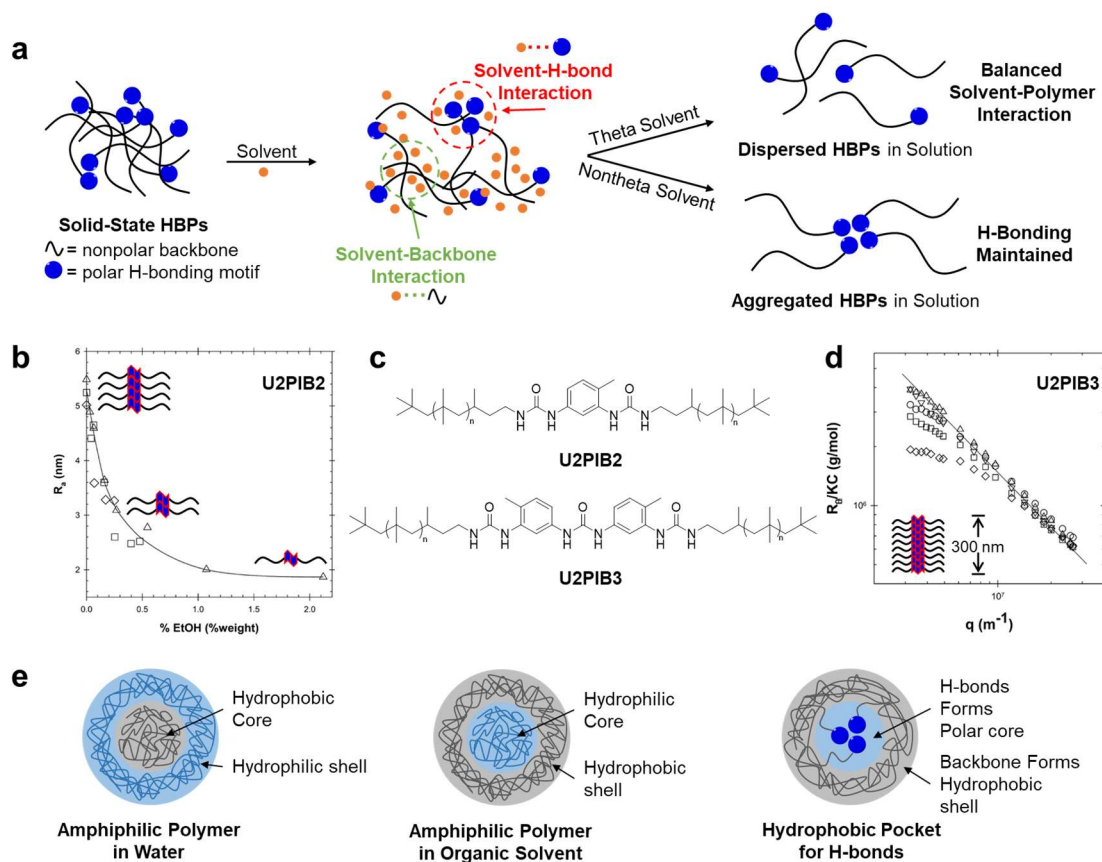
## **1.2. Impact of Polymers on the Dynamic Equilibria of Hydrogen-Bonds in Various Surroundings**

H-bonds, due to their dipolar nature, are highly sensitive to their molecular environment.<sup>139-141</sup> In solution, solvent molecules interact with both the H-bonding moieties and the polymer backbones, impacting the formation of assemblies or high-order structures.<sup>84,142,143</sup> Conversely, in the solid state, local confinement restricts H-bonding moieties from adopting their optimal geometry,<sup>144</sup> leading to aggregates distinct from their solution counterparts. Various factors influence the behavior of H-bonding motifs in different molecular contexts. Specific environments, such as ionic media, polymer blends, and phase-separated hydrogels or organogels, present unique challenges for analyzing and predicting H-bonding behavior due to their complex molecular interactions in such HBPs consisting of low-molecular-weight H-bonding units or oligomeric/polymeric building blocks functionalized with associative, reversible H-bonding motifs. This part focuses on the latter category of HBPs, where H-bonding motifs are integrated onto polymer backbones, and examines how local molecular environments influence their properties and behavior, particularly from the perspective of polymer backbones and H-bond interactions.

### **1.2.1. Assembly of H-bonded Supramolecular Polymers in Solution**

For noncharged polymers devoid of H-bonding motifs, solvent interactions can be categorized into theta solvents, poor solvents, and good solvents.<sup>121,145,146</sup> In contact with a solvent polymer chains interact with solvent molecules via noncovalent forces such as van der Waals interactions, dipole-dipole interactions, or H-bonding (if applicable), with additional interactions present as polymer-polymer interactions. With increasing amounts of solvent, solvent-polymer interactions gradually offset polymer-polymer interactions, reaching an equilibrium where polymer segments move freely relative to each other. Under theta-conditions, polymer chains conform to the Flory scaling law for ideal chains, with the radius of gyration ( $R_g$ ) proportional to  $N^{1/2}$ , where  $N$  represents the number of monomer units. In a poor solvent, polymer-solvent interactions are weak, causing polymer chains to collapse and potentially undergo phase separation, leading to polymer aggregation due to backbone-

solvent demixing. Conversely, in a good solvent, polymer chains exhibit stronger interactions with solvent molecules, adopting a swollen, extended



conformation.

**Figure 1.5** a) Schematic illustration of HBPs with polar H-bonding groups while the backbone may bear different nature of polarity, resulting in controversial dissolution process; b) the apparent hydrodynamic radius,  $R_a$ , of U2PIB2 supramolecular assemblies in ethanol/cyclohexane mixtures, (U2PIB2 concentrations of (◇) 2 g·L<sup>-1</sup>, (□) 4 g·L<sup>-1</sup>, and (△) 8 g·L<sup>-1</sup>), showing competitive association by ethanol to the bisurea thus deteriorating the assembly; c) structure of PIB with a bisurea (U2PIB2) or a trisurea core U3PIB2; d) the scattering wave vector  $q$  of U3PIB2 assembly in cyclohexane, demonstrating the giant U3PIB2 assembly up to 300 nm (polymer concentrations: (△) 0.08 g·L<sup>-1</sup>, (▽) 0.14 g·L<sup>-1</sup>, (○) 0.68 g·L<sup>-1</sup>, (□) 1.34 g·L<sup>-1</sup>, and (◇) 3.41 g·L<sup>-1</sup>; the solid line has a slope -1); Figure 1.4c&d are adapted with permission from reference,<sup>147</sup> Copyright 2013 American Chemical Society; e) the schematic illustration of amphiphilic polymer assembly in water and organic solvents, as well as the hydrophobic pocket to preserve H-bonds in aqueous system.

When polymer chains are functionalized with H-bonding motifs, their solvation behavior becomes more complex. While the attachment of H-bonding motifs induces only minor changes in interaction strength,<sup>62</sup> the integrity of

specific H-bonds can be preserved, unless cooperative effects<sup>148</sup> dominate or steric hindrance<sup>63,147,149</sup> from the attached backbone disrupts association. If under theta-conditions, solvent molecules not only balance polymer-polymer and solvent-polymer interactions but also compete with H-bonding motifs for solvation, partially disrupting H-bonds (**Figure 1.5a**). This competition introduces additional energy requirements and imposes stricter solvent selection criteria compared to non-H-bonded polymers, highlighting the sensitivity of H-bonding to molecular surroundings, particularly solvent properties.<sup>140,150</sup>

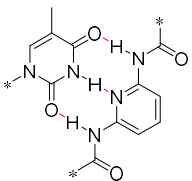
Researchers frequently manipulate solvent environments to direct the assembly of HBPs into distinct structures. Pensec et al.<sup>148</sup> synthesized a bisurea-functionalized polymer U2PIB2 with two pending PIB-arms (**Figure 1.5b-d**). The PIB arms ensure good solubility in both nonpolar solvents (heptane, toluene, chloroform) and polar solvents (THF). However, the bisurea core, which remains partially solvated and phase-separates from nonpolar solvents, drives the formation of higher-order structures. In contrast, low-molecular-weight bisurea U2PIB0 assembles into filaments or tubular structures depending on the nonpolar solvent used. Small-angle neutron scattering (SANS) and FT-IR analyses confirm that U2PIB2 consistently forms comb-like structures in all tested nonpolar solvents, with minimal assembly in polar solvents like THF. The observed filamentous, rather than tubular, assembly is likely due to steric hindrance from the PIB arms, preventing the formation of tubular structures. Building on this work, Catrouillet et al.<sup>147</sup> synthesized a trisurea-functionalized polymer U3PIB2 with stronger H-bonds and studied its assembly behavior. In a cyclohexane-ethanol mixture, increasing ethanol content progressively reduces the assembly of U2PIB2, underscoring the critical role of solvent polarity in H-bonded self-assembly. However, U3PIB2, with its stronger H-bonds, forms much larger bottle-brush-like structures. In contrast, U2PIB2 forms only short filaments, as its weaker H-bonds cannot sufficiently compensate for the conformational entropy penalty of the PIB side arms. Further extending this work, Catrouillet et al.<sup>149</sup> explored self-assembly in polystyrene-based systems, revealing that trisurea self-assembly is strongly influenced by both the molecular environment and the degree of polymerization of the polymer side chains.

HBPs can also self-assemble in aqueous environments, where hydrophobic

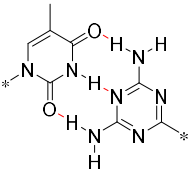
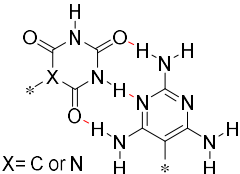
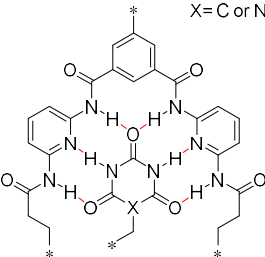
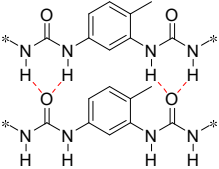
and hydrophilic interactions are key to structural organization. Amphiphilic block copolymers functionalized with H-bonding motifs are often designed to control these interactions.<sup>151</sup> To protect H-bonds from weakening or dissociating by water molecules,<sup>152</sup> the hydrophobic block encapsulates the H-bonding motifs, forming a hydrophobic core. The hydrophilic block surrounds this core, resulting in a core-shell structure, commonly referred to as a hydrophobic pocket<sup>153-155</sup> for H-bonds (**Figure 1.5e**), a structural feature frequently observed in proteins.<sup>156</sup> In certain systems, H-bonding motifs themselves can influence assembly behavior. Mandal et al.<sup>157</sup>, reported that TBA-functionalized PCL and PLA exhibit a unique assembly mechanism in water. Since TBA is more polar than the polymer backbone, the hydrophobic core is formed by the collapsed PCL or PLA chains, while the TBA motifs populate the outer shell, leading to droplet-like assemblies. Further analysis through dye release experiments revealed that at pH 5.5, the release rate of encapsulated dye significantly increased. This behavior was attributed to the disruption of H-bonds among TBA motifs in the acidic aqueous environment, demonstrating the pH-responsive nature of these assemblies as a functional material application.

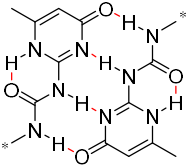
Though there are aforementioned confinements from the solvent, the H-bonding strength can be expressed by its  $K_a$  measured in solutions.<sup>158</sup> **Table 1** summarizes the H-bonding motifs, their  $K_a$  measured in solutions, and their  $K_a$  when modified with polymeric backbones.

**Table 1** The selected H-bonding motifs, their association constant, the polymeric backbone attached, and the association constant with the backbone.

Name	H-bonding Motifs and $K_a$	With Backbone and the Resulting $K_a$
<b>Thymine-Diaminopyridine (Thy-DAP)</b>	 $\sim 10^2 \text{ M}^{-1}$ (NMR titration, $\text{CDCl}_3$ ) <sup>27</sup>	PVAc-Thy+PVAc-DAP-PVAc <sup>64</sup> $1.4 \times 10^2 \text{ M}^{-1}$ (NMR titration, $\text{CDCl}_3$ )
		PVAc-Thy+PS-DAP-PS <sup>159</sup> $9.0 \times 10^1 \text{ M}^{-1}$ (NMR titration, $\text{CDCl}_3$ )
		PMMA-Thy+PS-DAP-PS <sup>159</sup> $8.5 \times 10^1 \text{ M}^{-1}$ (NMR titration, $\text{CDCl}_3$ )
		PI-Thy+PS-DAP-PS <sup>159</sup> $8.0 \times 10^1 \text{ M}^{-1}$ (NMR titration, $\text{CDCl}_3$ )



<b>Thymine- Diaminotriazine (Thy-DAT)</b>	 <p>~ 10<sup>2</sup> M<sup>-1</sup> (NMR titration, CDCl<sub>3</sub>)<sup>27</sup></p>	PIB-Bis-Thy+PEK-Bis-DAT <sup>160</sup> 10 <sup>0-3</sup> M <sup>-1</sup> (NMR titration, CDCl <sub>3</sub> ) PIB <sup>78</sup> 1.1 × 10 <sup>3</sup> M <sup>-1</sup> (NMR titration, CDCl <sub>3</sub> ) PnBA <sup>161</sup> 2.6 × 10 <sup>3</sup> M <sup>-1</sup> (NMR titration, CDCl <sub>3</sub> ) PPO-bisThy/DAT <sup>162</sup> 8.5 × 10 <sup>2</sup> M <sup>-1</sup> (NMR titration, CDCl <sub>3</sub> )
<b>Cyanurate /Barbiturate- Triaminopyrimidine (Cy/Ba-TAP)</b>	 <p>X = C or N ~ 10<sup>2</sup> M<sup>-1</sup> (NMR titration, CDCl<sub>3</sub>)<sup>163-165</sup></p>	PDMS <sup>166</sup> 1.3 × 10 <sup>2</sup> M <sup>-1</sup> (NMR titration, CDCl <sub>3</sub> )
<b>Hamilton Wedge- Cyanurate /Barbiturate (HW-Cy/Ba)</b>	 <p>X = C or N 2.1 × 10<sup>4</sup> M<sup>-1</sup> (NMR titration, CDCl<sub>3</sub>)<sup>21</sup>          2.5 × 10<sup>5</sup> M<sup>-1</sup>          (cyclic HW, Fluorescence/UV,          CH<sub>2</sub>Cl<sub>2</sub>)<sup>23</sup>          1.4 × 10<sup>6</sup> M<sup>-1</sup>          (cyclic HW, NMR titration,          CDCl<sub>3</sub>)<sup>21</sup></p>	PIB <sup>130</sup> 6 × 10 <sup>4</sup> M <sup>-1</sup> (NMR titration, CDCl <sub>3</sub> ) PMMA-Ba+HW-PNB <sup>167</sup> 2.9 × 10 <sup>3</sup> M <sup>-1</sup> (NMR titration, CDCl <sub>3</sub> ) PMAc-Ba+HW-PiC <sup>168</sup> 9.5 × 10 <sup>3</sup> M <sup>-1</sup> (NMR titration, CDCl <sub>3</sub> ) PMAc-Ba+HW-PiC <sup>169</sup> 3 × 10 <sup>4</sup> M <sup>-1</sup> (NMR titration, CDCl <sub>3</sub> ; ITC, DCE) PEO-HW+Ba <sup>170</sup> 2.8 × 10 <sup>4</sup> M <sup>-1</sup> (NMR titration, CDCl <sub>3</sub> ) PDMS <sup>166</sup> 4.3 × 10 <sup>4</sup> M <sup>-1</sup> (NMR titration, CDCl <sub>3</sub> )
<b>2,4-Toluene Bisurea Dimer</b>		PIB <sup>148</sup> 3.5 × 10 <sup>2</sup> M <sup>-1</sup> (ITC, CHCl <sub>3</sub> )

	$1.7 \times 10^3 \text{ M}^{-1}$ (ITC, $\text{CHCl}_3$ ) <sup>148</sup>	
<b>Ureidopyrimidinone (UPy) Dimer</b>	 $2.2 \times 10^6 \text{ M}^{-1}$ (NMR titration, $\text{CDCl}_3$ ) <sup>17</sup> $5.7 \times 10^7 \text{ M}^{-1}$ (Fluorescence, $\text{CDCl}_3$ ) <sup>171</sup> $5.9 \times 10^8 \text{ M}^{-1}$ (Fluorescence, toluene- $d_8$ ) <sup>171</sup>	$\text{PnBA}^{172}$ $\sim 10^{4-6} \text{ M}^{-1}$ (NMR titration, $\text{CDCl}_3$ )

### 1.2.2. In the Solid State of a Single Polymer

In bulk-polymers, where solvents and other mobile, low-molecular weight compounds are absent, the H-bonding motifs are then surrounded solely by the polymeric backbone. As a result, the chemical nature of the backbone plays a crucial role in modulating H-bond interactions, similar to solvent effects in (concentrated) solution. Additionally, in bulk polymers, the mobility of associative groups is highly restricted by local chain dynamics governed by segmental motion.<sup>121</sup> Consequently, H-bonds in the solid-state polymer matrix are rarely in their optimal configuration.<sup>144</sup> As supramolecular polymers often exhibit inhomogeneity at both local and global scales,<sup>173</sup> they introduce an additional driving force for H-bonding motifs to phase-segregate. In semi-crystalline polymers, crystalline regions impose further constraints on H-bonding interactions, while in covalently crosslinked polymer networks, long-range diffusion of H-bonding moieties is prohibited, preventing the formation of extended H-bonded aggregates. Thus, in solid-state polymers, both the chemical composition and physical chain dynamics dictate H-bonding behavior, influencing morphology, phase separation, and supramolecular organization.

#### **Influences from the Chemical Nature of the Polymeric Backbone**

Similar to low-molecular-weight compounds, the polarity of the polymer backbone significantly affects H-bond interactions in solid-state polymers. Since H-bonding motifs typically consist of carbon, polar atoms (O/N), and

protons, they exhibit moderate polarity. In solid-state polymers, polar backbones provide better solvation for H-bonding motifs than nonpolar backbones. **(Figure 1.6a)** Consequently, in polymers with increased polarity such as in PEO and its derivatives,<sup>71,137,174,175</sup> H-bonding motifs tend to exhibit weaker association, as confirmed by rheological study,<sup>137,175,176</sup> solid-state NMR,<sup>152,177,178</sup> and FT-IR spectroscopy.<sup>71,174,179</sup> This reduces association from competitive H-bonding interactions between the motifs and the polymer backbone, where O/N atoms act as additional H-bond acceptors, and -OH/-NH groups serve as additional H-bond donors, analogous to the effect observed in polar solvents.<sup>148,150,180,181</sup> Due to enhanced solvation by polar backbones, H-bonding motifs distribute more homogeneously within the polymer matrix, reducing the likelihood of phase-separated H-bonded aggregates<sup>176</sup> account for the mechanical properties of the modified polymer matrix.<sup>78,119,127,182</sup>

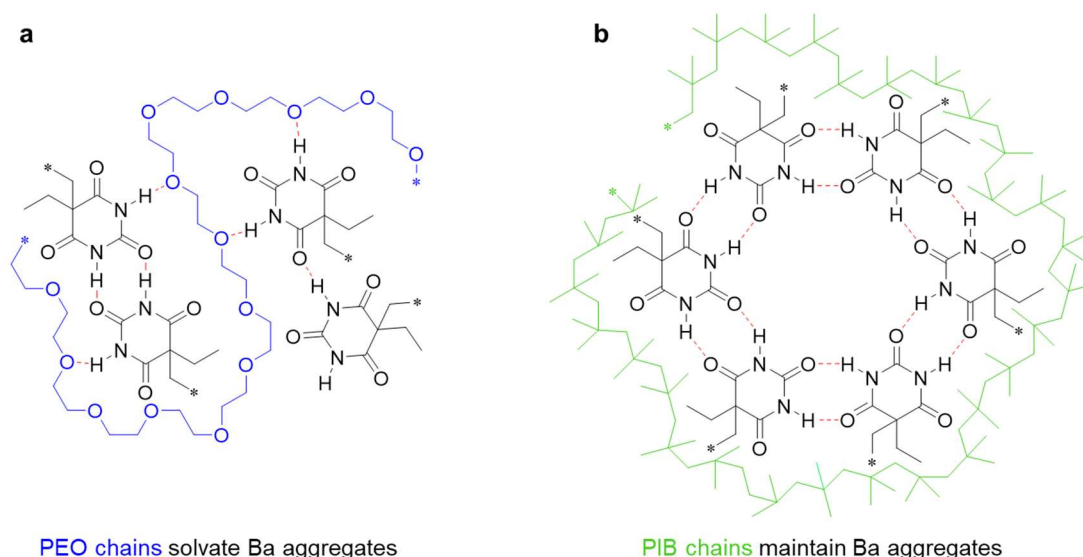


**Figure 1.6** a) Ba aggregates in the bulk PEO could be solvated and thus dissociated owing to the oxygen acting as the extra H-bonding acceptors; while b) in bulk PIB the Ba aggregates maintain their association owing to insufficient solvation by nonpolar PIB chains.

In contrast, in many nonpolar polymers, H-bonds usually display promoted association, as the motifs in the nonpolar solvents.<sup>183-185</sup> The nonpolar polymer backbones(**Figure 1.6b**), such as PIB, PE, and PP, lack polar groups like O/N, thus cannot solvate or completely solvate the polar H-bonding motifs covalently attached,<sup>186</sup> leading to a driving force steering the polar motifs to segregate from the polymeric backbones and gather together. Due to this tendency of

segregation from the backbone and assembly of H-bonding motifs, the H-bonded aggregates and further possible high-order structures can be generated.<sup>117,187</sup>

Steric hindrance from bulky polymer backbones significantly influences the molecular packing of H-bonding motifs, often resulting in unpredictable assembly in solid-state polymers.<sup>147-149</sup> This steric effect arises from multiple factors, including the molecular weight,<sup>188</sup> which determines chain length and chain entanglement, the backbone topology,<sup>84,189,190</sup> which dictates overall chain conformation and chemical composition at the surface, and the monomer structure,<sup>191-193</sup> which affects local packing constraints for instance in PA6 and PA66. By manipulating these parameters, it is possible to precisely control H-bond assembly and the consequent mechanical properties.

Aside from carbohydrate polymers, fluorinated polymers exhibit distinctive chemical properties due to the strength of the carbon-fluorine bond and the unique spatial arrangement of fluorine atoms. The incorporation of fluorinated monomers or blocks into a polymer chain alters its chemical and physical performance.<sup>194,195</sup> H-bonding motifs associated with (semi-) fluorinated polymers exhibit altered behavior due to the presence of fluorine atoms,<sup>190,196</sup> as the (semi-) fluorinated segments tend to associate with fluorinated regions,<sup>197</sup> the H-bonding motifs are repelled as a result of their hydrocarbon nature, so promoting the formation of the H-bonded aggregates. Moreover, fluorinated groups, such as trifluoromethyl, possess strong dipole moments that generate localized electric fields, influencing nearby H-bonding interactions, plus the electron-withdrawing nature weakens the H-bond acceptor ability, thereby impeding H-bond formation.<sup>198-200</sup> Furthermore, the pronounced electronegativity of fluorine withdraws electron density from H-bond donors, promoting their proton-donating ability and further enhancing weak  $\text{CH}\cdots\text{F}$  H-bonding.<sup>199</sup> Consequently, H-bond interactions in (semi-) fluorinated polymers exhibit complex sensitivities to their fluorinated environment, leading to unique material properties.

### **Influences from Physical Confinement by Backbone Dynamics**

Polymers typically contain amorphous regions where polymer chains are arranged in a disordered, random manner, and H-bonds formed within these regions are significantly influenced by chain dynamics. Amorphous polymers

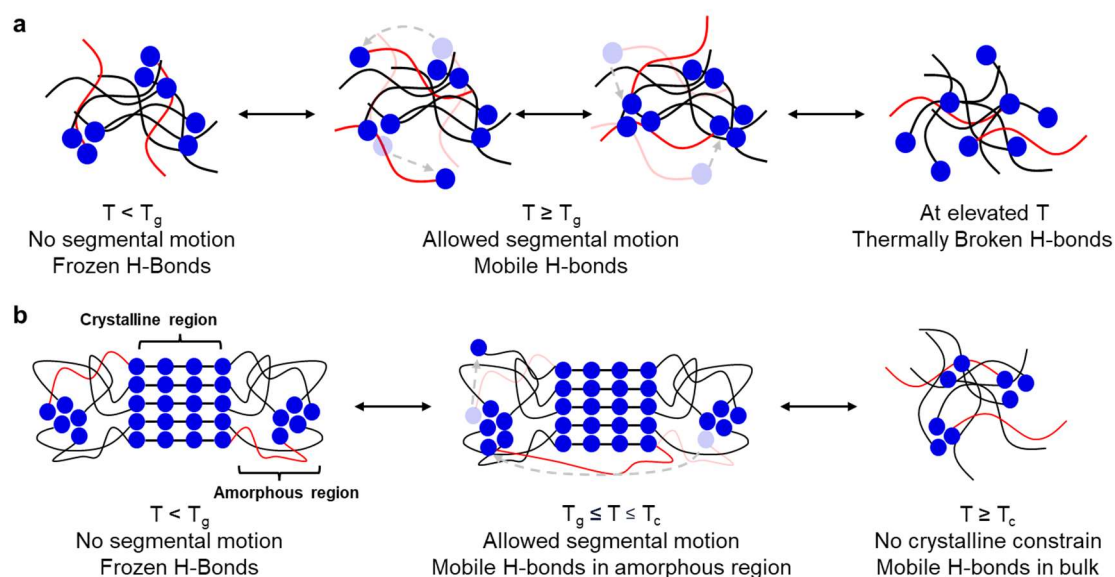


**Figure 1.7** a) In amorphous HBPs, increasing temperature gradually releases H-bonds from the constraints imposed by segmental motion governed by  $T_g$ , while at higher temperatures, thermal disruption weakens H-bonding; b) in semicrystalline HBPs, H-bonds first gain mobility within the amorphous regions as temperature rises, and upon thermal melting of the crystalline phase, the confined H-bonds become mobile throughout the entire polymer bulk.

can undergo a transition from a rigid, glassy state to a flexible, rubbery state at the glass transition temperature ( $T_g$ ).<sup>120-122</sup> Below  $T_g$ , the polymers exhibit glass-like rigidity, with segmental motions and cooperative movements of polymer chain segments being restricted, while localized motions, such as molecular vibrations or rotations, remain possible.<sup>120-122</sup> Consequently, H-bonding motifs in this state are effectively "frozen" due to limited long-range diffusion (**Figure 1.7a**). This phenomenon is commonly observed in H-bond-modified PS<sup>201-203</sup> and PMMA,<sup>204,205</sup> as these polymers have  $T_g$ s above room temperature. At  $T_g$ , polymers start to transition into a rubbery state with increased elasticity, allowing for greater segmental motion,<sup>120-122</sup> and enabling covalently attached H-bonding motifs to diffuse and associate over distances spanning several monomers. However, if chain entanglement is present, the intertwined chains hinder the migration of hydrogen-bonding motifs, thereby constraining their association.<sup>206,207</sup> Above  $T_g$ , polymer chains allow for long-range motion and flow on extended timescales,<sup>120-122</sup> facilitating the diffusion and interaction of H-bonding motifs, leading to the formation of H-bonded aggregates, provided that the H-bonds attached remain stable at the elevated temperatures. This behavior is commonly observed in polymer backbones with low  $T_g$ , such as

PIB,<sup>78,130,148</sup> PDMS,<sup>166,208</sup> and PnBA.<sup>161,172,209</sup> When modified with H-bonding motifs, these backbones provide a matrix that allows the motifs to diffuse and associate freely at room temperature, forming aggregates that contribute to the mechanical reinforcement of the polymer.<sup>116,119,210</sup>

Many polymers also contain crystalline regions, where polymer chains are tightly packed in an ordered, repetitive arrangement.<sup>89</sup> In semicrystalline polymers, H-bonding motifs selectively associate, contributing to the orderly packing of polymer chains and enhancing structural organization and material properties.<sup>191,192,211</sup> A well-known example of a semicrystalline polymer with H-bonds is polyamide 6 (PA6).<sup>193</sup> PA6 consists of repeating units comprising six methylene (-CH<sub>2</sub>-) groups and one amide (-CONH-) group. The flexible C6 chains adopt a highly regular, antiparallel crystalline structure (**Figure 1.7b**), while the amide groups, due to their strong associative nature, further stabilize this arrangement. The antiparallel alignment of C6 chains optimizes the number of H-bonds between adjacent amide groups (-NH and -C=O), minimizing thermal fluctuations and reinforcing structural stability.<sup>191-193</sup> Consequently, these H-bonds within the crystalline regions are effectively "frozen-in," maintaining permanent interchain interactions until thermal energy disrupts the crystalline structure.<sup>212</sup> Other synthetic semicrystalline polymers such as PVA,<sup>213</sup> and biopolymers like polysaccharides,<sup>214</sup> also show similar effects between H-bonds and their crystalline domains. Alternatively, when H-bonds are located at the termini of a semicrystalline polymer, blending with another polymer bearing complementary H-bonds can lead to the formation of a pseudo-block copolymer. This interaction modifies the crystallization behavior of the semicrystalline polymer due to the influence of the second polymer backbone, as demonstrated in Thy-DAP-modified PCL-PIB blends.<sup>79,211</sup>

### **Influences from Backbone Topology**

Polymer topology can significantly influence the cooperative behavior of H-bonds in the polymer (**Figure 1.8**). Main-chain HBPs bear H-bonding motifs integrated on the polymer backbone and these motifs are part of the repeating unit. Main-chain HBPs are composed of long, unbranched chains that facilitate tighter chain packing and molecular alignment, thereby maximizing H-bonding association due to reduced steric hindrance and greater accessibility of H-bonding groups, as often seen in polyamide,<sup>191,193</sup> polyurethane,<sup>51,75,215</sup> and

polyurea.<sup>35,37,208</sup> Main-chain HBPs often demonstrate promoted  $T_g$  and enhanced mechanical strength owing to the synergistic effect of compact chain alignment and reinforced H-bonding. This synergistic effect promotes structural rigidity and restricts chain mobility, contributing to the overall stability and mechanical resilience of the material.<sup>35,70,191-193</sup>

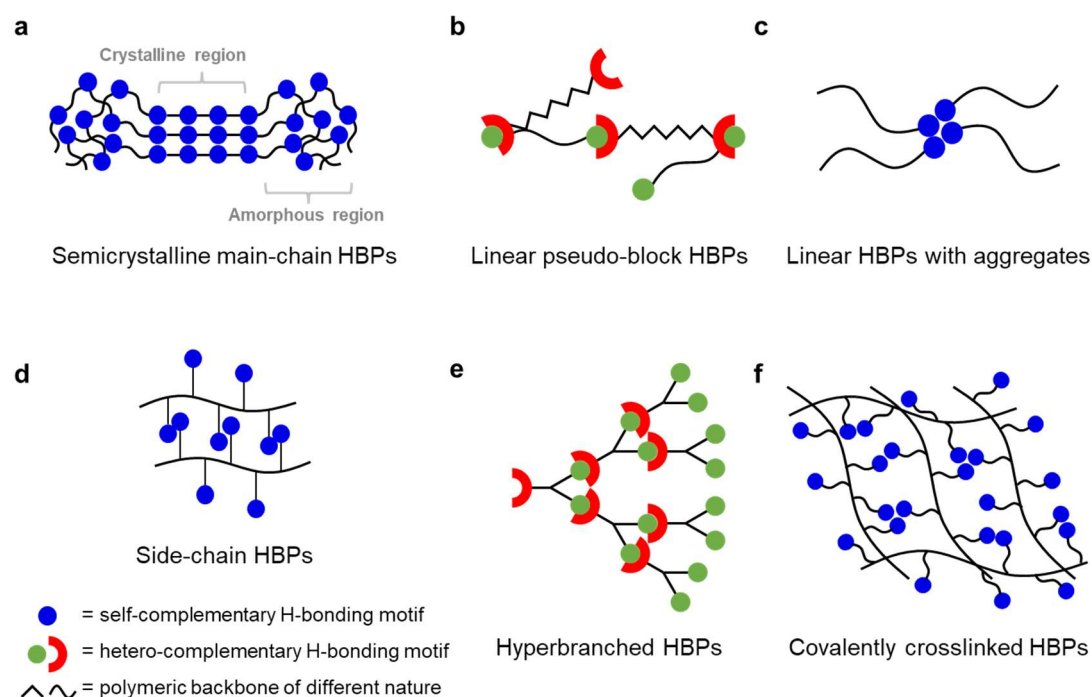


**Figure 1.8** Multiple topologies of HBPs: a) semicrystalline main-chain HBPs with crystalline and amorphous regions; b) pseudo-block HBPs with hetero-complementary H-bonding motifs; c) linear HBPs with the H-bonded aggregates; d) side-chain HBPs with interchain H-bonds; e) hyperbranched HBPs with hetero-complementary H-bonding motifs; and f) covalently crosslinked HBPs with locally confined H-bonds.

Linear termini-HBPs with H-bonding motifs equipped on the termini of the linear chain show distinct H-bonding behavior. If the backbone of termini-HBPs is flexible, as often seen in modified PIB,<sup>78,130,137</sup> PDMS,<sup>166,216,217</sup> and PnBA,<sup>161,172,209,218</sup> the H-bonding motifs at the chain ends are allowed to associate with each other so-forming aggregates in bulk. However, with increasing molecular weight, the abundance of H-bonding motifs in the polymer leads to a diminished contribution of H-bonding relative to chain relaxation.<sup>137,188</sup> As a result, the strengthening effect attributed to H-bonding is significantly reduced, as entanglement-driven constraints<sup>206,207</sup> gradually dominate the mechanical behavior of the material. In addition, owing to the

mobile binding site at the chain ends, the termini-HBPs can be used to create pseudo-block copolymer by mixing two distinct backbones equipped with H-bonding pairs, such as pseudo-block copolymer PEK-PIB by HW-Ba complex<sup>96</sup> and PCL-PIB by Thy-DAT complex.<sup>79</sup>

In contrast, branched polymers, characterized by side chains or branches extending from the main backbone, often exhibit increased steric hindrance and reduced packing efficiency, accounting for the lower viscosity and higher solubility of branched polymers.<sup>219-222</sup> A particularly distinct class of branched polymers are dendritic polymers, which possess a hyperbranched, tree-like architecture.<sup>223</sup> When H-bonding motifs are positioned at the branch termini, branched polymers and dendrimers can exhibit a high density of H-bonding sites on their surface, enhancing interactions with external molecules.<sup>189,224</sup> Their compact structure can also lead to chain overlap and packing frustration, thus intramolecular H-bonding or reduced overall H-bonding could also take place.<sup>225</sup>

Crosslinked polymers represent another unique topology, in which covalent crosslinking significantly restricts chain mobility.<sup>226,227</sup> This reduction in mobility could negatively impact H-bonding by limiting the optimal alignment of donors and acceptors, confining H-bonds unevenly throughout the polymer matrix.<sup>228</sup> While crosslinking may constrain overall H-bond density over long distances, the permanent confinement and random distribution of H-bonds may enhance local H-bonding density.<sup>229</sup> These static H-bonds can also function cooperatively as secondary noncovalent crosslinks, reinforcing the network and further slowing H-bond relaxation, thus affecting the polymer's viscoelasticity and mechanical strength.<sup>65</sup>

A distinct case is cyclic polymers, which feature a closed-loop structure without free chain ends. This cyclic topology restricts conformational freedom,<sup>230,231</sup> potentially enhancing H-bonding in localized regions. Cyclic peptides, such as cyclic diastereomers<sup>232</sup> and cyclosporine A,<sup>233</sup> exhibit well-defined H-bonding networks due to their constrained cyclic geometry accounting for their structural stability<sup>234-236</sup> and functional properties.<sup>237-239</sup> Man-made cyclic polymers are also created using H-bonding association, such as the HW-Cy complex<sup>240</sup>. However, the formation of these H-bonded cyclic polymers is highly entropically driven, and can only maintained at low



concentrations in nonpolar solvents where H-bonding interactions between the  $\alpha$ -donor and  $\omega$ -acceptor on the single polymer chain are promoted. Conversely, at higher concentrations, these polymer chains exhibit inter-chain aggregation rather than single-chain folding, which deteriorates the H-bonded cyclic structure.

### **Impact of the Relative Content of H-bonding Motifs**

The relative concentration of H-bonding motifs within the polymer significantly impacts the formation of H-bonded aggregates in the polymer bulk.<sup>123,241</sup> When the H-bonding motifs present with an insufficient amount, owing to the limited amount of associative moieties and uneven distribution of these motifs in the polymer matrix, the optimized association of these H-bonding motifs becomes less possible.<sup>155,176,207</sup> Further, the limited availability of the associative groups could demonstrate inadequate long-range interactions, unable to form well-defined aggregates, thus resulting in low-density and less stable aggregated structures. Consequently, the resulting morphology exhibits small and heterogeneous phase segregations,<sup>84,190</sup> in contrast to the formation of well-defined, uniformly separated phases observed when H-bonds are present in sufficient quantities and quality.<sup>166,242</sup>

### **1.2.3. In Other Novel Surroundings**

Beyond single-polymer systems, researchers have developed a variety of complex polymeric materials with H-bonds incorporated, including polymer blends,<sup>79,243,244</sup> polymeric ionic liquids (POILs),<sup>57,245,246</sup> and polymer gels such as hydrogels,<sup>247-249</sup> organogels,<sup>250-252</sup> and ionogels,<sup>245,253-255</sup> to explore diverse functionalities and applications. In these materials, H-bonds interact with multiple molecular components, including macromolecular backbones, solvent molecules that either solvate or expel, and novel low-molecular-weight ionic liquids (ILs). This intricate molecular environment introduces significant complexity, leading to an incomplete understanding of H-bonding behavior within such novel materials.

### **In Polymer Blends**

When chemically and physically distinct polymers are blended, they typically undergo phase segregation to minimize free energy, forming distinct domains. However, in blends of two HBPs with complementary H-bonding motifs, such as the poly(vinyl alcohol)-poly(vinylpyrrolidone) (PVA-PVP) system,<sup>256</sup> the -OH...O=C H-bonding between alcohol and pyrrolidone moieties along the polymer chains enhances miscibility by reducing interfacial tension and promoting interchain interactions. This intermolecular H-bonding drives originally immiscible polymer chains into proximity, stabilizing their interaction and enabling homogeneity at the molecular level.<sup>244,256,257</sup> (**Figure 1.9a**). In polymer blends, the dissociation on the one hand is guided by phase segregation between the blended polymeric backbones, characterized by their Hildebrand parameter for enthalpic immiscibility.<sup>146,258</sup> On the other hand, attractive H-bonding, accounting for the blend miscibility, depends on the strength of individual H-bonding pairs and the overall H-bond density along the polymer chains. Thus, the extent of phase segregation in polymer blends is primarily dictated by the balance between these opposing forces, i.e., the dissociative phase segregation and attractive H-bonding, which determine the final miscibility and structural integrity of the polymer blends.<sup>242,259</sup>

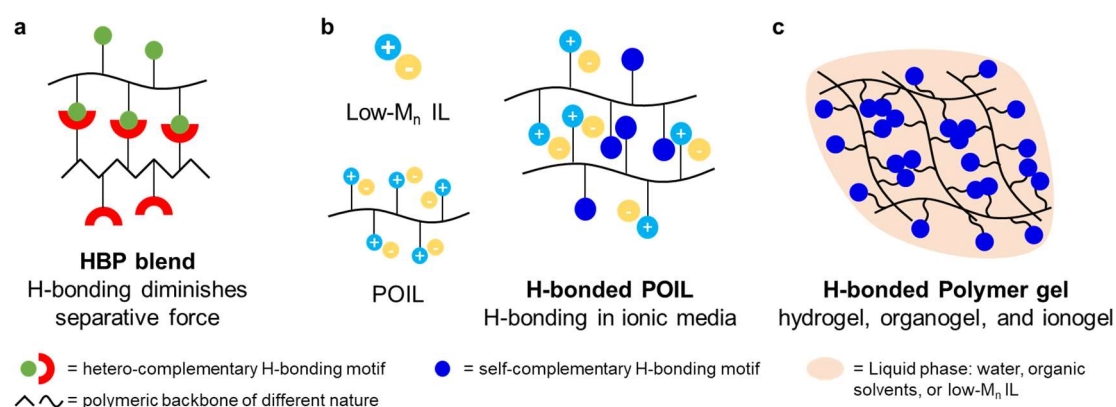


**Figure 1.9** a) Polymer blends of two HBPs with the hetero-complementary H-bonding diminishing the separative force, leading to homogenous polymer blends; b) low-molecular-weight ionic liquid (IL) and polymeric ionic liquid (POIL), and the H-bonded POIL with self-complementary H-bonds covalently tethered on the backbone, which introduces an ionic media to the H-bonds; c) H-bonded polymer gels with different liquid phase: hydrogel with water, organogel with organic solvents, and ionogel with IL.

### **In Polymeric Ionic Media**

When H-bonding motifs are incorporated into or copolymerized with a POIL, an H-bonded POIL is generated, preserving H-bonding within a polymeric ionic

medium (**Figure 1.9b**). POILs inherently combine the properties of their polymeric backbone and the tethered ionic liquid moieties, exhibiting both viscoelasticity and high ionicity. While viscoelastic behavior constrains H-bonds through chain dynamics, the chemical nature of the ionic liquid components significantly influences the dynamics and stability of these embedded H-bonds. Cations, such as imidazolium,<sup>260</sup> triazolium,<sup>261</sup> and protic tert-amine,<sup>262</sup> can serve as potential competitive H-bond donors, capable of interacting with H-bond acceptors like carbonyl groups, thereby weakening the intrinsic H-bonding within the system. Similarly, anions, such as OAc<sup>-</sup>,<sup>263</sup> BF<sub>4</sub><sup>-</sup>,<sup>264</sup> and Cl<sup>-</sup>,<sup>265</sup> can function as H-bond acceptors, interacting with donor groups such as -OH and -NH moieties, further diminishing the strength of embedded H-bonds. The presence of a permanently charged medium generates strong electrostatic fields that can affect H-bond donors or acceptors via electrostatic screening, dielectric shielding, and ion-dipole interactions,<sup>266-268</sup> ultimately reducing the overall H-bond strength. However, due to the ionic moieties, H-bonds within POILs remain highly dynamic,<sup>269,270</sup> constantly breaking and reforming, resulting in exceptionally material properties. This cooperativity between H-bonding and ionic interaction is further utilized for self-healing POILs,<sup>247,271</sup> electrolyte for battery,<sup>246,272</sup> and conductive adhesives.<sup>101,273</sup>

### **In Polymer Gels: Hydrogels, Organogels, and Ionogels**

Polymer gels are polymer-solvent systems characterized by a three-dimensional network of polymers or polymer aggregates capable of retaining substantial amounts of solvent, often exceeding tens to hundreds of times the polymer's weight.<sup>274</sup> Depending on the type of solvent encapsulated, polymer gels can be categorized into hydrogels, which entrap water; organogels, which retain liquid organic molecules; and ionogels, which incorporate low-molecular-weight ILs (**Figure 1.9c**). H-bonds in these materials are embedded into a complex surrounding due to the coexistence of crosslinked polymer backbones and liquid molecules of varying nature. The crosslinked network restricts H-bond dynamics through both chain motion constraints and the chemical properties of the polymer backbone,<sup>271,275,276</sup> while the liquid-rich domains introduce additional consideration. In hydrogels, water molecules can weaken H-bonding<sup>51,152,277,278</sup> due to their high polarity, small steric hindrance, high mobility, and dual role as both H-bond donors and acceptors. In organogels, the entrapped organic solvents may either enhance H-bonding cooperatively<sup>251</sup>

or engage in competitive association,<sup>279</sup> relying on the polarity and chemical composition of the entrapped solvents. In ionogels, the presence of a highly charged medium can weaken H-bonding due to its strong ionicity and the additional donor and acceptor sites provided by ionic species.<sup>260,261,266-268</sup> Besides, phase segregation, which localizes H-bonding, is manipulated to allocate H-bonds to solvophobic domains to boost their association,<sup>253</sup> thereby enhancing the mechanical strength of the gel.

### 1.3. Probing Hydrogen-Bonding Strength in Polymers

H-bonds play a crucial role in polymer systems, with embedded motifs significantly influencing the chemical and physical properties of the resulting materials. Consequently, H-bonding needs to be precisely analyzed to predict bulk material properties. However, detecting these subtle interactions in amorphous or semicrystalline polymers is considerably more challenging than studying H-bonds in small molecules, either in solution or in the solid state. To assess H-bond strength in polymer solutions, various analytical techniques have been developed, primarily relying on titration experiments via spectroscopy<sup>167,280,281</sup> or calorimetry<sup>168,282-284</sup>. In bulk polymers, the restricted diffusion of H-bonding motifs, coupled with the structural complexity of amorphous and semicrystalline backbones, makes such investigations particularly demanding. Nevertheless, advanced techniques such as solid-state NMR spectroscopy (ss NMR)<sup>50,177,285,286</sup> and Fourier-transform infrared spectroscopy (FT-IR)<sup>117,244,287</sup> provide valuable insights into H-bonding within bulk polymeric materials.

#### 1.3.1. Quantitative Analysis of Hydrogen-Bonding Strength in Solutions

Hydrogen-bonding motifs, such as self-complementary UPy dimer and hetero-complementary HW-Ba interaction, are typically studied in solution under a 1:1 equilibrium. A hetero-complementary H-bonding system generally consists of a host species (H) and a guest species (G), which associate in solution in a 1:1 ratio to form a bonded complex (HG), as illustrated below.



This process of H-bonding in an equilibria state is a thermodynamic process governed by the association constant  $K_a$ , which can be expressed as follows.

$$K_a = \frac{[HG]}{[H][G]} \quad (2)$$

Where [HG], [H], and [G] are the concentration of the bonded species, the host, and the guest. With these values in dynamic equilibrium and usually not measurable directly, the total concentration of such a system can help solve this equation. If the total concentration of the host is  $[H]_0$  and that of the guest is  $[G]_0$ , these total concentrations can be expressed as follows.

$$[H]_0 = [H] + [HG] \quad (3)$$

$$[G]_0 = [G] + [HG] \quad (4)$$

Taking (3) and (4) into (2) with [H] and [G] isolated, the expression of  $K_a$  can be expressed as follows.

$$K_a = \frac{[HG]}{[H]_0[G]_0 - [HG]([H]_0 + [G]_0) + [HG]^2} \quad (5)$$

If the [HG] is isolated and the equation (5) is rearranged, the equation (6) can be obtained as follows.

$$[HG]^2 - [HG]\left([H]_0 + [G]_0 + \frac{1}{K_a}\right) + [H]_0[G]_0 = 0 \quad (6)$$

And the real solution of (6) is (7).

$$[HG] = \frac{1}{2} \left\{ \left( [H]_0 + [G]_0 + \frac{1}{K_a} \right) - \sqrt{\left( [H]_0 + [G]_0 + \frac{1}{K_a} \right)^2 - 4[H]_0[G]_0} \right\} \quad (7)$$

Now equation (7) with the  $K_a$  being the only unknown quantity of interest offers a chance to determine the equilibrium constant  $K_a$ , while the direct detection of [HG] remains unrealistic. To solve this difficulty, a variety of indirect measurements via titration where the measurable physical properties change with substrate concentrations have been established, from NMR resonance ( $\delta$ ) to absorbance (A) in UV-vis spectroscopy, or thermal change (Q) in isothermal calorimetry (ITC).<sup>158,288</sup>

### **Spectroscopic Methods**

NMR spectroscopy is among the most informative techniques for studying H-bonding, able to provide both qualitative and quantitative insights. By leveraging NMR, atoms in distinct chemical environments can be detected, with proton NMR being particularly useful due to its direct observation of H-bond donor protons. In addition to proton ( $^1\text{H}$ ),<sup>171,289-292</sup> other nuclei such as  $^{13}\text{C}$ ,<sup>293-295</sup>  $^{19}\text{F}$ ,<sup>296-299</sup>, and other atoms,<sup>297,300-302</sup> can be analyzed to investigate H-bonding from the perspective of acceptor interactions. In a typical H-bonding study using the  $^1\text{H}$  nucleus, the chemical shifts of H-bonded protons are monitored, as their electronic environment changes upon association. By systematically varying the concentration of the H-bonding substrate, these chemical shifts can be recorded and mathematically fitted to determine the association constant  $K_a$ . This approach was first described in the early 1990s<sup>288</sup> and later comprehensively summarized by Prof. Thordarson in 2011.<sup>158</sup> With the assistance of mathematic fitting programs (such as *Origin*, or the online program *BindFit*<sup>303</sup>), the  $K_a$  can be calculated. Despite its efficiency and relatively simple sample preparation, NMR titration for  $K_a$  determination has inherent limitations. The concentration of the substrate must be maintained within a specific range (typically  $10^{-4} \text{ M} < [\text{Substrate}] < 10^{-1} \text{ M}$ ) to generate spectra with sufficient resolution, which may not always be feasible. Additionally, solubility constraints in nonpolar deuterated solvents, such as deuterated DCM, chloroform, and toluene, can further hinder accurate measurements. Moreover, the dynamic nature of H-bonding interactions may not always align with the NMR timescale, introducing uncertainty in  $K_a$  determination. As a result, NMR titration is generally limited to  $K_a$  values not exceeding  $10^5 \text{ M}^{-1}$ ,<sup>158</sup> beyond which the method becomes impractical due to signal broadening and exchange effects.

UV-vis spectroscopy is also a widely used method for determining H-bonding  $K_a$ , due to its affordability, rapid data acquisition, low concentration requirements, and resistance to minor impurities. However, this technique necessitates that the substrate molecules possess chromophoric structures, and within the titration concentration range, the absorbance peaks of interest for both the free substrates and the complex must adhere to Beer-Lambert's Law  $A = \epsilon lc$ , where  $A$  is the absorbance,  $\epsilon$  is the molar attenuation coefficient,  $l$  is the optical path length, and  $c$  is the concentration of the substrate molecule, with an optimal  $A < 1$ . Numerous studies have employed UV-vis spectroscopy to determine  $K_a$  values for H-bonding interactions.<sup>183,280,304,305</sup> Unlike NMR

spectroscopy, which operates on a much slower timescale, the transitions measured in UV-vis spectroscopy occur on the order of  $< 10^{-12}$  s, and the constant  $K_a$  up to  $10^9 \text{ M}^{-1}$  could be precisely determined by UV-Vis titration experiments.<sup>158</sup> As a result, the observed absorbance reflects the cumulative contributions from the host, the guest, and the complex in equilibrium. Mathematical considerations<sup>158,306</sup> for the determination of  $K_a$  via UV-Vis titration experiments are similar to NMR titration, which demands fitting programs such as *Origin* and online tools like *BindFit*.<sup>303</sup>

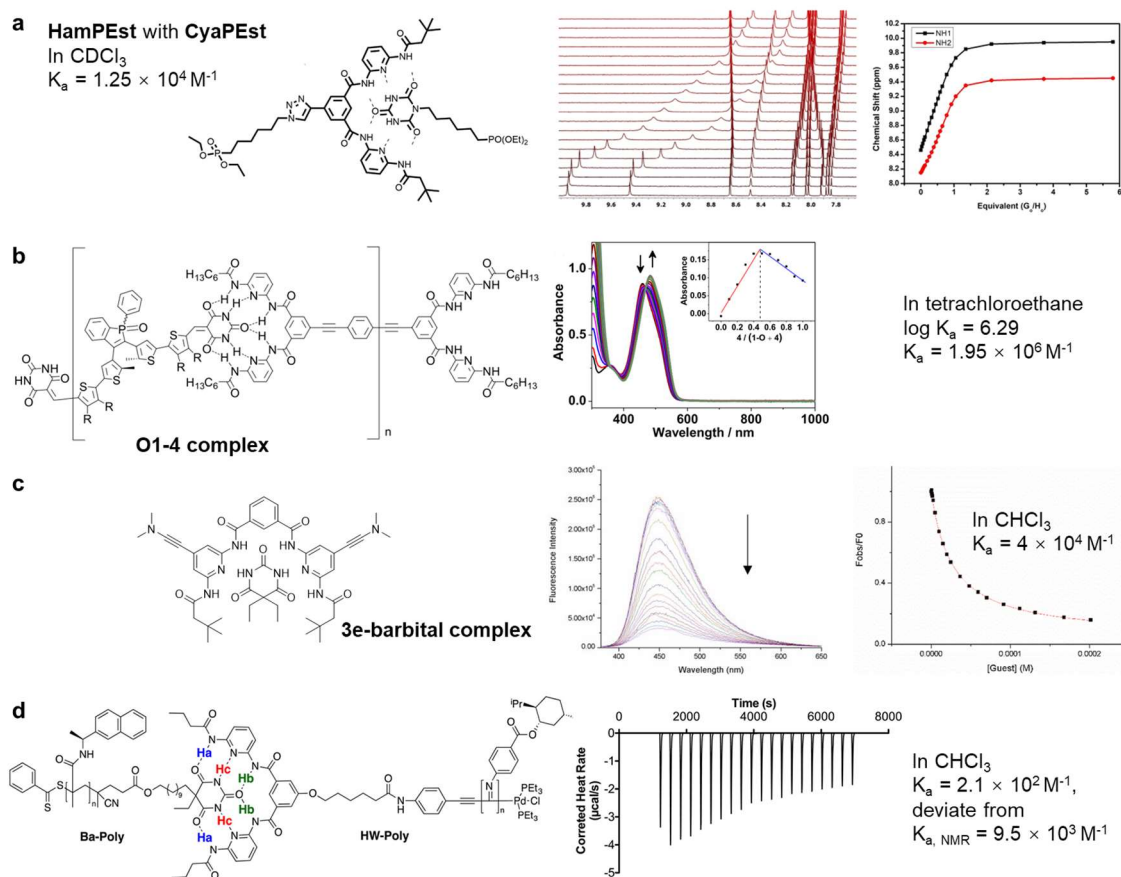


**Figure 1.10** Determination of association constant  $K_a$  via a) NMR spectroscopy (adapted with permissions from Wiley-VCH<sup>307</sup>), b) UV-Vis spectroscopy (adapted with permission from reference,<sup>280</sup> Copyright 2019 American Chemical Society), c) fluorescence spectroscopy (adapted with permission from reference,<sup>308</sup> Copyright 2019 American Chemical Society), and d) isothermal calorimetry (adapted with permission from reference,<sup>168</sup> Copyright 2016 American Chemical Society).

Fluorescence spectroscopy can also be employed to determine  $K_a$  of H-bonds, provided that the substrate molecule is fluorescent. Fluorescence spectroscopy could be the most sensitive method owing to the high quantum

yield and low solvent interference,<sup>309</sup> thereby allowing detection of  $K_a$  with substrate concentration even at the nanomolar range.<sup>281,308,310</sup> To maintain the linear relationship between the fluorescence absorbance/emission with the light absorbed, the concentration must be kept relatively low (sub-micro to nanomolar), which in turn enables the determination of the H-bonds with very large  $K_a$  ( $>10^6 \text{ M}^{-1}$ ).<sup>158</sup>

Practically, to measure the association constant  $K_a$  by NMR, UV-Vis, or fluorescence spectroscopy, isothermal titration calorimetry (ITC) can be employed. While one of the associative partners bears constant concentration, the other partner compound varies its concentration to obtain the physical changes. The resulting physical changes, such as NMR shift of the -NH of the modified HW HAMPEst with cyanurate CyaPEst,<sup>307</sup> UV absorption of O1-4 complex,<sup>280</sup> and the fluorescence intensity of the 3e-barbital complex<sup>308</sup> (**Figure 1.10a-c**), were plotted and analyzed for their association constant  $K_a$  using mathematical fitting. These techniques, combined with mathematical modeling, enable precise quantification of H-bonding interactions in various molecular systems.

### **Calorimetric Methods**

In addition to spectroscopic techniques, isothermal calorimetry (ITC) is a powerful method for determining the  $K_a$  of H-bonds.<sup>168,282-284</sup> This calorimetric approach measures thermal changes upon the addition of a defined amount of a binding partner, allowing for the determination of the enthalpic change  $\Delta H$  associated with binding. From the titration isotherm,  $K_a$  can be calculated, enabling further derivation of the free energy change  $\Delta G$  and, consequently, the entropic change  $\Delta S$  using the thermodynamic relation  $\Delta S = (\Delta H - \Delta G)/T$ . As shown in **Figure 1.10d**, when titrated, the thermal fluctuation of the system was recorded, and subsequently used for plotting and analysis for the association constant  $K_a$ .<sup>168</sup> However, the high cost of ITC equipment and its limited compatibility with organic solvents restrict its broader applications.

### **Other Methods**

Mass spectrometry (MS) has also been employed to determine binding constants in supramolecular chemistry. In 1998, Jolliffe, Timmerman, and Reinhoudt<sup>311</sup> introduced a novel  $\text{Ag}^+$ -labeling technique using matrix-assisted



laser desorption/ionization (MALDI) time-of-flight (ToF) MS to detect H-bonded assemblies. This method successfully identified the H-bonded complex between diethyl barbiturate and melamine in solution, leveraging Ag<sup>+</sup>'s high affinity for aromatic  $\pi$  donors and cyano groups. Later, in 2000, Kempen and Brodbelt<sup>312</sup> determined binding constants for crown ether–alkali metal cation complexes via competitive binding equilibria coupled with electrospray ionization (ESI) MS. In 2013, Su and Xie et al.<sup>313</sup> utilized desorption electrospray ionization (DESI) MS to analyze H-bonds between benzothiazoles and carboxylic acids, demonstrating a correlation between collision-induced dissociation (CID) data and H-bonding energies. This method quantifies H-bonding strengths by measuring the collision energy required to fully dissociate molecular complexes in the mass spectrometer. The energy needed for fragmentation is then correlated with H-bond lengths determined by X-ray crystallography or theoretical calculations, where shorter bonds generally indicate stronger interactions.

### 1.3.2. Probe Hydrogen-Bonding Strength in the Solid State

Probing hydrogen bonds in the solid state presents significant challenges. Unlike in solution, where H-bonds can adopt their optimal geometry, solid-state interactions are often constrained by the local environment,<sup>144</sup> leading to bond stretching, compression, or distortion, which introduces anisotropy. Additionally, the concept of “concentration” no longer exists in the solid state, complicating the application of solution-based H-bonding theories. For small organic molecules that crystallize, X-ray diffraction provides detailed insights into H-bond angles, lengths, and packing geometries.<sup>33,295,314</sup> Spectroscopic techniques such as ss NMR<sup>50,177,285,286</sup> and FT-IR<sup>117,244,287</sup> spectroscopy offer a direct observation of H-bonds, yielding valuable structural information in the solid phase. However, when H-bonding motifs are incorporated into a polymer matrix, the amorphous or semicrystalline nature of the material complicates traditional diffraction-based analysis. The relatively low content of H-bonding motifs per polymer chain weakens signal intensity in spectroscopic characterizations. Additionally, the lack of long-range order in the amorphous structure in polymers reduces contrast in diffraction patterns,<sup>315</sup> making precise structural characterization difficult. Despite these limitations, the influence of chain dynamics and polymer solvation on H-bonds can lead to phase separation<sup>79,211,242</sup> and unique aggregation behaviors<sup>116,166,316</sup> within the

polymer bulk. In turn, these H-bonding interactions induce notable changes in polymer properties, such as rheological behavior,<sup>179,317,318</sup> mechanical strength,<sup>56,208,319</sup> and morphology change,<sup>44,59,67</sup> which can serve as indirect indicators of H-bonding in complex polymer systems.

### **Solid-State (SS) NMR Spectroscopy**

Solid-state NMR (ss NMR) is a powerful technique for probing H-bonding in solid-phase polymers.<sup>242,320-326</sup> Often, protons serve as primary targets due to their favorable spectroscopic properties and direct involvement in the interaction. With the assistance of the magic angle spinning (MAS) technique, which improves resolution by narrowing broad signals, the accuracy of H-bond analysis could be enhanced.<sup>325</sup> By manipulating external stimuli such as temperature, humidity, or acidity, H-bond associations can be modulated, allowing proton chemical shifts to be recorded and evaluated accordingly (**Figure 1.11a**), as the chemical shift variations can be used to estimate the variation of the association strength.<sup>327</sup> H-bonding in PAA,<sup>286</sup> PMAA,<sup>177</sup> polymer-water interactions,<sup>178</sup> PAA-PVP blends,<sup>328</sup> PEO-urea assembly,<sup>329</sup> and UPy dimerization in crosslinked polyacrylate,<sup>50</sup> was studied by <sup>1</sup>H ss NMR to explore the solid phase constraints using such method. Similar solid-state studies have been conducted using other nuclei, such as <sup>13</sup>C<sup>152,213,330</sup> but remain relatively scarce. Although ss NMR aids in the thermal fluctuation of H-bonds, the anisotropy of polymers and the lack of a thermodynamic model prevent the precise measurement of absolute H-bonding strength.<sup>144,322</sup>

Beyond chemical shift analysis, ss NMR determines proton distances by measuring dipolar couplings, providing insights into internuclear distances.<sup>331</sup> Unlike diffraction methods, which are constrained by the amorphous polymer matrix, ss NMR directly analyzes the atoms involved in H-bonding, enabling more precise structural characterization. Such a method was first explored using UPy motifs in solution studies,<sup>19,171</sup> and then extended by <sup>1</sup>H double-quantum (DQ) MAS ss NMR spectroscopy for solid-state study.<sup>291</sup> The H-bonded protons of UPy motifs exhibit chemical shifts above 10 ppm, free from interference from aliphatic or aromatic proton signals. Additionally, the DQ signal pattern directly reveals spatial proximities between protons of different species, enabling the identification of UPy tautomers and the distances between H-bonded protons and receptor atoms (**Figure 1.11b**). This study was

further expanded for UPy motifs in a crosslinked polyacrylate.<sup>292</sup> Using selective saturation DQ ss NMR under ultrafast MAS rates exceeding 60 kHz, the aliphatic signals from the polymer backbone were effectively suppressed, allowing for a clear illustration of amidic proton proximities in the 2D spectra with a low overall UPy content of 4.7%, which reveals a distinct DDAA H-bonding array of UPy motifs within the solid-phase polymer matrix.

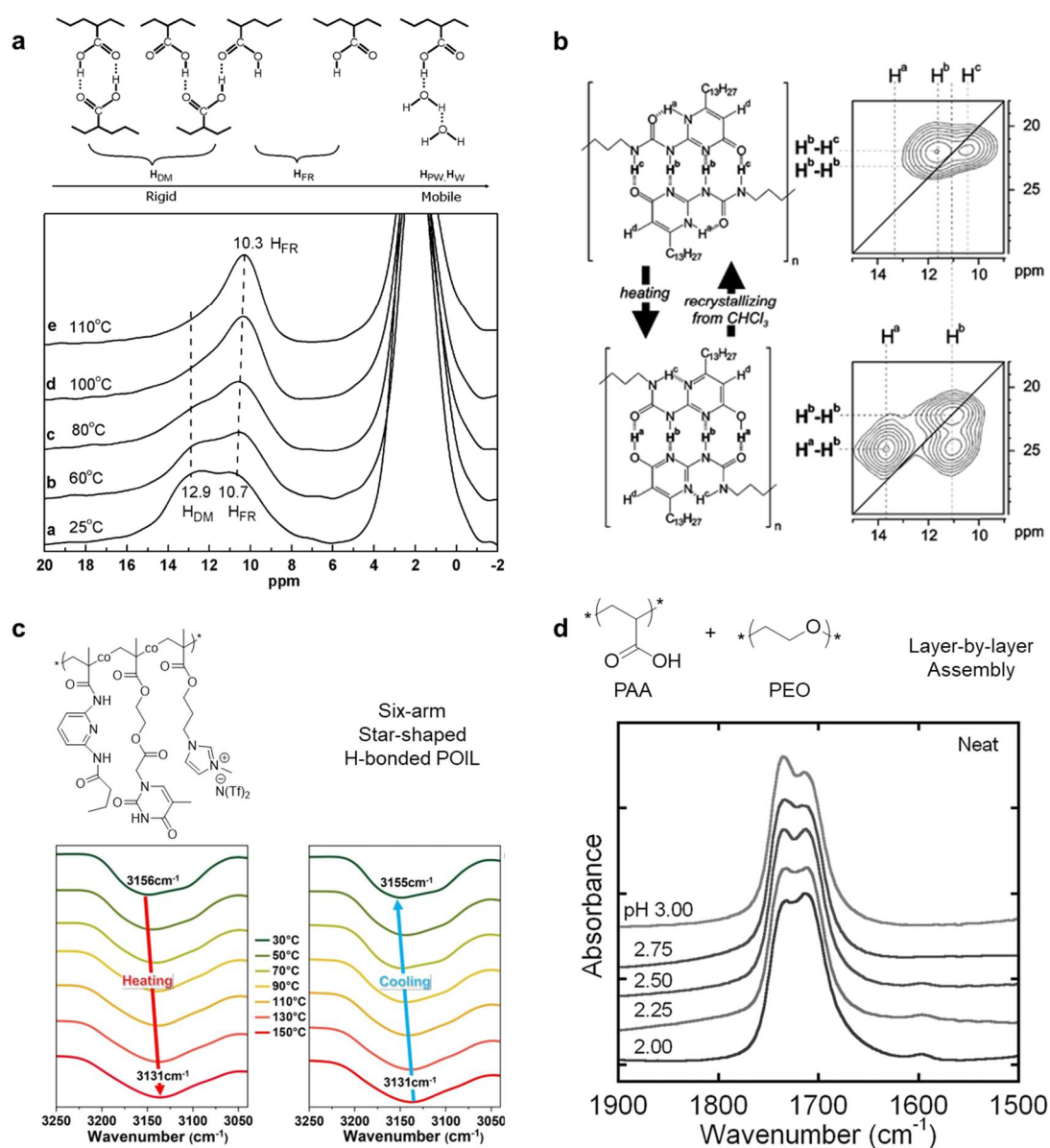


**Figure 1.11** a) Variable-temperature (VT) ss NMR spectra of dry PAA: as the temperature rises, the proton ( $H_{DM}$ ) of carboxylic dimer gradually merges with free proton ( $H_{FR}$ ) of carboxylic acid groups (adapted with permission from reference,<sup>286</sup> Copyright 2007 American Chemical Society); b)  $^1H$  double-quantum MAS ss NMR spectra of UPy tautomers: the double-quantum signals directly reveal the variation of the proton–proton

proximities in keto-keto and enol-enol H-bonding array. (reproduced from reference <sup>285</sup> with permission from the Royal Society of Chemistry); c) Variable-temperature (VT) FT-IR spectra of the H-bonded POIL with Thy-DAP motifs (adapted with the permissions from Wiley-VCH<sup>57</sup>); d) FT-IR spectra of PEO-PAA layer-by-layer assembly with acidity as the external stimuli (adapted with permission from reference,<sup>174</sup> Copyright 2007 American Chemical Society).

### **Fourier-Transform Infrared Spectroscopy**

Fourier-transform infrared (FT-IR) spectroscopy is a well-established technique for probing chemical bonds and intermolecular interactions, including H-bonding. While extensively applied to study H-bonding behavior in solution,<sup>332-336</sup> FT-IR has also been used in solid-state studies,<sup>35,117,187,337,338</sup> often coupled with temperature variations. The stretching vibration of the donor D–H bond is particularly informative, typically exhibiting redshift and broadening upon H-bonding formation. Similarly, acceptor groups such as C=O and C≡N undergo redshifts as H-bonding extends bond lengths and lowers their vibrational energy. Although FT-IR does not directly measure absolute bond dissociation energies, it allows for the estimation of H-bond enthalpy  $\Delta H$  through spectral variations, including frequency shifts,<sup>339,340</sup> peak broadening, and intensity changes.<sup>341</sup> Extensive efforts have correlated these spectral variations with various low-molecular-weight compounds, including solid-state carbohydrates, nucleobases, nucleosides,<sup>339,340,342-346</sup> amino acids, and small peptides.<sup>340,347</sup> Further, H-bond lengths in nucleobase crystals, such as hypoxanthine, xanthine, adenine, and guanine, have been correlated to their respective H-bond enthalpies.<sup>348</sup>

Despite the generally low H-bond content in HBPs, FT-IR remains a reliable technique for characterizing H-bonding in solid-phase polymers. Techniques such as attenuated total reflection (ATR),<sup>244</sup> peak deconvolution,<sup>349</sup> and 2D IR spectroscopy<sup>287</sup> further enhance their applicability in probing H-bonds in HBPs. Studies on H-bonding in HBPs typically focus on specific donors (-NH, -OH), as their distinct stretching vibrations appear at high wavenumbers with minimal overlap, and acceptors (C=O) for the strong sensitivity to H-bonding interactions in FT-IR spectra.<sup>46,244,334,337,350</sup> Coupled with temperature-dependent experiments<sup>57,83,351,352</sup> or other external stimuli,<sup>71,174</sup> FT-IR enables the observation of H-bonding trends (**Figure 1.11c&d**), providing insights into H-bond stability. However, the precise determination of absolute association

constants remains unattainable.

### **Other Indirect Methods**

Rheology is a fundamental technique for investigating the viscoelasticity of solid-state or melt-state HBPs, as H-bonding significantly influences their mechanical properties.<sup>319,353,354</sup> H-bonded networks contribute to strain-dependent viscosity,<sup>123</sup> dynamic crosslinking,<sup>212</sup> and stress relaxation,<sup>176</sup> all of which can be effectively analyzed through frequency-dependent viscoelastic measurements. These measurements, in turn, provide insights into H-bond dynamics, reflecting their stability and network behavior.<sup>206,241</sup> Dynamic oscillatory rheology is commonly used to determine the timescale and strength of H-bonds in HBPs by assessing their role as reversible crosslinks over varying timescales. The storage modulus ( $G'$ ) represents elasticity, while the loss modulus ( $G''$ ) indicates viscous behavior, with strong H-bonds often imparting a solid-like character ( $G' > G''$ ). Time-temperature superposition is applied to construct a master curve on which the crossover of  $G'$  and  $G''$  reveals the relaxation of interactions among polymer chains, indicating the H-bond lifetime when the Rouse model applies.<sup>241</sup> The activation energy for H-bond dissociation can be derived from the shift factor  $a_T$ ,<sup>316,326</sup> while temperature sweeps assess thermal stability and reversibility.<sup>355</sup> Creep tests measure deformation under constant stress, whereas stress-relaxation tests monitor stress decay over time, both indirectly indicating H-bond strength.<sup>356</sup> Nonlinear rheology, particularly large amplitude oscillatory shear (LAOS), explores nonlinear viscoelasticity and H-bond rupture,<sup>210,357,358</sup> which leads to mechanical weakening under high strain. Therefore, the dynamics of the H-bonds can be determined by rheology, indicative of the stability of the H-bonds and the H-bonding network.<sup>176,241,359</sup>

Dielectric spectroscopy is a powerful analytical technique for investigating H-bonds of dipolar nature in solid-state polymers, elucidating H-bonding cooperativity, relaxation dynamics, and phase transitions in polymeric materials.<sup>175,360-362</sup> Although dielectric spectroscopy alone does not provide direct H-bond strength measurements and is best used alongside other techniques such as FT-IR, ss NMR, and ITC/DSC, to obtain a more comprehensive understanding of H-bonding in polymeric systems.

Mechanical analysis reveals the relationship between molecular interactions

and macroscopic mechanical strength, indirectly comparing the H-bonding strength. Stress-strain analysis<sup>56,208,319</sup> provides direct insights into the role of H-bonding in polymer elasticity and plastic deformation, while creep and stress relaxation tests<sup>319,356,363</sup> reveal the time-dependent dissociation and reformation of H-bonding interactions. Temperature-dependent mechanical analysis<sup>364-367</sup> further elucidates how H-bonding affects  $T_g$  and thermal relaxation, indirectly expressing the H-bonding stability.

Morphology reflects phase transitions in HBPs, driven by the aggregation of polymer backbones and attached H-bonding motifs. It indirectly indicates whether H-bonds are strong enough to induce or suppress phase segregation.<sup>242</sup> Additionally, molecular packing derived from morphology provides insights into H-bond geometry. Techniques such as X-ray scattering,<sup>78,116,166,242</sup> neutron scattering,<sup>368,369</sup> and microscopy<sup>370-372</sup> are used for morphological analysis. With the temperature being the common variable, the morphological studies in turn offer information on the variation of H-bonding in the solid-state HBPs.

## 2. Scope of the Thesis

### 2.1. Aim of Thesis

This thesis aims to investigate the behavior of multiple hydrogen bonds in different polymeric materials. The central H bonding systems for investigation are modified barbiturates (Ba), Hamilton wedges (HW), and ureido-pyrimidinone (UPy), either as low-molecular-weight compounds or as sticker groups attached to distinct polymeric backbones. The focus is to understand the strength and variation of this set of hydrogen bonds (H-bonds) in different molecular environments, including organic solvents, novel ionic media, and bulk polymer matrices (**Figure 2.1**).

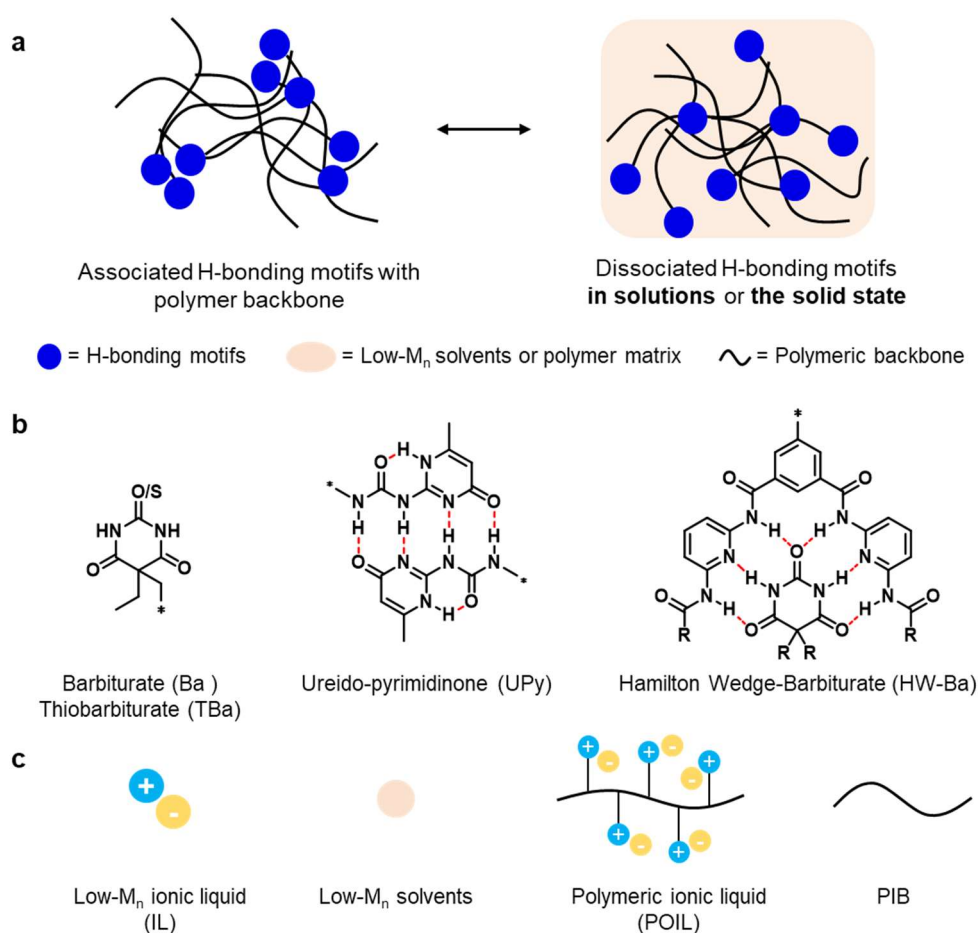


**Figure 2.1** a) Proposed proximity effects from molecular surroundings to the H-bonds: effect could arise from the H-bonding motif, the polymeric backbone, or the low-molecular-weight compounds in adjacent; b) the H-bonding motifs used in this thesis; c) the possible low-molecular-weight compounds and polymeric backbone to create novel molecular surroundings.

The focus is to understand and modify the stability of these H-bonds at a molecular level to facilitate further applications of H-bonds in advanced material systems.

The specific objectives of this thesis are shown as follows:

1. Investigation of H-bonding in modified barbiturates and 2-thiobarbiturates both in solutions and in nonpolar polymer:

Thiourea exhibits distinct H-bonding characteristics compared to urea,<sup>29,33,373</sup> resulting in unique material properties.<sup>35,49</sup> Similarly, barbiturates are known to impart self-healing capabilities and enhanced mechanical strength to polymer matrices.<sup>59,137</sup> However, the H-bonding behavior of the sulfur analog, 2-thiobarbiturate (TBa), remains largely unexplored. This study aims to examine the H-bonding behavior of modified Ba and TBa in solution, the solid state, and within nonpolar polyisobutylene matrices.

2. Investigation of stability of quadruple H-bonds in polymeric ionic liquids containing UPy moieties:

The ureido-pyrimidinone (UPy) motif, with its capacity to form quadruple H-bonds, has been extensively employed in designing multifunctional materials,<sup>51,218,374</sup> including polymeric ionic liquids (POILs).<sup>245,246,272</sup> However, the stability and behavior of UPy H-bonds in highly charged ionic media remain insufficiently understood. This study focuses on the synthesis of POIL copolymers containing UPy moieties and investigates the stability and dynamics of quadruple H-bonds within these charged systems.

3. Investigation of H-bonding behavior of novel Hamilton wedges and barbiturates in various solutions:

The Hamilton wedge barbiturate (HW-Ba) H-bonding complex with programmable sextuple H-bonds, has been explored in various smart materials.<sup>83,130,168</sup> Due to the ease of modification of HW and Ba, this research aims to study the structural variability of HWs for covalent fixation of H-bonds with Ba. Additionally, the H-bonding interactions between modified HW and Ba will be analyzed in various solutions to elucidate their structural and functional implications.



## 2.2. Scientific Approach

This thesis investigates the structural variability of Hamilton wedge (HW), barbiturate (Ba), thiobarbiturate (TBa), and ureido-pyrimidinone (UPy) through chemical modifications. These H-bonding motifs were incorporated into various polymer matrices via post-polymerization modification or direct polymerization of acrylate-based H-bonding monomers. Both solution and solid-state analytical techniques were employed to examine their H-bonding behaviors under diverse conditions and molecular environments. The specific methodologies are outlined as follows:

### 1. Investigation of H-bonding in modified barbiturates and 2-thiobarbiturates both in solutions and in nonpolar polymer:

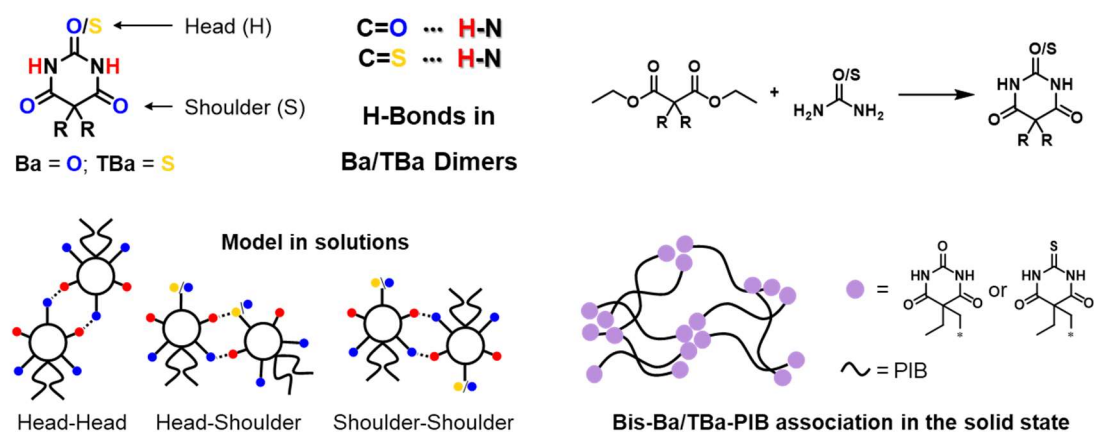


**Figure 2.2** Synthesis of Ba and TBa, and proposed H-bonding pattern as low-molecular-weight compounds and association as H-bonding stickers in PIB matrix.

The first part of this thesis is published as “Comparing C2=O and C2=S Barbiturates: Different Hydrogen-Bonding Patterns of Thiobarbiturates in Solution and the Solid State, **Chenming Li**, Philipp Hilgeroth, Nazmul Hasan, Dieter Ströhl, Jörg Kressler, and Wolfgang H. Binder\*, *Int. J. Mol. Sci.* **2021**, 22(23), 12679”.<sup>375</sup> Ba and TBa are synthesized, and their association behavior is investigated both as low-molecular-weight compounds and as adhesive motifs within the PIB matrix (**Figure 2.2**). TBa is synthesized via the condensation of thiourea with modified malonate, following a method analogous to Ba, with an alternative synthesis route explored using Lawesson’s reagent or other reagents. NMR titration and variable-temperature (VT) NMR spectroscopy are expected to reveal distinct association behaviors of TBa in

solution compared to Ba, while DSC and VT FT-IR spectroscopy will provide insights into the thermodynamics of H-bonding. Differences in monolayer assembly at the water surface between TBa and Ba are anticipated due to their unique H-bonding characteristics. Both compounds are subsequently conjugated to the termini of a PIB backbone via CuAAC reaction to form telechelic H-bonded PIB. Rheological analysis will indicate variations in viscoelastic behavior, further elucidating the distinct H-bonding properties of TBa and Ba within the PIB matrix.

## 2. Investigation of stability of UPy quadruple H-bonds in polymeric ionic liquids:

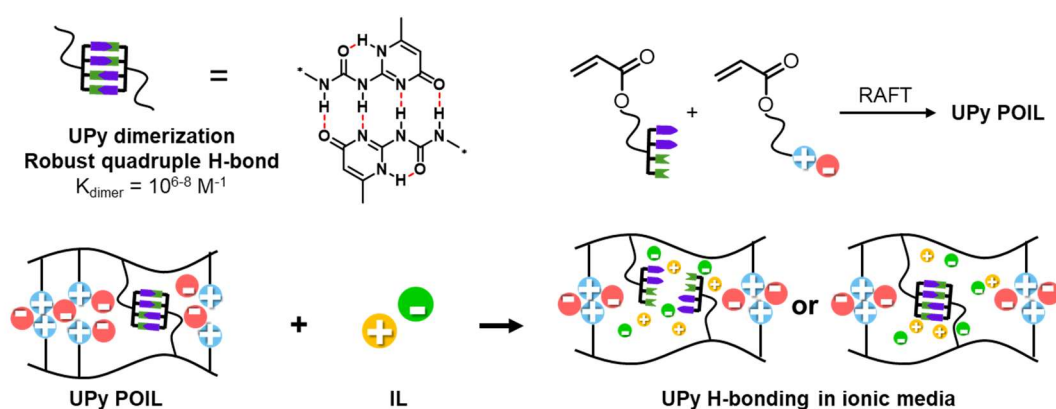


**Figure 2.3** UPy POIL synthesis and UPy H-bonds in an ionic media.

The second part of this thesis is published as “Synthesis and Characterization of Quadrupolar-Hydrogen-Bonded Polymeric Ionic Liquids for Potential Self-Healing Electrolytes, **Chenming Li**, Rajesh Bhandary, Anja Marinow, Dmitrii Ivanov, Mengxue Du, René Androsch, and Wolfgang H. Binder\*, *Polymers* **2022**, 14(19), 4090”<sup>376</sup> and “Stability of Quadruple Hydrogen Bonds in an Ionic Liquid Environment, **Chenming Li**, Rajesh Bhandary, Anja Marinow, Stephanie Bachmann, Ann-Christin Pöppler, and Wolfgang H. Binder\*, *Macromol. Rapid Commun.* **2024**, 45, 2300464”.<sup>377</sup> To synthesize novel polymeric ionic liquids (POILs) incorporating UPy motifs, pyrrolidinium-based ILs, and UPy units are functionalized with polymerizable acrylate groups (**Figure 2.3**). Using RAFT polymerization, UPy motifs are embedded in POILs at varying ratios relative to IL groups. Further mixing of low-molecular-weight ionic liquid (IL) increases the ionicity of the POIL matrix, allowing exploring the influence of ionic media on the UPy H-bonds. VT Solid-state NMR and FT-IR spectroscopy will provide insights into the thermodynamics and stability of UPy

quadruple H-bonds within the ionic environment, while DSC and rheological analysis will further investigate the dynamics and structural variations of these H-bonds under ionic conditions.

### 3. Investigation of H-bonds and aggregates of novel Hamilton wedge-barbiturate complex:

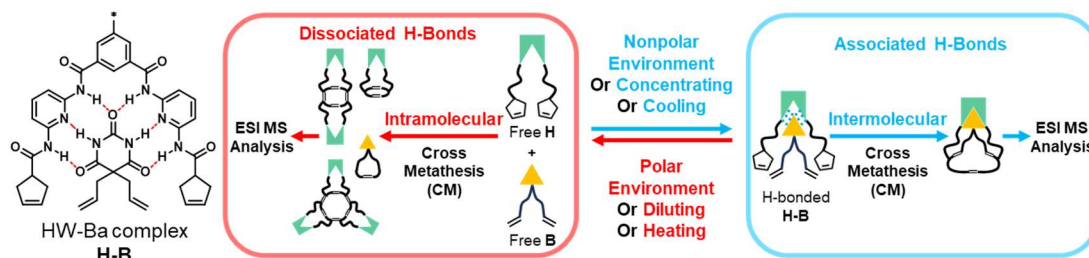


**Figure 2.4** Structure of Hamilton wedge H, barbiturate B, and Hamilton wedge-barbiturate complex H-B with groups able to crosslink via cross-metathesis; the proposed methods to manipulate the H-bonding between H-b complex.

The third part of this thesis is published as “Proximity Effects and Aggregation of Hamilton-Receptor Barbiturate Host-Guest Complexes Probed by Cross-Metathesis and ESI MS Analysis. **Chenming Li**, Pascal Mai, Niclas Festag, Anja Marinow, and Wolfgang H. Binder\*, *Chem. Eur. J.* **2024**, e202403939”.<sup>378</sup> The Hamilton wedge H is modified with cyclopentene moieties and the barbiturate B with allyl groups to enable cross-metathesis (CM) for covalent fixation of the H-bonded H-B complex (**Figure 2.4**). By varying conditions like temperature, solvents of different polarity, or concentration, the H-bonding between the H-B complex can be manipulated. UV-Vis titration in various solvents and temperatures examines the influence of molecular surroundings on H-bond stability, thermodynamics, and aggregate formation. Grubbs catalyst is employed to initiate CM under multiple conditions, ensuring covalent fixation of HW-Ba aggregates. Subsequent ESI MS analysis quantifies aggregate sizes by determining the mass distribution, providing insight into how temperature, solvent polarity, and additional donors/acceptors affect H-bond interactions within H-H, H-B, and B-B associations. This method is further applied to the H-B complex in a PIB matrix, where solvent-free conditions lead to distinct aggregation behavior influenced by polymeric confinement, demonstrating the impact of nonpolar polymeric environments on H-bonded assembly.

### 3. List of Publications

The outcomes of this thesis are published in the following four publications and used as part of this cumulative thesis with no special permission required from MDPI<sup>375,376</sup> (under the terms and conditions of the Creative Commons Attribution (CC BY) license) and with the permissions from Wiley-VCH.<sup>377,378</sup>

#### **[P1] Comparing C2=O and C2=S Barbiturates: Different Hydrogen-Bonding Patterns of Thiobarbiturates in Solution and the Solid State<sup>375</sup>**

Chenming Li, Philipp Hilgeroth, Nazmul Hasan, Dieter Ströhl, Jörg Kressler, and Wolfgang H. Binder\*

*Int. J. Mol. Sci.* **2021**, 22(23), 12679; <https://doi.org/10.3390/ijms222312679>

Author contributions: conceptualization, C.L. and W.H.B.; methodology, C.L., P.H., N.H. and D.S.; investigation, C.L., P.H. and N.H.; writing—original draft preparation, C.L. and W.H.B.; writing—review and editing, C.L., J.K. and W.H.B.; supervision, W.H.B.; project administration, W.H.B.; funding acquisition, W.H.B. All authors have read and agreed to the published version of the manuscript.

#### **[P2] Synthesis and Characterization of Quadrupolar-Hydrogen-Bonded Polymeric Ionic Liquids for Potential Self-Healing Electrolytes<sup>376</sup>**

Chenming Li, Rajesh Bhandary, Anja Marinow, Dmitrii Ivanov, Mengxue Du, René Androsch, and Wolfgang H. Binder\*

*Polymers* **2022**, 14(19), 4090; <https://doi.org/10.3390/polym14194090>

Author contributions: conceptualization, W.H.B., A.M. and C.L.; methodology, C.L., R.B., D.I. and M.D.; writing—original draft preparation, C.L.; writing—review and editing, W.H.B., A.M. and R.A.; supervision, project administration, and funding acquisition, W.H.B. and A.M. All authors have read and agreed to the published version of the manuscript.

#### **[P3] Stability of Quadruple Hydrogen Bonds in an Ionic Liquid Environment<sup>377</sup>**

Chenming Li, Rajesh Bhandary, Anja Marinow, Stephanie Bachmann, Ann-Christin Pöppler, and Wolfgang H. Binder\*

*Macromol. Rapid Commun.* **2024**, *45*, 2300464;  
<https://doi.org/10.1002/marc.202300464>

Author contributions: conceptualization, W.H.B., A.M. and C.L.; methodology, C.L., R.B., and S.B.; writing—original draft preparation, C.L.; writing—review and editing, W.H.B., A.M. and A.C.P.; supervision, project administration, and funding acquisition, W.H.B. and A.M. All authors have read and agreed to the published version of the manuscript.

**[P4] Proximity Effects and Aggregation of Hamilton-Receptor Barbiturate Host-Guest Complexes Probed by Cross-Metathesis and ESI MS Analysis<sup>378</sup>**

Chenming Li, Pascal Mai, Niclas Festag, Anja Marinow, and Wolfgang H. Binder\*

*Chem. Eur. J.* **2024**, e202403939; <https://doi.org/10.1002/chem.202403939>

Author contributions: conceptualization, W.H.B., A.M. and C.L.; methodology, C.L., P.M., and N.F.; writing—original draft preparation, C.L.; writing—review and editing, W.H.B. and A.M.; supervision, project administration, and funding acquisition, W.H.B. and A.M. All authors have read and agreed to the published version of the manuscript.



Article

# Comparing C2=O and C2=S Barbiturates: Different Hydrogen-Bonding Patterns of Thiobarbiturates in Solution and the Solid State

Chenming Li <sup>1</sup>, Philipp Hilgeroth <sup>1</sup>, Nazmul Hasan <sup>2</sup>, Dieter Ströhl <sup>3</sup>, Jörg Kressler <sup>2</sup>  
and Wolfgang H. Binder <sup>1,\*</sup>

- <sup>1</sup> Macromolecular Chemistry, Institute of Chemistry, Martin-Luther University Halle-Wittenberg, Von-Danckelmann-Platz 4, D-06120 Halle (Saale), Germany; chenming.li@chemie.uni-halle.de (C.L.); philipp.hilgeroth@chemie.uni-halle.de (P.H.)
- <sup>2</sup> Physical Chemistry, Institute of Chemistry, Martin-Luther University Halle-Wittenberg, Von-Danckelmann-Platz 4, D-06120 Halle (Saale), Germany; nazmul.hasan@chemie.uni-halle.de (N.H.); joerg.kressler@chemie.uni-halle.de (J.K.)
- <sup>3</sup> Organic Chemistry, Institute of Chemistry, Martin-Luther University Halle-Wittenberg, Kurt-Mothes-Str. 2, 06120 Halle (Saale), Germany; dieter.stroehl@chemie.uni-halle.de
- \* Correspondence: wolfgang.binder@chemie.uni-halle.de

**Abstract:** Carbonyl-centered hydrogen bonds with various strength and geometries are often exploited in materials to embed dynamic and adaptive properties, with the use of thiocarbonyl groups as hydrogen-bonding acceptors remaining only scarcely investigated. We herein report a comparative study of C2=O and C2=S barbiturates in view of their differing hydrogen bonds, using the 5,5-disubstituted barbiturate **B** and the thiobarbiturate **TB** as model compounds. Owing to the different hydrogen-bonding strength and geometries of C2=O vs. C2=S, we postulate the formation of different hydrogen-bonding patterns in C2=S in comparison to the C2=O in conventional barbiturates. To study differences in their association in solution, we conducted concentration- and temperature-dependent NMR experiments to compare their association constants, Gibbs free energy of association  $\Delta G_{\text{assn.}}$ , and the coalescence behavior of the N-H...S=C bonded assemblies. In Langmuir films, the introduction of C2=S suppressed 2D crystallization when comparing **B** and **TB** using Brewster angle microscopy, also revealing a significant deviation in morphology. When embedded into a hydrophobic polymer such as polyisobutylene, a largely different rheological behavior was observed for the barbiturate-bearing **PB** compared to the thiobarbiturate-bearing **PTB** polymers, indicative of a stronger hydrogen bonding in the thioanalogue **PTB**. We therefore prove that H-bonds, when affixed to a polymer, here the thiobarbiturate moieties in **PTB**, can reinforce the nonpolar PIB matrix even better, thus indicating the formation of stronger H-bonds among the thiobarbiturates in polymers in contrast to the effects observed in solution.

**Keywords:** (2-thio)barbiturates; hydrogen bonds; supramolecular association; polyisobutylene; Langmuir film



**Citation:** Li, C.; Hilgeroth, P.; Hasan, N.; Ströhl, D.; Kressler, J.; Binder, W.H. Comparing C2=O and C2=S Barbiturates: Different Hydrogen-Bonding Patterns of Thiobarbiturates in Solution and the Solid State. *Int. J. Mol. Sci.* **2021**, *22*, 12679. <https://doi.org/10.3390/ijms222312679>

Academic Editor: James K. Bashkin

Received: 2 November 2021

Accepted: 20 November 2021

Published: 24 November 2021

**Publisher's Note:** MDPI stays neutral with regard to jurisdictional claims in published maps and institutional affiliations.



**Copyright:** © 2021 by the authors. Licensee MDPI, Basel, Switzerland. This article is an open access article distributed under the terms and conditions of the Creative Commons Attribution (CC BY) license (<https://creativecommons.org/licenses/by/4.0/>).

## 1. Introduction

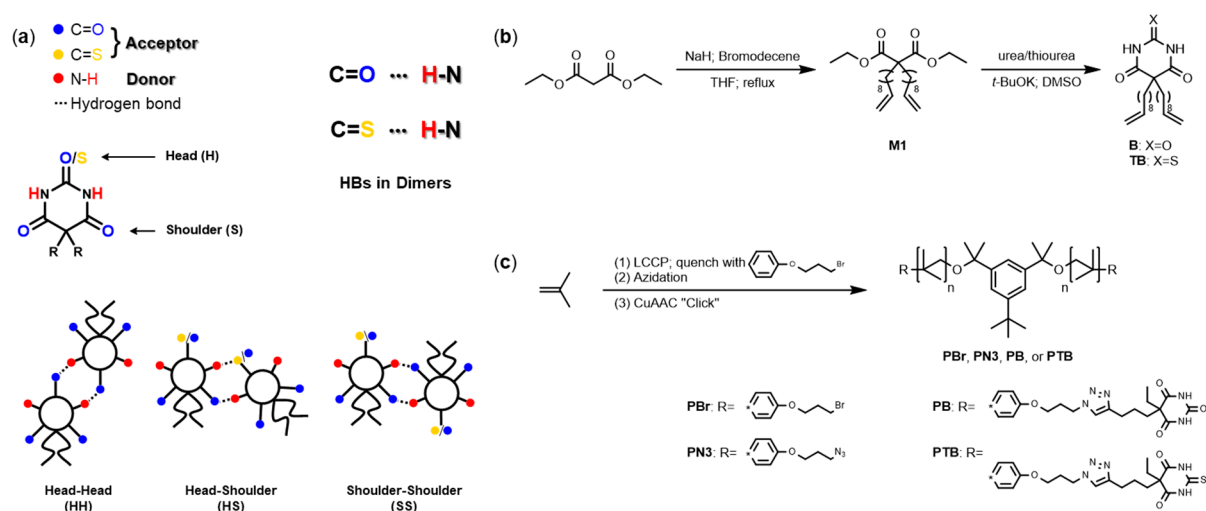
Hydrogen bonds (H-bonds) are non-covalent attractive interactions between hydrogen atoms and electronegative elements/groups [1] and are very prominent in supramolecular science to achieve molecular ordering effects and recognition. The formation of simple H-bonds is described as a proton-sharing process ( $\text{D-H} \cdots \text{A} \leftrightarrow \text{D}^- \cdots \text{H-A}^+$ ) between a Lewis acid (donor) and a Lewis base (acceptor) [2], where often oxygen or nitrogen act as a H-bond acceptor element. However, also other main group elements like sulfur [3–7] and selenium [7,8] were reported as potential acceptors despite their comparatively lower electronegativity. The use of thiocarbonyl groups (C=S) as hydrogen-bonding (H-bonding) acceptors instead of the carbonyl group (C=O) displays significantly different assembly

behavior, as they form tilted H-bonding patterns, subsequently useful for organocatalysis [9]. The use of thioamides to replace natural amides as a weaker H-bonding acceptor can change the folding mechanisms in proteins [10], and different oblique H-bonding layers can form as Langmuir films when using thioureas instead of ureas [11]. In the area of materials displaying adaptive [12–14] and dynamic properties [15,16], the use of H-bonds bearing thiocarbonyl moieties has also become attractive due to their unique assembly pattern. Thus the replacement of urea groups by thiourea groups generates non-linear H-bonds, which promote dynamic crosslinking, reduce crystallization, and thus can impart improved self-healing properties to materials [15]. Several biomimetic polymer networks were therefore designed based on thiourea bonds, which exhibit solid-state plasticity and reprocessability in addition to the formation of stiff, strong, tough, and resilient mechanical properties [16].

When looking towards multiple carbonyl groups, barbiturates display a well-known H-bonding entity featuring an ADA/DA motive (D = donor; A = acceptor). They can bind specifically and strongly towards artificial receptors like the Hamilton Wedge [17–19], triazines [20], and diaminopyridines [21], display self-association [22–24], and generate transient H-bonds networks in barbiturate-bearing polymers [25,26], despite their comparatively low association constant in nonpolar solvents of only  $23.6 \text{ M}^{-1}$  (allobarbitol) [22]. When attaching them onto (macro-)molecules, unique dynamic properties via their distinctive H-bonding in functional materials can be achieved, such as in monolayers [27–29], in coordination complexes [30,31], in 3D printing [32], or as self-healing-polymers [25,26,32–34] in self-assembled materials [35,36].

While the H-bonds in native barbiturates were systematically studied widely before, the molecular exchange of thiocarbonyl moieties (C=S) in barbiturates to understand H-bonds has not been intensely exploited yet [37–39]. This motivated us to investigate thio-barbiturates and their H-bonding behavior in more detail. We herein report a comparative study of C=O and C=S barbiturates in view of their divergent H-bonds, using the 5,5-disubstituted barbiturate **B** and the thiobarbiturate **TB** as model compounds. We expected the formation of different H-bonding patterns due to the fixation of the C=S group in comparison to the C=O group in normal barbiturates as shown in Scheme 1. To study differences in their association in solution and the solid state, we conducted investigations on the association constants of **B** and **TB** via concentration-dependent NMR experiments to compare their Gibbs free energy of association  $\Delta G_{\text{assn.}}$ . Furthermore, we generated Langmuir films as a 2D material, where both **B** and **TB** displayed a different aggregation behavior observed by Brewster angle microscopy (BAM). To understand the H-bonds' behavior in the melt state, we also affixed the (thio-)barbiturate moieties onto bulk polyisobutylene (named as **PB** for barbiturate-bearing polyisobutylene and **PTB** for thiobarbiturate-bearing polyisobutylene), revealing a largely different rheological behavior, again indicative for the distinct H-bonding of the C=S-moieties in comparison to the C=O-barbiturates.





**Scheme 1.** (a) The possible association of (thio-)barbiturates via H-bonding between N-H and C=O/S; (b) synthesis of the model compounds **B** and **TB**; and (c) the polyisobutylene (PIB)-based model polymers **PB** and **PTB**. THF: tetrahydrofuran; *t*-BuOK: potassium tert-butoxide; DMSO: dimethyl sulfoxide; LCCP: living carbocationic polymerization; CuAAC: copper(I)-catalyzed alkyne-azide cycloaddition "click" reaction.

## 2. Results

### Synthesis

We firstly prepared the model compounds **B** and **TB**, differing only in the C2 position, either containing a C=O or a C=S group. The syntheses (for details, see Supplementary Materials) were accomplished using diethyl malonate and 10-bromo-1-decene as starting materials, followed by condensation with an excess amount of either urea or thiourea in DMSO. For the model polymers **PB** and **PTB**, the diethyl ethylmalonate was charged with 5-chloro-1-pentyne to synthesize the (thio-)barbiturates for CuAAC "click" reaction with a telechelic diazidopolyisobutylene, thus affixing two thiobarbiturate moieties to either end of the polymer chain. The structure of the two model systems **B** and **TB** and **PB** and **PTB** were unambiguously proven by NMR-, IR spectroscopy, and ESI- or MALDI-ToF mass spectroscopy (for spectra, see Figures S3–S11), thus allowing for further investigations of H-bonding, which are discussed in the next chapters.

## 3. Discussion

### 3.1. Hydrogen Bonding of Model Compounds in Solution

As a first step to understand the behavior of the H-bonds in solution, we studied the low molecular weight systems via the model compounds **B** and **TB** to understand basic differences in strength and dynamics of association in non-competing chloroform.

#### 3.1.1. Concentration-Dependent Assembly Studies in Solution

Barbiturates can form dimeric assemblies in inert solvents like chloroform [17,25] with a  $K_{assn.} < 100 \text{ M}^{-1}$  or even lower. Using NMR spectroscopy under diluting conditions the association constant can be determined and compared to reported values of the self-association of barbitals [22]. For both model compounds **B** and **TB** the chemical shifts of their NH protons were observed by NMR spectroscopy, in turn determining their association constants (dimerization) by nonlinear fitting of the chemical shifts, as shown in Figure 1 (for fitting details, see Supplementary Materials).



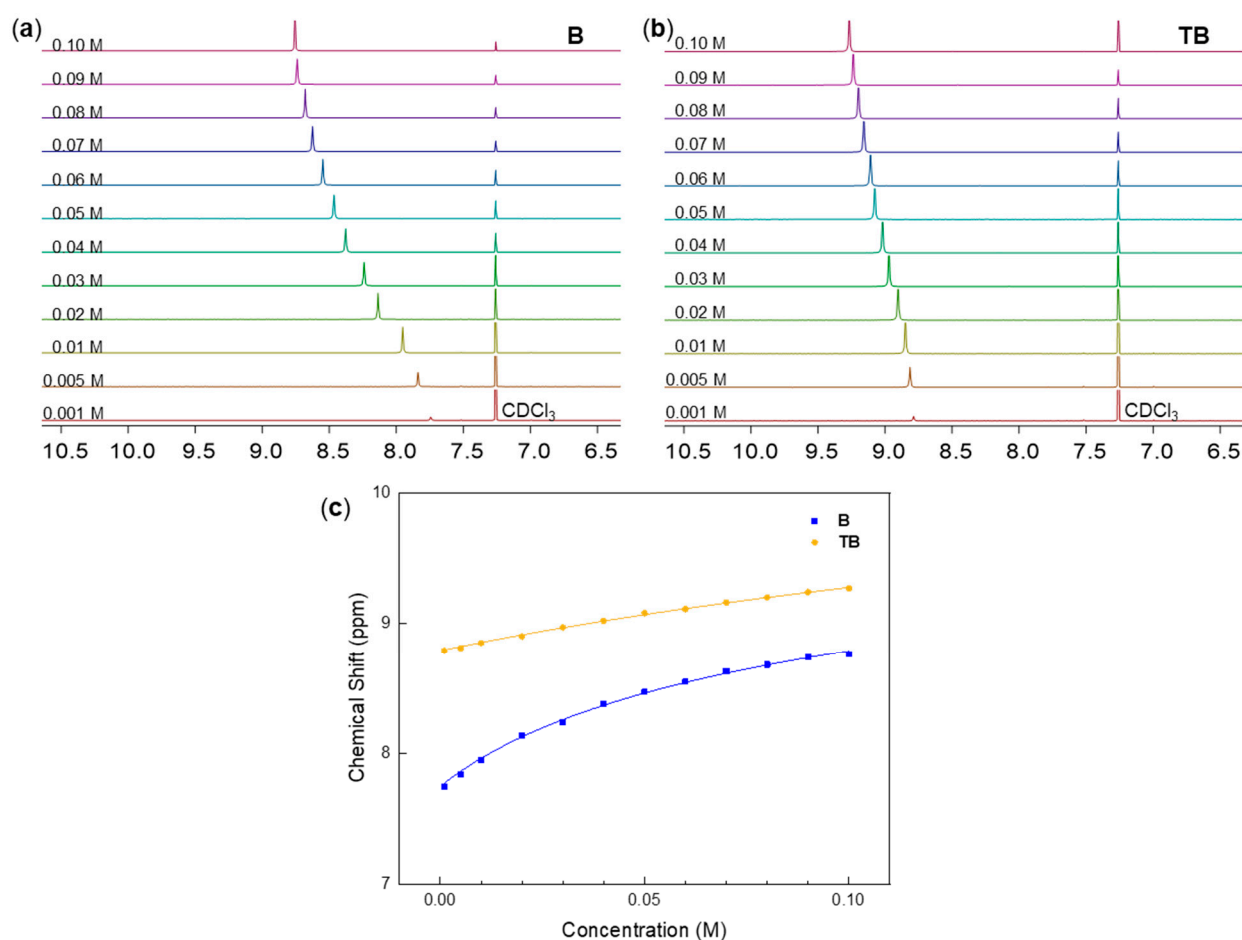


**Figure 1.** (a,b) Concentration-dependent NMR spectra of model compounds **B** and **TB** in CDCl<sub>3</sub> measured at 27 °C and (c) their fitting curves of the chemical shifts of the N-H (for fitting details, see Supplementary Materials).

From these nonlinear fitting of the N-H proton chemical shifts, the association constants (see Table 1) were determined as  $4.26 \text{ M}^{-1}$  (for **B**) and  $0.94 \text{ M}^{-1}$  (for **TB**), counting to a nearly 4-fold decrease by the introduction of the C=S group. This clearly indicates a weaker H-bonding with the C=S group, in line with our expectations. Looking at the donor-capabilities of the N-H in **TB**, it could be regarded as more acidic than in **B** ( $pK_{\text{HA,Urea}} = 26.9$  and  $pK_{\text{HA,Thiourea}} = 21.0$  [40]), thus placing **TB** as a better H-bond donor as, e.g., reported for thioamides [41]. Herein, self-consistent reaction-field calculations (SCRF) showed that a (C=S)N-H  $\cdots$  O=C-(NH) interaction in thioacetamides is  $3.3\text{--}4.6 \text{ kcal}\cdot\text{mol}^{-1}$  more stable than the (C=O)N-H  $\cdots$  S=C-(NH) orientation, but also more stable (by  $1.5 \text{ kcal}\cdot\text{mol}^{-1}$ ) when compared to the (C=O)N-H  $\cdots$  O=C-(NH) H-bond (present in conventional acetamide) [41]. Although the  $\pi$ -system in thiocarbonyls is regarded an effective acceptor and could form out-of-plan H-bonds [5]. Thio-compounds generally bear a lower H-bonding basicity than their oxo-analogues [42,43], resulting in a weaker acceptor nature of the thio-species. Based on the observed 4-fold decrease in the association constant of **TB**, the latter thus seems to surpass the former argument about the H-bonding in **TB**. When comparing the tendency towards the hydrogen-bonded (H-bonded) assemblies, the negative Gibbs free energy of association  $\Delta G_{\text{assn.}}$  of **B** evidences stronger H-bonds, whereas nearly equilibrated associated/free N-H in **TB** at 27 °C in chloroform can be observed.

**Table 1.** Association constant  $K_{assn.}$ , maximum chemical shift of N-H  $\delta_{max}$ , Gibbs free energy of association  $\Delta G_{assn.}$ , coalescence rate constant  $k_C$ , Gibbs free energy of coalescence  $\Delta G_c^\ddagger$ , and exchange equilibrium constant  $K_{-15^\circ\text{C}}$  of model compounds **B** and **TB**.

	$K_{assn.}/\text{M}^{-1}$	$\delta_{max}/\text{ppm}$	$\Delta G_{assn.}/\text{kJ}\cdot\text{mol}^{-1}$	$k_C/\text{s}^{-1}$	$\Delta G_c^\ddagger/\text{kJ}\cdot\text{mol}^{-1}$	$K_{-15^\circ\text{C}}/\text{M}^{-1}$
<b>B</b>	$4.26 \pm 0.40$	$10.67 \pm 0.15$	$-3.61 \pm 2.29$	-	-	-
<b>TB</b>	$0.94 \pm 0.16$	$12.27 \pm 0.46$	$0.15 \pm 4.57$	205.08	54.57	0.32

### 3.1.2. Temperature-Dependent Association Behavior

As demonstrated in Scheme 1 and Figure 2d, (thio-)barbiturates can form several dimeric H-bonding patterns via the N1/3-H with the C2=O/S and C4/6=O carbonyls, forming dimers via “head-head” (HH), “head-shoulder” (HS), and “shoulder-shoulder” (SS) orientations. While the purely C=O-based barbiturates could form all three possible arrangements, dimers of the thiobarbiturates could have preferred orientations due to the lower H-bonding acceptor qualities of the thiocarbonyl group [42,43] and the different lone-pair electron density at the sulfur atom [44]. Due to the dynamic nature of aggregates, the H-bonding arrangements are continuously exchanging, expecting a significant change in dynamics at reduced temperatures. To detect the dynamic H-bonding of the N-H  $\cdots$  O/S=C in the dimer of the model compounds **B** and **TB**, temperature-dependent NMR experiments were conducted to evaluate an eventual coalescence behavior of the dynamic assemblies.

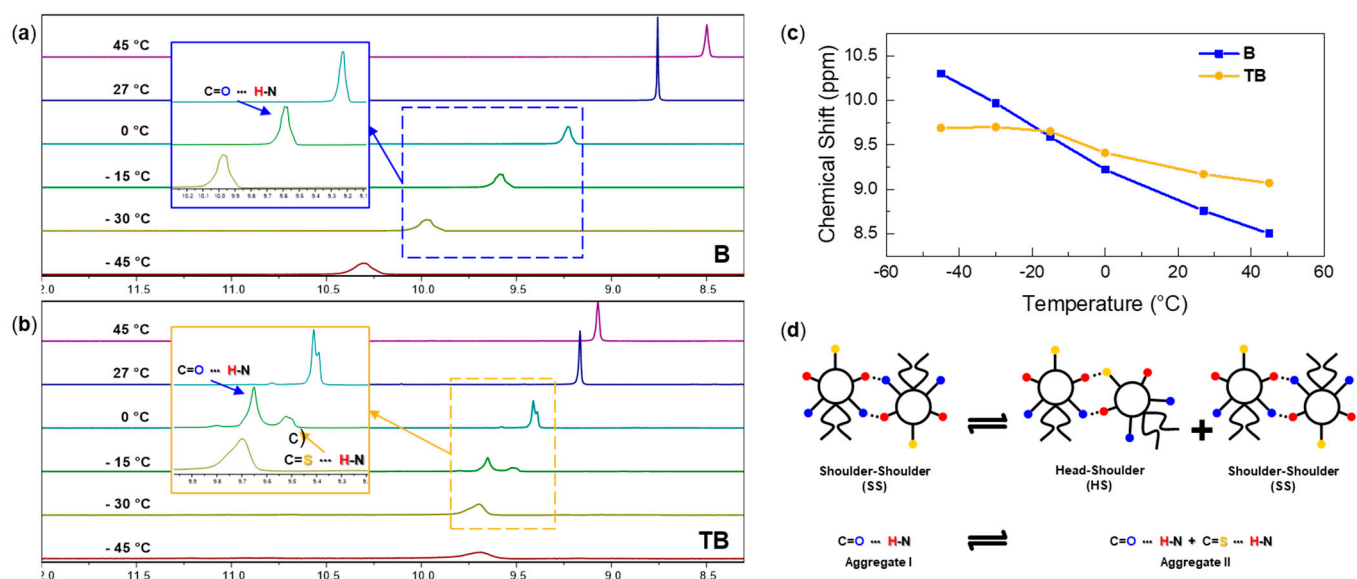


**Figure 2.** (a,b) Temperature-dependent  $^1\text{H}$  NMR spectra of model compounds **B** and **TB** in  $\text{CDCl}_3$ , (c) chemical shifts of N-H vs. temperature of the model compounds **B** and **TB**, and (d) the possible exchangeable assemblies in thiobarbiturate **TB** in  $\text{CDCl}_3$  at  $T_{\text{Coalescence}} = 0^\circ\text{C}$ .

In Figure 2a,b, the temperature-dependent  $^1\text{H}$  NMR spectra of both model compounds **B** and **TB** are shown. Starting from 0 °C for the thiobarbiturate **TB**, we clearly observe a splitting of the NH protons, indicative for two differently ordered arrangements—a behavior that was not observed for the native barbiturate **B**. It can be hypothesized that this is an indication for the formation of the two types of aggregates, I and II (see Figure 2d), which contain SS orientation or both HS and SS orientations, respectively. A coalescence temperature of  $T_{\text{Coalescence}} = 0^\circ\text{C}$  is observed, above which the two arrangements HS and SS would interchange faster compared to the NMR timescale and, thus, we found coalescence with a rate constant  $k_C = 205.1 \text{ s}^{-1}$  (for calculation details, see Supplementary Materials).

By calculating the ratio between the integral of the two isolated N-H peaks, the exchange equilibrium constant  $K_{-15^\circ\text{C}}$  of the aggregates I and II at  $-15^\circ\text{C}$  could be

obtained (see Table 1). With  $K_{-15^{\circ}\text{C}} = 0.32 \text{ M}^{-1}$ , we concluded that, at a temperature lower than  $T_{\text{Coalescence}}$ , **TB** tends to form dimers with a predominant N-H  $\cdots$  O=C instead of the N-H  $\cdots$  S=C orientation. At temperatures around  $-30^{\circ}\text{C}$ , the peak representing the N-H  $\cdots$  S=C bond, believed to be the weaker H-bonds and in an even slower exchange regime, is no longer detectable by NMR spectroscopy, presumably by peak broadening and overlap. There is no significant change of the N-H chemical shift of **TB** at temperatures lower than  $-15^{\circ}\text{C}$  (see Figure 2c), indicative that the equilibrium is frozen in **TB**, while the still decreasing N-H chemical shift of **B** demonstrates the dynamic nature of the H-bonded aggregates in **B** in this temperature range.

Overall, we see an indication for the participation of the C=S thiocarbonyl groups in the dimerization of **TB**, in total resulting in a 4-fold decrease in its overall dimerization in chloroform. While the timescale of the exchangeable aggregates in **B** is too fast to be monitored by NMR spectroscopy, the coalescence behavior of **TB** aggregates is observed, indicating aggregates in **TB** with a preferred “SS” orientation at temperatures below  $T_{\text{Coalescence}}$ . Thus, by replacing C2=O with C2=S, there is a change in the molecular arrangements and the overall strength of the H-bonds.

### 3.2. Hydrogen Bonding of Model Compounds in the Solid State

As the strength and arrangement of H-bonds differs significantly when moving to the solid state, we also studied the behavior of **B** vs. **TB** in the solid state. Here, the H-bonds in the bulk model compounds **B** and **TB** were first investigated via temperature-dependent ATR FT-IR experiments, and subsequently as Langmuir monolayers in a 2D arrangement.

#### 3.2.1. Hydrogen Bonds in Model Compounds **B** and **TB** at Elevated Temperatures

To understand the potential contribution of the C=S moiety in these H-bonding arrangements, we used temperature-dependent FT-IR spectroscopy for clarification. Due to the presence of the two 10-carbon hydrocarbon chains at the C5 position in both model compounds, **B** and **TB** show a glass transition ( $T_g$ ) (for **B** and **TB**) (see Figure 3a), with only **B** displaying crystallization ( $T_c$ ) and melting ( $T_m$ ). To study the H-bonds in the solid state at elevated temperatures, temperatures around the melting peak of **B** and the glass transition of **TB** were selected to see how the H-bonds vary below and above the respective  $T_g$ , where molecular motions are either frozen or enabled. Below the melting in **B**, the free N-H stretching at  $\sim 3400 \text{ cm}^{-1}$  is absent, whereas it is present in **TB** even at temperatures below its  $T_g$ , which is an indication for the weaker association of the thiobarbiturates. While for **B**, the H-bonded N-H stretching shows a dual peak at  $3200$  and  $3100 \text{ cm}^{-1}$  [45], denoting the ordered H-bonds in barbiturates, in **TB**, the H-bonded N-H shows a much broader peak centered at  $\sim 3200 \text{ cm}^{-1}$  with weak N-H symmetric stretching at  $\sim 3075 \text{ cm}^{-1}$ , indicating a more complex H-bonding pattern due to the existence of the C2=S [46–48] in the thiobarbiturates. The red-shifted resonance of the C=S band clearly proves that the C2=S is indeed H-bonded with the N-H [24,47–49]. As temperature rises above  $85^{\circ}\text{C}$ , **B** melts partially, showing the free N-H stretching at  $\sim 3400 \text{ cm}^{-1}$ , together with a blueshift of the carbonyl stretching from  $1692$  to  $1706 \text{ cm}^{-1}$ , demonstrating that the H-bonds in **B** are partially broken at elevated temperatures. As for **TB**, the IR spectra remain almost identical to those at room temperature, similar to the spectra of **B** in the melt state, indicative for an already dynamic character with more broken H-bonds in thiobarbiturates **TB** within the whole temperature range.

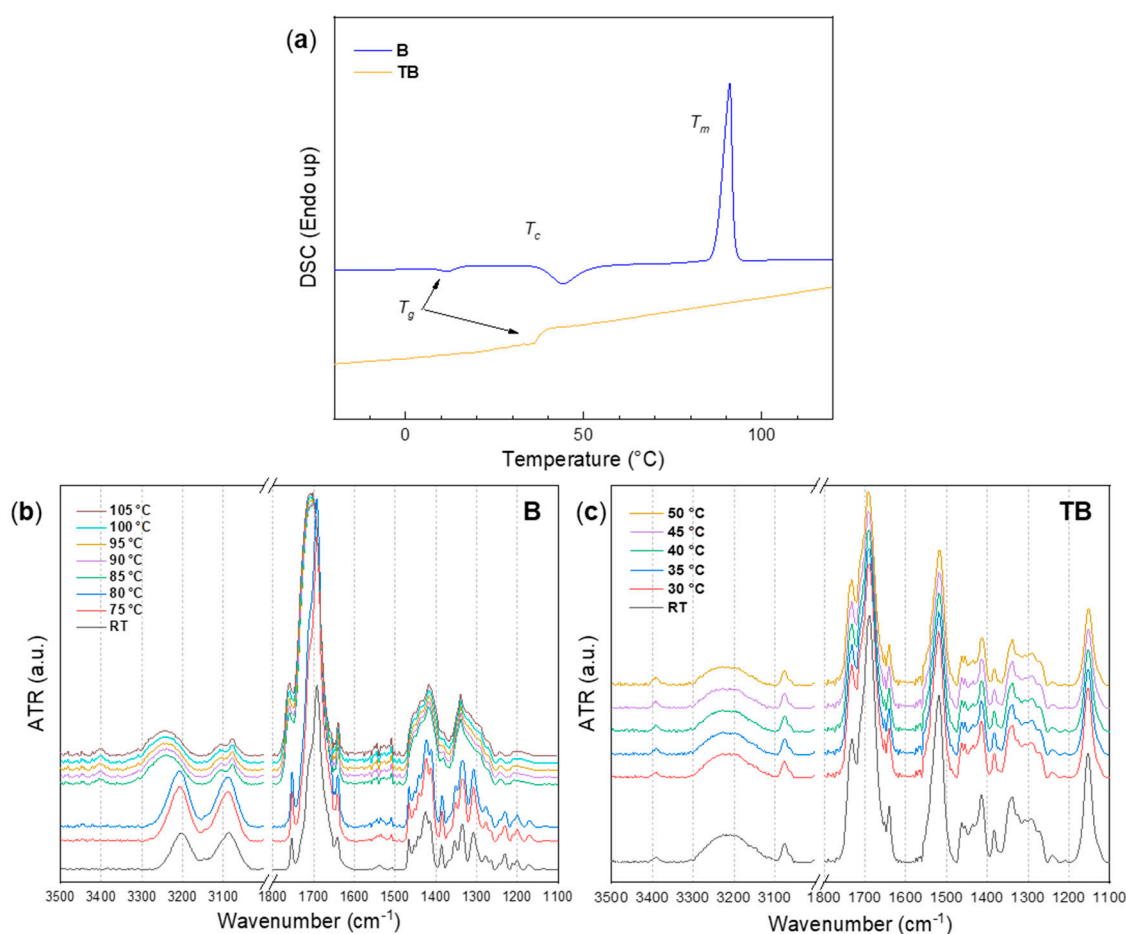


**Figure 3.** (a) DSC curves (heating rate of 5 K/min, the thermal history was cancelled by the preheating and cooling circle); (b,c) the ATR FT-IR spectra at various temperatures of model compounds **B** and **TB**.  $T_g$ : glass transition temperature;  $T_c$ : crystallization temperature;  $T_m$ : melting temperature.

Owing to the strong and ordered H-bonds in barbiturates, barbiturate **B** presents as a white powder that can form crystals, which is consistent with previous reports to use the H-bonds to engineer its ordering via crystallization [15,50,51]. Thiobarbiturate **TB**, in contrast, presents itself as a highly viscous liquid at room temperature. This difference again gives evidence for the significantly different dynamic nature of C2=O vs. C2=S in barbiturates, as the H-bonds change from an ordered crystalline nature to a rather amorphous behavior when introduced into solid materials.

### 3.2.2. Hydrogen Bonds in 2D-Ordered Films

It was reported [27–29] that barbiturates can form Langmuir films on a water subphase; however, there is no report regarding their thio-analogues. Thus, a Langmuir film of either **B** and **TB** was generated by spreading the compound solutions on the water subphase, evaporating the solvent, and compressing the films by moving the barriers of the Langmuir trough. The surface pressure-mean molecular area ( $\pi$ - $mmA$ ) isotherms of the model compounds **B** and **TB** are shown in Figure 4a.

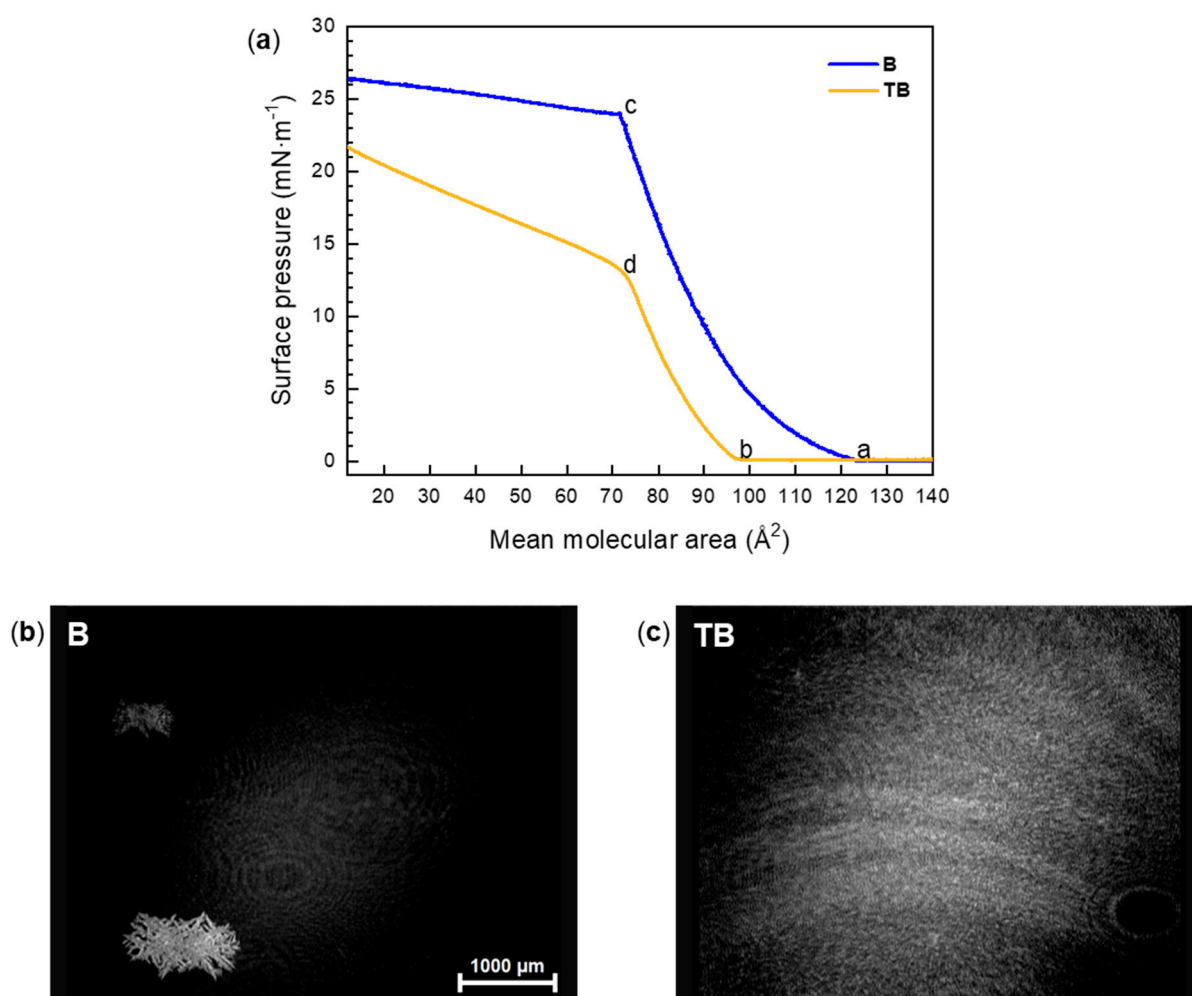


**Figure 4.** (a)  $\pi$ - $mmA$  isotherm recorded on the water subphase at 20 °C with the compression rate of 1.5 Å<sup>2</sup> / (molecule·min); Table 124 Å<sup>2</sup>, b = ~97 Å<sup>2</sup>, c = ~71 Å<sup>2</sup>, and d = ~73 Å<sup>2</sup>. (b,c) BAM images of the Langmuir films at 15 Å<sup>2</sup> of model compounds B and TB.

When compression starts from 140 Å<sup>2</sup>, both B and TB do not display an increase in surface pressure, indicating a gas-like state of the molecules on the water subphase. When the area reduces to ~124 Å<sup>2</sup>, the surface pressure of B starts to rise, which by coincidence roughly matches the theoretically calculated mean molecular area of 120 Å<sup>2</sup> for a vertically lying head group on the water surface, with the hydrocarbon chains oriented into the air (for a space filling model, see Figure S2). For TB, the increase takes place at ~97 Å<sup>2</sup>, explained by the formation of molecular stacks of the film when compressed. After an increase with an almost identical slope, the transition occurs at 71 Å<sup>2</sup> and 73 Å<sup>2</sup> for B and TB, respectively, which could either be explained by crystallization or multilayer formation, since it was reported that the nature of the H-bonds can change during crystallization [15,50,51]. As shown in Figure 4b, several crystalline domains can clearly be observed for B, but most parts of the film remain amorphous. An explanation could be that the crystallization is the result from compression and the amorphous part of B is not visible due to the poor contrast against the water subphase, which is the limitation of BAM. Meanwhile for TB, clearly there is no crystallization and only ribbon-like structures are observed. Thus, we think that the strong H-bonds within the polar head group barbiturates in B indeed contribute to crystallization, which is also in line with the investigations reported above, where B shows a higher tendency to crystallize than TB owing to the stronger and more ordered H-bonds. Thus, by introducing the C2=S, the H-bonds are weakened and lead to the formation of amorphous aggregates even under compression. The observation



of distinct domains in BAM motivates further, more detailed investigations to be reported in future work.

### 3.3. Hydrogen Bonding of Model Polymers

Based on our previous work on barbiturate-modified polyisobutylene [25,26,34,52,53], we were curious how the use of C=S-modified barbiturates would change the materials properties. Especially the formation of different H-bonding patterns with the now known weaker association was expected to change their assembly behavior significantly. We therefore prepared the C=S-modified model polymer analogues similar to those prepared previously and studied their association behavior by melt rheology, where the C=O-containing barbiturates form aggregates as reported previously [25,26,52,53]. Thus, we prepared the polymers **PB** and **PTB**, both featuring a molecular weight  $M_n = \sim 3.2$  kDa, bearing two identical (thio-)barbiturates at either of the chain ends. The synthesis was based on the strategy via living carbocationic polymerization, followed by end group modification and subsequent CuAAC “click” reaction to attach the (thio-)barbiturate moieties [25] (for synthesis, see Figure S2). Purity and properties of the so-modified model polymers **PB** and **PTB** were proven by NMR, GPC, and MALDI-ToF mass spectroscopy (for spectra and characterization data, see Figures S5,S6,S10 and S11, and Table S1).

To understand differences of the H-bonding in the polymer matrix, the polymers modified with barbiturates (**PB**) and 2-thiobarbiturates (**PTB**) were subjected to melt rheology. As known from the model compounds in solution, we sought to analyze their clustering behavior as shown in Figure 5. At room temperature, while the precursor polymer **PBr** (telechelic dibromo PIB) is a viscous liquid, both the model polymer **PB** and **PTB** present themselves as rubbery materials due to the clustering of the end groups induced by the H-bonds. In both polymers, the glass transition temperature was only slightly increased from  $-58.8$  °C (for **PBr**) to  $-61.3$  °C and  $-59.6$  °C for **PB** and **PTB**, respectively (for DSC curves, see Figure S12). The rubbery nature originates from the association of the barbiturate/thiobarbiturate end groups via their H-bonds acting as “stickers”, which connect the soft polyisobutylene chains into transient H-bonding networks. The lifetime  $\tau$  of the “stickers”, namely the lifetime of the aggregates bonded via their H-bonds, can be characterized by the crossover point in frequency sweep rheological measurement [54]. Interestingly, as shown in Figure 5a, **PB** shows terminal flow at 20 °C with a crossover point at  $\tau = 5.27 \times 10^{-3} \text{ s}^{-1}$ , with the dynamic viscosity  $\eta'$  being increased to  $\sim 10^7$  Pa·s. However, for **PTB**, terminal flow is not observed at 20 °C. Due to the absence of the crossover within the given frequency range, one can conclude that the thiobarbiturate aggregates in **PTB** display a longer lifetime compared to that of the native barbiturate aggregates in **PB**. Besides their longer lifetime, H-bonds in thiobarbiturates are indeed more tolerant against a low frequency (of shear) than those in barbiturates at frequency lower than  $\sim 53 \text{ s}^{-1}$ , evidenced by a lower loss tangent value of **PTB** than that of **PB** (for the loss tangent vs. frequency curve, see Figure S13). As represented in Figure 5a,b, during the frequency sweep, the **PB** chains, connected via the H-bonding network, are gradually opened by the shear-stress, causing an overall decrease in viscosity. The H-bonding network in **PTB**, to some extent, was also dynamized, but within the given frequency range the H-bonds network can still persist in the “more closed” state, indicating that at a certain frequency range the H-bonds in **TB** may be even as strong (or even stronger) inside the polymer when compared to the native barbiturate moieties.

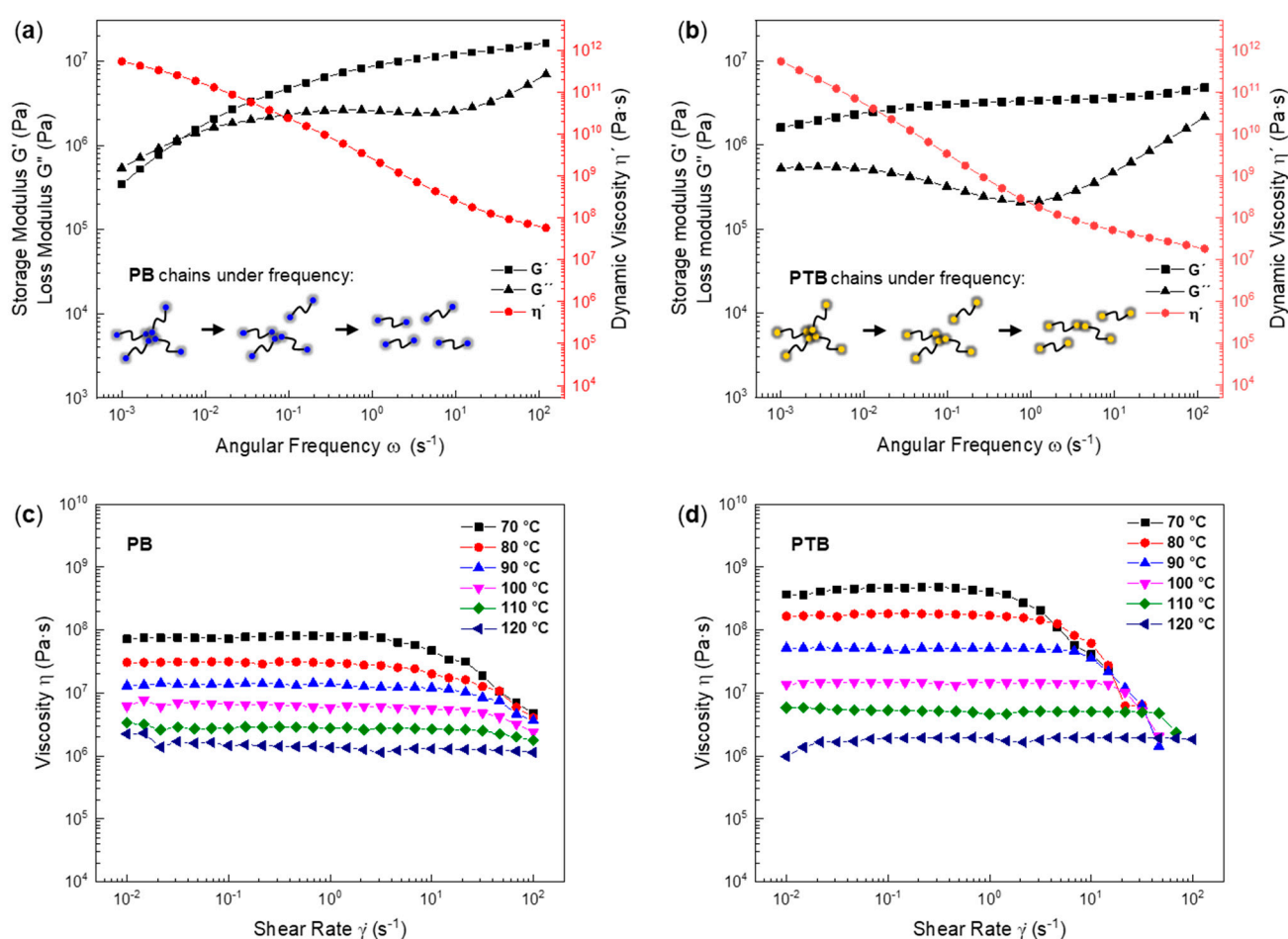


**Figure 5.** Storage modulus  $G'$ , loss modulus  $G''$ , and dynamic viscosity  $\eta'$  vs. angular frequency  $\omega$  measured at 20 °C, and viscosity  $\eta$  vs. shear rate  $\dot{\gamma}$  at elevated temperatures of the model polymer **PB** (a,c) and **PTB** (b,d).

Due to the rubbery nature of the model polymers at room temperature, the viscosities were determined from 70 °C to 120 °C and the viscosity vs. shear rate at elevated temperatures is shown in Figure 5c,d. Both polymers show a shear-thinning behavior, which is in line with the behavior observed in the melt extrusion of these polymers, as required for 3D printing [32]. At a temperature between 70 °C and 110 °C, **PTB** always demonstrates a higher zero-shear viscosity (for the zero-shear viscosity vs. temperature curve, see Figure S14) than that of **PB**, which could be another proof of the in view of stronger rheology H-bonds in thiobarbiturates than those in barbiturates, when applied in the nonpolar polyisobutylene matrix. The shear-thinning behavior disappears after the temperature reaches 120 °C, indicative for a complete rupture of the H-bonds within the network. Therefore, if free from H-bonding, the (thio-)barbiturate-modified **PB** and **PTB** show an almost identical native viscosity, and the unexpected higher viscosity in **PTB** may be a result of the weaker and more discrete H-bonds in thiobarbiturates instead of the stronger and more ordered H-bonds, which deviates from the observation in model compound solutions.

#### 4. Materials and Methods

Urea was purchased from Merck; thiourea was purchased from Apolda (DDR); diethyl ethylmalonate was purchased from J&K (Germany); sodium azide, sodium hydride, copper(I) iodide, and potassium tert-butoxide were purchased from Sigma Aldrich (Germany); diethyl malonate, 10-bromo-1-decene, 5-chloro-1-pentyne, and diisopropylethylamine were purchased from TCI (Belgium). All chemicals listed here were used without any purifica-

tion unless otherwise stated. Solvents handling and the chemicals that are not mentioned here can be found in the Supplementary Materials.

#### 4.1. Nuclear Magnetic Resonance Spectroscopy (NMR)

All  $^1\text{H}$ -NMR and  $^{13}\text{C}$ -NMR spectra were measured on a Varian FT-NMR spectrometer (500 and 101 MHz, respectively), Agilent Technologies (Agilent Technologies Germany GmbH & Co. KG, Waldbronn, Germany). All samples were measured at 27 °C using deuterated chloroform ( $\text{CDCl}_3$ ) or DMSO- $\text{d}_6$ . Chemical shifts ( $\delta$ ) were recorded in parts per million (ppm) relative to the remaining solvent signals ( $\text{CDCl}_3$ : 7.26 ppm ( $^1\text{H}$ ) and 77.0 ppm ( $^{13}\text{C}$ ), DMSO- $\text{d}_6$ : 2.50 ppm ( $^1\text{H}$ ) and 39.5 ppm ( $^{13}\text{C}$ )). Chemical shifts were reported with the following notations: s, singlet; d, doublet; t, triplet; q, quartlet; p, pentlet; m, a more complex multiplet or overlapping multiplets. The data analysis was performed on the software MestReNova (version 9.0.1-13254).

#### 4.2. Differential Scanning Calorimetry (DSC)

DSC measurements were accomplished on a Netzsch DSC 204 F1 Phoenix (NETZSCH-Gerätebau GmbH, Selb, Germany). Samples pieces with a mass of 5–10 mg were placed into aluminum crucibles and were heated under nitrogen atmosphere. The thermal history was cancelled by a preheating circle to 150 °C with a rate of 10 K/min, then keeping the sample for 20 min at 150 °C, followed by cooling to −50 °C with a rate of 5 K/min, then keeping the sample for 20 min at −50 °C. The DSC data were collected from the second heating circle from −50 °C to 150 °C with a heating rate of 5 K/min. Data analysis was performed on the software NETZSCH Proteus (version 5.2.1.) and Origin 2018 (version b9.5.0.193).

#### 4.3. ATR FT-IR Spectroscopy

ATR-FTIR spectra were recorded using a Bruker Tensor vertex 70 (Bruker Optik GmbH, Bremen, Germany) equipped with a Golden Gate Heated Diamond ATR top plate (Specac Ltd, Orpington, UK). All wavenumbers are given in  $\text{cm}^{-1}$ . For FT-IR measurements at elevated temperatures, samples were heated with the heating rate of 10 K/min, and equilibrated at the desired temperature for 10 min before the measurement started. Data analysis was performed via the software OPUS (version 8.2) and Origin 2018 (version b9.5.0.193).

#### 4.4. Langmuir Isotherm

The  $\pi$ - $\text{m}^2\text{A}$  isotherms were recorded using a Langmuir trough (Riegler & Kirstein GmbH, Potsdam, Germany) with a maximum trough area of 545  $\text{cm}^2$ . The trough was equipped with two moveable barriers and a Wilhelmy plate made of filter paper. The entire trough was covered by a Plexiglas box to maintain an equilibrium environment. Millipore water was used as a subphase for the experiment. The temperature of the subphase was kept at 20 °C using a thermostat. Before spreading the compound solutions, the purity of the subphase was checked by surface pressure measurement at a maximum barrier compression ( $\pi < 0.15 \text{ mN/m}$ ). Compound solutions with a concentration of  $\sim 1 \text{ mg/mL}$  were prepared in chloroform and spread dropwise in some random locations on the subphase using a Hamilton digital syringe. After a 20 min waiting time for complete solvent evaporation, the trough surface was compressed at a speed of  $1.5 \text{ \AA}^2/(\text{molecule} \cdot \text{min})$  to record the pressure–mean molecular area isotherms. Data analysis was performed via the software Origin 2018 (version b9.5.0.193).

#### 4.5. Brewster Angle Microscopy

To monitor the water surface during compression, a Brewster angle microscope (NFT Mini BAM, Nanofilm Technologies, Valley View, OH, USA) coupled with a Langmuir trough of 142  $\text{cm}^2$  was used. The lateral resolution of the microscopy was 20  $\mu\text{m}$  with a field view of  $4.8 \times 6.4 \text{ mm}^2$ . The images were captured using the software WinTV (Hauppauge Inc, Hauppauge, NY, USA). The imaging of the Langmuir film was done at different surface pressures during the film compression at a rate of  $1.5 \text{ \AA}^2/(\text{molecule} \cdot \text{min})$ .



#### 4.6. Rheology

Rheology experiments were performed on an MCR 101-DSO (Anton Paar Germany GmbH, Ostfildern-Scharnhausen, Germany) using a parallel plate–plate geometry (plate diameter 8 mm). All polymers were dried under high vacuum at 80 °C for 48 h before the rheology measurement. The solid samples were vacuum hot pressed into films at 80 °C, and then cut into discs of 8 mm with a punching tool. The sample temperature was regulated by thermoelectric cooling/heating in a Peltier chamber under a dry nitrogen atmosphere. At each temperature the sample was equilibrated for 20 min before the measurement was started. All measurements were performed in the dynamic mode and repeated for twice to ensure the precise viscosity values. The frequency sweeps were done within the linear viscoelastic regime (LVE) with 5% deformation applied. Data analysis was performed via the software Pheo Compass<sup>TM</sup> (version V1.30.1064) and Origin 2018 (version b9.5.0.193).

Methods which are not mentioned here can be found in the Supplementary Materials (Figures S1–S14, Table S1).

#### 5. Conclusions

In summary, we investigated the association behavior of the model compounds 5,5-disubstituted barbiturate **B** and thiobarbiturate **TB** in the nonpolar solvent chloroform. By replacing the C2=O with the C2=S group, a 4-fold decrease of the dimerization constant was observed. The observed coalescence behavior of the H-bonded aggregates in **TB** with a  $k_C = 205.1 \text{ s}^{-1}$  at 0 °C via NMR spectroscopy clearly indicates the formation of at least two different orientations of the H-bonding patterns—an effect not observed in the conventional barbiturate **B**. In the bulk, the H-bonds of the model system were investigated by ATR FT-IR spectroscopy, together with DSC, demonstrating more ordered H-bonds in native barbiturate **B** and more discrete H-bonds in the thiobarbiturate **TB** at room temperature as indicated by the crystalline nature of **B** and the purely amorphous nature of **TB**. The Langmuir isotherms of the model compounds again demonstrate the tendency of the barbiturate **B** to crystallize due to the more ordered and stronger H-bonds, while the weaker H-bonds in C2=S of the thiobarbiturate **TB** suppress crystallization and facilitate the formation of molecular stacks, as evidenced by the surface pressure isotherm and the BAM images. When covalently bound to both ends of a linear, nonpolar polymer, the thiobarbiturate-modified **PTB** shows a longer lifetime under frequency sweep, in line with the observation from the model system in solution. **PTB** shows a higher zero-shear viscosity when compared to **PB**, diverging from the observation in small molecule model system where **B** possesses a higher association constant in comparison to **TB**. Thus, within the bulk-polymer thiobarbiturates offer an “as strong” or “even stronger” “sticker effect” compared to the native barbiturate-modified **PB**—a point often misjudged by the results obtained for small molecules in solution. When turning towards bulk systems, such deviation in bonding strength and orientation can be significant, showing the necessity for studies in the solid state rather than the solution state to understand the formation of dynamic and adaptive effects in materials. This work proves that, while thiobarbiturates demonstrate a weaker association in chloroform, the discrete H-bonds in thiobarbiturate-modified **PTB** can at least equally, or even better, reinforce the nonpolar polymer matrix, thus indicating the formation of stronger H-bonds of the thiobarbiturates in polymers in contrast to effects observed in solution. In line with the already reported additional formation of additional (weaker) out-of-plane H-bonds [5], this altogether can explain why the H-bonds in **PTB** are overall stronger than in **TB**, but are still highly dynamic as they could “slide-along” several binding partners, similar to the observation by Aida et. al. for their self-healing thiourea system [15]. It also underscores that the presence of both, amide-type and thioamide-type groups could be regarded as advantageous, as both dynamic features are present and thus control the dynamics of the material. Overall, this gives a hint to the often superior properties of thio-based H-bonds in some self-healing materials, opening a potential tool to engineer such materials with adaptive and responsive properties.

**Supplementary Materials:** The following are available online at <https://www.mdpi.com/article/10.3390/ijms222312679/s1>.

**Author Contributions:** Conceptualization, C.L. and W.H.B.; methodology, C.L., P.H., N.H. and D.S.; investigation, C.L., P.H. and N.H.; writing—original draft preparation, C.L. and W.H.B.; writing—review and editing, C.L., J.K. and W.H.B.; supervision, W.H.B.; project administration, W.H.B.; funding acquisition, W.H.B. All authors have read and agreed to the published version of the manuscript.

**Funding:** We thank the International Graduate School AGRIPOLY supported by the European Regional Development Fund (ERDF) and the Federal State Saxony-Anhalt; the DFG-Graduate College GRK 2670 (German research foundation—project ID 43649874, TP B2, RTG 2670); the DFG SFB TRR 102, TP A03, Nr 189853844; and the BAT4EVER project founded by the European Union in the scope of H2020-LC-BAT-2020-3 for financial support.

**Institutional Review Board Statement:** Not applicable.

**Informed Consent Statement:** Not applicable.

**Data Availability Statement:** Data are contained within the article.

**Conflicts of Interest:** The authors declare no conflict of interest.

## References




1. Arunan, E.; Desiraju, G.R.; Klein, R.A.; Sadlej, J.; Scheiner, S.; Alkorta, I.; Clary, D.C.; Crabtree, R.H.; Dannenberg, J.J.; Hobza, P.; et al. Definition of the hydrogen bond (IUPAC Recommendations 2011). *Pure Appl. Chem.* **2011**, *83*, 1637–1641. [\[CrossRef\]](#)
2. Weinhold, F.; Klein, R.A. What is a hydrogen bond? Resonance covalency in the supramolecular domain. *Chem. Educ. Res. Pract.* **2014**, *15*, 276–285. [\[CrossRef\]](#)
3. Biswal, H.S.; Chakraborty, S.; Wategaonkar, S. Experimental evidence of O—H—S hydrogen bonding in supersonic jet. *J. Chem. Phys.* **2008**, *129*, 184311. [\[CrossRef\]](#) [\[PubMed\]](#)
4. Zheng, W.; Fu, Y.; Liu, L.; Guo, Q. Hydrogen Bonding Interaction between Ureas or Thioureas and Carbonyl Compounds. *Acta Phys.-Chim. Sin.* **2007**, *23*, 1018–1024. [\[CrossRef\]](#)
5. Lenthall, J.T.; Foster, J.A.; Anderson, K.M.; Probert, M.R.; Howard, J.A.K.; Steed, J.W. Hydrogen bonding interactions with the thiocarbonyl  $\pi$ -system. *CrystEngComm* **2011**, *13*, 3202–3212. [\[CrossRef\]](#)
6. Mundlapati, V.R.; Gautam, S.; Sahoo, D.K.; Ghosh, A.; Biswal, H.S. Thioamide, a Hydrogen Bond Acceptor in Proteins and Nucleic Acids. *J. Phys. Chem. Lett.* **2017**, *8*, 4573–4579. [\[CrossRef\]](#)
7. Chand, A.; Sahoo, D.K.; Rana, A.; Jena, S.; Biswal, H.S. The Prodigious Hydrogen Bonds with Sulfur and Selenium in Molecular Assemblies, Structural Biology, and Functional Materials. *Acc. Chem. Res.* **2020**, *53*, 1580–1592. [\[CrossRef\]](#) [\[PubMed\]](#)
8. Mundlapati, V.R.; Sahoo, D.K.; Ghosh, S.; Purame, U.K.; Pandey, S.; Acharya, R.; Pal, N.; Tiwari, P.; Biswal, H.S. Spectroscopic Evidences for Strong Hydrogen Bonds with Selenomethionine in Proteins. *J. Phys. Chem. Lett.* **2017**, *8*, 794–800. [\[CrossRef\]](#)
9. Jakab, G.; Tancon, C.; Zhang, Z.; Lippert, K.M.; Schreiner, P.R. (Thio)urea Organocatalyst Equilibrium Acidities in DMSO. *Org. Lett.* **2012**, *14*, 1724–1727. [\[CrossRef\]](#) [\[PubMed\]](#)
10. Culik, R.M.; Jo, H.; DeGrado, W.F.; Gai, F. Using Thioamides To Site-Specifically Interrogate the Dynamics of Hydrogen Bond Formation in  $\beta$ -Sheet Folding. *J. Am. Chem. Soc.* **2012**, *134*, 8026–8029. [\[CrossRef\]](#)
11. Stefaniu, C.; Zaffalon, P.-L.; Carmine, A.; Verolet, Q.; Fernandez, S.; Wesolowski, T.A.; Brezesinski, G.; Zumbuehl, A. Rigid Urea and Self-Healing Thiourea Ethanolamine Monolayers. *Langmuir* **2015**, *31*, 1296–1302. [\[CrossRef\]](#)
12. Tian, T.; Hu, R.; Tang, B.Z. Room Temperature One-Step Conversion from Elemental Sulfur to Functional Polythioureas through Catalyst-Free Multicomponent Polymerizations. *J. Am. Chem. Soc.* **2018**, *140*, 6156–6163. [\[CrossRef\]](#)
13. Wu, S.; Luo, M.; Darensbourg, D.J.; Zuo, X. Catalyst-Free Construction of Versatile and Functional CS<sub>2</sub>-Based Polythioureas: Characteristics from Self-Healing to Heavy Metal Absorption. *Macromolecules* **2019**, *52*, 8596–8603. [\[CrossRef\]](#)
14. Cao, W.; Dai, F.; Hu, R.; Tang, B.Z. Economic Sulfur Conversion to Functional Polythioamides through Catalyst-Free Multicomponent Polymerizations of Sulfur, Acids, and Amines. *J. Am. Chem. Soc.* **2020**, *142*, 978–986. [\[CrossRef\]](#) [\[PubMed\]](#)
15. Yanagisawa, Y.; Nan, Y.; Okuro, K.; Aida, T. Mechanically robust, readily repairable polymers via tailored noncovalent cross-linking. *Science* **2018**, *359*, 72–76. [\[CrossRef\]](#) [\[PubMed\]](#)
16. Lee, D.S.; Choi, Y.-S.; Hwang, J.H.; Lee, J.-H.; Lee, W.; Ahn, S.-k.; Park, S.; Lee, J.-H.; Kim, Y.S.; Kim, D.-G. Weldable and Reprocessable Biomimetic Polymer Networks Based on a Hydrogen Bonding and Dynamic Covalent Thiourea Motif. *ACS Appl. Polym. Mater.* **2021**, *3*, 3714–3720. [\[CrossRef\]](#)
17. Chang, S.K.; Hamilton, A.D. Molecular recognition of biologically interesting substrates: Synthesis of an artificial receptor for barbiturates employing six hydrogen bonds. *J. Am. Chem. Soc.* **1988**, *110*, 1318–1319. [\[CrossRef\]](#)
18. Chang, S.K.; Van Engen, D.; Fan, E.; Hamilton, A.D. Hydrogen bonding and molecular recognition: Synthetic, complexation, and structural studies on barbiturate binding to an artificial receptor. *J. Am. Chem. Soc.* **1991**, *113*, 7640–7645. [\[CrossRef\]](#)

19. McGrath, J.M.; Pluth, M.D. Understanding the Effects of Preorganization, Rigidity, and Steric Interactions in Synthetic Barbiturate Receptors. *J. Org. Chem.* **2014**, *79*, 711–719. [[CrossRef](#)] [[PubMed](#)]
20. Russell, K.C.; Lehn, J.M.; Kyritsakas, N.; DeCian, A.; Fischer, J. Self-assembly of hydrogen-bonded supramolecular strands from complementary melamine and barbiturate components with chiral selection. *New J. Chem.* **1998**, *22*, 123–128. [[CrossRef](#)]
21. Schneider, H.-J.; Juneja, R.K.; Simova, S. Solvent and Structural Effects on Hydrogen Bonds in Some Amides and Barbiturates. An Additive Scheme for the Stability of Corresponding Host-Guest Complexes. *Chem. Ber.* **1989**, *122*, 1211–1213. [[CrossRef](#)]
22. Yu, B.-S.; Jo, S.-B.; Kim, C.-K.; Hwang, Y.-S. Interaction between barbiturate and membrane components. *Arch. Pharmacol. Res.* **1990**, *13*, 246–251. [[CrossRef](#)]
23. Zuccarello, F.; Buemi, G.; Gandolfo, C.; Contino, A. Barbituric and thiobarbituric acids: A conformational and spectroscopic study. *Spectrochim. Acta Part A Mol. Biomol. Spectrosc.* **2003**, *59*, 139–151. [[CrossRef](#)]
24. Ramondo, F.; Pieretti, A.; Gontrani, L.; Bencivenni, L. Hydrogen bonding in barbituric and 2-thiobarbituric acids: A theoretical and FT-IR study. *Chem. Phys.* **2001**, *271*, 293–308. [[CrossRef](#)]
25. Herbst, F.; Seiffert, S.; Binder, W.H. Dynamic supramolecular poly(isobutylene)s for self-healing materials. *Polym. Chem.* **2012**, *3*, 3084–3092. [[CrossRef](#)]
26. Yan, T.; Schröter, K.; Herbst, F.; Binder, W.H.; Thurn-Albrecht, T. What Controls the Structure and the Linear and Nonlinear Rheological Properties of Dense, Dynamic Supramolecular Polymer Networks? *Macromolecules* **2017**, *50*, 2973–2985. [[CrossRef](#)]
27. Weck, M.; Fink, R.; Ringsdorf, H. Molecular Recognition via Hydrogen Bonding at the Air–Water Interface: An Isotherm and Fourier Transform Infrared Reflection Spectroscopy Study. *Langmuir* **1997**, *13*, 3515–3522. [[CrossRef](#)]
28. Huang, X.; Li, C.; Jiang, S.; Wang, X.; Zhang, B.; Liu, M. Self-Assembled Spiral Nanoarchitecture and Supramolecular Chirality in Langmuir–Blodgett Films of an Achiral Amphiphilic Barbituric Acid. *J. Am. Chem. Soc.* **2004**, *126*, 1322–1323. [[CrossRef](#)]
29. Kong, X.; Du, X. In Situ IRRAS Studies of Molecular Recognition of Barbituric Acid Lipids to Melamine at the Air–Water Interface. *J. Phys. Chem. B* **2011**, *115*, 13191–13198. [[CrossRef](#)]
30. Sun, M.; Zhou, Y.; Ye, Z.; Li, S.; Dong, A.; Zhang, J. Multifunctional polymer bearing malonylurea groups for the fabrication of coordination complexes and supramolecular assemblies. *Eur. Polym. J.* **2021**, *156*, 110616. [[CrossRef](#)]
31. Mahmudov, K.T.; Kopylovich, M.N.; Maharramov, A.M.; Kurbanova, M.M.; Gurbanov, A.V.; Pombeiro, A.J.L. Barbituric acids as a useful tool for the construction of coordination and supramolecular compounds. *Coord. Chem. Rev.* **2014**, *265*, 1–37. [[CrossRef](#)]
32. Rupp, H.; Döhler, D.; Hilgeroth, P.; Mahmood, N.; Beiner, M.; Binder, W.H. 3D Printing of Supramolecular Polymers: Impact of Nanoparticles and Phase Separation on Printability. *Macromol. Rapid Commun.* **2019**, *40*, 1900467. [[CrossRef](#)] [[PubMed](#)]
33. Chen, S.; Mahmood, N.; Beiner, M.; Binder, W.H. Self-Healing Materials from V- and H-Shaped Supramolecular Architectures. *Angew. Chem. Int. Ed.* **2015**, *54*, 10188–10192. [[CrossRef](#)] [[PubMed](#)]
34. Herbst, F.; Döhler, D.; Michael, P.; Binder, W.H. Self-Healing Polymers via Supramolecular Forces. *Macromol. Rapid Commun.* **2013**, *34*, 203–220. [[CrossRef](#)]
35. Chen, S.; Schulz, M.; Lechner, B.-D.; Appiah, C.; Binder, W.H. One-pot synthesis and self-assembly of supramolecular dendritic polymers. *Polym. Chem.* **2015**, *6*, 7988–7994. [[CrossRef](#)]
36. Chen, S.; Ströhl, D.; Binder, W.H. Orthogonal Modification of Polymers via Thio–Bromo “Click” Reaction and Supramolecular Chemistry: An Easy Method Toward Head-to-Tail Self-Assembled Supramolecular Polymers. *ACS Macro Lett.* **2015**, *4*, 48–52. [[CrossRef](#)]
37. Mane, S.R.; Sathyan, A.; Shunmugam, R. Barbiturate derived amphiphilic homopolymers: Synthesis, characterization, self-assembly and anticancer drug delivery. *Ther. Deliv.* **2019**, *10*, 419–431. [[CrossRef](#)]
38. Mane, S.R.; Rao, N.V.; Shunmugam, R. Reversible pH- and Lipid-Sensitive Vesicles from Amphiphilic Norbornene-Derived Thiobarbiturate Homopolymers. *ACS Macro Lett.* **2012**, *1*, 482–488. [[CrossRef](#)]
39. Mane, S.R.; Shunmugam, R. Hierarchical Self-Assembly of Amphiphilic Homopolymer into Unique Superstructures. *ACS Macro Lett.* **2014**, *3*, 44–50. [[CrossRef](#)]
40. Bordwell, F.G.; Algrim, D.J.; Harrelson, J.A. The relative ease of removing a proton, a hydrogen atom, or an electron from carboxamides versus thiocarboxamides. *J. Am. Chem. Soc.* **1988**, *110*, 5903–5904. [[CrossRef](#)]
41. Alemán, C. On the Ability of Modified Peptide Links to Form Hydrogen Bonds. *J. Phys. Chem. A* **2001**, *105*, 6717–6723. [[CrossRef](#)]
42. Abboud, J.L.M.; Roussel, C.; Gentric, E.; Sraidi, K.; Lauransan, J.; Guiheneuf, G.; Kamlet, M.J.; Taft, R.W. Studies on amphiprotic compounds. 3. Hydrogen-bonding basicity of oxygen and sulfur compounds. *J. Org. Chem.* **1988**, *53*, 1545–1550. [[CrossRef](#)]
43. Laurence, C.; Berthelot, M.; Le Questel, J.-Y.; El Ghomari, M.J. Hydrogen-bond basicity of thioamides and thioureas. *J. Chem. Soc. Perkin Trans.* **1995**, *2*, 2075–2079. [[CrossRef](#)]
44. Allen, F.H.; Bird, C.M.; Rowland, R.S.; Raithby, P.R. Resonance-Induced Hydrogen Bonding at Sulfur Acceptors in R1R2C=S and R1CS2- Systems. *Acta Crystallogr. Sect. B* **1997**, *53*, 680–695. [[CrossRef](#)]
45. Sun, C.; Xue, D. IR Spectral Study of Mesoscale Process during Urea Crystallization from Aqueous Solution. *Cryst. Growth Des.* **2015**, *15*, 2867–2873. [[CrossRef](#)]
46. Refat, M.S.; El-Korashy, S.A.; Ahmed, A.S. A convenient method for the preparation of barbituric and thiobarbituric acid transition metal complexes. *Spectrochim. Acta Part A Mol. Biomol. Spectrosc.* **2008**, *71*, 1084–1094. [[CrossRef](#)]
47. Srinivasan, K.; Gunasekaran, S.; Krishnan, S. Spectroscopic investigations and structural confirmation studies on thiourea. *Spectrochim. Acta Part A Mol. Biomol. Spectrosc.* **2010**, *75*, 1171–1175. [[CrossRef](#)] [[PubMed](#)]

- 
48. Śmiszek-Lindert, W.E.; Chelmecka, E.; Góralczyk, S.; Kaczmarek, M. Vibrational spectroscopic (FT-IR, FT-Raman) studies, Hirshfeld surfaces analysis, and quantum chemical calculations of m-acetotoluidide and m-thioacetotoluidide. *J. Mol. Struct.* **2017**, *1128*, 619–628. [[CrossRef](#)]
  49. Pegg, R.B.; Shahidi, F.; Jablonski, C.R. Interactions of sulfanilamide and 2-thiobarbituric acid with malonaldehyde: Structure of adducts and implications in determination of oxidative state of nitrite-cured meats. *J. Agric. Food Chem.* **1992**, *40*, 1826–1832. [[CrossRef](#)]
  50. Laventure, A.; Lauzon, D.; Pellerin, C.; Lebel, O. Triazine-based molecular glasses frustrate the crystallization of barbiturates. *CrystEngComm* **2019**, *21*, 1734–1741. [[CrossRef](#)]
  51. Hutzler, W.M.; Egert, E.; Bolte, M. One barbiturate and two solvated thiobarbiturates containing the triply hydrogen-bonded ADA/DAD synthon, plus one ansovate and three solvates of their cofomer 2,4-diaminopyrimidine. *Acta Crystallogr. Sect. C* **2016**, *72*, 705–715. [[CrossRef](#)] [[PubMed](#)]
  52. Yan, T.; Schröter, K.; Herbst, F.; Binder, W.H.; Thurn-Albrecht, T. Nanostructure and Rheology of Hydrogen-Bonding Telechelic Polymers in the Melt: From Micellar Liquids and Solids to Supramolecular Gels. *Macromolecules* **2014**, *47*, 2122–2130. [[CrossRef](#)]
  53. Yan, T.; Schröter, K.; Herbst, F.; Binder, W.H.; Thurn-Albrecht, T. Unveiling the molecular mechanism of self-healing in a telechelic, supramolecular polymer network. *Sci. Rep.* **2016**, *6*, 32356. [[CrossRef](#)] [[PubMed](#)]
  54. Feldman, K.E.; Kade, M.J.; Meijer, E.W.; Hawker, C.J.; Kramer, E.J. Model Transient Networks from Strongly Hydrogen-Bonded Polymers. *Macromolecules* **2009**, *42*, 9072–9081. [[CrossRef](#)]

## Article

# Synthesis and Characterization of Quadrupolar-Hydrogen-Bonded Polymeric Ionic Liquids for Potential Self-Healing Electrolytes

Chenming Li <sup>1</sup>, Rajesh Bhandary <sup>1</sup>, Anja Marinow <sup>1</sup>, Dmitrii Ivanov <sup>1</sup>, Mengxue Du <sup>2</sup>, René Androsch <sup>2</sup> and Wolfgang H. Binder <sup>1,\*</sup>

<sup>1</sup> Macromolecular Chemistry, Institute of Chemistry, Faculty of Natural Science II, Martin Luther University Halle-Wittenberg, Von-Danckelmann-Platz 4, 06120 Halle (Saale), Germany

<sup>2</sup> Interdisciplinary Center for Transfer-Oriented Research in Natural Sciences, Martin Luther University Halle-Wittenberg, 06099 Halle (Saale), Germany

\* Correspondence: wolfgang.binder@chemie.uni-halle.de

**Abstract:** Within the era of battery technology, the urgent demand for improved and safer electrolytes is immanent. In this work, novel electrolytes, based on pyrrolidinium-bistrifluoromethanesulfonylimide polymeric ionic liquids (POILs), equipped with quadrupolar hydrogen-bonding moieties of ureido-pyrimidinone (UPy) to mediate self-healing properties were synthesized. Reversible addition–fragmentation chain-transfer (RAFT) polymerization was employed using S,S-dibenzyl trithiocarbonate as the chain transfer agent to produce precise POILs with a defined amount of UPy and POIL-moieties. Kinetic studies revealed an excellent control over molecular weight and polydispersity in all polymerizations, with a preferable incorporation of UPy monomers in the copolymerizations together with the ionic monomers. Thermogravimetric analysis proved an excellent thermal stability of the polymeric ionic liquids up to 360 °C. By combining the results from differential scanning calorimetry (DSC), broadband dielectric spectroscopy (BDS), and rheology, a decoupled conductivity of the POILs from glass transition was revealed. While the molecular weight was found to exert the main influence on ionic conductivity, the ultimate strength and the self-healing efficiency (of up to 88%) were also affected, as quantified by tensile tests for both pristine and self-healed samples, evidencing a rational design of self-healing electrolytes bearing both hydrogen bonding moieties and low-molecular-weight polymeric ionic liquids.

**Keywords:** RAFT polymerization; hydrogen bonds; polymeric ionic liquids



**Citation:** Li, C.; Bhandary, R.; Marinow, A.; Ivanov, D.; Du, M.; Androsch, R.; Binder, W.H. Synthesis and Characterization of Quadrupolar-Hydrogen-Bonded Polymeric Ionic Liquids for Potential Self-Healing Electrolytes. *Polymers* **2022**, *14*, 4090. <https://doi.org/10.3390/polym14194090>

Academic Editor: Jason Bara

Received: 29 August 2022

Accepted: 23 September 2022

Published: 29 September 2022

**Publisher's Note:** MDPI stays neutral with regard to jurisdictional claims in published maps and institutional affiliations.



**Copyright:** © 2022 by the authors. Licensee MDPI, Basel, Switzerland. This article is an open access article distributed under the terms and conditions of the Creative Commons Attribution (CC BY) license (<https://creativecommons.org/licenses/by/4.0/>).

## 1. Introduction

Lithium-ion batteries (LIBs) as an alternative power source to traditional petrochemical energy have attracted researchers' interest owing to their excellent power density, reusability, and processability [1]. However in conventional liquid electrolytes, LIBs generally suffer drawbacks from lithium dendrites [2,3], leakage and flammability of the liquid electrolytes and the thus resulting poor thermal stability [4]. To solve such deficiencies in current electrolyte systems, polymeric ionic liquids (POILs), where ionic moieties are tethered onto a polymeric backbone, represent potential candidates as polymer electrolytes due to their good conductivity, thermal and mechanical stability, as well as their plasticity [5,6]. For next-generation electrolytes with battery applications, not only high ionic conductivity and good mechanical properties are required [7,8], but also properties such as self-healing can contribute to extending the lifespan of a polymer electrolyte, and thus of the battery as a whole. In the field of supramolecular materials, hydrogen bonds (HBs) play an important role because HBs can provide interchain forces, leading to material properties such as improved mechanical strength [9], shape memory behavior [10], stimulus responsiveness [11], and self-healing [12,13]. Thus in the field of polymer electrolyte chemistry, researchers are exploiting such HBs in POILs to exploit their generally proposed weaker strength and thus



to embed self-healing ability into the materials [14,15]. Among the diverse HB synthons, ureido-pyrimidinone (UPy) is widely applied to polymer matrices [16–19] owing to its facile synthesis and strong dimerization-abilities (with an association constant,  $K_{\text{assn.}} \geq 10^6 \text{ M}^{-1}$  in  $\text{CDCl}_3$ ) [20] via its quadrupolar HBs. There have been several approaches to introducing UPy into POIL to explore its self-healing property together with the conductive nature of POILs [15,17–19], which represents an advantageous strategy to design new-generation functional electrolytes.

While many POILs have been reported predominantly with polyimidazolium ions [17,21] or other POILs [18,22,23] as self-healing electrolytes, poly-pyrrolidinium-based self-healing electrolytes have been scarcely reported, despite the fact that pyrrolidinium-based ionic liquids generally have a higher electrochemical stability [24]. Moreover, in many publications POILs were synthesized via free radical polymerization, which offers no control over the molecular weight of POILs, thus yielding polymers with a broad polydispersity and a poor reproducibility, which significantly influences the final conductivity of the obtained polymer electrolytes [25–28]. While UPy was widely exploited in polymers synthesized via RAFT polymerization [29–31], only a few [32] RAFT kinetics studies regarding an acrylate-based UPy monomer were reported, let alone studies involving its copolymerization with ionic monomers.

Motivated by these findings, we herein report the synthesis and characterization of pyrrolidinium-bistrifluoromethanesulfonyl-imide-based POILs (**POIL-x**, with x being the entry number as provided in Table 1) and also the copolymers (**CPILU-y**, with y being the entry number) with an acrylate-based UPy monomer via RAFT polymerization. Kinetic studies were carried out firstly via the RAFT homopolymerization of the ionic monomer **ILA** in DMF, and subsequently the copolymerization kinetics with the acrylate-based UPy monomer **UPyA**. Homopolymers and copolymers with various molecular weights were prepared, and their thermal, electrical, rheological, and self-healing properties were discussed. Thermogravimetric analysis (TGA) revealed an extraordinarily high thermal stability of the homopolymers **POIL-x** and the copolymers **CPILU-y**, while differential scanning calorimetry (DSC) was employed to study the thermal transition of the homo- and co-polymers. Together with conductivity obtained via broadband dielectric spectroscopy (BDS) and zero shear viscosity determined by rheology, the relationship between conductivity and viscosity was explored. By combination with DSC data, an insight into the decoupled conductivity properties of both **POIL-x** and **CPILU-y** was revealed. To elucidate the self-healing ability, two copolymers with different molecular weights but identical UPy content were subjected to tensile tests, allowing the future rational design of self-healing electrolytes via HBs and with low molecular weight.

**Table 1.** Data from RAFT polymerizations of **ILA** and the resulting homopolymer **POIL-x**.

Sample	Entry	M/CTA <sup>a</sup>	T/°C	t/h	conv. <sup>b</sup>	$M_{n, \text{th}}$ <sup>c</sup>	$M_{n, \text{NMR}}$	PDI <sup>d</sup>
<b>POIL-</b>	1	20:1	70	7	38%	3900	8000	1.26
	2	20:1	80	7	62%	6100	11,000	1.26
	3	100:1	80	7	67%	32,500	40,100	1.34
	4	200:1	80	7	79%	75,800	82,100	1.36

<sup>a</sup> Polymerization was carried out in DMF with AIBN as the initiator, and the ratio of [DBTTC]/[AIBN] was kept to 1:0.1 while the monomer concentration was kept at 1 mmol monomer in 1 mL DMF; <sup>b</sup> conversion was detected by <sup>1</sup>H NMR using trioxane as reference; <sup>c</sup> the number-average molecular weight calculated by the equation:  $M_{n, \text{th}} = \text{conv.} \times ([M_{\text{ILA}}]/[\text{DBTTC}]) \times m_{\text{ILA}} + m_{\text{DBTTC}}$ ; <sup>d</sup> PDI was determined by DMF + LiTFSI (0.1 M) GPC with a PS standard.

## 2. Materials and Methods

Acryloyl chloride 96%, 2-cyanobutanyl-2-yl 3,5-dimethyl-1H-pyrazole-1-carbodithioate, 95% (PCDT), and calcium hydride coarse powder 92% were purchased from ABCR (Karl-sruhe, Germany); 3-chloro-1-propanol 98%, 1-methyl-pyrrolidine 98%, benzyl chloride 99%, carbon disulfide 99.9%, and  $\alpha, \alpha'$ -azoisobutyronitrile (AIBN) were purchased from Sigma-Aldrich (Taufkirchen, Germany); triethylamine 99% and molecular sieve 3 Å 1–2 mm

bead were purchased from Alfa Aesar (Kandel, Germany); 2-isocyanatoethyl acrylate 98% and 2-amino-4-hydroxy-6-methylpyrimidine (6-methylisocytosine) 98% were purchased from TCI (Eschborn, Germany); lithium bis(trifluoromethanesulfonyl)imide 99% was purchased from IoLiTech (Heilbronn, Germany); and potassium carbonate was purchased from Bernd Kraft (Oberhausen, Germany). Molecular sieve 3 Å was activated in a vacuum oven at 200 °C for one week before use. 1-Methyl-pyrrolidine was refluxed and distilled with calcium hydride for 48 h to dry and stored with molecular sieve 3 Å in a glovebox filled with nitrogen ( $O_2$ : 0.1 ppm,  $H_2O$ : 0.1 ppm). All the other chemicals were used as received unless otherwise stated. All other chemicals which are not described here can be found in the Supplementary Material Section S1.1.

Thermogravimetric analysis (TGA) was performed using a Netzsch Tarsus TG 209 F3 (NETZSCH-Gerätebau GmbH, Selb, Germany). Approximately 10 mg of samples was placed in aluminum oxide crucibles and measured from room temperature to 600 °C at 10 K·min<sup>−1</sup> under nitrogen with a flow rate of 20 mL min<sup>−1</sup>. The data analysis was performed via the NETSCH Proteus-Thermal Analysis (Germany, version 5.2.1) software.

Differential scanning calorimetry (DSC) measurements were performed on a calibrated heat-flux DSC (Mettler-Toledo, Greifensee, Switzerland) equipped with a FRS5 sensor, connected to a TC100 Intracooler (Huber, Offenbach, Germany). 5–10 mg of samples were placed in aluminum sealed crucibles for measurements. The thermal history was cancelled by heating the samples from 25 °C to 120 °C at 10 K·min<sup>−1</sup>, followed by isothermal annealing for 20 min, re-cooling to −60 °C at 5 K·min<sup>−1</sup>, and thermostating at −60 °C for another 20 min. The final DSC curves were then recorded from −60 °C to 120 °C at 5 K·min<sup>−1</sup>.

Preparations of samples applied in this work with specific geometry (bar or disc) were obtained via hot-vacuum press by a VCM Essential molding machine (MeltPrep GmbH, Graz, Austria). First, the raw polymers were dried in an oven at 80 °C at 5 mbar for 24 h and then dried thoroughly by an ultrahigh vacuum pump at 80 °C for 24 h to eliminate water traces. Second, the polymers were hot-vacuum-pressed into a bar or disc at 70 °C and the so prepared specimens were kept in a desiccator with phosphorous oxide before the measurements started. For disc samples with specific geometries, a punching tool was used. For the self-healing samples, the pristine samples were cut vertically at the middle of the long edge and brought back tightly before being put in an oven pre-conditioned at the temperature of interest and annealed for a certain time. After self-healing, the samples were cooled to room temperature in a desiccator containing phosphorous oxide before measurements were conducted.

Broadband dielectric spectroscopy (BDS) was performed on an Alpha analyzer dielectric spectrometer (Novocontrol Technologies GmbH & Co. KG, Hundsangen, Germany). Two different sample cells were used depending on the sample texture. For the gel samples, a cell consisting of two brass electrodes with a sample size of 20 mm diameter and a thickness of 0.25 mm was used. Gel samples were carefully inserted into the hollow space between the electrodes inside the sample holder, with air bubble formation avoided. For self-standing samples, the samples were firstly hot-vacuum-pressed into a disc of 20 mm in diameter and 0.2–0.8 mm in thickness and subsequently sandwiched between two brass electrodes for the dielectric measurement. The measurements were performed inside a cryostat with a constant flow of dry nitrogen gas during the measurements to avoid moisture. Measurements were performed in a frequency range from 1 Hz to 10<sup>6</sup> Hz. Values of the DC conductivity were extracted from the DC plateau of the log  $\sigma$  vs. log frequency plots.

Rheology measurements were performed on an MCR 101 DSO rheometer (Anton Paar Germany GmbH, Ostfildern-Scharnhausen, Germany) using a parallel plate–plate geometry (plate diameter: 8 mm). All polymers were dried under high vacuum at 80 °C for 24 h before the rheology measurement. While the gel samples were directly smeared on the lower plate of the sample holder, the solid samples were hot-vacuum-pressed into films at 70 °C, cut into discs of 8 mm with a punching tool, and subject to the measurement. The sample temperature was regulated by thermoelectric cooling/heating in a Peltier chamber

under a dry nitrogen atmosphere. At each temperature the sample was equilibrated for 20 min before measurement was initiated. All measurements were performed in the dynamic mode and repeated twice to ensure precise viscosity values. Data analysis was performed via Rheo Compass<sup>TM</sup> (Austria, version V1.30.1064).

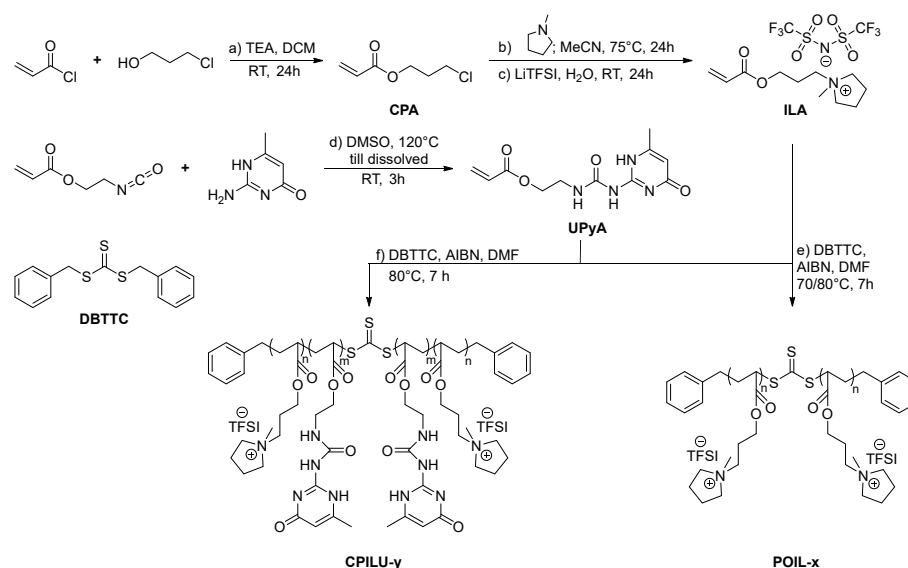
Tensile tests were performed on an INSTRON 5900 Series (INSTRON Deutschland GmbH, Darmstadt, Germany) tensile testing machine at room temperature at a strain rate of 20 mm·min<sup>−1</sup>. Data analysis was performed via Bluehill Universal (Germany, version 4.08).

All methods which are not mentioned here can be found in the Supplementary Material Section S1.1.

### 3. Results and Discussion

#### 3.1. Synthesis of Monomers and Polymers

To synthesize the ionic monomer **ILA**, firstly acryloyl chloride was reacted with chloropropanol in excess with triethylamine as the organic base in DCM to obtain chloropropyl acrylate (**CPA**) as a precursor. The precursor **CPA** was then used to quaternize 1-methyl pyrrolidine in MeCN to obtain pyrrolidinium-based acrylate with chloride as the counterion. Ion exchange was performed in water using an excessive amount of LiTFSI to afford the final ionic acrylate-base monomer **ILA**, with the pyrrolidinium-ion representing the cationic moiety and bistrifluoromethanesulfonyl imide (TFSI) constituting the anion (see Scheme 1). To link the UPy moiety to a polymerizable acrylate, 6-methylisocytosine was firstly dissolved in hot DMSO, whereafter an excessive amount of isocyanatoethyl acrylate was added, followed by immediate cooling in a water bath to prevent self-polymerization. After stirring for 3 h at room temperature and subsequent purification, the finely powdered UPy monomer **UPyA** was obtained (for synthetic details, see Supplementary Material Section S1.2).



**Scheme 1.** Synthetic route towards the **POIL-x** and **CPILU-y** (bearing the IL and the self-healing UPy moieties): (a) precursor **CPA**: acryloyl chloride with chloropropanol and triethylamine (TEA) at room temperature for 24 h; (b) ionic monomer **ILA**: **CPA** with 1-methyl pyrrolidine in MeCN at 75 °C for 24 h; (c) with LiTFSI in H<sub>2</sub>O at room temperature for 24 h; (d) HBs monomer **UPyA**: 6-methylisocytosine in DMSO at 120 °C, followed by isocyanatoethyl acrylate and stirring at room temperature for 3 h; (e) homopolymers **POIL-x**: DBTTC and AIBN in DMF at 70/80 °C for 7 h; (f) copolymers **CPILU-y**: DBTTC and AIBN in DMF at 80 °C.

In this work, S,S-dibenzyl trithiocarbonate (DBTTC) was used as a chain transfer agent (CTA) for the RAFT polymerization owing to its excellent control over acrylate monomers [33] and ionic monomers [34]. To make full use of the potential of DBTTC and



reach the maximum chain end fidelity, the ratio between DBTTC and AIBN was kept at 1:0.1 in all entries. Thanks to the nature of RAFT polymerization, by manipulation of the **ILA** to DBTTC ratio, the molecular weight of the final polymers can be adjusted, which enables precise studies on the influence of molecular weight on the final properties of the homopolymer **POIL-x** and the copolymers **CPILU-y**. RAFT polymerizations were carried out in DMF because it has been reported as an outstanding solvent for the polymerization of ionic liquids [35]. To obtain **POIL-x** with various molecular weights, the kinetics of RAFT homopolymerization of the **ILA** was investigated using DBTTC and AIBN as the initiator. The polymerization conditions, the monomer conversion into the final polymer, the calculated theoretical and practical number-averaged molecular weight via  $^1\text{H}$  NMR, as well as polydispersities determined by gel permeation chromatography (GPC) can be found in Table 1. As shown in Figure 1a), polymerization using  $[\text{ILA}]/[\text{DBTTC}] = 20:1$  at  $70^\circ\text{C}$  (red square) showed first-order kinetics within the investigated time (7 h), while increasing the reaction temperature to  $80^\circ\text{C}$  (blue circle) with the same monomer to CTA ratio drastically boosted the reaction rate, and the polymerization reached its maximum conversion within 3 h. As represented by the orange triangles in Figure 1a), when the  $[\text{ILA}]/[\text{DBTTC}]$  ratio was increased to 100:1, the polymerization at  $80^\circ\text{C}$  showed pseudo-first-order reaction kinetics, and after a 7-hour reaction, it reached a final conversion of 67%. As shown in Table 1, when the  $[\text{ILA}]/[\text{DBTTC}]$  ratio increased from 20: to 100:1, and subsequently to 200:1, the conversion also rose from 62% to 67%, and finally to 79%. Control over the molecular weight was also improved as the ratio increased, as evidenced by the decreasing deviation between the theoretical and experimental molecular weights calculated via  $^1\text{H}$  NMR (for calculation details and NMR spectra, see Supplementary Material Sections S1.2 and S4). In addition to the moderate control over molecular weight, the control over polydispersity decreased as the  $[\text{ILA}]/[\text{DBTTC}]$  ratio increased but still remained within the moderate range ( $\text{PDI} \leq 1.4$ ).

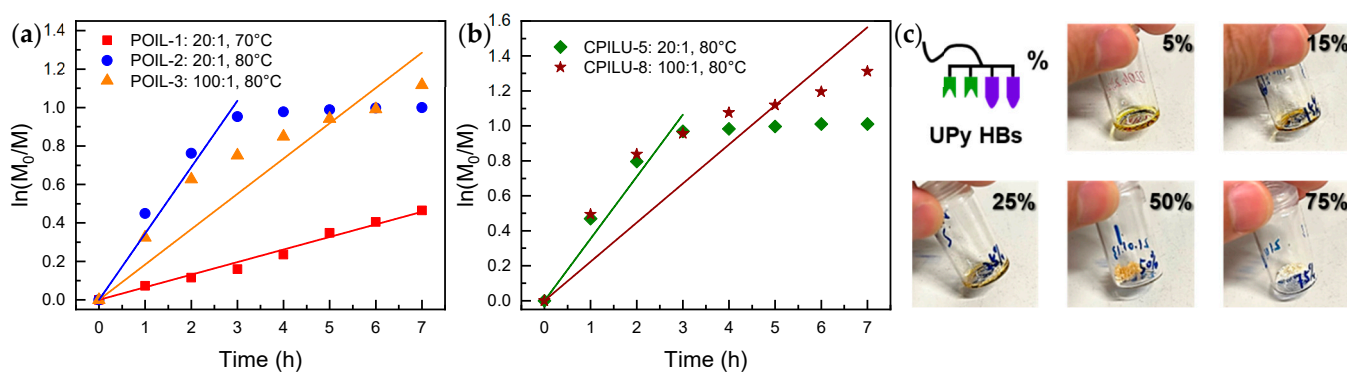


**Figure 1.** Kinetic plots of RAFT (a) homopolymerizations of **ILA** under the conditions:  $[\text{ILA}]/[\text{DBTTC}] = 20:1$  at  $70^\circ\text{C}$  (red square),  $[\text{ILA}]/[\text{DBTTC}] = 20:1$  at  $80^\circ\text{C}$  (blue circle), and  $[\text{ILA}]/[\text{DBTTC}] = 100:1$  at  $80^\circ\text{C}$  (orange triangle); (b) copolymerizations of **ILA** with **UPyA** under the conditions:  $[\text{ILA} + \text{UPyA}]/[\text{DBTTC}] = 20:1$  at  $80^\circ\text{C}$  (green rhombus) and  $[\text{ILA} + \text{UPyA}]/[\text{DBTTC}] = 100:1$  at  $80^\circ\text{C}$  (brown star); and (c) photos of the copolymers **CPILU-y** with various contents of UPy moieties.

Although GPC is a well-established method to characterize the molecular weight of many neutral polymers, the determination of the molecular weight of POILs via GPC remains challenging due to their unique hydrodynamic radius and interaction with the GPC column, as previously reported [36–38]. In 2013, He [38] reported a strategy to characterize the molecular weight of imidazolium-based POILs with various (counter)-anions by synthesizing a set of poly(4-vinylbenzyl chloride) with precise molecular weights via RAFT polymerization, followed by quaternization and ion exchange of the polymer precursors to obtain the final PS-based polybutylimidazolium with TFSI as the counterion. These polyimidazoliums were then used for calibration in a DMF GPC with LiTFSI as the additive

to reduce the interaction of POILs with the GPC column. The molecular weights detected by this GPC were compared with those obtained via  $^1\text{H}$  NMR, proving the preciseness of this strategy. Therefore we also prepared our acrylate-based polypyrrolidinium following this strategy (for synthesis details, see Supplementary Material Section S1.3). However, during the quaternization where 1-methylpyrrolidine was involved, side reactions took place, and the final POILs showed imperfect curves as detected by the GPC in DMF. This could be attributed to the hydrolysis of the ester moieties of the polymer [39,40] and the RAFT-active chain end [41] due to the presence of 1-methyl pyrrolidine (which is a base), which deteriorated the overall polydispersity and further impaired our GPC characterization with POIL calibration. Therefore, only the conventional PS standard calibration together with the 0.1 M LiTFSI as an additive was used in DMF GPC to establish the polydispersity (for GPC curves and data, see Supplementary Section S2).

To introduce the HB-moiety UPy into the POILs and also to study the RAFT copolymerization kinetics of the ionic monomer **ILA** with the quadrupolar hydrogen-bonded monomer **UPyA**, random copolymerizations of the two monomers were investigated. The copolymerization conditions, the monomer conversion into the final polymer, the initial molar fraction of **UPyA** in the monomer mixture and the final fraction on the polymer backbone, the degree of polymerization of both the **ILA** and the **UPyA**, the calculated theoretical and practical number-averaged molecular weight via  $^1\text{H}$  NMR, and the polydispersity determined by GPC are listed in Table 2.

**Table 2.** Data from RAFT copolymerizations of **ILA** with **UPyA** and the resulting copolymer **CPILU-y**.

Sample	Entry	M/CTA <sup>a</sup>	$f_{\text{UPy}}$ <sup>b</sup>	$T/^\circ\text{C}$	$t/\text{h}$	conv. <sup>c</sup>	$F_{\text{UPy, NMR}}$ <sup>d</sup>	$\text{DP}_{\text{IL}}$ <sup>e</sup>	$\text{DP}_{\text{UPy}}$ <sup>f</sup>	$M_{n, \text{th}}$ <sup>g</sup>	$M_{n, \text{NMR}}$	PDI <sup>h</sup>
CPILU-	5	20:1	5%	80	7	55%	4%	22.5	0.9	5400	11,800	1.35
	6	20:1	15%	80	7	77%	14%	18.6	2.6	7200	10,700	1.32
	7	20:1	25%	80	7	84%	24%	18.7	4.5	7400	10,500	1.25
	8	100:1	5%	80	7	65%	4%	90.1	3.6	30,700	44,400	1.36

<sup>a</sup> Polymerization was carried out in DMF with AIBN as the initiator, and the ratio of [DBTTC]/[AIBN] was kept to 1:0.1, while the monomer concentration was kept at 1 mmol monomer in 1 mL DMF; <sup>b</sup>  $f_{\text{UPy}}$  was the initial molar fraction of **UPyA** in the monomer mixture; <sup>c</sup> conversion was detected by  $^1\text{H}$  NMR using trioxane as reference; <sup>d</sup>  $F_{\text{UPy}}$  was the final molar fraction of **UPyA** on the polymer backbone, calculated from  $^1\text{H}$  NMR; <sup>e, f</sup> calculated from relative integral of protons from  $^1\text{H}$  NMR (for details see Supplementary Material Section S1.2); <sup>g</sup> the number-average molecular weight calculated by the equation:  $M_{n, \text{th}} = \text{conv.} \times [(M_{\text{ILA}})/(\text{DBTTC})] \times m_{\text{ILA}} + [(M_{\text{UPyA}})/(\text{DBTTC})] \times m_{\text{UPyA}} + m_{\text{DBTTC}}$ ; <sup>h</sup> PDI was determined by DMF + LiTFSI (0.1 M) GPC with PS standard.

As shown in Figure 1b, the copolymerization of **ILA** with a 5% feeding molar ratio of **UPyA** at 80 °C with  $[\text{ILA} + \text{UPyA}]/[\text{DBTTC}] = 20:1$  (green rhombus) showed similar kinetics as the homopolymerization entry 2 (blue circle in Figure 1a), and in 3 h the copolymerization reached its full conversion of 55%. Entry 8 with  $[\text{ILA} + \text{UPyA}]/[\text{DBTTC}] = 100:1$  also showed comparable kinetics (brown star in Figure 1b) as compared to the homopolymerization (entry 3) under the same conditions (orange triangle in Figure 1a)). As shown in Table 2, when the initial fraction of **UPyA** increased from 5% to 15% and to 25% the overall conversion of the two monomers also increased from 55% to 77% and to 84% respectively (see entry 5–7), this indicated a higher reactivity catalyzed by the HBs in monomer **UPyA**, presumably due to the attractive association of **UPyA** in compared to the repulsive ionic nature of **ILA**. Despite the difficulties of copolymerizing non-ionic and ionic monomers, the control over molecular weight by DBTTC remained moderate in all cases, while control over polydispersity was less pronounced compared to the homopolymerizations, which again was anticipated again due to the strong association among UPy moieties and ionic clusters of pyrrolidinium and TFSI ions.

In order to find the proper fraction of UPy on the polymer chain for application as self-healing electrolytes, **CPILU-y** with different UPy contents were prepared. As shown in Figure 1c, as the content of the strong dimerization of UPy moieties increased, the **CPILU-y** altered from a gel (5%) to a glassy solid (25%) and finally to a powdery material (>25%), indicating increased interchain forces due to the quadrupolar HBs of UPy moieties.

### 3.2. Thermal Characterization via Thermogravimetric Analysis (TGA) and Differential Scanning Calorimetry (DSC)

To understand the thermal stability of the POILs thermogravimetric analysis (TGA) was employed. The 5%-weight-loss temperature and the degradation onset temperature are listed in Table 3. The ionic monomer **ILA** demonstrated excellent thermal stability up to 348 °C as shown in the Figure 2a, while the non-ionic monomer **UPyA** showed lower stability until 198 °C. For the homopolymers **POIL-2** and **POIL-3** the thermal stabilities were slightly higher than that of the monomer, manifesting a minor influence by molecular weight on the thermal stability. The thermal stabilities of the **POIL-x** are comparable with those of similar polypyrrolidinium-polymers as previously reported [42]. However, when **UPyA** was incorporated into the polymer backbone the thermal stability showed a decreasing trend as the **UPyA** fraction increased. The degradation of the copolymer **CPILU-y** was found to be a two-step process, where the UPy moieties were decomposed first at around 200 °C, followed by the ionic moieties decomposing at around 360 °C (see Table 3, column **Onset  $T$ /°C**), indicating a reasonable thermal stability compared to the homopolymers.

**Table 3.** Thermal characterization data of **ILA**, **UPyA**, **POIL-x**, and **CPILU-y** via thermogravimetric analysis and differential scanning calorimetry.

Sample	Entry	Sample Info.	5 wt%-loss $T$ /°C	Onset $T$ /°C	$T_{g, DSC}$ /°C <sup>a</sup>
<b>ILA</b>	-	monomer	348	348	-
<b>UPyA</b>	-	monomer	201	198	-
<b>POIL-</b>	2	11 k	348	353	−13
	3	40 k	360	357	7
<b>CPILU-</b>	5	4%, 12 k	338	198, 360	9
	6	14%, 11 k	297	212, 365	13
	7	24%, 10 k	263	215, 363	30

<sup>a</sup> Glass transition temperature via DSC.

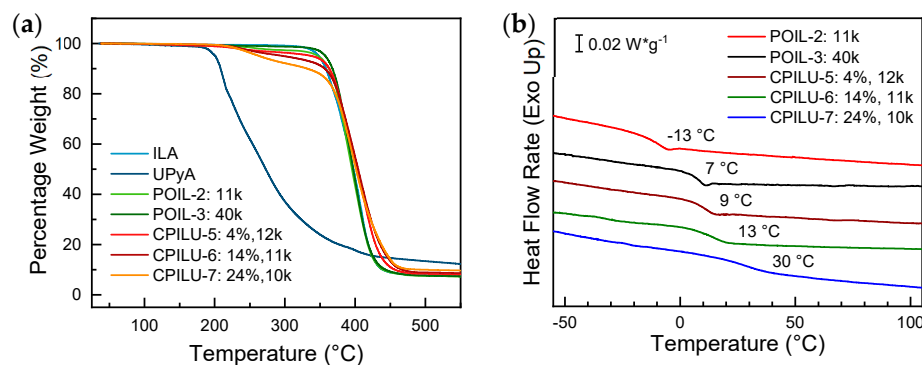


**Figure 2.** Thermal characterization of ionic monomer **ILA**, HBs monomer **UPyA**, homopolymers **POIL-x**, and copolymers **CPILU-y** via (a) thermogravimetric analysis measured at a heating rate of 10 K·min<sup>−1</sup> under N<sub>2</sub> atmosphere; and (b) differential scanning calorimetry measured at a heating rate of 5 K·min<sup>−1</sup> with the thermal history cancelled by a preheating/cooling circle (the baseline of **POIL-3** was corrected manually).

For the electrolytes used in batteries, it is often observed that the batteries can provide different local temperatures which could introduce a temperature-controlled structural transition of the electrolytes, causing changes in the physical and chemical properties of the electrolytes and further affecting the performance of the batteries, but also reaching temperatures sufficient to activate dynamic self-healing processes. Therefore, the thermal behavior of the polymers in this work was studied by differential scanning calorimetry (DSC). As shown in Figure 2b, the crystallization and melting peaks of the pyrrolidinium moieties [43] were not found in the DSC curves of all POILs, but only glass transitions were

observed. This could be advantageous for polymers applied as electrolytes, as a better conductivity value can be achieved both above and below the glass transition temperature in amorphous regions (analogous to higher conductivities achieved in amorphous region in PEO [44]). All  $T_g$ s are listed in Table 3 and are also shown in the plot. We found that the molecular weight of the **POIL-x** and the UPy content of the **CPILU-y** indeed influenced the glass transition temperature. When the molecular weight increased from 11 kDa to 40 kDa,  $T_g$  also increased from  $-13^\circ\text{C}$  (**POIL-2**) to  $7^\circ\text{C}$  (**POIL-3**), which is potentially indicative of more restricted chain motions. When only 4% of the UPy moieties were introduced into the polymers,  $T_g$  drastically increased from  $-13^\circ\text{C}$  to  $9^\circ\text{C}$ , revealing that the dimerizable UPy moieties act as a strong “chain-hardener” in comparison to the increase of molecular weight. If the UPy content increased from 4% to 14% and then to 24%,  $T_g$  increased further from  $9^\circ\text{C}$  to  $13^\circ\text{C}$  and to  $30^\circ\text{C}$ , respectively, this evidenced stiffer chain segments in **CPILU-6** and **CPILU-7** as a result of a denser UPy dimerization.

### 3.3. Conductivity via Broadband Dielectric Spectroscopy (BDS) and Zero Shear Viscosity via Rheology

To elucidate the potential of the polymers to be applied as electrolytes the DC conductivity was investigated by broadband dielectric spectroscopy (BDS). As shown in Figure 3a the low-molecular-weight **POIL-2** showed a higher conductivity compared to the high-molecular-weight **POIL-3**, matching the conclusions that—in line with expectations—low-molecular-weight POILs generally offer higher conductivity [25–28]. When 4% UPy moieties were introduced into the polymer backbone (**CPILU-5**), the conductivity was barely influenced by the non-conductive UPy moieties as compared to the homopolymer **POIL-2** (see red squares for **POIL-2** and blue triangles for **CPILU-5** in Figure 3a). However, when the UPy content continued increasing, a generally lower conductivity could be observed within the whole temperature range, as represented by **CPILU-6** and **CPILU-7**. It is often reported [45–47] that the conductivity of low-molecular-weight ionic liquids is affected by the viscosity of the conductive system, wherefore the zero shear viscosity  $\eta_0$  was determined to assist the interpretation of the conductivity behavior of the POILs. As shown in Figure 3b, an inverse relation was observed for the viscosity for those POILs, which can be explained by the higher molecular weight polymers also showing higher viscosity that further hinders ion transport.

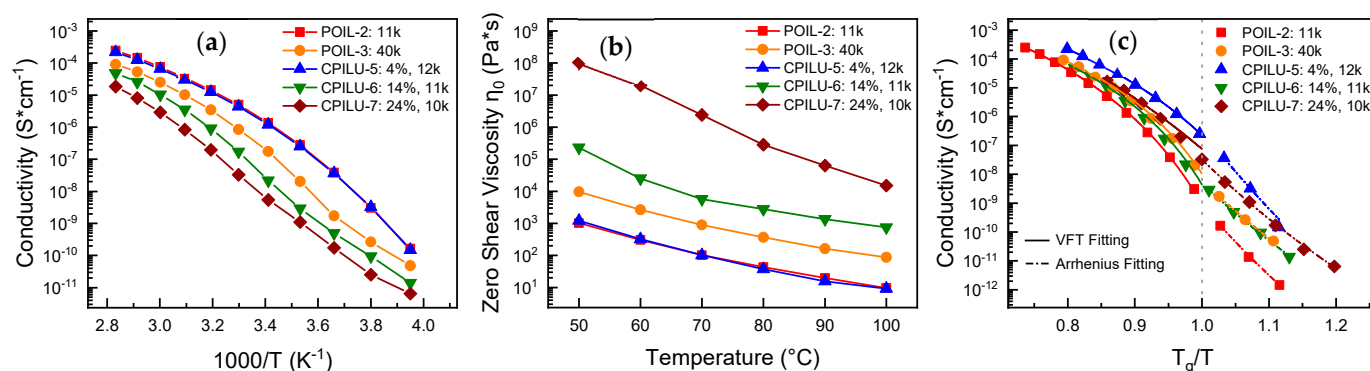


**Figure 3.** Conductivity  $\sigma$  of homo-/copolymer **POIL-x** and **CPILU-y** (a) as a function of inverse temperature  $1000/T$ ; (c) glass transition temperature divided by measurement temperature  $T_g/T$ ; and (b) zero shear viscosity  $\eta_0$  of homo-/copolymer **POIL-x** and **CPILU-y** versus temperature  $T$ .

In addition to the notable influence of the viscosity, the conductivity of polymer electrolytes before and after the thermal transition is significantly altered. Thus the conductivity of the polymers was plotted versus their glass transition temperature divided by the measurement temperature ( $T_g/T$ ), as shown in Figure 3c. The variation in conductivity of the polymers by temperature showed two distinct regions in the plot. When the temperature was higher than the polymers'  $T_g$ , segmental motion was enabled, and the conductivity was coupled with the segmental motion, thus following the Vogel–Fulcher–Tammann

(VFT) equation. At temperatures below  $T_g$ , segments were frozen, and the conductivity plot displayed Arrhenius behavior, which is comparable to the conductive behavior of inorganic glasses [48]. As previously reported [49,50], if the conductivity at  $T_g$  is roughly equal to  $10^{-15} \text{ S}\cdot\text{cm}^{-1}$  in an ionic system, the charge transport is then fully governed by the structural relaxation of the system, which is segmental motion in case of polymer electrolytes. For our polymers, the conductivities at  $T_g$ , as listed in Table 4, are all higher than the reported threshold value ( $10^{-15} \text{ S}\cdot\text{cm}^{-1}$ ) for the fully relaxation-coupled systems. As a consequence, the polymers in this work exhibited a certain degree of decoupled ion transport from the segmental dynamics. To clearly visualize this behavior, the decoupling index defined as  $R_{\sigma, T_g} = 15 + \log \sigma_{T_g}$  [51,52] was applied. Among our copolymers, those polymer with the strongest decoupling, ie those where the charge transport is least linked to the segmental relaxation, is the copolymer **CPILU-5** with 4% UPy moieties, with a decoupling index of 8.4. The least-decoupled homopolymer can be observed in the case of the homopolymer **POIL-2** (for  $R_{\sigma, T_g}$  of other polymers, see Table 4). Because the copolymers show a higher decoupling index, they could provide better conductivity and mechanical strength simultaneously. Therefore, a tensile test was employed to explore their mechanical strength and their self-healing ability, which is discussed in next chapter.

**Table 4.** Glass transition temperature and conductivity at glass transition temperature, and zero shear viscosity and conductivity at 80 °C of **POIL-x** and **CPILU-y**.

Sample	Entry	Sample Info.	$T_g, \text{DSC}/^\circ\text{C}^a$	$\sigma_{T_g}/\text{S}\cdot\text{cm}^{-1}^b$	$R_{\sigma, T_g}^c$	$\eta_{0, 80^\circ\text{C}} \text{ Pa}\cdot\text{s}^d$	$\sigma_{80^\circ\text{C}}/\text{S}\cdot\text{cm}^{-1}^e$
<b>POIL-</b>	2	11 k	−13	$3.07 \times 10^{-9}$ (−10 °C)	6.5	43	$2.46 \times 10^{-4}$
	3	40 k	7	$2.04 \times 10^{-8}$ (10 °C)	7.3	368	$9.09 \times 10^{-5}$
<b>CPILU-</b>	5	4%, 12 k	9	$2.55 \times 10^{-7}$ (10 °C)	8.4	37	$2.19 \times 10^{-4}$
	6	14%, 11 k	13	$2.19 \times 10^{-8}$ (20 °C)	7.3	$2.76 \times 10^3$	$4.85 \times 10^{-5}$
	7	24%, 10 k	30	$3.27 \times 10^{-8}$ (30 °C)	7.5	$2.84 \times 10^5$	$1.84 \times 10^{-5}$

<sup>a</sup> Glass transition temperature via DSC; <sup>b</sup> conductivity at glass transition temperature; <sup>c</sup> decoupling index calculated with  $R_{\sigma, T_g} = 15 + \log \sigma_{T_g}$ ; <sup>d</sup> zero shear viscosity at 80 °C; <sup>e</sup> and conductivity at 80 °C.

### 3.4. Mechanical and Self-Healing Characterization via Tensile Test

To evaluate the mechanical strength and the prominent self-healing ability, two copolymers, both with 7% UPy content but with different molecular weights, were synthesized, which are designated as **CPILU-9** (7% UPy, 10 kDa) and **CPILU-10** (7% UPy, 67 kDa) (for synthesis details, see Supplementary Material Section S1.2). The copolymers were hot-vacuum-pressed into bars or disc specimens, and self-healing ability tests were firstly performed with **CPILU-9**, as visualized in Figure 4a. A specimen was cut vertically at the long edge into two pieces and brought back with the freshly generated surface tightly and accurately matched. Owing to the quadrupolar HBs of the UPy moieties associating at the edge of the wound, self-healing was observed within 1 h at 40 °C or 24 h at room temperature. To quantify the mechanical strength and the self-healing ability, tensile tests of both pristine and self-healed bar specimens of **CPILU-9** and **CPILU-10** were performed at a strain rate of  $20 \text{ mm}\cdot\text{min}^{-1}$  at room temperature, as shown in Figure 4b.



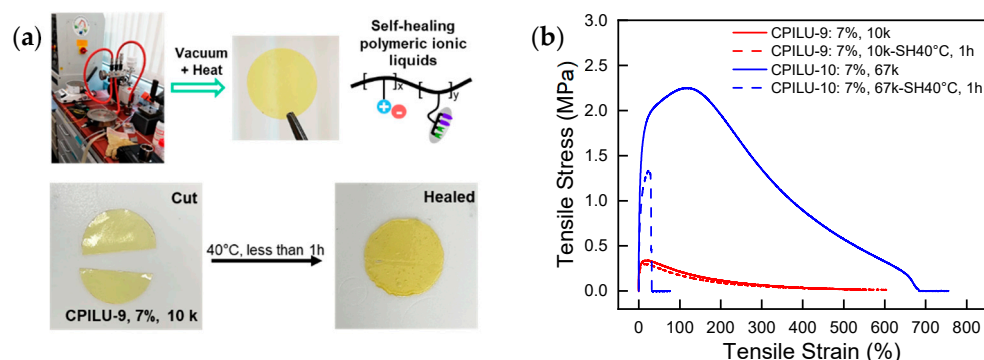


**Figure 4.** (a) Visualized self-healing of **CPILU-9**; and (b) stress–strain curves of pristine (solid line) and self-healed (at 40 °C for 1 h, dash line) **CPILU-9** and **CPILU-10** at a strain rate of 20 mm·min<sup>−1</sup> at room temperature.

For the pristine specimen, increasing the molecular weight from 10 kDa to 67 kDa indeed drastically enhanced the mechanical strength from 0.34 MPa (**CPILU-9**, red solid line in Figure 4b) to 2.25 MPa (**CPILU-10**, blue solid line in Figure 4b) in terms of ultimate stress. Both specimen showed good ductility, with roughly 550% and 650% in relation to the tensile strain for **CPILU-9** and **CPILU-10**, respectively. Regarding self-healing ability, the self-healed specimen of **CPILU-9** showed an almost identical tensile behavior (red dash line in Figure 4b) in comparison to the pristine specimen, with a slightly reduced ultimate stress (0.30 MPa) and a similar ductility. These results indicated efficient self-healing (88% in terms of ultimate stress compared to the pristine specimen) at 40 °C for 1 h which is the consequence of the flexible segments and the strong quadrupolar HBs of UPy moieties in **CPILU-9**. As for **CPILU-10**, with a molecular weight of 67 kDa, the self-healed specimen generated an ultimate stress of 1.33 MPa (59% in terms of ultimate stress compared to the pristine specimen) and a poor ductility at 32% tensile strain. This could be attributed to the more entangled segments in the high-molecular-weight **CPILU-10** which hindered self-healing by UPy dimerization.

#### 4. Conclusions

Novel polymeric ionic liquids **POIL-x** and copolymers **CPILU-y** bearing quadrupolar hydrogen bonds were synthesized via RAFT polymerization using DBTTC as chain transfer agent. Kinetic studies revealed that the HBs monomer **UPyA** showed preferable incorporation in a copolymerization of **ILA**, anticipated as the attractive association of **UPyA**. While the synthesized homopolymers were thermally stable up to 360 °C, the introduction of UPy moieties into the polymer chains decreased the thermal stability and altered the decomposition into a two-step process. Examining a combination of data from DSC, BDS, and rheology, a decoupling of conductivity from the glass transition was observed in all polymers, while the trend of the zero shear viscosity values of all the polymers matched that of their conductivity values. A copolymer with 4% UPy content displayed the highest decoupling index of 8.4, proving that both, self-healing and excellent conductivities can be embedded into the same type of a POIL using complex hydrogen-bonding. While copolymers with low molecular weights demonstrated both better conductivity and self-healing efficiency, the high-molecular-weight samples showed higher ultimate strength but lower healing efficiency and conductivity. This work proves that HBs are a useful tool for designing electrolytes with unique properties like decoupled conductivity and self-healing ability, which can contribute to battery science and electronic devices such as supercapacitors in the future.

**Supplementary Materials:** The following supporting information can be downloaded at: <https://www.mdpi.com/article/10.3390/polym14194090/s1>, Scheme S1: Synthesis route of monomers, RAFT chain transfer agent, and polymers; Scheme S2: Synthesis route of POILC-z for GPC calibration; Figure S1–S4: GPC curves of all the polymers; Figure S5–S12 NMR spectra of all the compounds and polymers; Table S1: Synthesis data of the copolymers CPILU-9 and CPILU-10 for tensile test; Table S2: GPC data of precursor polymers pCPA and final POILC-z, planned for calibration; Table S3: Conductivity of POIL-x and CPILU-y from  $-20\text{ }^{\circ}\text{C}$  to  $80\text{ }^{\circ}\text{C}$ , measured by BDS; Table S4: Zero shear viscosity of POIL-x and CPILU-y from  $50\text{ }^{\circ}\text{C}$  to  $100\text{ }^{\circ}\text{C}$ .

**Author Contributions:** Conceptualization, W.H.B., A.M. and C.L.; methodology, C.L., R.B., D.I. and M.D.; writing—original draft preparation, C.L.; writing—review and editing, W.H.B., A.M. and R.A.; supervision, project administration, and funding acquisition, W.H.B. and A.M. All authors have read and agreed to the published version of the manuscript.

**Funding:** This research was developed under the framework of the BAT4EVER project. This project has received funding from the European Union’s Horizon 2020 research and innovation program under grant agreement No. 957225.

**Data Availability Statement:** Not applicable.

**Acknowledgments:** The authors are grateful to Dieter Ströhl and his team for NMR measurements, Mario Beiner and his team for BDS measurement, Thomas Thurn-Albrecht for the molding machine, and all the members of AG Binder for their physical and mental support.

**Conflicts of Interest:** The authors declare no conflict of interest.

## References

1. Placke, T.; Kloepsch, R.; Dühnen, S.; Winter, M. Lithium ion, lithium metal, and alternative rechargeable battery technologies: The odyssey for high energy density. *J. Solid State Electrochem.* **2017**, *21*, 1939–1964. [\[CrossRef\]](#)
2. Lu, D.; Shao, Y.; Lozano, T.; Bennett, W.D.; Graff, G.L.; Polzin, B.; Zhang, J.; Engelhard, M.H.; Saenz, N.T.; Henderson, W.A.; et al. Failure Mechanism for Fast-Charged Lithium Metal Batteries with Liquid Electrolytes. *Adv. Energy Mater.* **2015**, *5*, 1400993. [\[CrossRef\]](#)
3. Li, Y.; Li, Y.; Pei, A.; Yan, K.; Sun, Y.; Wu, C.-L.; Joubert, L.-M.; Chin, R.; Koh, A.L.; Yu, Y.; et al. Atomic structure of sensitive battery materials and interfaces revealed by cryo-electron microscopy. *Science* **2017**, *358*, 506–510. [\[CrossRef\]](#)
4. Wang, Q.; Jiang, L.; Yu, Y.; Sun, J. Progress of enhancing the safety of lithium ion battery from the electrolyte aspect. *Nano Energy* **2019**, *55*, 93–114. [\[CrossRef\]](#)
5. Zhang, D.-Z.; Ren, Y.-Y.; Hu, Y.; Li, L.; Yan, F. Ionic Liquid/Poly (ionic liquid)-based Semi-solid State Electrolytes for Lithium-ion Batteries. *Chin. J. Polym. Sci.* **2020**, *38*, 506–513. [\[CrossRef\]](#)
6. Li, H.; Xu, Z.; Yang, J.; Wang, J.; Hirano, S.-I. Polymer electrolytes for rechargeable lithium metal batteries. *Sustain. Energy Fuels* **2020**, *4*, 5469–5487. [\[CrossRef\]](#)
7. Wang, J.; Li, S.; Zhao, Q.; Song, C.; Xue, Z. Structure Code for Advanced Polymer Electrolyte in Lithium-Ion Batteries. *Adv. Funct. Mater.* **2021**, *31*, 2008208. [\[CrossRef\]](#)
8. Meng, N.; Lian, F.; Cui, G. Macromolecular Design of Lithium Conductive Polymer as Electrolyte for Solid-State Lithium Batteries. *Small* **2021**, *17*, e2005762. [\[CrossRef\]](#)
9. Huang, X.; Nakagawa, S.; Houjou, H.; Yoshie, N. Insights into the Role of Hydrogen Bonds on the Mechanical Properties of Polymer Networks. *Macromolecules* **2021**, *54*, 4070–4080. [\[CrossRef\]](#)
10. Song, K.; Zhu, W.; Li, X.; Yu, Z. A novel mechanical robust, self-healing and shape memory hydrogel based on PVA reinforced by cellulose nanocrystal. *Mater. Lett.* **2020**, *260*, 126884. [\[CrossRef\]](#)
11. Lügger, S.J.D.; Houben, S.J.A.; Foelen, Y.; Debije, M.G.; Schenning, A.P.H.J.; Mulder, D.J. Hydrogen-Bonded Supramolecular Liquid Crystal Polymers: Smart Materials with Stimuli-Responsive, Self-Healing, and Recyclable Properties. *Chem. Rev.* **2022**, *122*, 4946–4975. [\[CrossRef\]](#)
12. Chen, S.; Mahmood, N.; Beiner, M.; Binder, W.H. Self-Healing Materials from V- and H-Shaped Supramolecular Architectures. *Angew. Chem. Int. Ed.* **2015**, *54*, 10188–10192. [\[CrossRef\]](#)
13. Herbst, F.; Seiffert, S.; Binder, W.H. Dynamic supramolecular poly(isobutylene)s for self-healing materials. *Polym. Chem.* **2012**, *3*, 3084–3092. [\[CrossRef\]](#)
14. Long, T.; Li, Y.; Fang, X.; Sun, J. Salt-Mediated Polyampholyte Hydrogels with High Mechanical Strength, Excellent Self-Healing Property, and Satisfactory Electrical Conductivity. *Adv. Funct. Mater.* **2018**, *28*, 1804416. [\[CrossRef\]](#)
15. Chen, J.; Peng, Q.; Thundat, T.; Zeng, H. Stretchable, Injectable, and Self-Healing Conductive Hydrogel Enabled by Multiple Hydrogen Bonding toward Wearable Electronics. *Chem. Mater.* **2019**, *31*, 4553–4563. [\[CrossRef\]](#)
16. Ligthart, G.B.W.L.; Ohkawa, H.; Sijbesma, A.R.P.; Meijer, E.W. Complementary Quadruple Hydrogen Bonding in Supramolecular Copolymers. *J. Am. Chem. Soc.* **2005**, *127*, 810–811. [\[CrossRef\]](#) [\[PubMed\]](#)

17. Guo, P.; Su, A.; Wei, Y.; Liu, X.; Li, Y.; Guo, F.; Li, J.; Hu, Z.; Sun, J. Healable, Highly Conductive, Flexible, and Nonflammable Supramolecular Ionogel Electrolytes for Lithium-Ion Batteries. *ACS Appl. Mater. Interfaces* **2019**, *11*, 19413–19420. [\[CrossRef\]](#)
18. Lin, Y.; Hu, H.; Yi, P.; Sun, S.; Li, Y.; Liu, X.; Li, G. Zwitterionic hydrogels formed via quadruple hydrogen-bonds with ultra-fast room-temperature self-healing ability. *Mater. Lett.* **2020**, *269*, 127665. [\[CrossRef\]](#)
19. Gan, H.; Zhang, Y.; Li, S.; Yu, L.; Wang, J.; Xue, Z. Self-Healing Single-Ion Conducting Polymer Electrolyte Formed via Supramolecular Networks for Lithium Metal Batteries. *ACS Appl. Energy Mater.* **2021**, *4*, 482–491. [\[CrossRef\]](#)
20. Beijer, F.H.; Sijbesma, R.P.; Kooijman, H.; Spek, A.L.; Meijer, E.W. Strong Dimerization of Ureidopyrimidones via Quadruple Hydrogen Bonding. *J. Am. Chem. Soc.* **1998**, *120*, 6761–6769. [\[CrossRef\]](#)
21. Guo, P.; Zhang, H.; Liu, X.; Sun, J. Counteranion-Mediated Intrinsic Healing of Poly (ionic liquid) Copolymers. *ACS Appl. Mater. Interfaces* **2018**, *10*, 2105–2113. [\[CrossRef\]](#)
22. D'Angelo, A.J.; Panzer, M.J. Design of Stretchable and Self-Healing Gel Electrolytes via Fully Zwitterionic Polymer Networks in Solvate Ionic Liquids for Li-Based Batteries. *Chem. Mater.* **2019**, *31*, 2913–2922. [\[CrossRef\]](#)
23. Sun, Y.; Ren, Y.-Y.; Li, Q.; Shi, R.-W.; Hu, Y.; Guo, J.-N.; Sun, Z.; Yan, F. Conductive, Stretchable, and Self-healing Ionic Gel Based on Dynamic Covalent Bonds and Electrostatic Interaction. *Chin. J. Polym. Sci.* **2019**, *37*, 1053–1059. [\[CrossRef\]](#)
24. McGrath, L.M.; Rohan, J.F. Pyrrolidinium Containing Ionic Liquid Electrolytes for Li-Based Batteries. *Molecules* **2020**, *25*, 6002. [\[CrossRef\]](#) [\[PubMed\]](#)
25. Keith, J.R.; Mogurampelly, S.; Aldukhi, F.; Wheatle, B.K.; Ganesan, V. Influence of molecular weight on ion-transport properties of polymeric ionic liquids. *Phys. Chem. Chem. Phys.* **2017**, *19*, 29134–29145. [\[CrossRef\]](#)
26. Zhao, Q.; Evans, C.M. Effect of Molecular Weight on Viscosity Scaling and Ion Transport in Linear Polymerized Ionic Liquids. *Macromolecules* **2021**, *54*, 3395–3404. [\[CrossRef\]](#)
27. Fan, F.; Wang, W.; Holt, A.P.; Feng, H.; Uhrig, D.; Lu, X.; Hong, T.; Wang, Y.; Kang, N.-G.; Mays, J.; et al. Effect of Molecular Weight on the Ion Transport Mechanism in Polymerized Ionic Liquids. *Macromolecules* **2016**, *49*, 4557–4570. [\[CrossRef\]](#)
28. Xu, H.; Mahanthappa, M.K. Ionic Conductivities of Broad Dispersity Lithium Salt-Doped Polystyrene/Poly (ethylene oxide) Triblock Polymers. *Macromolecules* **2021**, *54*, 8798–8809. [\[CrossRef\]](#)
29. Zhou, B.; He, D.; Hu, J.; Ye, Y.; Peng, H.; Zhou, X.; Xie, X.; Xue, Z. A flexible, self-healing and highly stretchable polymer electrolyte via quadruple hydrogen bonding for lithium-ion batteries. *J. Mater. Chem. A* **2018**, *6*, 11725–11733. [\[CrossRef\]](#)
30. Chen, X.; Yi, L.; Zou, C.; Liu, J.; Yu, J.; Zang, Z.; Tao, X.; Luo, Z.; Guo, X.; Chen, G.; et al. High-Performance Gel Polymer Electrolyte with Self-Healing Capability for Lithium-Ion Batteries. *ACS Appl. Energy Mater.* **2022**, *5*, 5267–5276. [\[CrossRef\]](#)
31. Cheng, Q.; Ding, S.; Zheng, Y.; Wu, M.; Peng, Y.-Y.; Diaz-Dussan, D.; Shi, Z.; Liu, Y.; Zeng, H.; Cui, Z.; et al. Dual Cross-Linked Hydrogels with Injectable, Self-Healing, and Antibacterial Properties Based on the Chemical and Physical Cross-Linking. *Biomacromolecules* **2021**, *22*, 1685–1694. [\[CrossRef\]](#) [\[PubMed\]](#)
32. Lewis, C.L.; Anthamatten, M. Synthesis, swelling behavior, and viscoelastic properties of functional poly(hydroxyethyl methacrylate) with ureidopyrimidinone side-groups. *Soft Matter* **2013**, *9*, 4058–4066. [\[CrossRef\]](#)
33. Chen, S.; Binder, W.H. Controlled copolymerization of n-butyl acrylate with semifluorinated acrylates by RAFT polymerization. *Polym. Chem.* **2015**, *6*, 448–458. [\[CrossRef\]](#)
34. Chen, S.; Funtan, A.; Gao, F.; Cui, B.; Meister, A.; Parkin, S.S.P.; Binder, W.H. Synthesis and Morphology of Semifluorinated Polymeric Ionic Liquids. *Macromolecules* **2018**, *51*, 8620–8628. [\[CrossRef\]](#)
35. Chen, M.; Dugger, J.; Li, X.; Wang, Y.; Kumar, R.; Meek, K.M.; Uhrig, D.W.; Browning, J.F.; Madsen, L.A.; Long, T.E.; et al. Polymerized ionic liquids: Effects of counter-anions on ion conduction and polymerization kinetics. *J. Polym. Sci. Part A Polym. Chem.* **2018**, *56*, 1346–1357. [\[CrossRef\]](#)
36. Rulkens, R.; Schulze, M.; Wegner, G. Rigid-rod polyelectrolytes: Synthesis of sulfonated poly(p-phenylene)s. *Macromol. Rapid Commun.* **1994**, *15*, 669–676. [\[CrossRef\]](#)
37. Huang, F.; Hou, L.; Wu, H.; Wang, X.; Shen, H.; Cao, W.; Yang, A.W.; Cao, Y. High-Efficiency, Environment-Friendly Electroluminescent Polymers with Stable High Work Function Metal as a Cathode: Green- and Yellow-Emitting Conjugated Polyfluorene Polyelectrolytes and Their Neutral Precursors. *J. Am. Chem. Soc.* **2004**, *126*, 9845–9853. [\[CrossRef\]](#)
38. He, H.; Zhong, M.; Adzima, B.; Luebke, D.; Nulwala, H.; Matyjaszewski, K. A Simple and Universal Gel Permeation Chromatography Technique for Precise Molecular Weight Characterization of Well-Defined Poly(ionic liquid)s. *J. Am. Chem. Soc.* **2013**, *135*, 4227–4230. [\[CrossRef\]](#)
39. Mori, H.; Müller, A.H. New polymeric architectures with (meth) acrylic acid segments. *Prog. Polym. Sci.* **2003**, *28*, 1403–1439. [\[CrossRef\]](#)
40. Zhu, L.; Tong, X.; Li, M.; Wang, E. Synthesis and solution properties of anionic linear-dendritic block amphiphiles. *J. Polym. Sci. Part A Polym. Chem.* **2000**, *38*, 4282–4288. [\[CrossRef\]](#)
41. Moad, G.; Chong, Y.; Postma, A.; Rizzardo, E.; Thang, S. Advances in RAFT polymerization: The synthesis of polymers with defined end-groups. *Polymer* **2005**, *46*, 8458–8468. [\[CrossRef\]](#)
42. Ogihara, W.; Washiro, S.; Nakajima, H.; Ohno, H. Effect of cation structure on the electrochemical and thermal properties of ion conductive polymers obtained from polymerizable ionic liquids. *Electrochimica Acta* **2006**, *51*, 2614–2619. [\[CrossRef\]](#)
43. A Henderson, W.; Young, V.G.; Pearson, W.; Passerini, S.; De Long, H.C.; Trulove, P.C. Thermal phase behaviour of N-alkyl-N-methylpyrrolidinium and piperidinium bis(trifluoromethanesulfonyl)imide salts. *J. Physics Condens. Matter* **2006**, *18*, 10377–10390. [\[CrossRef\]](#)



44. Berthier, C.; Gorecki, W.; Minier, M.; Armand, M.; Chabagno, J.; Rigaud, P. Microscopic investigation of ionic conductivity in alkali metal salts-poly (ethylene oxide) adducts. *Solid State Ionics* **1983**, *11*, 91–95. [[CrossRef](#)]
45. Qing-Shan, L.; Pei-Fang, Y.; Miao, Y.; Zhi-Cheng, T.; Chang-Ping, L.; Urs, W.-B. Dynamic Viscosity and Conductivity of Ionic Liquids [Cnpy] [NTf2] ( $n = 2, 4, 5$ ). *Acta Physico-Chimica Sin.* **2011**, *27*, 2762–2766. [[CrossRef](#)]
46. Chang-Ping, L.; Zhuo, L.; Ben-Xue, Z.; Qing-Shan, L.; Xiao-Xia, L. Density, Viscosity and Conductivity of Protic Ionic Liquid N,N-DimethylethanolammoniumPropionate. *Acta Physico-Chimica Sin.* **2013**, *29*, 2157–2161. [[CrossRef](#)]
47. Yuan, W.-L.; Yang, X.; He, L.; Xue, Y.; Qin, S.; Tao, G.-H. Viscosity, Conductivity, and Electrochemical Property of Dicyanamide Ionic Liquids. *Front. Chem.* **2018**, *6*, 59. [[CrossRef](#)]
48. Dyre, J.C.; Maass, P.; Roling, B.; Sidebottom, D.L. Fundamental questions relating to ion conduction in disordered solids. *Rep. Prog. Phys.* **2009**, *72*, 046501. [[CrossRef](#)]
49. Mizuno, F.; Belieres, J.-P.; Kuwata, N.; Pradel, A.; Ribes, M.; Angell, C. Highly decoupled ionic and protonic solid electrolyte systems, in relation to other relaxing systems and their energy landscapes. *J. Non-Crystalline Solids* **2006**, *352*, 5147–5155. [[CrossRef](#)]
50. Ansari, Y.; Ueno, K.; Zhao, Z.; Angell, C.A. Anhydrous Superprotonic Polymer by Superacid Protonation of Cross-linked (PNCl<sub>2</sub>)<sub>n</sub>. *J. Phys. Chem. C* **2013**, *117*, 1548–1553. [[CrossRef](#)]
51. Angell, C. Fast ion motion in glassy and amorphous materials. *Solid State Ionics* **1983**, *9–10*, 3–16. [[CrossRef](#)]
52. Wojnarowska, Z.; Feng, H.; Fu, Y.; Cheng, S.; Carroll, B.; Kumar, R.; Novikov, V.N.; Kisliuk, A.M.; Saito, T.; Kang, N.-G.; et al. Effect of Chain Rigidity on the Decoupling of Ion Motion from Segmental Relaxation in Polymerized Ionic Liquids: Ambient and Elevated Pressure Studies. *Macromolecules* **2017**, *50*, 6710–6721. [[CrossRef](#)]

# Stability of Quadruple Hydrogen Bonds in an Ionic Liquid Environment

Chenming Li, Rajesh Bhandary, Anja Marinow, Stephanie Bachmann, Ann-Christin Pöppler, and Wolfgang H. Binder\*

Hydrogen bonds (H-bonds) are highly sensitive to the surrounding environments owing to their dipolar nature, with polar solvents known to significantly weaken H-bonds. Herein, the stability of the H-bonding motif ureidopyrimidinone (UPy) is investigated, embedded into a highly polar polymeric ionic liquid (PIL) consisting of pendant pyrrolidinium bis(trifluoromethylsulfonyl)imide (IL) moieties, to study the influence of such ionic environments on the UPy H-bonds. The content of the surrounding IL is changed by addition of an additional low molecular weight IL to further boost the IL content around the UPy moieties in molar ratios of UPy/IL ranging from 1/4 up to 1/113, thereby promoting the polar microenvironment around the UPy-H-bonds. Variable-temperature solid-state MAS NMR spectroscopy and FT-IR spectroscopy demonstrate that the UPy H-bonds are largely present as (UPy-) dimers, but sensitive to elevated temperatures ( $>70\text{ }^{\circ}\text{C}$ ). Subsequent rheology and DSC studies reveal that the ILs only solvate the polymeric chains but do not interfere with the UPy-dimer H-bonds, thus accounting for their high stability and applicability in many material systems.

structures in peptides (such as  $\alpha$ -helices or  $\beta$ -folds);<sup>[2]</sup> mediate highly specific H-bonds in the duplex formation of DNA; mediate;<sup>[3]</sup> and impart self-healing properties in many polymers,<sup>[4]</sup> where the dynamics of the H-bonds allow crack healing and material reconstruction.<sup>[5]</sup> H-bonds display two important features, hardly reachable by other supramolecular bonding systems: they are strongly directional and thus highly dependent on spatial arrangements;<sup>[6]</sup> and they can be tuned over many orders of magnitude in their strength, which is expressed via their association constants ( $K_{\text{assn.}}$ ) in solution.<sup>[7]</sup> However, in many applications, as widespread in nature, there is one drawback: polar solvents and polar environments usually weaken H-bonds<sup>[8]</sup> by presenting alternative acceptors/donors, and thus often limit their applicability.<sup>[9]</sup> Cooperative effects in proteins can help overcome this drawback,<sup>[10]</sup> and the formation of hydrophobic

## 1. Introduction

Hydrogen bonds (H-bonds) are known to induce dynamic properties in many macromolecular assemblies and materials.<sup>[1]</sup> H-bonds, as in many supramolecular polymers and polypeptides, contribute to the formation of many assemblies or secondary

pockets or other noncovalent interactions<sup>[11]</sup> surrounding the H-bonds can also shield them from detrimental polar environments. Several such “hydrophobic shields” have led to quite stable H-bonding systems in synthetic polymers, protecting them even in aqueous environments.<sup>[12]</sup> However, most triple or multiple H-bonds fail in various strongly polar solvents,<sup>[13]</sup> stimulating the development of as-strong-as-possible H-bonding moieties like the quadruple ureidopyrimidinone (UPy), being powerful functional groups used to create functional materials with distinct properties such as shape-memory,<sup>[14]</sup> self-healing,<sup>[15]</sup> and ultra-tough-polymer properties.<sup>[16]</sup> In previous studies on H-bonds in solution,<sup>[17,18]</sup> UPy moieties were reported to self-associate into dimers with a  $K_{\text{assn.}} \cong 10^7\text{ M}^{-1}$  in chloroform, or a  $K_{\text{assn.}} \cong 10^8\text{ M}^{-1}$  in toluene, indicative of a strong influence by the polarity of the molecules near the UPy moieties. When embedded in a polymer matrix, it becomes difficult to directly measure changes in the association strength of these H-bond moieties, and only a few studies of changes in bonding strength in bulk polymers have been reported,<sup>[13,19–23]</sup> mainly focusing on the impact of organic solvents.<sup>[24]</sup>

We here report a systematic study on the influence of ionic liquids (ILs) on the association of the quadruple H-bonding motif UPy, by systematically embedding them into a microenvironment of increasing IL content. As the behavior of such UPy-system is crucial in the design of self-healing electrolytes or

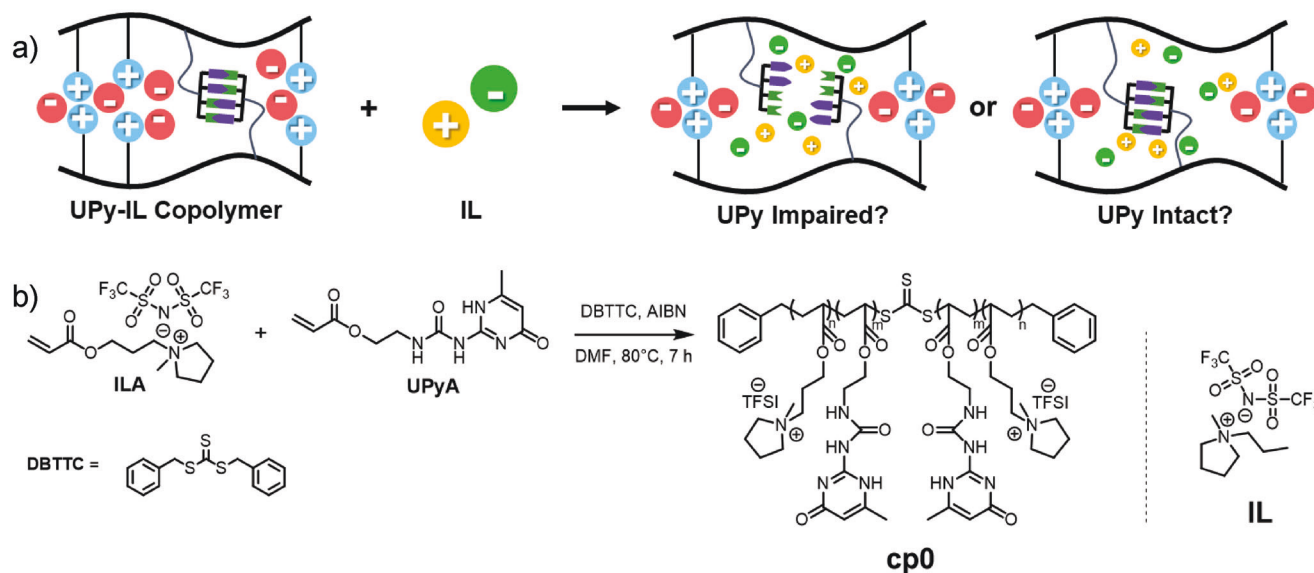
C. Li, R. Bhandary, A. Marinow, W. H. Binder  
Macromolecular Chemistry  
Institute of Chemistry  
Faculty of Natural Science II (Chemistry, Physics and Mathematics)  
Martin Luther University Halle-Wittenberg  
von-Danckelmann-Platz 4, D-06120 Halle (Saale), Germany  
E-mail: wolfgang.binder@chemie.uni-halle.de

S. Bachmann, A.-C. Pöppler  
Institute of Organic Chemistry  
Faculty of Chemistry and Pharmacy  
University of Würzburg  
Am Hubland, 97074 Würzburg, Germany

The ORCID identification number(s) for the author(s) of this article can be found under <https://doi.org/10.1002/marc.202300464>

© 2023 The Authors. Macromolecular Rapid Communications published by Wiley-VCH GmbH. This is an open access article under the terms of the Creative Commons Attribution-NonCommercial License, which permits use, distribution and reproduction in any medium, provided the original work is properly cited and is not used for commercial purposes.

DOI: 10.1002/marc.202300464



**Scheme 1.** a) Schematic representation of UPy dimer formation in ionic liquid environments: UPy moieties are copolymerized in a polymeric ionic liquid with extra added ionic liquid molecules; b) structure of the copolymer **cp0** ( $M_{n, NMR} = 11.5$  kDa, pyrrolidinium/UPy = 4.1:1) and the ionic liquid 1-methyl-1-propylpyrrolidinium bis(trifluoromethylsulfonyl) imide **IL** used in this work.

3D-printing,<sup>[25]</sup> knowledge of their stability in ILs is important. ILs are dipolar molecules that can offer strong polar molecular environments for UPy motifs, questioning their stability in such environments. However, since low molecular weight UPy molecules are poorly soluble in many ILs, such as pyrrolidinium-based ILs, we covalently embedded the UPy moieties into a polymeric ionic liquid (PIL) copolymer (see **Scheme 1**) composed of pyrrolidinium-ions along the chains via reversible addition-fragmentation chain-transfer (RAFT) polymerization. The adjacent pyrrolidinium moieties surrounding the UPy groups allow us to study the effects of this ionic microenvironment on the dissociation behavior of the quadruple UPy H-bonds. The chosen polymer also accomplishes the mixing of an additional pyrrolidinium-based IL to further increase the total amount of ILs around the UPy moieties systematically. Subsequent solid-state MAS NMR spectroscopy, FT-IR spectroscopy, differential scanning calorimetry (DSC), and rheology experiments then permit studying the binding state of the UPy moieties in these mixtures.

## 2. Results and Discussion

The pyrrolidinium-bis(trifluoromethylsulfonyl)imide-based copolymer **cp0** containing 20.7 pyrrolidinium moieties and 5.0 UPy moieties per polymer chain was synthesized via RAFT polymerization as reported<sup>[26]</sup> to reach a controllable molecular weight of 11.5 kDa (as determined by NMR spectroscopy; for the detailed calculation and spectra, see Section S1, Supporting Information). The neat polymer **cp0**, now containing  $\approx 4$  IL units for every UPy moiety, can be further mixed with different ratios of 1-methyl-1-propylpyrrolidinium bis(trifluoromethylsulfonyl)imide (**IL**) to prepare the samples **cp25**, **cp50**, and **cp75**, with a molar ratio of UPy/IL-moiety of 1:39.3 (**cp25**), 1:73.5 (**cp50**), and 1:113.2 (**cp75**) respectively. The synthesis of **cp0** and the structure of the

**Table 1.** Composition of the parent sample **cp0** with the ratio backbone-IL/UPy = 4.1/1; and the samples **cp25**, **cp50**, and **cp75**, with a molar ratio of UPy/IL-moiety of 1:39.3 (**cp25**), 1:73.5 (**cp50**), and 1:113.2 (**cp75**) respectively.

Sample ID	cp0 <sup>a)</sup>	cp25	cp50	cp75
Polymer: IL (weight ratio) <sup>a)</sup>	Neat	1:0.25	1:0.50	1:0.75
Polymer: IL <sup>a,b)</sup>	—	1:6.9	1:13.6	1:21.4
Backbone-IL: UPy: Free IL <sup>b)</sup>	4.1:1:—	4.1:1:35.2	4.1:1:69.4	4.1:1:109.1

<sup>a)</sup> For the detailed calculation of sample composition see Section S1 (Supporting Information); <sup>b)</sup> Molar ratio calculated by  $^1\text{H}$  NMR; <sup>c)</sup>  $M_{n, NMR} = 11.5$  kDa, backbone IL/UPy = 4.1:1.

added ionic liquid (**IL**) are shown in Scheme 1 and the sample information is listed in Table 1.

To study the behavior of the UPy H-bonds in such polar environments we firstly probed solid-state MAS NMR spectroscopy, as the bound/dissociated status of H-bonded protons can be directly detected by NMR spectroscopy both in solution<sup>[13,17,19,28,29]</sup> and in the solid state.<sup>[23,30–32]</sup> The  $^1\text{H}$  MAS NMR spectrum of **cp0** shown in Figure 1a reveals the intramolecular H-bond  $H_a$ , and the intermolecular H-bonds  $H_b$  and  $H_c$  of the UPy-NH protons (denoted by the two gray dashed lines) in the neat copolymer **cp0**, matching well with the reported solid-state NMR spectra of UPy compounds known for non-ionic surroundings.<sup>[23,33]</sup> Upon heating from 23 to 53 °C, these peaks do not shift to lower ppm values, forming evidence for still un-dissociated UPy moieties. As the actual temperature in the MAS rotor could be up to 30 °C higher than the set value due to the frictional heating upon rotation,<sup>[27]</sup> we can state that there is no observable shift of the H-bond peaks at the temperature of  $T_{\text{actual}} = 32\text{--}78$  °C. Similarly, the presence of still associated UPy moieties can be also evidenced by their immobility in their  $^{13}\text{C}$  NMR spectra (see  $^{13}\text{C}$  NMR spectra recorded under cross polarization (CP) and direct excitation (DE)

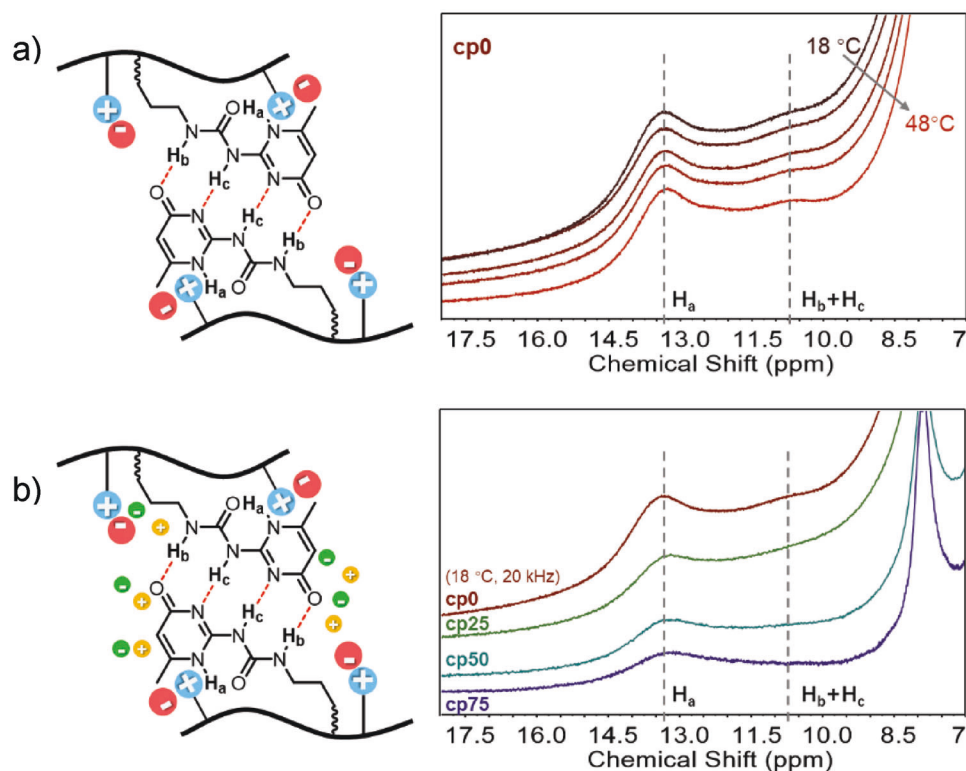


**Figure 1.** Schematic illustration of the UPy dimer in their DDAA (donor–donor–acceptor–acceptor) H-bonding array and extracts from  $^1\text{H}$  MAS NMR spectra of a) **cp0** at variable temperatures, measured at 20 kHz and  $T_{\text{set}} = 23, 33, 43, 48, 53^\circ\text{C}$  (with  $T_{\text{actual}}$  with an additional  $30^\circ\text{C}$  due to the frictional heating upon rotation<sup>[27]</sup>); b)  $^1\text{H}$  MAS NMR spectra of samples **cp0**, **cp25**, **cp50**, and **cp75** with different IL content (recorded at  $5^\circ\text{C}$  actual sample temperature and a maximum stable MAS frequency of 15 kHz due to their gel nature under rotation). Though the DADA (donor–acceptor–donor–acceptor) H-bonding array of UPy dimers is possible due to the tautomeric exchange, all the UPy dimers in this work are assumed to be in their most stable DDAA array.<sup>[17,23]</sup>

conditions in the Figure S2, Supporting Information). While polymeric backbone carbons, the pyrimidinone-carbonyls, and other UPy carbons appear in the CP-spectra, they are absent in the DE-spectra recorded with short interscan delays, where only the mobile moieties can be probed, indicating their immobility in the probed samples. To study whether a higher content of IL leads to changes in the dissociation state of the H-bonds, we have mixed the polymer samples with additional IL (see Table 1, samples **cp25**, **cp50**, **cp75**) to increase the ratio of IL/UPy. Upon mixing with the IL, the chemical shifts of the peaks remain unchanged as indicated by the gray dashed line in Figure 1b, demonstrating the invulnerability of the UPy dimers against the added IL up to a ratio UPy/IL  $\approx 1/113$ . The only observed change is the peak at  $\approx 10.8$  ppm, which becomes broader, less intense, or overlaps with the adjacent peaks. This might be a result of the exchange of the UPy keto-enol tautomer promoted by reduced chain friction via IL mixing. To distinguish possible tautomers double quantum 2D NMR spectra of the samples were recorded and compared with the reported spectra (for the 2D spectra, see Figure S3, Supporting Information),<sup>[23]</sup> which unfortunately did not provide further insight due to the poor spectral resolution and missing of the NH peaks. Analogous experiments at higher MAS frequency to obtain double quantum data with higher resolution were not successful due to the viscous nature of the gel samples,

as even upon cooling IL-containing samples pushed the cap out at MAS frequencies above 15 kHz.

We further probed FT-IR spectroscopy to reveal the open/close nature of the UPy H-bonds, since solid-state NMR spectroscopy was not applicable for all samples at elevated temperatures due to their reduced viscosities. Therefore, FT-IR analysis of the H-bonds at variable temperatures in a broader range ( $25$ – $150^\circ\text{C}$ ) was performed for all samples. For the neat copolymer **cp0** two features were observed when the temperature was increased (Figure 2a,b): the NH peaks at  $\approx 3200\text{ cm}^{-1}$  gradually became broader and increased in intensity when compared to the adjacent C–H peak ( $\approx 2975\text{ cm}^{-1}$ ), whereas the peaks at  $\approx 3400\text{ cm}^{-1}$  increased slightly, revealing indicative of an increase in free, dissociated N–H bonds in sample **cp0**. As the temperature was increased to  $70^\circ\text{C}$ , a new peak at  $\approx 1680\text{ cm}^{-1}$  was observed, separated from the main peak (at  $1663\text{ cm}^{-1}$ ) for the C = O of urea moieties of UPy (indicated by the gray dashed box), which is an indication of a weakening of the ureido H-bonds and a loss of the UPy stacking.<sup>[34,35]</sup> Blueshifting of the C = O (pyrimidinone) stretching ( $\approx 1702\text{ cm}^{-1}$ , denoted by the gray arrow) upon heating also indicates weakening of the UPy H-bonds at elevated temperatures ( $>70^\circ\text{C}$ ), in line with the previously reported temperature-dependency of UPy H-bonds.<sup>[36]</sup> However, mixing with IL does not interfere with the UPy H-bonds as indicated by the unshifted



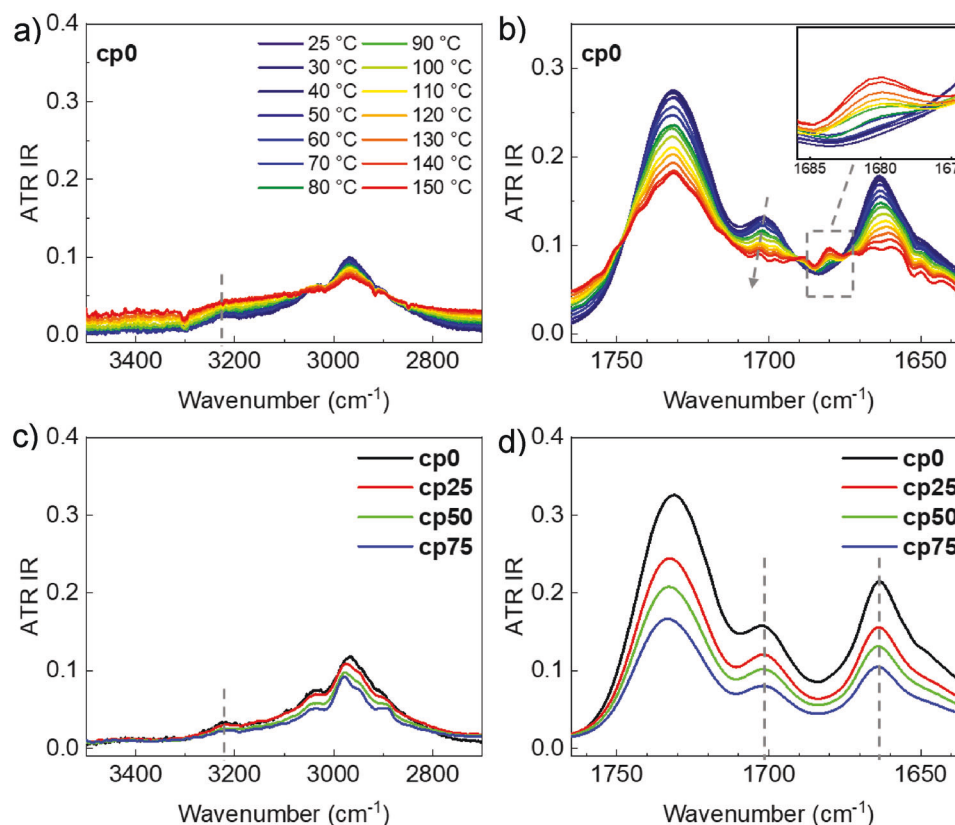


**Figure 2.** FT-IR analysis of a,b) **cp0** at variable temperatures and c,d) all samples at room temperature.

characteristic IR peaks of UPy in Figure 2c,d. Additionally, the samples with the added IL show similar FT-IR spectra compared to the sample **cp0** upon heating, which again proves the almost undisturbed H-bonds of UPy against the added IL (for detailed variable-temperature FT-IR spectra, see Figure S4, Supporting Information). Thus the UPy H-bonds are prone to dissociation at elevated temperatures ( $>70$  °C), but not sensitive to the charged IL molecules in the charged PIL matrix at ambient conditions.

We also searched for changes in the UPy-bonded copolymer upon the addition of IL by differential scanning calorimetry

(DSC). The neat sample **cp0**, when compared to the reported homopolymers, showed an increase in the glass transition temperature  $T_g$  from  $-13$  °C (homo PIL,  $M_n = 11.0$  kDa)<sup>[26]</sup> to  $22.4$  °C (**cp0**), suggesting closed UPy dimers in the charged PIL matrix that reduce the segmental motion and thus result in a higher  $T_g$ . When further IL is added, the  $T_g$ s of all samples were reduced from  $22.4$  °C (**cp0**), to  $-12.8$  °C (**cp25**), to  $-35.2$  °C (**cp50**), and to  $-56.1$  °C (**cp75**) (see Figure 3a), demonstrating that the added IL induced faster chain dynamics. For comparison, this is in contrast to effects observed by the addition of metal salts

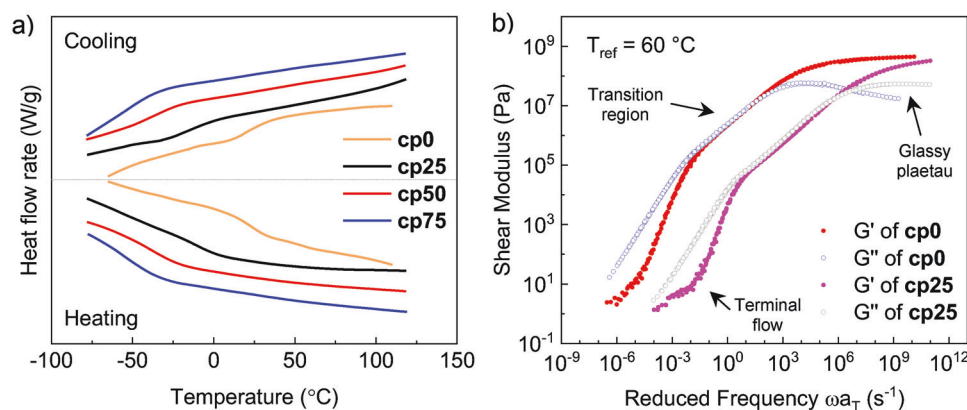


**Figure 3.** a) DSC analysis of all samples with a heating/cooling rate of  $3 \text{ K min}^{-1}$  and thermal history was canceled by a pre-heating cycle; b) the master curves of **cp0** and **cp25** measured from  $-10$  to  $120$  °C, with the reference temperature of  $60$  °C.

in UPy-containing polymers<sup>[37,38]</sup> where an increase of  $T_g$  can be observed via chain stiffening effects attributed to crosslinking by metal-carbonyl coordination. In DSC analysis, the number of glass transitions can be used as indirect proof of microphase separation if the formation of the separated domains can be excluded.<sup>[39–41]</sup> As shown in Figure 3a, there is only one glass transition occurred for every sample, suggesting that, though UPy forms dimers, there is no distinct microphase separation between the UPy dimers and the (poly-) ionic liquids moieties. To further test the influence of IL on the final H-bonded polymers, dynamic rheology measurements were performed. Owing to the technically too-low-to-detect viscosity of **cp50** and **cp75** at elevated temperatures, only the master curves of neat **cp0** and **cp25** were measured. As shown in Figure 3b, master curves of **cp0** and **cp25** demonstrate a typical Rouse behavior with a terminal flow, a transition region with a crossover of the storage modulus  $G'$  and the loss modulus  $G''$ , and a glassy plateau, though the rubbery plateau is absent due to lack of chain entanglements or permanent crosslinking. The terminal flow in the low-frequency region proves the dynamic nature of these two H-bonded samples over a long timescale, whereas according to the Rouse model the crossover of the  $G'$  and the  $G''$  reveal the loss of association among chains, where the material starts to flow, with the reciprocal of this crossover time representing the relaxation time ( $\tau_b$ ) of the polymer.<sup>[22]</sup> The relaxation time  $\tau_b$  of the sample added with IL in a 6.9 molar ratio (see Table 1 for sample compositions) is reduced from  $1.20 \times 10^{-1}$  s (**cp0**) to  $1.94 \times 10^{-6}$  s (**cp25**), indicative of the largely reduced total relaxation time by the added IL, resulting from synergic effects of the possible UPy H-bond relaxation and the solvation of the polymer chains by the added IL. Considering that **cp0** and **cp25** have the same parent polymer matrix (which is **cp0**), and their storage modulus at the glassy state, where all the segmental motion is frozen, are of similar value, we could thus further deduce that the associations that determine this modulus are also at a similar strength, which is most probably the association of UPy groups. Because **cp25** contains mobile IL molecules while **cp0** does not, and their modulus is of a similar value when segmental motion is frozen, we thus conclude that the UPy accounting for the mechanical strength is not influenced by the IL,<sup>[22,42]</sup> whereas the IL only promotes the chain motion by reducing the chain friction via chain solvation rather than breaking/weakening the UPy H-bonds. Therefore, the H-bonds of UPy dimers are largely independent of the addition of IL and thus the increased polar environment.

### 3. Conclusion

In summary, as proven by MAS NMR spectroscopy, the H-bonds of UPy at ambient temperature stay largely undisturbed in their dimeric state, also upon mixing with additional IL up to a molar ratio of UPy/IL =  $1/\approx 113$ . FT-IR analysis at elevated temperatures demonstrates a weakening of the UPy H-bonds at temperatures above 70 °C, although this is highly independent of the added IL at these temperatures (25–150 °C). We thus can prove that the UPy dimers remain stable in (poly-)ionic liquid environments, though the mobile IL molecules reduce chain friction and boost the chain dynamics of the polymeric ionic liquids matrix as evidenced by DSC and rheology. As the UPy-moieties

are used extensively in many materials systems, in recent times largely in poly(electrolytes) to impart self-healing properties, the findings here are important for the design of self-healing materials with strong polar surroundings, where UPy bonds are often used to generate transient crosslinks in highly charged media.

### 4. Experimental Section

**Materials:** 1-Methyl-1-propylpyrrolidinium bis(trifluoromethylsulfonil)imide 99% was purchased from IoLiTech (Heilbronn, Germany) and dried under ultrahigh vacuum at 80 °C for 48 h then stored in a glovebox ( $O_2 < 0.5$  ppm,  $H_2O < 0.5$  ppm); dimethyl formamide (DMF) were purchased from Grüssing (Filsum, Germany) and purified/dried via a solvent purification system; 2,2'-azobis(2-methylpropionitrile) (AIBN) was purchased from Sigma-Aldrich (Merck KGaA, Darmstadt, Germany), and recrystallized in methanol before use; deuterated dimethyl sulfoxide ( $DMSO-d_6$ ) were purchased from Chemotrade (Eckert and Ziegler Gruppe, Düsseldorf, Germany) and used as received.

**Synthesis of Monomer ILA and UPyA, and RAFT Agent DBTTC:** The synthesis was followed as described in reference.<sup>[26]</sup>

**The synthesis was followed as described in reference.<sup>[26]</sup>** The synthesis of ionic monomer **ILA**, UPy monomer **UPyA**, and the copolymer via RAFT polymerization was adapted from reference. The synthesis of ionic monomer **ILA**, UPy monomer **UPyA**, and the copolymer via RAFT polymerization was adapted from reference.<sup>[26]</sup> Briefly, **ILA** (2993 mg, 6.26 mmol), and **UPyA** (417 mg, 1.55 mmol) were placed in DMF (8 mL) in a Schlenk tube. The tube was sealed with a rubber septum and the reaction mixture was purged with nitrogen for 30 min to deoxygenate under vigorous stirring. After deoxygenation, the tube was heated in an oil bath at 120 °C till a clear solution was obtained, then the temperature of the oil bath was cooled to 80 °C. In the meantime, in a flask **DBTTC** (114.3 mg, 0.39 mmol) and AIBN (7.0 mg,  $4.26 \times 10^{-2}$  mmol) were dissolved in deoxygenated DMF (0.5 mL), then this solution was transferred to the reaction Schlenk tube by a syringe to initiate the polymerization. After 7 h, the reaction was stopped by opening the septum and subsequently precipitated into DCM three times to eliminate the monomer residue. The polymer was collected by centrifugation and decantation and finally dried at 80 °C under a high vacuum for 24 h. The molecular weight was evaluated by  $^1H$  NMR using the characteristic methyl protons of the pendent pyrrolidinium ( $\equiv N-CH_3$ , 3nH,  $\delta = 3.02$  ppm, with  $n$  being the degree of polymerization of **ILA**), the characteristic vinylic proton of the pendent UPy moiety ( $-(CH_3-C=CH-$ , mH,  $\delta = 5.80$  ppm, with  $m$  being the degree of polymerization of **UPyA**), and the characteristic aromatic protons of **DBTTC** (pH, 10H,  $\delta = 7.36$  ppm). For the NMR spectrum of **cp0** in  $DMSO-d_6$  and the detailed molecular weight calculation, see Figure S1 (Supporting Information). Briefly, **ILA** (2993 mg, 6.26 mmol), and **UPyA** (417 mg, 1.55 mmol) were placed in DMF (8 mL) in a Schlenk tube. The tube was sealed with a rubber septum and the reaction mixture was purged with nitrogen for 30 min to deoxygenate under vigorous stirring. After deoxygenation, the tube was heated in an oil bath at 120 °C till a clear solution was obtained, then the temperature of the oil bath was cooled to 80 °C. In the meantime, in a flask **DBTTC** (114.3 mg, 0.39 mmol) and AIBN (7.0 mg,  $4.26 \times 10^{-2}$  mmol) were dissolved in deoxygenated DMF (0.5 mL), then this solution was transferred to the reaction Schlenk tube by a syringe to initiate the polymerization. After 7 h, the reaction was stopped by opening the septum and subsequently precipitated into DCM three times to eliminate the monomer residue. The polymer was collected by centrifugation and decantation and finally dried at 80 °C under a high vacuum for 24 h. The molecular weight was evaluated by  $^1H$  NMR using the characteristic methyl protons of the pendent pyrrolidinium ( $\equiv N-CH_3$ , 3nH,  $\delta = 3.02$  ppm, with  $n$  being the degree of polymerization of **ILA**), the characteristic vinylic proton of the pendent UPy moiety ( $-(CH_3-C=CH-$ , mH,  $\delta = 5.80$  ppm, with  $m$  being the degree of polymerization of **UPyA**), and the characteristic aromatic protons of **DBTTC** (pH, 10H,

$\delta = 7.36$  ppm). For the NMR spectrum of **cp0** in DMSO- $d_6$  and the detailed molecular weight calculation, see Figure S1 (Supporting Information).

**Sample Preparation:** In a glovebox, neat **cp0** and the desired amount of **IL** were weighed in a vial with a magnetic stir bar, and then a small amount of dry MeCN ( $\approx 1$  mL) was added to support the mixing process. After homogeneity was reached, MeCN was firstly removed by heating the open vial in the glovebox at 120 °C overnight, then the vial was transferred to a closed heating kit with an ultrahigh vacuum applied and dried at 80 °C for 48 h before characterization.

**Differential scanning calorimetry (DSC)** measurements were performed on a calibrated heat-flux DSC (Mettler-Toledo, Greifensee, Switzerland) equipped with the FRSS sensor, connected to a TC100 Intracooler (Huber, Offenbach, Germany). About 0.5 mg of sample was placed in aluminum-sealed crucibles for measurements. The thermal history was canceled by heating the samples from 25 to 120 °C at 10 K min<sup>-1</sup>, followed by isothermal annealing for 20 min, re-cooling to -80 °C at 3 K min<sup>-1</sup>, and thermostating at -80 °C for another 10 min. The final DSC curves were then recorded from -80 to 120 °C at 3 K min<sup>-1</sup>.

**Rheology** measurements were performed on an MCR 101 DSO rheometer (Anton Paar Germany GmbH, Ostfildern-Scharnhausen, Germany) using a parallel plate geometry (plate diameter: 8 mm). All polymers were dried under an ultrahigh vacuum at 80 °C for 24 h before the rheology measurement. The samples were directly smeared on the lower plate of the sample holder at 80–100 °C, then thermostated for an hour before loading the upper kit. The sample temperature was regulated by thermoelectric cooling/heating in a Peltier chamber under a dry nitrogen atmosphere. At each temperature, the sample was equilibrated for 20 min before the measurement was initiated. All measurements were performed in the dynamic mode and repeated twice to ensure precise values. Data analysis was performed via Rheo Compass (version V1.30.1064).

**Liquid-State Nuclear Magnetic Resonance Spectroscopy** was performed on a Varian FT-NMR spectrometer (400 MHz for <sup>1</sup>H-NMR and 100 MHz for <sup>13</sup>C-NMR, respectively) (Agilent Technologies Germany GmbH & Co. KG, Waldbronn, Germany). All samples were measured at 27 °C using deuterated dimethyl sulfoxide (DMSO- $d_6$ ). Chemical shifts ( $\delta$ ) were recorded in parts per million (ppm) relative to the remaining protonated solvent signals (DMSO- $d_6$ : 2.50 ppm (<sup>1</sup>H) and 39.5 ppm (<sup>13</sup>C)). The data analysis was performed via MestReNova (version 9.0.1-13254).

**Solid-State Magic Angle Spinning Nuclear Magnetic Resonance Spectroscopy (MAS NMR)** was performed on a Bruker Avance III HD 600 MHz spectrometer using a 3.2 mm double-channel probe. The spinning rate was up to 20 kHz MAS and the temperature ranged from 263.0 to 326.4 K, although the sample temperature is up to 30 K higher due to frictional heating during magic angle spinning. The magic angle was optimized with KBr.  $\alpha$ -glycine was used to calibrate the <sup>1</sup>H 90° pulse and the <sup>13</sup>C cross-polarization conditions. For <sup>13</sup>C cross-polarization experiments, a 90 to 100 ramp and SPINAL64 heteronuclear decoupling were used. To get more insights into the mobile parts, <sup>13</sup>C NMR spectra with direct excitation and a short interscan delay of 1 s were measured. Adamantane was used to reference the chemical shift. Rotor-synchronized <sup>1</sup>H(SQ)-<sup>1</sup>H(DQ) BABA experiments were recorded.<sup>[43,44]</sup> The data analysis was performed via MestReNova (version 9.0.1-13254) or with TopSpin (Version 4.0.8).

**Variable-Temperature Attenuated Total Reflection (ATR) FT-IR Spectroscopy** was performed using a Bruker Tensor vertex 70 (Bruker Optik GmbH, Bremen, Germany) equipped with a Golden Gate Heated Diamond ATR top plate (Specac Ltd, Orpington, UK). All wavenumbers are given in cm<sup>-1</sup>. For FT-IR measurements at elevated temperatures, samples were heated with the heating rate of 10 K min<sup>-1</sup> and equilibrated at the desired temperature for 2 min before the measurement started. Data analysis was performed via the software OPUS (version 8.2) and Origin 2018 (version b9.5.0.193).

## Supporting Information

Supporting Information is available from the Wiley Online Library or from the author.

## Acknowledgements

The authors thank Prof. Dr.-Ing René Androsch and MSc. Mengxue Du for DSC analyses. The authors thank the DFG project BI 1337/14-1 (Mikrophasensegregierte polymere ionische Flüssigkeiten als Gating-Materialien), and the BA-T-4ever project (Horizon 2020, Grant agreement Nr 957225) for financial support.

Open access funding enabled and organized by Projekt DEAL.

## Conflict of Interest

The authors thank Prof. Dr.-Ing René Androsch and MSc. Mengxue Du for DSC analyses. The authors thank the DFG project BI 1337/14-1 (Mikrophasensegregierte polymere ionische Flüssigkeiten als Gating-Materialien), and the BA-T-4ever project (Horizon 2020, Grant agreement Nr 957225) for financial support.

## Data Availability Statement

The data that support the findings of this study are available in the supplementary material of this article.

## Keywords

hydrogen bonds, ionic liquids, polymeric ionic liquids, ureidopyrimidinone

Received: August 1, 2023  
Revised: October 2, 2023  
Published online: October 17, 2023

- [1] G. R. Desiraju, *Angew. Chem., Int. Ed.* **2011**, 50, 52.
- [2] K. A. Dill, *Biochemistry* **1990**, 29, 7133.
- [3] P. L. A. Popelier, L. Joubert, *J. Am. Chem. Soc.* **2002**, 124, 8725.
- [4] E. B. Stukalin, L.-H. Cai, N. A. Kumar, L. Leibler, M. Rubinstein, *Macromolecules* **2013**, 46, 7525.
- [5] A. Campanella, D. Döhler, W. H. Binder, *Macromol. Rapid Commun.* **2018**, 39, 1700739.
- [6] G. R. Desiraju, *Nature* **2001**, 412, 397.
- [7] W. H. Binder, R. Zirbs, in *Hydrogen Bonded Polymers*, (Ed: W. Binder), Springer, Berlin Heidelberg **2007**, p.1.
- [8] S. Pensec, N. Nouvel, A. Guilleman, C. Creton, F. Boué, L. Bouteiller, *Macromolecules* **2010**, 43, 2529.
- [9] F. Biedermann, H.-J. Schneider, *Chem. Rev.* **2016**, 116, 5216.
- [10] N. Dominelli-Whiteley, J. J. Brown, K. B. Muchowska, I. K. Mati, C. Adam, T. A. Hubbard, A. Elmi, A. J. Brown, I. A. W. Bell, S. L. Cockcroft, *Angew. Chem., Int. Ed.* **2017**, 56, 7658.
- [11] T. Steiner, G. Koellner, *J. Mol. Biol.* **2001**, 305, 535.
- [12] M. Tharcis, T. Breiner, J. Belleney, F. Boué, L. Bouteiller, *Polym. Chem.* **2012**, 3, 3093.
- [13] F. Herbst, W. H. Binder, *Polym. Chem.* **2013**, 4, 3602.
- [14] M. Guo, L. M. Pitet, H. M. Wyss, M. Vos, P. Y. W. Dankers, E. W. Meijer, *J. Am. Chem. Soc.* **2014**, 136, 6969.
- [15] P. Guo, A. Su, Y. Wei, X. Liu, Y. Li, F. Guo, J. Li, Z. Hu, J. Sun, *ACS Appl. Mater. Interfaces* **2019**, 11, 19413.
- [16] T. Liu, F. Wang, Q. Wu, T. Chen, P. Sun, *Mater. Horiz.* **2021**, 8, 3096.
- [17] S. H. M. Söntjens, R. P. Sijbesma, M. H. P. Van Genderen, E. W. Meijer, *J. Am. Chem. Soc.* **2000**, 122, 7487.
- [18] G. B. W. L. Ligthart, H. Ohkawa, R. P. Sijbesma, E. W. Meijer, *J. Am. Chem. Soc.* **2005**, 127, 810.
- [19] F. Herbst, K. Schröter, I. Gunkel, S. Gröger, T. Thurn-Albrecht, J. Balbach, W. H. Binder, *Macromolecules* **2010**, 43, 10006.

- [20] T. Yan, K. Schröter, F. Herbst, W. H. Binder, T. Thurn-Albrecht, *Macromolecules* **2014**, *47*, 2122.
- [21] R. Suriano, L. Brambilla, M. Tommasini, S. Turri, *Polym. Adv. Technol.* **2018**, *29*, 2899.
- [22] K. E. Feldman, M. J. Kade, E. W. Meijer, C. J. Hawker, E. J. Kramer, *Macromolecules* **2009**, *42*, 9072.
- [23] I. Schnell, B. Langer, S. H. M. Söntjens, R. P. Sijbesma, M. H. P. Van Genderen, H. Wolfgang Spiess, *Phys. Chem. Chem. Phys.* **2002**, *4*, 3750.
- [24] T. Naranjo, R. Álvarez-Asencio, P. Pedraz, B. Nieto-Ortega, S. M. Da Silva, E. Burzurí, M. W. Rutland, E. M. Pérez, *Sci. Rep.* **2020**, *10*, 15414.
- [25] Z. Katcharava, A. Marinow, R. Bhandary, W. H. Binder, *Nanomaterials* **2022**, *12*, 1859.
- [26] C. Li, R. Bhandary, A. Marinow, D. Ivanov, M. Du, R. Androsch, W. H. Binder, *Polymers* **2022**, *14*, 4090.
- [27] S. Scheidel, L. Östreicher, I. Mark, A.-C. Pöppler, *Magn. Reson. Chem.* **2022**, *60*, 572.
- [28] C. Dethlefs, J. Eckelmann, H. Kobarg, T. Weyrich, S. Brammer, C. Näther, U. Lüning, *Eur. J. Org. Chem.* **2011**, *2011*, 2066.
- [29] C. Li, P. Hilgeroth, N. Hasan, D. Ströhl, J. Kressler, W. H. Binder, *Int. J. Mol. Sci.* **2021**, *22*, 12679.
- [30] B. Li, L. Xu, Q. Wu, T. Chen, P. Sun, Q. Jin, D. Ding, X. Wang, G. i. Xue, A.-C. Shi, *Macromolecules* **2007**, *40*, 5776.
- [31] B. Fortier-McGill, V. Toader, L. Reven, *Macromolecules* **2012**, *45*, 6015.
- [32] Ü. Akbey, R. Graf, Y. G. Peng, P. P. Chu, H. W. Spiess, *J. Polym. Sci., Part B: Polym. Phys.* **2009**, *47*, 138.
- [33] B. Qin, S. Zhang, P. Sun, B. Tang, Z. Yin, X. Cao, Q. Chen, J.-F. Xu, X. Zhang, *Adv. Mater.* **2020**, *32*, 2000096.
- [34] F. Lortie, S. Boileau, L. Bouteiller, *Chemistry* **2003**, *9*, 3008.
- [35] W. P. J. Appel, G. Portale, E. Wisse, P. Y. W. Dankers, E. W. Meijer, *Macromolecules* **2011**, *44*, 6776.
- [36] K. E. Feldman, M. J. Kade, T. F. A. De Greef, E. W. Meijer, E. J. Kramer, C. J. Hawker, *Macromolecules* **2008**, *41*, 4694.
- [37] G. Venugopal, S. Krause, G. E. Wnek, *Polymer* **1993**, *34*, 3241.
- [38] T. Sako, A. Miyagawa, M. Yamaguchi, *J. Appl. Polym. Sci.* **2017**, *134*.
- [39] S. Chen, N. Mahmood, M. Beiner, W. H. Binder, *Angew. Chem., Int. Ed.* **2015**, *54*, 10188.
- [40] S. Chen, F. Frenzel, B. Cui, F. Gao, A. Campanella, A. Funtan, F. Kremer, S. S. P. Parkin, W. H. Binder, *J. Mater. Chem. C* **2018**, *6*, 8242.
- [41] S. Chen, A. Funtan, F. Gao, B. Cui, A. Meister, S. S. P. Parkin, W. H. Binder, *Macromolecules* **2018**, *51*, 8620.
- [42] M. Piest, X. Zhang, J. Trinidad, J. F. J. Engbersen, *Soft Matter* **2011**, *7*, 11111.
- [43] W. Sommer, J. Gottwald, D. E. Demco, H. W. Spiess, *J. Mag. Reson., Ser. A* **1995**, *113*, 131.
- [44] I. Schnell, A. Lupulescu, S. Hafner, D. E. Demco, H. W. Spiess, *J. Magn. Reson.* **1998**, *133*, 61.



# Chemistry A European Journal



**Chemistry  
Europe**

European Chemical  
Societies Publishing

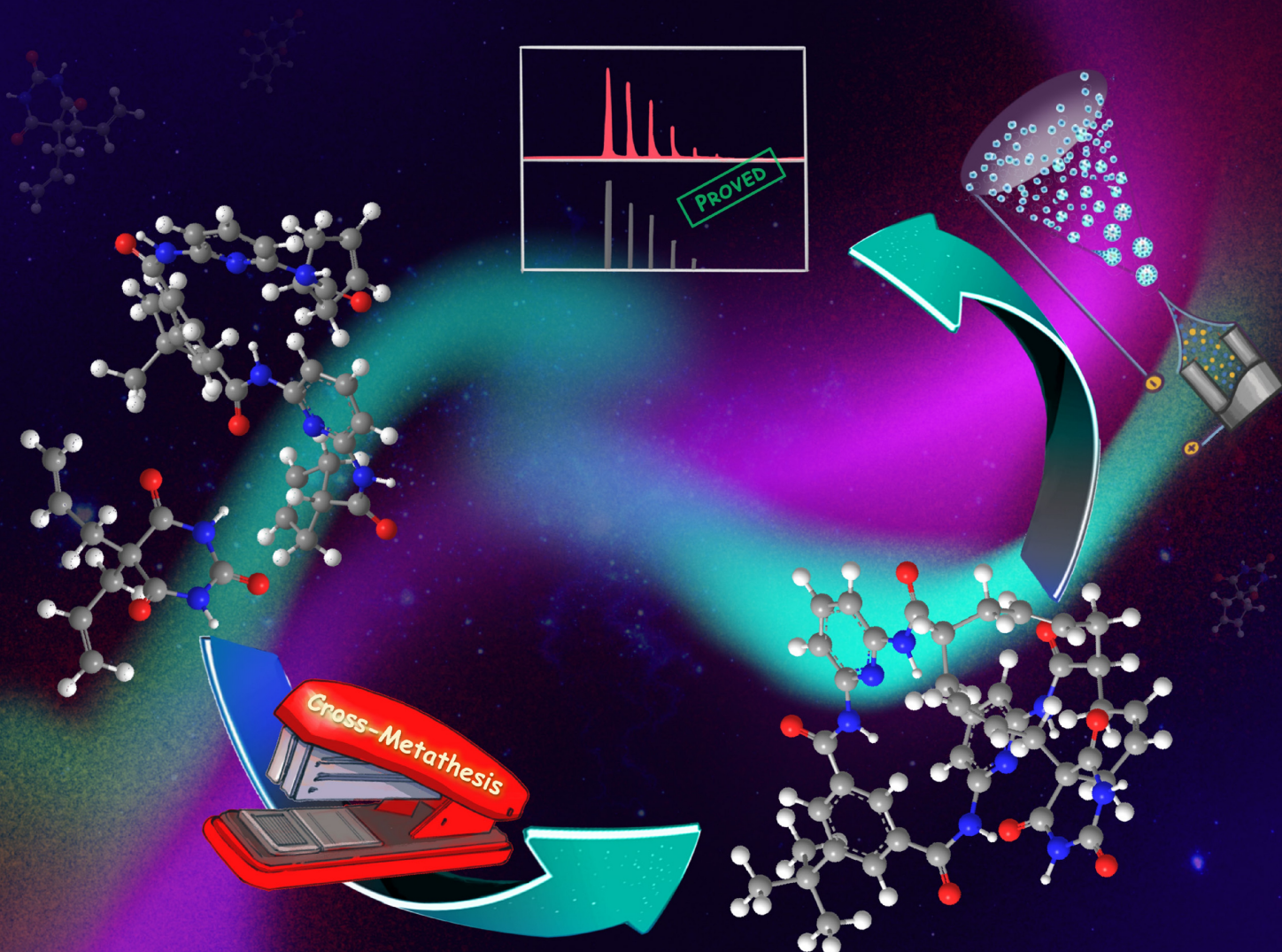
Celebrating  
**30** Years



**Cover Feature:**

*W. H. Binder and co-workers*

Proximity Effects and Aggregation of Hamilton-Receptor Barbiturate Host–Guest Complexes Probed by Cross-Metathesis and ESI MS Analysis





# Proximity Effects and Aggregation of Hamilton-Receptor Barbiturate Host–Guest Complexes Probed by Cross-Metathesis and ESI MS Analysis

Chenming Li,<sup>[a]</sup> Pascal Mai,<sup>[a]</sup> Niclas Festag,<sup>[a]</sup> Anja Marinow,<sup>[a]</sup> and Wolfgang H. Binder<sup>\*[a]</sup>

The molecular environment around supramolecular bonding systems significantly affects their stability and the assembly of host–guest complexes, most prominent for hydrogen bonds (H-bonds). Hamilton receptor–barbiturate host–guest complexes are well-known in solution, typically forming a 1:1 molar ratio complex. However, within a polymer matrix, these complexes can form higher-order assemblies, deviating from the standard 1:1 complex, which are challenging to characterize and often require lab-intensive methods. In this study, a novel Hamilton receptor (H) was equipped with cyclopentene moieties and used as a host to form host–guest complexes (H B) with allobarbital (B), followed by covalent crosslinking. UV-Vis spectroscopy titration experiments in different solvents and at

various temperatures revealed that polar solvents containing additional H-bonding sites significantly reduce the formation of the 1:1 H B complex, as indicated by a reduced association constant. Higher-order aggregates (HH-dimer, HHH-trimer) were subsequently detected via an alkene cross-metathesis (CM) reaction to fix the assemblies covalently, followed by analysis via electrospray ionization mass spectrometry (ESI MS). This two-step method, firstly via CM fixation followed by ESI MS, was extended to study the H B model complex within a polyisobutylene (PIB) matrix, presenting a direct method to analyze the complex host–guest assembly in solvent-free (polymer) environments.

## Introduction

Supramolecular structures, such as hydrogen bonding (H-bonding) systems, constitute highly relevant structural units of molecular self-assembly, bridging biological and synthetic sciences by implementing dynamic properties into materials and molecules. Similar to their behavior in solution, supramolecular bonds<sup>[1]</sup> in polymers also exhibit (partially) reversible formation and reformation via host–guest complexes, depending on their bonding strength, their exchange kinetics, as well as influences from the surrounding micro- and nano-environment. Phase segregation, crystallization, or the assembly of polymers is an additional structural principle where often limited diffusion is coupled to an anisotropic environment, with only rudimentary knowledge about the formation of host–guest complexes therein as both diffusion and spatial in-homogeneities, as well as anisotropy, prevail.<sup>[2]</sup> Therefore, when embedded into polymers, many host–guest complexes display an essentially modified exchange behavior compared to their solution

counterparts,<sup>[1b,c]</sup> often characterized by clustering and aggregation effects forming host–guest complexes different from the expected 1:1 stoichiometry.<sup>[3]</sup> Thus, for example, the effective strength of H-bonds is influenced by a subtle interplay between their intrinsic chemical structure (e.g., by substituent effects<sup>[4]</sup>), the surrounding polarity of the medium, their concentration as well as the microenvironment locally surrounding the H-bonds.<sup>[1c]</sup> Clusters of H-bonds are often formed in solid polymers, contributing most importantly to macroscopic effects, such as self-healing and reformation of the initial structures,<sup>[1c,3b,5]</sup> resulting in enormously different melt-flow behavior of the materials by their now changed relaxation behavior.<sup>[6]</sup> Whereas in most cases the same H-bonds, when affixed to larger groups such as polymer chains, do not differ in strength compared to the unsubstituted H-bond in well-solvating solvents,<sup>[7]</sup> a significant effect on the formation of different host–guest complexes observed from the local micro-environment on the associating H-bonds in case of attached polymers with reduced solubility.

We and others in the past have investigated the competing phase segregation effects in supramolecular polymers bearing H-bonds in both solutions and the solid state, wherein the molecular recognition elements are based on multiple H-bonding moieties (see Figure 1a), such as the thymine-diaminopyridine (THY-DAP), the thymine-diaminotriazine (THY-DAT), the ureidopyrimidinone dimers (UPy-UPy), and Hamilton-receptor-barbiturate (HW Ba) host–guest complexes.<sup>[1b,c,3,8]</sup> By tuning the segregation between the polymer chains, H-bonded supramolecular dendrons can be formed, displaying a complex assembly behavior into nanophases or the formation of (chain-extended) pseudo-block copolymers.<sup>[9]</sup> While attractive H-bond-

[a] C. Li, P. Mai, N. Festag, A. Marinow, W. H. Binder  
Faculty of Natural Science II, Institute of Chemistry, Macromolecular Chemistry, Martin Luther University Halle-Wittenberg, von-Danckelmann-Platz 4, Halle/Saale D-06120, Germany  
E-mail: wolfgang.binder@chemie.uni-halle.de

Supporting information for this article is available on the WWW under <https://doi.org/10.1002/chem.202403939>

© 2024 The Author(s). Chemistry - A European Journal published by Wiley-VCH GmbH. This is an open access article under the terms of the Creative Commons Attribution Non-Commercial License, which permits use, distribution and reproduction in any medium, provided the original work is properly cited and is not used for commercial purposes.



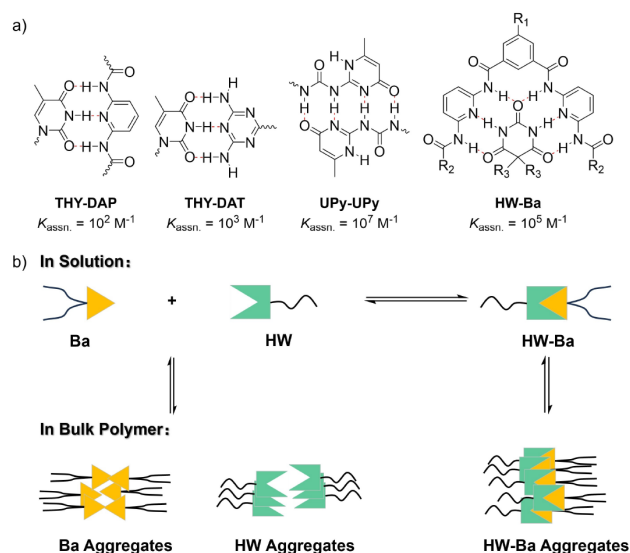


**Figure 1.** a) The molecular recognition elements of thymine-diaminopyridine (THY-DAP), thymine-diaminotriazine (THY-DAT), ureidopyrimidinone dimer (UPy-UPy), and Hamilton receptor-barbiturate (HW-Ba) host-guest complexes based on multiple H-bonds (values of the association constants  $K_{\text{assn.}}$  were taken from ref. [14]); b) possible association between HW and Ba in solution and bulk polymer forming aggregates and the backbone segregation during the assembly process.

ing in solution usually exceeds phase segregation effects between the polymer chains, the situation is different in polymers devoid of solvent, either in the melt state, the (semi-)crystalline or liquid crystalline state,<sup>[10]</sup> as now segregation can become dominant over the attractive H-bonding, also leading to clustering effects not observed in solution (see Figure 1b). Methods to study dynamics and thermodynamics of bond-breaking/reformation are currently only indirect ones, mainly using melt rheology<sup>[11]</sup> or magic-angle spinning (MAS) NMR spectroscopy<sup>[1b,12]</sup> with cluster sizes estimated by X-ray techniques.<sup>[1b,6c,11a,h,13]</sup>

Multiple H-bonding systems, such as the UPy-UPy or the HW-Ba, have become crucial for generating stable and reversible bonds in bulk-polymers. The HW-Ba host-guest complexes herein have been intensely studied in solutions, displaying a strong and specific assembly with an association constant  $K_{\text{assn.}}$  up to  $10^6 \text{ M}^{-1}$ <sup>[15]</sup> and a directional nature owing to the stereo-specified sextuple H-bonds, resulting in distinct 1:1 complexes in solution. Various chemical modifications have been accomplished to tune the assembly behavior of the HW receptor by modifying substituents at the outer rim<sup>[13f,16]</sup> or forming cyclic HW receptors.<sup>[16c,17]</sup> These modifications open the possibility of embedding further functionalities for a subsequent covalent modification to study the assembly processes between the HW-Ba system, as well as further by a covalent fixation after H-bonding formation, a strategy similar to the concept of Scherman and Meijer.<sup>[18]</sup> Herein, a cross-metathesis (CM) chemistry of adjacent ene-functionalities linked to the HW and Ba molecules was used to fix the specific H-bonded assembly of the HW-Ba host-guest complexes. We here present a method to investigate H-bond clustering effects in solutions

and bulk-polymers using covalent CM chemistry to tether transient or thermodynamically stable structures. This approach provides direct information that often is not accessible through spectroscopic methods. Our approach (see Figure 2) is based on a combination of supramolecular assembly via sextuple H-bonds between a novel Hamilton receptor (H) bearing cyclopentene moieties at the outer rim, and allobarbiturate (B) with allyl groups, followed by CM reactions to fix the formed assemblies covalently, which were subsequently analyzed by electrospray ionization mass spectrometry (ESI MS). We conducted this two-step covalent-fixation-ESI-analysis in different solvents at various concentrations of the H-B supramolecular binding partners as a proof-of-principle study, followed by a preliminary investigation inside a solvent-free polyisobutylene (PIB) matrix, finally aiming to understand the behavior of such supramolecular bonds in nonsolvating polymeric environments.

## Results and Discussion

### Model Hamilton Receptor-Barbiturate (H-B) Host-Guest Chemistry in Solution

Since the first reports on synthesizing the Hamilton receptor for barbiturates in the 1980s to 1990s,<sup>[15,19]</sup> variations of such receptors have been generated with multifold structures and functionalities.<sup>[13f,16b,d,17d,20]</sup> We herein designed a novel Hamilton receptor H bearing cyclopentene moieties at its outer rim (Figure 2), able to undergo a subsequent CM reaction with Grubbs catalysts. The cyclopentene moieties at the outer rim of the Hamilton receptor were expected to change the specific formation of the desired host-guest complex with barbiturates only slightly, analogous to other modifications of the Hamilton receptors reported previously.<sup>[17d,20b,e,21]</sup> Similarly, the bis-allyl-barbiturate B has been equipped with CM-reactive allyl groups on the C5 position, prepared as described in the supporting information (for the detailed synthesis, see *Supporting Informa-*

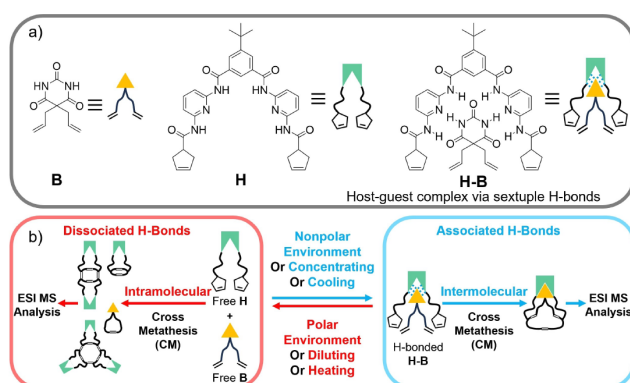


**Figure 2.** a) Chemical structures and schematic illustration of the model Hamilton receptor H and barbiturate B and their host-guest complex via sextuple H-bonds; b) the concept of this work: upon concentrating, cooling, or in a nonpolar environment, H and B associate to form a specific H-B assembly and higher-order assemblies (=aggregates); upon diluting, heating, or in a polar environment, H and B dissociate and cross-metathesis (CM) can be used to fix host/guest assemblies for subsequent ESI MS analysis.

tion, SI 1.3). Conceptually, the 1:1 H B host–guest complex can be fixed covalently after its formation. However, it also allows the detection of other formed complexes of different stoichiometry by ESI MS measurements to reveal their chemical nature and relative amounts. In bulk polymers, then devoid of solvents, we previously observed the formation of host–guest complexes different from the 1:1 stoichiometry in solution induced by phase segregation effects from the polymer chains.<sup>[1b,3b,13d,22]</sup> Here, the approach using covalent crosslinking via CM after forming the host–guest complexes presents a first step to reveal such host–guest structures inside the solvent-free environment.

To explore the influence (solvents, temperature) on the formation of the host–guest complexes of the modified H with B, the association constant  $K_{\text{assn.}}$  of the H B complex was determined in various solvents. As reported previously,<sup>[24]</sup> titration, in-situe followed by UV-Vis spectroscopy was employed due to its fast and sensitive determination and the low demand on the amount of the substrates. As depicted in Figure 3a), data collected from the UV titration were mathematically fitted to generate such a curve to obtain the  $K_{\text{assn.}}$  under different conditions using the online program BindFit (available via <http://supramolecular.org>;<sup>[24,25]</sup> for UV titration, fitting, and method details, see *Supporting Information*, SI 2). All the

determined  $K_{\text{assn.}}$ s are listed in Table 1. In Figure 3b), the association constants  $K_{\text{assn.}}$ s of H with B in various solvents are plotted against their dielectric constants,<sup>[23]</sup> indicative of the effects of solvent polarity on the stability of the H B complex. As expected, in toluene (Tol) the H B host–guest complex displays the highest stability with  $K_{\text{assn.}}$  equal to  $\sim 10^5 \text{ M}^{-1}$ , while in the halogenated solvents such as chloroform ( $\text{CHCl}_3$ ) and dichloromethane (DCM),  $K_{\text{assn.}}$  is reduced by an order of magnitude to  $\sim 10^4 \text{ M}^{-1}$ . In 1,2-dichloroethane (DCE), the H B association is further weakened to  $K_{\text{assn.}} \sim 10^3 \text{ M}^{-1}$ . Interestingly, in  $\alpha, \alpha, \alpha$ -trifluorotoluene (TFT), a solvent comparable to Tol but with an enhanced polarity and distinct fluorophilicity, the H B complex displays a surprising stability (see Entry S15 in Table 1), aligning with previously reported solvophobic interactions<sup>[26]</sup> that can enhance the H-bond strength. As expected, all other polar solvents (such as 1,4-dioxane, hexafluoro-2-propanol, isopropanol, acetonitrile, and THF, see Entry S4–S13) strongly reduce the stability of the host–guest complex, with association constants  $K_{\text{assn.}}$ s in the range of  $\sim 10^2 \text{ M}^{-1}$ . To further examine that the addition of extra donors/acceptors, besides polarity, leads to the reduction of H-bond strength,  $K_{\text{assn.}}$  of the H B complex was determined in toluene-methanol mixtures with increasing content of MeOH in Tol to detect the critical concentration of MeOH required to reduce the stability of the

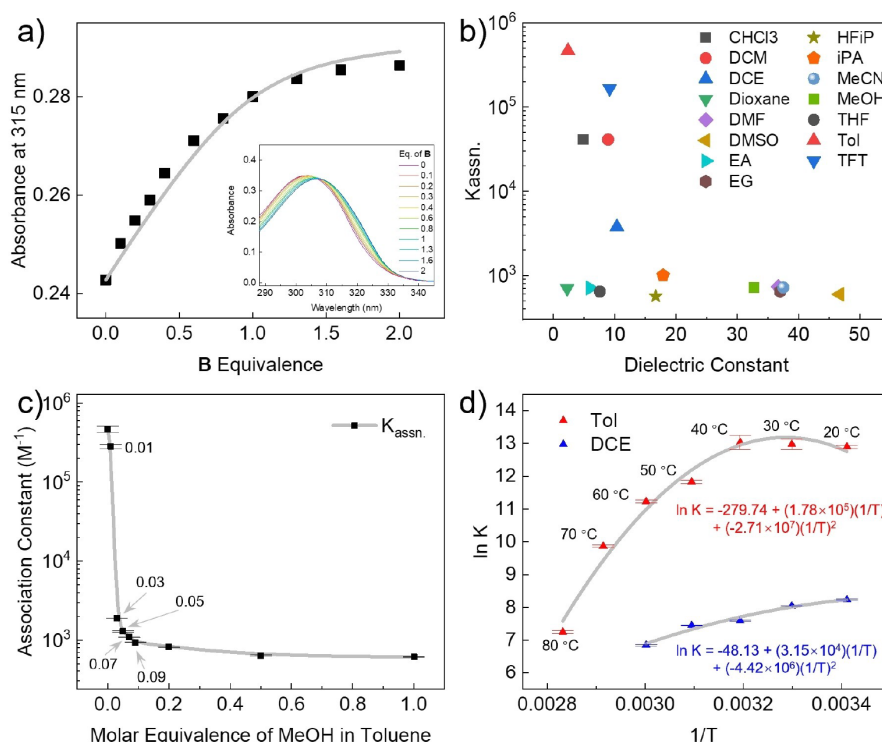


**Figure 3.** a) Data fitting from UV-Vis spectroscopy titration to determine the association constant  $K_{\text{assn.}}$  (figure-insert shows the UV-Vis spectrum at different [H]:[B] ratios); association constants  $K_{\text{assn.}}$  of the H B model host–guest complex in various solvents at 20 °C plotted against their dielectric constants taken from the literature [23]; the detailed  $K_{\text{assn.}}$ s are listed in Table 1 (each determination was repeated 3–5 times to ensure reproducibility; for titration, fitting, and method details, see *Supporting Information*, SI 2); c) association constants of the H B model in toluene + methanol mixtures (the line is a guide for the eye only; error bars are based on fitting errors); d) van't Hoff plot of association constants of the model compounds in toluene (Tol) and 1,2-dichloroethane (DCE) at various temperatures (grey curves and equations are from the fitting of data using a polynomial function; error bars are based on fitting errors; for fitting details, see *Supporting Information*, SI 2.2).

**Table 1.** Dielectric constants of solvents and association constants  $K_{\text{assn.}}$  and the Gibbs-energy ( $\Delta G$ ) of the **H B** model host–guest complex in various solvents.

Entry	Solvent	Abbreviation	Dielectric Constant <sup>[a]</sup>	$K_{\text{assn.}} / \text{M}^{-1}$ <sup>[b]</sup>	$\Delta G / \text{kJ mol}^{-1}$ <sup>[c]</sup>
S1	Chloroform	$\text{CHCl}_3$	4.8	$4.13 \times 10^4$	25.9
S2	Dichloromethane	DCM	8.9	$4.12 \times 10^4$	25.9
S3	1,2-Dichloroethane	DCE	10.4	$3.78 \times 10^3$	20.1
S4	1,4-Dioxane	Dioxane	2.2	$7.02 \times 10^2$	16.0
S5	N,N-Dimethylformamide	DMF	36.7	$7.34 \times 10^2$	16.1
S6	Dimethyl Sulfoxide	DMSO	46.7	$5.96 \times 10^2$	15.6
S7	Ethyl Acetate	EA	6.0	$7.08 \times 10^2$	16.0
S8	Ethylene Glycol	EG	37.0	$6.46 \times 10^2$	15.8
S9	Hexafluoro-2-propanol	HFiP	16.7	$5.66 \times 10^2$	15.4
S10	2-Propanol	iPA	17.9	$9.99 \times 10^2$	16.8
S11	Acetonitrile	MeCN	37.5	$7.18 \times 10^2$	16.0
S12	Methanol	MeOH	32.7	$7.12 \times 10^2$	16.0
S13	Tetrahydrofuran	THF	7.6	$6.44 \times 10^2$	15.8
S14	Toluene	Tol	2.4	$4.69 \times 10^5$	31.8
S15	$\alpha, \alpha, \alpha$ -Trifluorotoluene	TFT	9.2	$1.67 \times 10^5$	29.3

\* [a] The dielectric constants were taken from the ref. [23]; [b] determined by UV-Vis spectroscopy titration at 20 °C (each determination was repeated 3–5 times to ensure reproducibility; for details, see *Supporting Information*, SI 2); [c] calculated by  $\Delta G = RT \ln K_{\text{assn.}}$

host–guest complex. As demonstrated in Figure 3c), as the MeOH content increases up to a molar ratio of  $\text{MeOH}/\text{Tol} = 0.03$  ( $\text{MeOH} = 0.03$ ,  $\text{Tol} = 1$ ), the stability indicated by  $K_{\text{assn.}}$  is reduced significantly by two orders of magnitude. A further increase of the MeOH content to 0.2 equivalents further reduces the stability ( $K_{\text{assn.}}$  to  $\sim 10^2 \text{ M}^{-1}$ ) comparable to that in other polar or H-bonding-replacing solvents, such as HFiP, EA, and DMSO. This extreme reduction in  $K_{\text{assn.}}$  upon the addition of MeOH to Tol demonstrates that even a subtle change in the micromolecular environment, from a purely nonpolar aprotic medium to a slightly polar protic medium, can result in a significant weakening of the H-bonds in the **H B** model host–guest complex.

To probe the impact of the micro-environment on the thermodynamics of the **H B** host–guest complex, van't Hoff plots were employed as outlined in Figure 3d) in two different solvents (Tol, DCE) via temperature-dependent measurements. Similar to previously reported studies utilizing van't Hoff plot to analyze the thermodynamics of supramolecular systems,<sup>[27]</sup> including HW Ba complexes,<sup>[28]</sup> the  $K_{\text{assn.}}$  of the **H B** model host–guest complex obtained from UV titrations at various temperatures was fitted using a second-order polynomial function. This approach accounts for the nonlinearity arising from the non-constant standard enthalpy change over the selected temperature range (for fitting details, see *Supporting Information*, SI 2.2).<sup>[29]</sup> At temperatures of 20–40 °C the **H B** model complex remains stable with  $K_{\text{assn.}}$  unchanged but starts to decline at temperatures above 40 °C, while in DCE,  $K_{\text{assn.}}$  is steadily reduced as temperature increases, starting from 20 °C and thereon, indicating different contributions from enthalpic and entropic factors. Indeed, known from the enthalpy change  $\Delta H$  and the entropy change  $\Delta S$  (see Table 2) obtained from the fitting, at a temperature below 40 °C, the association of the **H B**

model complex in Tol is largely entropy-driven, while that in DCE is a largely enthalpy-driven process over the whole temperature range (20–60 °C). Additionally, as temperature increases, the absolute value of the Gibbs energy change  $\Delta G$  determined in Tol decreases, indicative of a reduced association between the model **H** and **B**. However, the temperature effect in DCE is less significant, evidenced by the barely changed  $\Delta G$  over the whole temperature range. Therefore, the molecular surroundings indeed affect the thermodynamics of the **H B** model complex by altering the contribution of the enthalpy and the entropy of the H-bonding process.

### Probing Covalent Fixation of the **H B** Host–Guest Complexes via Cross-Metathesis (CM) Chemistry

Several reactions were carried out to covalently fix the **H B** model host–guest complexes with a 1:1 stoichiometry  $[\text{H}]:[\text{B}]$  and aggregates with different stoichiometries (e.g., dimer **cm-HH**, trimer **cm-HHH**, and others as indicated) under various conditions (see Table 3) using cross-metathesis (**CM**) reaction. As illustrated in Figure 4a), the **H** and **B** model compounds, the Grubbs catalyst (10%mol), and the degassed solvent were placed in a vial in a glovebox with an  $\text{N}_2$  atmosphere. The vial was heated for 24 hours before  $^1\text{H}$  NMR spectroscopy was used to prove the conversion by monitoring the resonances of the initial alkenes at  $\delta = 5.62, 5.36, 4.95$ , and  $4.82$  ppm vs. the newly formed alkenes at  $\delta = 5.57, 5.25$ , and  $5.19$  ppm. Details of the reaction, the conversion, the catalysts, and the concentrations used are shown in Table 3. For Entry 1, the reaction was carried out at 100 °C in Tol with 0.01 M as the concentration of **H** or **B** in a ratio of 1:1. Grubbs catalyst 3<sup>rd</sup> generation (G3) was chosen



**Table 2.** Enthalpy  $\Delta H$ , entropy  $\Delta S$ , and the Gibbs energy  $\Delta G$  of the **H B** model host–guest complex in toluene (Tol) and 1,2-dichloroethane (DCE) at various temperatures.

T / °C	T / K	In Toluene (Tol)			In 1,2-Dichloroethane (DCE)		
		$\Delta H$ /kJ mol <sup>-1</sup>	$\Delta S$ /kJ mol <sup>-1</sup> K <sup>-1</sup>	$\Delta G$ /kJ mol <sup>-1</sup>	$\Delta H$ /kJ mol <sup>-1</sup>	$\Delta S$ /kJ mol <sup>-1</sup> K <sup>-1</sup>	$\Delta G$ /kJ mol <sup>-1</sup>
20	293	58.06	0.30	29.47	11.88	0.03	20.06
30	303	7.30	0.13	31.59	20.16	0.00	20.20
40	313	40.22	0.03	32.09	27.91	0.03	20.07
50	323	84.79	0.17	31.12	35.18	0.05	19.70
60	333	126.68	0.29	28.81	42.01	0.07	19.12
70	343	166.13	0.41	25.28	–	–	–
80	353	203.35	0.52	20.63	–	–	–

\* The enthalpy  $\Delta H$ , the entropy  $\Delta S$ , and the Gibbs energy  $\Delta G$  of the **H B** model host–guest complex were calculated from the constants obtained from the fitting of the Figure 3d); for fitting details, *Supporting Information*, SI 2.2.

**Table 3.** Reaction conditions for the cross-metathesis (CM) reaction to fix the **H B** model complex and their possible aggregates, and the conversion calculated by <sup>1</sup>H NMR spectra.

Entry	T / °C	Solvent	Concentration / M [a]	Catalyst [b]	Conversion [c]
1	100	Tol-d <sub>8</sub>	0.01	G3	100 %
2	50	Tol-d <sub>8</sub>	0.01	G3	89.4 %
3	50	DCE	0.1	G3	89.5 %
4	50	MeOD	0.01	G3	78.8 %
5	50	DCE	0.1	G2	97.6 %
6	50	PIB <sup>d)</sup>	–	G3	97.3 %

\* [a] Concentration refers to **H** or **B** in a 1:1 ratio; [b] G3: Grubbs catalyst 3<sup>rd</sup> generation; G2: Grubbs catalyst 2<sup>nd</sup> generation; catalyst load was kept at 10 % mol for all entries; all reactions were carried out in a glovebox under an N<sub>2</sub> atmosphere; [c] the conversion was calculated by the ratio of the integral of unreacted alkene and the product ene; for detailed calculations and NMR spectra for all entries, see *Supporting Information*, SI 3; [d] **PIB** was used as the reaction matrix; for detailed experimental conditions and process, see *Supporting Information*, SI 1.3.

due to its known fast initiation for **CM** reactions, allowing an efficient fixation of the **H B** model complex and its potential aggregates. As shown in Figure 4b), a complete conversion of model compounds could be observed as evidenced by the shifted <sup>1</sup>H resonances of the alkenes (from  $\delta$  = 5.62 in the black spectrum to  $\delta$  = 5.57 ppm in the red spectrum) and the disappearance of the alkene protons ( $\delta$  = 5.36, 4.95, and 4.82 in the red spectrum) and the newly formed alkene peak at  $\delta$  = 5.58 ppm as compared to the control NMR spectrum in black. At a reaction temperature of 100 °C, the stability of the H-bonds is strongly reduced, as is consequently the formation of the **H B** host–guest complex. Therefore, a reaction at 50 °C with other conditions was carried out, as shown in Entry 2. In Figure 4b), the NMR spectrum (shown in blue) shows a conversion of 89.4%, as demonstrated by the residual alkene protons from **B**. Owing to the limited solubility of the components at 50 °C, DCE was used as a non-H-bond-replacing solvent to offer a higher concentration of the **H** and **B** (Entry 3), expected to lead to higher stabilities of the host–guest complex

**H B**. We also conducted a trial in MeOH (Entry 4), anticipated to reduce the formation of specific **H B** host–guest complexes. Furthermore, Grubbs catalyst 2<sup>nd</sup> generation (G2) was also tested (Entry 5), which showed a slightly higher conversion at 50 °C. We further conducted the **CM** reaction of the **H** and **B** model compounds directly inside a bulk polyisobutylene (**PIB**) devoid of solvent to probe the formation of aggregates inside a solvent-free environment (Entry 6). In this reaction (see the experimental setup in Figure 7), the **H** and **B** model compounds were mixed with the Grubbs catalyst and the **PIB** polymer at room temperature using THF to reach homogeneity, followed by a quick evaporation of THF at room temperature in vacuum to avoid **CM** in the solution state. Subsequently, the reaction was heated at 50 °C in a glovebox under an N<sub>2</sub> atmosphere for 24 hours, and the conversion of this reaction (see Table 3, Entry 6) demonstrates a successful **CM** reaction inside the **PIB**. Overall, the data indicate that a successful **CM** reaction can be employed, both in solution and the solid state, to generate a conversion of **CM** ranging from 78–100 %, using either G3 or G2 catalysts at temperatures (50 °C) where the **H B** host–guest complexes are expected to be formed, together with potential formation of other aggregates.

### ESI MS Analysis of the Covalently Fixed Complexes from Cross-Metathesis (CM) Reactions

Subsequently, the reaction mixtures were analyzed using ESI MS to identify the products formed via the **CM** reaction. Potentially, these products can consist of a) the cyclic reactants (**cm-H** or **cm-B**) resulting from intramolecular **CM** reactions (macrocyclization of individual **H** or **B** model compounds); and b) from 1:1 host–guest complexes (**cm-HB**) or from other aggregates formed via H-bonds and fixed through intermolecular **CM** reactions (examples are **cm-HH**, **cm-HHH**). The analysis by ESI MS was conducted firstly qualitatively to identify specific forms. Using Entry 1 as an example, as shown in Figure 5a), the products via the intramolecular **CM** were found as cyclized **cm-B** and **cm-H**, resulting from the ring-closing of the allyl/

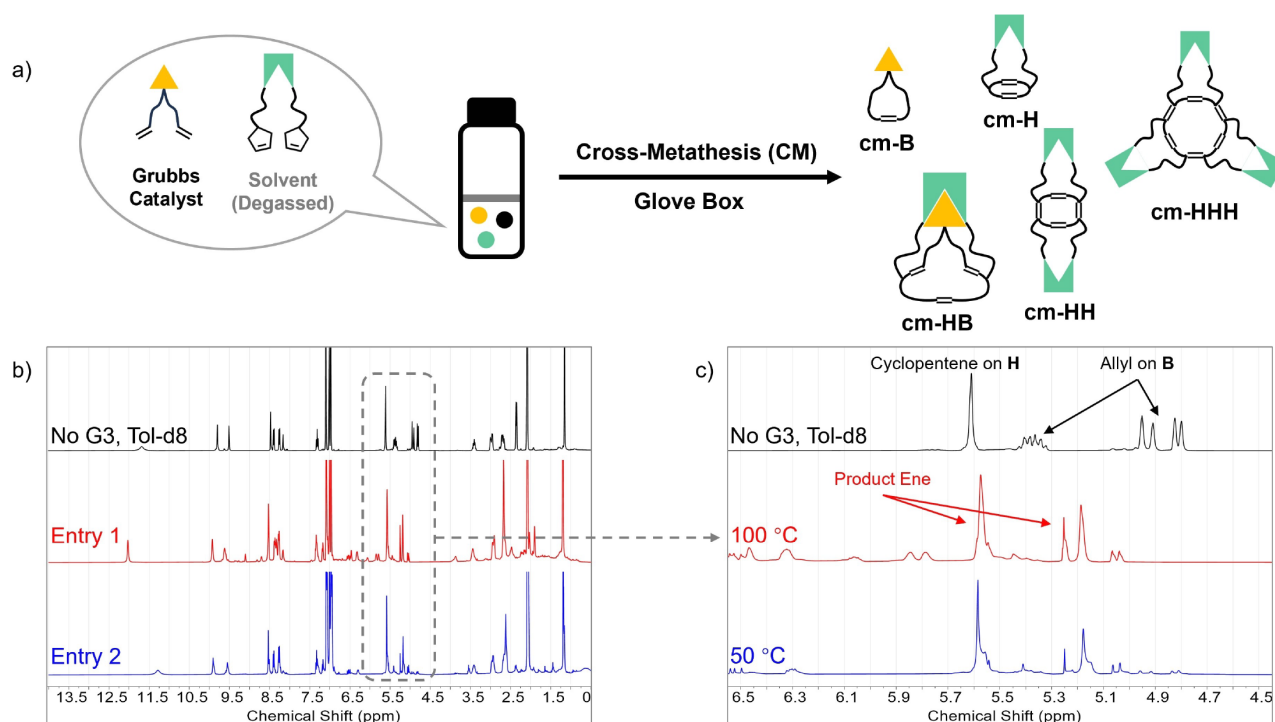


**Figure 4.** a) Schematic explanation to conduct cross-metathesis (CM) reactions to fix the H B model complexes; forming oligomers (representative structures cm-B, cm-H, cm-HB, cm-HH, cm-HHH are shown) b)  $^1\text{H}$  NMR spectrum of the reaction mixture from Entry 1 and 2, see Table 3; The zoom-in of the double bond region of the  $^1\text{H}$  NMR spectrum.

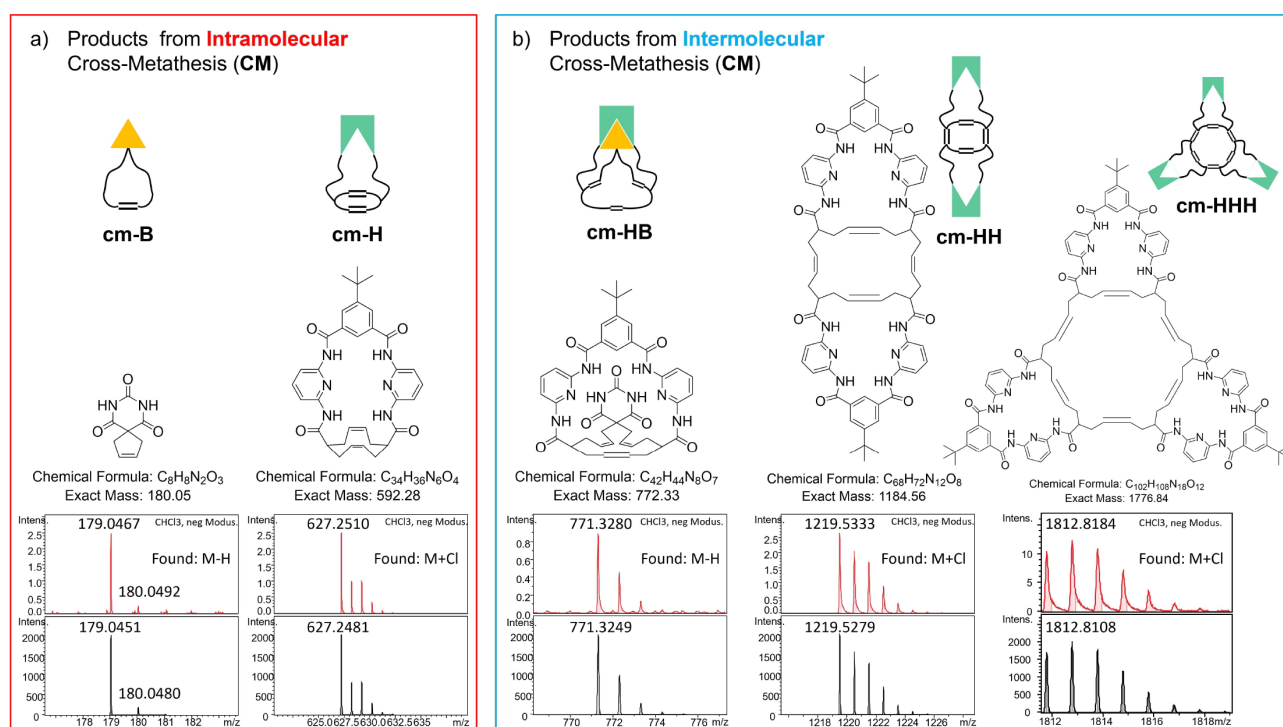


**Figure 5.** Representative products from Entry 1 (experimental condition: Tol-d<sub>8</sub>, H or B in a 1:1 ratio at 0.01 M, G3 catalyst) found by ESI MS using negative modus without salt (for simulation of all ions, constitutional isomers, and intermediates from cross-metathesis reactions for all entries, see the attached Supporting Information, SI 3 and SI PDF file: ESI Analysis\_All Entries).

cyclopentene moieties in a single molecule. As depicted in Figure 5b), the model host–guest complex fixed by the CM

reaction was found as cm-HB. Although the temperature was kept to 100 °C, a pretty harsh condition to maintain the host–

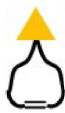




guest complex, **cm-HB**, **cm-HH**, and **cm-HHH** complexes were identified, with the dimers (**cm-HH**) and trimers (**cm-HHH**) being present, beyond our expectation, which were identified by the ESI MS analysis (the constitutional isomers of **cm-HH** and **cm-HHH** can be found in *Supporting Information*, SI 3). These oligomers can be attributed to the self-association of **H** and the potentially higher reactivity of the cyclopentene moieties compared to the allyl groups on **B**. Probing different reaction conditions (see Table 3), we could identify all those products with different temperatures and concentrations (as possible and partially limited by the reduced solubility of **H** and **B** under specific conditions). Nevertheless, the intermediate product bearing a styrene residue from the Grubbs catalyst was found for all entries, together demonstrating the successful **CM** reactions affording the similarly fixed individual model compounds and their possible aggregates (for the analysis of all products and intermediates for all entries, see *Supporting Information*, SI 3, and the attached PDF file: ESI Analysis\_All Entries).

We then went one step further to reveal the relative ratios of the different ions of the different host–guest complexes since ESI MS not only can qualitatively identify the products<sup>[30]</sup> but also allows us to semi-quantitatively extract the relative ratios among the **CM** products, which are essential to further study changes in response to different reaction conditions (concentration, solvent, temperature). In line with previous work on protein/lipid complexes,<sup>[31]</sup> we used the intensity of individual peaks representing a specific product to calculate the normalized product percentage within one measurement, provided that all **CM** products have similar structures and should demonstrate equal ionization in the ESI process. As there are multiple ions for one **CM** product, the intensity of all the relevant ion couplings for this respective product was summed as cumulative intensity and used for calculation (for calculation details, see *Supporting Information*, SI 3).

Indeed, the fixed H-bond-mediated products demonstrate different normalized product ratios due to the applied conditions influencing the H-bonds. The calculation and the analysis results for all entries are summarized in Table 4, with the schematic formulas provided therein, focusing on the major products detected and identified via ESI MS. In Entry 1–6, the **CM** product of **cm-B** is present in only a negligible percentage. This low percentage of **cm-B** could result from the low reactivity of the allyl group to form the target cyclopentene ring, impeding the ring-closing **CM** reactions catalyzed by the Grubbs catalyst. By contrast, due to the relatively low concentration applied and the high reactivity of cyclopentene moieties driven by the ring strain, the cyclic product **cm-H** shows the highest ratio among all products, ranging from 74.47% (Entry 4) to 95.22% (Entry 5). As the temperature was decreased from 100 °C (Entry 1) to 50 °C (Entry 2), expected to promote the formation of the **H B** host–guest complex via the intermolecular H-bonds, the amount of **cm-H** shows a decreasing ratio from 91.89% to 75.96%, with a concomitant increase of the fixed complex **cm-HB** from 1.62% to 4.62%. When concentration increased from 0.01 M (Entry 2) to 0.1 M (Entry 3), the formation of the **H B** complex should be favored, visible by the now changed product (**cm-HB**) ratio (4.62% vs. 9.07%), in line with expectations.

The experimental conditions (solvents, temperature) strongly influence the aggregation/association of the formed **CM** products. In Figure 6, the ratio of the fixed aggregated products, namely **cm-HB**, **cm-HH** for the dimer, and **cm-HHH** for the trimer, were plotted to illustrate the obtained product ratios. For Entry 1, using 100 °C in Tol-*d*<sub>8</sub> to fix the aggregates with a quantitative conversion, most H-bonds accounting for the formation of the host–guest complexes were also destroyed, showing the product **cm-HB** as a consequence with the lowest percentage of 1.63%, comparable to that in Entry 4 where the H-bond-replacing solvent MeOD was used though at 50 °C. These two comparable amounts of the **H B** host–guest

**Table 4.** Normalized product percentages calculated based on ESI MS intensities of each product.

Entry <sup>[a]</sup>	Experimental Conditions					
		cm-B	cm-H	cm-HH <sup>[b]</sup>	cm-HHH <sup>[b]</sup>	cm-HB
1	Tol- <i>d</i> <sub>8</sub> _100 °C_0.01 M	0.24 %	91.89 %	5.93 %	0.23 %	1.63 %
2	Tol- <i>d</i> <sub>8</sub> _50 °C_0.01 M	0.31 %	75.96 %	12.81 %	6.30 %	4.62 %
3	DCE_50 °C_0.1 M	–	87.98 %	2.55 %	0.40 %	9.07 %
4	MeOD_50 °C_0.01 M	0.08 %	74.47 %	15.25 %	8.35 %	1.84 %
5	DCE_50 °C_0.1 M_G2	–	95.22 %	2.16 %	0.32 %	2.30 %
6	PIB_50 °C	1.67 %	81.12 %	7.01 %	2.92 %	7.28 %

\* [a] The normalized percentages were calculated based on the cumulative intensity of the products in ESI MS spectra; for detailed calculation, see *Supporting Information*, SI 3; [b] the structures of **cm-HH** and **cm-HHH** here were selected as representatives, and their constitutional isomers can be found in the *Supporting Information*, SI 3.



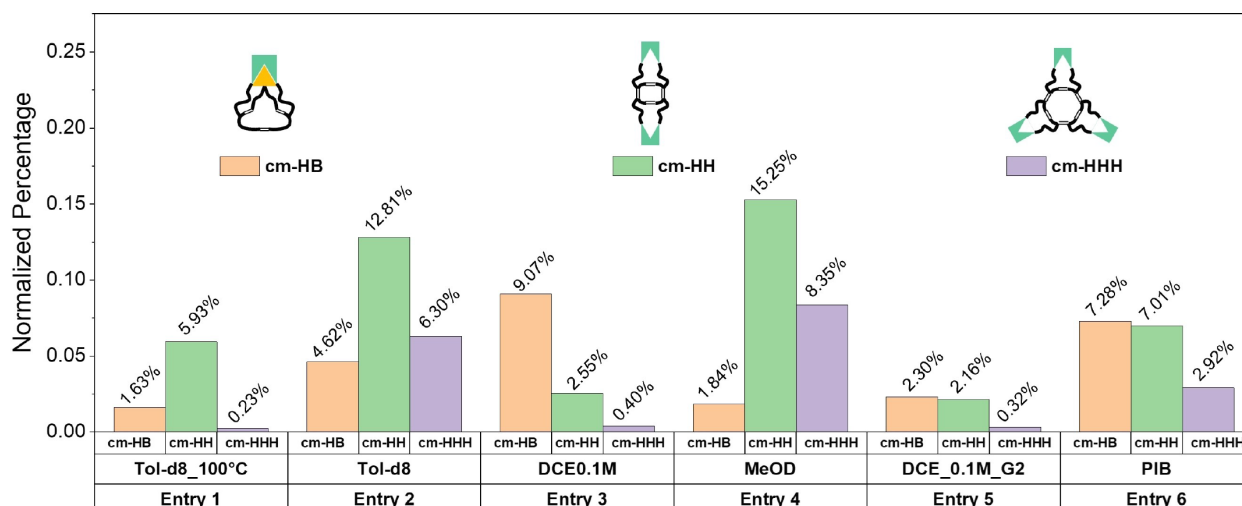


**Figure 6.** Normalized percentage of selected products for Entry 1–6 (the normalized percentage was calculated based on the cumulative intensity of the products in ESI MS spectra; for detailed calculation, see *Supporting Information*, SI 3; the structures of **cm-HH** and **cm-HHH** here were selected as representatives, and their constitutional isomers can be found in *Supporting Information*, SI 3.)

complex in Tol at 100 °C and in MeOH at 50 °C reveal that elevation of temperature weakens the H-bonds and the resulting host–guest complex in a similar manner as the change of the solvent from an H-bond-maintaining Tol-*d*<sub>8</sub> to an H-bond-replacing MeOD. When the temperature was reduced to 50 °C (Entry 2), the percentage of the dimeric aggregate, **cm-HH**, increased to 4.62%, as expected. Increasing the concentration of the reactants **H** and **B** to 0.1 M (Entry 3) led to an increase in the specific **H B** host–guest complex, yielding **cm-HB** with the highest percentage of 9.07% among all the products. Owing to the promoted reactivity of cyclopentene moieties on **H** in **CM** reaction compared to allyl groups on **B**, in Entry 1, 2, and 4, the aggregated **cm-HH** and **cm-HHH** demonstrate higher percentages than the associated **cm-HB**. However, this ratio is lower than **cm-HB** if the solvent is replaced by DCE (Entry 3 and 5). For Entry 4, though MeOH was added to the reaction medium, **cm-HH** and **cm-HHH** are formed in high percentages, which we attribute to the closer proximity among the aromatic rings driven by hydrophobic interaction from pi-pi stacking over the now strongly diminished H-bonds as destroyed by the polar protic nature of MeOH.

#### Cross-Metathesis (CM) Reaction in a Solvent-Free Polymeric Environment - inside a Polyisobutylene (PIB) Matrix

As described in Table 3 and Table 4, Entry 6 **CM** was conducted to fix the **H B** model host–guest complex and the possible aggregates inside a **PIB** matrix and further subject to the ESI MS analysis. As illustrated in Figure 7a), the **H** and **B** model compounds, the G3 catalyst, and the **PIB** matrix (*M<sub>n</sub>* = 1300 Da)

were placed in a vial, and degassed THF was added. After all components were dissolved, THF was removed at room temperature using a rotary evaporator, followed by an ultra-high vacuum to remove all THF residue. After refilling with argon, the vial was heated at 50 °C in a glovebox to promote the **CM** reaction. After 24 hours, the reaction was removed from the glovebox and diluted with a minimum amount of THF, followed by digestion in *n*-hexane and MeOH to separate the **PIB** matrix from the formed **CM** products in a separation funnel. After recovery from the MeOH phase, the herein soluble products (devoid of the **PIB** matrix, which was selectively removed by the *n*-hexane) were analyzed firstly via <sup>1</sup>H NMR spectroscopy to prove conversion (see Figures 7b&c). As the **CM** reaction was conducted without a solvent, different ratios of the host–guest complexes were expected to form. The chemical shifts of the alkene moieties at δ = 5.65 and 5.20 ppm of **B** vanished almost completely, and a new singlet peak at δ = 5.65 ppm was formed, indicative of a successful **CM** reaction. In addition, the starting resonances **H** at δ = 5.74 ppm vanished, with a new resonance appearing at δ = 5.72 ppm, demonstrating the conversion of the model compounds (97.3%, see Table 3, Entry 6). Further, the fixed complexes/aggregates were analyzed by the method developed previously using ESI MS. As depicted in Figure 6, the fixed host–guest **cm-HB** demonstrates a product ratio of 7.28%, comparable to that in Entry 3 using a 0.1 M model compound concentration. The fixed dimer **cm-HH** was found with a product ratio of 7.01% for the aggregated products. In comparison, the fixed trimer **cm-HHH** demonstrated the highest ratio of 2.92% among all entries due to the promoted aggregation by the nonpolar and non-H-bond-replacing **PIB** bulk.

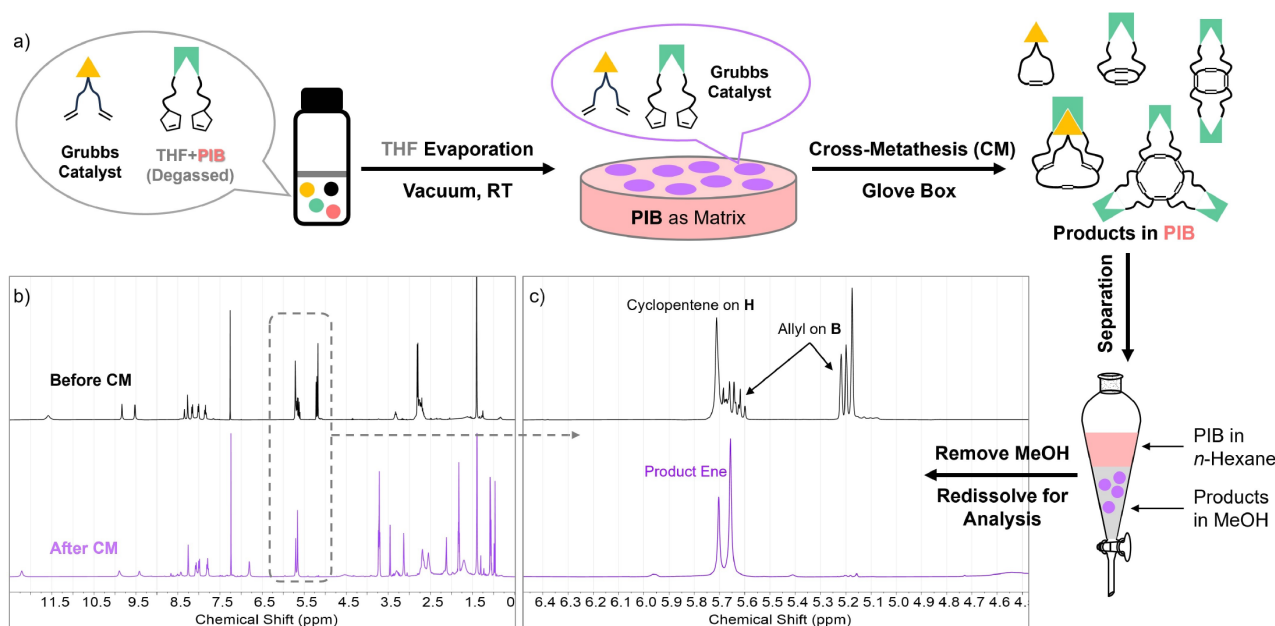


**Figure 7.** a) Schematic explanation of cross-metathesis (CM) reaction in a polyisobutylene (PIB) matrix and the workup to remove PIB matrix; b)  $^1\text{H}$  NMR (in  $\text{CDCl}_3$ ) of the products mixture before the addition of catalyst and after workup to remove PIB matrix; c) zoom-in of the double bond region of the  $^1\text{H}$  NMR spectrum; the vanish of the starting alkene shifts indicates the high conversion (97.3 %) of Entry 6 (see Table 3).

We further probed diffusion-ordered NMR spectroscopy (DOSY) to distinguish the different products based on their diffusion coefficients, similar to the reported identification of complex mixtures without separation.<sup>[32]</sup> After the workup, as described in Entry 6, the product mixture was directly probed. As shown in Figure 8, the newly formed alkene resonance at  $\delta = 5.65$  ppm and the peak at  $\delta = 5.72$  ppm can be clearly distinguished on the DOSY spectrum. Indicated by the yellow arrows, the resonances at  $\delta = 5.72$  & 3.25 and  $\delta = 1.0$ –1.5 ppm illustrate the CM products of barbiturate **cm-B** and the aggregated oligomers with a diffusion coefficient of  $6.50 \times 10^{-5} \text{ cm}^2 \text{ s}^{-1}$ . The alkene resonances at  $\delta = 5.68$  ppm (see

green arrows), together with the phenyl-resonances (Ph) at  $\delta = 7.5$ –8.5 ppm, demonstrate a reduced diffusion coefficient of  $5.50 \times 10^{-5} \text{ cm}^2 \text{ s}^{-1}$ , which can be assigned to the fixed host-guest complex **cm-HB** as well as the aggregated products **cm-HH** and **cm-HHH**. Thus, with the assistance of DOSY, various products can be further identified without separation. When our method for aggregate analysis is applied to study H-bonded aggregates in polymers, the resulting CM products with polymeric backbones can be distinguished by DOSY, hence facilitating the MS analysis which is typically more challenging when dealing with polymers.

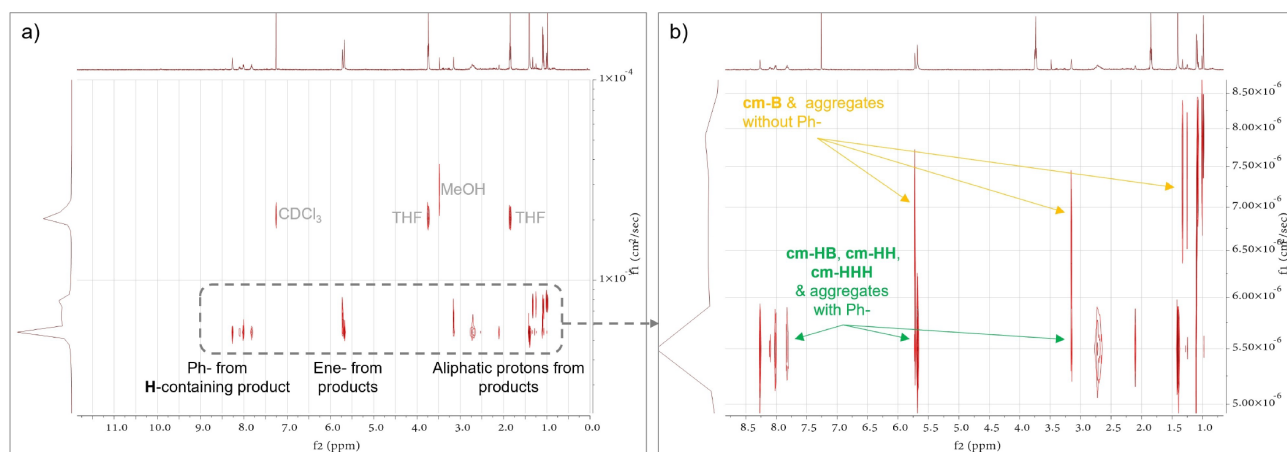


**Figure 8.** a) Diffusion-ordered NMR spectroscopy (DOSY) spectrum of the products mixture from Entry 6 directly after workup; b) the zoom-in of the region of product signals. (the alkene and other shifts referred by the yellow arrows are attributed to the fixed products of **cm-B** and possible aggregates as evidenced by a lack of phenyl (Ph) shifts, while the alkene and other shifts referred by the green arrows are attributed to the fixed products **cm-HB**, as well as the aggregated products **cm-HH** and **cm-HHH**).

## Conclusions

We here experimentally probed the formation of host–guest complexes of Hamilton receptor–barbiturate (**H B**) complexes, formed in solution and inside a polymer matrix, to probe the influence of a microenvironment on their supramolecular association behavior. A new method was developed to firstly covalently fix the H-bonded associates/aggregates via an alkene cross-metathesis (**CM**) reaction, followed by analysis of these then covalently linked aggregates using electrospray ionization mass spectrometry (ESI MS). To this end, a novel Hamilton receptor (**H**) was equipped with cyclopentene moieties and used as a host to form host–guest complexes with allobarbitol (**B**), as studied via UV-Vis spectroscopy titration experiments in different solvents and at various temperatures. These experiments allowed us to validate the formation of the specific host–guest complexes. Furthermore, it is observed that polar solvents containing additional H-bonding sites significantly reduce the formation of the 1:1 **H B** complex, indicated by an association constant of **H B**, weakened from  $K_{\text{assn.}} = \sim 10^5 \text{ M}^{-1}$  in toluene, to  $\sim 10^4 \text{ M}^{-1}$  in halogenated solvents (chloroform, DCM), further to  $\sim 10^3 \text{ M}^{-1}$  in 1,2-dichloroethane, and finally, to  $\sim 10^2 \text{ M}^{-1}$  in polar H-bonding-replacing solvents such as MeOH, HFIP, and DMSO. In addition, the presence of 0.2 equivalents of methanol in toluene significantly reduced  $K_{\text{assn.}}$  to  $\sim 10^2 \text{ M}^{-1}$ , comparable to other polar H-bonding-replacing solvents. To probe the cross-metathesis (**CM**) chemistry for covalent fixation of the H-bonded structures, we probed Grubbs 2<sup>nd</sup> and Grubbs 3<sup>rd</sup> generation catalysts under several reaction conditions (solvent, temperature, and concentration), identifying the optimal reaction conditions at 50 °C. Higher-order aggregates (dimers **cm-HH** and trimers **cm-HHH**, denoted after **CM** reactions) were covalently tethered via **CM** reaction, followed by electrospray ionization mass spectrometry (ESI MS) analysis. This two-step method, first a covalent **CM** fixation followed by ESI MS, was extended to study the **H B** model complex within a polyisobutylene (**PIB**) matrix, presenting a method to analyze the complex host–guest assemblies in solvent-free (polymeric) environments. The results indicated a higher percentage of H-bonded 1:1 **H B** assembly, **cm-HB**, and an increased amount of dimers, **cm-HH**, and trimers, **cm-HHH**, due to the closer proximity among the model compounds and the related segregation effects from the surrounding polymer matrix. This approach successfully established a two-step method to study H-bonded assemblies, allowing to be identified via ESI MS analysis, even inside concentrated or solvent-free systems, such as in a model polymer (polyisobutylene, **PIB**). This approach, therefore, opens a new perspective to reveal the formation of aggregates and complex assemblies, potentially avoiding the need for laborious physical characterizations such as SAXS/WAXS.

## Acknowledgements

The authors are grateful to the DFG project INST 271/444-1 FUGG for financial support; the DFG-Project BI1337/18-1,

BI1337/17-1, DFG-Project BI1337/16-1; BI1337/14-1 and the GRK 2670, W69000789, Project Nr 436494874. Open Access funding enabled and organized by Projekt DEAL.

## Conflict of Interests

The authors declare no conflict of interest.

## Data Availability Statement

The data that support the findings of this study are available in the supplementary material of this article.

**Keywords:** Aggregates · Association constants · Barbiturate · Hamilton receptor · Hydrogen bonds

- [1] a) T. Aida, E. W. Meijer, S. I. Stupp, *Science* **2012**, *335*, 813–817; b) S. Chen, T. Yan, M. Fischer, A. Mordvinkin, K. Saalwächter, T. Thurn-Albrecht, W. H. Binder, *Angew. Chem. Int. Ed.* **2017**, *56*, 13016–13020; c) S. Chen, W. H. Binder, *Acc. Chem. Res.* **2016**, *49*, 1409–1420; d) S. V. Wanasinghe, E. M. Schreiber, A. M. Thompson, J. L. Sparks, D. Konkolewicz, *Polym. Chem.* **2021**, *12*, 1975–1982.
- [2] A. J. Greenlee, C. I. Wendell, M. M. Cencer, S. D. Laffoon, J. S. Moore, *Trends Chem.* **2020**, *2*, 1043–1051.
- [3] a) C. Li, R. Bhandary, A. Marinow, D. Ivanov, M. Du, R. Androsch, W. H. Binder, *Polymers (Basel)* **2022**, *14*, 4090; b) S. Chen, Z. Li, Y. Wu, N. Mahmood, F. Lortie, J. Bernard, W. H. Binder, J. Zhu, *Angew. Chem. Int. Ed.* **2022**, *61*, e202203876; c) C. Li, P. Hilgeroth, N. Hasan, D. Ströhl, J. Kressler, W. H. Binder, *Int. J. Mol. Sci.* **2021**, *22*, 12679.
- [4] J. Sartorius, H.-J. Schneider, *Chem. Eur. J.* **1996**, *2*, 1446–1452.
- [5] S. Chen, N. Mahmood, M. Beiner, W. H. Binder, *Angew. Chem., Int. Ed.* **2015**, *54*, 10188–10192.
- [6] a) T. Yan, K. Schröter, F. Herbst, W. H. Binder, T. Thurn-Albrecht, *Macromolecules* **2017**, *50*, 2973–2985; b) X. Callies, C. Vechambre, C. Fonteneau, F. Herbst, J. M. Chenal, S. Pensec, L. Chazeau, W. H. Binder, L. Bouteiller, C. Creton, *Soft Matter* **2017**, *13*, 7979–7990; c) T. Yan, K. Schröter, F. Herbst, W. H. Binder, T. Thurn-Albrecht, *Macromolecules* **2014**, *47*, 2122–2130; d) F. Herbst, W. H. Binder, *Polym. Chem.* **2013**, *4*, 3602–3609.
- [7] a) F. Herbst, W. H. Binder, *Polym. Chem.* **2013**, *4*, 3602–3609; b) S. H. M. Söntjens, R. P. Sijbesma, M. H. P. van Genderen, E. W. Meijer, *J. Am. Chem. Soc.* **2000**, *122*, 7487–7493.
- [8] A. Mordvinkin, D. Döhler, W. H. Binder, R. H. Colby, K. Saalwächter, *Phys. Rev. Lett.* **2020**, *125*, 127801.
- [9] W. H. Binder, S. Bernstorff, C. Kluger, L. Petraru, M. J. Kunz, *Adv. Mater.* **2005**, *17*, 2824–2828.
- [10] S. Valkama, T. Ruotsalainen, A. Nykänen, A. Laiho, H. Kosonen, G. ten Brinke, O. Ikkala, J. Ruokolainen, *Macromolecules* **2006**, *39*, 9327–9336.
- [11] a) F. Herbst, K. Schröter, I. Gunkel, S. Gröger, T. Thurn-Albrecht, J. Balbach, W. H. Binder, *Macromolecules* **2010**, *43*, 10006–10016; b) M. Ahmadi, A. Jangizehi, S. Seiffert, *Macromolecules* **2022**, *55*, 5514–5526; c) X. Huang, S. Nakagawa, H. Houjou, N. Yoshie, *Macromolecules* **2021**, *54*, 4070–4080; d) M. Golkaram, K. Loos, *Macromolecules* **2019**, *52*, 9427–9444; e) A. Shabbir, H. Goldansaz, O. Hassager, E. van Ruymbeke, N. J. Alvarez, *Macromolecules* **2015**, *48*, 5988–5996; f) C. L. Lewis, K. Stewart, M. Anthamatten, *Macromolecules* **2014**, *47*, 729–740; g) K. E. Feldman, M. J. Kade, E. W. Meijer, C. J. Hawker, E. J. Kramer, *Macromolecules* **2009**, *42*, 9072–9081; h) T. Yan, K. Schröter, F. Herbst, W. H. Binder, T. Thurn-Albrecht, *Sci. Rep.* **2016**, *6*, 32356; i) S. Chen, D. Döhler, W. H. Binder, *Polymer* **2016**, *107*, 466–473.
- [12] a) R. Zhang, W. Chen, T. Miyoshi, *Macromolecules* **2024**, *57*, 1893–1918; b) F. Wang, P. Sun, *Acta Polym. Sin.* **2021**, *52*, 840–856; c) A. Mordvinkin, D. Döhler, W. H. Binder, R. H. Colby, K. Saalwächter, *Phys. Rev. Lett.* **2020**, *125*; d) B. Fortier-McGill, V. Toader, L. Reven, *Macromolecules* **2012**, *45*, 6015–6026; e) B. Li, L. Xu, Q. Wu, T. Chen, P. Sun, Q. Jin, D. Ding, X.



- Wang, G. Xue, A.-C. Shi, *Macromolecules* **2007**, *40*, 5776–5786; f) C. Li, R. Bhandary, A. Marinow, S. Bachmann, A.-C. Pöppler, W. H. Binder, *Macromol. Rapid Commun.* **2023**, *45*, 2300464.
- [13] a) A. Mordvinkin, D. Döhler, W. H. Binder, R. H. Colby, K. Saalwächter, *Macromolecules* **2021**, *54*, 5065–5076; b) A. R. Brás, C. H. Hövelmann, W. Antonius, J. Teixeira, A. Radulescu, J. Allgaier, W. Pyckhout-Hintzen, A. Wischniewski, D. Richter, *Macromolecules* **2013**, *46*, 9446–9454; c) E. Ostas, T. Yan, T. Thurn-Albrecht, W. H. Binder, *Macromolecules* **2013**, *46*, 4481–4490; d) S. Chen, Y. Wu, H. Wang, B. Zhu, B. Xiong, W. H. Binder, J. Zhu, *Polym. Chem.* **2021**, *12*, 4111–4119; e) B. N. Narasimhan, A. W. Dixon, B. Mansel, A. Taberner, J. Mata, J. Malmström, *J. Colloid Interface Sci.* **2023**, *630*, 638–653; f) S. Lettieri, P. Manesiotis, M. Slann, D. W. Lewis, A. J. Hall, *React. Funct. Polym.* **2021**, *167*, 105031.
- [14] S. Chen, W. H. Binder, *Acc. Chem. Res.* **2016**, *49*, 1409–1420.
- [15] S. K. Chang, A. D. Hamilton, *J. Am. Chem. Soc.* **1988**, *110*, 1318–1319.
- [16] a) D. T. Seidenkranz, M. D. Pluth, *J. Org. Chem.* **2019**, *84*, 8571–8577; b) D. T. Seidenkranz, J. M. McGrath, L. N. Zakharov, M. D. Pluth, *Chem. Commun.* **2017**, *53*, 561–564; c) J. M. McGrath, M. D. Pluth, *J. Org. Chem.* **2014**, *79*, 711–719; d) Y. Molard, D. M. Bassani, J.-P. Desvergne, P. N. Horton, M. B. Hursthouse, J. H. R. Tucker, *Angew. Chem. Int. Ed.* **2005**, *44*, 1072–1075; e) S. R. Collinson, J. H. R. Tucker, T. Gelbrich, M. B. Hursthouse, *Chem. Commun.* **2001**, 555–556; f) J. Westwood, S. J. Coles, S. R. Collinson, G. Gasser, S. J. Green, M. B. Hursthouse, M. E. Light, J. H. R. Tucker, *Organometallics* **2004**, *23*, 946–951.
- [17] a) J. J. Du, J. R. Hanrahan, V. R. Solomon, P. A. Williams, P. W. Groundwater, J. Overgaard, J. A. Platts, D. E. Hibbs, *J. Phys. Chem. A* **2018**, *122*, 3031–3044; b) T. Ema, K. Hamada, K. Sugita, Y. Nagata, T. Sakai, A. Ohnishi, *J. Org. Chem.* **2010**, *75*, 4492–4500; c) A. Tron, P. J. Thornton, B. Kauffmann, J. H. R. Tucker, N. D. McClenaghan, *Supramol. Chem.* **2016**, *28*, 733–741; d) S. Lakkakula, O. D. Mitkin, R. A. Valiulin, A. G. Kutateladze, *Org. Lett.* **2007**, *9*, 1077–1079; e) H. S. Sørensen, J. Larsen, B. S. Rasmussen, B. Laursen, S. G. Hansen, T. Skrydstrup, C. Amatore, A. Jutand, *Organometallics* **2002**, *21*, 5243–5253; f) M. H. Al-Sayah, R. McDonald, N. R. Branda, *Eur. J. Org. Chem.* **2004**, *2004*, 173–182.
- [18] O. A. Scherman, G. B. W. L. Ligthart, H. Ohkawa, R. P. Sijbesma, E. W. Meijer, *Proc. Natl. Acad. Sci.* **2006**, *103*, 11850–11855.
- [19] a) A. D. Hamilton, A. Muehldorf, S.-K. Chang, N. Pant, S. Goswami, D. van Engen, *J. Inclusion Phenom. Mol. Recognit. Chem.* **1989**, *7*, 27–38; b) S. K. Chang, D. Van Engen, E. Fan, A. D. Hamilton, *J. Am. Chem. Soc.* **1991**, *113*, 7640–7645.
- [20] a) K. Hager, U. Hartnagel, A. Hirsch, *Eur. J. Org. Chem.* **2007**, *2007*, 1942–1956; b) T. Ema, D. Tanida, K. Sugita, T. Sakai, K.-i. Miyazawa, A. Ohnishi, *Org. Lett.* **2008**, *10*, 2365–2368; c) M. Ali, E. Kataev, J. Müller, H. Park, M. Halik, A. Hirsch, *Chem. - Eur. J.* **2021**, *27*, 16429–16439; d) N. M.-W. Wu, V. W.-W. Yam, *ACS Appl. Mater. Interfaces* **2019**, *11*, 40290–40299; e) F. Wessendorf, B. Grimm, D. M. Guldi, A. Hirsch, *J. Am. Chem. Soc.* **2010**, *132*, 10786–10795; f) F. Wessendorf, A. Hirsch, *Tetrahedron* **2008**, *64*, 11480–11489.
- [21] a) A. Croom, K. B. Manning, M. Weck, *Macromolecules* **2016**, *49*, 7117–7128; b) R. Schmidt, M. Stolte, M. Grüne, F. Würthner, *Macromolecules* **2011**, *44*, 3766–3776.
- [22] S. Chen, B.-D. Lechner, A. Meister, W. H. Binder, *Nano Lett.* **2016**, *16*, 1491–1496.
- [23] I. M. Smallwood, *Handbook of Organic Solvent Properties*, Arnold, a member of the Hodder Headline Group, 338 Euston Road, London NW1 3BH, Great Britain, **1996**.
- [24] P. Thordarson, *Chem. Soc. Rev.* **2011**, *40*, 1305–1323.
- [25] D. Brynn Hibbert, P. Thordarson, *Chem. Commun.* **2016**, *52*, 12792–12805.
- [26] a) C. A. Hunter, *Angew. Chem. Int. Ed.* **2004**, *43*, 5310–5324; b) J. L. Cook, C. A. Hunter, C. M. R. Low, A. Perez-Velasco, J. G. Vinter, *Angew. Chem. Int. Ed.* **2007**, *46*, 3706–3709.
- [27] a) S. Alavi, R. Susilo, J. A. Ripmeester, *J. Chem Phys* **2009**, *130*, 174501; b) L. Wen, J. Zhang, T. Zhou, A. Zhang, *Vib. Spectrosc.* **2016**, *86*, 160–172; c) W. Suzuki, H. Kotani, T. Ishizuka, K. Ohkubo, Y. Shiota, K. Yoshizawa, S. Fukuzumi, T. Kojima, *Chem. - Eur. J.* **2017**, *23*, 4669–4679.
- [28] S.-I. Kondo, T. Hayashi, Y. Sakuno, Y. Takezawa, T. Yokoyama, M. Unno, Y. Yano, *Org. Biomol. Chem.* **2007**, *5*, 907.
- [29] a) T. Galaon, V. David, *J. Sep. Sci.* **2011**, *34*, 1423–1428; b) K. Ueda, K. Higashi, K. Moribe, L. S. Taylor, *Mol. Pharmaceutics* **2022**, *19*, 100–114.
- [30] a) H. Wang, S. Hanash, *Humana Press* **2009**, 227–242; b) D. T. Bui, Z. Li, P. I. Kitov, L. Han, E. N. Kitova, M. Fortier, C. Fuselier, P. Granger Joly de Boissel, D. Chatenet, N. Doucet, S. M. Tompkins, Y. St-Pierre, L. K. Mahal, J. S. Klassen, *ACS Cent. Sci.* **2022**, *8*, 963–974.
- [31] a) T. Kundlacz, C. Schmidt, *Anal. Chem.* **2023**, *95*, 17292–17299; b) W. Lu, X. Yin, X. Liu, G. Yan, P. Yang, *Sci. China: Chem.* **2014**, *57*, 686–694; c) S. Pérez-Rafael, S. Atrian, M. Capdevila, Ò. Palacios, *Talanta* **2011**, *83*, 1057–1061.
- [32] a) P. Groves, *Polym. Chem.* **2017**, *8*, 6700–6708; b) E. F. Dudás, A. Bodor, *Anal. Chem.* **2019**, *91*, 4929–4933; c) E. Ruzicka, P. Pellechia, B. C. Benicewicz, *Anal. Chem.* **2023**, *95*, 7849–7854.
- [33] a) P. C. Srivastava, A. P. Callahan, E. B. Cunningham, F. F. Knapp, Jr., *J. Med. Chem.* **1983**, *26*, 742–746; b) Mohammad, R. McDonald, Neil, *Eur. J. Org. Chem.* **2004**, *2004*, 173–182; c) H. Rupp, D. Döhler, P. Hilgeroth, N. Mahmood, M. Beiner, W. H. Binder, *Macromol. Rapid Commun.* **2019**, *40*, 1900467; d) R. Appel, *Angew. Chem., Int. Ed. Engl.* **1975**, *14*, 801–811.

Manuscript received: October 24, 2024

Accepted manuscript online: November 12, 2024

Version of record online: November 21, 2024

## 4. Conclusion

This cumulative thesis investigates the H-bonds of modified barbiturate (Ba), 2-thiobarbiturate (TBa), ureido-pyrimidinone (UPy), and the Hamilton wedge-barbiturate (HW-Ba) complex by manipulating molecular surroundings and extending the study to polymer matrices. The first approach explores the distinct H-bonding behavior of TBa compared to Ba in solution, solid-state, and within a polyisobutylene (PIB) matrix. The second approach examines the dynamics and stability of UPy quadruple H-bonds in polymerized ionic liquids (POILs) which is a highly charged ionic media, employing both solution-based and solid-state characterizations. The third approach investigates H-bonding in the HW-Ba complex across solvents with tailored polarity and H-bonding donor/acceptor abilities, establishing a two-step methodology that involves covalent fixation followed by ESI MS analysis to characterize H-bonded aggregates.

- **Investigation of H-bonding in modified barbiturate and 2-thiobarbiturate both in solutions and in nonpolar PIB:**

To explore the proximity effect arising from the receptor atom of H-bonds, barbiturate and 2-thiobarbiturate were prepared using a condensation reaction between C-2 modified malonate and urea or thiourea. NMR titration (**Figure 4.1**) using  $\text{CDCl}_3$  yielded the H-bonding strength with a  $K_a$  of  $4.26 \text{ M}^{-1}$  for B and  $0.94 \text{ M}^{-1}$  for TB. VT NMR spectroscopy revealed the slower dynamics of sulfur H-bonds of TB, as there appear two distinct -NH shifts representing  $\text{-NH}\cdots\text{O}=\text{C}$  and  $\text{-NH}\cdots\text{S}=\text{C}$  H-bonds at temperatures lower than  $0^\circ\text{C}$ . Meanwhile the slower dynamics by reduced temperature led to peak broadening of B as there is only  $\text{-NH}\cdots\text{O}=\text{C}$  H-bond. Therefore, the H-bonding in TB could involve both sulfur at the C-2 position and oxygen at the C-4/6 position. Solid-state characterization by DSC demonstrated a semicrystalline nature of B by the strong and highly ordered H-bonds of barbiturate that introduce a glass transition, a crystallization peak, and a melting peak. The weaker and less ordered sulfur H-bonds of TB result in a higher glass transition temperature than B, with no crystallization and melting peak observed. Further, VT FT-IR revealed the highly dynamic nature of TB H-bonds already at room temperature, demonstrated by the broad H-bonded -NH stretching at  $\sim 3200 \text{ cm}^{-1}$  and free -NH stretching at  $\sim 3390 \text{ cm}^{-1}$ . The H-bonds of B are “frozen” and became dynamic at a temperature higher than  $85^\circ\text{C}$ , as evidenced by the free -NH stretch at  $\sim 3400 \text{ cm}^{-1}$  and the

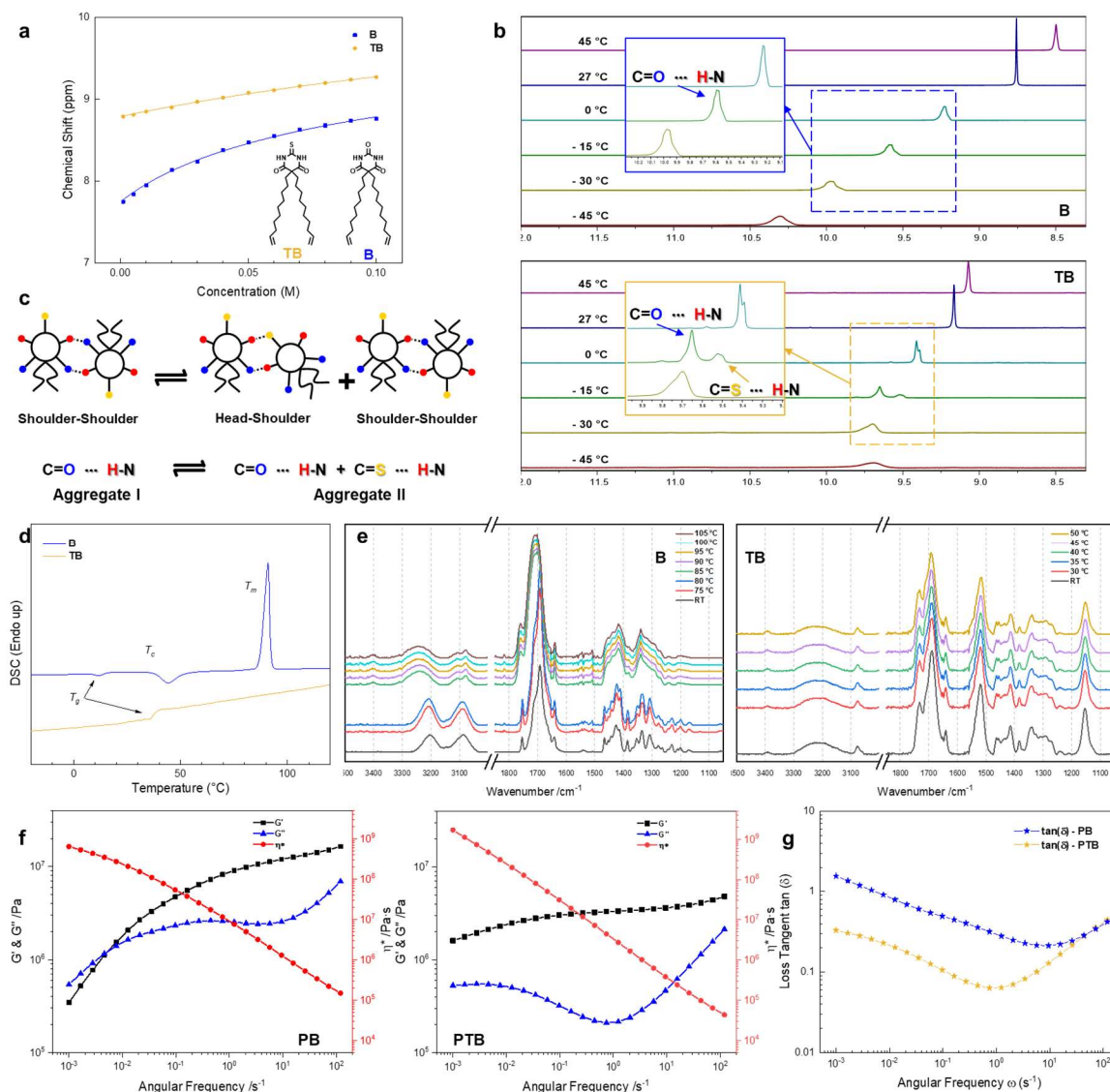


**Figure 4.1** a) NMR titration of B and TB in  $\text{CDCl}_3$ , yielding a  $K_a$  equal to  $4.26 \text{ M}^{-1}$  for B and for  $0.94 \text{ M}^{-1}$  TB; b) VT NMR spectra of B and TB, showing two distinct H-bonds of TB detected as temperature reduces; c) proposed H-bonding pattern of TB; d) DSC thermogram of B and TB, demonstrating the weaker H-bonds of TB introduces a higher  $T_g$ ; e) VT FT-IR spectra of B and TB, showing TB bears more dynamic H-bonds already at room temperature while B becomes dynamic only when the temperature rises above  $85 \text{ °C}$ ; f) frequency sweep of PB and PTB (two telechelic PIB modified with B or TB) at  $20 \text{ °C}$ , illustrating a faster dynamics of B than TB in the PIB matrix; g) loss tangent of PB and PTB, indicative for a more solid nature of PTB by the less order and weaker sulfur H-bonds.

broadened peak at  $\sim 3250 \text{ cm}^{-1}$  that was found at  $\sim 3200 \text{ cm}^{-1}$ . As for TB, its spectra remain almost identical to those at room temperature, similar to the spectra of B in the melt state, indicative of an already dynamic character with more broken H-bonds in thiobarbiturates TB within the whole temperature

range. Finally, the telechelic PIB was equipped with barbiturate or 2-thiobarbiturate using CuAAC click chemistry to afford PB and PTB, and the frequency sweep at 20 °C by a rheometer revealed their H-bonding in such nonpolar polymer matrix. As characterization by the crossover of the  $G'$  and  $G''$ , PB shows a relaxation at  $\tau = 5.27 \times 10^{-3} \text{ s}^{-1}$ . PTB demonstrated no terminal relaxation within the given frequency range, elucidating that thiobarbiturate aggregates in PTB display a longer lifetime compared to the native barbiturate aggregates in PB. Besides their longer lifetime, H-bonds in PTB are indeed more tolerant against a low frequency (of shear) than those in PB at a frequency lower than  $\sim 53 \text{ s}^{-1}$ , evidenced by a lower loss tangent value of PTB than that of PB. In summary, TB demonstrates a weak and slower association compared to B in solutions, and in the solid state, the less-ordered H-bonds of TB frustrate the crystallization but introduce glass transition at a higher temperature compared to B. When embedded at both ends of a nonpolar PIB, the faster dynamics of B result in an early terminal relaxation of the PIB matrix while the TB of slower dynamics results in a more robust H-bond against shear.

- **Investigation of stability of ureido-pyrimidinone quadruple H-bonds in ionic media:**

To introduce a (poly-) ionic environment to the ureido-pyrimidinone (UPy) quadruple H-bonding motif, the acrylate-based ionic liquid monomer (ILA) and UPy-bearing monomer (UPyA) were synthesized and polymerized via RAFT polymerization. Increasing the UPy content in the copolymer led to a transition from a gel to a powdery polymer (**Figure 4.2**), indicating stronger interchain interactions due to the UPy H-bonds. This effect was further confirmed by DSC analysis, which showed an elevated  $T_g$  with higher UPy content, resembling the effect of increased  $M_n$ . Due to the dynamic nature of H-bonding and ionic interactions in the copolymer, the material with  $M_n = 10 \text{ kDa}$  and 7 %mol UPy could be hot-pressed into disc (or stripe) specimens, demonstrating self-healing at 40 °C within an hour. Tensile strain-stress tests quantified this self-healing efficiency, showing that the low-molecular-weight copolymer ( $M_n = 10 \text{ kDa}$  and 7 %mol UPy) achieved nearly complete self-healing, whereas the high- $M_n$  counterpart ( $M_n = 67 \text{ kDa}$ , 7 %mol UPy) exhibited greater tensile strength (ultimate strength = 2.25 MPa). To investigate the influence of an ionic medium on UPy H-bonds, a neat copolymer ( $M_n = 11.5 \text{ kDa}$ , 25 %mol UPy, denoted as cp0) was mixed with varying amounts of pyrrolidinium bis(trifluoromethylsulfonyl)imide (IL), generating cp25, cp50, and cp75 (with the

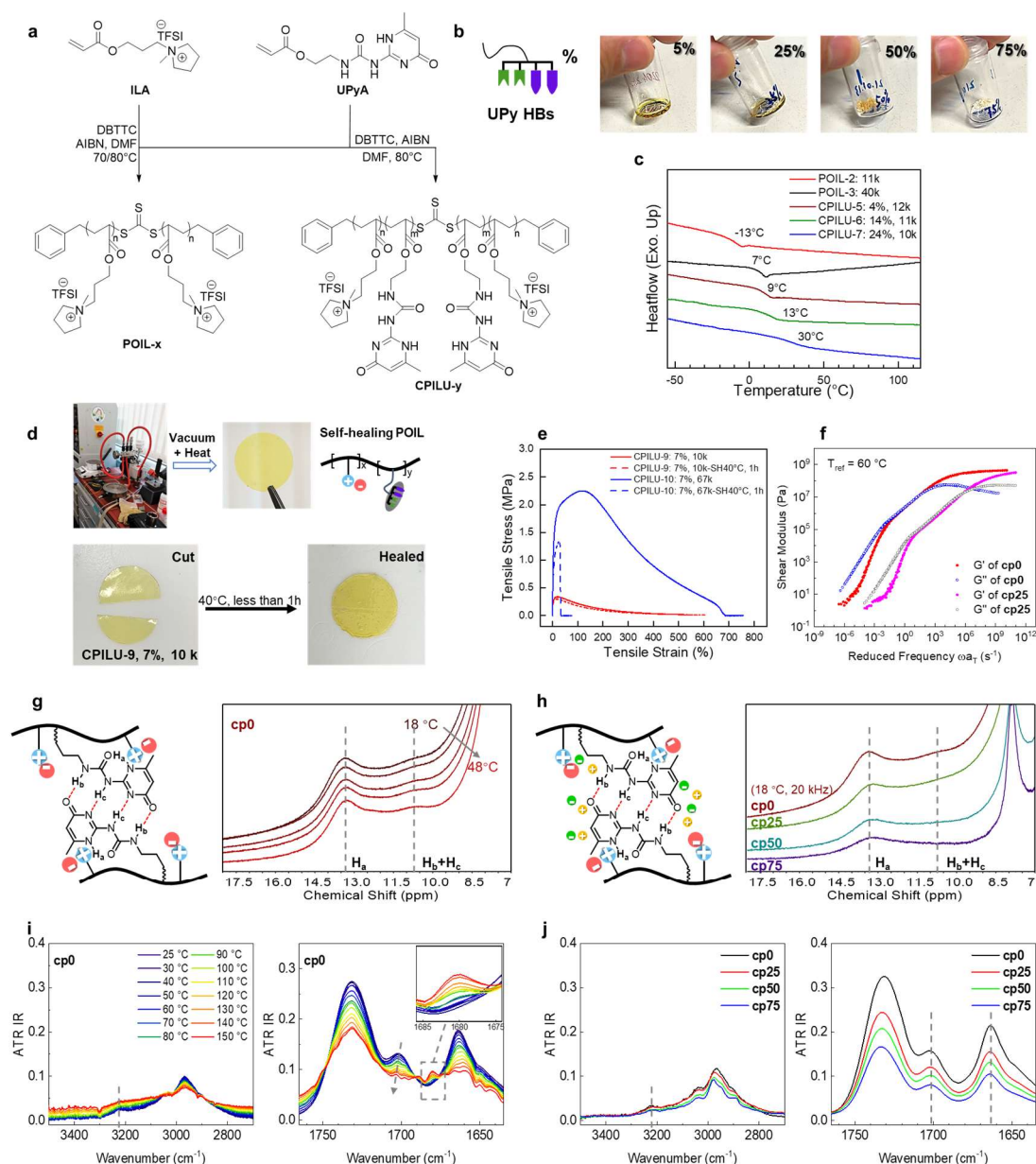


**Figure 4.2** a) Synthesis of polymeric ionic liquids (POIL-x) and UPy-containing POILs (CPILU-y) via RAFT polymerization; b) photos of CPILU with a increasing content of UPy motifs, showing the material status changes from gel to powdery; c) DSC thermogram of POIL and CPILU with different  $M_n$  and UPy content, demonstrating UPy H-bonds can increase the  $T_g$  which is a similar effect from increasing  $M_n$ ; d) manufacture of a disc sample of CPILU ( $M_n$  = 10 kDa, 7 %mol UPy) and the self-healing test at 40 °C; e) the tensile strain-stress curve of as-prepared and self-healed CPILU ( $M_n$  = 10 and 67 kDa, 7 %mol UPy), showing low-molecular-weight endows better self-healing while high- $M_n$  confers better tensile strength; f) master curve of neat CPILU (11.5 kDa and 25 %mol of UPy motifs, renamed "cp0") and CPILU + 25 %wt pyrrolidinium bis(trifluoromethylsulfonyl)imide (IL) (sample name = cp25), demonstrating the fastened but not altered polymer dynamics by mixing low-molecular-weight IL; g) the VT ss NMR



spectra of cp0, showing the stable UPy H-bonds till  $\sim 80\text{ }^{\circ}\text{C}$  (the  $T_{\text{actual}}$  with an additional  $30\text{ }^{\circ}\text{C}$  due to the frictional heating upon rotation); h) ss NMR of samples with different content of low-molecular-weight IL mixed (cp“z”, z is the %wt of IL mixed), showing the UPy H-bonds is stable upon mixing with IL; i) VT FT-IR spectra of neat cp0, revealing the partially broken UPy H-bonds at  $T > 70\text{ }^{\circ}\text{C}$ ; j) FT-IR spectra of cp25, cp50, and cp75, illustrating the stable UPy H-bonds in these samples.

number indicating the IL weight percentage). VT ss NMR spectra demonstrated the stability of UPy H-bonds in cp0 up to  $\sim 80\text{ }^{\circ}\text{C}$  (considering an additional  $30\text{ }^{\circ}\text{C}$  from frictional heating<sup>379</sup> during rotation). VT FT-IR spectra further indicated that UPy H-bonds began dissociating above  $70\text{ }^{\circ}\text{C}$ , as evidenced by a blue shift in C=O stretching and broadening of the -NH stretching band. Importantly, ss NMR confirmed that UPy H-bonds remained intact despite IL mixing, a finding further validated by FT-IR analysis. The master curve analysis of cp0 and cp25 revealed similar profiles with transitions occurring on different timescales, indicating accelerated polymer dynamics upon IL mixing but without altering fundamental behavior. This observation suggests that IL enhances chain mobility by reducing chain friction via solvation rather than disrupting UPy H-bonds, highlighting the independent stability of UPy H-bonds within the copolymer matrix.

- **Investigation of H-bonds and aggregates of novel Hamilton wedge-barbiturate complex:**

The host-guest association behavior between the modified barbiturate (B) and Hamilton wedge (H) was examined using UV titration experiments, to determine their  $K_a$  using different molecular proximity (**Figure 4.3**). By fitting the raw UV titration data, the  $K_a$ s in different solvents were calculated and plotted against the dielectric constants of each solvent, highlighting the effect of solvent polarity on the stability of the H-B complex. In the nonpolar hydrocarbon solvent toluene, the complex exhibited the highest stability ( $K_{a, \text{Tol}} = \sim 10^5\text{ M}^{-1}$ ), due to the absence of competing H-bond donors or acceptors and the low polarity. In contrast, chlorinated solvents (DCM,  $\text{CHCl}_3$ , DCE) weakened the association, with  $K_{a, \text{DCE}} = \sim 10^3\text{ M}^{-1}$ , as a result of their higher polarity and weak H-bond-accepting ability. Solvents containing oxygen or nitrogen atoms (dioxane, DMSO, DMF, EA, MeCN, THF) or hydroxyl groups (EG, HFIP, iPA, MeOH) significantly disrupted H-B binding (for instance,  $K_{a, \text{DMSO}} = \sim 10^2\text{ M}^{-1}$ ), due to their strong polarity and competitive H-bonding nature. Interestingly, in  $\alpha,\alpha,\alpha$ -trifluorotoluene (TFT), a solvent similar to toluene but with enhanced polarity

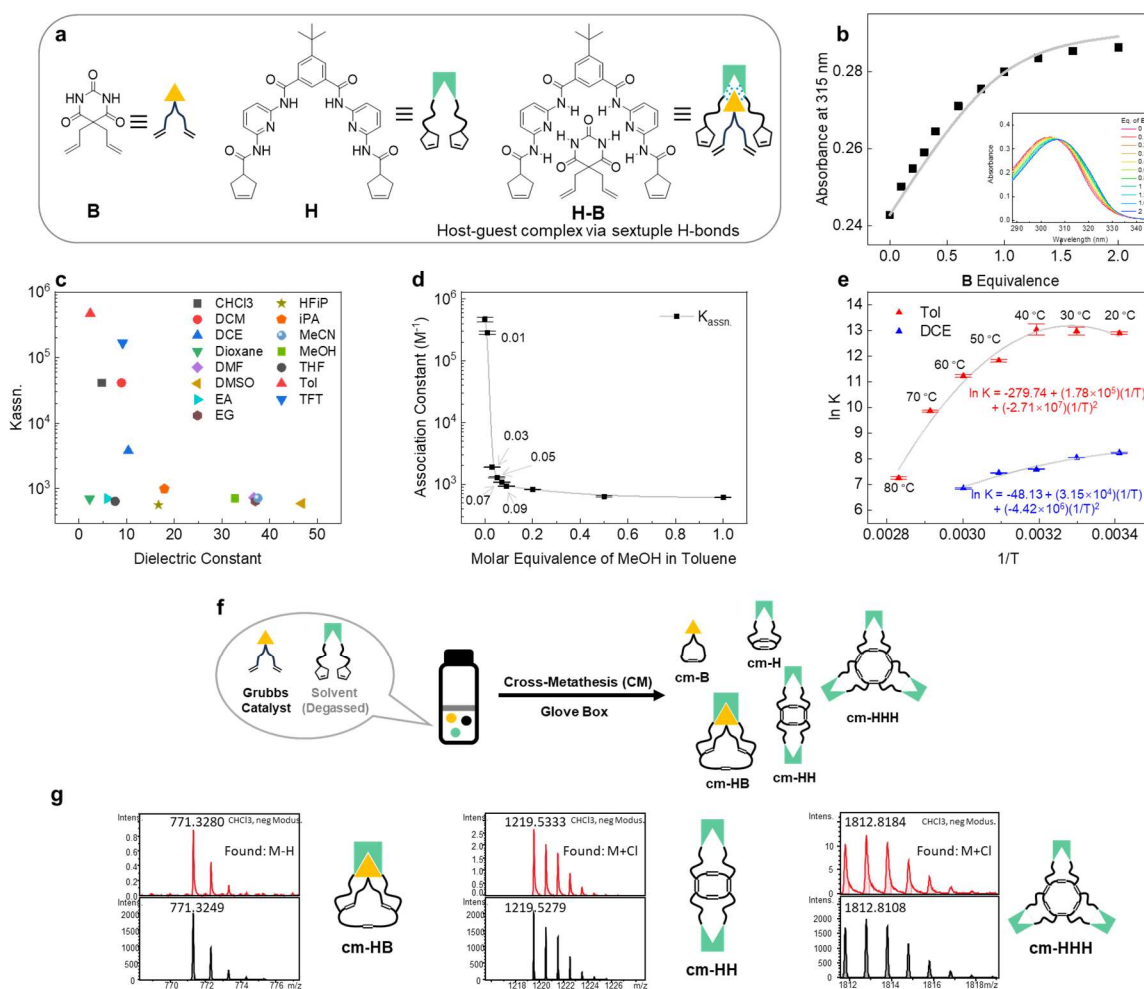


**Figure 4.3** a) Chemical structures of the modified barbiturate **B**, Hamilton wedge **H**, and the complex **H-B**, while the cyclopentene or allyl moieties allow for further chemical process; b) the UV titration plot with **B** equivalence, with the original UV spectra as the built-in figure; c) the association constant ( $K_a$ ) of the complex **H-B** determined with various solvents; d) the  $K_a$  of the complex **H-B** determined in toluene-methanol mixtures, showing the sensitivity of the **H-B** complex to the polar and H-bond-replacing molecular surrounding; e) van't Hoff plot of  $K_a$  in toluene (Tol) and 1,2-dichloroethane (DCE) at multiple temperatures, demonstrating the solvent-dependent thermodynamics of the H-bonds presenting in the **H-B** complex; f) the scheme showing the process to covalently fix the aggregated products by cross-metathesis reaction (CM); g) the ESI MS spectra of the selected aggregated products, showing the detection by ESI MS after CM is a feasible method for aggregates analysis.

and fluorophilicity, the **H-B** complex exhibited unexpectedly high stability, attributed to solvophobic interactions. Titration in toluene-methanol mixtures further illustrated the sensitivity of **H-B** H-bonds to the molecular environment. As methanol content increased to a MeOH/Tol molar ratio of 0.03, the  $K_a$

dropped by two orders of magnitude, demonstrating the pronounced effect of solvent polarity and competition on complex stability. A van't Hoff analysis of  $K_a$  across different temperatures provided thermodynamic insights into the H-B host-guest complex. In toluene, the association process was predominantly entropy-driven below 40°C, whereas in DCE, the binding remained largely enthalpy-driven across the entire temperature range (20 – 60 °C). This variation confirmed that molecular surroundings influence the thermodynamics of H-bonding by modulating enthalpic and entropic contributions. Further, the presence of cyclopentene or allyl moieties enabled covalent fixation of the H-B complex via cross-metathesis (CM), and the resulting aggregates were analyzed using ESI MS to determine molecular weight distribution and aggregation ratios under different conditions. This two-step strategy, covalent fixation via CM followed by ESI MS analysis, was extended to study H-B aggregates within a solvent-free PIB matrix, providing a novel approach for examining aggregate formation and complex assemblies in polymer matrices.

## 5. Reference

1. Gibb, B. C. The Centenary (Maybe) of the Hydrogen Bond. *Nature Chemistry*, **2020**, 12, 665-667. <https://doi.org/10.1038/s41557-020-0524-2>
2. Goymer, P. 100 Years of the Hydrogen Bond. *Nature Chemistry*, **2012**, 4, 863-864. <https://doi.org/10.1038/nchem.1482>
3. Moore, T. S. & Winmill, T. F. CLXXVII.—The State of Amines in Aqueous Solution. *Journal of the Chemical Society, Transactions*, **1912**, 101, 1635-1676. <https://doi.org/10.1039/CT9120101635>
4. Lewis, G. N. The Atom and the Molecule. *Journal of the American Chemical Society*, **1916**, 38, 762-785. <https://doi.org/10.1021/ja02261a002>
5. Langmuir, I. The Arrangement of Electrons in Atoms and Molecules. *Journal of the American Chemical Society*, **1919**, 41, 868-934. <https://doi.org/10.1021/ja02227a002>
6. Latimer, W. M. & Rodebush, W. H. Polarity and Ionization from the Standpoint of the Lewis Theory of Valence. *Journal of the American Chemical Society*, **1920**, 42, 1419-1433. <https://doi.org/10.1021/ja01452a015>
7. Pauling, L. The Structure and Entropy of Ice and of Other Crystals with Some Randomness of Atomic Arrangement. *Journal of the American Chemical Society*, **1935**, 57, 2680-2684. <https://doi.org/10.1021/ja01315a102>
8. Arunan, E., Desiraju, G. R., Klein, R. A., Sadlej, J., Scheiner, S., Alkorta, I., Clary, D. C., Crabtree, R. H., Dannenberg, J. J., Hobza, P., Kjaergaard, H. G., Legon, A. C., Mennucci, B. & Nesbitt, D. J. Definition of the Hydrogen Bond (IUPAC Recommendations 2011). *Pure and Applied Chemistry*, **2011**, 83, 1637-1641. <https://doi.org/10.1351/Pac-Rec-10-01-02>
9. Binder, W. H. & Zirbs, R. in *Hydrogen Bonded Polymers Advances in Polymer Science* (ed Wolfgang Binder) Ch. Chapter 109, 1-78 (Springer Berlin Heidelberg, 2006) [https://doi.org/10.1007/12\\_2006\\_109](https://doi.org/10.1007/12_2006_109)
10. Seidenkranz, D. T., McGrath, J. M., Zakharov, L. N. & Pluth, M. D. Supramolecular Bidentate Phosphine Ligand Scaffolds from Deconstructed Hamilton Receptors. *Chemical Communications*, **2017**, 53, 561-564. <https://doi.org/10.1039/c6cc09198a>
11. Tron, A., Rocher, M., Thornton, P. J., Tucker, J. H. R. & McClenaghan, N. D. Supramolecular Architectures Incorporating Hydrogen-Bonding Barbiturate Receptors. *Asian Journal of Organic Chemistry*, **2015**, 4, 192-202. <https://doi.org/10.1002/ajoc.201402243>
12. McGrath, J. M. & Pluth, M. D. Understanding the Effects of Preorganization, Rigidity, and Steric Interactions in Synthetic Barbiturate Receptors. *The Journal of Organic Chemistry*, **2014**, 79, 711-719. <https://doi.org/10.1021/jo402500a>

13. McGrath, J. M. & Pluth, M. D. Linear Free Energy Relationships Reveal Structural Changes in Hydrogen-Bonded Host-Guest Interactions. *The Journal of Organic Chemistry*, **2014**, 79, 11797-11801. <https://doi.org/10.1021/jo502325w>
14. Jorgensen, W. L. & Pranata, J. Importance of Secondary Interactions in Triply Hydrogen Bonded Complexes: Guanine-Cytosine vs Uracil-2,6-Diaminopyridine. *Journal of the American Chemical Society*, **1990**, 112, 2008-2010. <https://doi.org/10.1021/ja00161a061>
15. Pranata, J., Wierschke, S. G. & Jorgensen, W. L. OPLS Potential Functions for Nucleotide Bases. Relative Association Constants of Hydrogen-Bonded Base Pairs in Chloroform. *Journal of the American Chemical Society*, **1991**, 113, 2810-2819. <https://doi.org/10.1021/ja00008a002>
16. Karas, L. J., Wu, C. H., Das, R. & Wu, J. I. C. Hydrogen Bond Design Principles. *WIREs Computational Molecular Science*, **2020**, 10 <https://doi.org/10.1002/wcms.1477>
17. Sijbesma, R. P., Beijer, F. H., Brunsveld, L., Folmer, B. J., Hirschberg, J. H., Lange, R. F., Lowe, J. K. & Meijer, E. W. Reversible Polymers Formed from Self-Complementary Monomers Using Quadruple Hydrogen Bonding. *Science*, **1997**, 278, 1601-1604. <https://doi.org/10.1126/science.278.5343.1601>
18. Beijer, F. H., Kooijman, H., Spek, A. L., Sijbesma, R. P. & Meijer, E. W. Self-Complementarity Achieved through Quadruple Hydrogen Bonding. *Angewandte Chemie-International Edition*, **1998**, 37, 75-78. [https://doi.org/10.1002/\(SICI\)1521-3773\(19980202\)37:1/2<75::AID-ANIE75>3.0.CO;2-R](https://doi.org/10.1002/(SICI)1521-3773(19980202)37:1/2<75::AID-ANIE75>3.0.CO;2-R)
19. Beijer, F. H., Sijbesma, R. P., Kooijman, H., Spek, A. L. & Meijer, E. W. Strong Dimerization of Ureidopyrimidones via Quadruple Hydrogen Bonding. *Journal of the American Chemical Society*, **1998**, 120, 6761-6769. <https://doi.org/10.1021/ja974112a>
20. Blight, B. A., Hunter, C. A., Leigh, D. A., McNab, H. & Thomson, P. I. T. An AAAA-DDDD Quadruple Hydrogen-Bond Array. *Nature Chemistry*, **2011**, 3, 244-248. <https://doi.org/10.1038/nchem.987>
21. Chang, S. K. & Hamilton, A. D. Molecular Recognition of Biologically Interesting Substrates: Synthesis of an Artificial Receptor for Barbiturates Employing Six Hydrogen Bonds. *Journal of the American Chemical Society*, **1988**, 110, 1318-1319. <https://doi.org/10.1021/ja00212a065>
22. Hamilton, A. D., Muehldorf, A., Chang, S. K., Pant, N., Goswami, S. & Vanengen, D. Nucleotide Recognition by Macrocyclic Receptors. *Journal of Inclusion Phenomena*, **1989**, 7, 27-38. <https://doi.org/10.1007/Bf01112780>
23. Chang, S. K., Vanengen, D., Fan, E. & Hamilton, A. D. Hydrogen-Bonding and Molecular Recognition - Synthetic, Complexation, and Structural Studies on Barbiturate Binding to an Artificial Receptor. *Journal of the American Chemical Society*, **1991**, 113, 7640-7645. <https://doi.org/10.1021/ja00020a027>

24. Pekary, A. E. Pyridine Interactions with Phenolic Groups in Water: Evidence for Hydrogen Bonding and Hydrophobic Association. *Biophysical Chemistry*, **1978**, 7, 325-338. [https://doi.org/10.1016/0301-4622\(78\)85009-1](https://doi.org/10.1016/0301-4622(78)85009-1)
25. Williams, D. H., Gale, T. F. & Bardsley, B. The Increasing Tightness of Fully Associated States as a Function of Their Increasing Stability. The Dimerisation of Carboxylic Acids. *Journal of the Chemical Society, Perkin Transactions 2*, **1999**, 1331-1334. <https://doi.org/10.1039/a902147g>
26. Davies, M. & Thomas, D. K. Energies And Entropies Of Association For Amides In Benzene Solutions. Part II. *The Journal of Physical Chemistry*, **1956**, 60, 767-770. <https://doi.org/10.1021/j150540a014>
27. Beijer, F. H., Sijbesma, R. P., Vekemans, J. A. J. M., Meijer, E. W., Kooijman, H. & Spek, A. L. Hydrogen-Bonded Complexes of Diaminopyridines and Diaminotriazines: Opposite Effect of Acylation on Complex Stabilities. *The Journal of Organic Chemistry*, **1996**, 61, 6371-6380. <https://doi.org/10.1021/jo960612v>
28. Sivakova, S. & Rowan, S. J. Nucleobases as Supramolecular Motifs. *Chemical Society Reviews*, **2005**, 34, 9. <https://doi.org/10.1039/b304608g>
29. Custelcean, R. Crystal Engineering with Urea and Thiourea Hydrogen-Bonding Groups. *Chemical Communications*, **2008**, 295-307. <https://doi.org/10.1039/b708921j>
30. Biswal, H. S., Shirhatti, P. R. & Wategaonkar, S. O-H...O versus O-H...S Hydrogen Bonding I: Experimental and Computational Studies on the p-Cresol x H<sub>2</sub>O and p-Cresol x H<sub>2</sub>S Complexes. *The Journal of Physical Chemistry A*, **2009**, 113, 5633-5643. <https://doi.org/10.1021/jp9009355>
31. Biswal, H. S., Shirhatti, P. R. & Wategaonkar, S. O-H...O versus O-H...S Hydrogen Bonding. 2. Alcohols and Thiols as Hydrogen Bond Acceptors. *The Journal of Physical Chemistry A*, **2010**, 114, 6944-6955. <https://doi.org/10.1021/jp102346n>
32. Biswal, H. S. & Wategaonkar, S. OH...X (X = O, S) Hydrogen Bonding in the Tetrahydrofuran and Tetrahydrothiophene. *The Journal of Chemical Physics*, **2011**, 135, 134306. <https://doi.org/10.1063/1.3645107>
33. Stefaniu, C., Zaffalon, P. L., Carmine, A., Verolet, Q., Fernandez, S., Wesolowski, T. A., Brezesinski, G. & Zumbuehl, A. Rigid Urea and Self-Healing Thiourea Ethanolamine Monolayers. *Langmuir*, **2015**, 31, 1296-1302. <https://doi.org/10.1021/la5039987>
34. Lee, D. S., Choi, Y. S., Hwang, J. H., Lee, J. H., Lee, W., Ahn, S. K., Park, S., Lee, J. H., Kim, Y. S. & Kim, D. G. Weldable and Reprocessable Biomimetic Polymer Networks Based on a Hydrogen Bonding and Dynamic Covalent Thiourea Motif. *Acs Applied Polymer Materials*, **2021**, 3, 3714-3720. <https://doi.org/10.1021/acsapm.1c00667>
35. Yanagisawa, Y., Nan, Y., Okuro, K. & Aida, T. Mechanically Robust, Readily Repairable Polymers via Tailored Noncovalent Cross-Linking. *Science*, **2018**, 359, 72-76.

<https://doi.org/10.1126/science.aam7588>

36. Chen, K., Xie, H. M. & Liu, J. Self-Healing and Mechanically Robust Poly(Thiourea-Disulfide) Elastomers Based on Three Types of Synergistic Dynamic Bonding. *Polymer Chemistry*, **2024**, 15, 2370-2376. <https://doi.org/10.1039/d4py00322e>
37. Zhao, X., Wang, L., Zhou, G., Feng, S. & Li, L. Stiff, Tunable and Reprocessable Polythiourea Supramolecular Materials by Manipulating Hydrogen-Bonding and Metal-Coordinating Interactions. *Polymer*, **2024**, 290, 126596. <https://doi.org/10.1016/j.polymer.2023.126596>
38. Biswal, H. S., Gloaguen, E., Loquais, Y., Tardivel, B. & Mons, M. Strength of NH...S Hydrogen Bonds in Methionine Residues Revealed by Gas-Phase IR/UV Spectroscopy. *The Journal of Physical Chemistry Letters*, **2012**, 3, 755-759. <https://doi.org/10.1021/jz300207k>
39. Roy, G., Sarma, B. K., Phadnis, P. P. & Mughesh, G. Selenium-Containing Enzymes in Mammals: Chemical Perspectives. *Journal of Chemical Sciences*, **2005**, 117, 287-303. <https://doi.org/10.1007/BF02708441>
40. Adman, E., Watenpaugh, K. D. & Jensen, L. H. NH---S Hydrogen Bonds in Peptococcus Aerogenes Ferredoxin, Clostridium Pasteurianum Rubredoxin, and Chromatium High Potential Iron Protein. *Proceedings of the National Academy of Sciences*, **1975**, 72, 4854-4858. <https://doi.org/10.1073/pnas.72.12.4854>
41. Gómez-Tamayo, J. C., Cordoní, A., Olivella, M., Mayol, E., Fourmy, D. & Pardo, L. Analysis of the Interactions of Sulfur-Containing Amino Acids in Membrane Proteins. *Protein Science*, **2016**, 25, 1517-1524. <https://doi.org/10.1002/pro.2955>
42. Dai, S. Q., He, J. X., Chen, X. P., Cui, J. Y., Zhao, H. Q., Zhang, R. C., Lei, H. Y., Yin, J. F., Cai, L. K., Ye, F., Kong, X., Hu, R. R. & Huang, M. J. Polythiourea Superionic Conductors for Solid-State Batteries. *Macromolecules*, **2023**, 56, 3660-3667. <https://doi.org/10.1021/acs.macromol.3c00116>
43. He, X. Y., Liu, Z., Yang, Y. L., Wang, Z. Y., Chen, Y. M., Zhang, Q. C., Shi, Z. Q., Tan, Y. H., Yue, X. Y. & Liang, Z. A Polythiourea Protective Layer for Stable Lithium Metal Anodes. *Journal of Materials Chemistry A*, **2023**, 11, 10155-10163. <https://doi.org/10.1039/d3ta01343j>
44. Liu, Y. N., Chen, J., Jiang, X. S., Jiang, P. K. & Huang, X. Y. All-Organic Cross-Linked Polysiloxane-Aromatic Thiourea Dielectric Films for Electrical Energy Storage Application. *Acs Applied Energy Materials*, **2020**, 3, 5198-5207. <https://doi.org/10.1021/acsaem.9b02521>
45. Feng, H., Zheng, N., Peng, W., Ni, C., Song, H., Zhao, Q. & Xie, T. Upcycling of Dynamic Thiourea Thermoset Polymers by Intrinsic Chemical Strengthening. *Nature Communications*, **2022**, 13, 397. <https://doi.org/10.1038/s41467-022-28085-2>



46. Li, Y. M., Zhang, Z. P., Rong, M. Z. & Zhang, M. Q. Tailored Modular Assembly Derived Self-Healing Polythioureas with Largely Tunable Properties Covering Plastics, Elastomers and Fibers. *Nature Communications*, **2022**, 13, 2633. <https://doi.org/10.1038/s41467-022-30364-x>
47. Yoo, S., Park, H., Kim, Y. S., Won, J. C., Kim, D. G. & Kim, Y. H. A Dual Cross-Linked Aromatic Polythiourea Gate Dielectric with Multifunctional Capabilities for Organic Field-Effect Transistors. *Journal of Materials Chemistry C*, **2021**, 9, 77-81. <https://doi.org/10.1039/d0tc03617j>
48. Burlingame, Q., Wu, S., Lin, M. R. & Zhang, Q. M. Conduction Mechanisms and Structure-Property Relationships in High Energy Density Aromatic Polythiourea Dielectric Films. *Advanced Energy Materials*, **2013**, 3, 1051-1055. <https://doi.org/10.1002/aenm.201201110>
49. Feng, Y., Hasegawa, Y., Suga, T., Nishide, H., Yang, L. Q., Chen, G. & Li, S. T. Tuning Conformational H-Bonding Arrays in Aromatic/Alicyclic Polythiourea toward High Energy-Storable Dielectric Material. *Macromolecules*, **2019**, 52, 8781-8787. <https://doi.org/10.1021/acs.macromol.9b01785>
50. Zhang, C., Yang, Z. J., Duong, N. T., Li, X. H., Nishiyama, Y., Wu, Q., Zhang, R. C. & Sun, P. C. Using Dynamic Bonds to Enhance the Mechanical Performance: From Microscopic Molecular Interactions to Macroscopic Properties. *Macromolecules*, **2019**, 52, 5014-5025. <https://doi.org/10.1021/acs.macromol.9b00503>
51. Guo, M., Pitet, L. M., Wyss, H. M., Vos, M., Dankers, P. Y. W. & Meijer, E. W. Tough Stimuli-Responsive Supramolecular Hydrogels with Hydrogen-Bonding Network Junctions. *Journal of the American Chemical Society*, **2014**, 136, 6969-6977. <https://doi.org/10.1021/ja500205v>
52. Chen, S., Mahmood, N., Beiner, M. & Binder, W. H. Self-Healing Materials from V- and H-Shaped Supramolecular Architectures. *Angewandte Chemie International Edition*, **2015**, 54, 10188-10192. <https://doi.org/10.1002/anie.201504136>
53. Gauthier, M. A., Gibson, M. I. & Klok, H. A. Synthesis of Functional Polymers by Post-Polymerization Modification. *Angewandte Chemie International Edition*, **2009**, 48, 48-58. <https://doi.org/10.1002/anie.200801951>
54. Du, Y., Zeng, Q., Yuan, L. & He, L. Post-Polymerization Modification Based on Reactive Fluorinated Polymers Reaction. *Journal of Macromolecular Science, Part A*, **2021**, 58, 521-538. <https://doi.org/10.1080/10601325.2021.1903328>
55. Zhou, D., Zhu, L.-W., Wu, B.-H., Xu, Z.-K. & Wan, L.-S. End-Functionalized Polymers by Controlled/Living Radical Polymerizations: Synthesis and Applications. *Polymer Chemistry*, **2022**, 13, 300-358. <https://doi.org/10.1039/d1py01252e>
56. Cummings, S. C., Dodo, O. J., Hull, A. C., Zhang, B. R., Myers, C. P., Sparks, J. L. & Konkolewicz, D. Quantity or Quality: Are Self-Healing Polymers and Elastomers Always



Tougher with More Hydrogen Bonds? *Acs Applied Polymer Materials*, **2020**, 2, 1108-1113. <https://doi.org/10.1021/acsapm.9b01095>

57. Deng, Q., Han, S., Wu, Y., Chen, Y., Zhang, Y., Zhao, Y., Chen, S. & Zhu, J. Robust and Reversible Thermal/Electro-Responsive Supramolecular Polymeric Adhesives via Synergistic Hydrogen-Bonds and Ionic Junctions. *Angewandte Chemie International Edition*, **2024**, <https://doi.org/10.1002/anie.202415386>

58. Huerta, E., Van Genabeek, B., Stals, P. J. M., Meijer, E. W. & Palmans, A. R. A. A Modular Approach to Introduce Function into Single-Chain Polymeric Nanoparticles. *Macromolecular Rapid Communications*, **2014**, 35, 1320-1325. <https://doi.org/10.1002/marc.201400213>

59. Chen, S. B., Geng, Z., Zheng, X. H., Xu, J. P., Binder, W. H. & Zhu, J. T. Engineering the Morphology of Hydrogen-Bonded Comb-Shaped Supramolecular Polymers: from Solution Self-Assembly to Confined Assembly. *Polymer Chemistry*, **2020**, 11, 4022-4028. <https://doi.org/10.1039/d0py00570c>

60. Zhang, G., Ngai, T., Deng, Y. & Wang, C. An Injectable Hydrogel with Excellent Self-Healing Property Based on Quadruple Hydrogen Bonding. *Macromolecular Chemistry and Physics*, **2016**, 217, 2172-2181. <https://doi.org/10.1002/macp.201600319>

61. Sirekanyan, I. N., Kalantaryan, A. V., Akopyan, G. V. & Eripyan, M. L. Copolymerization of Acrylic Acid with Acrylamide Biuret Derivatives. *Russian Journal of Applied Chemistry*, **2014**, 87, 1570-1574. <https://doi.org/10.1134/s1070427214100267>

62. Chen, S., Rocher, M., Ladavière, C., Gérard, J.-F., Lortie, F. & Bernard, J. AB/ABC/ABCD Supramolecular Block Copolymers from Hamilton Wedge and Barbiturate-Functionalized RAFT Agents. *Polymer Chemistry*, **2012**, 3, 3157. <https://doi.org/10.1039/c2py20340e>

63. Pahnke, K., Altintas, O., Schmidt, F. G. & Barner-Kowollik, C. Entropic Effects on the Supramolecular Self-Assembly of Macromolecules. *ACS Macro Letters*, **2015**, 4, 774-777. <https://doi.org/10.1021/acsmacrolett.5b00335>

64. Bernard, J., Lortie, F. & Fenet, B. Design of Heterocomplementary H-Bonding RAFT Agents – Towards the Generation of Supramolecular Star Polymers. *Macromolecular Rapid Communications*, **2009**, 30, 83-88. <https://doi.org/10.1002/marc.200800586>

65. Ren, Y. & Dong, X. Dynamic Polymeric Materials via Hydrogen-Bond Cross-Linking: Effect of Multiple Network Topologies. *Progress in Polymer Science*, **2024**, 158, 101890. <https://doi.org/10.1016/j.progpolymsci.2024.101890>

66. Feldman, K. E., Kade, M. J., de Greef, T. F. A., Meijer, E. W., Kramer, E. J. & Hawker, C. J. Polymers with Multiple Hydrogen-Bonded End Groups and Their Blends. *Macromolecules*, **2008**, 41, 4694-4700. <https://doi.org/10.1021/ma800375r>

67. Chen, S. B., Wang, K., Geng, Z., Chen, Y., Zheng, X. H., Wang, H. Y. & Zhu, J. T.

Construction and Morphology of Non-Covalently Double-Crosslinked Supramolecular Polymer Networks. *Polymer Chemistry*, **2019**, *10*, 4740-4745. <https://doi.org/10.1039/c9py00681h>

68. Altintas, O., Lejeune, E., Gerstel, P. & Barner-Kowollik, C. Bioinspired Dual Self-Folding of Single Polymer Chains via Reversible Hydrogen Bonding. *Polymer Chemistry*, **2012**, *3*, 640-651. <https://doi.org/10.1039/c1py00392e>

69. Mansfeld, U., Hager, M. D., Hoogenboom, R., Ott, C., Winter, A. & Schubert, U. S. Advanced Supramolecular Initiator for Nitroxide-Mediated Polymerizations Containing Both Metal-Ion Coordination and Hydrogen-Bonding Sites. *Chemical Communications*, **2009**, 3386. <https://doi.org/10.1039/b902636c>

70. Qin, B., Zhang, S., Sun, P., Tang, B., Yin, Z., Cao, X., Chen, Q., Xu, J. F. & Zhang, X. Tough and Multi-Recyclable Cross-Linked Supramolecular Polyureas via Incorporating Noncovalent Bonds into Main-Chains. *Advanced Materials*, **2020**, *32*, e2000096. <https://doi.org/10.1002/adma.202000096>

71. Rupp, H., Bhandary, R., Kulkarni, A. & Binder, W. Printable Electrolytes: Tuning 3D-Printing by Multiple Hydrogen Bonds and Added Inorganic Lithium-Salts. *Advanced Materials Technologies*, **2022**, *7*, 2200088. <https://doi.org/10.1002/admt.202200088>

72. Moad, G., Rizzardo, E. & Thang, S. H. End-Functional Polymers, Thiocarbonylthio Group Removal/Transformation and Reversible Addition–Fragmentation–Chain Transfer (RAFT) Polymerization. *Polymer International*, **2011**, *60*, 9-25. <https://doi.org/10.1002/pi.2988>

73. Chen, X. & Michinobu, T. Postpolymerization Modification: A Powerful Tool for the Synthesis and Function Tuning of Stimuli-Responsive Polymers. *Macromolecular Chemistry and Physics*, **2022**, *223*, 2100370. <https://doi.org/10.1002/macp.202100370>

74. Ezzah, Khan, A. & Stuparu, M. C. Post-Polymerization Modification Reactions of Poly(Glycidyl Methacrylate)s. *RSC Advances*, **2017**, *7*, 55874-55884. <https://doi.org/10.1039/c7ra11093f>

75. Mackanic, D. G., Yan, X., Zhang, Q., Matsuhisa, N., Yu, Z., Jiang, Y., Manika, T., Lopez, J., Yan, H., Liu, K., Chen, X., Cui, Y. & Bao, Z. Decoupling of Mechanical Properties and Ionic Conductivity in Supramolecular Lithium Ion Conductors. *Nature Communications*, **2019**, *10* <https://doi.org/10.1038/s41467-019-13362-4>

76. Liu, K., Cheng, L., Zhang, N., Pan, H., Fan, X., Li, G., Zhang, Z., Zhao, D., Zhao, J., Yang, X., Wang, Y., Bai, R., Liu, Y., Liu, Z., Wang, S., Gong, X., Bao, Z., Gu, G., Yu, W. & Yan, X. Biomimetic Impact Protective Supramolecular Polymeric Materials Enabled by Quadruple H-Bonding. *Journal of the American Chemical Society*, **2021**, *143*, 1162-1170. <https://doi.org/10.1021/jacs.0c12119>

77. Kushner, A. M., Vossler, J. D., Williams, G. A. & Guan, Z. A Biomimetic Modular Polymer with Tough and Adaptive Properties. *Journal of the American Chemical Society*,

**2009**, 131, 8766-8768. <https://doi.org/10.1021/ja9009666>

78. Herbst, F., Schröter, K., Gunkel, I., Gröger, S., Thurn-Albrecht, T., Balbach, J. & Binder, W. H. Aggregation and Chain Dynamics in Supramolecular Polymers by Dynamic Rheology: Cluster Formation and Self-Aggregation. *Macromolecules*, **2010**, 43, 10006-10016. <https://doi.org/10.1021/ma101962y>

79. Ostas, E., Yan, T. Z., Thurn-Albrecht, T. & Binder, W. H. Crystallization of Supramolecular Pseudoblock Copolymers. *Macromolecules*, **2013**, 46, 4481-4490. <https://doi.org/10.1021/ma400622w>

80. Lee, J. H., Bae, J., Hwang, J. H., Choi, M. Y., Kim, Y. S., Park, S., Na, J. H., Kim, D. G. & Ahn, S. K. Robust and Reprocessable Artificial Muscles Based on Liquid Crystal Elastomers with Dynamic Thiourea Bonds. *Advanced Functional Materials*, **2022**, 32, 2110360. <https://doi.org/10.1002/adfm.202110360>

81. Liu, H., Maugein, V. A. & Haddleton, D. M. Radical Polymerisation and Thiol–Ene Post-Polymerisation Functionalisation of Terpenoid Acrylates in Conventional and Renewably Sourced Organic Solvents. *Polymer Chemistry*, **2024**, 15, 2862-2872. <https://doi.org/10.1039/d4py00340c>

82. Lee, H. W. & Kim, J. G. Multifunctional Polymer Synthesis via Sequential Postpolymerization Modification Using a Single Aldehyde Repeat Unit: Allylation and Orthogonal Esterification and Thiol–ene Reaction. *ACS Macro Letters*, **2024**, 13, 1418-1424. <https://doi.org/10.1021/acsmacrolett.4c00618>

83. Chen, S., Li, Z., Wu, Y., Mahmood, N., Lortie, F., Bernard, J., Binder, W. H. & Zhu, J. Hydrogen-Bonded Supramolecular Polymer Adhesives: Straightforward Synthesis and Strong Substrate Interaction. *Angewandte Chemie International Edition*, **2022**, 61, e202203876. <https://doi.org/10.1002/anie.202203876>

84. Chen, S. B., Schulz, M., Lechner, B. D., Appiah, C. & Binder, W. H. One-pot Synthesis and Self-Assembly of Supramolecular Dendritic Polymers. *Polymer Chemistry*, **2015**, 6, 7988-7994. <https://doi.org/10.1039/c5py01329a>

85. Beyer, V. P., Cattoz, B., Strong, A., Phillips, D. J., Schwarz, A. & Remzi Becer, C. Fast Track Access to Multi-Block Copolymers via Thiol-Bromo Click Reaction of Telechelic Dibromo Polymers. *Polymer Chemistry*, **2019**, 10, 4259-4270. <https://doi.org/10.1039/c9py00775j>

86. Chen, L., Zheng, Y., Meng, X., Wei, G., Dietliker, K. & Li, Z. Delayed Thiol-Epoxy Photopolymerization: A General and Effective Strategy to Prepare Thick Composites. *ACS Omega*, **2020**, 5, 15192-15201. <https://doi.org/10.1021/acsomega.0c01170>

87. Biedermann, F., Appel, E. A., del Barrio, J., Gruending, T., Barner-Kowollik, C. & Scherman, O. A. Postpolymerization Modification of Hydroxyl-Functionalized Polymers with Isocyanates. *Macromolecules*, **2011**, 44, 4828-4835. <https://doi.org/10.1021/ma2008018>

88. Folmer, B. J. B., Sijbesma, R. P., Versteegen, R. M., Van Der Rijt, J. A. J. & Meijer, E. W. Supramolecular Polymer Materials: Chain Extension of Telechelic Polymers Using a Reactive Hydrogen-Bonding Synthon. *Advanced Materials*, **2000**, 12, 874-878. [https://doi.org/10.1002/1521-4095\(200006\)12:12<874::aid-adma874>3.0.co;2-c](https://doi.org/10.1002/1521-4095(200006)12:12<874::aid-adma874>3.0.co;2-c)
89. Yang, J. H., Lee, J., Lim, S., Jung, S., Jang, S. H., Jang, S. H., Kwak, S. Y., Ahn, S., Jung, Y. C., Priestley, R. D. & Chung, J. W. Understanding and Controlling the Self-Healing Behavior of 2-Ureido-4[1H]-Pyrimidinone-Functionalized Clustery and Dendritic Dual Dynamic Supramolecular Network. *Polymer*, **2019**, 172, 13-26. <https://doi.org/10.1016/j.polymer.2019.03.027>
90. Chen, H., Wang, L., Feng, S. & Li, L. Efficient and Facile Dual Post-Polymerization Modification Using Acetoacetate-Acrylate Michael Addition. *European Polymer Journal*, **2024**, 220, 113463. <https://doi.org/10.1016/j.eurpolymj.2024.113463>
91. Hoffmann, C., Stuparu, M. C., Daugaard, A. & Khan, A. Aza-Michael Addition Reaction: Post-Polymerization Modification and Preparation of PEI/PEG-Based Polyester Hydrogels from Enzymatically Synthesized Reactive Polymers. *Journal of Polymer Science Part A: Polymer Chemistry*, **2015**, 53, 745-749. <https://doi.org/10.1002/pola.27498>
92. Dai, Y., Zhang, X. & Xia, F. Click Chemistry in Functional Aliphatic Polycarbonates. *Macromolecular Rapid Communications*, **2017**, 38, 1700357. <https://doi.org/10.1002/marc.201700357>
93. Hirao, A., Tohoyama, M. & Nakahama, S. Synthesis of End-Functionalized Polymers by Means of Living Anionic Polymerization. 8. Reactions of Living Anionic Polymers with  $\alpha,\omega$ -Dihaloalkanes. *Macromolecules*, **1997**, 30, 3484-3489. <https://doi.org/10.1021/ma970138a>
94. Hadjichristidis, N., Pispas, S. & Pitsikalis, M. End-Functionalized Polymers with Zwitterionic End-Groups. *Progress in Polymer Science*, **1999**, 24, 875-915. [https://doi.org/10.1016/S0079-6700\(99\)00018-0](https://doi.org/10.1016/S0079-6700(99)00018-0)
95. Nifant'Ev, I. E., Korchagina, S. A., Chinova, M. S. & Tsvetkov, A. N. Polyisobutylenes with Controlled Molecular Weight and Chain-End Structure: Synthesis and Actual Applications. *Polymers*, **2023**, 15, 3415. <https://doi.org/10.3390/polym15163415>
96. Binder, W. H., Kunz, M. J., Kluger, C., Hayn, G. & Saf, R. Synthesis and Analysis of Telechelic Polyisobutylenes for Hydrogen-Bonded Supramolecular Pseudo-Block Copolymers. *Macromolecules*, **2004**, 37, 1749-1759. <https://doi.org/10.1021/ma034924t>
97. Rossow, T. & Seiffert, S. 1-46 (Springer International Publishing, 2015) [https://doi.org/10.1007/978-3-319-15404-6\\_1](https://doi.org/10.1007/978-3-319-15404-6_1)
98. Beingessner, R. L., Fan, Y. & Fenniri, H. Molecular and Supramolecular Chemistry of Rosette Nanotubes. *RSC Advances*, **2016**, 6, 75820-75838. <https://doi.org/10.1039/c6ra16315g>

99. Gruschwitz, F. V., Klein, T., Catrouillet, S. & Brendel, J. C. Supramolecular Polymer Bottlebrushes. *Chemical Communications*, **2020**, 56, 5079-5110. <https://doi.org/10.1039/d0cc01202e>
100. Zhang, M., Kim, M., Choi, W., Choi, J., Kim, D. H., Liu, Y. & Lin, Z. Chiral Macromolecules and Supramolecular Assemblies: Synthesis, Properties and Applications. *Progress in Polymer Science*, **2024**, 151, 101800. <https://doi.org/10.1016/j.progpolymsci.2024.101800>
101. Zhang, K., Wu, Y., Chen, S. & Zhu, J. Programmable Reconfiguration of Supramolecular Bottlebrush Block Copolymers: From Solution Self-Assembly to Co-Crystallization-Assistant Self-Assembly. *Angewandte Chemie International Edition*, **2024**, 136 <https://doi.org/10.1002/anie.202408730>
102. Wang, H. Y., Chen, Q., Geng, Z., Rao, J. Y., Xiong, B. J., Lortie, F., Bernard, J., Binder, W. H., Chen, S. B. & Zhu, J. T. Hydrogen-Bonding Mediated Self-Assembly of Amphiphilic ABA Triblock Copolymers into Well-Defined Giant Vesicles. *Polymer Chemistry*, **2021**, 12, 6300-6306. <https://doi.org/10.1039/d1py01061a>
103. Watson, J. D. & Crick, F. H. C. Molecular Structure of Nucleic Acids: A Structure for Deoxyribose Nucleic Acid. *Nature*, **1953**, 171, 737-738. <https://doi.org/10.1038/171737a0>
104. Watson, J. D. & Crick, F. H. C. Genetical Implications of the Structure of Deoxyribonucleic Acid. *Nature*, **1953**, 171, 964-967. <https://doi.org/10.1038/171964b0>
105. Crick, F. H. C. & Watson, J. D. The Complementary Structure of Deoxyribonucleic Acid. *Proceedings of the Royal Society of London. Series A. Mathematical and Physical Sciences*, **1954**, 223, 80-96. <https://doi.org/10.1098/rspa.1954.0101>
106. Baker, E. N. & Hubbard, R. E. Hydrogen Bonding in Globular Proteins. *Progress in Biophysics and Molecular Biology*, **1984**, 44, 97-179. [https://doi.org/10.1016/0079-6107\(84\)90007-5](https://doi.org/10.1016/0079-6107(84)90007-5)
107. Dill, K. A. & MacCallum, J. L. The Protein-Folding Problem, 50 Years On. *Science*, **2012**, 338, 1042-1046. <https://doi.org/10.1126/science.1219021>
108. Yang, A.-S. & Honig, B. Free Energy Determinants of Secondary Structure Formation: I.  $\alpha$ -Helices. *Journal of Molecular Biology*, **1995**, 252, 351-365. <https://doi.org/10.1006/jmbi.1995.0502>
109. Chen, G., Ge, X., Sun, Y., Sui, W., Jin, Y., Geng, J., Zhang, M. & Wu, T. Identification of Two Novel  $\alpha$ -Amylase Inhibitory Activity Peptide from Russian Sea Cucumber Body Wallprotein Hydrolysate. *International Journal of Biological Macromolecules*, **2025**, 295, 139499. <https://doi.org/10.1016/j.ijbiomac.2025.139499>
110. Zhu, B., Zhang, M., Li, M., Pan, K., Yao, P., Zhang, X. & Wu, X. Genome-Wide Identification and Gene Expression Pattern Reveal Dominant Digestive Enzyme Genes Contributing to Major Enzyme Activities During the Molting Cycle of the Chinese Mitten

- Crab, Eriocheir Sinensis. *Aquaculture*, **2025**, 597, 741944.  
<https://doi.org/10.1016/j.aquaculture.2024.741944>
111. Silberstein, M., Dennis, S., Brown, L., Kortvelyesi, T., Clodfelter, K. & Vajda, S. Identification of Substrate Binding Sites in Enzymes by Computational Solvent Mapping. *Journal of Molecular Biology*, **2003**, 332, 1095-1113.  
<https://doi.org/10.1016/j.jmb.2003.08.019>
112. Pace, C. N., Fu, H., Fryar, K. L., Landua, J., Trevino, S. R., Shirley, B. A., Hendricks, M. M., Iimura, S., Gajiwala, K., Scholtz, J. M. & Grimsley, G. R. Contribution of Hydrophobic Interactions to Protein Stability. *Journal of Molecular Biology*, **2011**, 408, 514-528.  
<https://doi.org/10.1016/j.jmb.2011.02.053>
113. Xiao, F., Chen, Z., Wei, Z. & Tian, L. Hydrophobic Interaction: A Promising Driving Force for the Biomedical Applications of Nucleic Acids. *Advanced Science*, **2020**, 7, 2001048. <https://doi.org/10.1002/advs.202001048>
114. Sun, T., Korolev, N., Lyubartsev, A. P. & Nordenskiöld, L. CG Modeling of Nucleosome Arrays Reveals the Salt-Dependent Chromatin Fiber Conformational Variability. *The Journal of Chemical Physics*, **2025**, 162 <https://doi.org/10.1063/5.0242509>
115. Zhao, X., Zhang, Y., Wang, X., Fu, Z., Zhong, Z. & Deng, C. Multivalent Ionizable Lipid-Polypeptides for Tumor-Confined mRNA Transfection. *Bioactive Materials*, **2025**, 46, 423-433. <https://doi.org/10.1016/j.bioactmat.2024.12.032>
116. Yan, T. Z., Schröter, K., Herbst, F., Binder, W. H. & Thurn-Albrecht, T. Nanostructure and Rheology of Hydrogen-Bonding Telechelic Polymers in the Melt: From Micellar Liquids and Solids to Supramolecular Gels. *Macromolecules*, **2014**, 47, 2122-2130.  
<https://doi.org/10.1021/ma402007f>
117. Appel, W. P. J., Portale, G., Wisse, E., Dankers, P. Y. W. & Meijer, E. W. Aggregation of Ureido-Pyrimidinone Supramolecular Thermoplastic Elastomers into Nanofibers: A Kinetic Analysis. *Macromolecules*, **2011**, 44, 6776-6784.  
<https://doi.org/10.1021/ma201303s>
118. Terashima, T., Mes, T., De Greef, T. F. A., Gillissen, M. A. J., Besenius, P., Palmans, A. R. A. & Meijer, E. W. Single-Chain Folding of Polymers for Catalytic Systems in Water. *Journal of the American Chemical Society*, **2011**, 133, 4742-4745.  
<https://doi.org/10.1021/ja2004494>
119. Kim, J., Jung, H. Y. & Park, M. J. End-Group Chemistry and Junction Chemistry in Polymer Science: Past, Present, and Future. *Macromolecules*, **2020**, 53, 746-763.  
<https://doi.org/10.1021/acs.macromol.9b02293>
120. Ebnesajjad, S. in *Chemical Resistance of Engineering Thermoplastics* (eds Erwin Baur, Katja Ruhrberg, & William Woishnis) xiii-xxv (William Andrew Publishing, 2016)  
<https://doi.org/10.1016/B978-0-323-47357-6.00021-0>



121. Rubinstein, M. & Colby, R. H. *Polymer Physics*. (Oxford University Press, **2003**), ISBN: 9780198520597. <https://doi.org/10.1093/oso/9780198520597.001.0001>
122. Mark, J., Ngai, K., Graessley, W., Mandelkern, L., Samulski, E., Koenig, J. & Wignall, G. in *Physical Properties of Polymers* (eds James Mark, Kia Ngai, William Graessley, Leo Mandelkern, Edward Samulski, Jack Koenig, & George Wignall) 72-152 (Cambridge University Press, 2004) <https://doi.org/10.1017/CBO9781139165167.003>
123. Chen, S. B., Döhler, D. & Binder, W. H. Rheology of Hydrogen-Bonded Dendritic Supramolecular Polymer Networks in the Melt State. *Polymer*, **2016**, 107, 466-473. <https://doi.org/10.1016/j.polymer.2016.08.046>
124. Chen, S. & Binder, W. H. Dynamic Ordering and Phase Segregation in Hydrogen-Bonded Polymers. *Accounts of Chemical Research*, **2016**, 49, 1409-1420. <https://doi.org/10.1021/acs.accounts.6b00174>
125. Cortese, J., Soulié-Ziakovic, C., Cloitre, M., Tencé-Girault, S. & Leibler, L. Order–Disorder Transition in Supramolecular Polymers. *Journal of the American Chemical Society*, **2011**, 133, 19672-19675. <https://doi.org/10.1021/ja209126a>
126. Cortese, J., Soulié-Ziakovic, C., Tencé-Girault, S. & Leibler, L. Suppression of Mesoscopic Order by Complementary Interactions in Supramolecular Polymers. *Journal of the American Chemical Society*, **2012**, 134, 3671-3674. <https://doi.org/10.1021/ja2119496>
127. Jangizehi, A., Ghaffarian, S. R. & Ahmadi, M. Dynamics of Entangled Supramolecular Polymer Networks in Presence of High-Order Associations of Strong Hydrogen Bonding Groups. *Polymers for Advanced Technologies*, **2018**, 29, 726-735. <https://doi.org/10.1002/pat.4178>
128. L. Brunsveld, J. A. J. M. V., J. H. K. K. Hirschberg, R. P. Sijbesma, and E. W. Meijer. Hierarchical Formation of Helical Supramolecular Polymers via Stacking of Hydrogen-Bonded Pairs in Water. *Proceedings of the National Academy of Sciences of the United States of America*, **2002**, 99 <https://doi.org/10.1073/pnas.072659099>
129. Hirschberg, J. H. K. K., Brunsveld, L., Ramzi, A., Vekemans, J. A. J. M., Sijbesma, R. P. & Meijer, E. W. Helical Self-Assembled Polymers from Cooperative Stacking of Hydrogen-Bonded Pairs. *Nature*, **2000**, 407, 167-170. <https://doi.org/10.1038/35025027>
130. Herbst, F., Seiffert, S. & Binder, W. H. Dynamic Supramolecular Poly(Isobutylene)s for Self-Healing Materials. *Polymer Chemistry*, **2012**, 3, 3084-3092. <https://doi.org/10.1039/c2py20265d>
131. Kang, Y., Lu, A., Ellington, A., Jewett, M. C. & O'Reilly, R. K. Effect of Complementary Nucleobase Interactions on the Copolymer Composition of RAFT Copolymerizations. *ACS Macro Letters*, **2013**, 2, 581-586. <https://doi.org/10.1021/mz4001833>
132. Binder, W. H., Petraru, L., Roth, T., Groh, P. W., Pálfi, V., Keki, S. & Ivan, B. Magnetic



and Temperature-Sensitive Release Gels from Supramolecular Polymers. *Advanced Functional Materials*, **2007**, 17, 1317-1326. <https://doi.org/10.1002/adfm.200601084>

133. Piest, M., Zhang, X. L., Trinidad, J. & Engbersen, J. F. J. PH-Responsive, Dynamically Restructuring Hydrogels Formed by Reversible Crosslinking of PVA with Phenylboronic Acid Functionalised PPO-PEO-PPO Spacers (Jeffamines®). *Soft Matter*, **2011**, 7, 11111-11118. <https://doi.org/10.1039/c1sm06230a>

134. Mane, S. R., Rao, N. V. & Shunmugam, R. Reversible pH- and Lipid-Sensitive Vesicles from Amphiphilic Norbornene-Derived Thiobarbiturate Homopolymers. *ACS Macro Letters*, **2012**, 1, 482-488. <https://doi.org/10.1021/mz2002092>

135. Liu, Y., Wang, L., Zhao, L., Zhang, Y., Li, Z.-T. & Huang, F. Multiple Hydrogen Bonding Driven Supramolecular Architectures and Their Biomedical Applications. *Chemical Society Reviews*, **2024**, 53, 1592-1623. <https://doi.org/10.1039/d3cs00705g>

136. Wu, Y. G., Wang, H. Y., Liu, Q. Q., Lortie, F., Bernard, J., Binder, W. H., Chen, S. B. & Zhu, J. T. Hydrogen-Bonded Supramolecular Polymer Micelles with pH/Photothermal-Responsive Carmofur Release and Combined Chemo-Photothermal Therapy. *Polymer Chemistry*, **2022**, 13, 1010-1014. <https://doi.org/10.1039/d1py01634b>

137. Rupp, H., Dohler, D., Hilgeroth, P., Mahmood, N., Beiner, M. & Binder, W. H. 3D Printing of Supramolecular Polymers: Impact of Nanoparticles and Phase Separation on Printability. *Macromol Rapid Commun*, **2019**, 40, e1900467. <https://doi.org/10.1002/marc.201900467>

138. Xiang, W. & Xia, J. Synthesis of Novel (Meth)acrylates with Variable Hydrogen Bond Interaction and Their Application in a Clear Viscoelastic Film. *ACS Omega*, **2024**, 9, 13644-13654. <https://doi.org/10.1021/acsomega.3c07566>

139. Spencer, J. N., Campanella, C. L., Harris, E. M. & Wolbach, W. S. Solvent Effects on Hydrogen-Bond Formation .2. *Journal of Physical Chemistry*, **1985**, 89, 1888-1891. <https://doi.org/10.1021/j100256a015>

140. Cook, J. L., Hunter, C. A., Low, C. M., Perez-Velasco, A. & Vinter, J. G. Solvent Effects on Hydrogen Bonding. *Angewandte Chemie International Edition*, **2007**, 46, 3706-3709. <https://doi.org/10.1002/anie.200604966>

141. Cabot, R., Hunter, C. A. & Varley, L. M. Hydrogen Bonding Properties of Non-Polar Solvents. *Organic & Biomolecular Chemistry*, **2010**, 8, 1455-1462. <https://doi.org/10.1039/b921003b>

142. Selin, V., Aliakseyeu, A., Ankner, J. F. & Sukhishvili, S. A. Effect of a Competitive Solvent on Binding Enthalpy and Chain Intermixing in Hydrogen-Bonded Layer-by-Layer Films. *Macromolecules*, **2019**, 52, 4432-4440. <https://doi.org/10.1021/acs.macromol.9b00650>

143. Wurthner, F. Solvent Effects in Supramolecular Chemistry: Linear Free Energy

- Relationships for Common Intermolecular Interactions. *The Journal of Organic Chemistry*, **2022**, 87, 1602-1615. <https://doi.org/10.1021/acs.joc.1c00625>
144. Steiner, T. The Hydrogen Bond in the Solid State. *Angewandte Chemie International Edition*, **2002**, 41, 49-76. [https://doi.org/10.1002/1521-3773\(20020104\)41:1<48::aid-anie48>3.0.co;2-u](https://doi.org/10.1002/1521-3773(20020104)41:1<48::aid-anie48>3.0.co;2-u)
145. Strobl, G. The Physics of Polymers. 3 edn, (Springer Berlin, **2007**), ISBN: 978-3-540-68411-4. <https://doi.org/10.1007/978-3-540-68411-4>
146. Teraoka, I. Polymer Solutions: An Introduction to Physical Properties. (Wiley, **2002**), ISBN: 9780471224518. <https://doi.org/10.1002/0471224510>
147. Catrouillet, S., Fonteneau, C., Bouteiller, L., Delorme, N., Nicol, E., Nicolai, T., Pensec, S. & Colombani, O. Competition Between Steric Hindrance and Hydrogen Bonding in the Formation of Supramolecular Bottle Brush Polymers. *Macromolecules*, **2013**, 46, 7911-7919. <https://doi.org/10.1021/ma401167n>
148. Pensec, S., Nouvel, N., Guilleman, A., Creton, C., Boué, F. & Bouteiller, L. Self-Assembly in Solution of a Reversible Comb-Shaped Supramolecular Polymer. *Macromolecules*, **2010**, 43, 2529-2534. <https://doi.org/10.1021/ma901709e>
149. Catrouillet, S., Bouteiller, L., Nicol, E., Nicolai, T., Pensec, S., Jacquette, B., Le Bohec, M. & Colombani, O. Self-Assembly and Critical Solubility Temperature of Supramolecular Polystyrene Bottle-Brushes in Cyclohexane. *Macromolecules*, **2015**, 48, 1364-1370. <https://doi.org/10.1021/ma5024022>
150. Aquino, A. J. A., Tunega, D., Haberhauer, G., Gerzabek, M. H. & Lischka, H. Solvent Effects on Hydrogen Bonds A Theoretical Study. *The Journal of Physical Chemistry A*, **2002**, 106, 1862-1871. <https://doi.org/10.1021/jp013677x>
151. Sikder, A. & Ghosh, S. Hydrogen-Bonding Regulated Assembly of Molecular and Macromolecular Amphiphiles. *Materials Chemistry Frontiers*, **2019**, 3, 2602-2616. <https://doi.org/10.1039/c9qm00473d>
152. Fortier-McGill, B., Toader, V. & Reven, L. <sup>13</sup>C MAS NMR Study of Poly(Methacrylic Acid)-Polyether Complexes and Multilayers. *Macromolecules*, **2014**, 47, 4298-4307. <https://doi.org/10.1021/ma401673n>
153. Saif, M. S., Waqas, M., Hussain, R., Ahmed, M. M., Tariq, T., Batool, S., Liu, Q., Mustafa, G. & Hasan, M. Potential of CME@ZIF-8 MOF Nanoformulation: Smart Delivery of Silymarin for Enhanced Performance and Mechanism in Albino Rats. *ACS Applied Bio Materials*, **2024**, 7, 6919-6931. <https://doi.org/10.1021/acsabm.4c01019>
154. Wang, J., Zhou, Y., Zhang, J., Tong, Y., Abbas, Z., Zhao, X., Li, Z., Zhang, H., Chen, S., Si, D., Zhang, R. & Wei, X. Peptide TaY Attenuates Inflammatory Responses by Interacting with Myeloid Differentiation 2 and Inhibiting NF-κB Signaling Pathway. *Molecules*, **2024**, 29, 4843. <https://doi.org/10.3390/molecules29204843>

155. Chang, X., Geng, Y., Cao, H., Zhou, J., Tian, Y., Shan, G., Bao, Y., Wu, Z. L. & Pan, P. Dual-Crosslink Physical Hydrogels with High Toughness Based on Synergistic Hydrogen Bonding and Hydrophobic Interactions. *Macromolecular Rapid Communications*, **2018**, 39, 1700806. <https://doi.org/10.1002/marc.201700806>
156. Lombardi, A., Summa, C. M., Geremia, S., Randaccio, L., Pavone, V. & Degrado, W. F. Retrostructural Analysis of Metalloproteins: Application to the Design of a Minimal Model for Diiron Proteins. *Proceedings of the National Academy of Sciences*, **2000**, 97, 6298-6305. <https://doi.org/10.1073/pnas.97.12.6298>
157. Mandal, P., Patra, D. & Shunmugam, R. Hierarchical Self-Assembled Nanostructures of Lactone-Derived Thiobarbiturate Homopolymers for Stimuli-Responsive Delivery Applications. *Polymer Chemistry*, **2020**, 11, 3340-3348. <https://doi.org/10.1039/d0py00367k>
158. Thordarson, P. Determining Association Constants from Titration Experiments in Supramolecular Chemistry. *Chemical Society Reviews*, **2011**, 40, 1305-1323. <https://doi.org/10.1039/c0cs00062k>
159. Chen, S., Bertrand, A., Chang, X., Alcouffe, P., Ladavière, C., Gérard, J.-F., Lortie, F. & Bernard, J. Heterocomplementary H-Bonding RAFT Agents as Tools for the Preparation of Supramolecular Miktoarm Star Copolymers. *Macromolecules*, **2010**, 43, 5981-5988. <https://doi.org/10.1021/ma101044y>
160. Binder, W. H., Kunz, M. J. & Ingolic, E. Supramolecular Poly(Ether Ketone)–Polyisobutylene Pseudo-Block Copolymers. *Journal of Polymer Science Part A: Polymer Chemistry*, **2004**, 42, 162-172. <https://doi.org/10.1002/pola.10979>
161. Herbst, F. & Binder, W. H. Comparing Solution and Melt-State Association of Hydrogen Bonds in Supramolecular Polymers. *Polymer Chemistry*, **2013**, 4, 3602-3609. <https://doi.org/10.1039/c3py00362k>
162. Cortese, J., Soulié-Ziakovic, C. & Leibler, L. Binding and Supramolecular Organization of Homo- and Heterotelechelic Oligomers in Solutions. *Polymer Chemistry*, **2014**, 5, 116-125. <https://doi.org/10.1039/c3py00638g>
163. Bielejewska, A. G., Marjo, C. E., Prins, L. J., Timmerman, P., de Jong, F. & Reinhoudt, D. N. Thermodynamic Stabilities of Linear and Crinkled Tapes and Cyclic Rosettes in Melamine–Cyanurate Assemblies: A Model Description. *Journal of the American Chemical Society*, **2001**, 123, 7518-7533. <https://doi.org/10.1021/ja010664o>
164. Würthner, F., Thalacker, C., Sautter, A., Schärfl, W., Ibach, W. & Hollricher, O. Hierarchical Self-Organization of Perylene Bisimide–Melamine Assemblies to Fluorescent Mesoscopic Superstructures. *Chemistry – A European Journal*, **2000**, 6, 3871-3886. [https://doi.org/10.1002/1521-3765\(20001103\)6:21<3871::aid-chem3871>3.0.co;2-4](https://doi.org/10.1002/1521-3765(20001103)6:21<3871::aid-chem3871>3.0.co;2-4)
165. Motloch, P. & Hunter, C. A. Quantification of Cooperativity in the Self-Assembly of H-Bonded Rosettes. *Organic & Biomolecular Chemistry*, **2020**, 18, 1602-1606.

<https://doi.org/10.1039/d0ob00068j>

166. Chen, S. B., Wu, Y. G., Wang, H. Y., Zhu, B. G., Xiong, B. J., Binder, W. H. & Zhu, J. T. Synthesis and Self-Aggregated Nanostructures of Hydrogen-Bonding Polydimethylsiloxane. *Polymer Chemistry*, **2021**, 12, 4111-4119. <https://doi.org/10.1039/d1py00513h>
167. Lye, D. S., Xia, Y., Wong, M. Z., Wang, Y., Nieh, M.-P. & Weck, M. ABC Supramolecular Triblock Copolymer by ROMP and ATRP. *Macromolecules*, **2017**, 50, 4244-4255. <https://doi.org/10.1021/acs.macromol.7b00169>
168. Croom, A., Manning, K. B. & Weck, M. Supramolecular Helix–Helix Block Copolymers. *Macromolecules*, **2016**, 49, 7117-7128. <https://doi.org/10.1021/acs.macromol.6b01410>
169. Deng, R., Milton, M., Pomarico, S. K. & Weck, M. Synthesis of a Heterotelechelic Helical Poly(Methacrylamide) and its Incorporation into a Supramolecular Triblock Copolymer. *Polymer Chemistry*, **2019**, 10, 5087-5093. <https://doi.org/10.1039/c9py01047e>
170. Lu, J., Deng, Y., Zhong, K., Huang, Z. & Jin, L. Y. Construction of Nanoaggregates from Amphiphilic Supramolecules Containing Barbiturate and Hamilton Wedge Units. *Polymer International*, **2021**, 71, 478-486. <https://doi.org/10.1002/pi.6318>
171. Söntjens, S. H. M., Sijbesma, R. P., van Genderen, M. H. P. & Meijer, E. W. Stability and Lifetime of Quadruply Hydrogen Bonded 2-Ureido-4[1H]-Pyrimidinone Dimers. *Journal of the American Chemical Society*, **2000**, 122, 7487-7493. <https://doi.org/10.1021/ja000435m>
172. De Greef, T. F. A., Kade, M. J., Feldman, K. E., Kramer, E. J., Hawker, C. J. & Meijer, E. W. Spacer-Length-Dependent Association in Polymers with Multiple-Hydrogen-Bonded End Groups. *Journal of Polymer Science Part A: Polymer Chemistry*, **2011**, 49, 4253-4260. <https://doi.org/10.1002/pola.24868>
173. Ahmadi, M., Löser, L., Fischer, K., Saalwächter, K. & Seiffert, S. Connectivity Defects and Collective Assemblies in Model Metallo-Supramolecular Dual-Network Hydrogels. *Macromolecular Chemistry and Physics*, **2020**, 221, 1900400. <https://doi.org/10.1002/macp.201900400>
174. Lutkenhaus, J. L., McEnnis, K. & Hammond, P. T. Tuning the Glass Transition of and Ion Transport within Hydrogen-Bonded Layer-by-Layer Assemblies. *Macromolecules*, **2007**, 40, 8367-8373. <https://doi.org/10.1021/ma0713557>
175. Brás, A. R., Arizaga, A., Sokolova, D., Agirre, U., Viciosa, M. T., Radulescu, A., Prévost, S. F., Kruteva, M., Pyckhout-Hintzen, W. & Schmidt, A. M. Influence of Polymer Polarity and Association Strength on the Properties of Poly(Alkyl Ether)-Based Supramolecular Melts. *Macromolecules*, **2022**, 55, 10014-10030. <https://doi.org/10.1021/acs.macromol.2c01116>
176. Ahmadi, M., Jangizehi, A. & Seiffert, S. Backbone Polarity Tunes Sticker Clustering in

- Hydrogen-Bonded Supramolecular Polymer Networks. *Macromolecules*, **2022**, *55*, 5514-5526. <https://doi.org/10.1021/acs.macromol.2c00645>
177. Fortier-McGill, B., Toader, V. & Reven, L. <sup>1</sup>H Solid State NMR Study of Poly(Methacrylic Acid) Hydrogen-Bonded Complexes. *Macromolecules*, **2012**, *45*, 6015-6026. <https://doi.org/10.1021/ma300534t>
178. Fortier-McGill, B., Toader, V. & Reven, L. Chain Dynamics of Water-Saturated Hydrogen-Bonded Polymer Complexes and Multilayers. *Macromolecules*, **2011**, *44*, 2755-2765. <https://doi.org/10.1021/ma102907w>
179. Liu, Q. H., Wang, C., Guo, Y. H., Peng, C., Narayanan, A., Kaur, S., Xu, Y., Weiss, R. A. & Joy, A. Opposing Effects of Side-Chain Flexibility and Hydrogen Bonding on the Thermal, Mechanical, and Rheological Properties of Supramolecularly Cross-Linked Polyesters. *Macromolecules*, **2018**, *51*, 9294-9305. <https://doi.org/10.1021/acs.macromol.8b01781>
180. Scheiner, S. & Kar, T. Effect of Solvent upon CH $\cdots$ O Hydrogen Bonds with Implications for Protein Folding. *The Journal of Physical Chemistry B*, **2005**, *109*, 3681-3689. <https://doi.org/10.1021/jp0446736>
181. Cai, W., Xu, D., Zhang, F., Wei, J., Lu, S., Qian, L., Lu, Z. & Cui, S. Intramolecular Hydrogen Bonds in a Single Macromolecule: Strength in High Vacuum Versus Liquid Environments. *Nano Research*, **2022**, *15*, 1517-1523. <https://doi.org/10.1007/s12274-021-3696-1>
182. Lewis, C. L., Stewart, K. & Anthamatten, M. The Influence of Hydrogen Bonding Side-Groups on Viscoelastic Behavior of Linear and Network Polymers. *Macromolecules*, **2014**, *47*, 729-740. <https://doi.org/10.1021/ma402368s>
183. Fagnani, D. E., Bou Zerdan, R. & Castellano, R. K. Synthesis, Optoelectronic Properties, Self-Association, and Base Pairing of Nucleobase-Functionalized Oligothiophenes. *The Journal of Organic Chemistry*, **2018**, *83*, 12711-12721. <https://doi.org/10.1021/acs.joc.8b02138>
184. Jordan, A., Stoy, P. & Sneddon, H. F. Chlorinated Solvents: Their Advantages, Disadvantages, and Alternatives in Organic and Medicinal Chemistry. *Chemical Reviews*, **2021**, *121*, 1582-1622. <https://doi.org/10.1021/acs.chemrev.0c00709>
185. Meredith, N. Y., Borsley, S., Smolyar, I. V., Nichol, G. S., Baker, C. M., Ling, K. B. & Cockroft, S. L. Dissecting Solvent Effects on Hydrogen Bonding. *Angewandte Chemie International Edition*, **2022**, *61*, e202206604. <https://doi.org/10.1002/anie.202206604>
186. Crago, M., Lee, A., Hoang, T. P., Talebian, S. & Naficy, S. Protein Adsorption on Blood-Contacting Surfaces: A Thermodynamic Perspective to Guide the Design of Antithrombogenic Polymer Coatings. *Acta Biomaterialia*, **2024**, *180*, 46-60. <https://doi.org/10.1016/j.actbio.2024.04.018>

- 187.van Beek, D. J. M., Spiering, A. J. H., Peters, G. W. M., te Nijenhuis, K. & Sijbesma, R. P. Unidirectional Dimerization and Stacking of Ureidopyrimidinone End Groups in Polycaprolactone Supramolecular Polymers. *Macromolecules*, **2007**, *40*, 8464-8475. <https://doi.org/10.1021/ma0712394>
- 188.Ahmadi, M., Jangizehi, A., van Ruymbek, E. & Seiffert, S. Deconvolution of the Effects of Binary Associations and Collective Assemblies on the Rheological Properties of Entangled Side-Chain Supramolecular Polymer Networks. *Macromolecules*, **2019**, *52*, 5255-5267. <https://doi.org/10.1021/acs.macromol.9b00323>
- 189.Wang, H., Liu, H., Cao, Z., Li, W., Huang, X., Zhu, Y., Ling, F., Xu, H., Wu, Q., Peng, Y., Yang, B., Zhang, R., Kessler, O., Huang, G. & Wu, J. Room-Temperature Autonomous Self-healing Glassy Polymers with Hyperbranched Structure. *Proceedings of the National Academy of Sciences*, **2020**, *117*, 11299-11305. <https://doi.org/10.1073/pnas.2000001117>
- 190.Chen, S., Meister, A. & Binder, W. H. Supramolecular Semifluorinated Dendrons Glued by Weak Hydrogen-Bonds. *Chemical Communications*, **2017**, *53*, 8699-8702. <https://doi.org/10.1039/c7cc04683a>
- 191.Krishna, S., Sreedhar, I. & Patel, C. M. Molecular Dynamics Simulation of Polyamide-Based Materials – A Review. *Computational Materials Science*, **2021**, *200*, 110853. <https://doi.org/10.1016/j.commatsci.2021.110853>
- 192.Qin, Y., Summerscales, J., Graham-Jones, J., Meng, M. & Pemberton, R. Monomer Selection for In Situ Polymerization Infusion Manufacture of Natural-Fiber Reinforced Thermoplastic-Matrix Marine Composites. *Polymers*, **2020**, *12*, 2928. <https://doi.org/10.3390/polym12122928>
- 193.Seguela, R. Overview and Critical Survey of Polyamide6 Structural Habits: Misconceptions and Controversies. *Journal of Polymer Science*, **2020**, *58*, 2971-3003. <https://doi.org/10.1002/pol.20200454>
- 194.Chen, S. B., Frenzel, F., Cui, B., Gao, F., Campanella, A., Funtan, A., Kremer, F., Parkin, S. S. P. & Binder, W. H. Gating Effects of Conductive Polymeric Ionic Liquids. *Journal of Materials Chemistry C*, **2018**, *6*, 8242-8250. <https://doi.org/10.1039/c8tc01936c>
- 195.Chen, S. B., Funtan, A., Gao, F., Cui, B., Meister, A., Parkin, S. S. P. & Binder, W. H. Synthesis and Morphology of Semifluorinated Polymeric Ionic Liquids. *Macromolecules*, **2018**, *51*, 8620-8628. <https://doi.org/10.1021/acs.macromol.8b01624>
- 196.Chen, S., Lechner, B. D., Meister, A. & Binder, W. H. Hierarchical Micelles via Polyphilic Interactions: Hydrogen-Bonded Supramolecular Dendrons and Double Immiscible Polymers. *Nano Letters*, **2016**, *16*, 1491-1496. <https://doi.org/10.1021/acs.nanolett.5b05203>
- 197.Hillmyer, M. A. & Lodge, T. P. Synthesis and Self-Assembly of Fluorinated Block Copolymers. *Journal of Polymer Science Part A: Polymer Chemistry*, **2002**, *40*, 1-8. <https://doi.org/10.1002/pola.10074>



198. Tian, F.-X. & Qu, J. Studies on the Origin of the Stabilizing Effects of Fluorinated Alcohols and Weakly Coordinated Fluorine-Containing Anions on Cationic Reaction Intermediates. *The Journal of Organic Chemistry*, **2022**, *87*, 1814-1829. <https://doi.org/10.1021/acs.joc.1c02361>
199. Alcívar León, C. D., Echeverría, G. A., Piro, O. E., Ulic, S. E., Jíos, J. L., Pereañez, J. A., Henao Castañeda, I. C. & Pérez, H. The Role of Non-Covalent Interactions in Some 2-Trifluoromethylchromones in the Solid State. *New Journal of Chemistry*, **2017**, *41*, 14659-14674. <https://doi.org/10.1039/c7nj00481h>
200. Hierso, J.-C. Indirect Nonbonded Nuclear Spin–Spin Coupling: A Guide for the Recognition and Understanding of “Through-Space” NMR J Constants in Small Organic, Organometallic, and Coordination Compounds. *Chemical Reviews*, **2014**, *114*, 4838-4867. <https://doi.org/10.1021/cr400330g>
201. Karatzas, A., Talelli, M., Vasilakopoulos, T., Pitsikalis, M. & Hadjichristidis, N. Micellization of  $\omega$ -Functionalized Diblock Copolymers in Selective Solvent. Study on the Effect of Hydrogen Bonds. *Macromolecules*, **2006**, *39*, 8456-8466. <https://doi.org/10.1021/ma061396n>
202. Wrue, M. H., McUmbler, A. C. & Anthamatten, M. Atom Transfer Radical Polymerization of End-Functionalized Hydrogen-Bonding Polymers and Resulting Polymer Miscibility. *Macromolecules*, **2009**, *42*, 9255-9262. <https://doi.org/10.1021/ma901822k>
203. Sharma, A. K., Caricato, M., Quartarone, E., Edizer, S., Schieroni, A. G., Mendichi, R. & Pasini, D. Polystyrene-Based Self-Aggregating Polymers Based on UPy Units. *Polymer Bulletin*, **2012**, *69*, 911-923. <https://doi.org/10.1007/s00289-012-0844-5>
204. Kuo, S. W. & Tsai, H. T. Self-Complementary Multiple Hydrogen Bonding Interactions Increase the Glass Transition Temperatures to Supramolecular Poly(Methyl Methacrylate) Copolymers. *Journal of Applied Polymer Science*, **2012**, *123*, 3275-3282. <https://doi.org/10.1002/app.35001>
205. Street, D. P., Ledford, W. K., Allison, A. A., Patterson, S., Pickel, D. L., Lokitz, B. S., Messman, J. M. & Kilbey, S. M., II. Self-Complementary Multiple Hydrogen-Bonding Additives Enhance Thermomechanical Properties of 3D-Printed PMMA Structures. *Macromolecules*, **2019**, *52*, 5574-5582. <https://doi.org/10.1021/acs.macromol.9b00546>
206. Jangizehi, A., Ghaffarian, S. R., Schmolke, W. & Seiffert, S. Dominance of Chain Entanglement over Transient Sticking on Chain Dynamics in Hydrogen-Bonded Supramolecular Polymer Networks in the Melt. *Macromolecules*, **2018**, *51*, 2859-2871. <https://doi.org/10.1021/acs.macromol.7b02180>
207. Jangizehi, A., Ahmadi, M. & Seiffert, S. Dynamics of Supramolecular Associative Polymer Networks at the Interplay of Chain Entanglement, Transient Chain Association, and Chain-Sticker Clustering. *Journal of Polymer Science Part B: Polymer Physics*, **2019**, *57*, 1209-1223. <https://doi.org/10.1002/polb.24782>



208. Döhler, D., Kang, J., Cooper, C. B., Tok, J. B. H., Rupp, H., Binder, W. H. & Bao, Z. Tuning the Self-Healing Response of Poly(Dimethylsiloxane)-Based Elastomers. *Acs Applied Polymer Materials*, **2020**, 2, 4127-4139. <https://doi.org/10.1021/acsapm.0c00755>
209. Bobade, S., Wang, Y., Mays, J. & Baskaran, D. Synthesis and Characterization of Ureidopyrimidone Telechelics by CuAAC “Click” Reaction: Effect of Tg and Polarity. *Macromolecules*, **2014**, 47, 5040-5050. <https://doi.org/10.1021/ma5007705>
210. Yan, T., Schroter, K., Herbst, F., Binder, W. H. & Thurn-Albrecht, T. Unveiling the Molecular Mechanism of Self-Healing in a Telechelic, Supramolecular Polymer Network. *Scientific Reports*, **2016**, 6, 32356. <https://doi.org/10.1038/srep32356>
211. Ostas, E., Schröter, K., Beiner, M., Yan, T. Z., Thurn-Albrecht, T. & Binder, W. H. Poly( $\epsilon$ -Caprolactone)-Poly(Isobutylene): A Crystallizing, Hydrogen-Bonded Pseudo-Block Copolymer. *Journal of Polymer Science Part a-Polymer Chemistry*, **2011**, 49, 3404-3416. <https://doi.org/10.1002/pola.24777>
212. Tellers, J., Canossa, S., Pinalli, R., Soliman, M., Vachon, J. & Dalcanale, E. Dynamic Cross-Linking of Polyethylene via Sextuple Hydrogen Bonding Array. *Macromolecules*, **2018**, 51, 7680-7691. <https://doi.org/10.1021/acs.macromol.8b01715>
213. Masuda, K., Kaji, H. & Horii, F. CP/MAS<sup>13</sup>C NMR Analyses of Hydrogen Bonding and the Chain Conformation in the Crystalline and Noncrystalline Regions for Poly(Vinyl Alcohol) Films. *Journal of Polymer Science Part B: Polymer Physics*, **2000**, 38, 1-9. [https://doi.org/10.1002/\(sici\)1099-0488\(20000101\)38:1<1::aid-polb1>3.0.co;2-z](https://doi.org/10.1002/(sici)1099-0488(20000101)38:1<1::aid-polb1>3.0.co;2-z)
214. Cheng, Y., Prud'homme, R. K., Chik, J. & Rau, D. C. Measurement of Forces between Galactomannan Polymer Chains: Effect of Hydrogen Bonding. *Macromolecules*, **2002**, 35, 10155-10161. <https://doi.org/10.1021/ma020887e>
215. Wang, F., Yang, Z., Li, J., Zhang, C. & Sun, P. Bioinspired Polyurethane Using Multifunctional Block Modules with Synergistic Dynamic Bonds. *ACS Macro Letters*, **2021**, 10, 510-517. <https://doi.org/10.1021/acsmacrolett.1c00054>
216. Xing, K., Tress, M., Cao, P., Cheng, S., Saito, T., Novikov, V. N. & Sokolov, A. P. Hydrogen-Bond Strength Changes Network Dynamics in Associating Telechelic PDMS. *Soft Matter*, **2018**, 14, 1235-1246. <https://doi.org/10.1039/c7sm01805c>
217. Xing, K., Chatterjee, S., Saito, T., Gainaru, C. & Sokolov, A. P. Impact of Hydrogen Bonding on Dynamics of Hydroxyl-Terminated Polydimethylsiloxane. *Macromolecules*, **2016**, 49, 3138-3147. <https://doi.org/10.1021/acs.macromol.6b00262>
218. Hilton, E. M., Jhons, Y., Warren, N. J. & Wilson, A. J. Polymers with Quadruple Hydrogen-Bonding End Groups: Controlling Molecular Weight Using a Small Molecule Photoswitch. *Polymer Chemistry*, **2024**, 15, 4115-4121. <https://doi.org/10.1039/d4py00835a>
219. Frey, H. Universal Glue for Cells. *Nature Materials*, **2012**, 11, 359-360.

<https://doi.org/10.1038/nmat3320>

220. Cheng, K.-C. Effect of Feed Rate on Structure of Hyperbranched Polymers Formed by Stepwise Addition of AB<sub>2</sub> Monomers into Multifunctional Cores. *Polymer*, **2003**, *44*, 1259-1266. [https://doi.org/10.1016/S0032-3861\(02\)00846-7](https://doi.org/10.1016/S0032-3861(02)00846-7)
221. Litvinenko, G. I. & Müller, A. H. E. Molecular Weight Averages and Degree of Branching in Self-Condensing Vinyl Copolymerization in the Presence of Multifunctional Initiators. *Macromolecules*, **2002**, *35*, 4577-4583. <https://doi.org/10.1021/ma012063n>
222. Wilms, D., Stiriba, S.-E. & Frey, H. Hyperbranched Polyglycerols: From the Controlled Synthesis of Biocompatible Polyether Polyols to Multipurpose Applications. *Accounts of Chemical Research*, **2010**, *43*, 129-141. <https://doi.org/10.1021/ar900158p>
223. Tomalia, D. A. & Fréchet, J. M. J. in *Dendrimers and Other Dendritic Polymers* 1-44 (2001) <https://doi.org/10.1002/0470845821.ch1>
224. Sztandera, K., Gorzkiewicz, M., Dias Martins, A. S., Pallante, L., Zizzi, E. A., Miceli, M., BaTal, M., Reis, C. P., Deriu, M. A. & Klajnert-Maculewicz, B. Noncovalent Interactions with PAMAM and PPI Dendrimers Promote the Cellular Uptake and Photodynamic Activity of Rose Bengal: The Role of the Dendrimer Structure. *Journal of Medicinal Chemistry*, **2021**, *64*, 15758-15771. <https://doi.org/10.1021/acs.jmedchem.1c01080>
225. Schubert, C., Osterwinter, C., Tonhauser, C., Schömer, M., Wilms, D., Frey, H. & Friedrich, C. Can Hyperbranched Polymers Entangle? Effect of Hydrogen Bonding on Entanglement Transition and Thermorheological Properties of Hyperbranched Polyglycerol Melts. *Macromolecules*, **2016**, *49*, 8722-8737. <https://doi.org/10.1021/acs.macromol.6b00674>
226. Yokota, K., Abe, A., Hosaka, S., Sakai, I. & Saitô, H. A <sup>13</sup>C Nuclear Magnetic Resonance Study of Covalently Cross-Linked Gels. Effect of Chemical Composition, Degree of Cross-Linking, and Temperature to Chain Mobility. *Macromolecules*, **1978**, *11*, 95-100. <https://doi.org/10.1021/ma60061a017>
227. Spruell, J. M., Wolffs, M., Leibfarth, F. A., Stahl, B. C., Heo, J., Connal, L. A., Hu, J. & Hawker, C. J. Reactive, Multifunctional Polymer Films through Thermal Cross-linking of Orthogonal Click Groups. *Journal of the American Chemical Society*, **2011**, *133*, 16698-16706. <https://doi.org/10.1021/ja207635f>
228. Mauritz, K. A., Blackwell, R. I. & Beyer, F. L. Viscoelastic Properties and Morphology of Sulfonated Poly(Styrene-*b*-Ethylene/Butylene-*b*-Styrene) Block Copolymers (sBCP), and sBCP/[Silicate] Nanostructured Materials. *Polymer*, **2004**, *45*, 3001-3016. <https://doi.org/10.1016/j.polymer.2003.12.078>
229. Zheng, X., Guo, Y., Douglas, J. F. & Xia, W. Competing Effects of Cohesive Energy and Cross-Link Density on the Segmental Dynamics and Mechanical Properties of Cross-Linked Polymers. *Macromolecules*, **2022**, *55*, 9990-10004. <https://doi.org/10.1021/acs.macromol.2c01719>

230. Bielawski, C. W., Benitez, D. & Grubbs, R. H. An "Endless" Route to Cyclic Polymers. *Science*, **2002**, 297, 2041-2044. <https://doi.org/10.1126/science.1075401>
231. Zhang, L., Elupula, R., Grayson, S. M. & Torkelson, J. M. Major Impact of Cyclic Chain Topology on the Tg-Confinement Effect of Supported Thin Films of Polystyrene. *Macromolecules*, **2016**, 49, 257-268. <https://doi.org/10.1021/acs.macromol.5b02474>
232. Rezai, T., Yu, B., Millhauser, G. L., Jacobson, M. P. & Lokey, R. S. Testing the Conformational Hypothesis of Passive Membrane Permeability Using Synthetic Cyclic Peptide Diastereomers. *Journal of the American Chemical Society*, **2006**, 128, 2510-2511. <https://doi.org/10.1021/ja0563455>
233. Gray, A. L. H., Steren, C. A., Haynes, I. W., Bermejo, G. A., Favretto, F., Zweckstetter, M. & Do, T. D. Structural Flexibility of Cyclosporine A Is Mediated by Amide Cis–Trans Isomerization and the Chameleonic Roles of Calcium. *The Journal of Physical Chemistry B*, **2021**, 125, 1378-1391. <https://doi.org/10.1021/acs.jpcb.0c11152>
234. Beck, J. G., Chatterjee, J., Laufer, B., Kiran, M. U., Frank, A. O., Neubauer, S., Ovadia, O., Greenberg, S., Gilon, C., Hoffman, A. & Kessler, H. Intestinal Permeability of Cyclic Peptides: Common Key Backbone Motifs Identified. *Journal of the American Chemical Society*, **2012**, 134, 12125-12133. <https://doi.org/10.1021/ja303200d>
235. Poteau, R. & Trinquier, G. All-Cis Cyclic Peptides. *Journal of the American Chemical Society*, **2005**, 127, 13875-13889. <https://doi.org/10.1021/ja052342g>
236. Awada, H., Grison, C. M., Charnay-Pouget, F., Baltaze, J.-P., Brisset, F., Guillot, R., Robin, S., Hachem, A., Jaber, N., Naoufal, D., Yazbeck, O. & Aitken, D. J. Conformational Effects through Hydrogen Bonding in a Constrained  $\gamma$ -Peptide Template: From Intraresidue Seven-Membered Rings to a Gel-Forming Sheet Structure. *The Journal of Organic Chemistry*, **2017**, 82, 4819-4828. <https://doi.org/10.1021/acs.joc.7b00494>
237. Kuhn, B., Mohr, P. & Stahl, M. Intramolecular Hydrogen Bonding in Medicinal Chemistry. *Journal of Medicinal Chemistry*, **2010**, 53, 2601-2611. <https://doi.org/10.1021/jm100087s>
238. Song, Q., Cheng, Z., Kariuki, M., Hall, S. C. L., Hill, S. K., Rho, J. Y. & Perrier, S. Molecular Self-Assembly and Supramolecular Chemistry of Cyclic Peptides. *Chemical Reviews*, **2021**, 121, 13936-13995. <https://doi.org/10.1021/acs.chemrev.0c01291>
239. Kurita, T. & Numata, K. The Structural and Functional Impacts of Rationally Designed Cyclic Peptides on Self-Assembly-Mediated Functionality. *Physical Chemistry Chemical Physics*, **2024**, 26, 28776-28792. <https://doi.org/10.1039/d4cp02759k>
240. Altintas, O., Gerstel, P., Dingenouts, N. & Barner-Kowollik, C. Single Chain Self-Assembly: Preparation of  $\alpha,\omega$ -Donor–Acceptor Chains via Living Radical Polymerization and Orthogonal Conjugation. *Chemical Communications*, **2010**, 46, 6291. <https://doi.org/10.1039/c0cc00702a>

241. Feldman, K. E., Kade, M. J., Meijer, E. W., Hawker, C. J. & Kramer, E. J. Model Transient Networks from Strongly Hydrogen-Bonded Polymers. *Macromolecules*, **2009**, *42*, 9072-9081. <https://doi.org/10.1021/ma901668w>
242. Chen, S., Yan, T., Fischer, M., Mordvinkin, A., Saalwachter, K., Thurn-Albrecht, T. & Binder, W. H. Opposing Phase-Segregation and Hydrogen-Bonding Forces in Supramolecular Polymers. *Angewandte Chemie International Edition*, **2017**, *56*, 13016-13020. <https://doi.org/10.1002/anie.201707363>
243. Chen, H.-L., Wang, S.-F. & Lin, T.-L. Morphological Structure of Crystalline Polymer Blend Involving Hydrogen Bonding: Polycaprolactone/Poly(4-vinylphenol) System. *Macromolecules*, **1998**, *31*, 8924-8930. <https://doi.org/10.1021/ma9811019>
244. Mitani, E., Ozaki, Y. & Sato, H. Two Types of C O...HO Hydrogen Bonds and OH...OH (Dimer, Trimer, Oligomer) Hydrogen Bonds in PVA with 88% Saponification/PMMA and PVA with 99% Saponification/PMMA Blends and Their Thermal Behavior Studied by Infrared Spectroscopy. *Polymer*, **2022**, *246*, 124725. <https://doi.org/10.1016/j.polymer.2022.124725>
245. Guo, P., Su, A., Wei, Y., Liu, X., Li, Y., Guo, F., Li, J., Hu, Z. & Sun, J. Healable, Highly Conductive, Flexible, and Nonflammable Supramolecular Ionogel Electrolytes for Lithium-Ion Batteries. *ACS Applied Materials & Interfaces*, **2019**, *11*, 19413-19420. <https://doi.org/10.1021/acsami.9b02182>
246. Gan, H., Zhang, Y., Li, S., Yu, L., Wang, J. & Xue, Z. Self-Healing Single-Ion Conducting Polymer Electrolyte Formed via Supramolecular Networks for Lithium Metal Batteries. *Acs Applied Energy Materials*, **2021**, *4*, 482-491. <https://doi.org/10.1021/acsaem.0c02384>
247. Lin, Y., Hu, H., Yi, P., Sun, S., Li, Y., Liu, X. & Li, G. Zwitterionic Hydrogels Formed via Quadruple Hydrogen-Bonds with Ultra-Fast Room-Temperature Self-Healing Ability. *Materials Letters*, **2020**, *269*, 127665. <https://doi.org/10.1016/j.matlet.2020.127665>
248. Chen, J., Peng, Q., Thundat, T. & Zeng, H. Stretchable, Injectable, and Self-Healing Conductive Hydrogel Enabled by Multiple Hydrogen Bonding toward Wearable Electronics. *Chemistry of Materials*, **2019**, *31*, 4553-4563. <https://doi.org/10.1021/acs.chemmater.9b01239>
249. Cui, J. & Campo, A. d. Multivalent H-bonds for Self-Healing Hydrogels. *Chemical Communications*, **2012**, *48*, 9302-9304. <https://doi.org/10.1039/C2CC34701F>
250. Shirakawa, M., Kawano, S.-i., Fujita, N., Sada, K. & Shinkai, S. Hydrogen-Bond-Assisted Control of H versus J Aggregation Mode of Porphyrins Stacks in an Organogel System. *The Journal of Organic Chemistry*, **2003**, *68*, 5037-5044. <https://doi.org/10.1021/jo0341822>
251. Pirner, D., Dulle, M., E. J. Mauer, M. & Förster, S. Reinforcement of Nanostructured Organogels by Hydrogen Bonds. *RSC Advances*, **2016**, *6*, 42730-42738.

<https://doi.org/10.1039/c6ra03567a>

252. Wang, J., Hao, X., Yan, H., Jiang, Q., Peng, H., Xiong, B., Liao, Y. & Xie, X. Hydrogen Bond Driven Self-Supporting Organogels from Main-Chain Liquid Crystalline Polymers. *Polymer*, **2020**, 188, 122148. <https://doi.org/10.1016/j.polymer.2019.122148>
253. Wang, M., Zhang, P., Shamsi, M., Thelen, J. L., Qian, W., Truong, V. K., Ma, J., Hu, J. & Dickey, M. D. Tough and Stretchable Ionogels by in situ Phase Separation. *Nature Materials*, **2022**, 21, 359-365. <https://doi.org/10.1038/s41563-022-01195-4>
254. Tamate, R., Hashimoto, K., Horii, T., Hirasawa, M., Li, X., Shibayama, M. & Watanabe, M. Self-Healing Micellar Ion Gels Based on Multiple Hydrogen Bonding. *Advanced Materials*, **2018**, 30, 1802792. <https://doi.org/10.1002/adma.201802792>
255. Kim, S., Park, S., Kim, M. S., Lee, H., Lee, H., Lee, K. H. & Kim, M. Supramolecular Association of a Block Copolymer via Strong Hydrogen Bonding to Form Self-Healable Ionogels. *ACS Applied Materials & Interfaces*, **2024**, 16, 51459-51468. <https://doi.org/10.1021/acsami.4c09988>
256. Lewandowska, K. The Miscibility of Poly(Vinyl Alcohol)/Poly(N-Vinylpyrrolidone) Blends Investigated in Dilute Solutions and Solids. *European Polymer Journal*, **2005**, 41, 55-64. <https://doi.org/10.1016/j.eurpolymj.2004.08.016>
257. Rao, J., Ma, H., Baettig, J., Woo, S., Stuparu, M. C., Bang, J. & Khan, A. Self-Assembly of an Interacting Binary Blend of Diblock Copolymers in Thin Films: a Potential Route to Porous Materials with Reactive Nanochannel Chemistry. *Soft Matter*, **2014**, 10, 5755. <https://doi.org/10.1039/c4sm01029a>
258. Krause, S. Polymer-Polymer Miscibility. *Pure and Applied Chemistry*, **1986**, 58, 1553-1560. <https://doi.org/10.1351/pac198658121553>
259. He, Y., Zhu, B. & Inoue, Y. Hydrogen Bonds in Polymer Blends. *Progress in Polymer Science*, **2004**, 29, 1021-1051. <https://doi.org/10.1016/j.progpolymsci.2004.07.002>
260. Dong, K., Zhang, S. & Wang, J. Understanding the Hydrogen Bonds in Ionic Liquids and Their Roles in Properties and Reactions. *Chemical Communications*, **2016**, 52, 6744-6764. <https://doi.org/10.1039/c5cc10120d>
261. Liu, S.-h., Wang, H., Sun, J.-k., Antonietti, M. & Yuan, J. Smart Hydrogen Atoms in Heterocyclic Cations of 1,2,4-Triazolium-Type Poly(ionic liquid)s. *Accounts of Chemical Research*, **2022**, 55, 3675-3687. <https://doi.org/10.1021/acs.accounts.2c00430>
262. Hoque, M., Morgan, Miran, M. S., Akiyama, M., Marium, M., Ueno, K., Dokko, K. & Watanabe, M. Protic Ionic Liquids with Primary Alkylamine-Derived Cations: the Dominance of Hydrogen Bonding on Observed Physicochemical Properties. *RSC Advances*, **2018**, 8, 9790-9794. <https://doi.org/10.1039/c8ra00402a>
263. Brehm, M., Pulst, M., Kressler, J. & Sebastiani, D. Triazolium-Based Ionic Liquids: A Novel Class of Cellulose Solvents. *The Journal of Physical Chemistry B*, **2019**, 123, 3994-



4003. <https://doi.org/10.1021/acs.jpcb.8b12082>
264. Giron, R. G. P. & Ferguson, G. S. Tetrafluoroborate and Hexafluorophosphate Ions are not Interchangeable: A Density Functional Theory Comparison of Hydrogen Bonding. *ChemistrySelect*, **2017**, 2, 10895-10901. <https://doi.org/10.1002/slct.201702176>
265. Pethes, I., Bakó, I. & Pusztai, L. Chloride Ions as Integral Parts of Hydrogen Bonded Networks in Aqueous Salt Solutions: the Appearance of Solvent Separated Anion Pairs. *Physical Chemistry Chemical Physics*, **2020**, 22, 11038-11044. <https://doi.org/10.1039/d0cp01806f>
266. Efremov, R. G. Dielectric-Dependent Strength of Interlipid Hydrogen Bonding in Biomembranes: Model Case Study. *Journal of Chemical Information and Modeling*, **2019**, 59, 2765-2775. <https://doi.org/10.1021/acs.jcim.9b00193>
267. Srivastava, K. R., Goyal, B., Kumar, A. & Durani, S. Scrutiny of Electrostatic-Driven Conformational Ordering of Polypeptide Chains in DMSO: a Study with a Model Oligopeptide. *RSC Advances*, **2017**, 7, 27981-27991. <https://doi.org/10.1039/c7ra02137b>
268. Feng, W. & Jia, G.-z. The Hydrogen Bonding Dynamics and Cooperative Interactions in Aqueous N,N-Dimethyl Formamide Solution Studied by Dielectric Relaxation Spectroscopy. *Physica A: Statistical Mechanics and its Applications*, **2014**, 404, 315-322. <https://doi.org/10.1016/j.physa.2014.02.049>
269. Anderson, J. L., Armstrong, D. W. & Wei, G.-T. Ionic Liquids in Analytical Chemistry. *Analytical Chemistry*, **2006**, 78, 2892-2902. <https://doi.org/10.1021/ac069394o>
270. Frenzel, F., Guterman, R., Anton, A. M., Yuan, J. & Kremer, F. Molecular Dynamics and Charge Transport in Highly Conductive Polymeric Ionic Liquids. *Macromolecules*, **2017**, 50, 4022-4029. <https://doi.org/10.1021/acs.macromol.7b00554>
271. Cheng, Q., Ding, S., Zheng, Y., Wu, M., Peng, Y.-Y., Diaz-Dussan, D., Shi, Z., Liu, Y., Zeng, H., Cui, Z. & Narain, R. Dual Cross-Linked Hydrogels with Injectable, Self-Healing, and Antibacterial Properties Based on the Chemical and Physical Cross-Linking. *Biomacromolecules*, **2021**, 22, 1685-1694. <https://doi.org/10.1021/acs.biomac.1c00111>
272. Katcharava, Z., Orlamünde, T. E., Tema, L. T., Hong, H., Beiner, M., Iliev, B., Marinow, A. & Binder, W. H. Designing Conductive Pyrrolidinium-Based Dual Network Gel Electrolytes: Tailoring Performance with Dynamic and Covalent Crosslinking. *Advanced Functional Materials*, **2024**, 34 <https://doi.org/10.1002/adfm.202403487>
273. Zhang, J., Wang, W., Zhang, Y., Wei, Q., Han, F., Dong, S., Liu, D. & Zhang, S. Small-Molecule Ionic Liquid-Based Adhesive with Strong Room-Temperature Adhesion Promoted by Electrostatic Interaction. *Nature Communications*, **2022**, 13 <https://doi.org/10.1038/s41467-022-32997-4>
274. Hassan, P. A., Verma, G. & Ganguly, R. in *Functional Materials* (eds S. Banerjee & A. K. Tyagi) 1-59 (Elsevier, 2012) <https://doi.org/10.1016/B978-0-12-385142-0.00001-5>



275. Zhang, G., Kim, J., Hassan, S. & Suo, Z. Self-Assembled Nanocomposites of High Water Content and Load-Bearing Capacity. *Proceedings of the National Academy of Sciences*, **2022**, 119 <https://doi.org/10.1073/pnas.2203962119>
276. Li, X., Cui, K., Zheng, Y., Ye, Y. N., Yu, C., Yang, W., Nakajima, T. & Gong, J. P. Role of Hierarchy Structure on the Mechanical Adaptation of Self-Healing Hydrogels under Cyclic Stretching. *Science Advances*, **2023**, 9 <https://doi.org/10.1126/sciadv.adj6856>
277. Liu, X., Zhang, Q., Gao, Z., Hou, R. & Gao, G. Bioinspired Adhesive Hydrogel Driven by Adenine and Thymine. *ACS Applied Materials & Interfaces*, **2017**, 9, 17645-17652. <https://doi.org/10.1021/acsami.7b04832>
278. Lu, L., Zhou, W., Chen, Z., Hu, Y., Yang, Y., Zhang, G. & Yang, Z. A Supramolecular Hydrogel Enabled by the Synergy of Hydrophobic Interaction and Quadruple Hydrogen Bonding. *Gels*, **2022**, 8, 244. <https://doi.org/10.3390/gels8040244>
279. Tang, J., He, Y., Xu, D., Zhang, W., Hu, Y., Song, H., Zhang, Y., Chen, Y. M., Yang, Y. & Zhang, K. Tough, Rapid Self-Recovery and Responsive Organogel-Based Ionotronic for Intelligent Continuous Passive Motion System. *npj Flexible Electronics*, **2023**, 7 <https://doi.org/10.1038/s41528-023-00259-y>
280. Wu, N. M. & Yam, V. W. Photochromic Barbiturate Pendant-Containing Benzo[b]phosphole Oxides with Co-Assembly Property and Photoinduced Morphological Changes. *ACS Applied Materials & Interfaces*, **2019**, 11, 40290-40299. <https://doi.org/10.1021/acsami.9b13900>
281. Kiebal, D. J., Doder, A., Weder, C. & Schreittl, S. Optical Monitoring of Supramolecular Interactions in Polymers. *Angewandte Chemie International Edition*, **2024**, 63, e202405922. <https://doi.org/10.1002/anie.202405922>
282. Dethlefs, C., Eckelmann, J., Kobarg, H., Weyrich, T., Brammer, S., Näther, C. & Luning, U. Determination of Binding Constants of Hydrogen-Bonded Complexes by ITC, NMR CIS, and NMR Diffusion Experiments. *European Journal of Organic Chemistry*, **2011**, 2011, 2066-2074. <https://doi.org/10.1002/ejoc.201001684>
283. Schmidtchen, F. P. in *Supramolecular Chemistry* (2012) <https://doi.org/10.1002/9780470661345.smc024>
284. Chen, S. B., Deng, Y. M., Chang, X. J., Barqawi, H., Schulz, M. & Binder, W. H. Facile Preparation of Supramolecular (ABAC) Multiblock Copolymers from Hamilton Wedge and Barbiturate-Functionalized RAFT Agents. *Polymer Chemistry*, **2014**, 5, 2891-2900. <https://doi.org/10.1039/c3py01482g>
285. Schnell, I., Langer, B., Söntjens, S. H. M., Sijbesma, R. P., van Genderen, M. H. P. & Spiess, H. W. Quadruple Hydrogen Bonds of Ureido-Pyrimidinone Moieties Investigated in the Solid State by  
H Double-Quantum MAS NMR Spectroscopy. *Physical Chemistry Chemical Physics*, **2002**,

4, 3750-3758. <https://doi.org/10.1039/b203333j>

286. Li, B., Xu, L., Wu, Q., Chen, T., Sun, P., Jin, Q., Ding, D., Wang, X., Xue, G. & Shi, A. C. Various Types of Hydrogen Bonds, Their Temperature Dependence and Water-Polymer Interaction in Hydrated Poly(Acrylic Acid) as Revealed by <sup>1</sup>H Solid-State NMR Spectroscopy. *Macromolecules*, **2007**, *40*, 5776-5786. <https://doi.org/10.1021/ma070485c>

287. Giubertoni, G., Hilbers, M., Caporaletti, F., Laity, P., Groen, H., Van der Weide, A., Bonn, D. & Woutersen, S. Hydrogen Bonds under Stress: Strain-Induced Structural Changes in Polyurethane Revealed by Rheological Two-Dimensional Infrared Spectroscopy. *The Journal of Physical Chemistry Letters*, **2023**, *14*, 940-946. <https://doi.org/10.1021/acs.jpclett.2c03109>

288. Macomber, R. S. An Introduction to NMR Titration for Studying Rapid Reversible Complexation. *Journal of Chemical Education*, **1992**, *69*, 375-378. <https://doi.org/10.1021/ed069p375>

289. Martinez-Cuezva, A., Berna, J., Orenes, R. A., Pastor, A. & Alajarin, M. Small-Molecule Recognition for Controlling Molecular Motion in Hydrogen-Bond-Assembled Rotaxanes. *Angewandte Chemie International Edition*, **2014**, *53*, 6762-6767. <https://doi.org/10.1002/anie.201402962>

290. Yamauchi, M., Adhikari, B., Prabhu, D. D., Lin, X., Karatsu, T., Ohba, T., Shimizu, N., Takagi, H., Haruki, R., Adachi, S. I., Kajitani, T., Fukushima, T. & Yagai, S. Supramolecular Polymerization of Supramacrocycles: Effect of Molecular Conformations on Kinetics and Morphology. *Chemistry*, **2017**, *23*, 5270-5280. <https://doi.org/10.1002/chem.201605873>

291. Schnell, I., Langer, B., Söntjens, S. H. M., Sijbesma, R. P., van Genderen, M. H. P. & Wolfgang Spiess, H. Quadruple Hydrogen Bonds of Ureido-Pyrimidinone Moieties Investigated in the Solid State by <sup>1</sup>H Double-Quantum MAS NMR Spectroscopy. *Physical Chemistry Chemical Physics*, **2002**, *4*, 3750-3758. <https://doi.org/10.1039/B203333J>

292. Zhang, C., Yang, Z., Duong, N. T., Li, X., Nishiyama, Y., Wu, Q., Zhang, R. & Sun, P. Using Dynamic Bonds to Enhance the Mechanical Performance: From Microscopic Molecular Interactions to Macroscopic Properties. *Macromolecules*, **2019**, *52*, 5014-5025. <https://doi.org/10.1021/acs.macromol.9b00503>

293. Jena, S., Routray, C., Dutta, J. & Biswal, H. S. Hydrogen Bonding Directed Reversal of (<sup>13</sup>C NMR Chemical Shielding. *Angewandte Chemie International Edition*, **2022**, *61*, e202207521. <https://doi.org/10.1002/anie.202207521>

294. Guo, J., Tolstoy, P. M., Koeppe, B., Golubev, N. S., Denisov, G. S., Smirnov, S. N. & Limbach, H. H. Hydrogen Bond Geometries and Proton Tautomerism of Homoconjugated Anions of Carboxylic Acids Studied via H/D Isotope Effects on <sup>13</sup>C NMR Chemical Shifts. *The Journal of Physical Chemistry A*, **2012**, *116*, 11180-11188. <https://doi.org/10.1021/jp304943h>

295. Tsuchiya, K., Takahashi, A., Takeda, N., Asakawa, N., Kuroki, S., Ando, I., Shoji, A. &

- Ozaki, T. Hydrogen-Bonding Effect on  $^{13}\text{C}$  NMR Chemical Shifts of Amino Acid Residue Carbonyl Carbons of Some Peptides in the Crystalline State. *Journal of Molecular Structure*, **1995**, 350, 233-240. [https://doi.org/10.1016/0022-2860\(94\)08476-x](https://doi.org/10.1016/0022-2860(94)08476-x)
296. Dalvit, C., Invernizzi, C. & Vulpetti, A. Fluorine as a Hydrogen-Bond Acceptor: Experimental Evidence and Computational Calculations. *Chemistry*, **2014**, 20, 11058-11068. <https://doi.org/10.1002/chem.201402858>
297. Milic, M., Targos, K., Tellez Chavez, M., Thompson, M. A. M., Jennings, J. J. & Franz, A. K. NMR Quantification of Hydrogen-Bond-Accepting Ability for Organic Molecules. *The Journal of Organic Chemistry*, **2021**, 86, 6031-6043. <https://doi.org/10.1021/acs.joc.0c02876>
298. Dalvit, C., Veronesi, M. & Vulpetti, A.  $^1\text{H}$  and  $^{19}\text{F}$  NMR Chemical Shifts for Hydrogen Bond Strength Determination: Correlations between Experimental and Computed Values. *Journal of Magnetic Resonance*, **2022**, 12-13, 100070. <https://doi.org/10.1016/j.jmro.2022.100070>
299. Tang, B., Pauls, M., Bannwarth, C. & Hecht, S. Photoswitchable Quadruple Hydrogen-Bonding Motif. *Journal of the American Chemical Society*, **2024**, 146, 45-50. <https://doi.org/10.1021/jacs.3c10401>
300. Giba, I. S., Mulloyarova, V. V., Denisov, G. S. & Tolstoy, P. M. Sensitivity of  $(^{31}\text{P})$  NMR Chemical Shifts to Hydrogen Bond Geometry and Molecular Conformation for Complexes of Phosphinic Acids with Pyridines. *Magn Reson Chem*, **2021**, 59, 465-477. <https://doi.org/10.1002/mrc.5123>
301. Vogt, F. G., Yin, H., Forcino, R. G. & Wu, L.  $^{17}\text{O}$  Solid-State NMR as a Sensitive Probe of Hydrogen Bonding in Crystalline and Amorphous Solid Forms of Diflunisal. *Molecular Pharmaceutics*, **2013**, 10, 3433-3446. <https://doi.org/10.1021/mp400275w>
302. Rowlands, L. J., Marks, A., Sanderson, J. M. & Law, R. V.  $(^{17}\text{O})$  NMR Spectroscopy as a Tool to Study Hydrogen Bonding of Cholesterol in Lipid Bilayers. *Chemical Communications*, **2020**, 56, 14499-14502. <https://doi.org/10.1039/d0cc05466f>
303. Hübler, C. SupraFit – An Open Source Qt Based Fitting Application to Determine Stability Constants from Titration Experiments\*\*. *Chemistry-Methods*, **2022**, 2, e202200006. <https://doi.org/10.1002/cmtd.202200006>
304. Kondo, S., Hayashi, T., Sakuno, Y., Takezawa, Y., Yokoyama, T., Unno, M. & Yano, Y. Synthesis of Cyclic Bis- and Trismelamine Derivatives and Their Complexation Properties with Barbiturates. *Organic & Biomolecular Chemistry*, **2007**, 5, 907-916. <https://doi.org/10.1039/b615537e>
305. Schmidt, R., Stolte, M., Grüne, M. & Würthner, F. Hydrogen-Bond-Directed Formation of Supramolecular Polymers Incorporating Head-to-Tail Oriented Dipolar Merocyanine Dyes. *Macromolecules*, **2011**, 44, 3766-3776. <https://doi.org/10.1021/ma2004184>

306. Brynn Hibbert, D. & Thordarson, P. The Death of the Job Plot, Transparency, Open Science and Online Tools, Uncertainty Estimation Methods and Other Developments in Supramolecular Chemistry Data Analysis. *Chemical Communications*, **2016**, 52, 12792-12805. <https://doi.org/10.1039/c6cc03888c>
307. Ali, M., Kataev, E., Muller, J., Park, H., Halik, M. & Hirsch, A. Host-Guest Systems on the Surface of Functionalized Superparamagnetic Iron Oxide Nanoparticles (SPIONs) Utilizing Hamilton Receptors and Cyanurate Derivative Molecules. *Chemistry*, **2021**, 27, 16429-16439. <https://doi.org/10.1002/chem.202102581>
308. Seidenkranz, D. T. & Pluth, M. D. Fluorescent Arylethynyl Hamilton Receptors for Barbiturate Sensing. *The Journal of Organic Chemistry*, **2019**, 84, 8571-8577. <https://doi.org/10.1021/acs.joc.9b00978>
309. Lakowicz, J. Principles of Fluorescence Spectroscopy. Vol. 1 (**2006**), ISBN: 978-0-387-31278-1. <https://doi.org/10.1007/978-0-387-46312-4>
310. Wessendorf, F., Grimm, B., Guldi, D. M. & Hirsch, A. Pairing Fullerenes and Porphyrins: Supramolecular Wires That Exhibit Charge Transfer Activity. *Journal of the American Chemical Society*, **2010**, 132, 10786-10795. <https://doi.org/10.1021/ja101937w>
311. Jolliffe, K. A., Calama, M. C., Fokkens, R., Nibbering, N. M. M., Timmerman, P. & Reinhoudt, D. N. Characterization of Hydrogen-Bonded Supramolecular Assemblies by MALDI-TOF Mass Spectrometry after Ag(+) Labeling. *Angewandte Chemie International Edition*, **1998**, 37, 1247-1251. [https://doi.org/10.1002/\(SICI\)1521-3773\(19980518\)37:9<1247::AID-ANIE1247>3.0.CO;2-7](https://doi.org/10.1002/(SICI)1521-3773(19980518)37:9<1247::AID-ANIE1247>3.0.CO;2-7)
312. Kempen, E. C. & Brodbelt, J. S. A Method for the Determination of Binding Constants by Electrospray Ionization Mass Spectrometry. *Analytical Chemistry*, **2000**, 72, 5411-5416. <https://doi.org/10.1021/ac000540e>
313. Su, H. F., Xue, L., Li, Y. H., Lin, S. C., Wen, Y. M., Huang, R. B., Xie, S. Y. & Zheng, L. S. Probing Hydrogen Bond Energies by Mass Spectrometry. *Journal of the American Chemical Society*, **2013**, 135, 6122-6129. <https://doi.org/10.1021/ja312133k>
314. Rozenberg, M., Shoham, G., Reva, I. & Fausto, R. Spontaneous Self-association of Adenine and Uracil in Polycrystals from Low Temperature FTIR Spectra in the Range below 1000 cm<sup>-1</sup>. *Spectrochimica Acta Part A: Molecular and Biomolecular Spectroscopy*, **2005**, 62, 233-238. <https://doi.org/10.1016/j.saa.2004.12.037>
315. Murthy, N. S. 14-36 (John Wiley & Sons, Inc, 2016) <https://doi.org/10.1002/9781118892756.ch2>
316. Mordvinkin, A., Döhler, D., Binder, W. H., Colby, R. H. & Saalwächter, K. Rheology, Sticky Chain, and Sticker Dynamics of Supramolecular Elastomers Based on Cluster-Forming Telechelic Linear and Star Polymers. *Macromolecules*, **2021**, 54, 5065-5076. <https://doi.org/10.1021/acs.macromol.1c00655>

317. Yang, Z. & Han, C. D. Rheology of Miscible Polymer Blends with Hydrogen Bonding. *Macromolecules*, **2008**, *41*, 2104-2118. <https://doi.org/10.1021/ma7025385>
318. Zhang, Z., Liu, C., Cao, X., Gao, L. & Chen, Q. Linear Viscoelastic and Dielectric Properties of Strongly Hydrogen-Bonded Polymers near the Sol–Gel Transition. *Macromolecules*, **2016**, *49*, 9192-9202. <https://doi.org/10.1021/acs.macromol.6b02017>
319. Huang, X., Nakagawa, S., Houjou, H. & Yoshie, N. Insights into the Role of Hydrogen Bonds on the Mechanical Properties of Polymer Networks. *Macromolecules*, **2021**, *54*, 4070-4080. <https://doi.org/10.1021/acs.macromol.1c00120>
320. Brunner, E. & Sternberg, U. Solid-State NMR Investigations on the Nature of Hydrogen Bonds. *Progress in Nuclear Magnetic Resonance Spectroscopy*, **1998**, *32*, 21-57. [https://doi.org/10.1016/S0079-6565\(97\)00018-6](https://doi.org/10.1016/S0079-6565(97)00018-6)
321. Schnell, I. & Spiess, H. W. High-Resolution <sup>1</sup>H NMR Spectroscopy in the Solid State: Very Fast Sample Rotation and Multiple-Quantum Coherences. *Journal of Magnetic Resonance*, **2001**, *151*, 153-227. <https://doi.org/10.1006/jmre.2001.2336>
322. Aliev, A. E. & Harris, K. D. M. in *Supramolecular Assembly via Hydrogen Bonds I* (ed D. Michael P. Mingos) 1-53 (Springer Berlin Heidelberg, 2004) <https://doi.org/10.1007/b14136>
323. Xu, Y. J., Szell, P. M. J., Kumar, V. & Bryce, D. L. Solid-State NMR Spectroscopy for the Analysis of Element-Based Non-Covalent Interactions. *Coordination Chemistry Reviews*, **2020**, *411*, 213237. <https://doi.org/10.1016/j.ccr.2020.213237>
324. Wang, F. & Sun, P. Solid-state NMR Characterization of Polymers. *Acta Polymerica Sinica*, **2021**, *52*, 840-856. <https://doi.org/10.11777/j.issn1000-3304.2020.20254>
325. Zhang, R. C., Chen, W. & Miyoshi, T. Elucidations of Structure and Molecular Dynamics of Complex Polymers by State-of-the-Art Solid-State NMR Spectroscopy. *Macromolecules*, **2024**, *57*, 1893-1918. <https://doi.org/10.1021/acs.macromol.3c02535>
326. Mordvinkin, A., Dohler, D., Binder, W. H., Colby, R. H. & Saalwachter, K. Terminal Flow of Cluster-Forming Supramolecular Polymer Networks: Single-Chain Relaxation or Micelle Reorganization? *Physical Review Letters*, **2020**, *125*, 127801. <https://doi.org/10.1103/PhysRevLett.125.127801>
327. Del Bene, J. E., Perera, S. A. & Bartlett, R. J. Hydrogen Bond Types, Binding Energies, and <sup>1</sup>H NMR Chemical Shifts. *The Journal of Physical Chemistry A*, **1999**, *103*, 8121-8124. <https://doi.org/10.1021/jp9920444>
328. Akbey, U., Graf, R., Peng, Y. G., Chu, P. P. & Spiess, H. W. Solid-State NMR Investigations of Anhydrous Proton-Conducting Acid-Base Poly(Acrylic Acid)-Poly(4-Vinyl Pyridine) Polymer Blend System: A Study of Hydrogen Bonding and Proton Conduction. *Journal of Polymer Science Part B-Polymer Physics*, **2009**, *47*, 138-155. <https://doi.org/10.1002/polb.21623>

329. Miyoshi, T., Hu, W. & Li, Y. Dynamic Geometry and Kinetics of Polymer Confined in Self-Assembly via Cooperative Hydrogen Bonding: A Solid-State NMR Study under Paramagnetic Doping. *Macromolecules*, **2010**, 43, 4435-4437. <https://doi.org/10.1021/ma100449n>
330. Yuan, X., Xiang, T. X., Anderson, B. D. & Munson, E. J. Hydrogen Bonding Interactions in Amorphous Indomethacin and Its Amorphous Solid Dispersions with Poly(vinylpyrrolidone) and Poly(vinylpyrrolidone-co-vinyl acetate) Studied Using <sup>13</sup>C Solid-State NMR. *Molecular Pharmaceutics*, **2015**, 12, 4518-4528. <https://doi.org/10.1021/acs.molpharmaceut.5b00705>
331. Rajput, L., Banik, M., Yarava, J. R., Joseph, S., Pandey, M. K., Nishiyama, Y. & Desiraju, G. R. Exploring the Salt-Cocrystal Continuum with Solid-State NMR Using Natural-Abundance Samples: Implications for Crystal Engineering. *IUCrJ*, **2017**, 4, 466-475. <https://doi.org/10.1107/S205225251700687X>
332. Lortie, F., Boileau, S. & Bouteiller, L. N,N'-Disubstituted Ureas: Influence of Substituents on the Formation of Supramolecular Polymers. *Chemistry*, **2003**, 9, 3008-3014. <https://doi.org/10.1002/chem.200304801>
333. Sun, C. T. & Xue, D. F. IR Spectral Study of Mesoscale Process during Urea Crystallization from Aqueous Solution. *Crystal Growth & Design*, **2015**, 15, 2867-2873. <https://doi.org/10.1021/acs.cgd.5b00293>
334. Ma, B., Wang, L., Han, L., Cai, W. & Shao, X. Understanding the Effect of Urea on the Phase Transition of Poly(N-Isopropylacrylamide) in Aqueous Solution by Temperature-Dependent Near-Infrared Spectroscopy. *Spectrochimica Acta Part A: Molecular and Biomolecular Spectroscopy*, **2021**, 253, 119573. <https://doi.org/10.1016/j.saa.2021.119573>
335. Han, L., Sun, Y., Wang, Y., Fu, H., Duan, C., Wang, M., Cai, W. & Shao, X. Ultra-High Resolution Near-Infrared Spectrum by Wavelet Packet Transform Revealing the Hydrogen Bond Interactions. *Spectrochimica Acta Part A: Molecular and Biomolecular Spectroscopy*, **2023**, 289, 122233. <https://doi.org/10.1016/j.saa.2022.122233>
336. Sun, C. T., Chen, X. Y. & Xue, D. F. Hydrogen Bonding Paradigm in the Formation of Crystalline KH<sub>2</sub>PO<sub>4</sub> from Aqueous Solution. *Crystal Growth & Design*, **2017**, 17, 3178-3184. <https://doi.org/10.1021/acs.cgd.7b00139>
337. Suriano, R., Brambilla, L., Tommasini, M. & Turri, S. A Deep Insight into the Intrinsic Healing Mechanism in Ureido-Pyrimidinone Copolymers. *Polymers for Advanced Technologies*, **2018**, 29, 2899-2908. <https://doi.org/10.1002/pat.4409>
338. Gupta, S., Yuan, X., Mike Chung, T. C., Cakmak, M. & Weiss, R. A. Influence of Hydrogen Bonding on the Melt Rheology of Polypropylene. *Polymer*, **2016**, 107, 223-232. <https://doi.org/10.1016/j.polymer.2016.11.027>
339. Rozenberg, M., Loewenschuss, A. & Marcus, Y. An Empirical Correlation between Stretching Vibration Redshift and Hydrogen Bond Length. *Physical Chemistry Chemical*



*Physics*, **2000**, 2, 2699-2702. DOI 10.1039/b002216k

340. Rozenberg, M., Shoham, G., Reva, I. & Fausto, R. A Correlation between the Proton Stretching Vibration Red Shift and the Hydrogen Bond Length in Polycrystalline Amino Acids and Peptides. *Physical Chemistry Chemical Physics*, **2005**, 7, 2376-2383. <https://doi.org/10.1039/b503644e>

341. Ilogansen, A. V. Direct Proportionality of the Hydrogen Bonding Energy and the Intensification of the Stretching  $\nu(\text{XH})$  Vibration in Infrared Spectra. *Spectrochimica Acta Part A: Molecular and Biomolecular Spectroscopy*, **1999**, 55, 1585-1612. [https://doi.org/10.1016/s1386-1425\(98\)00348-5](https://doi.org/10.1016/s1386-1425(98)00348-5)

342. Rozenberg, M., Loewenschuss, A. & Marcus, Y. Infrared Spectra and Hydrogen Bonding of Pentitols and Pyranosides at 20 to 300 K. *Carbohydrate Research*, **2000**, 328, 307-319. [https://doi.org/10.1016/s0008-6215\(00\)00117-8](https://doi.org/10.1016/s0008-6215(00)00117-8)

343. Rozenberg, M., Shoham, G., Reva, I. & Fausto, R. Low-Temperature Fourier Transform Infrared Spectra and Hydrogen Bonding in Polycrystalline L-Alanine. *Spectrochimica Acta Part A: Molecular and Biomolecular Spectroscopy*, **2003**, 59, 3253-3266. [https://doi.org/10.1016/s1386-1425\(03\)00159-8](https://doi.org/10.1016/s1386-1425(03)00159-8)

344. Rozenberg, M., Shoham, G., Reva, I. & Fausto, R. Low Temperature FTIR Spectroscopy and Hydrogen Bonding in Cytosine Polycrystals. *Spectrochimica Acta Part A: Molecular and Biomolecular Spectroscopy*, **2004**, 60, 463-470. [https://doi.org/10.1016/s1386-1425\(03\)00251-8](https://doi.org/10.1016/s1386-1425(03)00251-8)

345. Rozenberg, M., Shoham, G., Reva, I. & Fausto, R. Low Temperature Fourier Transform Infrared Spectra and Hydrogen Bonding in Polycrystalline Uracil and Thymine. *Spectrochimica Acta Part A: Molecular and Biomolecular Spectroscopy*, **2004**, 60, 2323-2336. <https://doi.org/10.1016/j.saa.2003.12.006>

346. Rozenberg, M., Jung, C. & Shoham, G. Ordered and Disordered Hydrogen Bonds in Adenosine, Cytidine and Uridine Studied by Low Temperature FT Infrared Spectroscopy. *Physical Chemistry Chemical Physics*, **2003**, 5, 1533-1535. <https://doi.org/10.1039/b300210c>

347. Rozenberg, M. & Shoham, G. FTIR Spectra of Solid Poly-L-Lysine in the Stretching NH Mode Range. *Biophysical Chemistry*, **2007**, 125, 166-171. <https://doi.org/10.1016/j.bpc.2006.07.008>

348. Rozenberg, M., Fausto, R. & Reva, I. Variable Temperature FTIR Spectra of Polycrystalline Purine Nucleobases and Estimating Strengths of Individual Hydrogen Bonds. *Spectrochimica Acta Part A: Molecular and Biomolecular Spectroscopy*, **2021**, 251, 119323. <https://doi.org/10.1016/j.saa.2020.119323>

349. Djikanović, D., Devečerski, A., Steinbach, G., Simonović, J., Matović, B., Garab, G., Kalauzi, A. & Radotić, K. Comparison of Macromolecular Interactions in the Cell Walls of Hardwood, Softwood and Maize by Fluorescence and FTIR Spectroscopy, Differential

Polarization Laser Scanning Microscopy and X-Ray Diffraction. *Wood Science and Technology*, **2015**, 50, 547-566. <https://doi.org/10.1007/s00226-015-0792-y>

350. Brela, M. Z., Wójcik, M. J., Boczar, M., Onishi, E., Sato, H., Nakajima, T. & Ozaki, Y. Study of Hydrogen Bond Dynamics in Nylon 6 Crystals Using IR Spectroscopy and Molecular Dynamics Focusing on the Differences between  $\alpha$  and  $\gamma$  Crystal Forms. *International Journal of Quantum Chemistry*, **2018**, 118, e25595. <https://doi.org/10.1002/qua.25595>

351. Wen, L., Zhang, J. H., Zhou, T. & Zhang, A. M. Hydrogen Bonding in Micro-Phase Separation of Poly(Polyamide 12-Block-Polytetrahydrofuran) Alternating Block Copolymer: Enthalpies and Molecular Movements. *Vibrational Spectroscopy*, **2016**, 86, 160-172. <https://doi.org/10.1016/j.vibspec.2016.07.001>

352. Zhang, D.-D., Ruan, Y.-B., Zhang, B.-Q., Qiao, X., Deng, G., Chen, Y. & Liu, C.-Y. A Self-healing PDMS Elastomer Based on Acylhydrazone Groups and the Role of Hydrogen Bonds. *Polymer*, **2017**, 120, 189-196. <https://doi.org/10.1016/j.polymer.2017.05.060>

353. Brás, A., Arizaga, A., Agirre, U., Dorau, M., Houston, J., Radulescu, A., Kruteva, M., Pyckhout-Hintzen, W. & Schmidt, A. M. Chain-End Effects on Supramolecular Poly(Ethylene Glycol) Polymers. *Polymers*, **2021**, 13, 2235. <https://doi.org/10.3390/polym13142235>

354. Goldansaz, H., Fustin, C.-A., Wübberhorst, M. & van Ruymbeke, E. How Supramolecular Assemblies Control Dynamics of Associative Polymers: Toward a General Picture. *Macromolecules*, **2016**, 49, 1890-1902. <https://doi.org/10.1021/acs.macromol.5b01535>

355. Wittenberg, E., Meyer, A., Eggers, S. & Abetz, V. Hydrogen Bonding and Thermoplastic Elastomers – A Nice Couple with Temperature-Adjustable Mechanical Properties. *Soft Matter*, **2018**, 14, 2701-2711. <https://doi.org/10.1039/c8sm00296g>

356. Qiu, H. N., Lin, J., Hou, L. X., Xiao, R., Zheng, Q. & Wu, Z. L. Stress Relaxation and Creep Response of Glassy Hydrogels with Dense Physical Associations. *ACS Applied Materials & Interfaces*, **2025**, <https://doi.org/10.1021/acsami.4c22398>

357. Yan, T., Schröter, K., Herbst, F., Binder, W. H. & Thurn-Albrecht, T. What Controls the Structure and the Linear and Nonlinear Rheological Properties of Dense, Dynamic Supramolecular Polymer Networks? *Macromolecules*, **2017**, 50, 2973-2985. <https://doi.org/10.1021/acs.macromol.6b02507>

358. Shabbir, A., Goldansaz, H., Hassager, O., van Ruymbeke, E. & Alvarez, N. J. Effect of Hydrogen Bonding on Linear and Nonlinear Rheology of Entangled Polymer Melts. *Macromolecules*, **2015**, 48, 5988-5996. <https://doi.org/10.1021/acs.macromol.5b00757>

359. Li, H., Wang, Y., Zhang, W., Ma, R., Zhao, X., Liu, X., Zhang, L. & Gao, Y. Structure, Dynamics, and Rheological Behavior of Associative Polymers Formed by Hydrogen Bonds. *Macromolecules*, **2024**, 57, 1106-1117. <https://doi.org/10.1021/acs.macromol.3c01794>

360. Tu, C.-H., Fastow, E. J., John Chethalen, R., Papamokos, G. V., Coughlin, E. B. & Winey, K. I. Coupling and Decoupling between Stickers and Backbones in Associating Polymers with Terminally Functionalized Side Chains. *Macromolecules*, **2024**, 57, 8067-8081. <https://doi.org/10.1021/acs.macromol.4c00983>
361. Arrese-Igor, S., Alegría, A. & Colmenero, J. Signature of Hydrogen Bonding Association in the Dielectric Signal of Polyalcohols. *Journal of Molecular Liquids*, **2020**, 318, 114215. <https://doi.org/10.1016/j.molliq.2020.114215>
362. Tress, M., Xing, K., Ge, S., Cao, P., Saito, T. & Sokolov, A. What Dielectric Spectroscopy Can Tell Us about Supramolecular Networks. *The European Physical Journal E*, **2019**, 42, 133. <https://doi.org/10.1140/epje/i2019-11897-4>
363. Qin, B. & Xia, J. Silicone-Polyurea Based Clear Viscoelastic Films for Flexible Displays, Impact of Diisocyanate, Chain Extender, Soft Segment Molecular Weight, and Hard Segment Contents. *European Polymer Journal*, **2024**, 219, 113392. <https://doi.org/10.1016/j.eurpolymj.2024.113392>
364. Liu, B., Chen, X., Spiering, G. A., Moore, R. B. & Long, T. E. Quadruple Hydrogen Bond-Containing A-AB-A Triblock Copolymers: Probing the Influence of Hydrogen Bonding in the Central Block. *Molecules*, **2021**, 26, 4705. <https://doi.org/10.3390/molecules26154705>
365. Panov, Y. N., Stalevich, A. M., Tiranov, V. G., Yakovenko, L. K. & Frenkel, S. Y. Effect of Hydrogen-Bond Network on the Thermomechanical and Relaxation Properties of Block Copolymers. *Polymer Mechanics*, **1971**, 3, 268-271. <https://doi.org/10.1007/BF00858763>
366. Chen, M., Inglefield, D. L., Zhang, K., Hudson, A. G., Talley, S. J., Moore, R. B. & Long, T. E. Synthesis of Urea-Containing ABA Triblock Copolymers: Influence of Pendant Hydrogen Bonding on Morphology and Thermomechanical Properties. *Journal of Polymer Science Part A: Polymer Chemistry*, **2018**, 56, 1844-1852. <https://doi.org/10.1002/pola.29066>
367. Chavan, J. G., Rath, S. K., Praveen, S., Kalletla, S. & Patri, M. Hydrogen Bonding and Thermomechanical Properties of Model Polydimethylsiloxane Based Poly(Urethane-Urea) Copolymers: Effect of Hard Segment Content. *Progress in Organic Coatings*, **2016**, 90, 350-358. <https://doi.org/10.1016/j.porgcoat.2015.06.015>
368. Narasimhan, B. N., Dixon, A. W., Mansel, B., Taberner, A., Mata, J. & Malmstrom, J. Hydrogen Bonding Sissipating Hydrogels: The Influence of Network Structure Design on Structure-Property Relationships. *Journal of Colloid and Interface Science*, **2023**, 630, 638-653. <https://doi.org/10.1016/j.jcis.2022.10.029>
369. Brás, A. R., Hövelmann, C. H., Antonius, W., Teixeira, J., Radulescu, A., Allgaier, J., Pyckhout-Hintzen, W., Wischnewski, A. & Richter, D. Molecular Approach to Supramolecular Polymer Assembly by Small Angle Neutron Scattering. *Macromolecules*, **2013**, 46, 9446-9454. <https://doi.org/10.1021/ma401714r>

370. Chen, J., Wu, M., Gong, L., Zhang, J., Yan, B., Liu, J., Zhang, H., Thundat, T. & Zeng, H. Mechanistic Understanding and Nanomechanics of Multiple Hydrogen-Bonding Interactions in Aqueous Environment. *The Journal of Physical Chemistry C*, **2019**, 123, 4540-4548. <https://doi.org/10.1021/acs.jpcc.8b11790>
371. Giessibl, F. J. Probing the Nature of Chemical Bonds by Atomic Force Microscopy. *Molecules*, **2021**, 26, 4068. <https://doi.org/10.3390/molecules26134068>
372. Chen, J., Peng, Q., Peng, X., Zhang, H. & Zeng, H. Probing and Manipulating Noncovalent Interactions in Functional Polymeric Systems. *Chemical Reviews*, **2022**, 122, 14594-14678. <https://doi.org/10.1021/acs.chemrev.2c00215>
373. Lenthall, J. T., Foster, J. A., Anderson, K. M., Probert, M. R., Howard, J. A. K. & Steed, J. W. Hydrogen Bonding Interactions with the Thiocarbonyl  $\pi$ -System. *Crystengcomm*, **2011**, 13, 3202-3212. <https://doi.org/10.1039/c0ce00680g>
374. Verjans, J., André, A., Van Ruymbeke, E. & Hoogenboom, R. Physically Cross-Linked Polybutadiene by Quadruple Hydrogen Bonding through Side-Chain Incorporation of Ureidopyrimidinone with Branched Alkyl Side Chains. *Macromolecules*, **2022**, 55, 928-941. <https://doi.org/10.1021/acs.macromol.1c01908>
375. Li, C., Hilgeroth, P., Hasan, N., Strohl, D., Kressler, J. & Binder, W. H. Comparing C2=O and C2=S Barbiturates: Different Hydrogen-Bonding Patterns of Thiobarbiturates in Solution and the Solid State. *International Journal of Molecular Sciences*, **2021**, 22, 12679. <https://doi.org/10.3390/ijms222312679>
376. Li, C., Bhandary, R., Marinow, A., Ivanov, D., Du, M., Androsch, R. & Binder, W. H. Synthesis and Characterization of Quadrupolar-Hydrogen-Bonded Polymeric Ionic Liquids for Potential Self-Healing Electrolytes. *Polymers*, **2022**, 14, 4090. <https://doi.org/10.3390/polym14194090>
377. Li, C., Bhandary, R., Marinow, A., Bachmann, S., Poppler, A. C. & Binder, W. H. Stability of Quadruple Hydrogen Bonds in an Ionic Liquid Environment. *Macromol Rapid Commun*, **2024**, 45, e2300464. <https://doi.org/10.1002/marc.202300464>
378. Li, C., Mai, P., Festag, N., Marinow, A. & Binder, W. H. Proximity Effects and Aggregation of Hamilton-Receptor Barbiturate Host–Guest Complexes Probed by Cross-Metathesis and ESI MS Analysis. *Chemistry – A European Journal*, **2024**, <https://doi.org/10.1002/chem.202403939>
379. Scheidel, S., Ostreicher, L., Mark, I. & Poppler, A. C. You Cannot Fight the Pressure: Structural Rearrangements of Active Pharmaceutical Ingredients under Magic Angle Spinning. *Magn Reson Chem*, **2022**, 60, 572-582. <https://doi.org/10.1002/mrc.5267>

## Appendix

Supporting Information to:

Comparing C2=O and C2=S Barbiturates: Different Hydrogen-Bonding Patterns of Thiobarbiturates in Solution and the Solid State

*Int. J. Mol. Sci.* **2021**, 22(23), 12679;  
<https://doi.org/10.3390/ijms222312679>

Synthesis and Characterization of Quadrupolar-Hydrogen-Bonded Polymeric Ionic Liquids for Potential Self-Healing Electrolytes

*Polymers* **2022**, 14(19), 4090  
<https://doi.org/10.3390/polym14194090>

Stability of Quadruple Hydrogen Bonds in an Ionic Liquid Environment

*Macromol. Rapid Commun.* **2024**, 45, 2300464  
<https://doi.org/10.1002/marc.202300464>

Proximity Effects and Aggregation of Hamilton-Receptor Barbiturate Host-Guest Complexes Probed by Cross-Metathesis and ESI MS Analysis

*Chem. Eur. J.* **2024**, e202403939  
<https://doi.org/10.1002/chem.202403939>

# Supporting Information

## Comparing C2=O and C2=S Barbiturates: Different Hydrogen Bonding Patterns of Thiobarbiturates in Solution and the Solid State

Chenming Li<sup>1</sup>, Phillip Hilgeroth<sup>1</sup>, Nazmul Hasan<sup>2</sup>, Dieter Ströhl<sup>3</sup>, Jörg Kressler<sup>2</sup>, and Wolfgang H. Binder<sup>1\*</sup>

<sup>1</sup> Institute of Chemistry, Martin-Luther-University Halle-Wittenberg, Von-Danckelmann-Platz 4, D-06120 Halle (Saale), Germany; chenming.li@chemie.uni-halle.de

<sup>2</sup> Institute of Chemistry, Martin Luther University Halle-Wittenberg, Von-Danckelmann-Platz 4, D-06120 Halle (Saale), Germany; nazmul.hasan@chemie.uni-halle.de

<sup>3</sup> Institute of Chemistry, Martin Luther University Halle-Wittenberg, Kurt-Mothes-Str. 2, 06120 Halle (Saale), Germany; dieter.stroehl@chemie.uni-halle.de

\* Correspondence: wolfgang.binder@chemie.uni-halle.de



<b>1.</b>	<b>EXPERIMENTAL PART</b>	<b>1</b>
1.1.	SOLVENTS AND MATERIALS	1
1.2.	METHODS	1
1.3.	SYNTHESIS	3
1)	Synthesis of Diethyl 2,2-Di(dec-9-en-1-yl)malonate ( <b>M1</b> )	3
2)	Synthesis of Diethyl 2,2-Di(dec-9-en-1-yl)malonate ( <b>M2</b> )	4
	General Synthesis of Barbiturate and 2-Thiobarbiturate	4
3)	Synthesis of 5,5-Di(dec-9-en-1-yl)pyrimidine-2,4,6(1H,3H,5H)-trione ( <b>B</b> )	5
4)	Synthesis of 5,5-Di(dec-9-en-1-yl)-2-thioxodihydropyrimidine-4,6(1H,5H)-dione ( <b>TB</b> )	5
5)	Synthesis of 5-Ethyl-5-(pent-4-yn-1-yl)pyrimidine-2,4,6(1H,3H,5H)-trione ( <b>B2</b> )	5
6)	Synthesis of 5-Ethyl-5-(pent-4-yn-1-yl)-2-thioxodihydropyrimidine-4,6(1H,5H)-dione ( <b>TB2</b> )	5
	Synthesis of Telechelic Polyisobutylenes	6
7)	Synthesis of Dimethyl-5-(tert-butyl)isophthalate ( <b>1</b> )	6
8)	Synthesis of 2,2-(5-(Tert-butyl)-1,3-phenylene)bis(propan-2-ol) ( <b>2</b> )	6
9)	Synthesis of 1-(Tert-butyl)-3,5-bis(2-methoxypropan-2-yl)benzene ( <b>3</b> )	7
10)	Synthesis of Telechelic Dibromopolyisobutylene ( <b>PBr</b> )	7
11)	Synthesis of Telechelic Diazidopolyisobutylene ( <b>PN3</b> )	8
12)	Synthesis of Telechelic Dibarbiturate Polyisobutylene ( <b>PB</b> )	8
13)	Synthesis of Telechelic Dithiobarbiturate Polyisobutylene ( <b>PTB</b> )	9
<b>2.</b>	<b>NONLINEAR FITTING OF NH CHEMICAL SHIFT FOR ASSOCIATION CONSTANTS</b>	<b>10</b>
<b>3.</b>	<b>CALCULATION OF COALESCENCE CONSTANT</b>	<b>10</b>
<b>4.</b>	<b>MOLECULE MODEL OF B IN LANGMUIR FILM</b>	<b>11</b>
<b>5.</b>	<b>SUMMARY OF CHARACTERIZATION OF MODEL POLYMERS</b>	<b>11</b>
<b>6.</b>	<b>NMR SPECTRA OF MODEL COMPOUNDS AND POLYMERS</b>	<b>12</b>
<b>7.</b>	<b>ESI-TOF MS SPECTRA OF MODEL COMPOUNDS</b>	<b>15</b>
<b>8.</b>	<b>MALDI-TOF MS SPECTRA OF MODEL POLYMERS</b>	<b>16</b>
8.1.	SPECTRA OF <b>PB</b>	16
8.2.	SPECTRA OF <b>PTB</b>	17
<b>9.</b>	<b>DSC CURVES OF MODEL POLYMERS</b>	<b>18</b>
<b>10.</b>	<b>LOSS TANGENT VS FREQUENCY CURVE OF MODEL POLYMERS</b>	<b>18</b>
<b>11.</b>	<b>ZERO-SHEAR VISCOSITY VS TEMPERATURE CURVE OF MODEL POLYMERS</b>	<b>19</b>
<b>12.</b>	<b>REFERENCE</b>	<b>20</b>

## 1. Experimental Part

### 1.1. Solvents and Materials

Chloroform from VWR, ethyl acetate from Overlack, methanol from Brenntag, and toluene from Roth were purchased in technical grade and distilled at least once prior use. Deuterium chloroform ( $\text{CDCl}_3$ -*d*) and deuterium dimethyl sulfoxide ( $\text{DMSO}$ -*d*6), from Chemotrade, were used as NMR deuterium solvents.

Dry solvents were prepared as follows: tetrahydrofuran (THF), from Roth, was predried over potassium hydroxide for several days and refluxed over sodium and benzophenone under inert atmosphere and distilled freshly before use; *n*-hexane, from Roth, was refluxed over concentrated sulfuric acid and oleum to remove olefins and subsequently distilled over sodium and benzophenone under an inert gas atmosphere for several hours; dichloromethane (DCM), from Overlack, was predried over calcium chloride for several days and then refluxed over calcium hydride for several hours; diethyl ether, from Overlack, was passed through a column filled with sodium sulfate to remove moisture; dimethyl sulfoxide (DMSO), from Grüssing, was stored over molecular sieves (pore diameters 4Å) for several days before use; N,N-dimethylformamide (DMF) from Grüssing was stored over calcium hydride for several days before use.

1-Bromo-3-phenoxypropane was purchased from Alfa Aesar; titanium tetrachloride, magnesium chips, iodomethane, N,N-dimethylacetamide, 2,6-di-*tert*-butyl pyridine, and isobutylene were purchased from Sigma Aldrich; 5-(*tert*-butyl)isophthalic acid were purchased from TCI. All chemicals listed here were used without any purification unless otherwise stated.

### 1.2. Methods

#### *Thin-layer Chromatography (TLC)*

TLC was performed on “Merck silica gel 60” plates. Spots on TLC plate were visualized using UV light (254 or 366 nm), oxidizing agent “blue stain”, or potassium

permanganate solution. “Blue stain” was prepared as follow:  $(\text{NH}_4)_6\text{Mo}_7\text{O}_{24}\cdot 4\text{H}_2\text{O}$  (1 g) and  $\text{Ce}(\text{SO}_4)_2\cdot 4\text{H}_2\text{O}$  (1 g) were dissolved in a mixture of distilled water (90 mL) and concentrated sulfuric acid (6 mL). Potassium permanganate solution was prepared as follow:  $\text{KMnO}_4$  (3 g) and  $\text{K}_2\text{CO}_3$  (10 g) were dissolved in distilled water (300 mL).

#### *Electrospray Ionization Time-of-Flight Mass Spectroscopy (ESI-ToF MS)*

ESI-ToF MS measurements were performed using a Bruker Daltonics microTOF. 0.1 mg of samples were dissolved in HPLC grade methanol. All spectra were obtained by means of direct injection with a flow rate of  $180\ \mu\text{L h}^{-1}$  in the negative mode with an acceleration voltage of 4.5 kV.

#### *Gel Permeation Chromatography*

GPC measurements were performed at  $40\ ^\circ\text{C}$  on a Viscotek GPCmax VE 2002 from Viscotek<sup>TM</sup> applying a HHRH Guard-17369 and a GMHHR-N-18055 column. As solvent THF was used and the sample concentration was adjusted to  $3\ \text{mg}\cdot\text{mL}^{-1}$  while applying a flow rate of  $1\ \text{mL}\cdot\text{min}^{-1}$ . For determination of the molecular weights the refractive index of the investigated sample was detected with a VE 3580 RI detector of Viscotek<sup>TM</sup> and PIB-standards ( $320\ \text{g}\cdot\text{mol}^{-1}$  to  $578,000\ \text{g}\cdot\text{mol}^{-1}$ ) were used as reference from Viscotek<sup>TM</sup>.

#### *Matrix-assisted Laser Desorption / Ionization Time-of-Flight Mass Spectrometry (MALDI-ToF MS)*

MALDI-ToF MS was done on a Bruker Autoflex III system in the reflection mode. Formation of ions was obtained by laser desorption (smart beam laser at 355, 532, 808, and  $1064 \pm 6.5\ \text{nm}$ ; 3 ns pulse width; up to 2500 Hz repetition rate). Ions were accelerated by a voltage of 20 kV, and detected as positive ions. 1,8-dihydroxy-9,10-dihydroanthracen-9-one (Dithranol,  $20\ \text{mg}\cdot\text{mL}^{-1}$  in THF) was used as matrix and sodium iodide (NaI,  $20\ \text{mg}\cdot\text{mL}^{-1}$  in THF) was used as salts for ionizing polymers functionalized with hydrogen-bonding moieties (model polymer PB or PTB,  $20\ \text{mg}\cdot\text{mL}^{-1}$  in THF) while applying a volume ratio of 100:20:1.

### 1.3. Synthesis

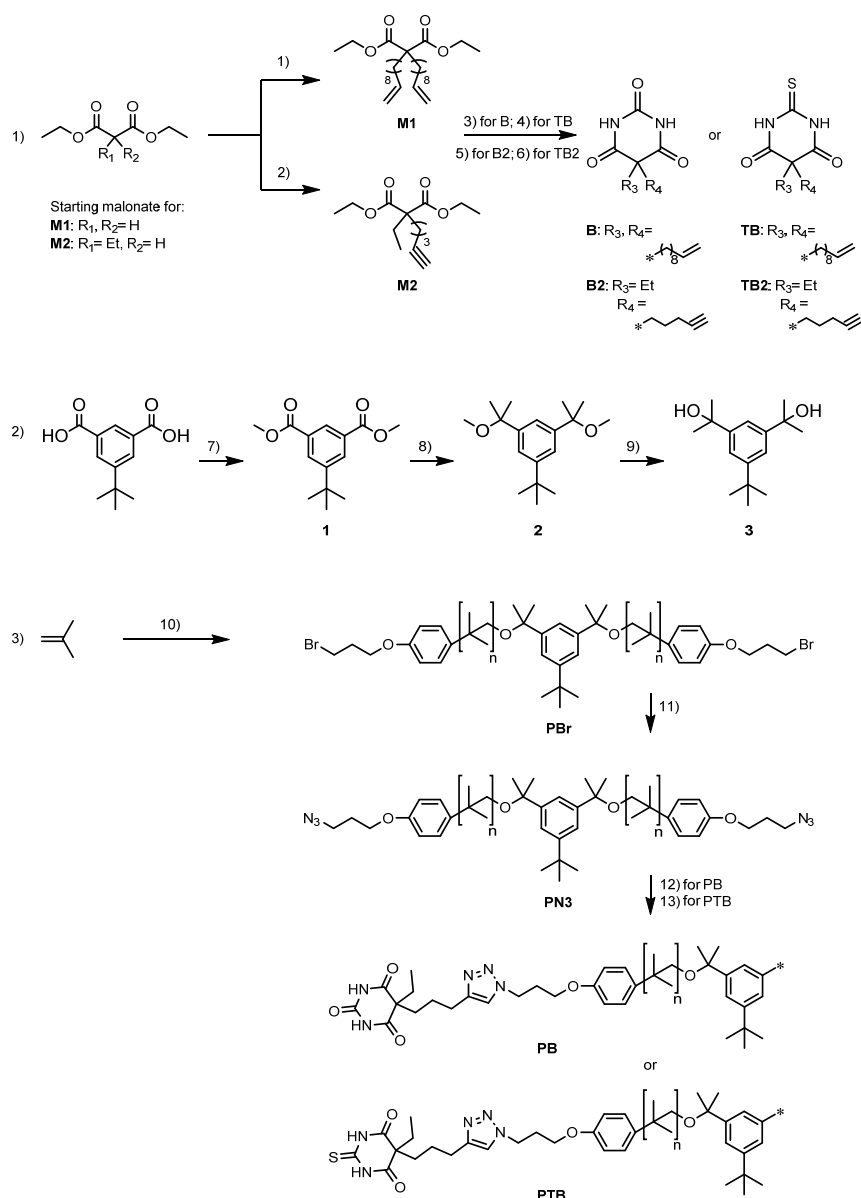


**Figure S1** Synthetic procedure of 1) barbiturates **B/B2** and 2-thiobarbiturate **TB/TB2**; 2) the initiator **3** for LCCP of isobutylene; 3) telechelic dibarbiturate/dithiobarbiturate polyisobutylene **PB/PTB**.

#### 1) Synthesis of Diethyl 2,2-Di(dec-9-en-1-yl)malonate (**M1**)

The synthesis of **M1** was modified according to reference [1]. To a two-necked flask, sodium hydride (0.88g, 60% wt dispersion in oil, 110 mmol) was placed followed by adding 20 ml dry THF. While the flask was cooled in an ice bath, diethyl malonate (1.52 ml, 10 mmol) dissolved in 5 ml dry THF was added dropwise. The reaction mixture was stirred for 30 minutes till clear, then treated with 10-bromo-1-decene (4.02 ml, 22 mmol) dissolved in 5 ml dry THF. The reaction mixture was heated to reflux

(temperature of oil bath was 85 °C) for 72 hours, monitored by TLC. After reaction was finished, the mixture was quenched with 50 ml 1 M hydrochloric acid, and was extracted with ethyl acetate (3 × 30 ml). The combined organic layers were washed with brine, dried with sodium sulfate, filtered and concentrated under reduced pressure. Column chromatography on silica with hexane/diethyl ether 100:10 was performed. After drying under vacuum, **M1** as a colorless liquid was obtained. Yield: 2.98 g (68 %). <sup>1</sup>H-NMR (500 MHz, CDCl<sub>3</sub>): 5.78 (2 H, ddt, J 16.9, 10.1, 6.7), 5.02 – 4.85 (4 H, m), 4.15 (4 H, q, J 7.1), 2.06 – 1.98 (4 H, m), 1.87 – 1.80 (4 H, m), 1.40 – 1.05 (31 H, m). <sup>13</sup>C-NMR (101 MHz, CDCl<sub>3</sub>): 171.97, 139.12, 114.07, 60.85, 57.51, 33.75, 32.09, 29.79, 29.33, 29.24, 29.05, 28.88, 23.87, 14.08.

## 2) *Synthesis of Diethyl 2,2-Di(dec-9-en-1-yl)malonate (M2)*

The **M2** was synthesized according to reference [2]. <sup>1</sup>H-NMR (400 MHz, DMSO-*d*<sub>6</sub>): δ ppm 4.12 (q, *J* = 7.1 Hz, 4H), 2.77 (t, *J* = 2.6 Hz, 1H), 2.18 (td, *J* = 6.8, 2.7 Hz, 2H), 1.92 – 1.74 (m, 4H), 1.31 – 1.21 (m, 2H), 1.16 (t, *J* = 7.1 Hz, 6H). <sup>13</sup>C-NMR (101 MHz, DMSO-*d*<sub>6</sub>): δ ppm 171.29, 84.37, 71.90, 61.17, 57.44, 30.59, 25.07, 23.10, 18.31, 14.37, 8.52.

## *General Synthesis of Barbiturate and 2-Thiobarbiturate*

To synthesize different barbiturates and 2-thiobarbiturates by condensation of malonate substrates with urea or thiourea, the general synthesis was modified according to reference [2,3] as follow: to a flask cooled in an ice bath finely grounded urea (10 equivalence) or thiourea (6 equivalence) and potassium tert-butoxide (2.2 equivalence) were added. Dry DMSO was added to dissolve the solids, followed by stirring for 30 minutes till the mixture turned clear. Then the malonate (**M1** or **M2**, 1 equivalence) was added and the mixture was stirred at different temperature for different time, monitored by TLC. After reaction the reaction mixture was diluted with 1 M hydrochloric acid (the pH of the mixture was checked to be 2). The mixture was extracted with ethyl acetate for three times. The combined organic extracts were washed with water, dried with sodium sulfate, filtered, and concentrated under reduced pressure. Further purification was performed by column chromatography on silica or recrystallization in

toluene at 75 °C.

### 3) *Synthesis of 5,5-Di(dec-9-en-1-yl)pyrimidine-2,4,6(1H,3H,5H)-trione (B)*

General synthesis was followed. Urea (3.00 g, 50 mmol), potassium tert-butoxide (1.23 g, 11.0 mmol) and diethyl 2,2-di(dec-9-en-1-yl)malonate **M 1** (2.18 g, 5.0 mmol) were mixed in 20 ml DMSO and stirred at 40 °C for 48 hours. Column chromatography on silica with ethyl acetate/*n*-hexane 1:4 was performed. After drying under high vacuum, **B1** as a white solid was obtained. Yield: 1.05 g (52 %). M.p.: 91°C (DSC). <sup>1</sup>H-NMR (500 MHz, CDCl<sub>3</sub>): δ ppm 8.75 (2 H, s), 5.79 (2 H, ddt, *J* 16.9, 10.2, 6.7), 5.02 – 4.89 (4 H, m), 2.07 – 1.90 (8 H, m), 1.42 – 1.10 (24 H, m). <sup>13</sup>C-NMR (101 MHz, CDCl<sub>3</sub>): δ ppm 172.93 , 149.14 , 139.23 , 114.31 , 56.87 , 39.33 , 33.88 , 29.55 , 29.40 , 29.23 , 29.12 , 28.97 , 25.22. ESI-ToF MS: [M-H]<sup>-</sup> calculated for C<sub>24</sub>H<sub>40</sub>N<sub>2</sub>O<sub>3</sub>, 403.60; found, 403.29.

### 4) *Synthesis of 5,5-Di(dec-9-en-1-yl)-2-thioxodihydropyrimidine-4,6(1H,5H)-dione (TB)*

General synthesis was followed. Thiourea (1.14 g, 15.0 mmol), potassium tert-butoxide (617 mg, 5.5 mmol) and **M1** (1.10 g, 2.5 mmol) were mixed in 10 ml DMSO and stirred at room temperature for 24 hours. Column chromatography on silica with diethyl ether/*n*-hexane 1:4 was performed. After drying under high vacuum, **TB** as a slight yellowish high viscous liquid was obtained. Yield: 0.65 g (62 %). <sup>1</sup>H-NMR (500 MHz, CDCl<sub>3</sub>): δ ppm 9.23 (2 H, s), 5.79 (2 H, ddt, *J* 16.9, 10.2, 6.7), 5.02 – 4.89 (4 H, m), 2.06 – 1.88 (8 H, m), 1.43 – 1.11 (24 H, m). <sup>13</sup>C-NMR (101 MHz, CDCl<sub>3</sub>): δ ppm 176.09 , 170.80 , 139.24 , 114.32 , 57.04 , 39.41 , 33.89 , 29.55 , 29.38 , 29.20 , 29.11 , 28.97 , 25.19. ESI-ToF MS: [M-H]<sup>-</sup> calculated for C<sub>24</sub>H<sub>40</sub>N<sub>2</sub>O<sub>2</sub>S, 419.66; found, 419.26.

### 5) *Synthesis of 5-Ethyl-5-(pent-4-yn-1-yl)pyrimidine-2,4,6(1H,3H,5H)-trione (B2)*

The **B2** was synthesized according to reference [2]. <sup>1</sup>H-NMR (400 MHz, DMSO-*d*<sub>6</sub>): δ ppm 11.53 (s, 2H), 2.77 (t, *J* = 2.6 Hz, 1H), 2.12 (td, *J* = 6.9, 2.7 Hz, 2H), 1.91 – 1.78 (m, 4H), 1.30 – 1.21 (m, 2H), 0.74 (t, *J* = 7.4 Hz, 3H). <sup>13</sup>C-NMR (101 MHz, DMSO-*d*<sub>6</sub>): δ ppm 173.29, 150.23, 83.95, 72.12, 55.86, 37.26, 31.78, 24.06, 18.04, 9.51. ESI-ToF MS: [M-H]<sup>-</sup> calculated for C<sub>11</sub>H<sub>14</sub>N<sub>2</sub>O<sub>3</sub>, 221.24; found, 221.10.

### 6) *Synthesis of 5-Ethyl-5-(pent-4-yn-1-yl)-2-thioxodihydropyrimidine-4,6(1H,5H)-*



### ***dione (TB2)***

General synthesis was followed. Thiourea (6.45 g, 84.71 mmol), potassium tert-butoxide (3.67 g, 31.06 mmol) and **M2** (3.59 g, 14.12 mmol) were mixed in 15 ml DMSO and stirred at room temperature for 24 hours. Column chromatography on silica with ethyl acetate/chloroform 1:8 was performed then the crude **TB2** was recrystallized in toluene. After drying under high vacuum, **TB2** as a slight yellowish solid was obtained. Yield: 1.85 g (56 %). <sup>1</sup>H-NMR (400 MHz, DMSO-*d*6): δ ppm 12.61 (s, 2H), 2.78 (t, *J* = 2.6 Hz, 1H), 2.13 (td, *J* = 6.9, 2.7 Hz, 2H), 1.93 – 1.81 (m, 4H), 1.32 – 1.20 (m, 2H), 0.75 (t, *J* = 7.4 Hz, 3H). <sup>13</sup>C-NMR (101 MHz, DMSO-*d*6): δ ppm 179.23, 171.31, 83.91, 72.17, 56.45, 37.20, 31.81, 24.03, 18.02, 9.50. ESI-ToF MS: [M-H]<sup>-</sup> calculated for C<sub>11</sub>H<sub>14</sub>N<sub>2</sub>O<sub>2</sub>S, 237.31; found, 237.08.

### ***Synthesis of Telechelic Polyisobutylenes***

#### ***7) Synthesis of Dimethyl-5-(tert-butyl)isophthalate (1)***

5-(tert-butyl)isophthalic acid (2.5 g, 11.25 mmol) was dissolved in methanol (100 ml). Then sulfuric acid (1.25 ml, 22.6 mmol) was added and the reaction mixture was heated to reflux for 48 hours. After cooling down to room temperature, the solvent was removed under reduced pressure. The product was purified using column chromatography (chloroform) and allowed to crystallize in the freezer. After drying under vacuum, **1** as a white solid was obtained. Yield: 2.4 g (85 %). <sup>1</sup>H NMR (400 MHz, CDCl<sub>3</sub>): δ 8.50 (t, *J* = 1.6 Hz, 1H), 8.26 (d, *J* = 1.6 Hz, 2H), 3.95 (s, 6H), 1.38 (s, 9H). <sup>13</sup>C NMR (100 MHz, CDCl<sub>3</sub>): δ 166.63, 152.13, 130.91, 130.35, 128.02, 52.27, 34.98, 31.16.

#### ***8) Synthesis of 2,2-(5-(Tert-butyl)-1,3-phenylene)bis(propan-2-ol) (2)***

A 500 ml flask was heated and flushed with nitrogen thrice. Magnesium chips (4.6 g, 0.19 mol) were dissolved in dry diethyl ether (100 ml) and a small portion of iodomethane (2 ml, 32 mmol) was added. The mixture was allowed to react until a color change was observed. The reaction mixture was held at 0°C, while the rest of iodomethane (12.5 ml, 200 mmol) was added. In a second flask **1** (9.5 g, 38 mmol) was dissolved in dry diethyl ether (150 ml) and was added to the reaction mixture over 2

hours and stirred for 16 hours. The solvent was evaporated und the crude product was recrystallized from hot ethyl acetate at 80°C. After drying under vacuum, **2** as a white solid was obtained. Yield: 8.0 g (84 %). <sup>1</sup>H NMR (400 MHz, CDCl<sub>3</sub>): δ 7.43 (m, 3H), 1.75 (s, 2H), 1.60 (s, 12H), 1.35 (s, 9H). <sup>13</sup>C NMR (100 MHz, CDCl<sub>3</sub>): δ 150.98, 148.63, 119.83, 117.65, 72.88, 35.01, 31.88, 31.50.

**9) Synthesis of 1-(Tert-butyl)-3,5-bis(2-methoxypropan-2-yl)benzene (3)**

**2** (1.9 g, 7.6 mmol) was dissolved in methanol (30 ml). Then sulfuric acid (0.004 ml, 72.3 μmol) was added and the reaction mixture was heated to refluxed for 24 hours. After cooling down to room temperature. The solution was adjusted to pH 7 using sodium bicarbonate, then extracted with hexane (50 ml) twice. The organic phase was then washed with distilled water (50 ml) four times, then dried with sodium sulfate. The solvent was removed under vacuum. After drying under vacuum, **3** as a white solid was obtained. Yield: 1.5 g (80 %). <sup>1</sup>H NMR (400 MHz, CDCl<sub>3</sub>): δ 7.32 (d, *J* = 1.7 Hz, 2H), 7.23 (t, *J* = 1.7 Hz, 1H), 3.07 (s, 6H), 1.54 (s, 12H), 1.33 (s, 9H). <sup>13</sup>C NMR (100 MHz, CDCl<sub>3</sub>): δ 150.76, 145.20, 121.19, 120.35, 77.24, 50.56, 34.84, 31.51, 28.13.

**10) Synthesis of Telechelic Dibromopolyisobutylene (PBr)**

A 250 ml flask was heated and flushed with nitrogen thrice. A stock solution of DCM (1 ml), N,N-dimethylacetamide (21 μl, 0.23 μmol), di-tert-butyl pyridine (50 μl, 0.23 μmol) and **3** (244 mg, 0.8 mmol) were prepared in a separate flask. Hexane and DCM (45 ml; 60:40) and the stock solution were added to the reaction flask via septum and cooled down to -80°C. Isobutylene (3.4 ml, 35.6 mmol) was condensed at -70°C in a separate flask and added to the reaction flask via septum. Titanium tetrachloride (1.2 ml, 10.9 mmol) was added and the mixture was stirred for 10 min. The reaction was quenched with 1-bromo-3-phenoxypropane (803 μl, 5.1 μmol) and stirred for 3 hours. The solvent was removed under reduced pressure, and the crude polymer was subsequently dissolved in hexane and precipitated into methanol (400 ml). After drying under high vacuum, **PBr** as a colorless viscous liquid was obtained. Yield: 2.7 g (90 %). *M<sub>n</sub>*, GPC = 2981. <sup>1</sup>H NMR (400 MHz, CDCl<sub>3</sub>): δ 7.26 (m, 4H), 7.17 (s, 3H), 6.82 (m, 4H), 4.08 (t, *J* = 5.8 Hz, 4H), 3.60 (t, *J* = 6.5 Hz, 4H), 2.31 (p, *J* = 6.2 Hz, 4H), 1.83 (s, 6H), 1.80 (s, 6H), 1.42 (m, 85H), 1.10 (m, 256H).

### 11) Synthesis of Telechelic Diazidopolyisobutylene (PN3)

Telechelic dibromo-PIB **PBr** ( $M_n$  was assumed to 3000) (1.15 g, 0.383 mmol) was dissolved in a 80 ml *n*-heptane/DMF mixture (1:1 v/v), then sodium azide (506 mg, 7.7 mmol) was added. The reaction mixture was heated to 90 °C for 8 h. After the reaction mixture was cooled down, the *n*-heptane layer was separated and washed with water (3 x 50 ml). The organic layer was dried over sodium sulfate and the solvent was removed. The crude polymer was redissolved in *n*-hexane and then precipitated into methanol (3 x 400 ml). After drying under high vacuum **PN3** as a yellowish viscous liquid was obtained. Yield: 1.05 g (94 %).  $M_{n, GPC} = 2818$ .  $^1H$  NMR (400 MHz,  $CDCl_3$ ):  $\delta$  7.26 (d,  $J = 8.8$  Hz, 4H), 7.17 (s, 3H), 6.81 (d,  $J = 8.8$  Hz, 4H), 4.03 (t,  $J = 5.9$  Hz, 4H), 3.51 (t,  $J = 6.7$  Hz, 4H), 2.04 (p,  $J = 6.3$  Hz, 4H), 1.83 (s, 6H), 1.80 (s, 6H), 1.44 – 1.36 (m, 85H), 1.18 – 0.95 (m, 256H).

### 12) Synthesis of Telechelic Dibarbiturate Polyisobutylene (PB)

The synthesis was modified according to reference [4,5]. Telechelic diazido-PIB (**PN3**) ( $M_n$  was assumed to 3000) (506.4 mg, 0.169 mmol), **B2** (87.68 mg, 0.371 mmol), and *N,N*-diisopropylethylamine (174.2  $\mu$ l, 1.016 mmol) were dissolved in 15 ml dry THF. The mixture was purged with argon for 30 minutes to remove oxygen. Cu(I)iodide (6.56 mg, 0.0338 mmol) was added under counterflow of argon then stirred at 50 °C for 48 hours. The reaction was checked by TLC. After reaction was finished, 30 ml 1 M hydrochloric acid was added and the mixture was extracted with DCM (3 x 30 ml). The combined organic mixture was washed with water (1 x 30 ml) and dried over sodium sulfate. Then DCM was removed under reduced pressure and the raw product was purified by column chromatography on silica with ethyl acetate/hexane (1:1,  $R_{f, BA} = 0.5$ ,  $R_{f, PI} = 0$ ) then chloroform/methanol (1:20,  $R_{f, PI} = 0.5$ ), followed by precipitation into methanol (400 ml). After drying under high vacuum **PB** as a yellowish rubbery solid was obtained. Yield: 265 mg (45 %).  $M_{n, GPC} = 3165$ .  $^1H$  NMR (400 MHz,  $CDCl_3$ ): 8.88 (s, 4H), 7.29 (s, 2H), 7.26 (d,  $J = 8.8$  Hz, 4H), 7.17 (s, 3H), 6.80 (d,  $J = 8.8$  Hz, 4H), 4.53 (t,  $J = 6.8$  Hz, 4H), 3.95 (t,  $J = 5.7$  Hz, 4H), 2.68 (t,  $J = 7.5$  Hz, 4H), 2.35 (p,  $J = 6.4$  Hz, 4H), 2.03 (dq, 4H), 1.83 (s, 6H), 1.80 (s, 6H), 1.70 – 1.53 (m, 8H), 1.43

– 1.30 (m, 85H), 1.14 – 1.00 (m, 256H), 0.88 (t,  $J = 7.4$  Hz, 6H).

### ***13) Synthesis of Telechelic Dithiobarbiturate Polyisobutylene (PTB)***

The synthesis was modified according to reference [4,5]. Telechelic diazido-PIB (**PN3**) ( $M_n$  was assumed to 3000) (434.6 mg, 0.145 mmol), **TB2** (78.64 mg, 0.33 mmol), and N,N-diisopropylethylamine (257.67  $\mu$ l, 1.5 mmol) were dissolved in 15 ml dry THF. The mixture was purged with argon for 30 minutes to remove oxygen. Cu(I)iodide (5.83 mg, 0.033 mmol) was added under counterflow of argon then stirred at 50 °C for 48 hours. The reaction was checked by TLC. After reaction was finished, 30 ml 1 M hydrochloric acid was added and the mixture was extracted with DCM (3 x 30 ml). The combined organic mixture was washed with water (1 x 30 ml) and dried over sodium sulfate. Then DCM was removed under reduced pressure and the raw product was purified by column chromatography on silica with chloroform/hexane (1:4,  $R_f$ , PTB = 0,  $R_f$ , TB2 = 0,  $R_f$ , PN3 = 1), then chloroform ( $R_f$ , PTB = 0,  $R_f$ , TBA = 0.25), and final methanol/chloroform (1:20,  $R_f$ , PTB = 0.5) followed by precipitation into methanol (3 x 400 ml). After drying under high vacuum **PTB** as a brown rubbery solid was obtained. Yield: 230 mg (49 %).  $M_n$ , GPC = 3165.  $^1\text{H}$  NMR (400 MHz,  $\text{CDCl}_3$ )  $\delta$  9.24 (s, 4H), 7.27 (d,  $J = 8.5$  Hz, 6H), 7.17 (s, 3H), 6.80 (d,  $J = 8.7$  Hz, 4H), 4.54 (t,  $J = 6.7$  Hz, 4H), 3.95 (t,  $J = 5.6$  Hz, 4H), 2.74 – 2.60 (m, 4H), 2.36 (p,  $J = 6.4$  Hz, 4H), 2.04 (dq,  $J = 16.0, 8.4$  Hz, 4H), 1.83 (s, 6H), 1.80 (s, 6H), 1.61 (s, 8H), 1.47 – 1.29 (m, 1036H), 1.15 – 0.99 (m, 2345H), 0.89 (t, 25H).

## 2. Nonlinear Fitting of NH Chemical Shift for Association Constants

For determination of the dimerization constant of the barbiturate **B** and thiobarbiturate **TB**, the stock solutions in CDCl<sub>3</sub> were prepared and the exact concentration was calculated. The NMR samples were prepared by diluting the exact amount of the stock solutions with CDCl<sub>3</sub> to reach the desired concentration, varying from 0.005 to 0.1 M. Then the N-H chemical shifts were recorded and plotted vs concentration as shown in the main text in Figure 1c). The association constant was calculated using the following equation (1):

$$\delta = \delta_{NH,free} + \frac{\delta_{NH,max} - \delta_{NH,free}}{[B]_0} \left( [B]_0 + \frac{1}{4K_{assn.}} - \sqrt{([B]_0 + \frac{1}{4K_{assn.}})^2 - [B]_0^2} \right) \quad (1)$$

Where

$\delta$  is the experimental N-H chemical shift;

$\delta_{NH,free}$  is the N-H chemical shift for the species free from hydrogen bonds (the N-H chemical shift from the sample with 0.005 M was used here);

$\delta_{NH,max}$  is the N-H chemical shift for the fully hydrogen bonded species;

$[B]_0$  is the concentration of the NMR sample;

$K_{assn.}$  is the association constant.

## 3. Calculation of Coalescence Constant

Using the equation (2), the coalescence rate constant at the  $T_{Coalescence} = 0$  °C can be calculated.

$$k_c = \frac{\pi \Delta \nu}{\sqrt{2}} \approx 2.22 \sqrt{\Delta \nu^2 + J_{AB}^2} \quad (2)$$

Where

$\Delta \nu$  is the difference of frequency of the two isolated peaks;

$J_{AB}$  is the  $J$ -coupling of the two isolated peaks

If we apply the coalescence rate constant to Eyring equation (3), the free enthalpy of coalescence can be calculated.

$$k_c = \chi \frac{k_B T}{h} e^{\Delta G_c^\ddagger / RT} \quad (3)$$

Where

$k_B$  is the Boltzmann constant;

$\chi$  is the transmission coefficient, assumed equal to 1;

$h$  is the Planck constant:

$\Delta G_c^\ddagger$  is the Gibbs free energy of activation.

#### 4. Space Filling Model of B in Langmuir Film

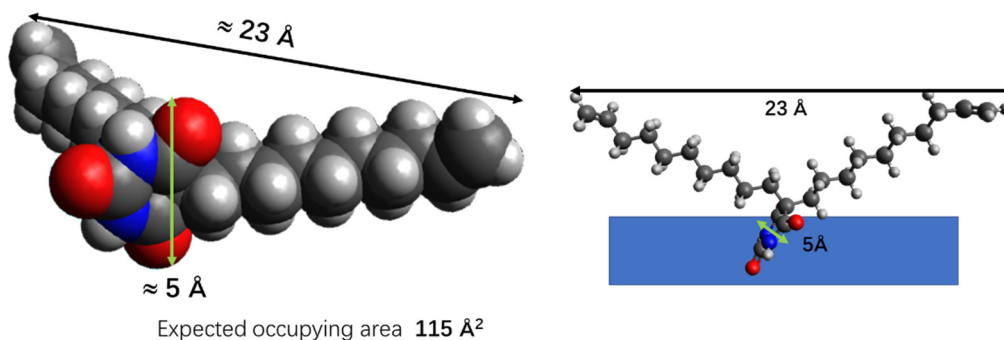


**Figure S2** The space filling model of **B** and the hypothesized arrangement on the water subphase. For the molecule **TB**, the model is identical except a larger C2=S thus is not shown here.

#### 5. Summary of Characterization of Model Polymers

**Table S1** Molecular weight and PDI from NMR, GPC, and MALDI-ToF MS; glass transition temperature; and melt viscosity at 80 °C of polymer precursor **PBr** and model polymer **PB** and **PTB**.

	$M_n$ NMR	$M_n$ GPC	$M_n$ MALDI	PDI GPC	$T_g$ DSC (°C)	Viscosity 80°C (Pa·s)
<b>PBr</b>	3512	2981	-	1.32	-58.8	6.43
<b>PB</b>	3741	3165	2800	1.43	-61.3	$3.03 \times 10^7$
<b>PTB</b>	3971	3244	3091	1.78	-59.6	$1.63 \times 10^8$



## 6. NMR Spectra of Model Compounds and Polymers

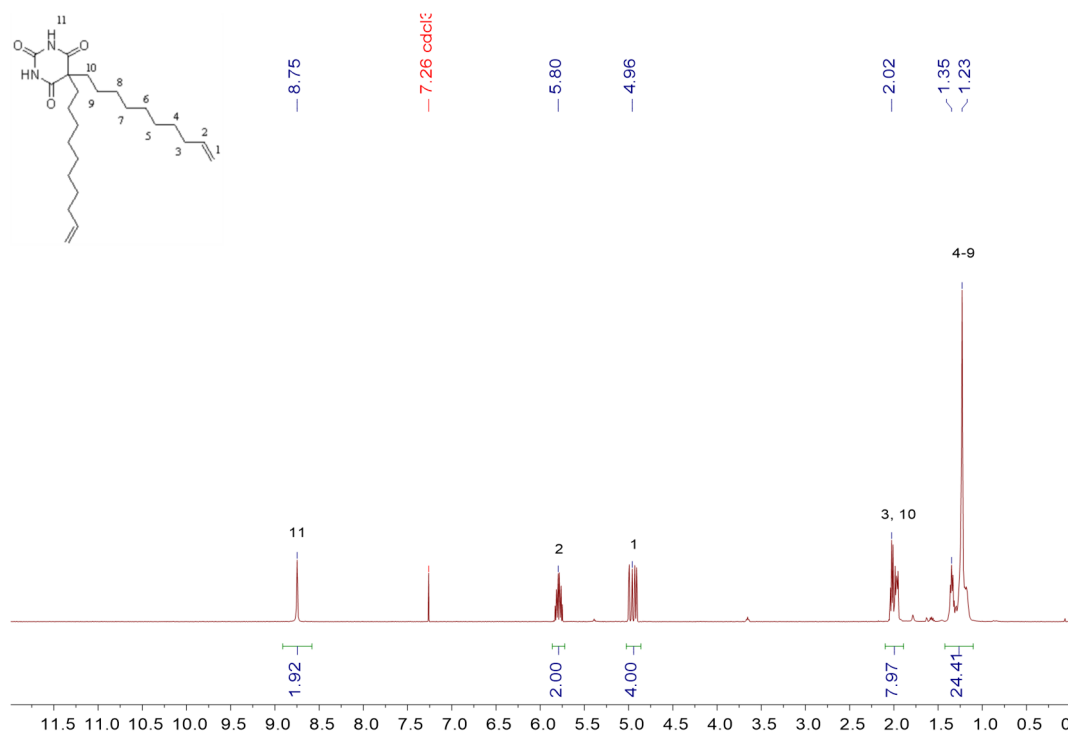


Figure S3  $^1\text{H}$  NMR spectrum of B.

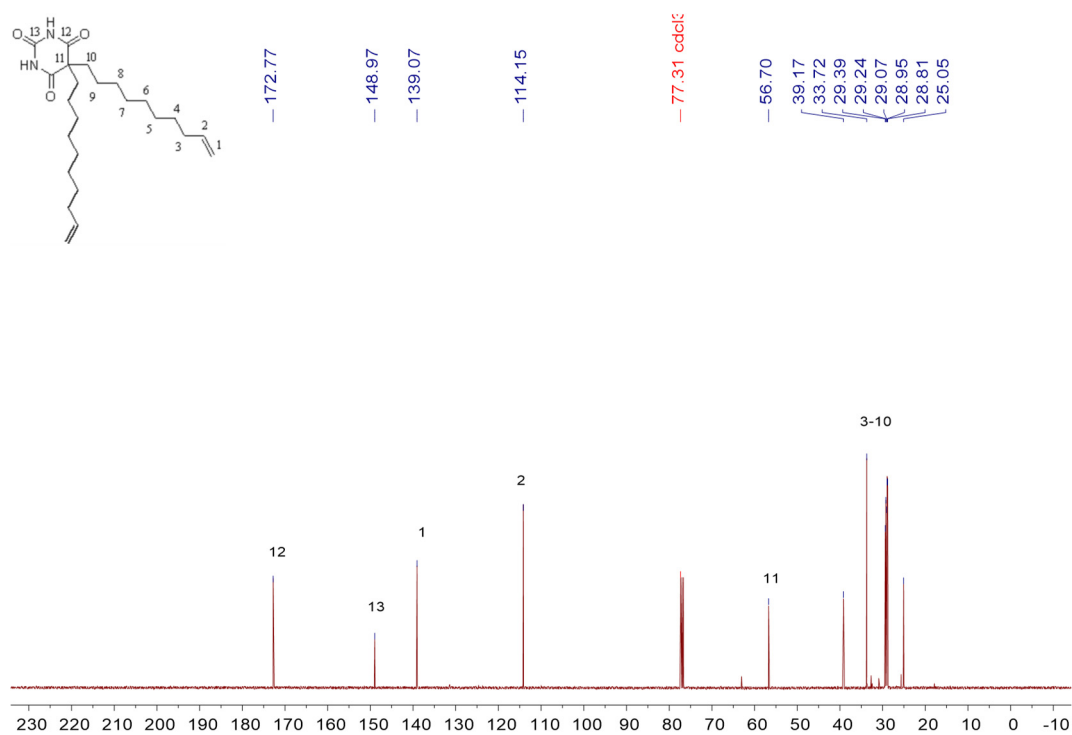
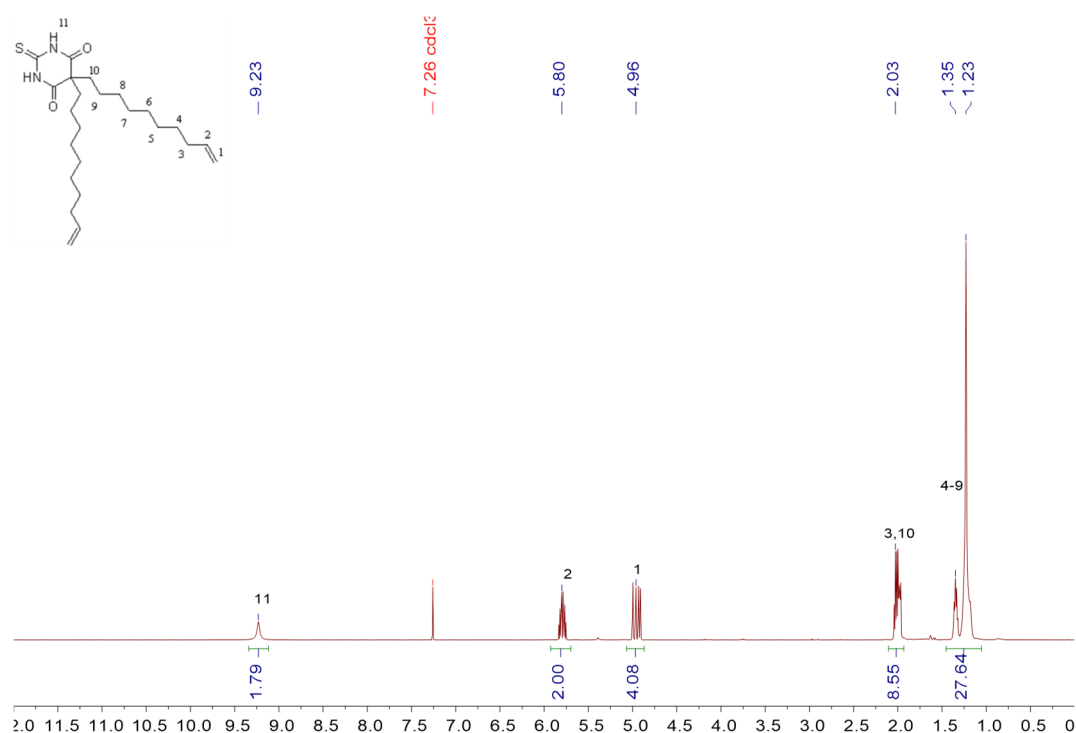
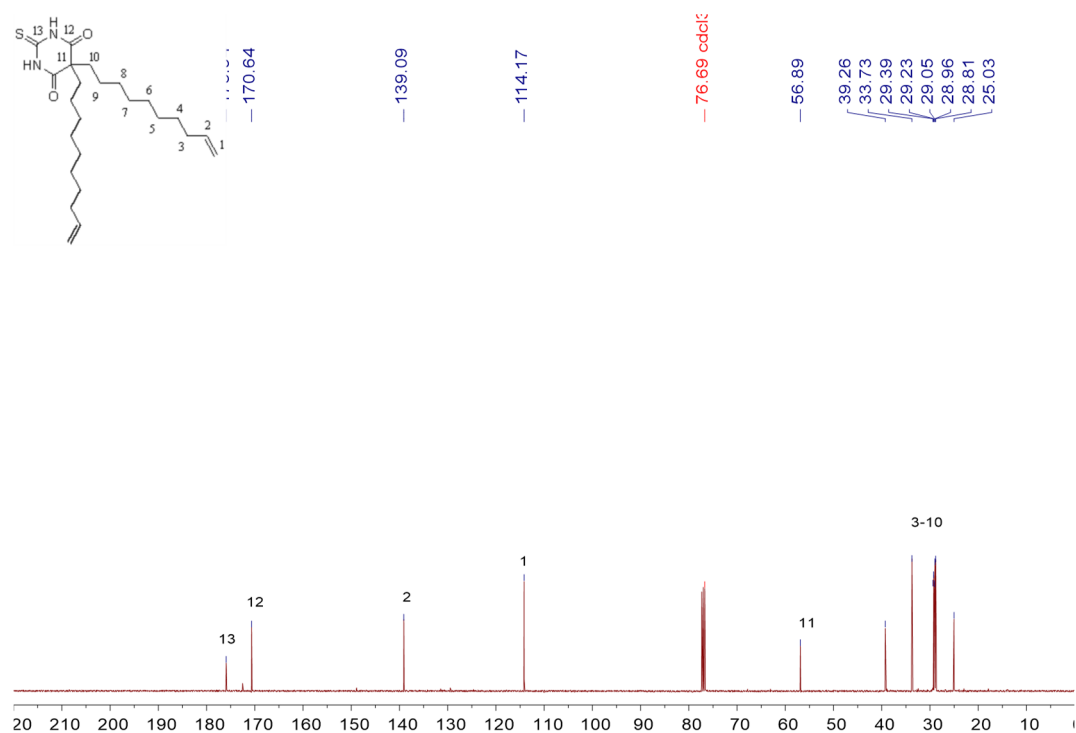


Figure S4  $^{13}\text{C}$  NMR spectrum of B.



**Figure S5 <sup>1</sup>H NMR spectrum of TB.**



**Figure S6 <sup>13</sup>C NMR spectrum of TB.**

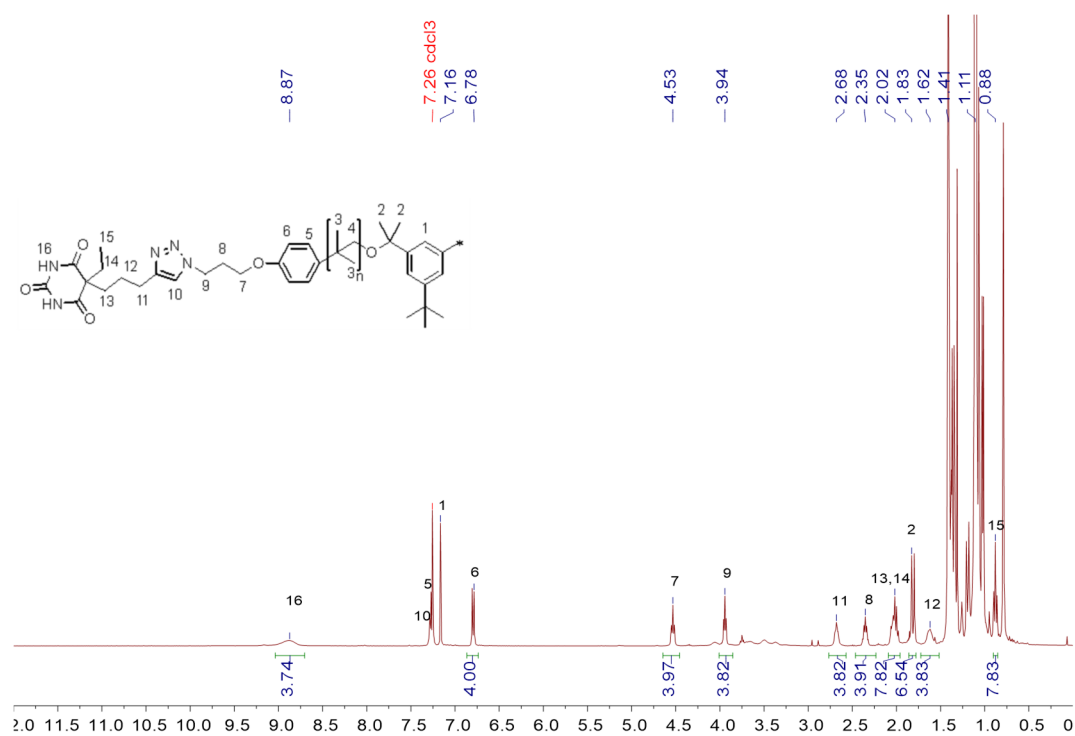


Figure S7  $^1\text{H}$  NMR spectrum of PB.

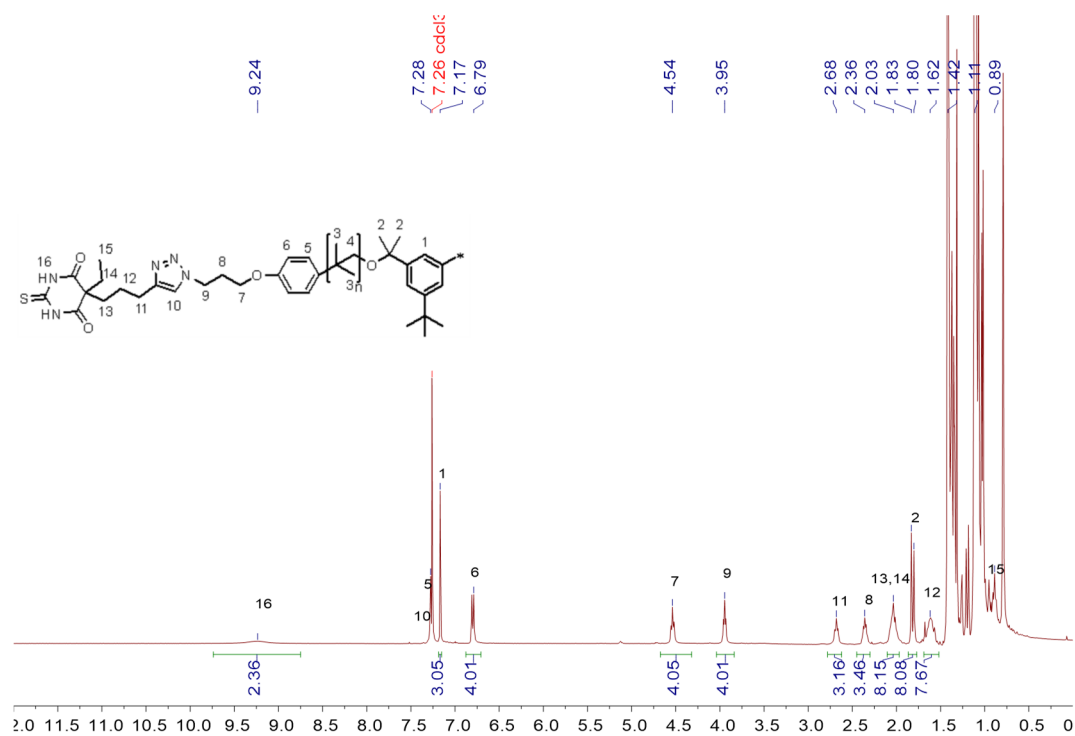
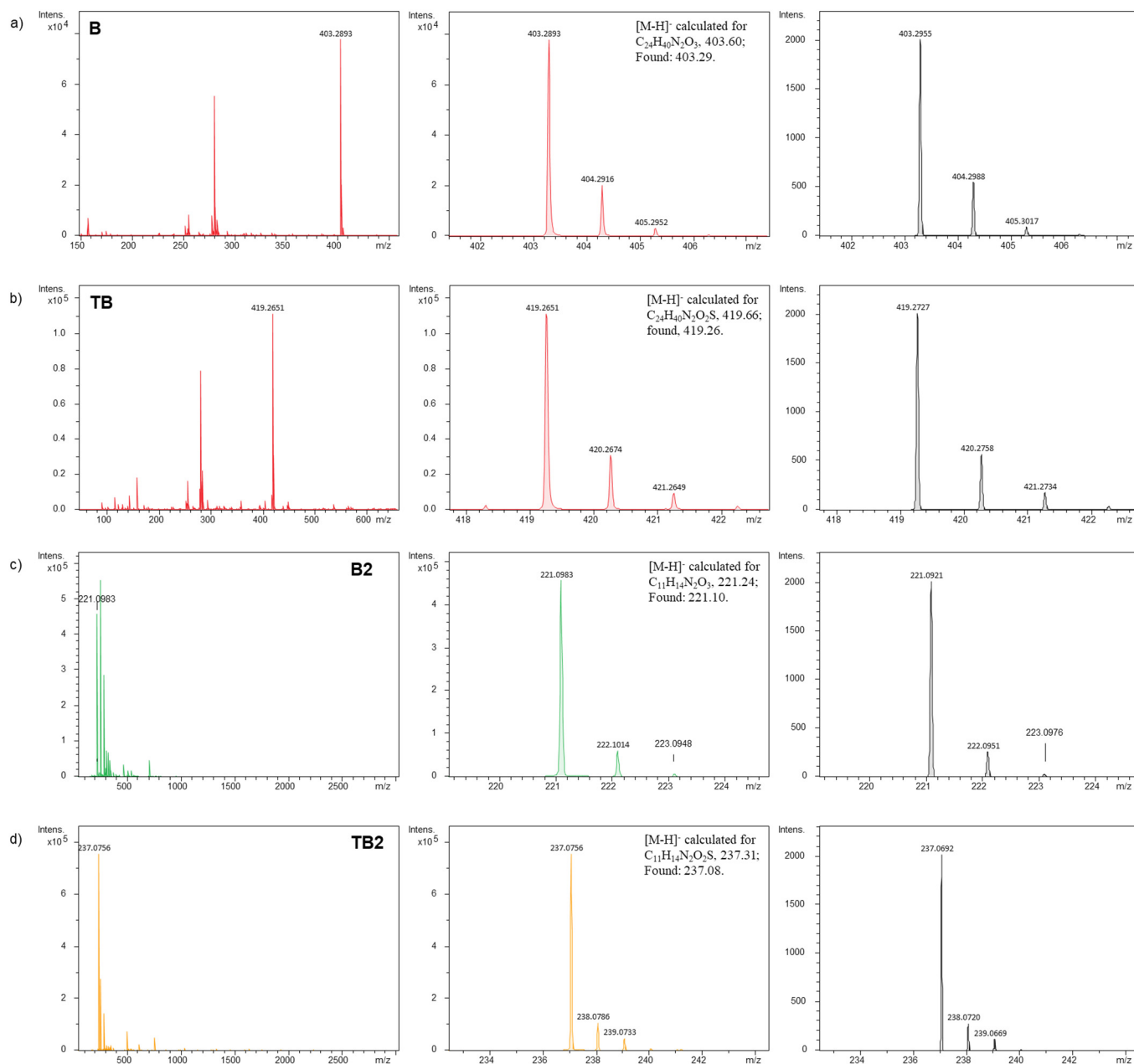


Figure S8  $^1\text{H}$  NMR spectrum of PTB.

## 7. ESI-ToF MS Spectra of Model Compounds



**Figure S9** Left: the full experimental ESI-ToF MS spectra; middle: the compound spectra; and right : the simulated isotope pattern of a) **B**, b) **TB**, c) **B2**, and d) **TB2**.

## 8. MALDI-ToF MS Spectra of Model Polymers

1,8-dihydroxy-9,10-dihydroanthracen-9-one (Dithranol, 20 mg·mL<sup>-1</sup> in THF) was used as matrix and sodium iodide (NaI, 20 mg·mL<sup>-1</sup> in THF) was used as salts for ionizing polymers functionalized with hydrogen-bonding moieties (model polymer **PB** or **PTB**, 20 mg·mL<sup>-1</sup> in THF) while applying a volume ratio of 100:20:1 in reflection mode.

### 8.1. Spectra of PB

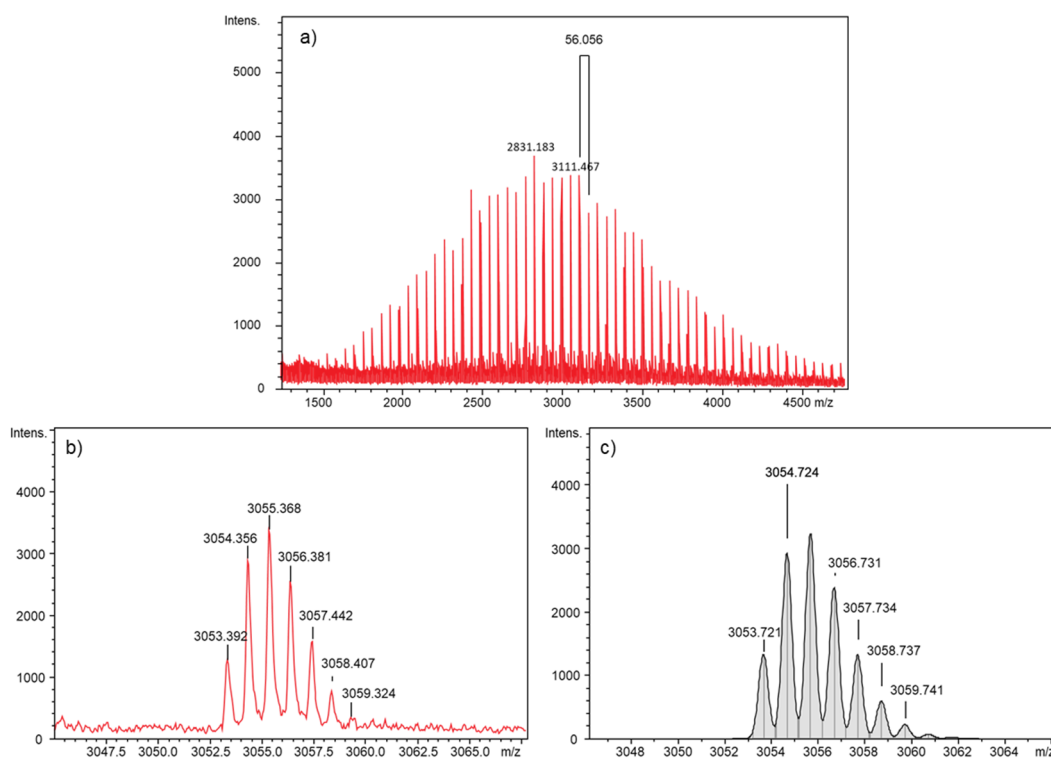


**Figure S10** a) MALDI-ToF spectra of **PB**; b) the zoom-in of the peak at 3055.37; and c) the simulated isotope pattern for  $[C_{36}H_{48}N_5O_6(C_4H_8)_3C_{20}H_{24}N_5O_4]+[Na_2+H]^+$ .

## 8.2. Spectra of PTB

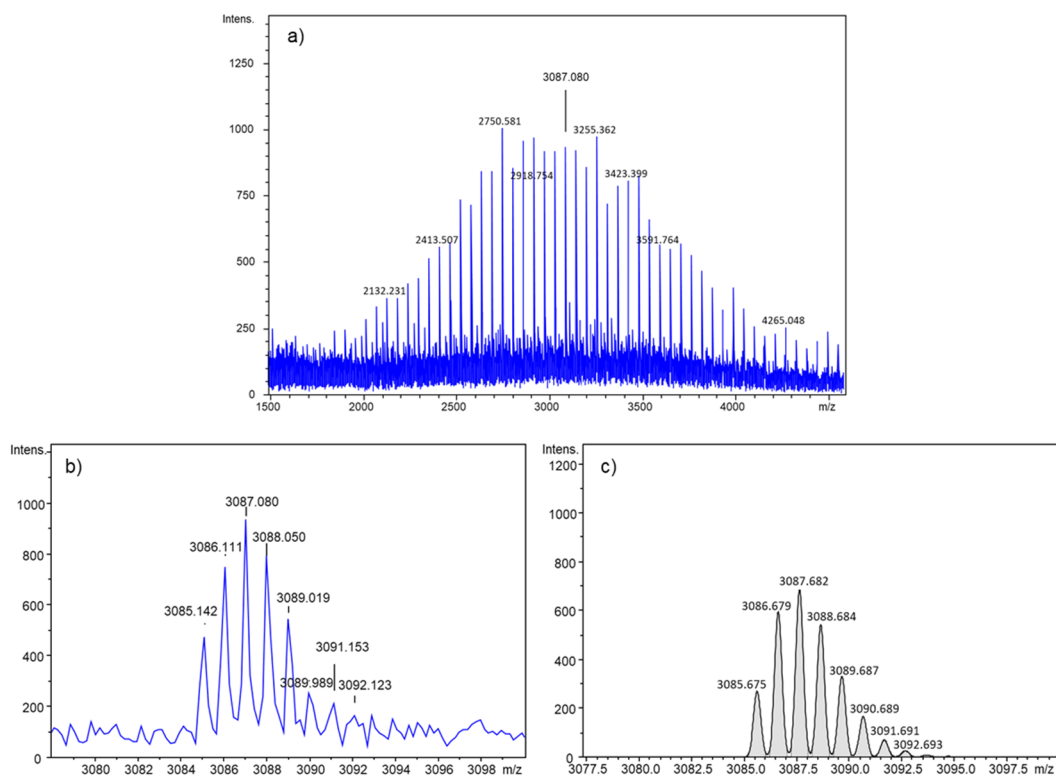


**Figure S11** a) MALDI-ToF spectra of PTB; b) the zoom-in of the peak at 3087.08; and c) the simulated isotope pattern for  $[C_{36}H_{48}N_5O_5S(C_4H_8)_{35}C_{20}H_{24}N_5O_3S]^+[Na_2+H]^+$ .



## 9. DSC Curves of Model Polymers

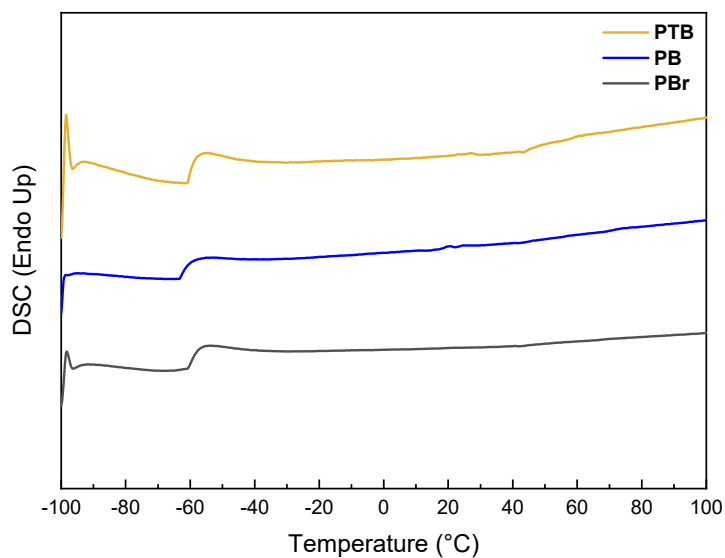


**Figure S12** DSC curves of telechelic dibromo PIB **PBr**, model polymer **PB** and **PTB** (curves are vertically shifted).

## 10. Loss Tangent vs Frequency Curve of Model Polymers

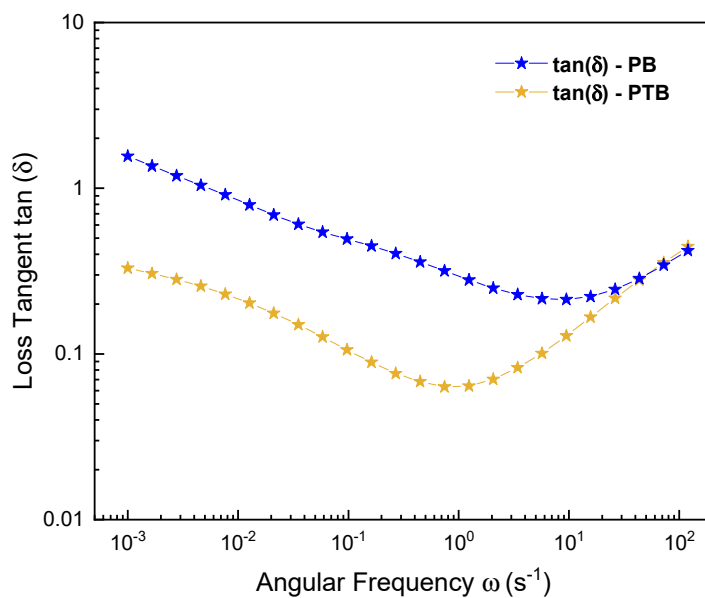


**Figure S13** Loss tangent vs frequency curve of model polymer **PB** and **PTB**.

## 11. Zero-shear Viscosity vs Temperature Curve of Model Polymers

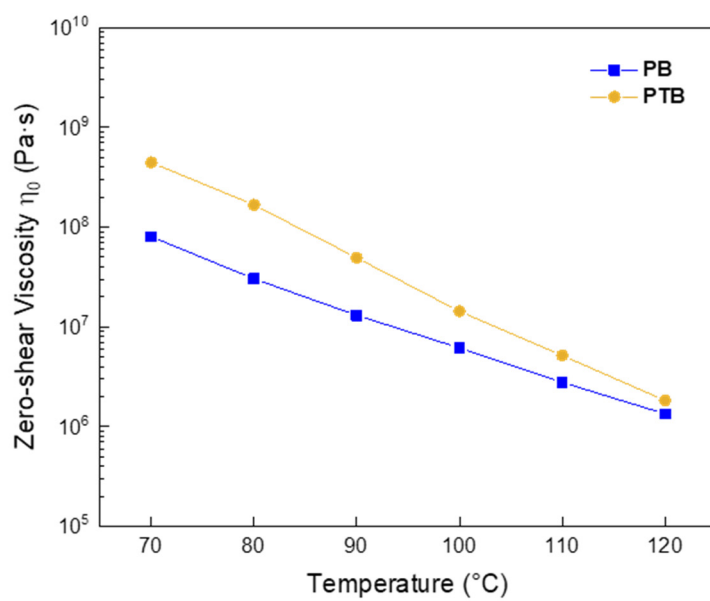


**Figure S14** Zero-shear viscosity vs temperature curve of model polymer **PB** and **PTB**.

## 12. Reference

1. Kotha, S.D., Ashoke Chandra. Design and synthesis of spiro-heterocycles by ring-closing metathesis. *Indian Journal of Chemistry* **2008**, *47 B*, 1120-1134.
2. Srivastava, P.C.; Callahan, A.P.; Cunningham, E.B.; Knapp, F.F. Potential cerebral perfusion agents: synthesis and evaluation of a radioiodinated vinylalkylbarbituric acid analog. *Journal of Medicinal Chemistry* **1983**, *26*, 742-746, doi:10.1021/jm00359a020.
3. Bouhlel, A.; Curti, C.; Vanelle, P. New methodology for the synthesis of thiobarbiturates mediated by manganese(III) acetate. *Molecules* **2012**, *17*, 4313-4325, doi:10.3390/molecules17044313.
4. Schulz, M.; Glatte, D.; Meister, A.; Scholtysek, P.; Kerth, A.; Blume, A.; Bacia, K.; Binder, W.H. Hybrid lipid/polymer giant unilamellar vesicles: effects of incorporated biocompatible PIB–PEO block copolymers on vesicle properties. *Soft Matter* **2011**, *7*, 8100-8110, doi:10.1039/C1SM05725A.
5. Rupp, H.; Döhler, D.; Hilgeroth, P.; Mahmood, N.; Beiner, M.; Binder, W.H. 3D Printing of Supramolecular Polymers: Impact of Nanoparticles and Phase Separation on Printability. *Macromolecular Rapid Communications* **2019**, *40*, 1900467, doi:10.1002/marc.201900467.

# ***Supporting Information***

*for*

## **Synthesis and Characterization of Quadrupolar-Hydrogen-Bonded Polymeric Ionic Liquids for Potential Self-Healing Electrolytes**

Chenming Li <sup>1</sup>, Rajesh Bhandary <sup>1</sup>, Anja Marinow <sup>1</sup>, Dmitrii Ivanov <sup>1</sup>, Mengxue Du <sup>2</sup>, René Androsch <sup>2</sup>, Wolfgang H. Binder <sup>1,\*</sup>

<sup>1</sup> Macromolecular Chemistry, Institute of Chemistry, Faculty of Natural Science II, Martin Luther University Halle-Wittenberg, Von-Danckelmann-Platz 4, 06120 Halle (Saale), Germany

<sup>2</sup> Interdisciplinary Center for Transfer-oriented Research in Natural Sciences, Martin Luther University Halle-Wittenberg, 06099 Halle (Saale), Germany

\* Correspondence: [wolfgang.binder@chemie.uni-halle.de](mailto:wolfgang.binder@chemie.uni-halle.de) (W.H.B.)

## Table of Content

<b>1. EXPERIMENTAL PROCEDURE</b>	<b>1</b>
1.1. Materials and Methods	1
1.2. Synthesis of Monomers and Polymers	2
a) Synthesis of 3-Chloropropyl Acrylate (CPA)	2
b) Synthesis of 1-(3-(Acryloyloxy)propyl)-1-methylpyrrolidin-1-ium Bis(trifluoromethyl sulfonyl)imide (ILA)	2
c) Synthesis of 2-(3-(6-Methyl-4-oxo-1,4-dihydropyrimidin-2-yl)ureido)ethyl Acrylate (UPyA)	3
d) Synthesis of Dibenzyl Carbonotrithioate (DBTTC)	4
e) RAFT Homopolymerization of ILA for POIL-x	4
f) RAFT Copolymerization of ILA with UPyA for CPILU-y	4
1.3. Synthesis of POILC-z for GPC Calibration	5
g) RAFT Polymerization of CPA for pCPA	5
h) Quaternization and Ion Exchange of pCPA for POILC-z	5
2. GPC CURVES AND DATA	7
3. CONDUCTIVITY AND VISCOSITY DATA	9
4. NMR SPECTRA	10
5. REFERENCE	16

# 1. Experimental Procedure

## 1.1. Materials and Methods

### *Solvents*

Acetonitrile (MeCN), dimethyl sulfoxide (DMSO) and dimethyl formamide (DMF) were purchased from Grüssing (Filsum, Germany); methylene chloride (DCM), acetone and *n*-hexane were purchased from Overlack (OQEMA GmbH, Mönchengladbach, Germany); tetrahydrofuran (THF) was purchased from Carl Roth (Karlsruhe, Germany); and dimethyl sulfoxide 99.7+ % extra dry was purchased from Fisher Scientific (Schwerte, Germany). All the volatile solvents were purchased in technical grade and redistilled at least once before use. The DMF for polymerization was dried over a solvent purification system and the dimethyl sulfoxide 99.7+ % extra dry was used as received. NMR solvents deuterated chloroform (chloroform-*d*) and deuterated dimethyl sulfoxide (DMSO-*d*<sub>6</sub>) were purchased from Chemotrade (Eckert & Ziegler Gruppe, Düsseldorf, Germany) and used as received.

### *Methods*

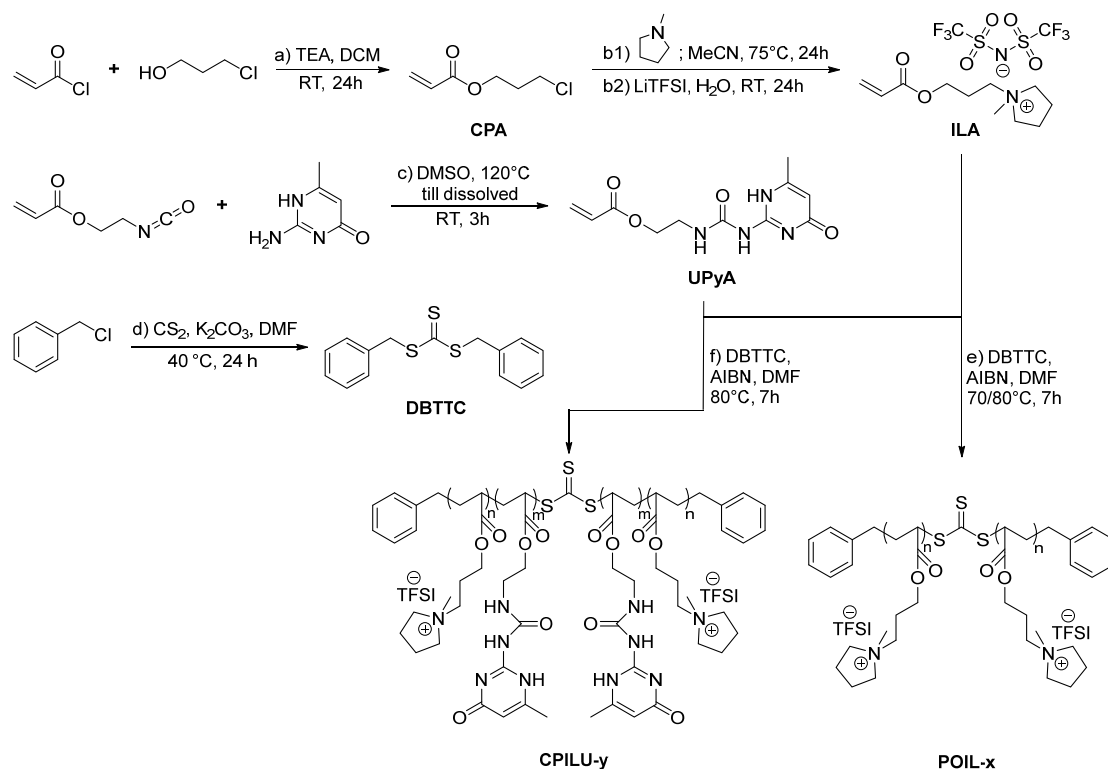
#### *Nuclear Magnetic Resonance*

All <sup>1</sup>H-NMR and <sup>13</sup>C-NMR spectra were measured on a Varian FT-NMR spectrometer (500 and 101 MHz, respectively) (Agilent Technologies Germany GmbH & Co. KG, Waldbronn, Germany). All samples were measured at 27 °C using deuterated chloroform (chloroform-*d*) or deuterated dimethyl sulfoxide (DMSO-*d*<sub>6</sub>). Chemical shifts (δ) were recorded in parts per million (ppm) relative to the remaining solvent signals (chloroform-*d*: 7.26 ppm (<sup>1</sup>H) and 77.0 ppm (<sup>13</sup>C), DMSO-*d*<sub>6</sub>: 2.50 ppm (<sup>1</sup>H) and 39.5 ppm (<sup>13</sup>C)). Chemical shifts were reported with the following notations: s, singlet; d, doublet; t, triplet; q, quartet; p, pentlet; m, a more complex multiplet or overlapping multiplets. The data analysis was performed via MestReNova (version 9.0.1-13254).

#### *Gel Permeation Chromatography*

GPC (THF) measurements were performed on a Viscotek GPCmax VE 2002 (Malvern Panalytical GmbH, Kassel, Germany) GPC machine with a CLM3008 (Tguard, Org Guard 10×4.6) and a CLM3011 (Range:1000 – 400000 g·mol<sup>-1</sup>) main column at 30 °C. Detection of the refractive index was realized via a VE 3580 RI detector (Malvern Panalytical GmbH, Kassel, Germany) at 35 °C. Poly(styrene) (PS) was used as the external calibration standards with a molecular weight range from 300 to 170000 g·mol<sup>-1</sup>. GPC (DMF+0.1M LiTFSI) measurements were performed on a Viscotek GPCmax VE 2001 (Malvern Panalytical GmbH, Kassel, Germany) GPC machine with a CLM3008 precolumn and a GMH<sub>HR</sub>-N-18055 main column in DMF with LiTFSI (0.1 M) at 60 °C. Detection of the refractive index was realized via a VE 3580 RI detector (Malvern Panalytical GmbH, Kassel, Germany) at 35 °C. Poly(styrene) (PS) was used as the external calibration standards with a molecular weight range from 1050 to 115000 g·mol<sup>-1</sup>. The data analysis was performed via OminSEC4.5 and Origin 2018 (version b9.5.0.193).

## 1.2. Synthesis of Monomers and Polymers



**Scheme S1** Synthetic route of monomers, RAFT chain transfer agent, and polymers.

### a) Synthesis of 3-Chloropropyl Acrylate (CPA)

The synthesis was adopted from the reference [1] with slight modification. 3-Chloro-1-propanol (20.0 mL, 236.3 mmol) was dissolved in 150 mL dry DCM in a three neck flask and cooled at 0 °C. Triethylamine (33.3 mL, 236.3 mmol) dissolved in 75 mL dry DCM was added dropwise via a separation funnel under vigorous stirring over 1 hour. Then acryloyl chloride (18.3 mL, 214.8 mmol) dissolved in 75 mL dry DCM was added in the same way as triethylamine. The reaction mixture was stirred at 0 °C for about 1 hour and subsequently at room temperature for 24 hours. After the reaction was finished, the reaction mixture was filtered and the organic liquid was washed with 1 M hydrochloric acid (150 mL  $\times$  1), DI water (150 mL  $\times$  3), and brine (150 mL  $\times$  1). The organic layer was collected, dried over sodium sulfate, filtered, and concentrated under reduced pressure. The crude product was then distilled at 55 °C (vapor temperature = 31 °C) at 0.015 mbar. The purified 3-chloropropyl acrylate (**CPA**) was afforded as colorless liquids with the yield of 27.7 g (87 %). <sup>1</sup>H NMR (400 MHz, Chloroform-*d*)  $\delta$  6.41 (dd, *J* = 17.4, 1.5 Hz, 1H), 6.12 (dd, *J* = 17.4, 10.4 Hz, 1H), 5.84 (ddd, *J* = 10.5, 1.5, 0.5 Hz, 1H), 4.31 (t, *J* = 6.1 Hz, 2H), 3.63 (t, *J* = 6.4 Hz, 2H), 2.14 (p, *J* = 6.3 Hz, 2H). <sup>13</sup>C NMR (101 MHz, Chloroform-*d*)  $\delta$  165.95, 130.94, 128.17, 61.20, 41.13, 31.59.

### b) Synthesis of 1-(3-(Acryloyloxy)propyl)-1-methylpyrrolidin-1-ium Bis(trifluoromethanesulfonyl)imide (ILA)

The synthesis was adopted from the reference [1] with slight modification and was carried out in two steps:



*First step b1):*

**CPA** (7.5 g, 50.7 mmol) was dissolved in MeCN (30 mL) and heated to 75 °C, followed by adding 1-methylpyrrolidine (5.6 mL, 53.3 mmol). After 24 hours, the reaction mixture was cooled down to room temperature and MeCN was removed by a rotary evaporator at 35 °C. Then a little amount of water (5 to 10 mL) was added to dissolve the raw product and the water solution was washed with DCM (50 mL × 3), whereafter the water phase was concentrated under reduced pressure. The crude product was afforded as a viscous brownish oil and was used directly in next step without further purification.

*Second step b2):*

The product from the *first step b1)* was dissolved in water (10 mL) and added to a water solution (10 mL) of lithium bis(trifluoromethanesulfonyl)imide (15.5 g, 53.3 mmol). The reaction mixture was then stirred at room temperature for 24 hours. After the reaction was finished, the reaction mixture was extracted with DCM (50 mL × 3). Then the combined organic layers were washed with water (50 mL × 3) and dried over sodium sulfate. The sodium sulfate was filtered and active charcoal was added to the organic solution and stirred at room temperature for 5 hours to decolorize the product. After decolorization the active charcoal was filtered and DCM was evaporated under reduced pressure. The product 1-(3-(acryloyloxy)propyl)-1-methylpyrrolidin-1-ium bis(trifluoromethanesulfonyl)imide (**IIA**) was afforded as a transparent viscous yellowish oil with the total yield of 31.9 g (80%). <sup>1</sup>H NMR (400 MHz, DMSO-*d*<sub>6</sub>) δ 6.38 (dd, *J* = 17.3, 1.5 Hz, 1H), 6.18 (dd, *J* = 17.3, 10.4 Hz, 1H), 5.99 (dd, *J* = 10.4, 1.5 Hz, 1H), 4.19 (t, *J* = 6.2 Hz, 2H), 3.55 – 3.37 (m, 6H), 3.00 (s, 3H), 2.20 – 2.01 (m, 6H). <sup>13</sup>C NMR (101 MHz, DMSO-*d*<sub>6</sub>) δ 165.74, 132.34, 128.48, 124.73, 121.53, 118.32, 115.12, 64.03, 61.74, 60.78, 47.97, 23.30, 21.51. <sup>19</sup>F NMR (376 MHz, DMSO-*d*<sub>6</sub>) δ -78.74.

**c) Synthesis of 2-(3-(6-Methyl-4-oxo-1,4-dihydropyrimidin-2-yl)ureido)ethyl Acrylate (UPyA)**

The synthesis was adopted from the reference [2] with slight modification. 6-Methylisocytosine (5.0 g, 40.0 mmol) was placed in 100 mL DMSO and the mixture was heated at 120 °C till a clear solution was obtained. Then the flask was removed from the oil bath and 2-isocyanatoethyl acrylate (5.2 mL, 42.0 mmol) was added immediately to the flask, followed by cooling in a water bath to inhibit polymerization. The reaction mixture was stirred for 3 hours at room temperature. After reaction was finished, the white solid was filtered and washed thoroughly with *n*-hexane and dried under reduced pressure. Then the product was dried via a freeze-drier to remove residual DMSO. The purified product was afforded as a white powder with a yield of 9.5 g (87 %). <sup>1</sup>H NMR (400 MHz, Chloroform-*d*) δ 12.95 (s, 1H), 11.94 (s, 1H), 10.47 (s, 1H), 6.44 (dd, *J* = 17.4, 1.5 Hz, 1H), 6.13 (dd, *J* = 17.3, 10.4 Hz, 1H), 5.88 – 5.70 (m, 2H), 4.29 (t, *J* = 5.7 Hz, 2H), 3.57 (q, *J* = 5.6 Hz, 2H), 2.23 (s, 2H). <sup>13</sup>C NMR (126 MHz, Chloroform-*d*) δ 173.00, 166.22, 156.97, 154.68, 148.39, 131.00, 128.52, 106.93, 63.03, 38.96, 19.11.

*d) Synthesis of Dibenzyl Carbonotrithioate (DBTTC)*

The synthesis was performed according to reference [3].  $^1\text{H}$  NMR (400 MHz, Chloroform-*d*)  $\delta$  7.40 – 7.24 (m, 10H), 4.64 (s, 4H).  $^{13}\text{C}$  NMR (101 MHz, Chloroform-*d*)  $\delta$  222.86, 135.07, 129.39, 128.84, 127.91, 41.68.

*e) RAFT Homopolymerization of ILA for POIL-x*

RAFT homopolymerization of **ILA** was carried out in DMF using **DBTTC** as the RAFT chain transfer agent and ABIN as the initiator. Typically, **ILA** (1086.0 mg, 2.3 mmol), **DBTTC** (5.6 mg,  $2.3 \times 10^{-2}$  mmol), AIBN (0.4 mg,  $2.3 \times 10^{-3}$  mmol) were dissolved in DMF (2.3 mL) inside a Schlenk tube. Trioxane was added as the NMR reference to monitor the monomer conversion. The Schlenk tube was sealed with a rubber septum and the reaction mixture was purged with nitrogen for 30 minutes to deoxygenate under vigorous stirring. The tube was then quickly immersed in an oil bath thermostated at 80 °C. Aliquots were taken at certain time intervals and measured  $^1\text{H}$  NMR to study the kinetics of the polymerization by calculating the integral of vinylenic protons of **ILA** to the integral of trioxane protons. The reaction was stopped by opening the septum and subsequently precipitated into DCM twice to eliminate the monomer residue. The polymer was collected and finally dried at 80 °C under vacuum for 24 hours. The molecular weight was evaluated by  $^1\text{H}$  NMR using the characteristic methyl protons of the pendent pyrrolidinium ( $\equiv\text{N-CH}_3$ , 3nH,  $\delta$  = 3.02 ppm, with n being the degree of polymerization) and the characteristic aromatic protons of **DBTTC** (pH, 10H,  $\delta$  = 7.37 ppm).

*f) RAFT Copolymerization of ILA with UPyA for CPILU-y*

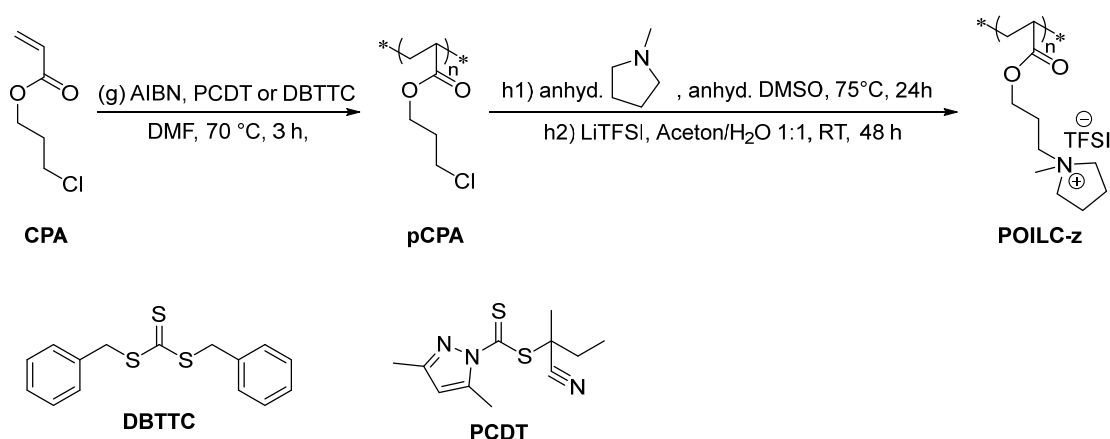
RAFT copolymerization of **ILA** with **UPyA** was carried out in DMF using **DBTTC** as the RAFT chain transfer agent and ABIN as the initiator. Typically, **ILA** (1043.0 mg, 2.2 mmol), and **UPyA** (29 mg, 0.109 mmol) were placed in DMF (2 mL) in a Schlenk tube. The tube was sealed with a rubber septum and the reaction mixture was purged with nitrogen for 30 minutes to deoxygenate under vigorous stirring. After deoxygenation the tube was heated in an oil bath at 120 °C till a clear solution was obtained, then the temperature of the oil bath was cooled to 80 °C. In the meantime, to a flask **DBTTC** (33.2 mg,  $1.1 \times 10^{-1}$  mmol), AIBN (1.88 mg,  $1.1 \times 10^{-2}$  mmol), and trioxane as the NMR reference were dissolved in deoxygenated DMF (0.29 mL), and this solution was transferred to the reaction Schlenk tube by a syringe to initiate the polymerization. Aliquots were taken at certain time intervals and measured  $^1\text{H}$  NMR to study the kinetics of the polymerization by calculating the integral of vinylenic protons of **ILA** and **UPyA** to the integral of trioxane protons. The reaction was stopped by opening the septum and subsequently precipitate into DCM thrice to remove the monomer residue. The polymer was collected and finally dried at 80 °C under vacuum for 24 hours. The molecular weight was evaluated by  $^1\text{H}$  NMR using the characteristic methyl protons of the pendent pyrrolidinium ( $\equiv\text{N-CH}_3$ , 3nH,  $\delta$  = 3.02 ppm, with n being the degree of polymerization of **ILA**), the characteristic vinylenic proton of the pendent UPy moiety ( $-(\text{CH}_3)\text{C}=\text{CH}-$ , mH,  $\delta$  = 5.80 ppm, with m being the degree of polymerization of **UPyA**), and the characteristic aromatic protons of **DBTTC** (pH,

10H,  $\delta = 7.36$  ppm).

**Table S1** Synthetic data of the copolymers **CPILU-9** and **CPILU-10** for tensile test.

Sample	Entry	M/CTA	Solvent	M <sub>mon.</sub> /M	f <sub>UPy</sub>	T	t	conv.	F <sub>UPy</sub> , NMR	DP <sub>IL</sub>	DP <sub>UPy</sub>	M <sub>n, th</sub>	M <sub>n</sub> , NMR	M <sub>n</sub> , GPC	PDI
<b>cpILU</b>	<b>9</b>	20:1	DMSO	1	8%	80°C	16	97%	7%	20.7	1.4	9540	10452	2985	1.32
	<b>10</b>	200:1	DMSO	1	8%	80°C	16	98%	7%	133.8	9.4	96380	66798	3454	1.52

### 1.3. Synthesis of POILC-z for GPC Calibration



**Scheme S2** Synthesis rout of POILC-z for GPC calibration.

#### g) RAFT Polymerization of CPA for pCPA

RAFT polymerization of **CPA** was carried out in DMF using **DBTTC** as the RAFT chain transfer agent and AIBN as the initiator. Typically, **CPA** (447.0 mg, 3.0 mmol), **PCDT** (8.03 mg,  $3.0 \times 10^{-2}$  mmol) AIBN (0.5 mg,  $3.0 \times 10^{-3}$  mmol) were dissolved in DMF (4.5 mL) in a Schlenk tube. The Schlenk tube was sealed with a rubber septum and the reaction mixture was purged with nitrogen for 30 minutes to deoxygenate under vigorous stirring. The tube was then heated in an oil bath thermostated at 70 °C. The reaction was stopped by opening the septum and subsequently precipitated into MeOH twice to eliminate the monomer residue. The molecular weight was evaluated by THF GPC with PS standard.

#### h) Quaternization and Ion Exchange of pCPA for POILC-z

The synthesis was adopted from references [4-6] with modification and was carried out in two steps:

*First step h1):*

In a glovebox, **pCPA** (122.0 mg, 0.8 mmol, calculated based on the molecular weight of repeating unit) and pre-distilled anhydrous 1-methylpyrrolidine (0.5 mL, 4.1 mmol) were dissolved in anhydrous DMSO (1.0 mL) in a vial. The vial was sealed and heated at 75 °C for 24 hours. After reaction was finished, the reaction mixture was precipitated into THF twice. The crude product was afforded as viscous oil due to its hygroscopic nature and was used directly in next step without further purification.

*Second step h2):*

The product from *first step h1)* was dissolved in water (1.0 mL) and added to the water solution (1.0 mL) of lithium bis((trifluoromethyl)sulfonyl)imide (2.3 g, 8.0 mmol). After precipitation was observed, acetone (2.0 mL) was added to reach a homogeneous reaction mixture. The reaction mixture was then stirred at room temperature for 24 hours. After reaction was finished, the reaction mixture was precipitated into DCM thrice. The polymer was collected and finally dried at 80 °C under vacuum for 24 hours.

## 2. GPC Curves and Data

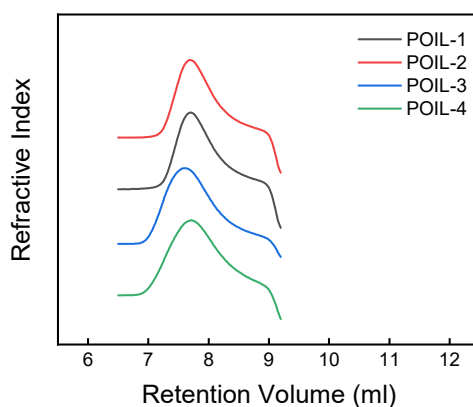


**Figure S1** GPC (DMF+LiTFSI, 0.1 M) curves of **POIL-x** using a PS standard calibration.

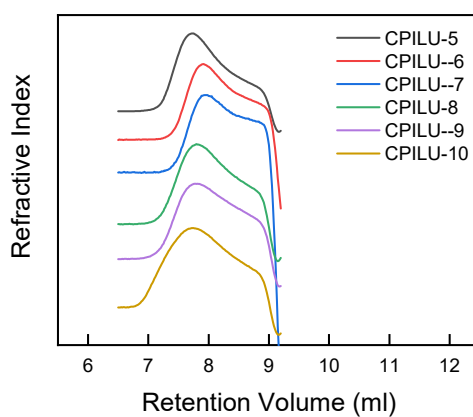


**Figure S2** GPC (DMF+LiTFSI, 0.1 M) curves of **CPILU-y** using a PS standard calibration.

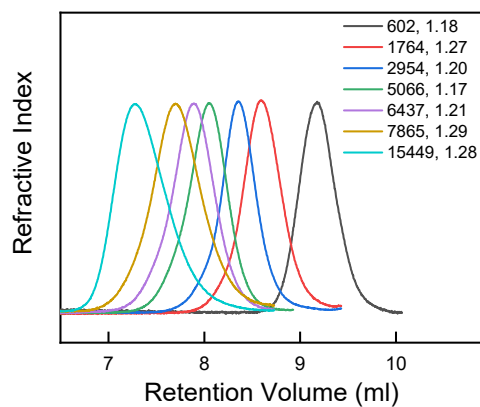


**Figure S3** GPC (THF) curves of precursor polymer pCPA using a PS standard calibration.

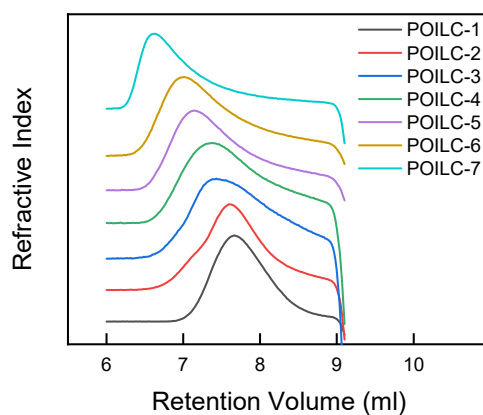


**Figure S4** GPC (DMF+LiTFSI, 0.1 M) curves of **POILC-z** supposed to be calibration.

**Table S2** GPC data of precursor polymers **pCPA** and final **POILC-z** supposed to be calibration.

pCPA (in THF)	Peak Rv /mL	Mn (PS-calibration)	PDI	Mp	DP, Mp
pCPA-1	9.17	600	1.18	690	2.3
pCPA-2	8.59	1800	1.27	2100	10.2
pCPA-3	8.35	3000	1.2	3300	18.2
pCPA-4	8.05	5100	1.17	5300	32.4
pCPA-5	7.89	6400	1.21	6900	41.6
pCPA-6	7.70	7900	1.29	9500	51.2
pCPA-7	7.28	15400	1.28	21100	102.0
Calibration POILC-z (in DMF+0.1 M LiTFSI)	Peak Rv /mL	Mn (PS-calibration)	PDI	Mp (calculated based on DP, Mp of pCPA)	
POILC-1	7.67	4200	1.26	1400	
POILC-2	7.60	4500	1.49	5100	
POILC-3	7.40	4300	1.73	9000	
POILC-4	7.37	4700	1.68	15700	
POILC-5	7.13	5500	1.81	20200	
POILC-6	7.00	6200	1.99	24800	
POILC-7	6.62	9200	2.12	49100	

### 3. Conductivity and Viscosity Data

**Table S3** Conductivity of **POIL-x** and **CPILU-y** from -20 °C to 80 °C, measured by BDS

Sample	Entry	Conductivity $\sigma$ / S*cm <sup>-1</sup>										
		-20 °C	-10 °C	0 °C	10 °C	20 °C	30 °C	40 °C	50 °C	60 °C	70 °C	80 °C
<b>POIL-x</b>	<b>2</b>	1.64E-10	3.07E-09	3.89E-08	2.80E-07	1.35E-06	5.03E-06	1.43E-05	3.45E-05	7.56E-05	1.46E-04	2.46E-04
	<b>3</b>	4.86E-11	2.67E-10	1.71E-09	2.04E-08	1.75E-07	8.56E-07	3.49E-06	1.03E-05	2.52E-05	5.32E-05	9.09E-05
<b>CPILU-y</b>	<b>5</b>	1.49E-10	3.24E-09	3.68E-08	2.55E-07	1.22E-06	4.40E-06	1.27E-05	3.02E-05	6.61E-05	1.26E-04	2.19E-04
	<b>6</b>	1.38E-11	9.48E-11	4.98E-10	2.90E-09	2.19E-08	1.72E-07	9.03E-07	3.52E-06	1.05E-05	2.57E-05	4.85E-05
	<b>7</b>	6.42E-12	2.50E-11	1.72E-10	1.10E-09	5.43E-09	3.27E-08	1.95E-07	8.42E-07	2.89E-06	8.05E-06	1.84E-05

**Table S4** Zero shear viscosity of **POIL-x** and **CPILU-y** from 50 °C to 100 °C.

Sample	Entry	Zero Shear Viscosity $\eta_0$ Pa*s					
		50 °C	60 °C	70 °C	80 °C	90 °C	100 °C
<b>POIL-x</b>	<b>2</b>	1.01E3	301	102	43	20	10
	<b>3</b>	9.57E3	2.63E3	896	368	163	87
	<b>5</b>	1.20E3	323	102	37	16	9
<b>CPILU-y</b>	<b>6</b>	2.30E5	2.52E4	5.72E3	2.76E3	1.35E3	755
	<b>7</b>	1.03E8	1.99E7	2.42E6	2.84E5	6.30E4	1.51E4



## 4. NMR Spectra

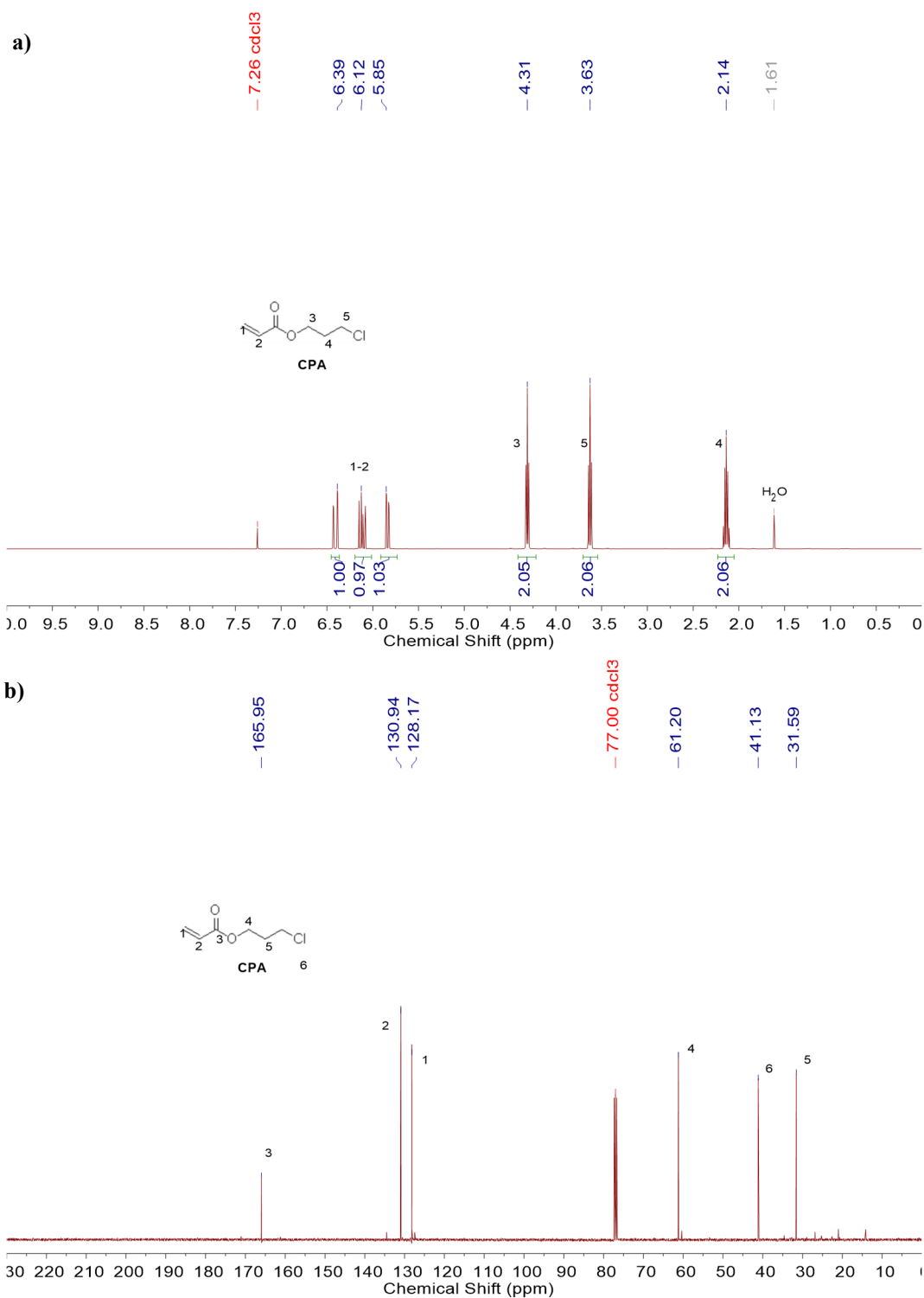


**Figure S5** a)  $^1\text{H}$  and b)  $^{13}\text{C}$  NMR spectra of compound CPA.

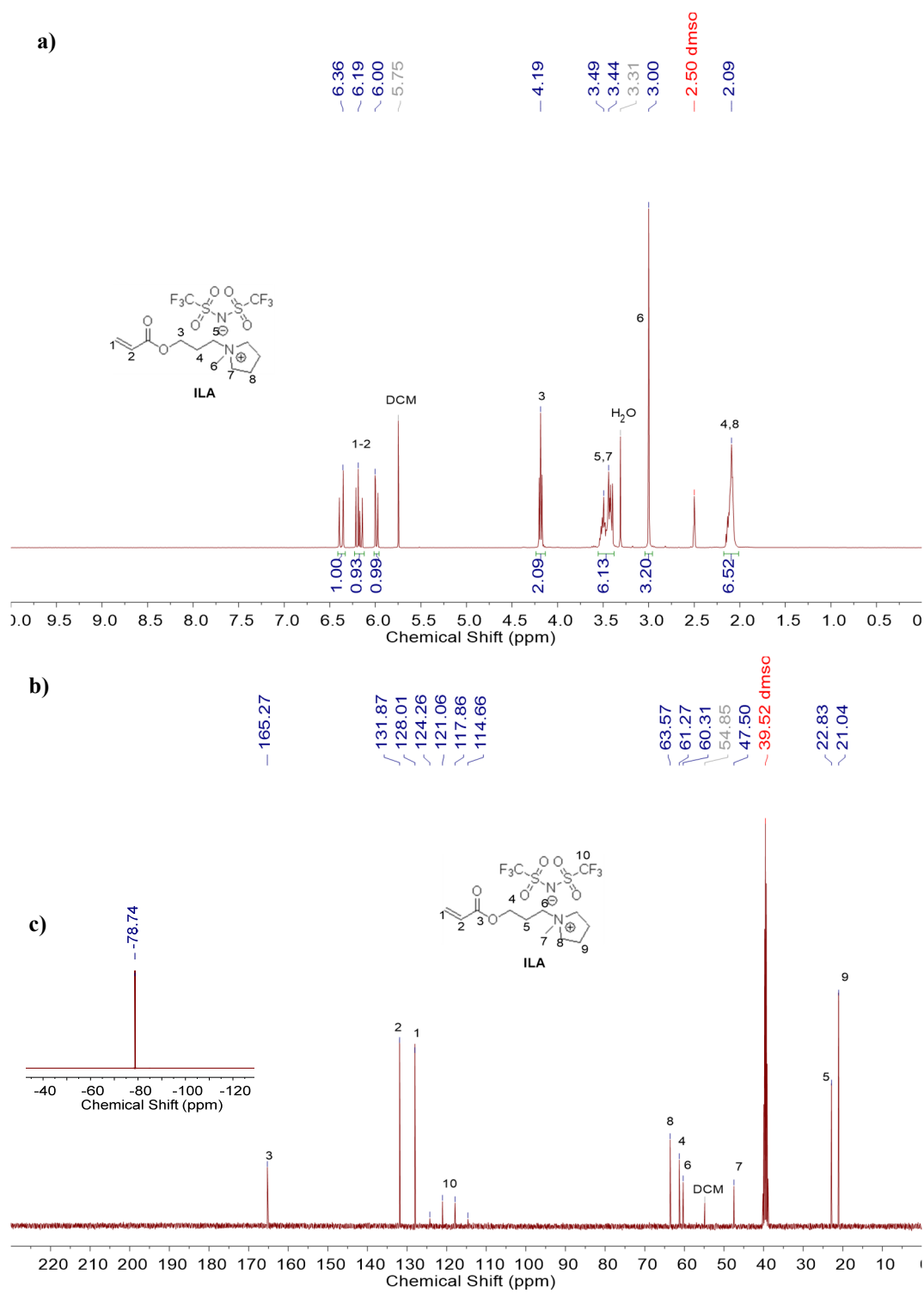


**Figure S6** a)  $^1\text{H}$ , b)  $^{13}\text{C}$ , and c)  $^9\text{F}$  NMR spectra of compound **ILA**.

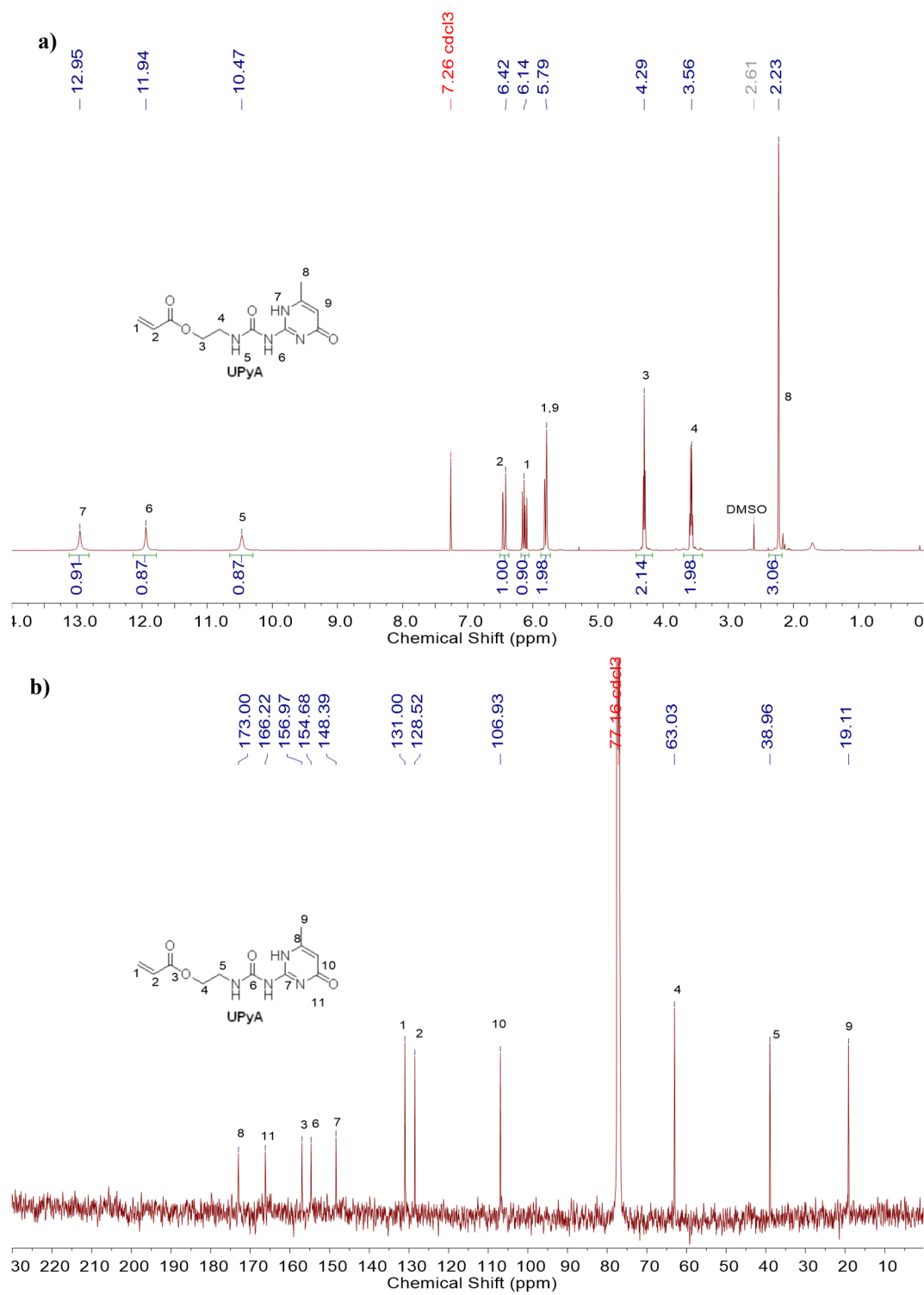


**Figure S7** a) <sup>1</sup>H and b) <sup>13</sup>C NMR spectra of compound UPyA.

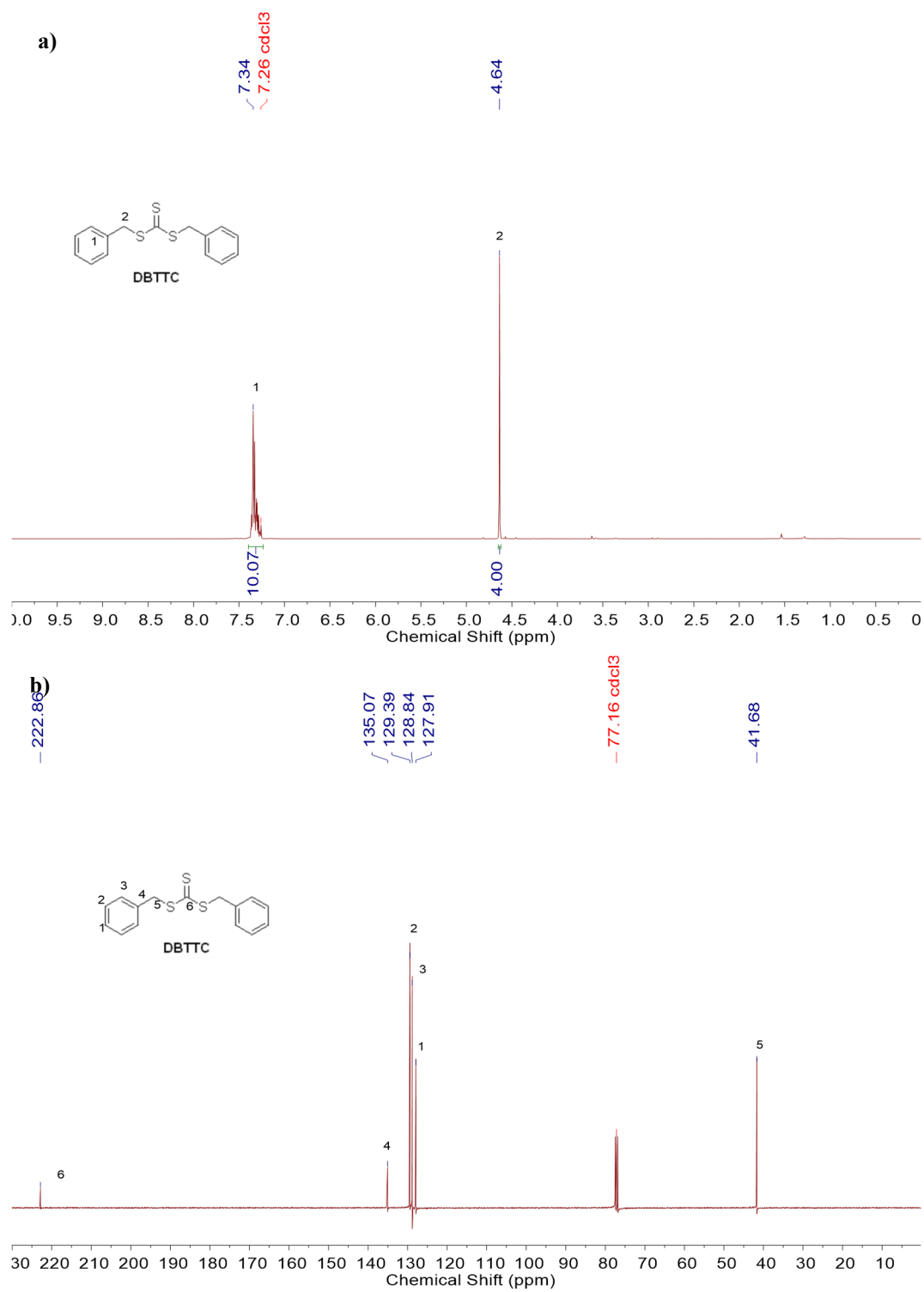


**Figure S8** a)  $^1\text{H}$  and b)  $^{13}\text{C}$  NMR spectra of compound DBTTC.



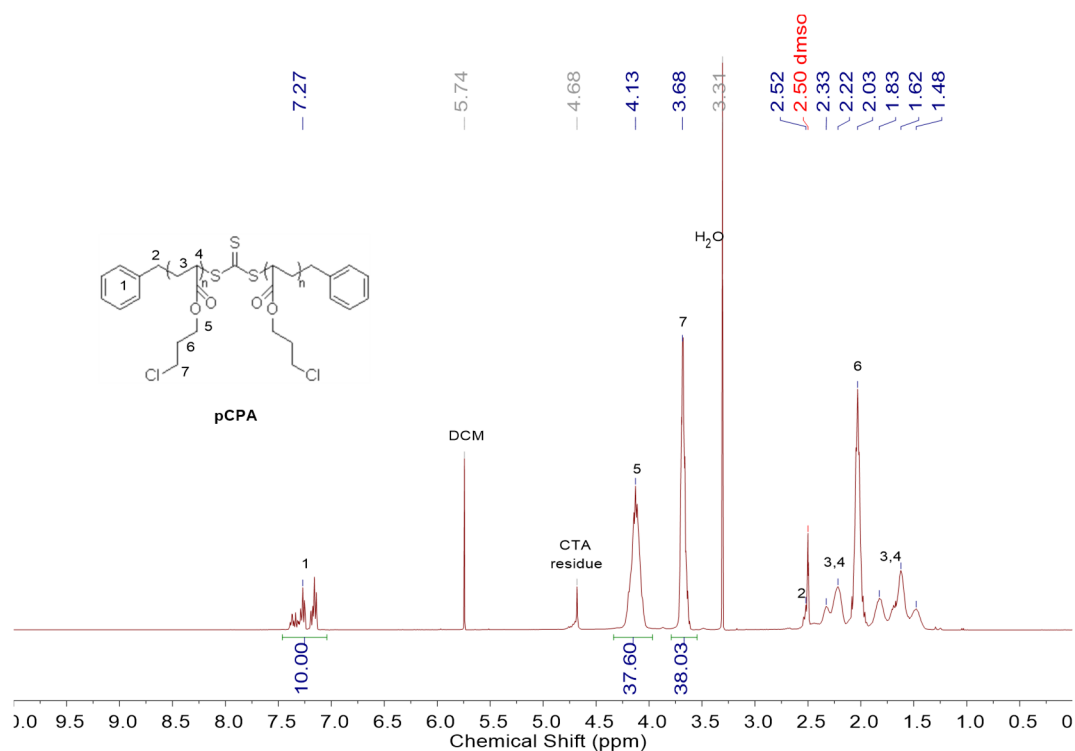


**Figure S11** <sup>1</sup>H NMR spectra of polymer pCPA.

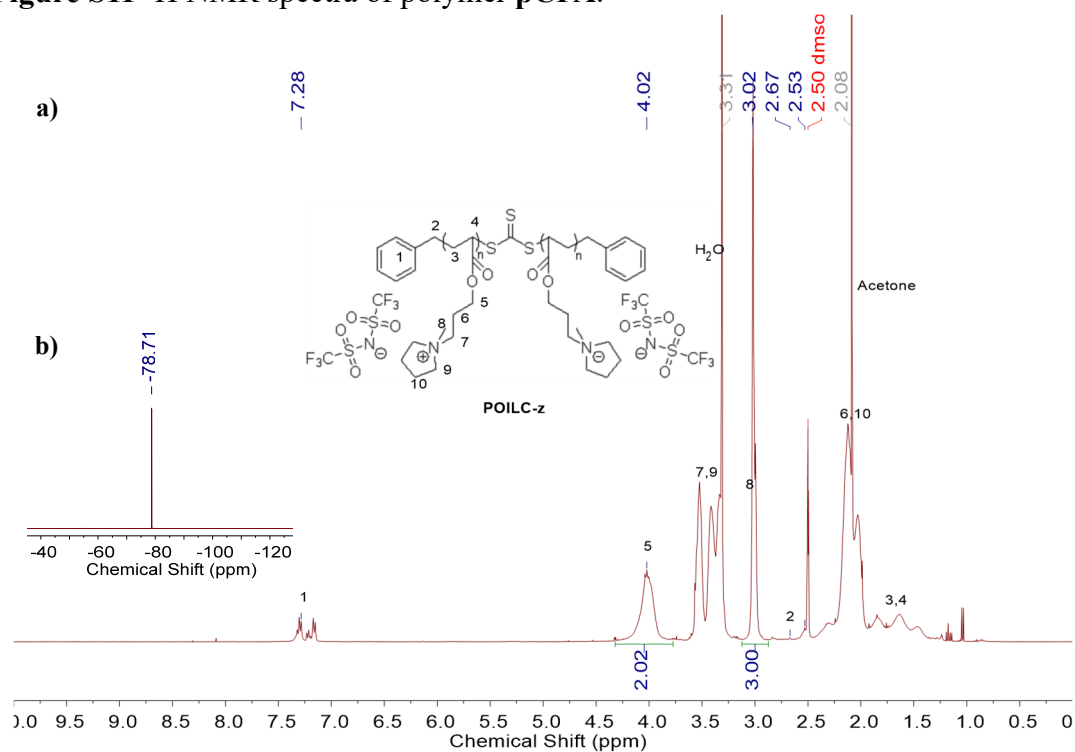


**Figure S12** a) <sup>1</sup>H and b) <sup>19</sup>F NMR spectra of polymer POILC-z.

## 5. Reference

1. Chen, S.; Funtan, A.; Gao, F.; Cui, B.; Meister, A.; Parkin, S.S.P.; Binder, W.H. Synthesis and Morphology of Semifluorinated Polymeric Ionic Liquids. *Macromolecules* **2018**, *51*, 8620-8628, doi:10.1021/acs.macromol.8b01624.
2. Yamauchi, K.; Lizotte, J.R.; Long, T.E. Thermoreversible Poly(alkyl acrylates) Consisting of Self-Complementary Multiple Hydrogen Bonding. *Macromolecules* **2003**, *36*, 1083-1088, doi:10.1021/ma0212801.
3. Aoyagi, N.; Endo, T. Functional RAFT agents for radical-controlled polymerization: Quantitative synthesis of trithiocarbonates containing functional groups as RAFT agents using equivalent amount of CS<sub>2</sub>. *Journal of Polymer Science Part A: Polymer Chemistry* **2009**, *47*, 3702-3709, doi:10.1002/pola.23410.
4. Cao, W.; Tan, L.; Wang, H.; Yuan, J. Dual-Cationic Poly(ionic liquid)s Carrying 1,2,4-Triazolium and Imidazolium Moieties: Synthesis and Formation of a Single-Component Porous Membrane. *ACS Macro Letters* **2021**, *10*, 161-166, doi:10.1021/acsmacrolett.0c00784.
5. Choi, J.-H.; Ye, Y.; Elabd, Y.A.; Winey, K.I. Network Structure and Strong Microphase Separation for High Ion Conductivity in Polymerized Ionic Liquid Block Copolymers. *Macromolecules* **2013**, *46*, 5290-5300, doi:10.1021/ma400562a.
6. Meek, K.M.; Elabd, Y.A. Alkaline Chemical Stability of Polymerized Ionic Liquids with Various Cations. *Macromolecules* **2015**, *48*, 7071-7084, doi:10.1021/acs.macromol.5b01223.



# acro- molecular Rapid Communications

## Supporting Information

for *Macromol. Rapid Commun.*, DOI 10.1002/marc.202300464

Stability of Quadruple Hydrogen Bonds in an Ionic Liquid Environment

*Chenming Li, Rajesh Bhandary, Anja Marinow, Stephanie Bachmann, Ann-Christin Pöppler  
and Wolfgang H. Binder\**

# ***Supporting Information***

*for*

## **Stability of Quadruple Hydrogen Bonds in an Ionic Liquid Environment**

Chenming Li <sup>1</sup>, Rajesh Bhandary <sup>1</sup>, Anja Marinow <sup>1</sup>, Stephanie Bachmann <sup>2</sup>,  
Ann-Christin Pöppler <sup>2</sup>, Wolfgang H. Binder <sup>1,\*</sup>

<sup>1</sup> Macromolecular Chemistry, Institute of Chemistry, Faculty of Natural Science II,  
Martin Luther University Halle-Wittenberg, Von-Danckelmann-Platz 4, 06120 Halle  
(Saale), Germany;

chenming.li@chemie.uni-halle.de (C.L.);

raj17.chem@gmail.com (R.B.);

anja.marinow@chemie.uni-halle.de (A.M.)

\* Correspondence: wolfgang.binder@chemie.uni-halle.de (W.H.B.)

<sup>2</sup> Institute of Organic Chemistry, Faculty of Chemistry and Pharmacy, University of  
Würzburg, Am Hubland, 97074 Würzburg, Germany

stephanie.bachmann@uni-wuerzburg.de

ann-christin.poeppler@uni-wuerzburg.de

## 1. NMR Spectrum of CP0 and Calculation of Sample Composition

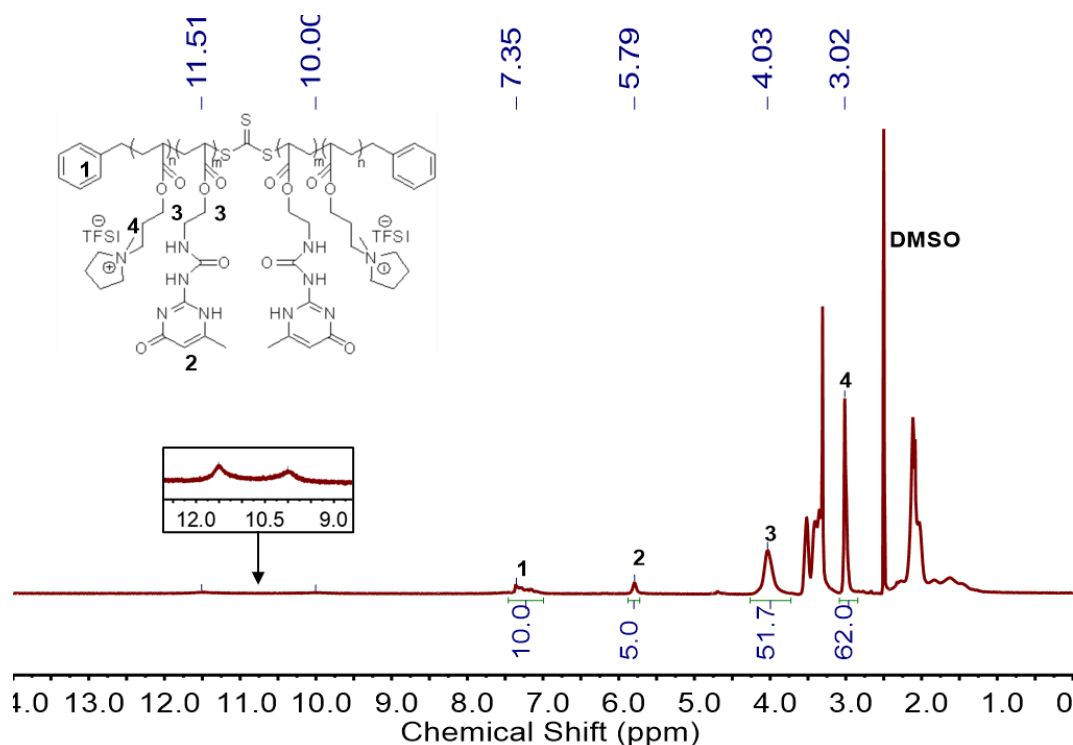


**Figure S1.** The  $^1\text{H}$  NMR spectrum of **cp0** in  $\text{DMSO-}d_6$ .

The molecular weight of **cp0** was calculated according to its NMR spectrum measured in  $\text{DMSO-}d_6$  as shown in Figure S1. The “m” and “n” in the structure refer to the degree of polymerization (DP) of the ILA ( $\text{DP}_{\text{IL}} = 2m$ ) and UPyA ( $\text{DP}_{\text{UPy}} = 2n$ ), and the detailed calculation is listed in Table S1 as follows:

**Table S1.** The calculation of the molecular weight of **cp0** via its  $^1\text{H}$  NMR spectrum.

Proton	1	2	3	4
Peak /ppm	7.35	5.79	4.03	3.02
Integral	10.0	5.0	51.7	62.0
Information	Reference peak			The calculated integral
		DP <sub>UPy</sub> = 5/1 = 5,	DP <sub>IL</sub> = 51.7/3 =	5*2+20.7*2=51.4 ≈ the
		namely 5 UPy	20.7, namely	real integral 51.7,
		per chain.	20.7 IL per chain.	proving the precise
				calculation

So the molecular weight of the synthesized **cp0** is

$$M_{n,\text{NMR}} = 290.47 + 478.42 \times 20.7 + 266.26 \times 5 = 11525 \text{ Da}$$

Then the composition of the sample can be calculated as follows:

**Table S2.** The calculation of sample compositions

	% wt	cp0 /mg	cp0 /mmol	IL /mg	IL /mmol	molar ratio
<b>cp25</b>	1:0.25	218	0.0189	53	0.1298	1:6.9
<b>cp50</b>	1:0.50	211	0.0183	102	0.2498	1:13.6
<b>cp75</b>	1:0.75	211	0.0183	160	0.3918	1:21.4

## 2. MAS NMR Spectra

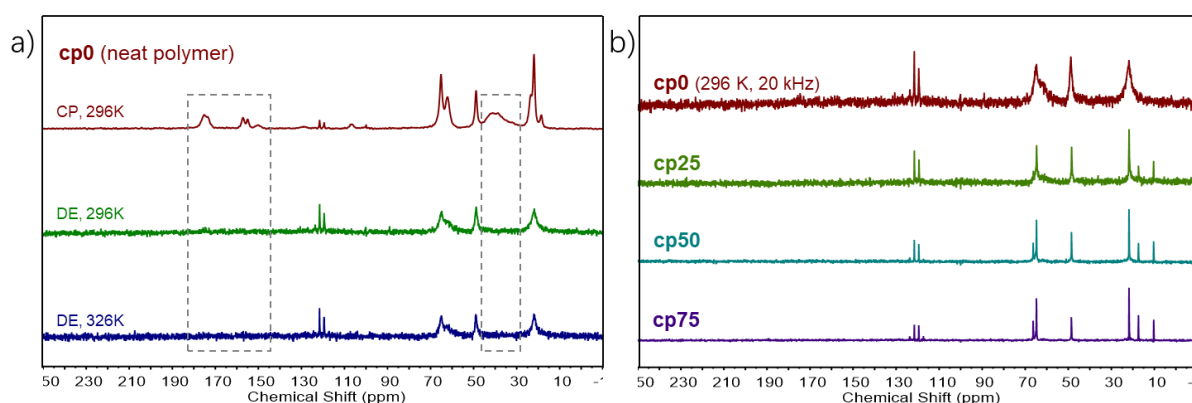


**Figure S2** a) Cross polarization (CP) and direct excitation (DE)  $^{13}\text{C}$  NMR spectra of **cp0** measured at 20 kHz MAS rate, and b) direct excitation  $^{13}\text{C}$  NMR spectra of all samples measured at 263 K and 15 kHz MAS rate (except for **cp0** as indicated).

In Figure S2a) the left dashed box refers to the carbonyls of the backbone ester, ureido moieties, and pyrimidinone moieties, and the right box refers to the polymeric backbone carbons. While the carbonyls and backbone carbons can be seen in the cross polarization (CP) spectrum, the lack of them in the direct excitation (DE) spectra (even at 326 K) proves their immobility, evidencing rigid UPy moieties locked by the quadrupolar H-bonds. Similarly, in Figure S2b), the carbonyls and backbone carbons are missing in the DE spectra of all the samples mixed with **IL**, indicative of the invulnerable H-bonds of UPy against **IL**. The quadruplet peaks at 120 ppm are the  $-\text{CF}_3$  carbons in the mobile TFSI (trifluoromethanesulfonyl imide) anions in the samples. All the sharpened peaks are due to the promoted mobility of these moieties resulting from the addition of the **IL**.

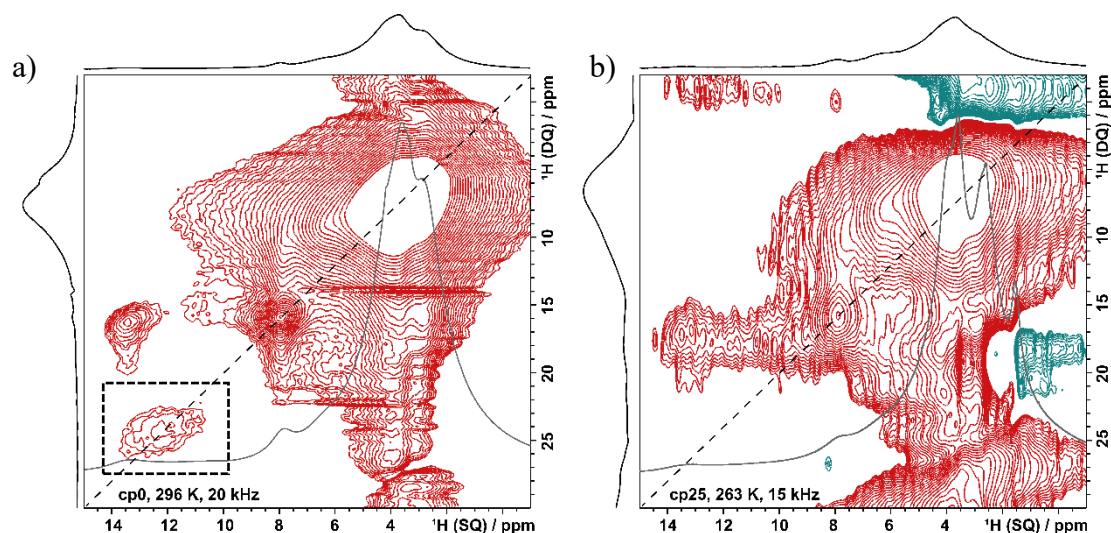
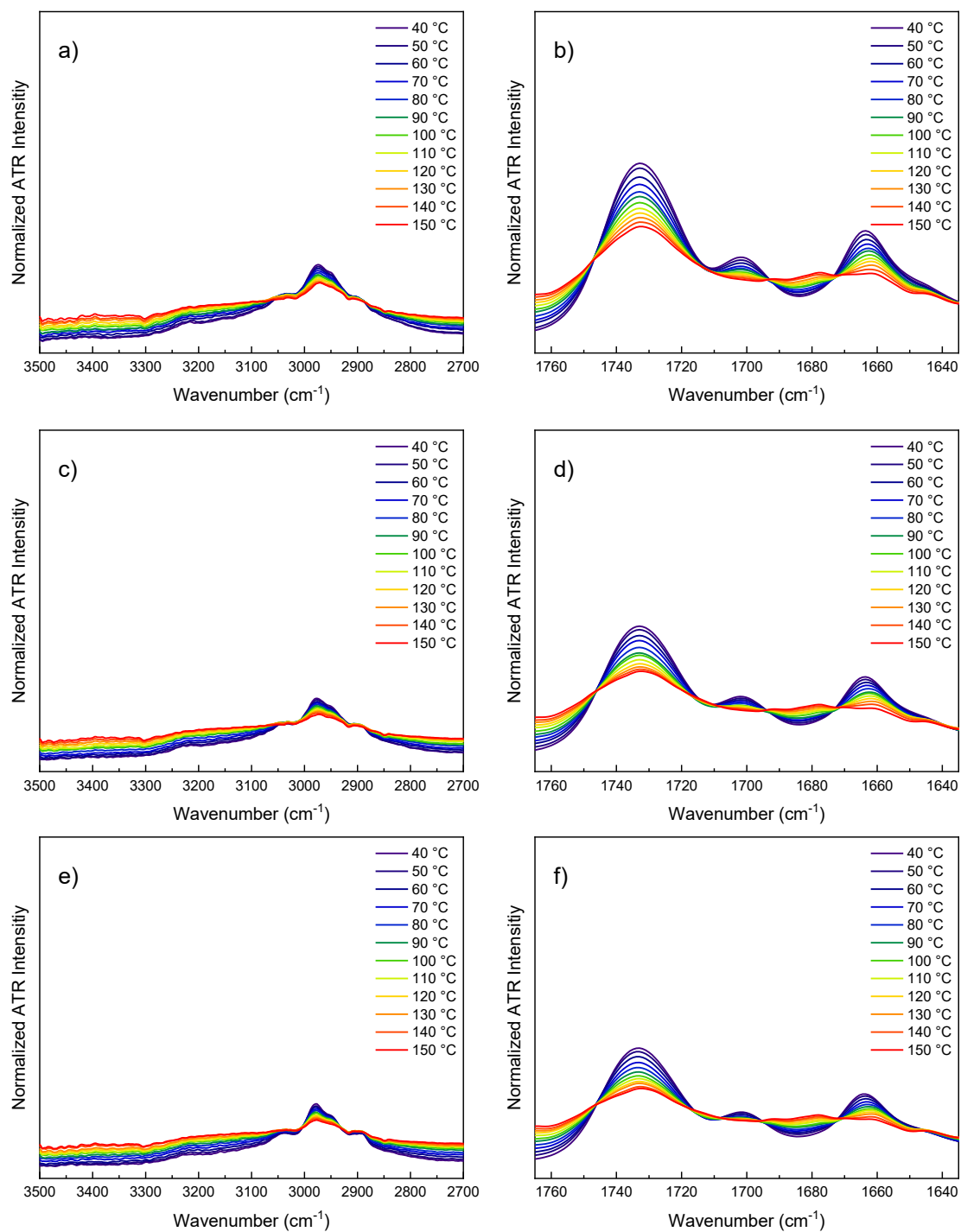


**Figure S3**  $^1\text{H}(\text{SQ})$ - $^1\text{H}(\text{DQ})$  BABA spectra alongside corresponding 1D  $^1\text{H}$  solid-state NMR spectra (blue) of a) **cp0** measured at 296 K and 20 kHz MAS rate, and b) **cp25** measured at 263 K and 15 kHz MAS rate.

In Figure S3 the 2D  $^1\text{H}$  MAS NMR spectra of **cp0** and **cp25** are shown. As indicated by the black dashed box, upon mixing with **IL**, the signal of the ureido and pyrimidinonyl H-bonding protons was slightly deformed, however, if compared with the reported spectra,<sup>[1]</sup> the tautomers exchange (enol-keto) of the UPy moieties cannot be concluded due to the poor spectra resolution and missing of corresponding peaks.

[1] I. Schnell, B. Langer, S. H. M. Söntjens, R. P. Sijbesma, M. H. P. van Genderen, H. Wolfgang Spiess, *Physical Chemistry Chemical Physics* **2002**, 4, 3750.



### 3. ATR FT-IR Spectra

**Figure S4** Variable-temperature ATR FT-IR Spectra of a) & b) **cp25**, c) & d) **cp50**, and e) & f) **cp75**.

# Chemistry–A European Journal

Supporting Information

## **Proximity Effects and Aggregation of Hamilton-Receptor Barbiturate Host–Guest Complexes Probed by Cross-Metathesis and ESI MS Analysis**

Chenming Li, Pascal Mai, Niclas Festag, Anja Marinow, and Wolfgang H. Binder\*



# *Supporting Information*

---

## Table of Content

1. EXPERIMENTAL PARTS .....	2
1.1. INSTRUMENTS .....	2
1.2. MATERIALS .....	3
1.3. SYNTHESIS .....	4
2. UV-VIS TITRATION FOR BINDING CONSTANT OF H-B .....	10
2.1. GENERAL PROCEDURES .....	10
2.2. AT DIFFERENT TEMPERATURES FOR VAN'T HOFF PLOT .....	11
2.3. LINKS OF ONLINE PROGRAM FOR UV-VIS TITRATION DETAILS .....	13
3. ANALYSIS OF PRODUCTS FROM CM REACTION VIA ESI MS .....	15
4. CONVERSION CALCULATION BY NMR SPECTROSCOPY .....	18
5. NMR SPECTRA OF COMPOUNDS .....	25
6. REFERENCE .....	30

---

## 1. Experimental Parts

### 1.1. Instruments

*Nuclear Magnetic Resonance Spectroscopy* (NMR) measurements were performed on a VNMRS (400 MHz) and a DD2 (500 MHz) NMR spectrometer (Agilent Technologies Germany GmbH & Co. KG, Waldbronn, Germany). Samples were measured at 27 °C using deuterated chloroform (CDCl<sub>3</sub>) or dimethyl sulfoxide (DMSO-*d*<sub>6</sub>). Chemical shifts ( $\delta$ ) were recorded in parts per million (ppm) relative to the remaining protonated solvent signals (CDCl<sub>3</sub>: 7.26 ppm for <sup>1</sup>H spectra and 77.0 ppm for <sup>13</sup>C spectra; DMSO-*d*<sub>6</sub>: 2.50 ppm for <sup>1</sup>H spectra and 39.5 ppm for <sup>13</sup>C spectra). The data analysis was performed via MestReNova (version 9.0.1-13254).

*Diffusion-ordered spectroscopy* (DOSY) *NMR Spectroscopy* measurements were performed on a DD2 (500 MHz) NMR spectrometer (Agilent Technologies Germany GmbH & Co. KG, Waldbronn, Germany). The experiment was performed under OpenVnmrJ 1.1 and equipped with a 5 mm PFG One NMR probe, z-gradient, and temperature unit. Diffusion-ordered NMR data were acquired by means of the Agilent pulse program DgcsteSL\_cc using a stimulated echo with self-compensating gradient schemes and conventional compensation. The length of the gradient pulse was set to 3.0 ms for <sup>1</sup>H in combination with a diffusion period of 50 – 200 ms (CDCl<sub>3</sub>). Data were systematically accumulated by linearly varying the diffusion encoding gradients over a range from 2% to 95% for 64 gradient increment values.

*UV-Vis Spectroscopy* measurements were on a Perkin Elmer LAMBDA 365 UV/Vis Spectrophotometer (PerkinElmer U.S. LLC, Shelton, United States) using Helma analytics quartz glass cuvettes (d = 10 mm). Temperature control was achieved using the Perkin Elmer Peltier System L365 (PerkinElmer U.S. LLC, Shelton, United States). All measurements were conducted at 20 °C unless otherwise stated. All measurements were repeated three to five times to ensure reproducibility.

*Electrospray Ionization Time of Flight Mass Spectrometry* (ESI MS) measurements were performed on a Bruker Daltonics microTOF (Bruker Daltonics GmbH & Co. K.G., Bremen, Germany) via direct injection at a flow rate of 180  $\mu\text{L}\cdot\text{h}^{-1}$  in positive mode with an acceleration voltage of 4.5 kV. Samples were prepared by dissolving/diluting in LC-MS grade acetonitrile or chloroform. The instrument was calibrated using the ESI-L low-concentration tuning mix from Agilent Technologies (product no. G1969-85000). The software Data Analysis (version 4.0) was used for data evaluation.

---

## 1.2. Materials

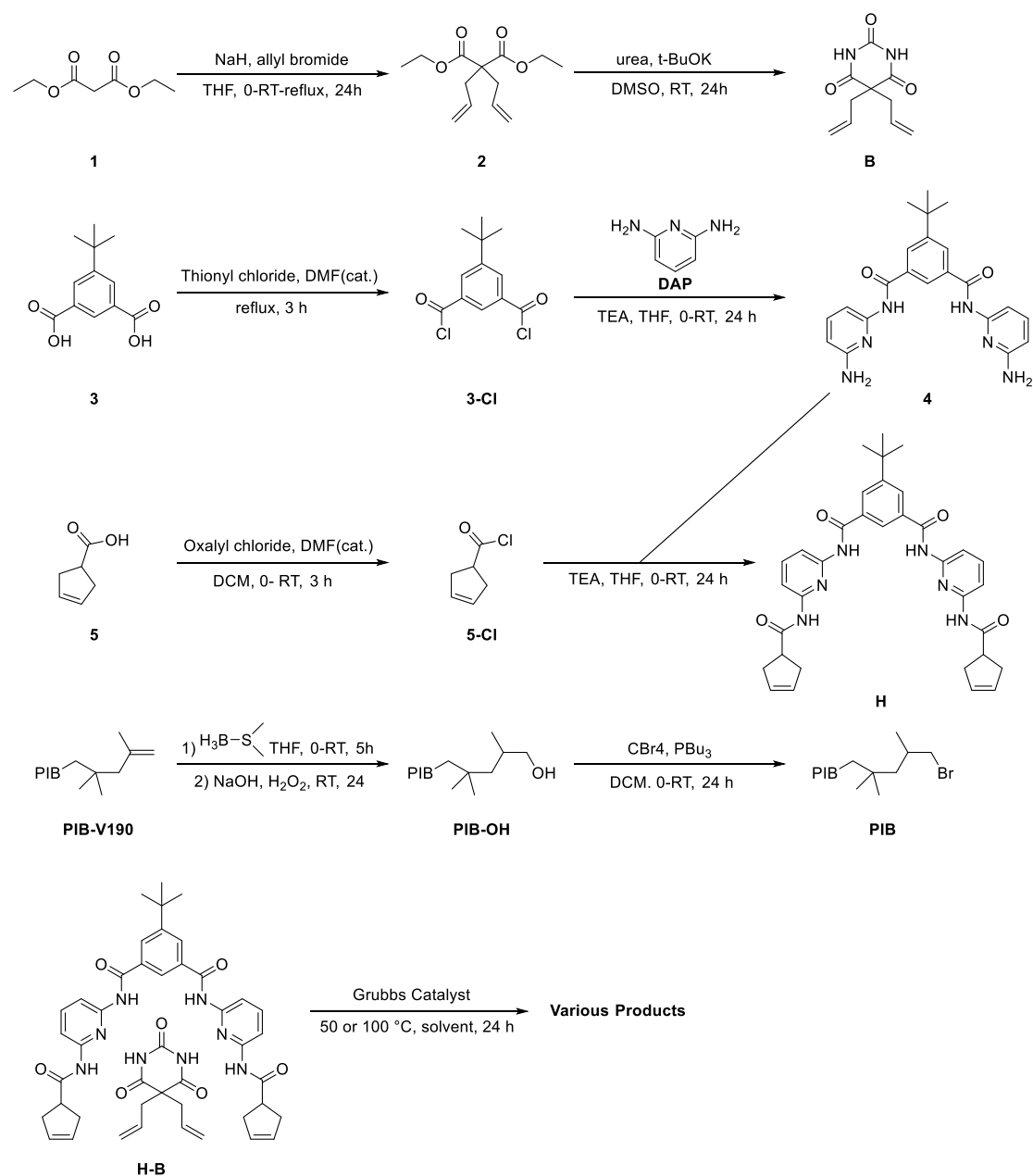
All chemicals were used as received unless otherwise specified. Urea 99%, sodium hydride 60% dispersion in mineral oil, potassium tert-butoxide 95%, allyl bromide 97%, thionyl chloride, triethylamine 99%, Grubbs catalyst 2<sup>nd</sup> generation, Grubbs catalyst 3<sup>rd</sup> generation, hydrogen peroxide solution 30 %wt, carbon tetrabromide 99%, tributylphosphine 97% (mixture of isomers), 1,2-dichloroethane water-free 99.8%, ethylene glycol 99%, and  $\alpha,\alpha,\alpha$ -trifluorotoluene anhydrous 99% were purchased from Sigma Aldrich (Steinheim, Germany); diethylmalonate 99% (G.C.), 5-(tert-butyl)isophthalic acid 98% and borane dimethyl sulfide complex 98% were purchased from TCI (Zwijndrecht, Belgium); 2,6-diaminopyridine 98% and cyclopent-3-enecarboxylic acid 99.8% were purchased from BLD Pharm (Kaiserslautern, Germany); oxalyl chloride 98% were purchased from abcr (Karlsruhe, Germany); dimethyl sulfoxide anhydrous 99.8% and formic acid LC-MS grade were purchased from Fisher Scientific (Schwerte, Germany). Polyisobutylene V190 85 %exo was purchased from Caldic (Hemiksem, Belgium).

Technical solvents cyclohexane, ethyl acetate, and dichloromethane were purchased from Overlack (Korschenbroich, Germany), and redistilled before use.

HPLC/LC grade solvents *n*-hexane and 1,4-dioxan were purchased from Roth (Karlsruhe, Germany); N,N-dimethylformamide (DMF), ethyl acetate (E.A.), tetrahydrofuran (THF), acetonitrile (MeCN), methanol (MeOH), isopropanol (iPA) and chloroform (CHCl<sub>3</sub>) were purchased from VWR - Prolabo (Dresden, Germany); hexafluoro-2-propanol (HFIP) was purchased from Carbolution Chemicals (Sankt Ingbert, Germany).

Deuterated solvents Chloroform-d 99.8% Atom%D stabilized with Ag (CDCl<sub>3</sub>), dimethylsulfoxide-d<sub>6</sub> 99.8 atom%D (DMSO-d<sub>6</sub>), methanol-d<sub>4</sub> 99.8 atom%D (MeOD), and toluene-d<sub>8</sub> 99.8 atom%D (Tol-d<sub>8</sub>) were purchased from Chemotrade (Düsseldorf, Germany).

### 1.3. Synthesis



**Scheme S1** Synthesis of **B**, **H**, and **PIB**.

#### *Synthesis of Diethyl 2,2-Diallylmalonate (2)*

The synthesis was adapted from literature<sup>[1]</sup>. Sodium hydride (4.40 g, 110 mmol) was suspended in dry THF (100 mL) in a pre-dried two-necked flask at 0 °C. A solution of **1** (7.59 mL, 50 mmol) in dry THF (15 mL) was added dropwise. After the addition, the reaction mixture was stirred for 30 minutes until gas evolution ceased. Allyl bromide (9.51 mL, 110 mmol) was then added, and the reaction was refluxed for 24 hours. After the reaction was complete, 1 M aq. HCl was slowly added to quench the reaction, and

---

the resulting solid was vacuum-filtered. The filtrate was extracted with diethyl ether, and the combined organic layers were dried over Na<sub>2</sub>SO<sub>4</sub>. The solvent was removed using a rotary evaporator. The crude product was then purified by column chromatography on silica gel using a hexane/diethyl ether mixture as the eluent (with hexane/diethyl ether 100/15, R<sub>f</sub> = 0.48), yielding **2** as transparent liquid (yield = 83 %). <sup>1</sup>H NMR (CDCl<sub>3</sub>): δ ppm 5.61(m, 2H), 5.04(m, 4H), 4.13(q, J = 7.1 Hz, 4H), 2.58(dt, 4H), 1.20(t, 6H).

<sup>13</sup>C NMR (CDCl<sub>3</sub>): δ ppm 170.71, 132.31, 119.07, 61.18, 57.23, 36.37, 14.09.

### ***Synthesis of 5,5-Diallylpyrimidine-2,4,6(1H,3H,5H)-trione (B)***

The synthesis was adapted from literature<sup>[1-2]</sup>. A pre-dried two-necked flask was charged with urea (5 g, 83.2 mmol) and potassium tert-butoxide (2.05 g, 18.3 mmol). A solution of **2** (2 g, 8.32 mmol) in deoisturized DMSO (35 mL) was added slowly to dissolve all solids. The reaction mixture was stirred at room temperature for 24 hours. After the reaction was completed, the pH of the reaction mixture was adjusted to 10 using 1 M aq. NaOH, followed by the addition of deionized water (100 mL). The mixture was washed with chloroform, and the pH of the aq. phase was then adjusted to 1 using concentrated HCl. The product was extracted with ethyl acetate, and the organic layer was washed with aq. NaHCO<sub>3</sub> and brine, then dried over Na<sub>2</sub>SO<sub>4</sub>. The solvent was removed using a rotary evaporator, and the crude product was purified by recrystallization from hot xylene, yielding **B** as white crystals (yield = 80%).

<sup>1</sup>H NMR (CDCl<sub>3</sub>): δ ppm 8.39 (s, 2H), 5.61 (m, 2H), 5.16 (m, 4H), 2.56 (d, 4H).

<sup>13</sup>C NMR (CDCl<sub>3</sub>): δ ppm 172.4, 150.2, 131.8, 120.6, 55.4, 42.0.

ESI MS: calculated for [C<sub>10</sub>H<sub>2</sub>N<sub>2</sub>O<sub>3</sub>] = 208.08; found: [M-H]<sup>-</sup> = 207.08.

### ***Synthesis of N1,N3-Bis(6-aminopyridin-2-yl)-5-(tert-butyl)isophthalamide (4)***

The synthesis was adapted from literature<sup>[3]</sup>. **4** was prepared in two steps. First, **3-Cl** was prepared. A two-necked flask was charged with **3** (5 g, 22.5 mmol) and cooled to 0 °C. Thionyl chloride (50 mL) was slowly added to the flask, followed by the addition of a catalytic amount of DMF. The reaction mixture was then allowed to warm to room temperature and refluxed for 3 hours. After the reaction was complete, the flask was cooled to room temperature, and the thionyl chloride was removed using a rotary evaporator. The crude product was then dried under a high vacuum, yielding **3-Cl** as a transparent yellowish oil, which was used without further purification.

Second, **4** was prepared. A two-necked flask was charged with DAP (12.3 g, 112.5 mmol), TEA (15.8 mL, 112.5 mmol), and dry THF (250 mL). The flask was then cooled to 0 °C, and a solution of **3-Cl** in dry THF (50 mL) was added dropwise. After the

---

addition was complete, the reaction mixture was allowed to warm to room temperature and stirred for 24 hours. After the reaction was complete, the solution was filtered, and the filtrate was concentrated to one-third of its volume. The concentrated solution was then precipitated into hot water (2 L, 60-70 °C). The resulting suspension was vacuum-filtered, and the solid was washed with hot water. The crude product was then dried and purified by column chromatography on silica gel using hexane/ethyl acetate as the eluent (with ethyl acetate,  $R_{f, 4} = 0.68$ ), yielding **4** as a white powder (yield = 63 %).

$^1\text{H}$  NMR (DMSO- $d_6$ ):  $\delta$  ppm 10.28 (s, 2H), 8.33 (s, 1H), 8.11 (s, 2H), 7.52 – 7.32 (m, 4H), 6.26 (dd, 2H), 5.78 (s, 4H), 1.37 (s, 9H).

$^{13}\text{C}$  NMR (DMSO- $d_6$ ):  $\delta$  ppm 165.12, 158.56, 151.35, 150.38, 138.97, 134.11, 127.97, 124.26, 104.05, 101.82, 34.79, 30.91.

### ***Synthesis of 5-(Tert-butyl)-N1,N3-bis(6-(cyclopent-3-ene-1-carboxamido)pyridin-2-yl)isophthalamide (H)***

**H** was prepared in two steps. First, **5-Cl** was prepared. A two-necked flask was charged with a solution of **5** (1.07 mL, 10 mmol) and a catalytic amount of DMF in DCM (2 mL), and the mixture was cooled to 0 °C. A solution of oxalyl chloride (0.98 mL, 11 mmol) in DCM (3 mL) was then added dropwise. The reaction mixture was allowed to warm to room temperature and stirred for 3 hours. The resulting solution of **5-Cl** was used directly in the next step without further purification.

Second, **H** was prepared. A two-necked flask was charged with **4** (808.94 mg, 2 mmol), TEA (10 mL, 1.4 mmol), and dry THF (30 mL). The flask was cooled to 0 °C, and the solution of **3-Cl** from the previous step was added dropwise. After the addition was complete, the reaction mixture was allowed to warm to room temperature and stirred for 24 hours. After the reaction was complete, ethyl acetate (100 mL) was added to the mixture, then filtered and washed sequentially with 1 M aqueous HCl, concentrated aqueous  $\text{NaHCO}_3$ , and brine. The organic phase was dried over  $\text{Na}_2\text{SO}_4$ , and the solvent was removed using a rotary evaporator. The crude product was then purified by column chromatography on silica gel using a hexane/ethyl acetate mixture as the eluent (with hexane/ethyl acetate 1/1,  $R_{f, H.W.} = 0.5$ ), yielding **H** as a white powder (yield = 72 %).

$^1\text{H}$  NMR ( $\text{CDCl}_3$ ):  $\delta$  ppm 10.55 (s, 2H), 10.14 (s, 2H), 8.37 (s, 1H), 8.20 (s, 2H), 7.87 – 7.79 (m, 6H), 5.67 (s, 4H), 3.40 – 3.33 (m, 2H), 2.66 – 2.53 (m, 8H), 1.40 (s, 9H).

$^{13}\text{C}$  NMR ( $\text{CDCl}_3$ ):  $\delta$  ppm 174.63, 165.38, 151.48, 150.60, 150.17, 140.02, 134.03, 128.98, 128.04, 125.05, 110.51, 109.93, 42.57, 39.52, 36.41, 34.92, 30.91.

ESI MS: calculated for  $[\text{C}_{34}\text{H}_{36}\text{N}_6\text{O}_4] = 592.28$ ; found:  $[\text{M}-\text{H}]^- = 591.27$ .

### ***Synthesis of Terminal Hydroxyl Polyisobutylene (PIB-OH)***



---

The synthesis was adapted from literature<sup>[4]</sup>. A 250 mL pre-dried, two-necked flask was charged with a solution of **PIB-V190** (8.73 g, 66.48 mmol, exo-ene-terminated,  $M_{n, NMR} = 1050$  Da) in dry THF (50 mL) and cooled to 0 °C. Borane dimethylsulfide (7.72 mL, 73.13 mmol) was added dropwise, slowly (Caution: heat and gas formation). After the addition, the reaction mixture was allowed to warm to room temperature and stirred vigorously for 24 hours. The reaction was then cooled to 0 °C, and aqueous NaOH (5.37 g, 132.96 mmol, in 10 mL deionized water) was slowly added, followed by 30% aqueous H<sub>2</sub>O<sub>2</sub> (20.4 mL, 664.8 mmol). The reaction was stirred vigorously at room temperature for another 24 hours. Upon completion, the mixture was transferred to a separatory funnel, and cyclohexane (100 mL) was added. The organic phase was separated and dried over Na<sub>2</sub>SO<sub>4</sub>, and the solvent was removed using a rotary evaporator. The crude product was purified by column chromatography on silica gel, first with hexane and then with chloroform as the eluent (with hexane,  $R_{f, PIB-V190} = 0.95$ ,  $R_{f, PIB-OH} = 0$ ; with chloroform,  $R_{f, PIB-OH} = 0.95$ ), yielding **PIB-OH** as a colorless viscous liquid (yield = 75 %).

<sup>1</sup>H NMR (CDCl<sub>3</sub>):  $\delta$  ppm 3.46 (q, 1H), 3.32 (q, 1H), 1.78 – 1.64 (m, 1H), 1.58 (d, J = 13.5 Hz, 2H), 1.53 – 1.24 (m, 50H), 1.24 – 0.74 (m, 150H).

### ***Synthesis of Terminal Bromide Polyisobutylene (PIB)***

The synthesis was adapted from literature<sup>[5]</sup>. A pre-dried two-necked flask was charged with a solution of **PIB-OH** (6.3 g, 5.73 mmol) in dry DCM (150 mL) and carbon tetrabromide (19.18 g, 57.3 mmol), then cooled to 0 °C. After dissolution, tributyl phosphine (14.75 mL, 57.3 mmol) was added dropwise. The reaction mixture was then allowed to warm to room temperature and stirred vigorously for 24 hours. Upon completion, 150 g of silica was added, and the DCM was removed using a rotary evaporator. Cyclohexane (300 mL) was then added, and the mixture was stirred vigorously for 30 minutes, followed by vacuum filtration and thorough washing of the solid with cyclohexane. The filtrate was combined, and the solvent was removed using a rotary evaporator. The crude product was precipitated in methanol (200 mL) and further purified by column chromatography on silica gel with cyclohexane as the eluent (with hexane,  $R_{f, PIB} = 0.90$ ), yielding **PIB** as a colorless viscous liquid (yield = 83 %).

<sup>1</sup>H NMR (CDCl<sub>3</sub>):  $\delta$  ppm 3.39 (q, 1H), 3.27 (q, 1H), 1.98 – 1.85 (m, 1H), 1.55 (d, J = 15.8 Hz, 2H), 1.49 – 1.31 (m, 50H), 1.21 – 0.97 (m, 150H).

$M_{n, NMR} = 1533$  Da

$M_{n, GPC, THF, P.S. standard} = 1324$  Da

### ***General Cross-Metathesis (CM) Reaction to Fix H+B Aggregates***

All cross-metathesis (CM) reactions were performed following the general CM procedure, with variations in conditions as specified, except Entry 6. Typically, a screw-capped vial was charged with **H**, **B**, and Grubbs catalyst inside a glovebox. A degassed solvent was added to the vial, and then the cap was secured. The vial was heated to the desired temperature to initiate the CM reaction. After 24 hours, the vial was cooled to room temperature, removed from the glovebox, and exposed to air to terminate the reaction. The reaction mixture was then directly analyzed by NMR spectroscopy and ESI-MS without further purification.

**Table S1** Summary of cross-metathesis reaction to fix **H+B** aggregates

Entry	T /°C	Solvent	Conc. /M	Cat.	Conv. total ene
(1)	100	Tol-d8	0.01	G3	100 %.
(2)	50	Tol-d8	0.01	G3	89.4 %
(3)	50	DCE	0.1	G3	89.5 %
(4)	50	MeOD	0.01	G3	78.8 %
(5)	50	DCE	0.1	G2	97.6 %
(6)	50	<b>PIB</b>	-	G3	97.3 %

***CM Reaction Entry 1 in Table S1***

General procedure was followed. **H** (6.00 mg, 0.01012 mmol), **B** (2.11 mg, 0.01012 mmol), the Grubbs catalyst 3<sup>rd</sup> generation (0.89 mg 0.001012 mmol), and toluene-d<sub>8</sub> (1 mL) were used.

***CM Reaction Entry 2 in Table S1***

General procedure was followed. **H** (6.00 mg, 0.01012 mmol), **B** (2.11 mg, 0.01012 mmol), the Grubbs catalyst 3<sup>rd</sup> generation (0.89 mg 0.001012 mmol), and toluene-d<sub>8</sub> (1 mL) were used.

***CM Reaction Entry 3 in Table S1***

General procedure was followed. **H** (6.00 mg, 0.01012 mmol), **B** (2.11 mg, 0.01012 mmol), the Grubbs catalyst 3<sup>rd</sup> generation (0.89 mg 0.001012 mmol), and 1,2-dichloroethane (0.1 mL) were used.

***CM Reaction Entry 4 in Table S1***

General procedure was followed. **H** (6.00 mg, 0.01012 mmol), **B** (2.11 mg, 0.01012 mmol), the Grubbs catalyst 3<sup>rd</sup> generation (0.89 mg 0.001012 mmol), and MeOD (1

---

mL) were used.

***CM Reaction Entry 5 in Table S1***

General procedure was followed. **H** (6.00 mg, 0.01012 mmol), **B** (2.11 mg, 0.01012 mmol), the Grubbs catalyst 2<sup>rd</sup> generation (0.86 mg 0.001012 mmol), and 1,2-dichloroethane (0.1 mL) were used.

***CM Reaction Entry 6 in Table S1***

A vial was charged with **H** (4.3 mg, 0.0072 mmol), **B** (1.6 mg, 0.0072 mmol), **PIB** (12.3 mg), the Grubbs catalyst 3<sup>rd</sup> generation (2.6 mg, 0.0029 mmol), and degassed THF (1 mL). The vial was then transferred into a flask, and THF was removed using a rotary evaporator over 30 minutes. Argon was introduced to restore the vacuum conditions. The cap was secured, and the vial was heated to the desired temperature to initiate the cross-metathesis reaction in a glovebox. After 24 hours, the vial was cooled to room temperature, removed from the glovebox, and THF (1 mL) was added to dissolve the reaction mixture. The reaction mixture was then transferred to a separatory funnel, and *n*-hexane (20 mL) and methanol (20 mL) were added, mixed, and separated, extracting all the product into the methanol layer. The methanol layer was transferred to a flask, and the methanol was removed using a rotary evaporator. The product mixture was dissolved in CDCl<sub>3</sub> for NMR analysis or in acetonitrile for ESI MS analysis.

## 2. UV-Vis Titration for Binding Constant of H-B

### 2.1. General Procedures

To measure the binding constant  $K_{\text{assn.}}$  between **H** and **B**, stock solutions were first prepared in different solvents (volume changes upon dissolution were considered negligible and treated as a systematic error, diminished when fitting for the binding constant). Typically, **H** was dissolved in an HPLC-grade solvent in flask A to reach its target concentration, while **B** was dissolved in the same solvent in flask B to reach its target concentration. After measuring the background with the neat solvent, 3 mL of the **H** solution was added to an empty cuvette and measured as the initial (0<sup>th</sup>) spectrum. A specific amount of **B** solution was then added to the cuvette, which was shaken to mix thoroughly, and the mixture was measured as the 1<sup>st</sup> sample. Subsequently, additional amounts of **B** solution were added incrementally to the cuvette, with each mixture measured accordingly as the 2<sup>nd</sup>, 3<sup>rd</sup>, and subsequent samples. This process was repeated to collect data for 10 samples, following the protocol outlined in the accompanying **Table S2**.

**Table S2** The profile of UV Vis spectroscopy titration for measurements of binding constant of **H** with **B**.

	<b>H</b>		<b>B</b>				
No.	mmol Based on 3 mL solution in the cuvette	conc. / mmol/mL	<b>B</b> Equivalence	mmol	to reach eq., the <i>theoretical</i> <i>amount</i> of stock solution needed /mL	μL	the <i>real</i> <i>amount</i> <i>needed</i> to add to the cuvette /μL
0	7.50E-05	2.50E-05	0	0.00E+00	0		
1			0.1	7.50E-06	5.00E-03	5	5
2			0.2	1.50E-05	1.00E-02	10	5
3			0.3	2.25E-05	1.50E-02	15	5
4			0.4	3.00E-05	2.00E-02	20	5
5			0.6	4.50E-05	3.00E-02	30	10
6			0.8	6.00E-05	4.00E-02	40	10
7			1.0	7.50E-05	5.00E-02	50	10
8			1.3	9.75E-05	6.50E-02	65	15
9			1.6	1.20E-04	8.00E-02	80	15
10			2.0	1.50E-04	1.00E-01	100	20
			<b>Sum</b>	-	-	-	80

After collecting the U.V. spectra, the data were fitted using the online fitting program BindFit (<http://supramolecular.org>). Fundamental information about UV-Vis spectroscopy titration and the use of BindFit can be found in the literature.<sup>[6]</sup> Titrations for each solvent were repeated 3-5 times to ensure reproducibility. A summary of the fitted binding constants is provided in **Table S3**.

For measurements in a toluene/methanol mixture, the solvents were prepared in the desired molar ratio and used as described above.

## 2.2. At Different Temperatures for Van't Hoff Plot

For measurements at different temperatures, each sample was equilibrated at the desired temperature for 5 minutes before measurement.

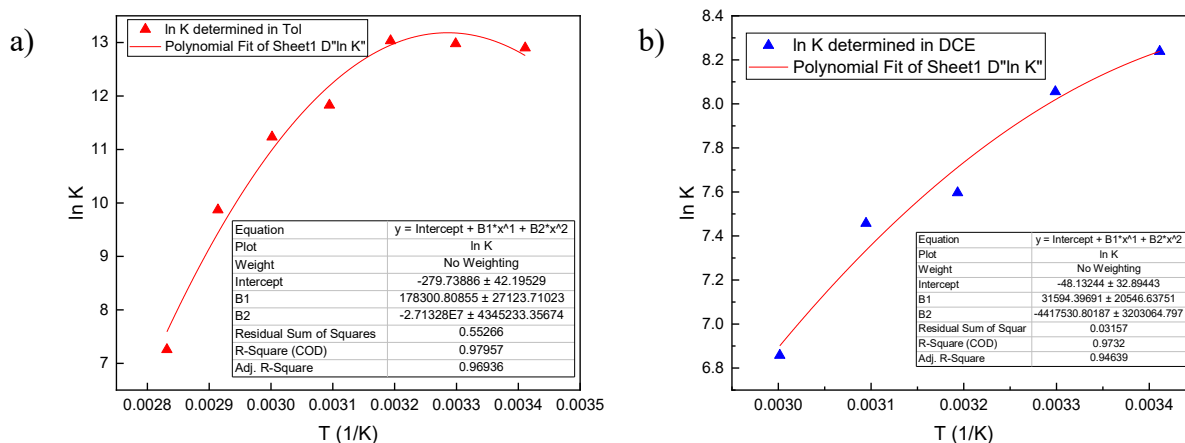


**Figure S1** Fitting of the association constants of **H** and **B** determined in a) toluene and b) 1,2-dichloroethane at various temperatures, using a polynomial function to generate Vann't Hoff plot.

The  $K_{\text{assn.}}$ s were plotted against  $1/T$  and fitted using the following equation as previously reported:

$$\ln K_{\text{assn.}} = a + \frac{b}{T} + \frac{c}{T^2}$$

Where

$K_{\text{assn.}}$  is the association constant measure at the specified temperature;

$T$  is the specific temperature in Kelvin;

$a$ ,  $b$ , and  $c$  are constants obtained from the polynomial fitting, as following

	a	b	c
Tol	-279.74	$1.78 \times 10^5$	$-2.71 \times 10^7$
DCE	-48.13	$3.15 \times 10^4$	$-4.42 \times 10^6$

---

Then the change in enthalpy ( $\text{kJ}\cdot\text{mol}^{-1}$ ) and entropy ( $\text{J}\cdot\text{mol}^{-1}\text{K}^{-1}$ ) at a given temperature can be calculated using the following equation:

$$\Delta H = -R\left(b + \frac{2c}{T}\right)$$

$$\Delta S = R\left(a - \frac{c}{T^2}\right)$$

Where

R is the gas constant ( $8.314 \text{ J}\cdot\text{mol}^{-1}\text{K}^{-1}$ ).

### 2.3. Links of Online Program for UV-Vis Titration Details

**Table S3 H-B Titration Results and Fitting Links**

<b>Solvent</b>	<b>Kassn /M<sup>-1</sup></b>	<b>Error</b>	<b>Links for Fitting Data</b>
CHCl <sub>3</sub>	4.13E+04	0.73%	<a href="http://app.supramolecular.org/bindfit/view/b1fbd083-f441-4c81-b29f-2f6278951853">http://app.supramolecular.org/bindfit/view/b1fbd083-f441-4c81-b29f-2f6278951853</a>
DCM	4.12E+04	1.92%	<a href="http://app.supramolecular.org/bindfit/view/baa00347-e69a-4336-ba6a-23af54054aa4">http://app.supramolecular.org/bindfit/view/baa00347-e69a-4336-ba6a-23af54054aa4</a>
DCE	3.78E+03	2.21%	<a href="http://app.supramolecular.org/bindfit/view/b7190d75-1131-4164-b232-c6b511701790">http://app.supramolecular.org/bindfit/view/b7190d75-1131-4164-b232-c6b511701790</a>
Dioxane	7.02E+02	2.56%	<a href="http://app.supramolecular.org/bindfit/view/fe5e0449-4ca5-41c0-9e27-380210ebc17d">http://app.supramolecular.org/bindfit/view/fe5e0449-4ca5-41c0-9e27-380210ebc17d</a>
DMF	7.34E+02	1.58%	<a href="http://app.supramolecular.org/bindfit/view/ebf50628-94e4-4114-ab3a-aa21f4e499e7">http://app.supramolecular.org/bindfit/view/ebf50628-94e4-4114-ab3a-aa21f4e499e7</a>
DMSO	5.96E+02	3.12%	<a href="http://app.supramolecular.org/bindfit/view/cbeabd06-5474-4de1-aadd-a66e4c780623">http://app.supramolecular.org/bindfit/view/cbeabd06-5474-4de1-aadd-a66e4c780623</a>
E.A.	7.08E+02	1.42%	<a href="http://app.supramolecular.org/bindfit/view/55badf10-cbc9-42c4-a739-d797171951bd">http://app.supramolecular.org/bindfit/view/55badf10-cbc9-42c4-a739-d797171951bd</a>
EG	6.46E+02	1.71%	<a href="http://app.supramolecular.org/bindfit/view/6debd171-052e-4c54-9153-28aa2e39bac0">http://app.supramolecular.org/bindfit/view/6debd171-052e-4c54-9153-28aa2e39bac0</a>
HFiP	5.66E+02	4.00%	<a href="http://app.supramolecular.org/bindfit/view/082d2fed-c3d8-46a8-8b0f-70b3a90fadb8">http://app.supramolecular.org/bindfit/view/082d2fed-c3d8-46a8-8b0f-70b3a90fadb8</a>
iPrA	9.99E+02	2.03%	<a href="http://app.supramolecular.org/bindfit/view/840e4300-4c1a-4b74-aba1-694e960e1c4c">http://app.supramolecular.org/bindfit/view/840e4300-4c1a-4b74-aba1-694e960e1c4c</a>
MeCN	7.18E+02	1.89%	<a href="http://app.supramolecular.org/bindfit/view/0f5614aa-fbfe-4c05-8394-3065eea46b04">http://app.supramolecular.org/bindfit/view/0f5614aa-fbfe-4c05-8394-3065eea46b04</a>
MeOH	7.12E+02	1.63%	<a href="http://app.supramolecular.org/bindfit/view/47efb1d6-b99d-478d-b677-913db75d7d91">http://app.supramolecular.org/bindfit/view/47efb1d6-b99d-478d-b677-913db75d7d91</a>
THF	6.44E+02	2.64%	<a href="http://app.supramolecular.org/bindfit/view/675a601f-59de-4b49-b315-a31cc41349f2">http://app.supramolecular.org/bindfit/view/675a601f-59de-4b49-b315-a31cc41349f2</a>
Tol	4.69E+05	8.43%	<a href="http://app.supramolecular.org/bindfit/view/0b93e6a2-c22b-438f-9a7a-5d64776ef892">http://app.supramolecular.org/bindfit/view/0b93e6a2-c22b-438f-9a7a-5d64776ef892</a>
TFT	1.67E+05	2.14%	<a href="http://app.supramolecular.org/bindfit/view/1ce9ead9-2b6e-415d-b6e7-6e5739f2c3d8">http://app.supramolecular.org/bindfit/view/1ce9ead9-2b6e-415d-b6e7-6e5739f2c3d8</a>
<b>In DCE at various T</b>	<b>Kassn /M<sup>-1</sup></b>	<b>Error</b>	<b>Links for Fitting Data</b>
20 °C	3.78E+03	2.21%	<a href="http://app.supramolecular.org/bindfit/view/b7190d75-1131-4164-b232-c6b511701790">http://app.supramolecular.org/bindfit/view/b7190d75-1131-4164-b232-c6b511701790</a>
30 °C	3.15E+03	0.54%	<a href="http://app.supramolecular.org/bindfit/view/f512a7c3-64cd-427c-9278-d15e48411faf">http://app.supramolecular.org/bindfit/view/f512a7c3-64cd-427c-9278-d15e48411faf</a>
40 °C	1.99E+03	1.19%	<a href="http://app.supramolecular.org/bindfit/view/a181d472-3e7f-42bc-9e33-55ee40179a23">http://app.supramolecular.org/bindfit/view/a181d472-3e7f-42bc-9e33-55ee40179a23</a>
50 °C	1.73E+03	1.28%	<a href="http://app.supramolecular.org/bindfit/view/8a1d17f0-d742-4563-a8f4-ebfb9f290ae4">http://app.supramolecular.org/bindfit/view/8a1d17f0-d742-4563-a8f4-ebfb9f290ae4</a>
60 °C	9.52E+02	2.61%	<a href="http://app.supramolecular.org/bindfit/view/a77ecc5d-3348-48a0-a853-7b502e10c37c">http://app.supramolecular.org/bindfit/view/a77ecc5d-3348-48a0-a853-7b502e10c37c</a>
<b>In Tol at various T</b>	<b>Kassn /M<sup>-1</sup></b>	<b>Error</b>	<b>Links for Fitting Data</b>
20 °C	4.00E+05	5.32%	<a href="http://app.supramolecular.org/bindfit/view/f4c0de05-4d88-40a0-8376-56de7111f25a">http://app.supramolecular.org/bindfit/view/f4c0de05-4d88-40a0-8376-56de7111f25a</a>
30 °C	4.33E+05	15.91%	<a href="http://app.supramolecular.org/bindfit/view/8ef698b1-35cc-4376-ae7b-75f292785614">http://app.supramolecular.org/bindfit/view/8ef698b1-35cc-4376-ae7b-75f292785614</a>
40 °C	4.58E+05	21.46%	<a href="http://app.supramolecular.org/bindfit/view/de436de3-0dcb-4665-8726-e8f41197c62d">http://app.supramolecular.org/bindfit/view/de436de3-0dcb-4665-8726-e8f41197c62d</a>
50 °C	1.35E+05	5.14%	<a href="http://app.supramolecular.org/bindfit/view/c63b06ab-36cb-4c89-a083-4a61de1fc38d">http://app.supramolecular.org/bindfit/view/c63b06ab-36cb-4c89-a083-4a61de1fc38d</a>
60 °C	7.56E+04	3.86%	<a href="http://app.supramolecular.org/bindfit/view/3cda4c9a-4c97-4bf6-8344-b84f20fce763">http://app.supramolecular.org/bindfit/view/3cda4c9a-4c97-4bf6-8344-b84f20fce763</a>
70 °C	1.93E+04	3.66%	<a href="http://app.supramolecular.org/bindfit/view/1c7f9618-c7c2-48ab-9ca9-fbe02ca08e7e">http://app.supramolecular.org/bindfit/view/1c7f9618-c7c2-48ab-9ca9-fbe02ca08e7e</a>
80 °C	1.42E+03	4.22%	<a href="http://app.supramolecular.org/bindfit/view/188d7826-175c-4e9a-8524-9fc268e52573">http://app.supramolecular.org/bindfit/view/188d7826-175c-4e9a-8524-9fc268e52573</a>



---

**(Continued) Table S3** Titration Results and Fitting Links

<b>Tol/MeOH</b>	<b>K<sub>assn</sub> /M<sup>-1</sup></b>	<b>Error</b>	<b>Links for Fitting Data</b>
Molar ratio			
1 : 0	4.69E+05	8.43%	<a href="http://app.supramolecular.org/bindfit/view/0b93e6a2-c22b-438f-9a7a-5d64776ef892">http://app.supramolecular.org/bindfit/view/0b93e6a2-c22b-438f-9a7a-5d64776ef892</a>
1 : 0.01	2.84E+05	5.76%	<a href="http://app.supramolecular.org/bindfit/view/42278c75-9c03-4fcb-b74a-fedfc787a1e9">http://app.supramolecular.org/bindfit/view/42278c75-9c03-4fcb-b74a-fedfc787a1e9</a>
1 : 0.03	1.89E+03	0.62%	<a href="http://app.supramolecular.org/bindfit/view/607ca93f-45de-4654-ac63-878516e0cd90">http://app.supramolecular.org/bindfit/view/607ca93f-45de-4654-ac63-878516e0cd90</a>
1 : 0.05	1.29E+03	1.89%	<a href="http://app.supramolecular.org/bindfit/view/a586d25f-e3af-4f99-bff6-d276d1f48c9c">http://app.supramolecular.org/bindfit/view/a586d25f-e3af-4f99-bff6-d276d1f48c9c</a>
1 : 0.07	1.09E+03	1.26%	<a href="http://app.supramolecular.org/bindfit/view/f13d6148-3123-494c-9f14-9ed1930c7af0">http://app.supramolecular.org/bindfit/view/f13d6148-3123-494c-9f14-9ed1930c7af0</a>
1 : 0.09	9.33E+02	2.11%	<a href="http://app.supramolecular.org/bindfit/view/ff8539e3-8b62-46db-b241-f26db7a2b7e2">http://app.supramolecular.org/bindfit/view/ff8539e3-8b62-46db-b241-f26db7a2b7e2</a>
1 : 0.2	8.22E+02	1.11%	<a href="http://app.supramolecular.org/bindfit/view/ea6c6e91-8a73-4890-8968-21b57326c1b5">http://app.supramolecular.org/bindfit/view/ea6c6e91-8a73-4890-8968-21b57326c1b5</a>
1 : 0.5	5.36E+02	1.66%	<a href="http://app.supramolecular.org/bindfit/view/5425ff64-6d56-4ad7-a570-eb7b96e7d2c4">http://app.supramolecular.org/bindfit/view/5425ff64-6d56-4ad7-a570-eb7b96e7d2c4</a>
1 : 1	6.99E+02	0.77%	<a href="http://app.supramolecular.org/bindfit/view/2692654a-95fe-46a9-879d-06adc227a8fb">http://app.supramolecular.org/bindfit/view/2692654a-95fe-46a9-879d-06adc227a8fb</a>

---

### 3. Analysis of Products from CM Reaction via ESI MS

The normalized ratio between products was calculated as follows:

The products were first found by ESI MS and simulated with all possible ion couplings ([M-H], [M+Cl], [M-H+Na+CH<sub>3</sub>CN-H], etc, as specified in each spectrum). Then, the relative intensity of all the matched peaks for one product was summed up and used to calculate the cumulative intensity of such compound (*I<sub>c</sub>*). The intensity of all products with all relevant ion coupling was summed up and used as intensity (*I<sub>all</sub>*) for all products. All the ratios are only calculated based on one spectrum and compared within this spectrum. The normalized ratio of this compound was calculated using the following equations:

*Cumulative intensity of one product I<sub>c</sub>*

*= sum (intensity of peaks with different simulation of one compound)*

*Total intensity of all products I<sub>all</sub>*

*= sum (intensity of peaks with different simulation of one compound)*

$$\text{normalized ratio } R = \frac{I_c}{I_{all}}$$

The analysis of products from CM reaction is listed as follows, and the results of the product ratio calculation are summarized in **Table S4**.

For analysis of EIS MS spectra of products from all entries, see the attached PDF file “ESI Analysis\_All Entries” as attached separately.

The following structures are the possible isomers of **cm-HH** and **cm-HHH**:

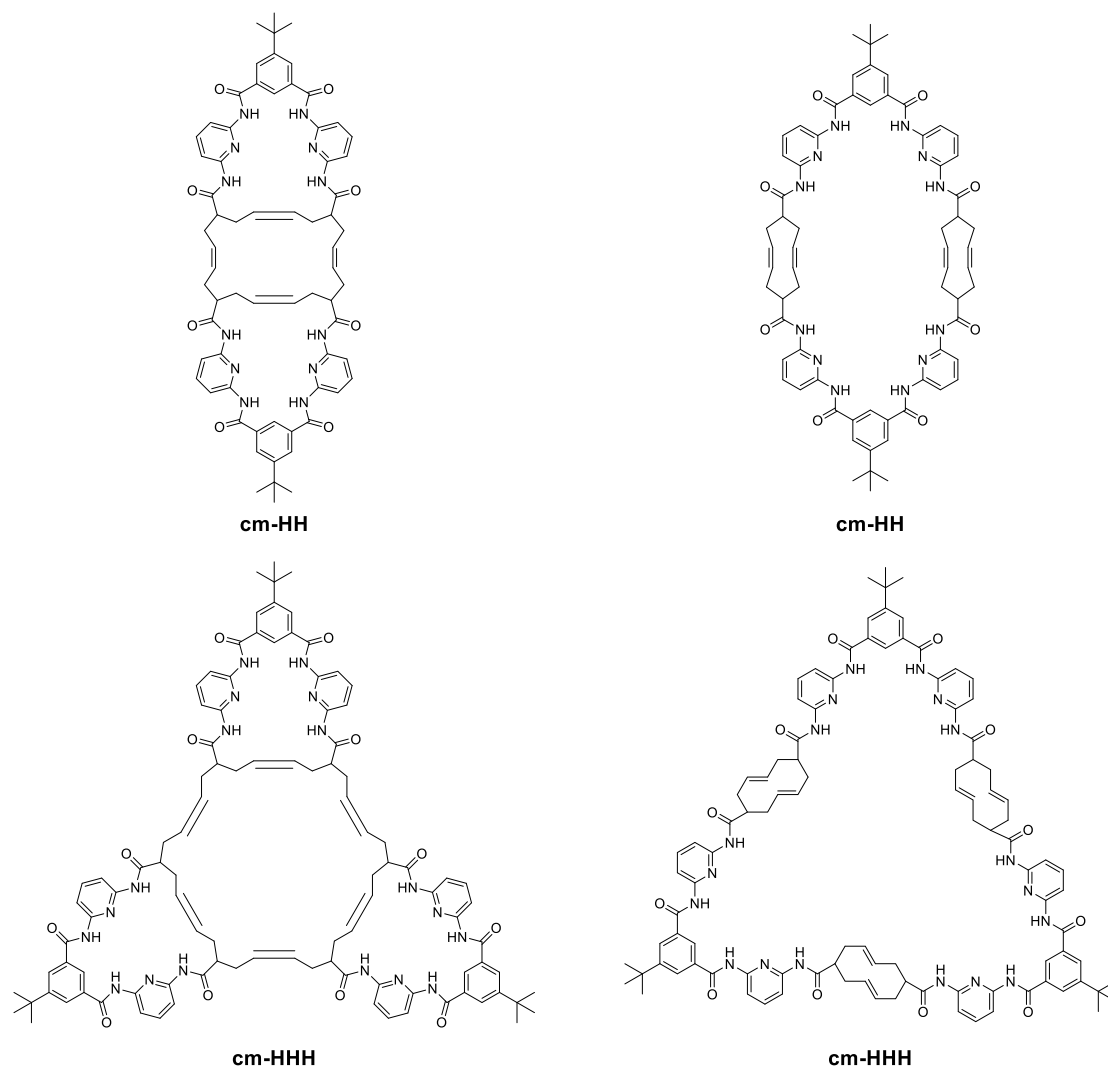


**Figure S2** the possible constitutional isomers of **cm-HH** and **cm-HHH**.

**Table S4** Relative intensity taken from ESI MS spectra and the calculated normalized ratio among products.

		Relative Intensity from ESI MS Spectra					
Entry	Exp.	cm-B	cm-H	cm-HH	cm-HHH	cm-HB	Sum
1	Tol_100°C_0.01M	0.51	197.5	12.74	0.5	3.5	214.75
2	Tol_50°C_0.01M	0.5	121.22	20.44	10.05	7.37	159.58
3	DCE_50°C_0.1M	0	111.23	3.22	0.5	11.47	126.42
4	MeOD_50°C_0.01M	0.12	106.62	21.84	11.96	2.63	143.17
5	DCE_50°C_0.1M_G2	0	202.45	4.59	0.68	4.9	212.62
6	PIB_50°C	2.35	114.48	9.89	4.12	10.28	141.12
		Normalized Ratio					
Entry	Exp.	cm-B	cm-H	cm-HH	cm-HHH	cm-HB	
1	Tol_100°C_0.01M	0.24%	91.97%	5.93%	0.23%	1.63%	
2	Tol_50°C_0.01M	0.31%	75.96%	12.81%	6.30%	4.62%	
3	DCE_50°C_0.1M	0.00%	87.98%	2.55%	0.40%	9.07%	
4	MeOD_50°C_0.01M	0.08%	74.47%	15.25%	8.35%	1.84%	
5	DCE_50°C_0.1M_G2	0.00%	95.22%	2.16%	0.32%	2.30%	
6	PIB_50°C	1.67%	81.12%	7.01%	2.92%	7.28%	

#### 4. Conversion Calculation by NMR Spectroscopy

To calculate the conversion of the cross-metathesis reactions, the integral of the residue vinylenic protons (at ~4.9 ppm in Tol-d<sub>8</sub> and ~ 5.2 ppm in CDCl<sub>3</sub>) of **B** was set to 1, then the integral of another vinylenic proton (at ~5.4 ppm in Tol-d<sub>8</sub> and ~ 5.6 ppm in CDCl<sub>3</sub>) of **B** was determined, followed by determination of vinylenic protons of products. The integral of vinylenic protons and the integral of vinylenic protons of products were summed up, respectively, and the ratio between these two values is the ratio between unreacted starting barbiturate and all products. As the conversion of **H** was almost quantitative, this ratio can be used to calculate the total conversion of all vinylene groups and further the overall conversion as follows:

$$\begin{aligned} & \text{Integral of residue Ba vinylenic protons } I_{\text{residue}} \\ &= \text{sum (integral of peaks at } \sim 4.9 \text{ ppm in Tol} \\ &\quad \text{– d8 and } \sim 5.2 \text{ ppm in CDCl}_3 \text{ )} \\ & \text{Integral of all products vinylenic protons } I_{\text{product}} \\ &= \text{sum (integral of new vinylenic peaks)} \end{aligned}$$

$$\text{conversion} = \frac{I_{\text{residue}}}{I_{\text{product}}}$$

**Table S5** Calculation of conversions of all cross-metathesis reactions by NMR spectroscopy.

Entry	T /°C	Solvent	Conc. /M	Cat.	I <sub>residue</sub>	I <sub>product</sub>	Conv. ene
(1)	100	Tol-d <sub>8</sub>	0.01	G3	0	-	100 %.
(2)	50	Tol-d <sub>8</sub>	0.01	G3	2.21	18.59	89.4 %
(3)	50	DCE	0.1	G3	1	8.5	89.5 %
(4)	50	MeOD	0.01	G3	11.22	41.77	78.8 %
(5)	50	DCE	0.1	G2	1	41.33	97.6 %
(6)	50	PIB	-	G3	1	36.74	97.3 %

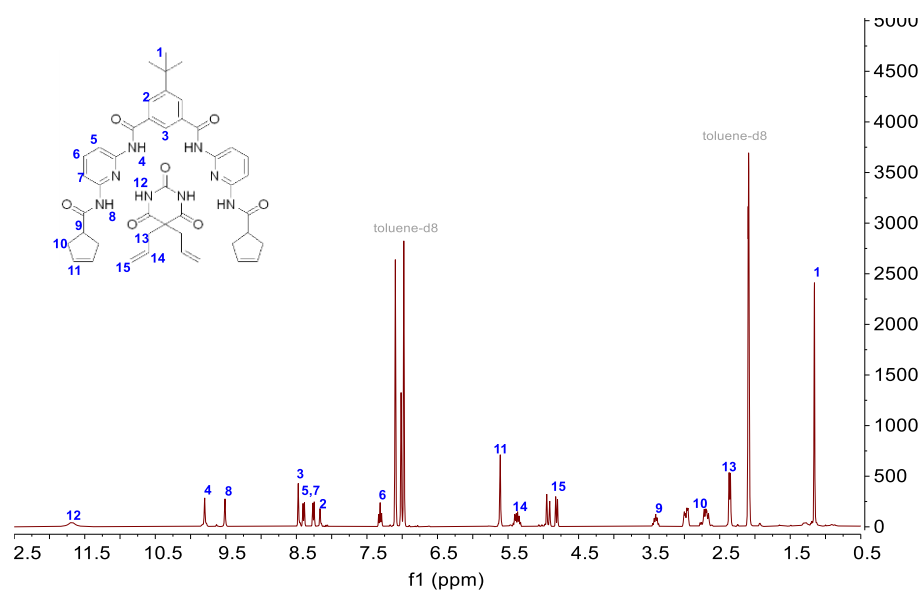


**Figure S3**  $^1\text{H}$  NMR spectrum of **H-B** 1:1 without catalyst in  $\text{Tol-d}_8$ .

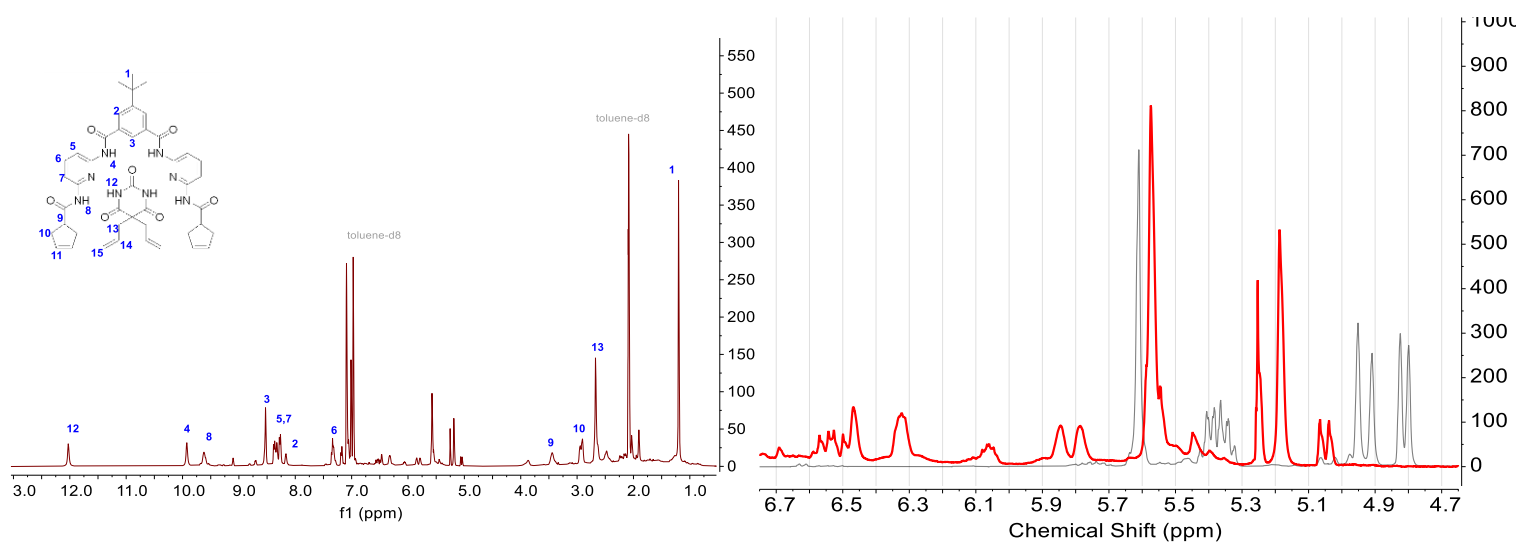


**Figure S4**  $^1\text{H}$  NMR spectrum of the reaction mixture from **Entry 1** in  $\text{Tol-d}_8$  and zoom-in of vinylene region with **H-B** 1:1 without catalyst as the background (the grey spectrum).

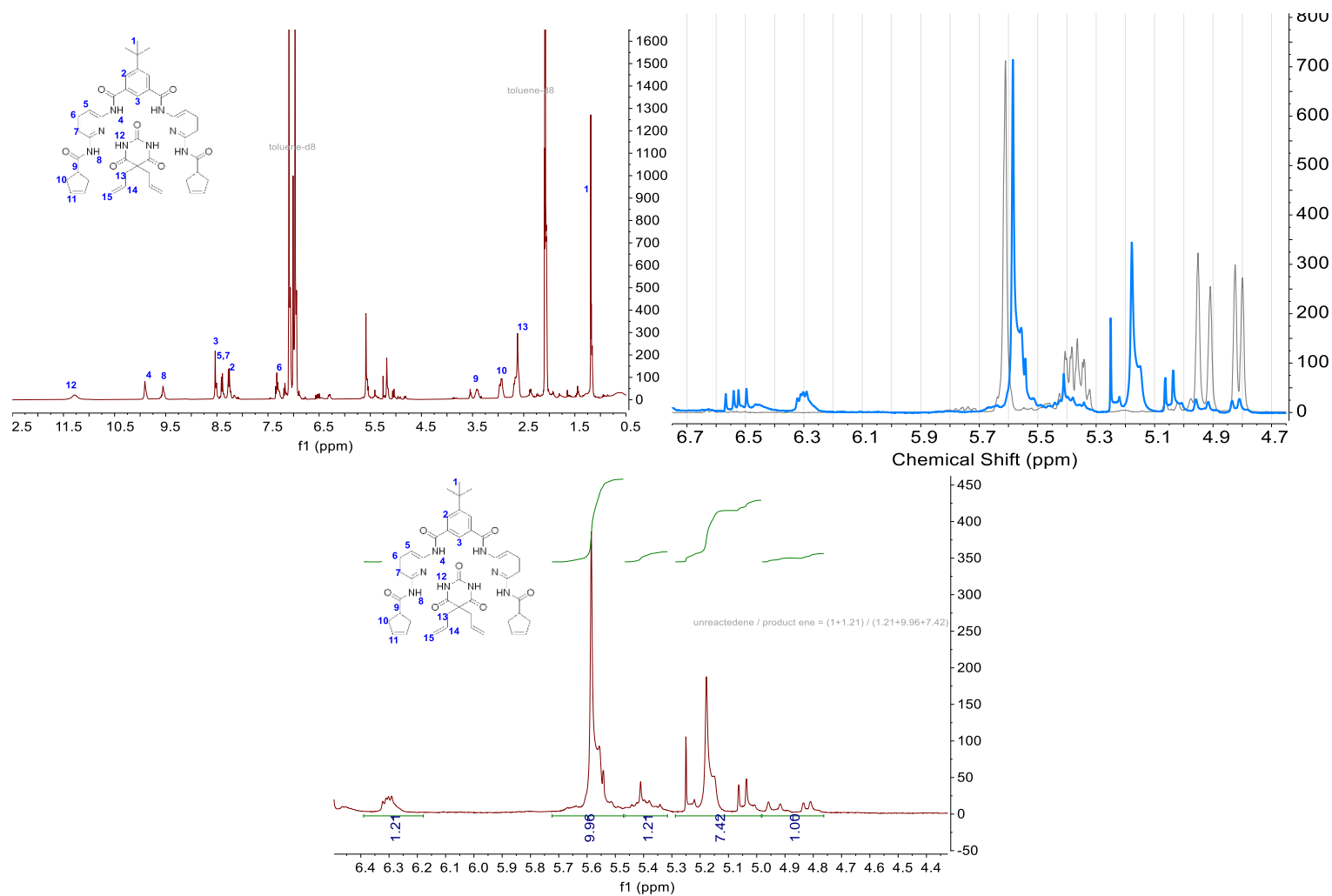


**Figure S5**  $^1\text{H}$  NMR spectrum of a) the reaction mixture from **Entry 2** in  $\text{Tol-d}_8$ , b) zoom-in of vinylene region with **H-B** 1:1 without catalyst as the background (the grey spectrum), and c) the integral of relevant protons for conversion calculation.



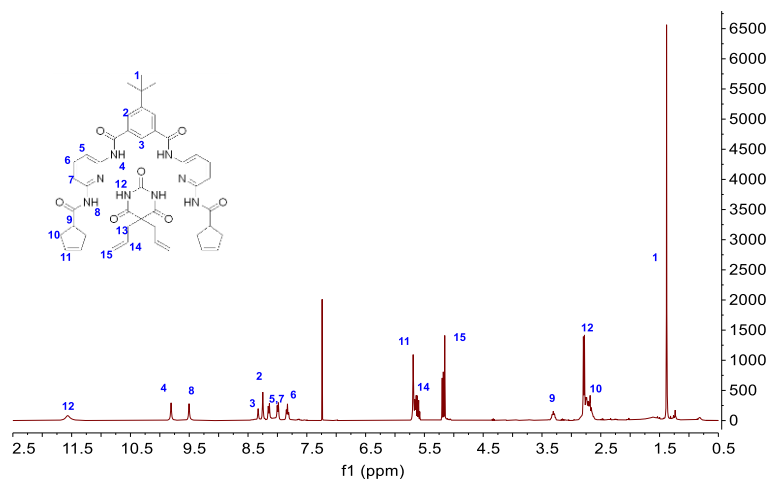


**Figure S6**  $^1\text{H}$  NMR spectrum of **H-B** 1:1 without catalyst in  $\text{CDCl}_3$ .

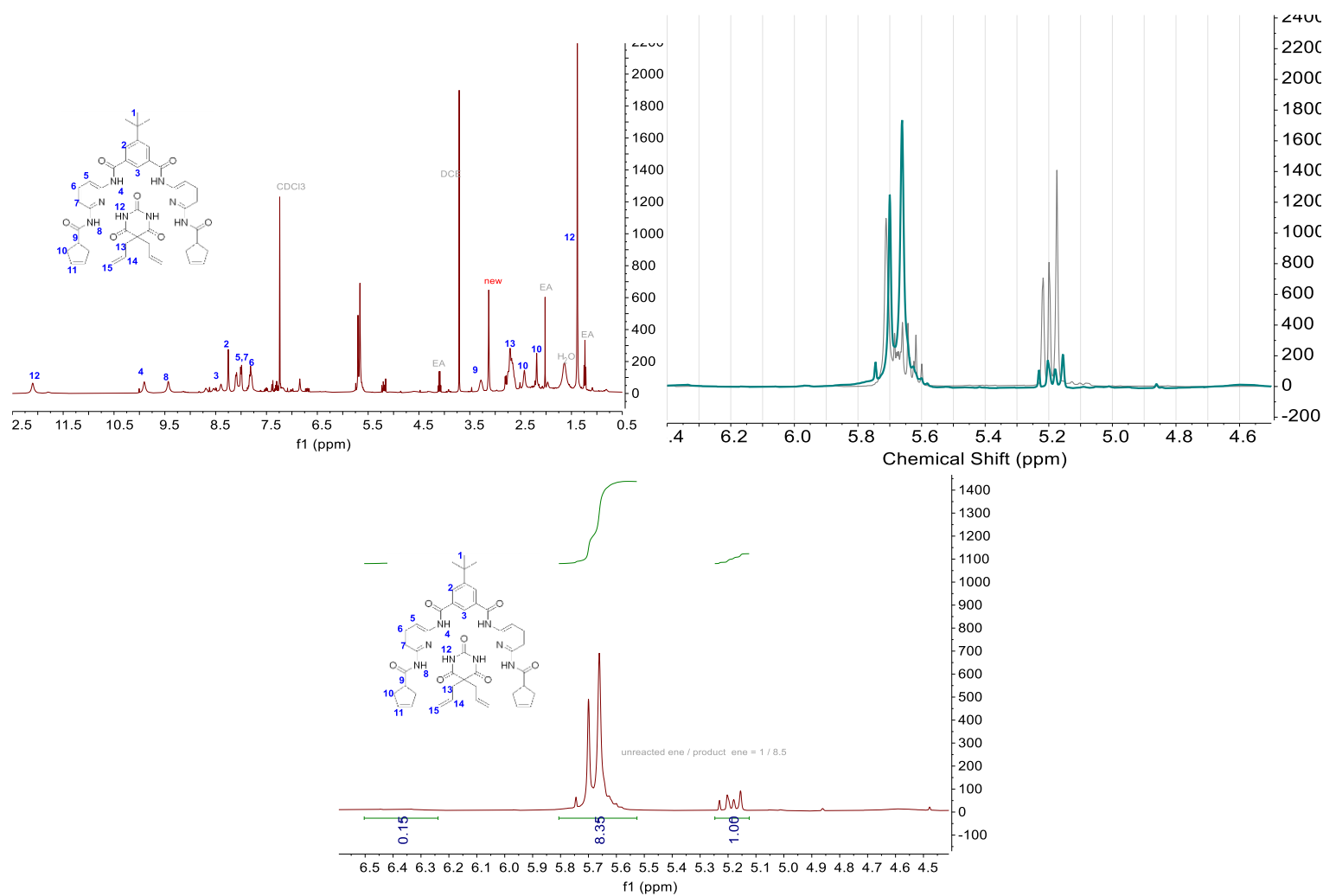


**Figure S7**  $^1\text{H}$  NMR spectrum of a) the reaction mixture from **Entry 3** in  $\text{CDCl}_3$ , b) zoom-in of vinylene region with **H-B** 1:1 without catalyst as the background (the grey spectrum), and c) the integral of relevant protons for conversion calculation.

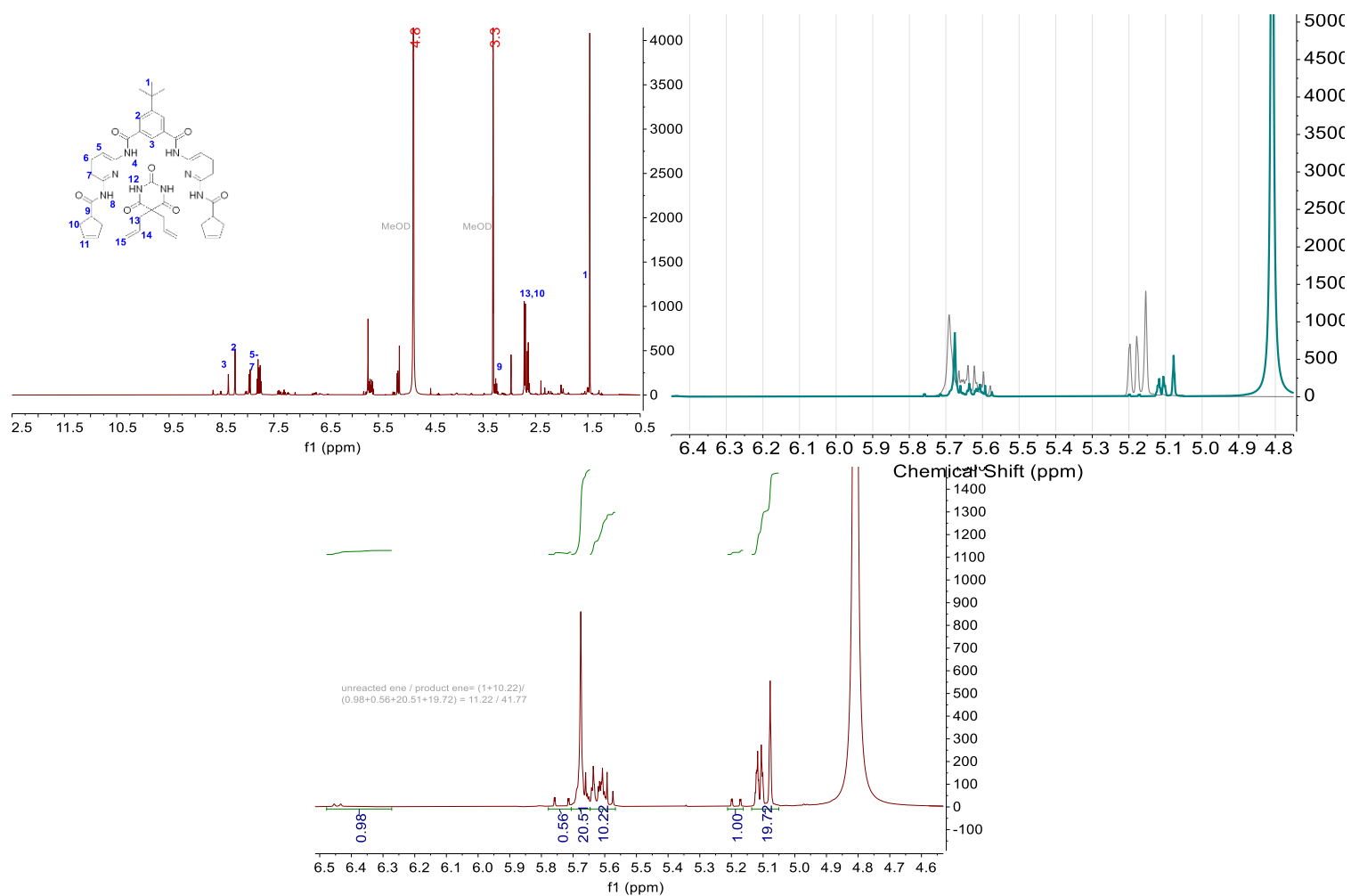


**Figure S8**  $^1\text{H}$  NMR spectrum of a) the reaction mixture from **Entry 4** in MeOD, b) zoom-in of vinylene region with **H-B** 1:1 without catalyst as the background (the grey spectrum), and c) the integral of relevant protons for conversion calculation.

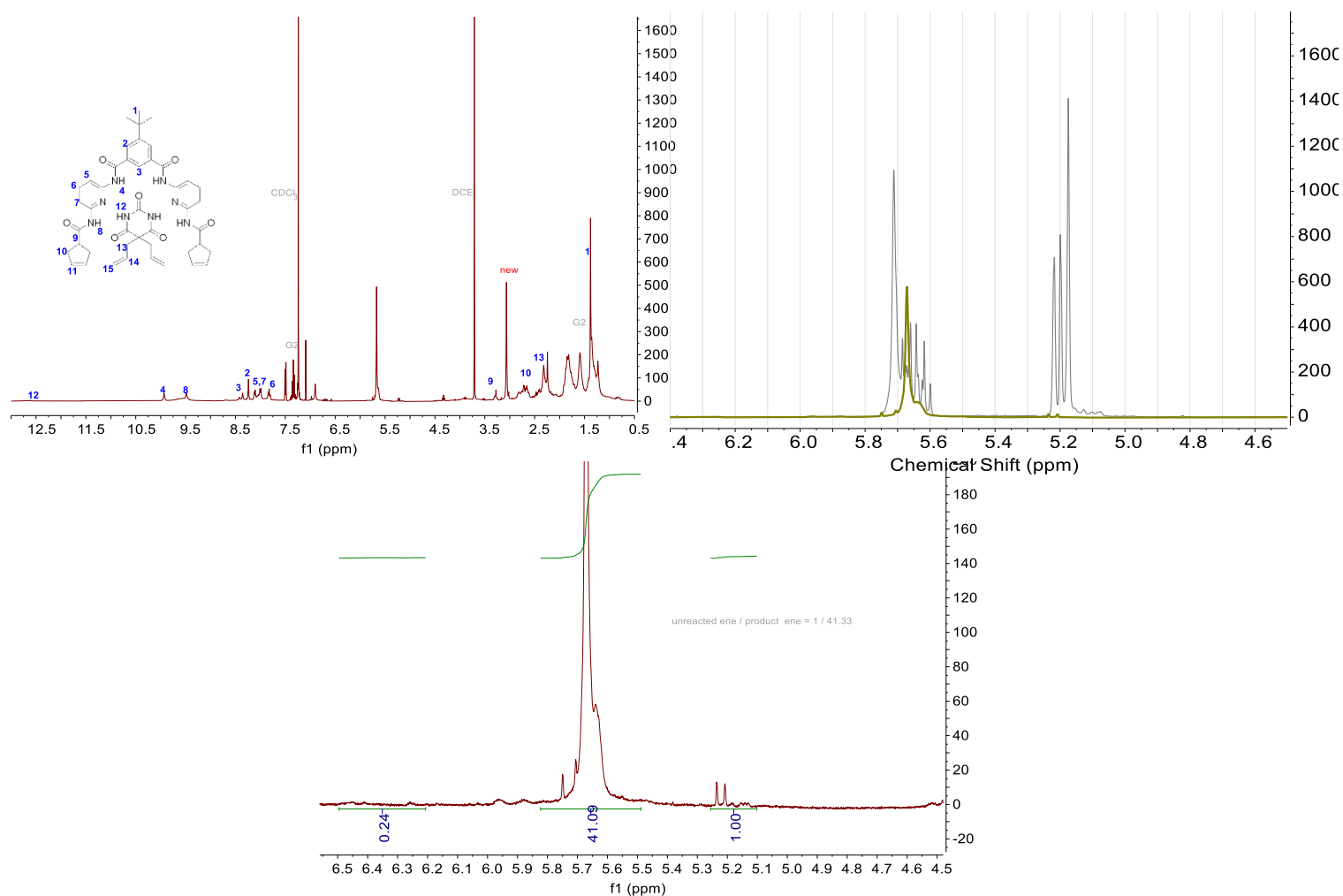


**Figure S9**  $^1\text{H}$  NMR spectrum of a) the reaction mixture from **Entry 5** in  $\text{CDCl}_3$ , b) zoom-in of vinylene region with **H-B** 1:1 without catalyst as the background (the grey spectrum), and c) the integral of relevant protons for conversion calculation.

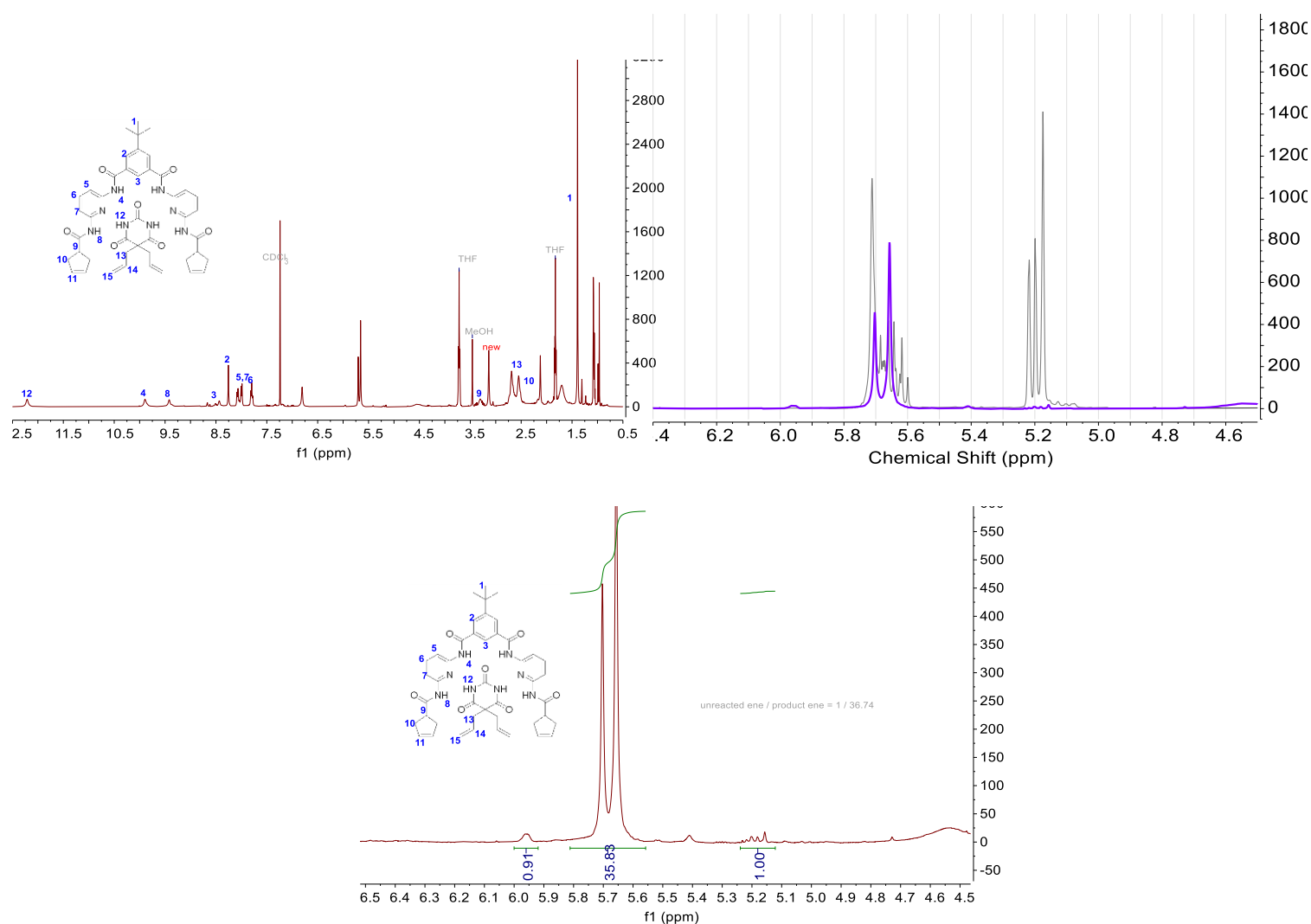


**Figure S10**  $^1\text{H}$  NMR spectrum of a) the reaction mixture from **Entry 6** in  $\text{CDCl}_3$ , b) zoom-in of vinylene region with **H-B** 1:1 without catalyst as the background (the grey spectrum), and c) the integral of relevant protons for conversion calculation.

## 5. NMR Spectra of Compounds

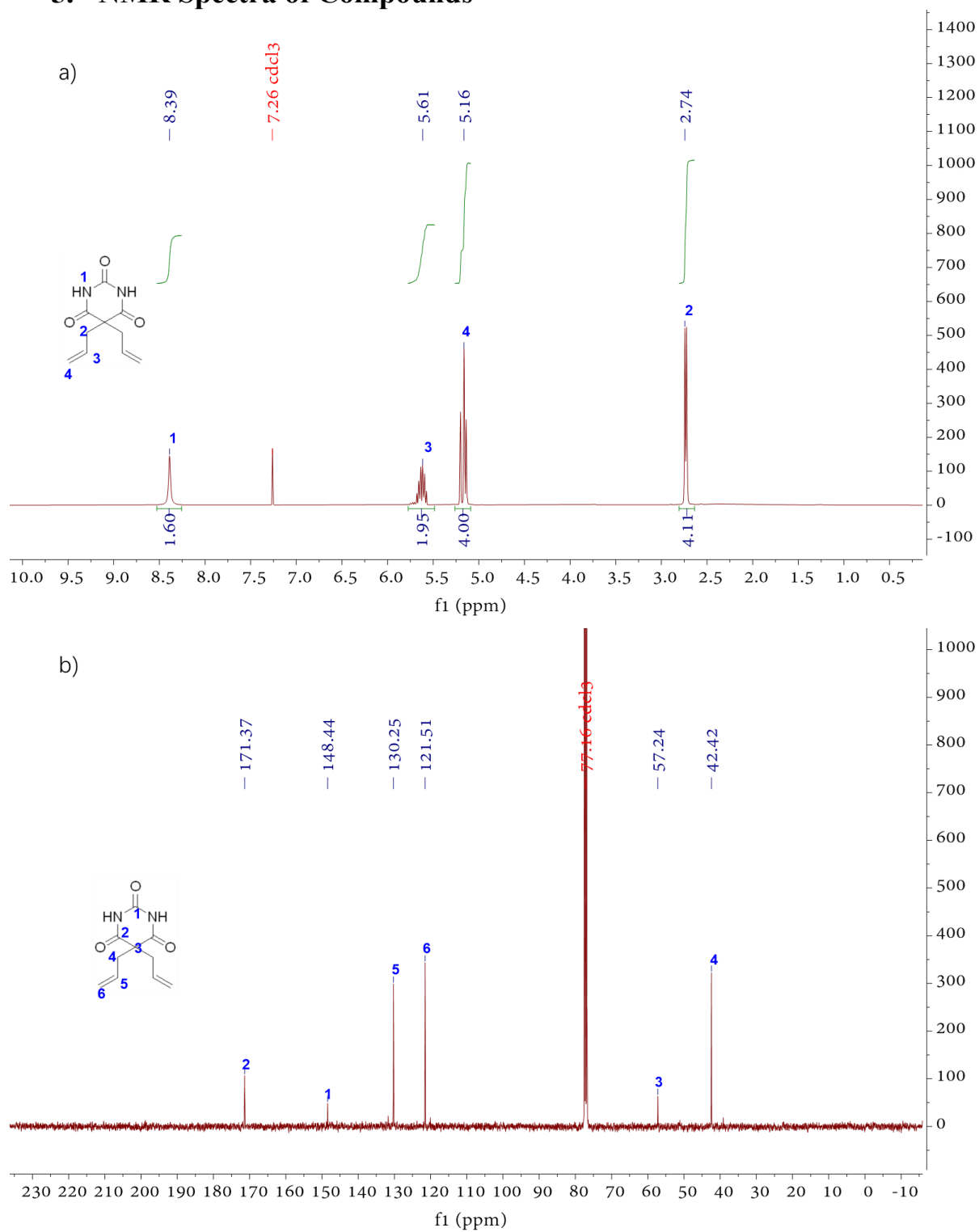


**Figure S11** a)  $^1\text{H}$  NMR and b)  $^{13}\text{C}$  NMR spectrum of **B** in CDCl<sub>3</sub>.

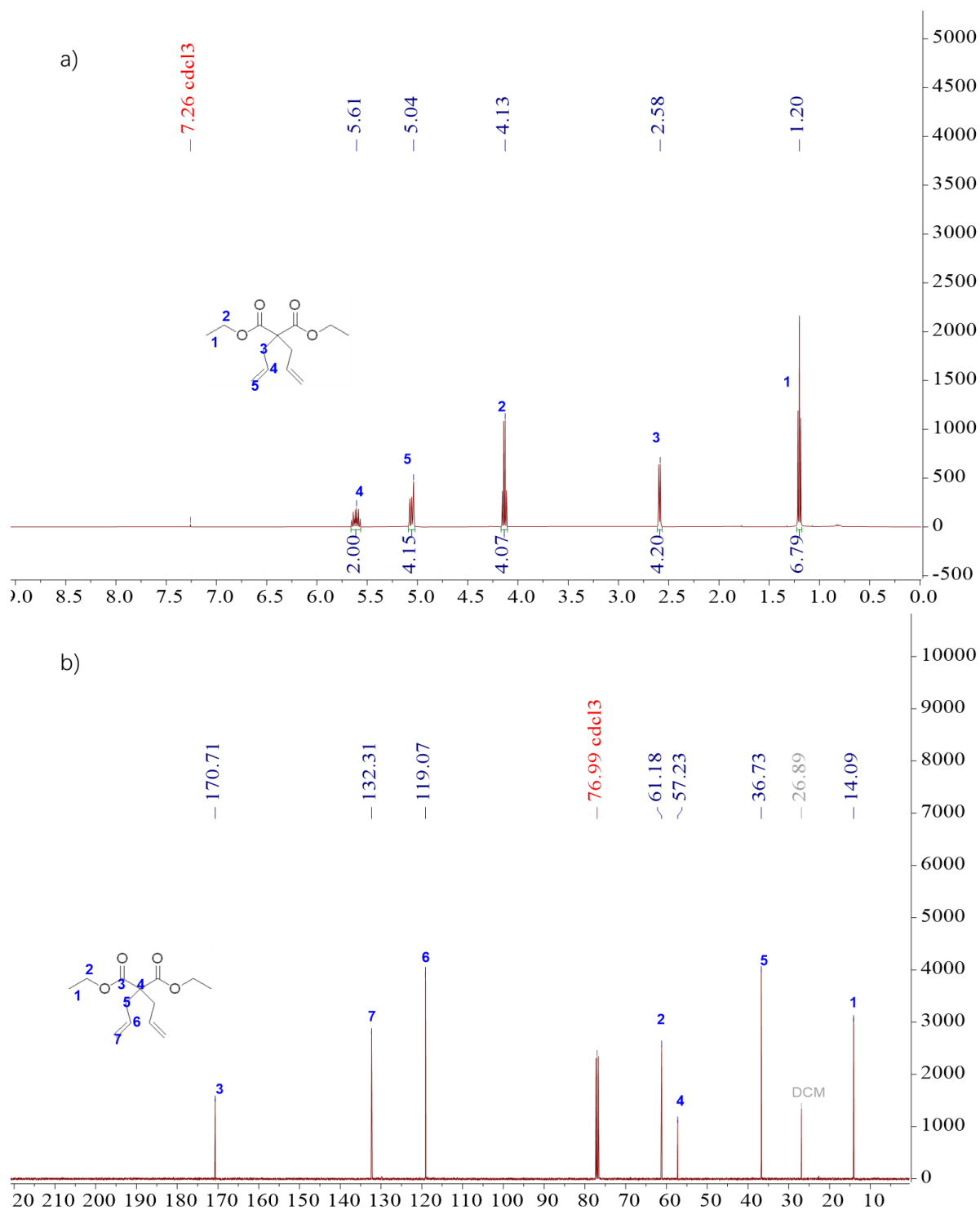


**Figure S12** a)  $^1\text{H}$  NMR and b)  $^{13}\text{C}$  NMR spectrum of **2** in CDCl<sub>3</sub>.

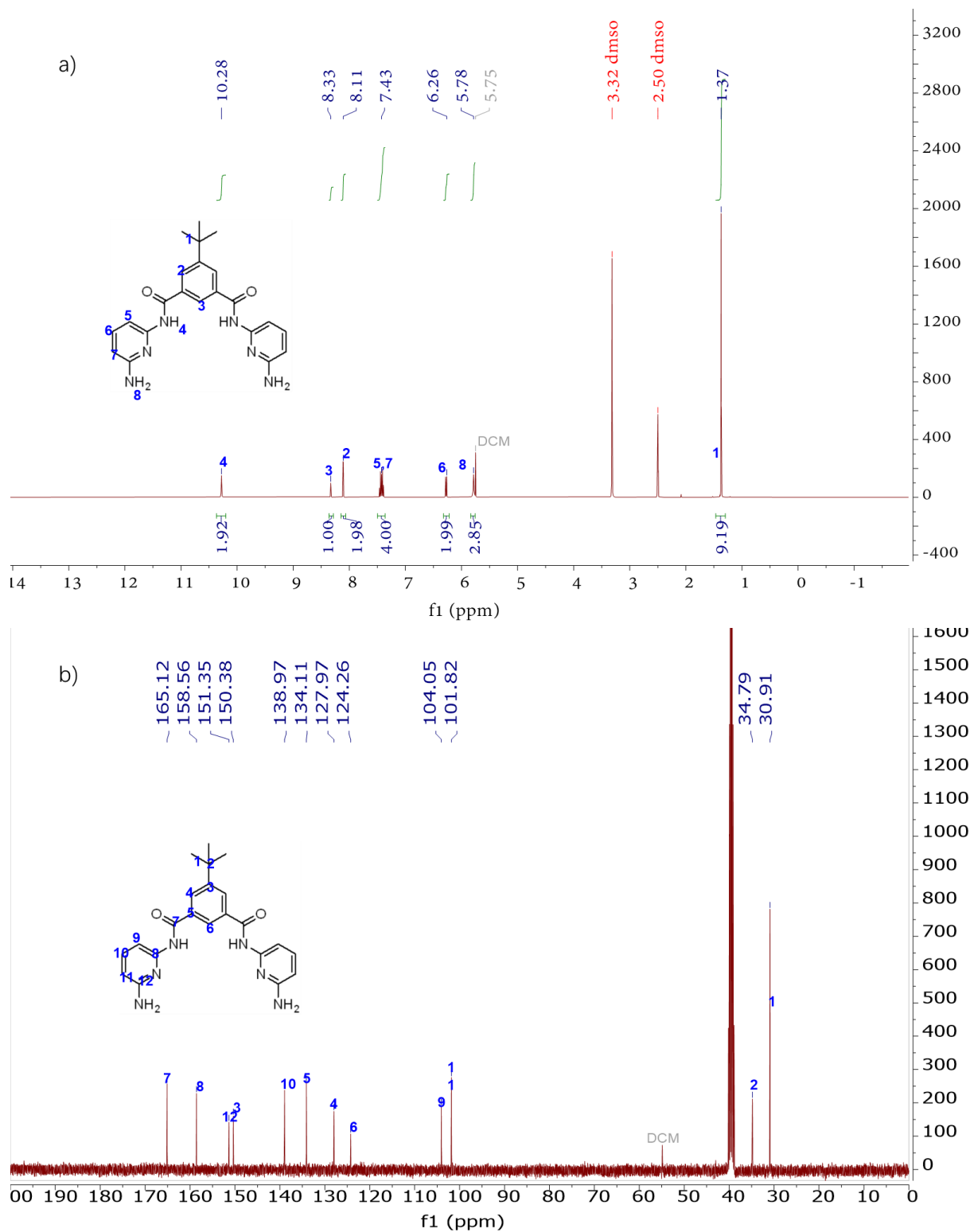


**Figure S13** a)  $^1\text{H}$  NMR and b)  $^{13}\text{C}$  NMR spectrum of **4** in DMSO- $d_6$ .

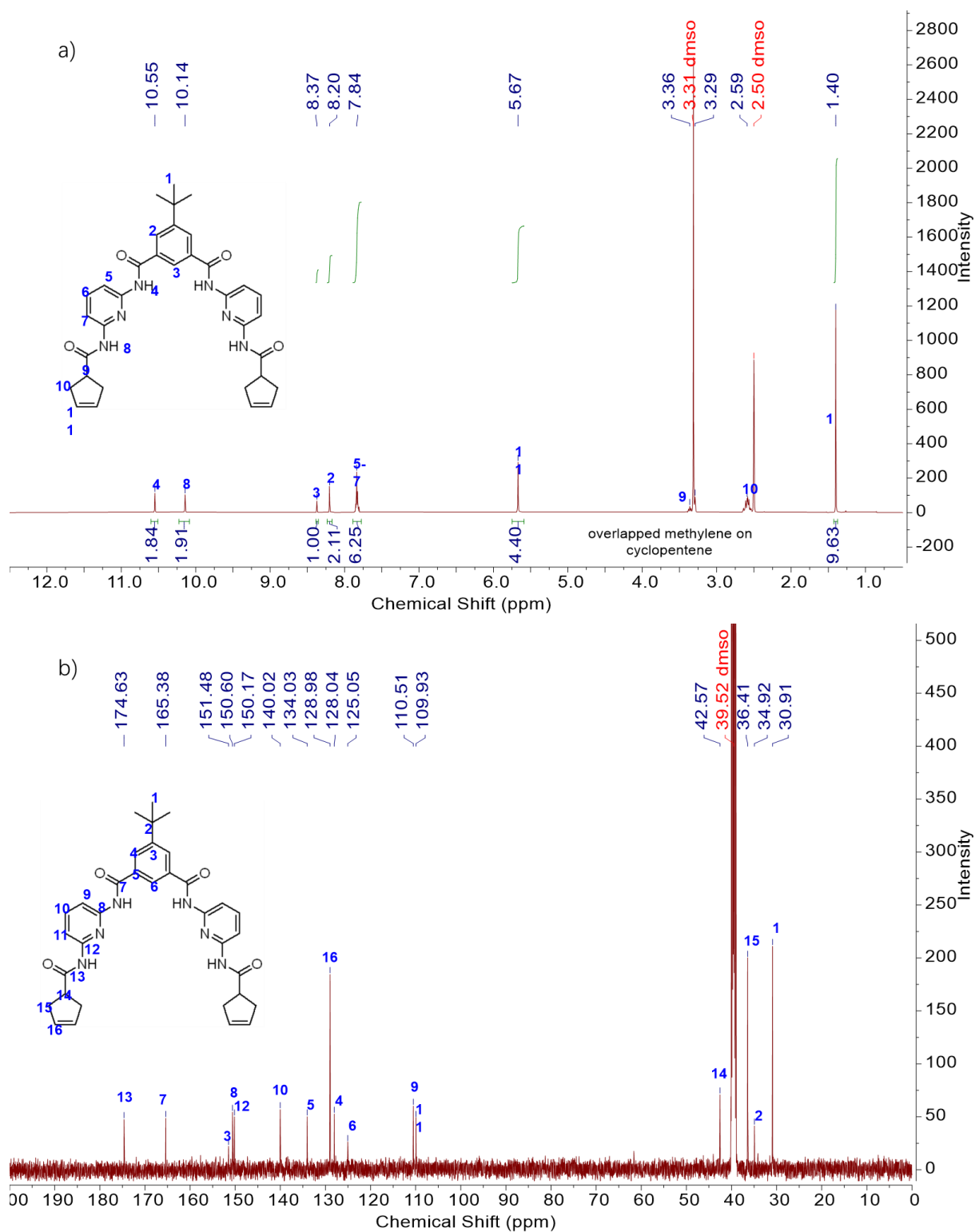


**Figure S14** a)  $^1\text{H}$  NMR and b)  $^{13}\text{C}$  NMR spectrum of **H** in DMSO- $d_6$ .



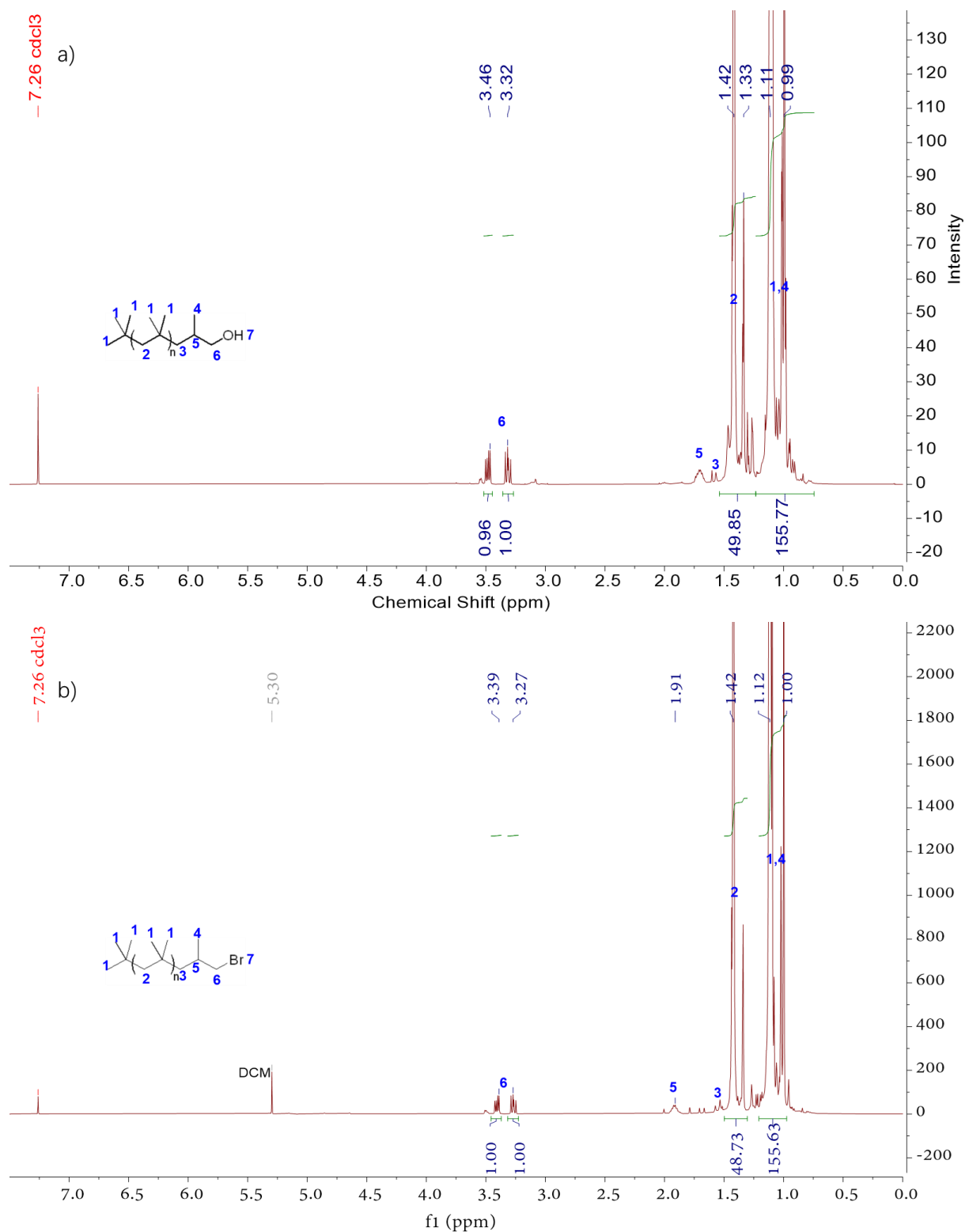


Figure S15 <sup>1</sup>H NMR spectrum of a) PIB-OH and b) PIB in CDCl<sub>3</sub>.

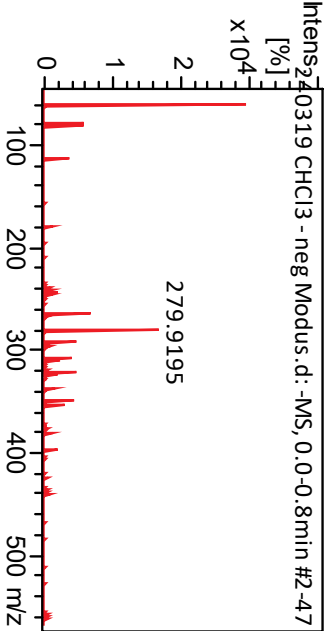
---

## 6. Reference

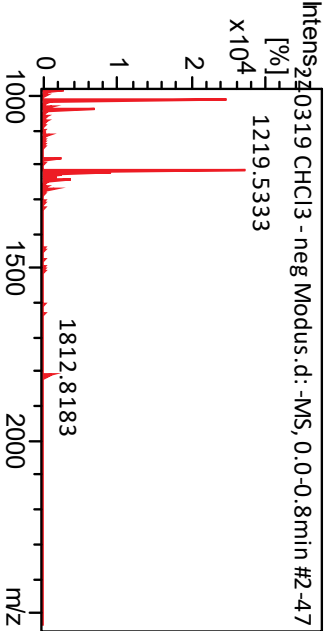
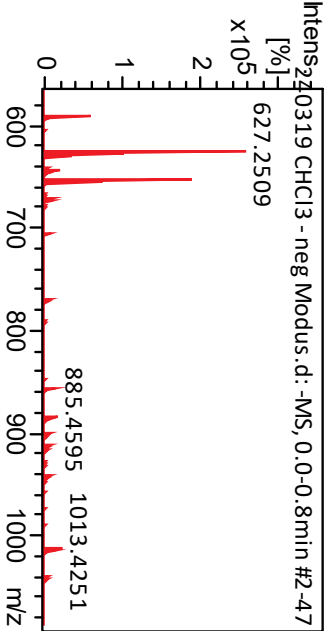
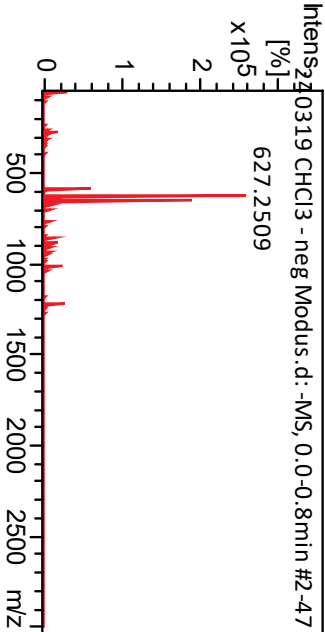
- [1] C. Li, P. Hilgeroth, N. Hasan, D. Ströhl, J. Kressler, W. H. Binder, *International Journal of Molecular Sciences* **2021**, 22, 12679.
- [2] P. C. Srivastava, A. P. Callahan, E. B. Cunningham, F. F. Knapp, Jr., *Journal of Medicinal Chemistry* **1983**, 26, 742-746.
- [3] a) Mohammad, R. McDonald, Neil, *European Journal of Organic Chemistry* **2004**, 2004, 173-182; b) S. Lettieri, P. Manesiotis, M. Slann, D. W. Lewis, A. J. Hall, *Reactive and Functional Polymers* **2021**, 167, 105031.
- [4] H. Rupp, D. Döhler, P. Hilgeroth, N. Mahmood, M. Beiner, W. H. Binder, *Macromolecular Rapid Communications* **2019**, 40, 1900467.
- [5] R. Appel, *Angewandte Chemie International Edition in English* **1975**, 14, 801-811.
- [6] a) P. Thordarson, *Chemical Society Reviews* **2011**, 40, 1305-1323; b) D. Brynn Hibbert, P. Thordarson, *Chemical Communications* **2016**, 52, 12792-12805.

# ESI MS spectrum for products from Entry 1

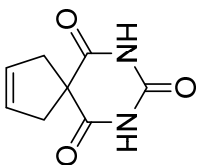
Selected range



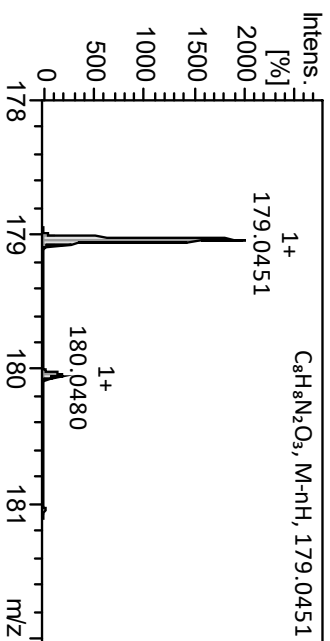
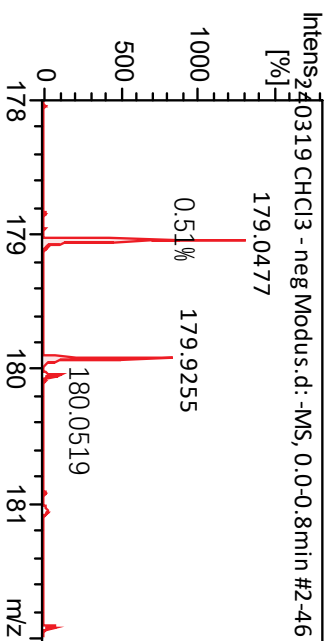
All range



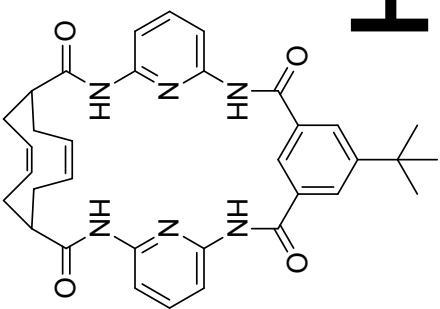
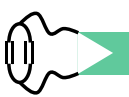
# cm-B



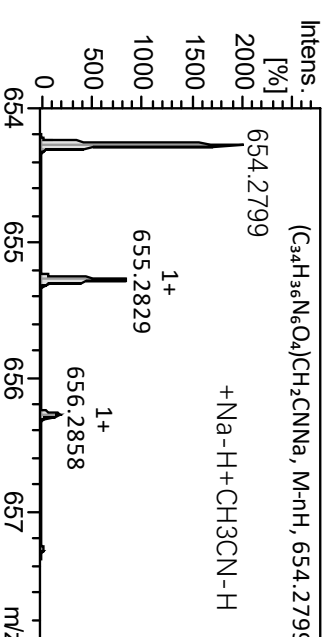
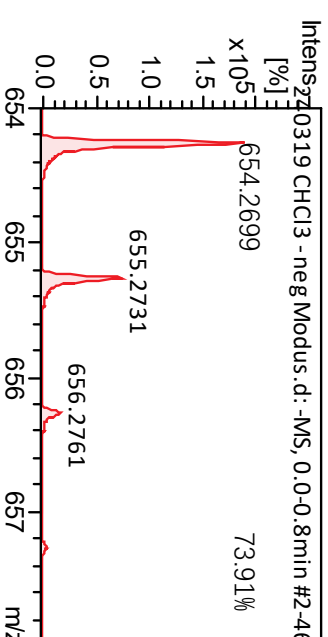
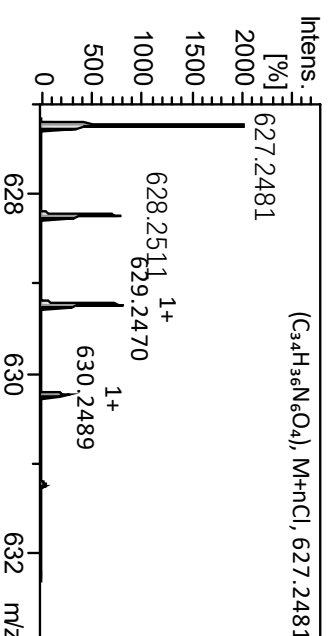
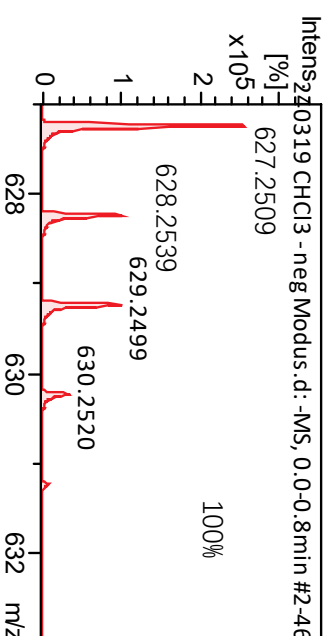
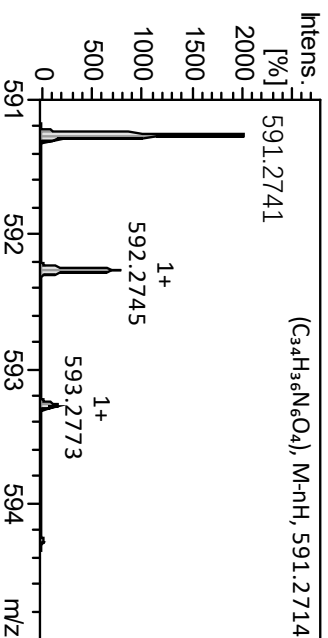
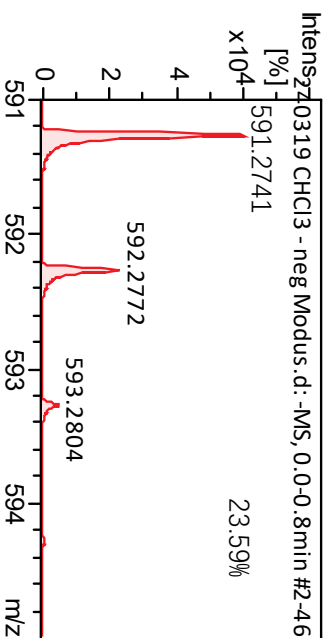
Chemical Formula: C<sub>8</sub>H<sub>8</sub>N<sub>2</sub>O<sub>3</sub>  
Molecular Weight: 180.16



# cm-H



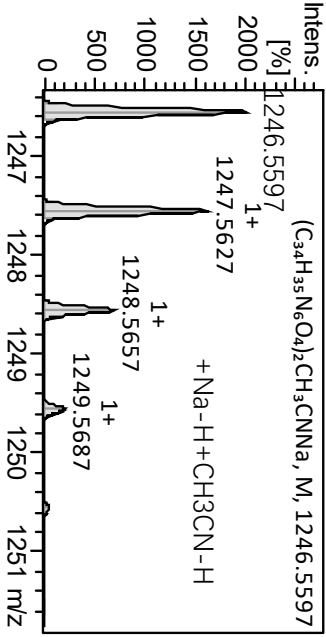
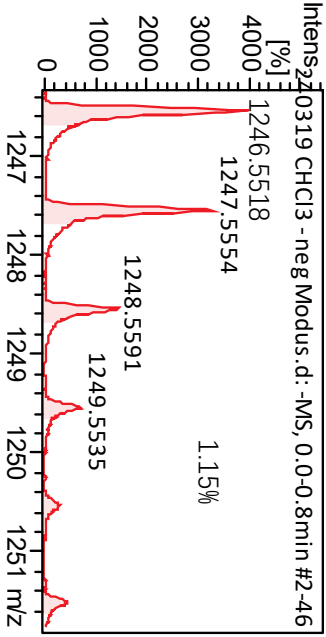
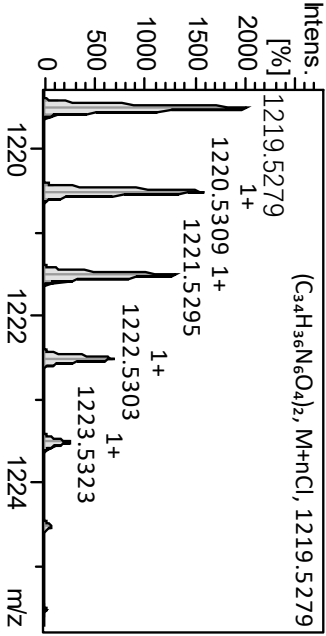
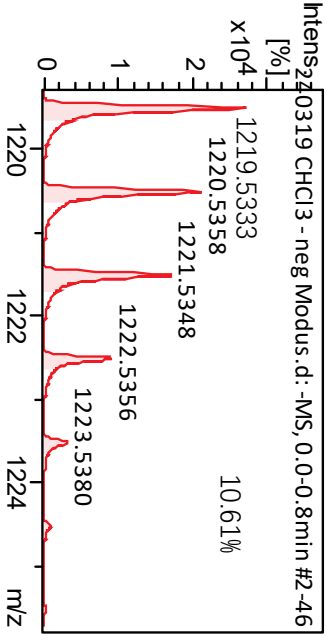
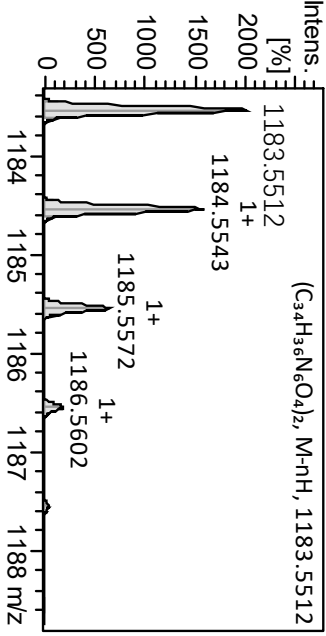
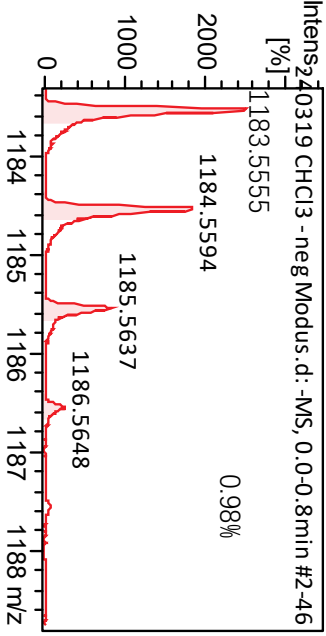
Chemical Formula:  $C_{34}H_{36}N_6O_4$   
Molecular Weight: 592.70



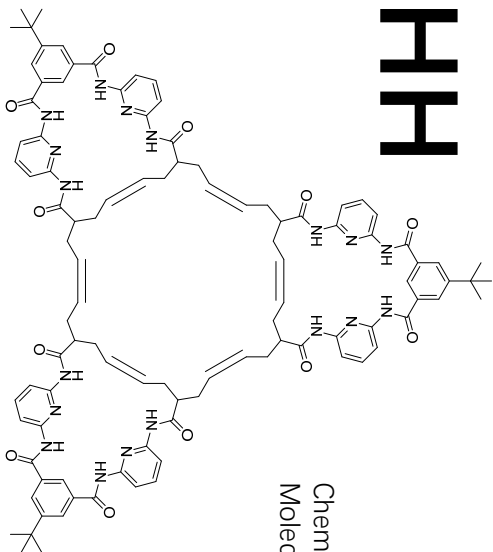
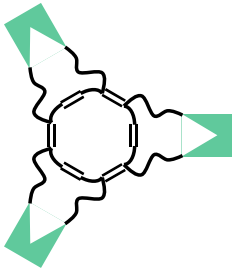
# cm-HH



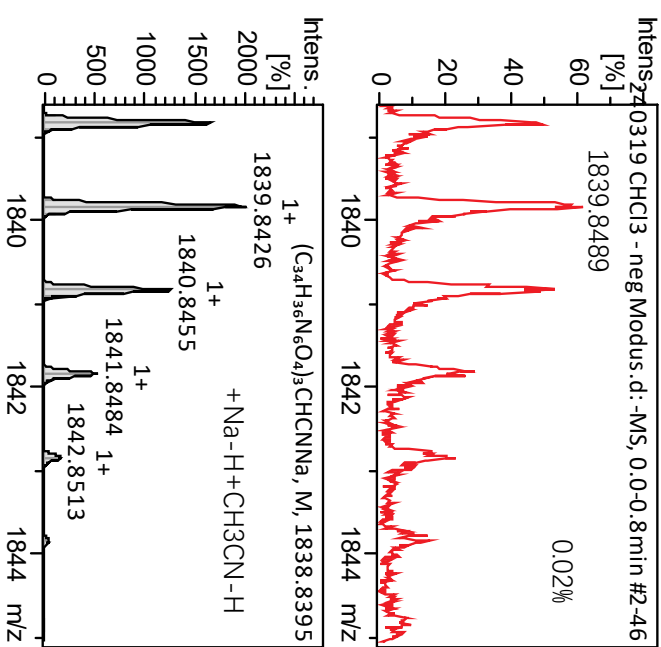
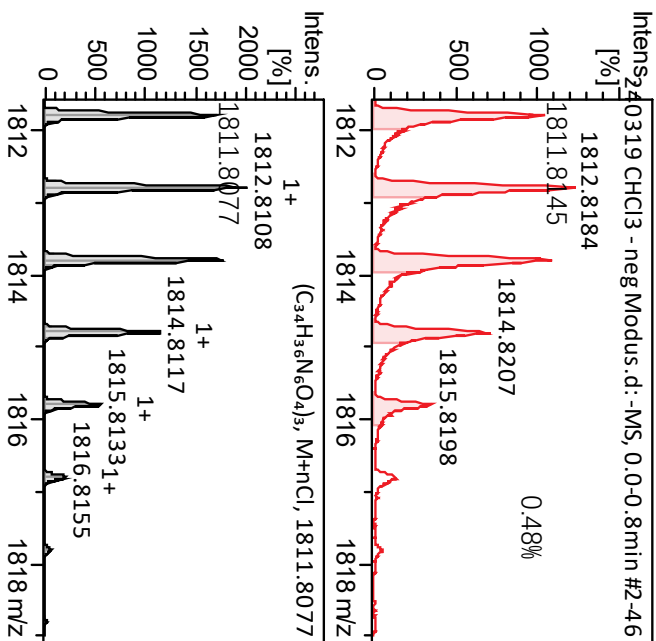
Chemical Formula: C<sub>68</sub>H<sub>72</sub>N<sub>12</sub>O<sub>8</sub>  
Molecular Weight: 1185.40



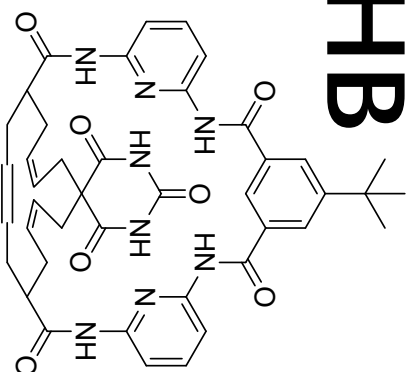
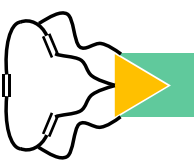
# cm-HHH



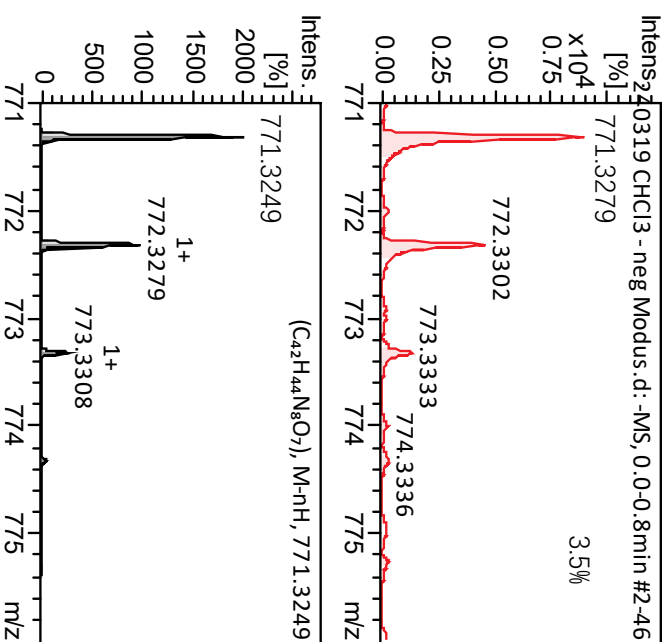
Chemical Formula:  $(C_{34}H_{36}N_6O_4)_3$   
Molecular Weight:  $592.70 \times 3 = 1778.07$



# cm-HB

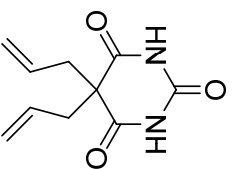


Chemical Formula: C<sub>42</sub>H<sub>44</sub>N<sub>8</sub>O<sub>7</sub>  
Molecular Weight: 772.86



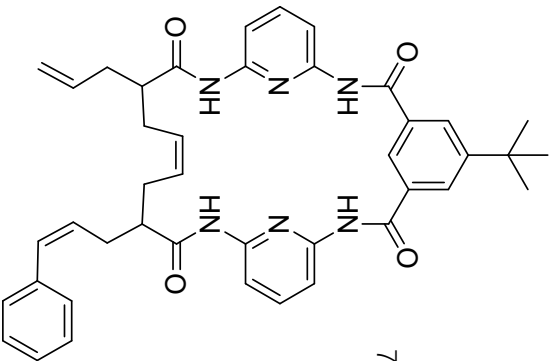
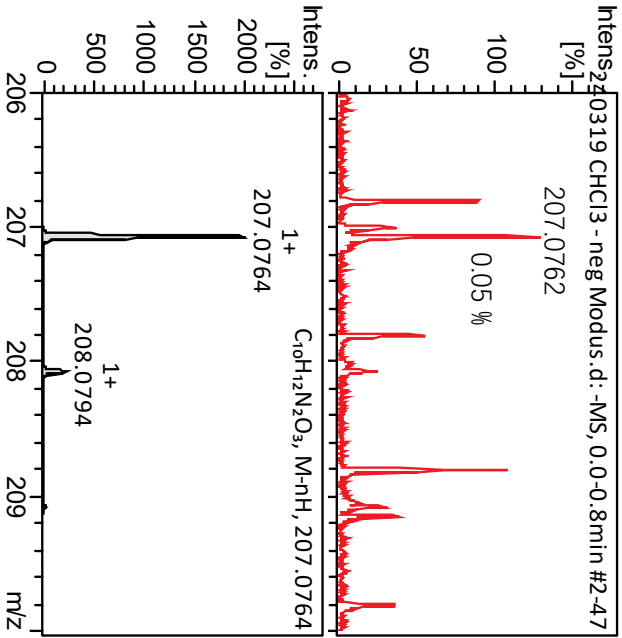


# Intermediates and Starting Materials



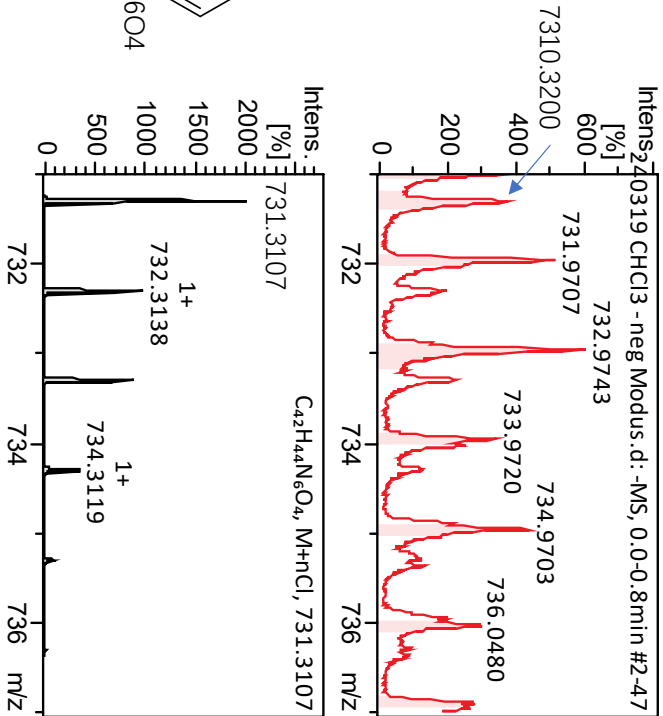
Chemical Formula:  $C_{10}H_{12}N_2$   
Exact Mass: 208.08

**Ba**



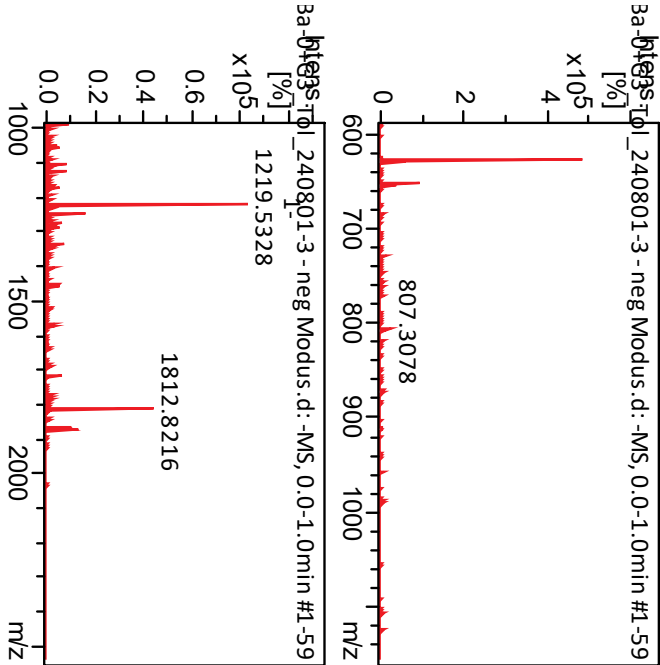
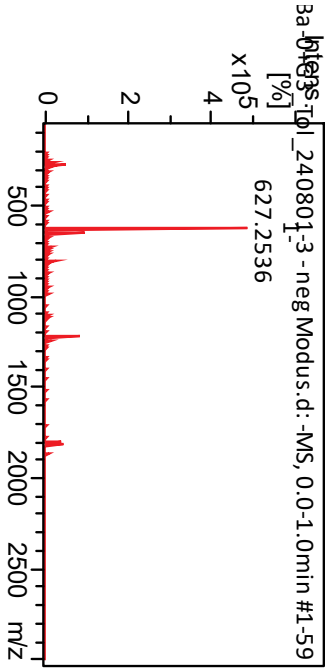
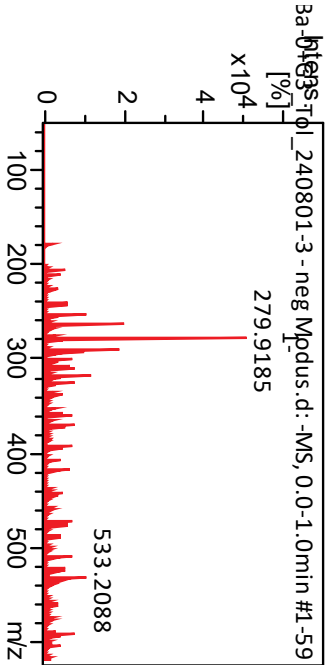
Chemical Formula:  $C_{42}H_{44}N_6O_4$   
Exact Mass: 696.34

**Int-H1**

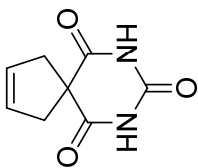


# ESI MS spectrum for products from Entry 2

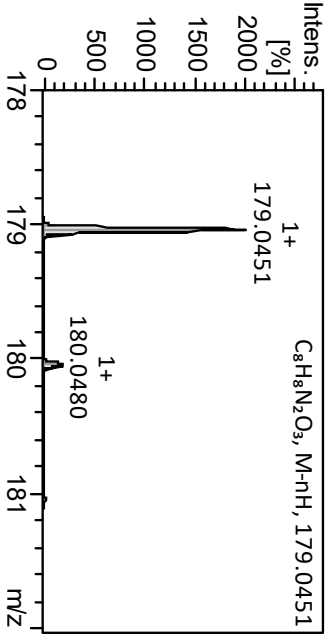
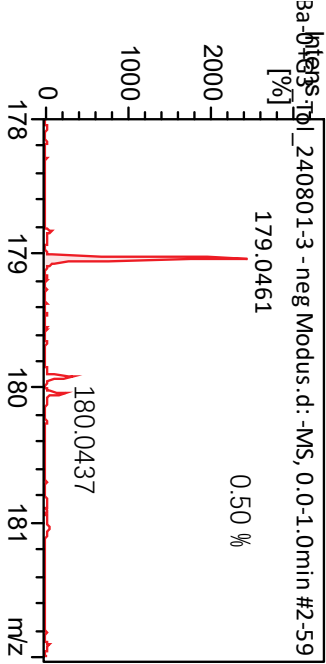
Selected range



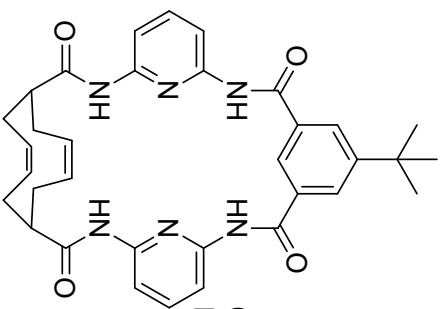
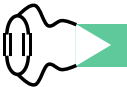
# cm-B



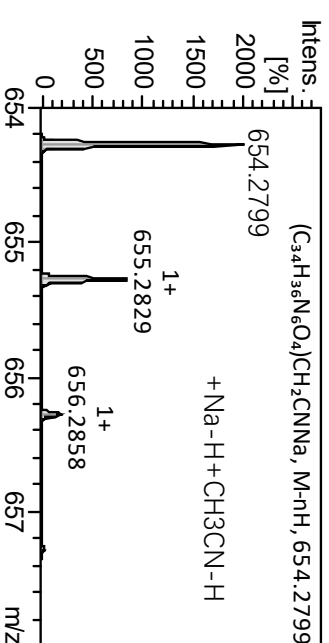
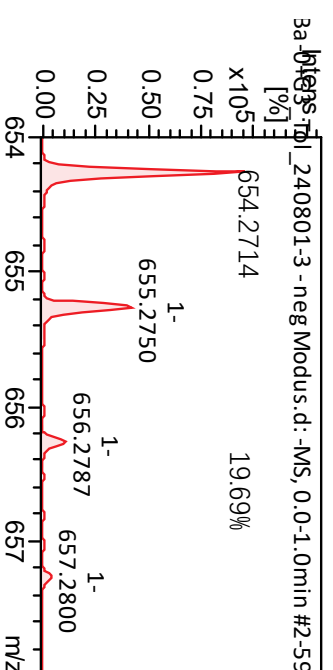
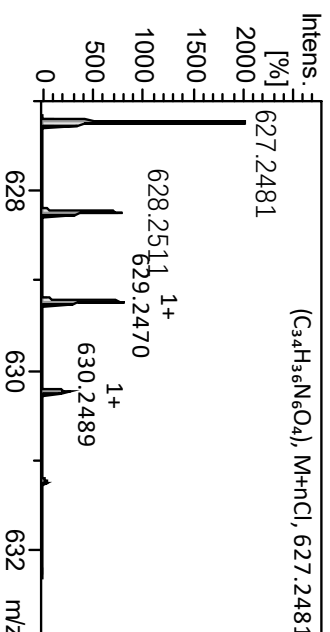
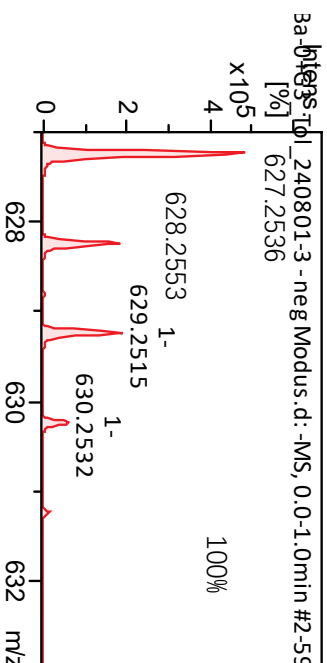
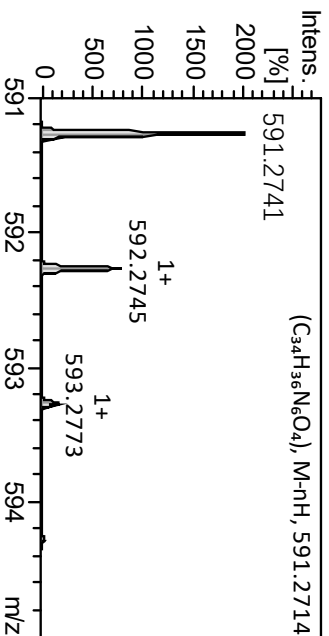
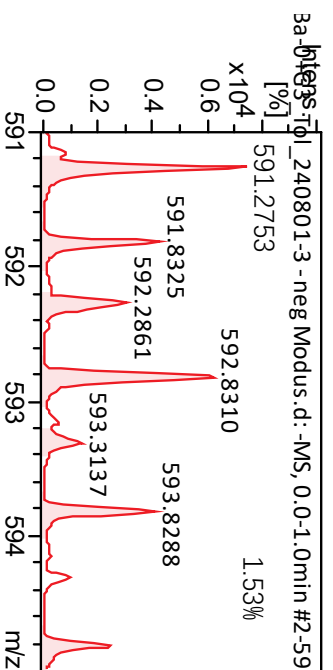
Chemical Formula: C<sub>8</sub>H<sub>8</sub>N<sub>2</sub>O<sub>3</sub>  
Molecular Weight: 180.16



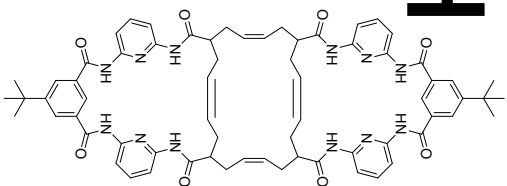
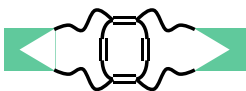
# cm-H



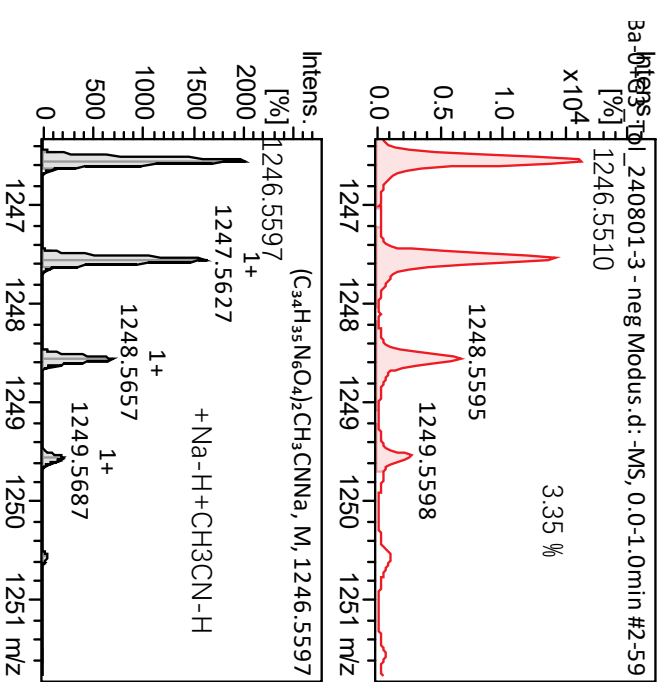
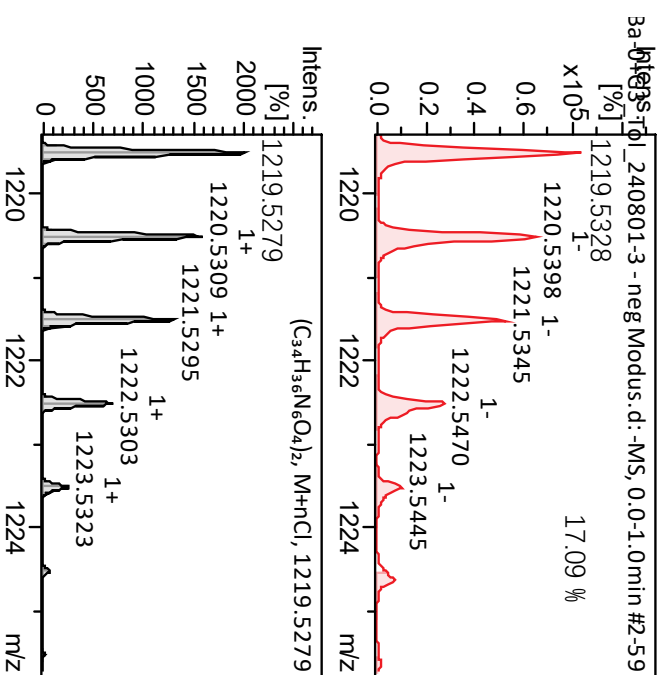
Chemical Formula:  $C_{34}H_{36}N_6O_4$   
Molecular Weight: 592.70



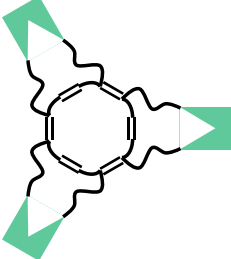
# cm-HH



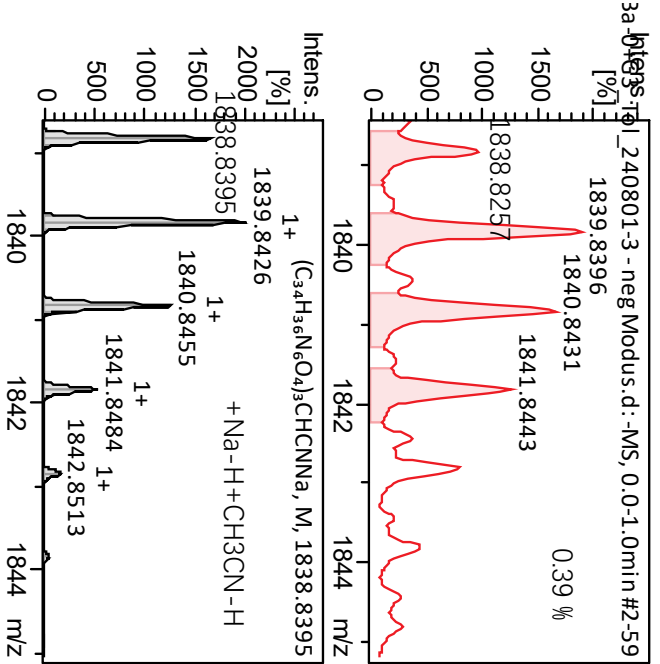
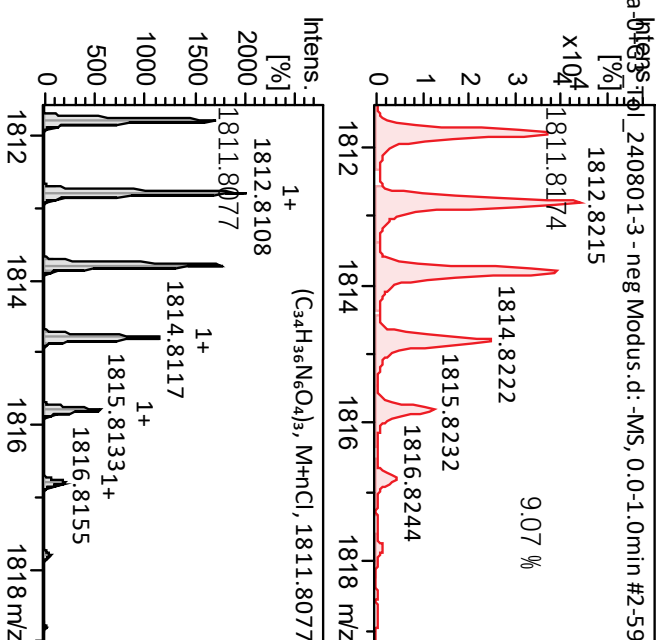
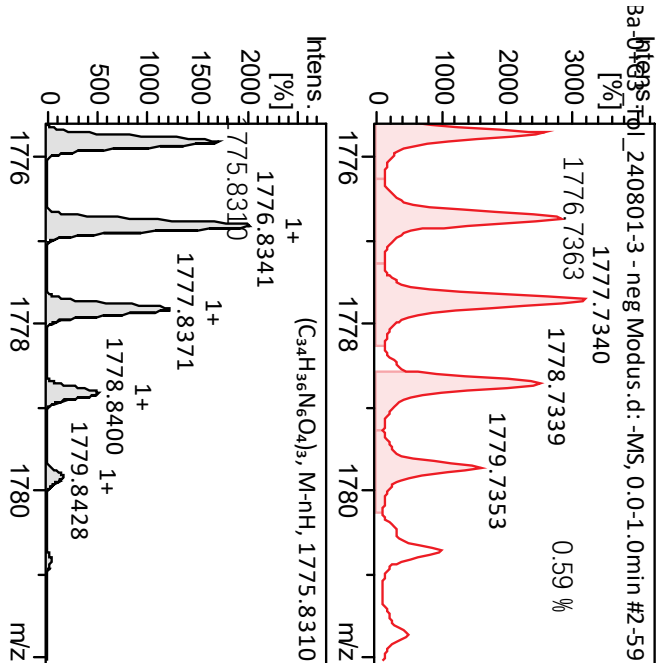
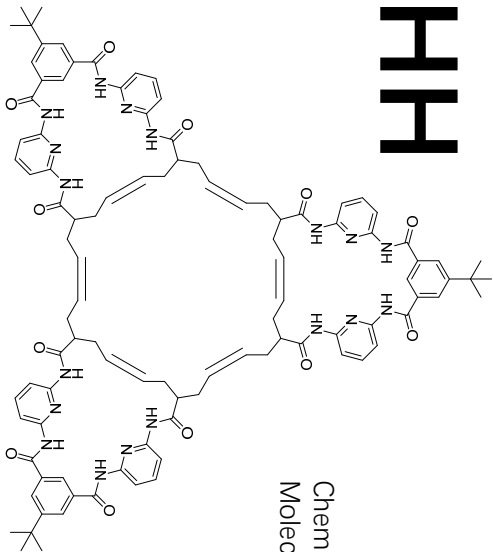
Chemical Formula: C<sub>68</sub>H<sub>72</sub>N<sub>12</sub>O<sub>8</sub>  
Molecular Weight: 1185.40



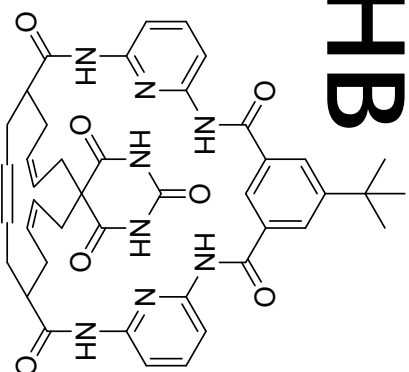
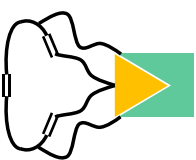
# cm-HHH



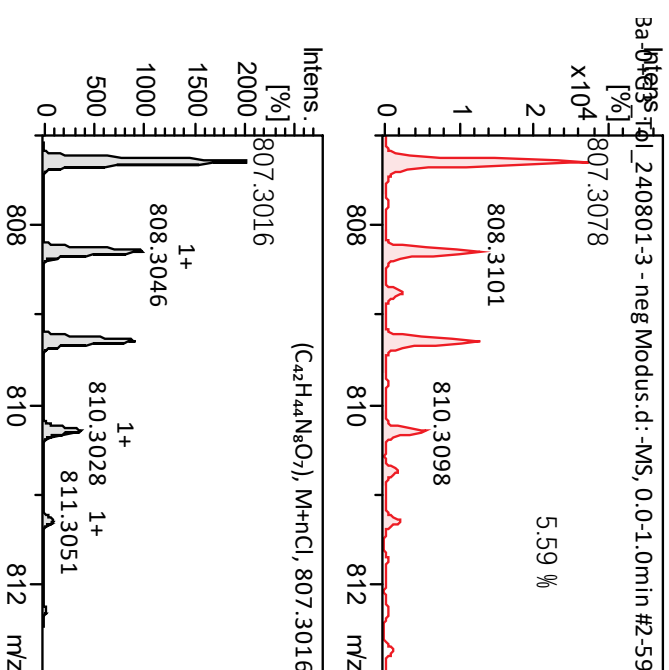
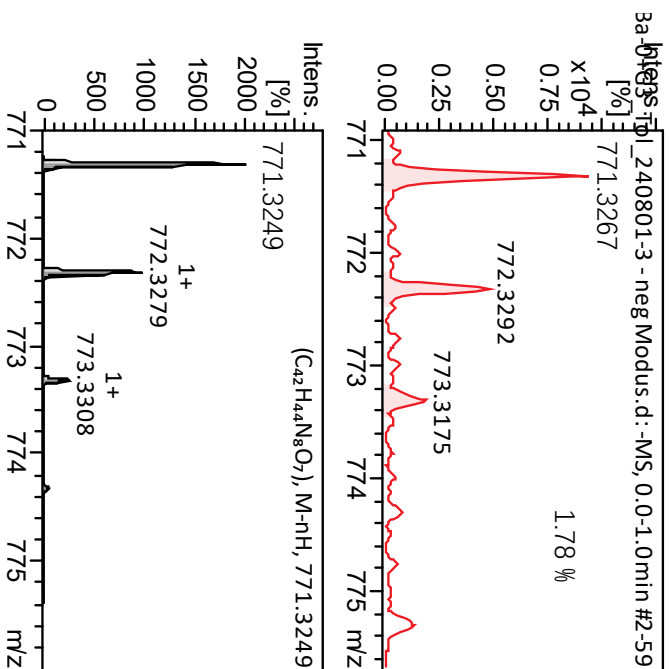
Chemical Formula: (C<sub>34</sub>H<sub>36</sub>N<sub>6</sub>O<sub>4</sub>)<sub>3</sub>  
Molecular Weight: 592.70\*3=1778.07



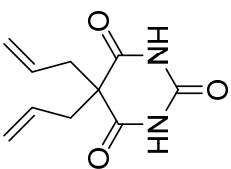
# cm-HB



Chemical Formula: C<sub>42</sub>H<sub>44</sub>N<sub>8</sub>O<sub>7</sub>  
Molecular Weight: 772.86

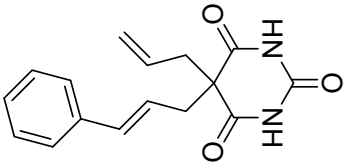
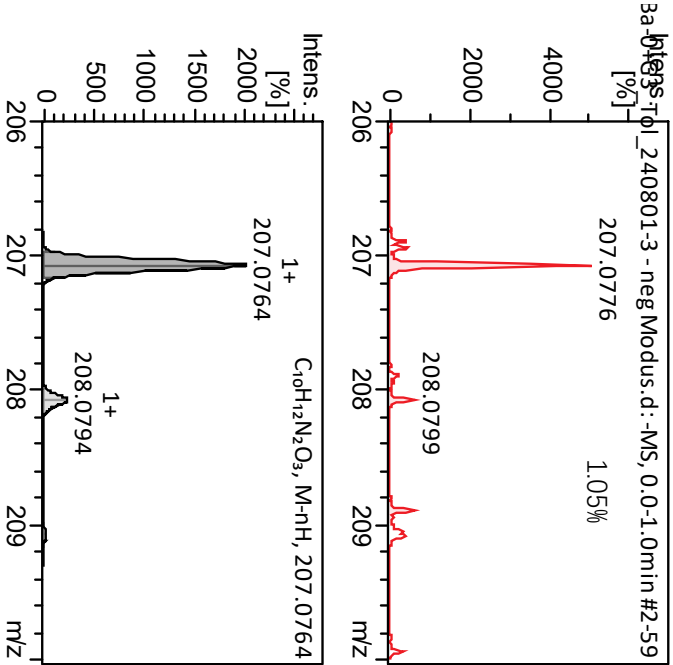


# Intermediates and Starting Materials



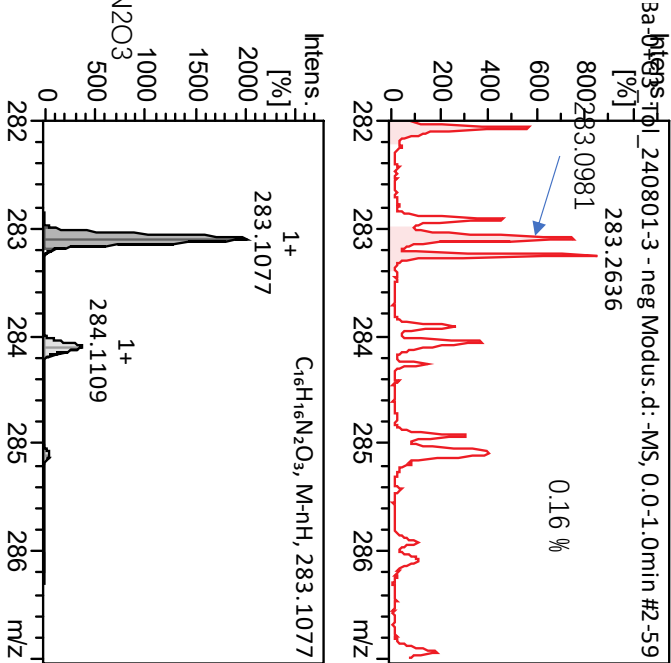
Chemical Formula: C<sub>10</sub>H<sub>12</sub>N<sub>2</sub>O<sub>3</sub>  
Exact Mass: 208.08

Ba



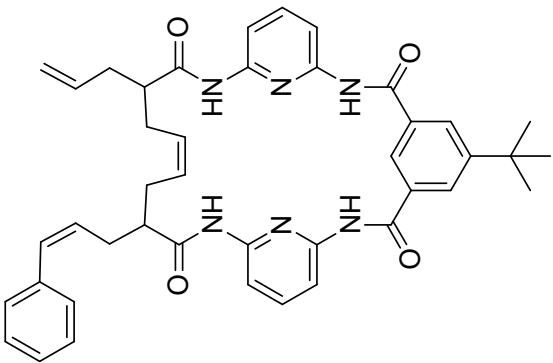
Chemical Formula: C<sub>16</sub>H<sub>16</sub>N<sub>2</sub>O<sub>3</sub>  
Exact Mass: 284.1161

Int-B1



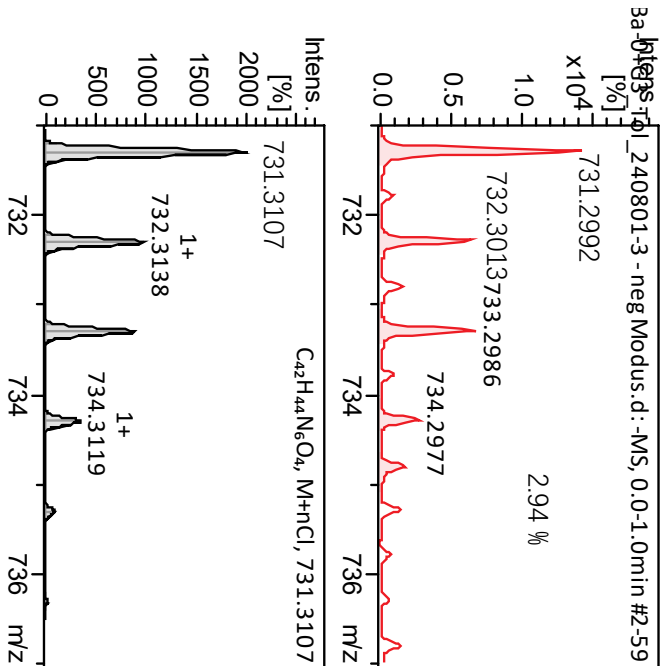
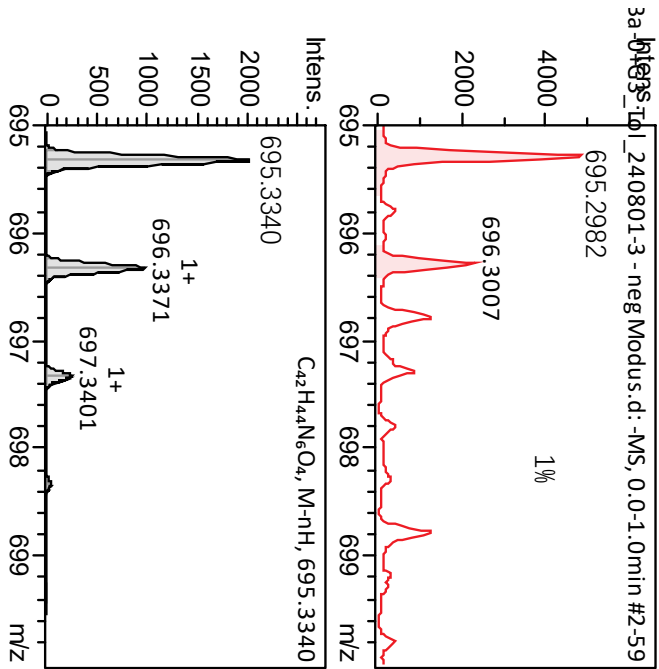


Intermediates and Starting Materials



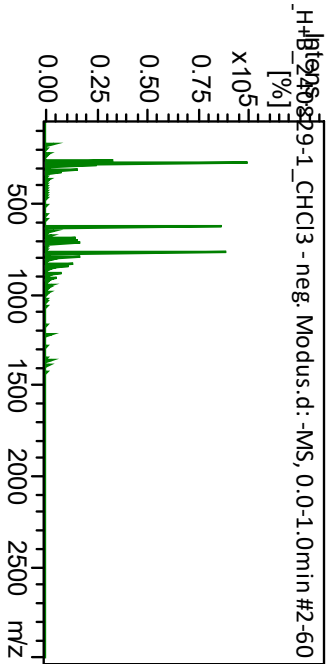
Chemical Formula:  $\text{C}_{42}\text{H}_{44}\text{N}_6\text{O}_4$   
Exact Mass: 696.34

Int-H1

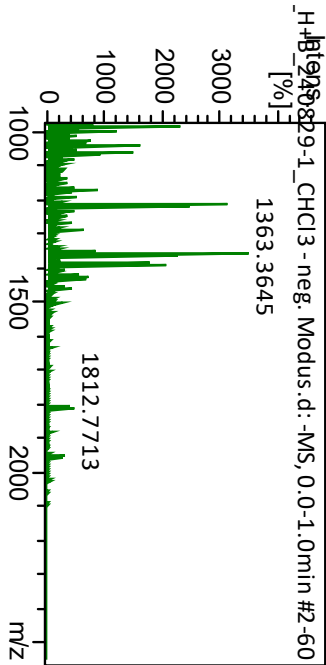
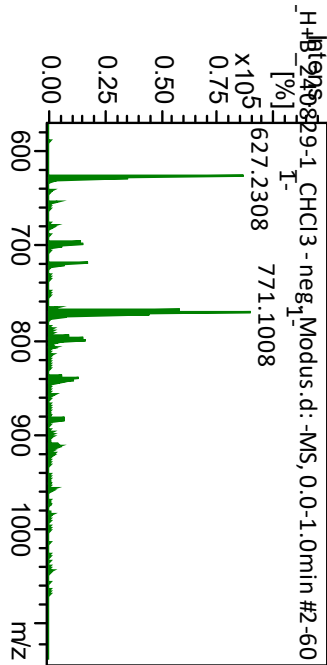
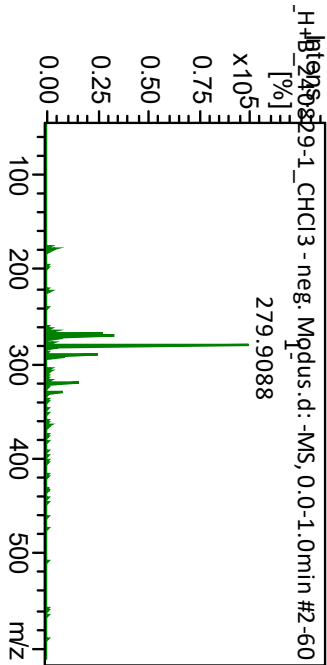


ESI MS spectrum for products from Entry 3

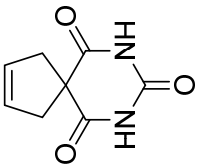
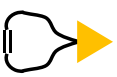
All range



Selected range



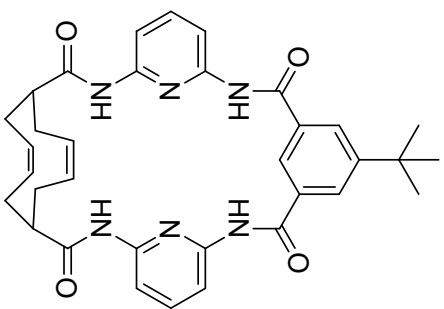
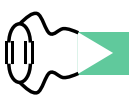
# CM-B



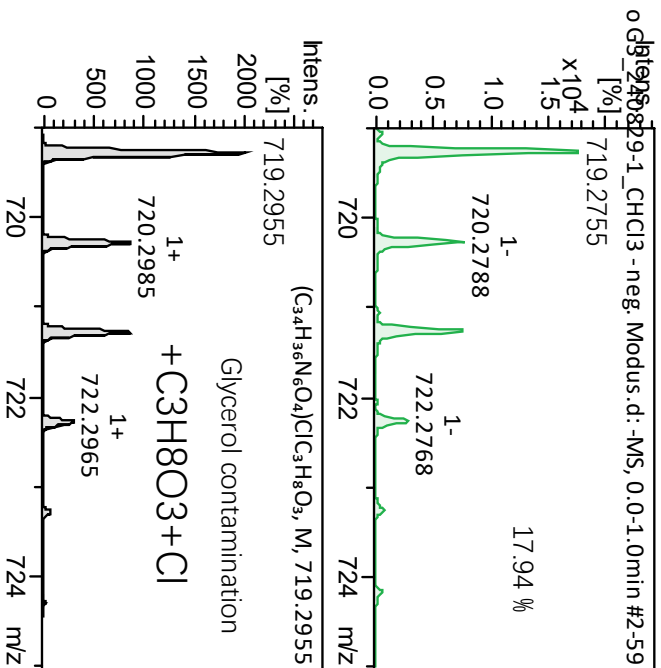
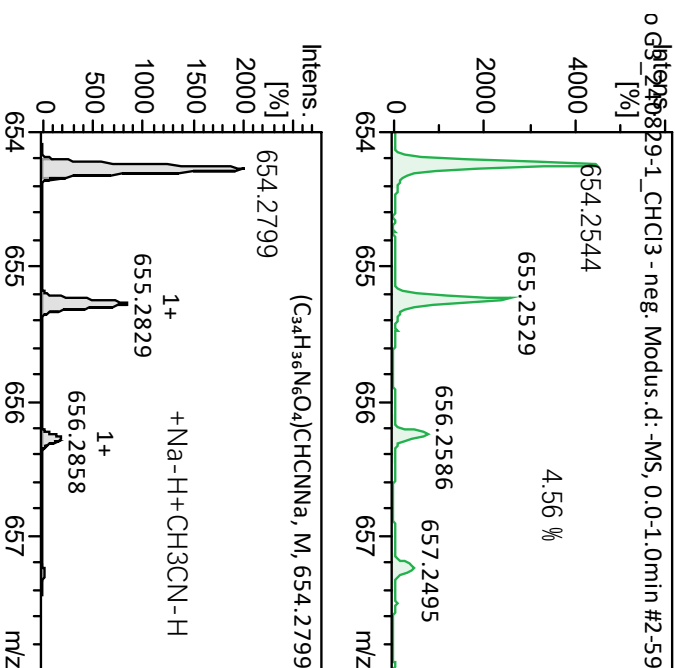
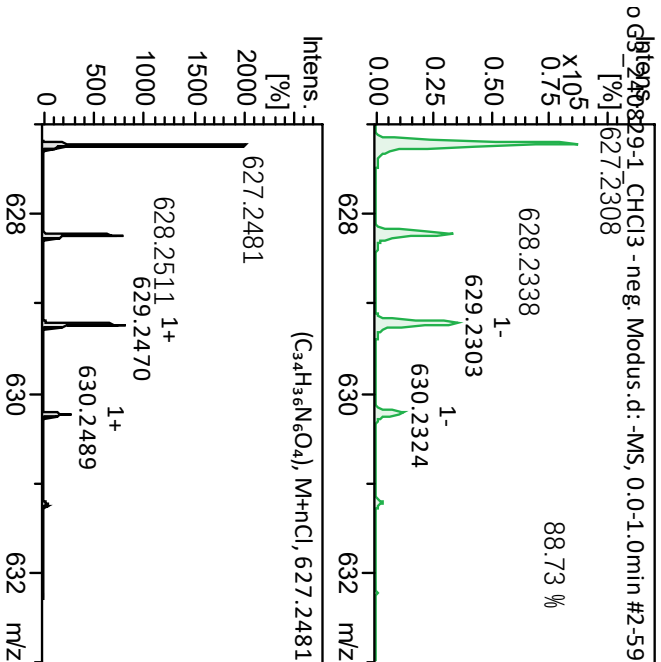
Chemical Formula: C<sub>8</sub>H<sub>8</sub>N<sub>2</sub>O<sub>3</sub>  
Molecular Weight: 180.16

Na

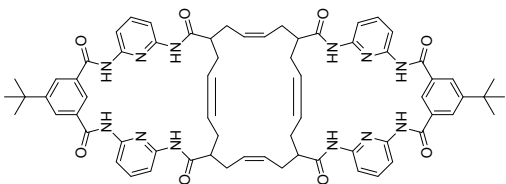
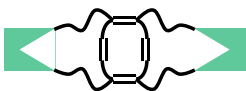
# cm-H



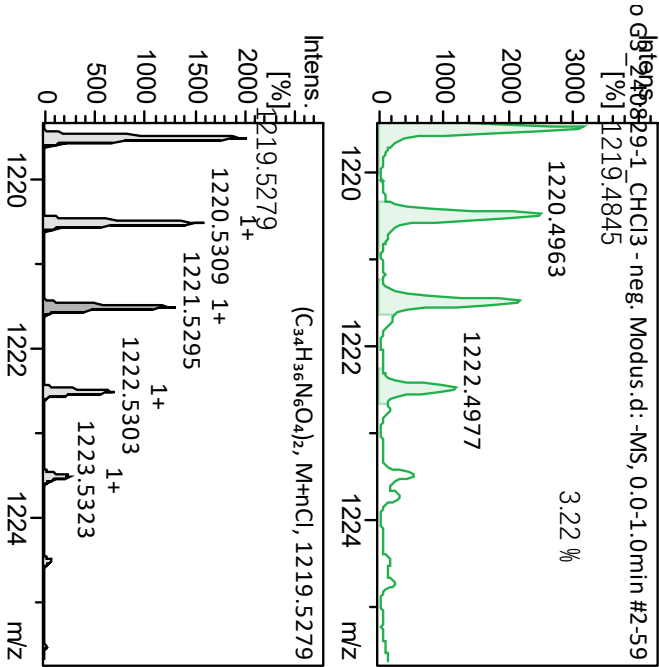
Chemical Formula: C<sub>34</sub>H<sub>36</sub>N<sub>6</sub>O<sub>4</sub>  
Molecular Weight: 592.70



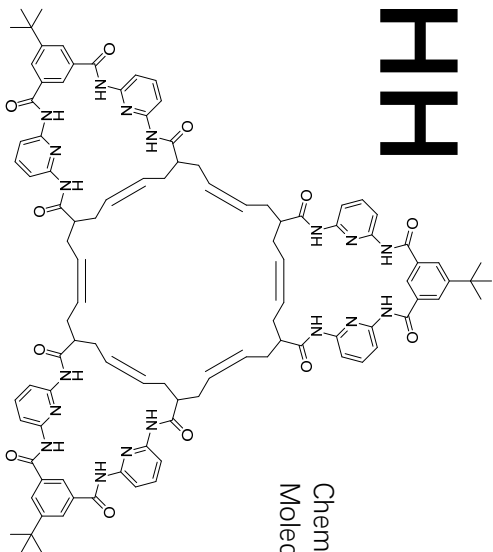
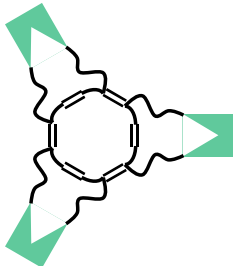
# cm-HH



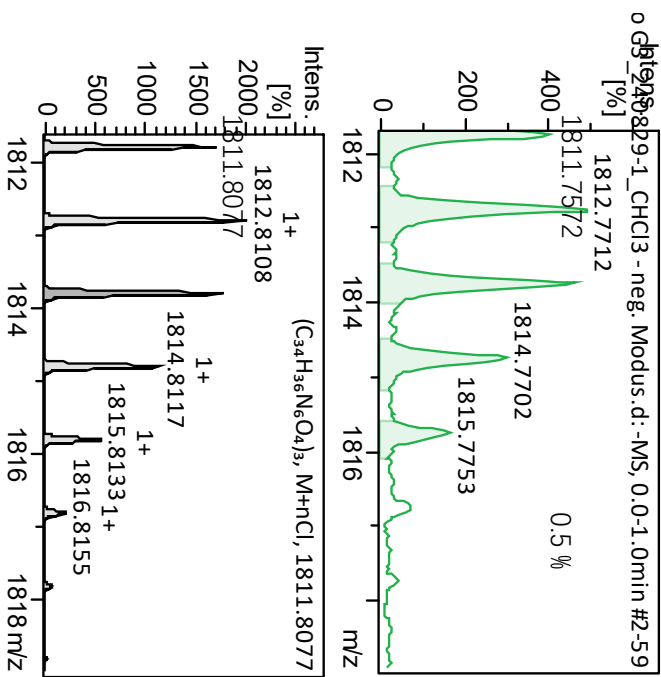
Chemical Formula: C<sub>68</sub>H<sub>72</sub>N<sub>12</sub>O<sub>8</sub>  
Molecular Weight: 1185.40



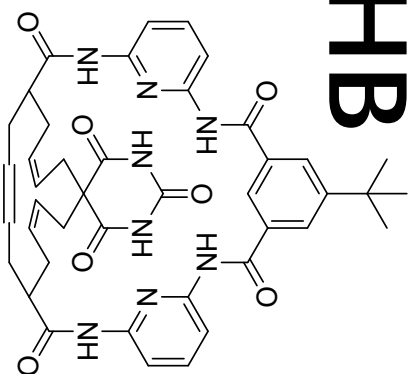
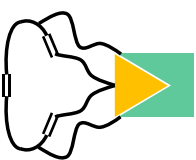
# cm-HHH



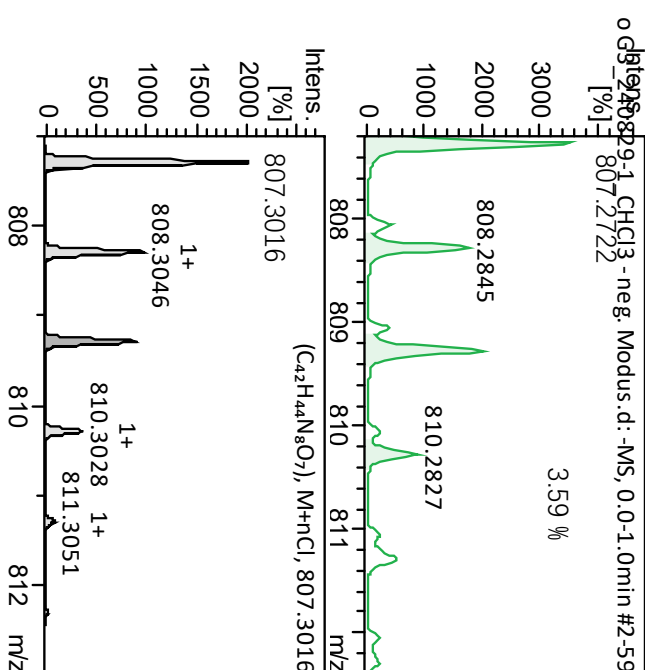
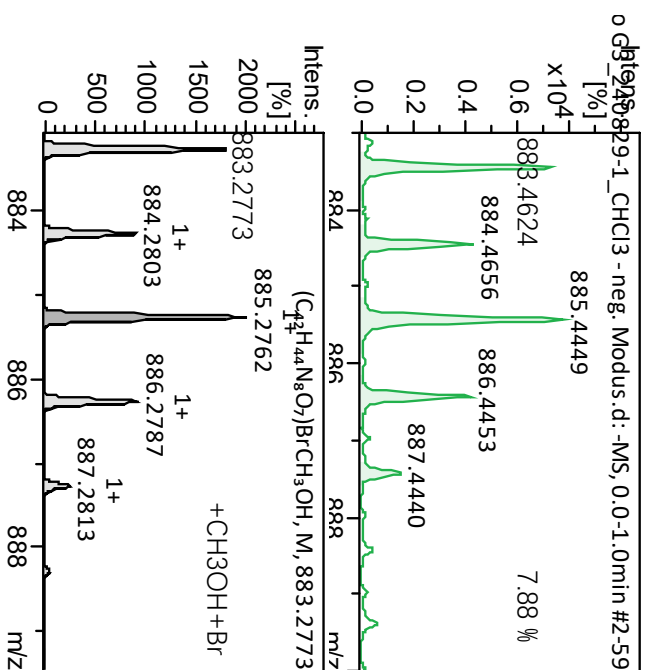
Chemical Formula:  $(C_{34}H_{36}N_6O_4)_3$   
Molecular Weight:  $592.70 \times 3 = 1778.07$



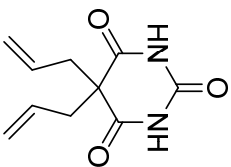
# cm-HB



Chemical Formula:  $C_{42}H_{44}N_8O_7$   
Molecular Weight: 772.86



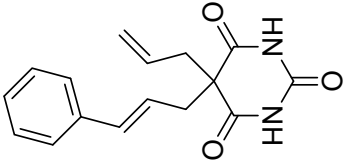
Intermediates and Starting Materials



N a

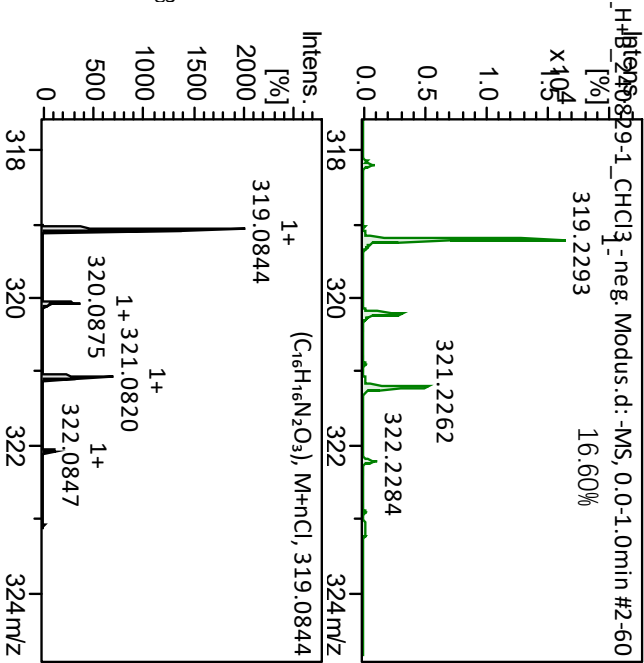
Chemical Formula: C<sub>10</sub>H<sub>12</sub>N<sub>2</sub>O<sub>3</sub>  
Exact Mass: 208.08

Ba



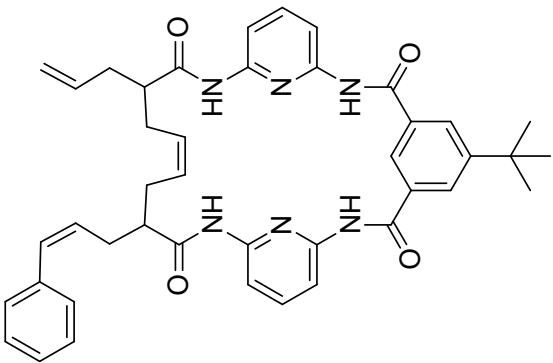
Chemical Formula: C<sub>16</sub>H<sub>16</sub>N<sub>2</sub>O<sub>3</sub>  
Exact Mass: 284.1161

Int-B1



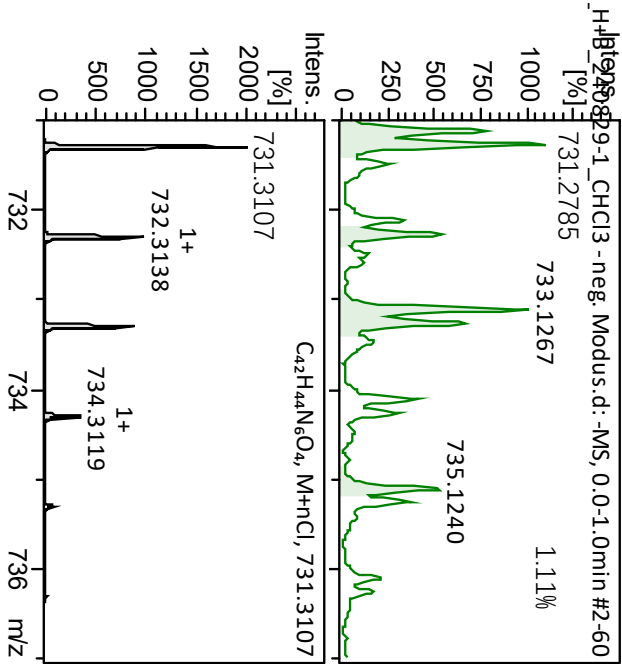


Intermediates and Starting Materials



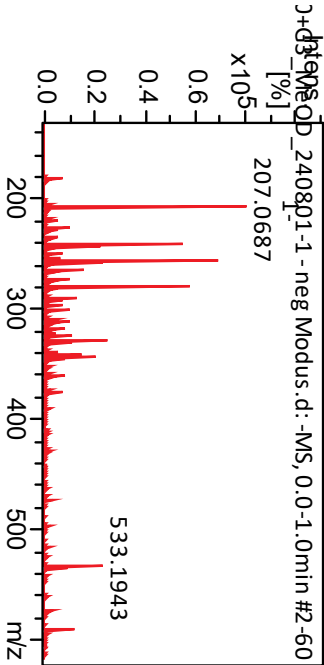
Chemical Formula: C<sub>42</sub>H<sub>44</sub>N<sub>6</sub>O<sub>4</sub>  
Exact Mass: 696.34

Int-H1

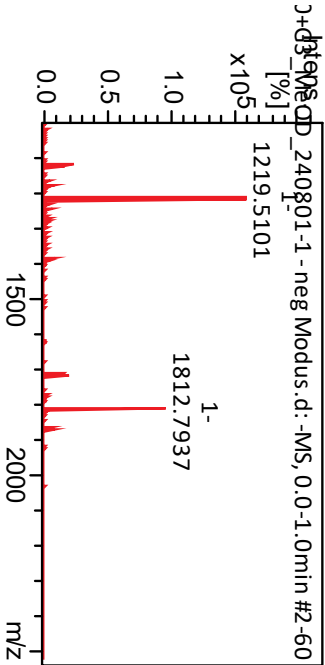
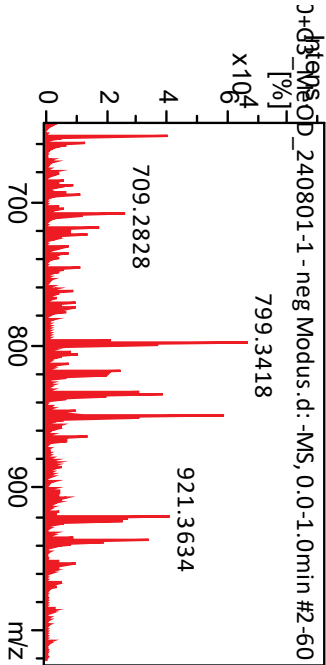
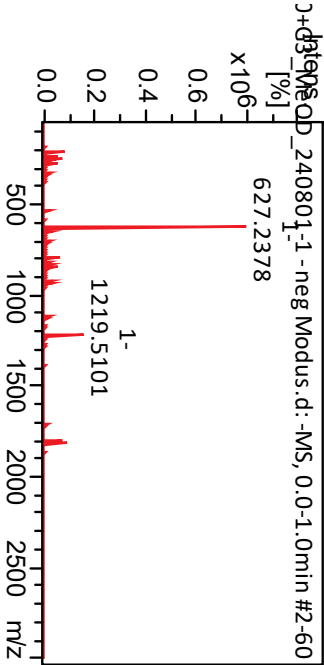


# ESI MS spectrum for products from Entry 4

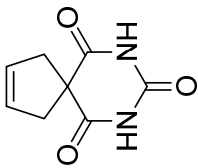
Selected range



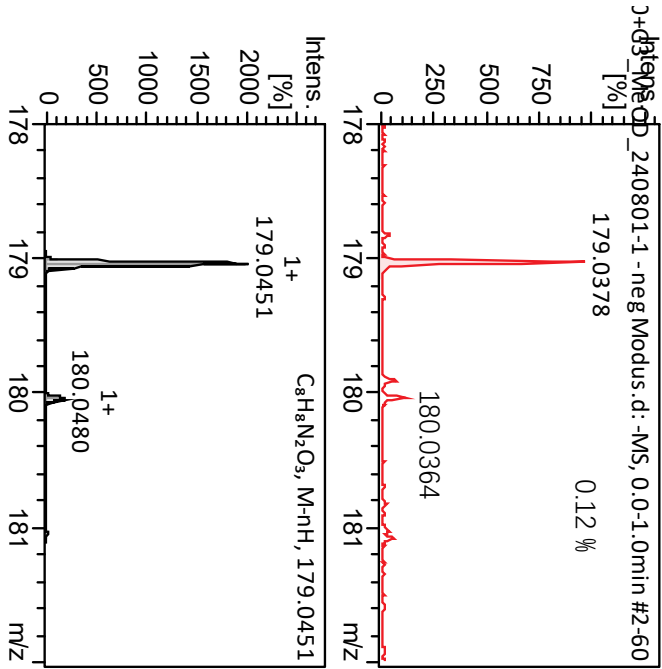
All range



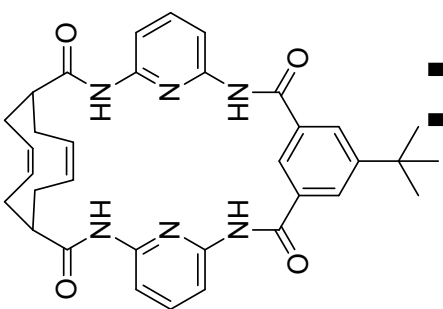
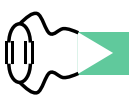
# cm-B



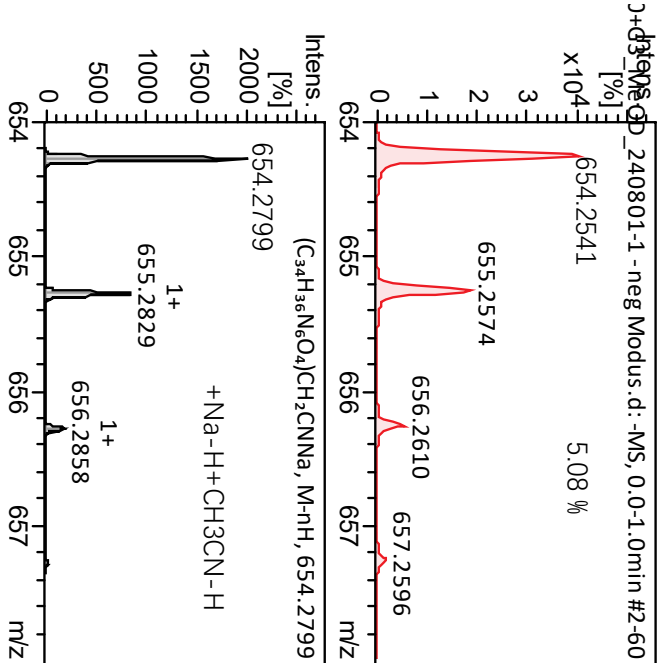
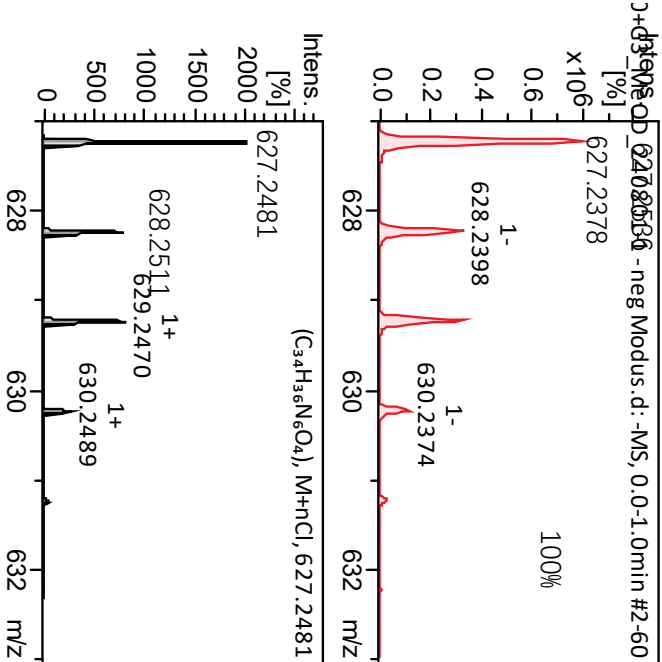
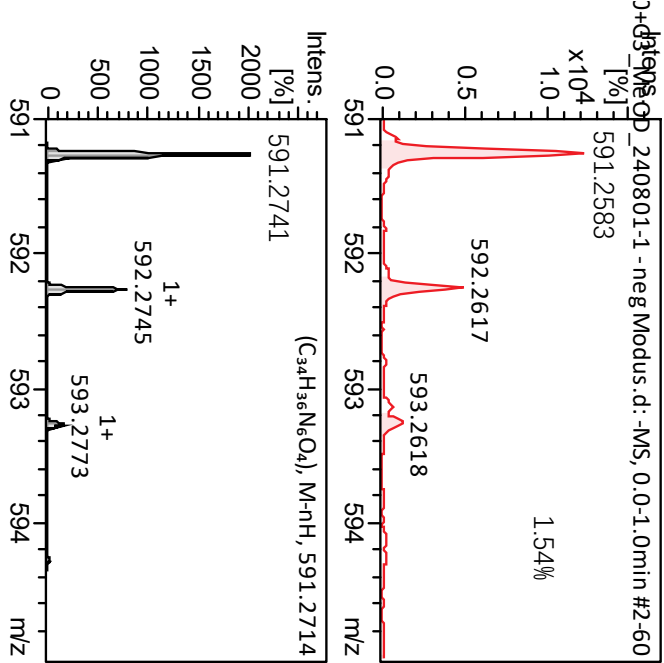
Chemical Formula: C<sub>8</sub>H<sub>8</sub>N<sub>2</sub>O<sub>3</sub>  
Molecular Weight: 180.16



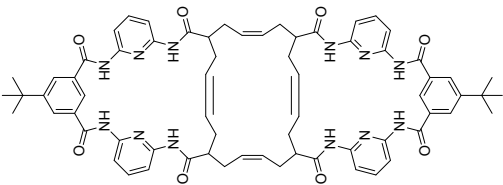
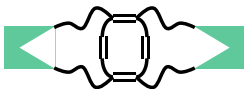
# cm-H



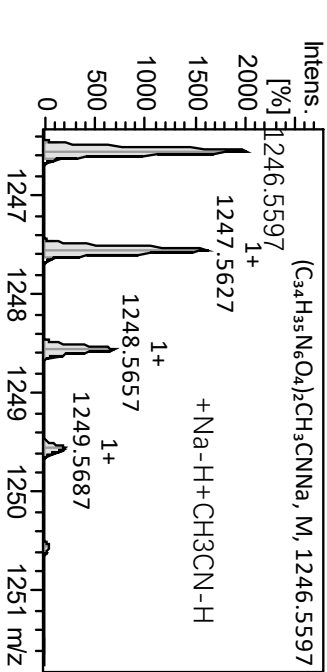
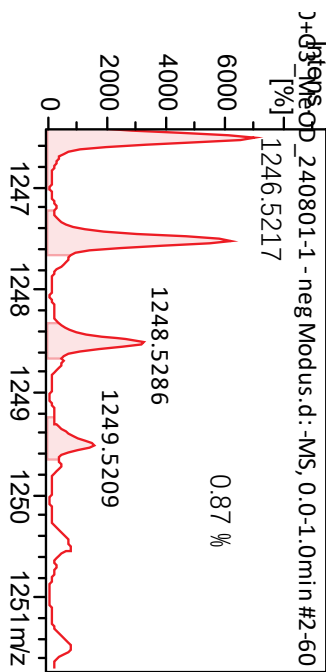
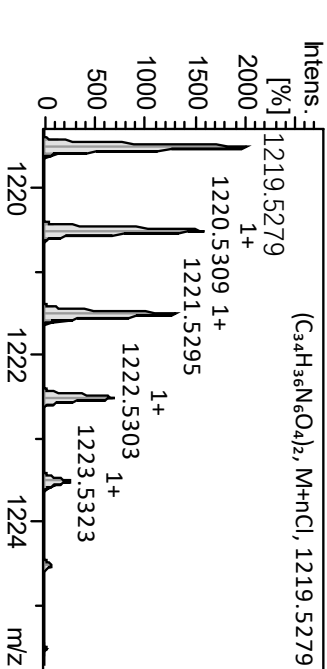
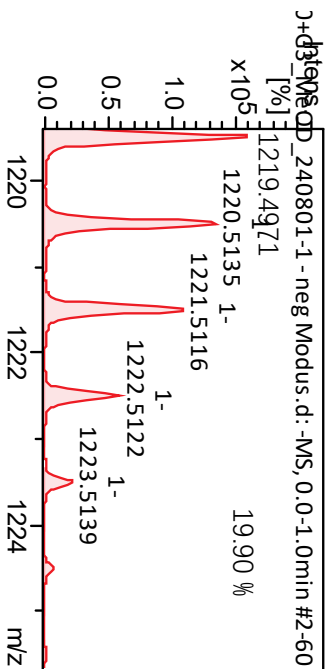
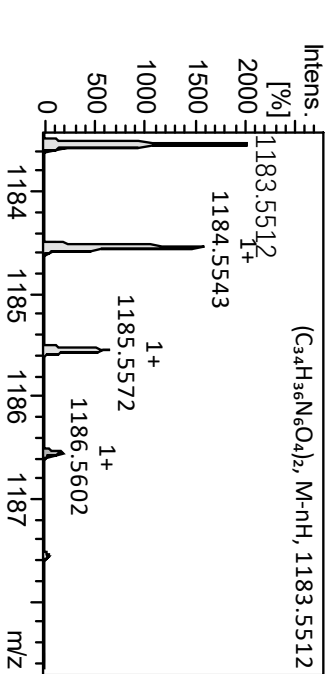
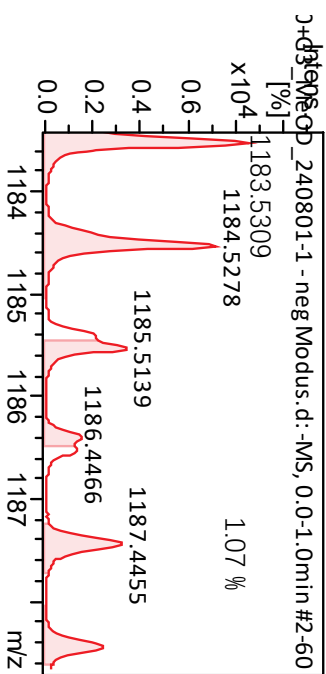
Chemical Formula: C<sub>34</sub>H<sub>36</sub>N<sub>6</sub>O<sub>4</sub>  
Molecular Weight: 592.70



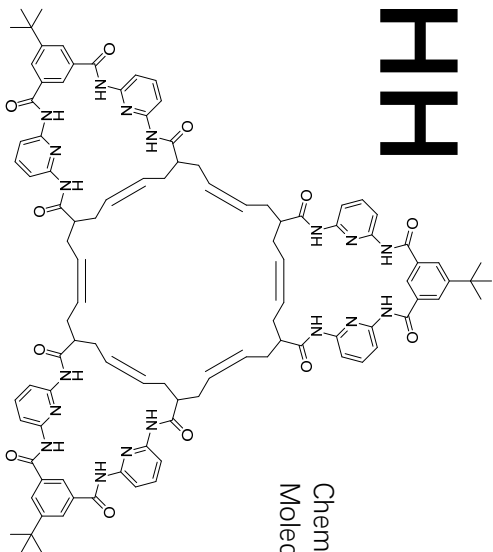
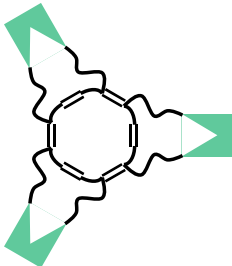
# cm-HH



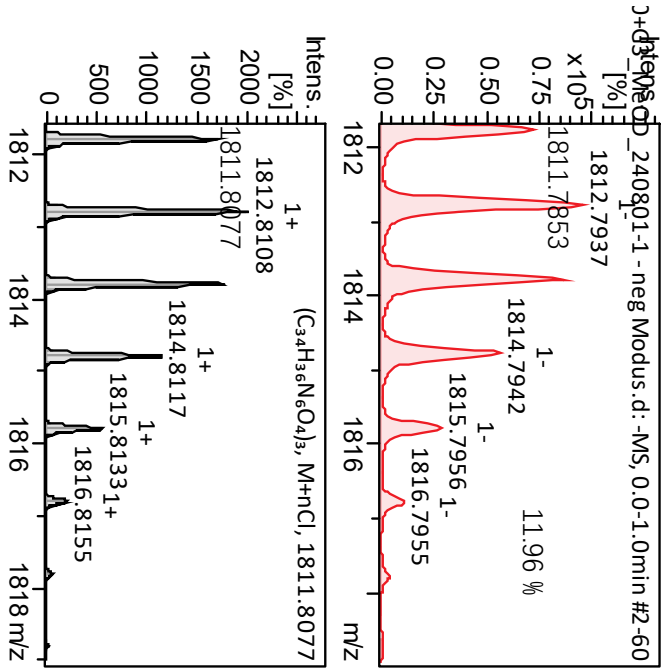
Chemical Formula: C<sub>68</sub>H<sub>72</sub>N<sub>12</sub>O<sub>8</sub>  
Molecular Weight: 1185.40

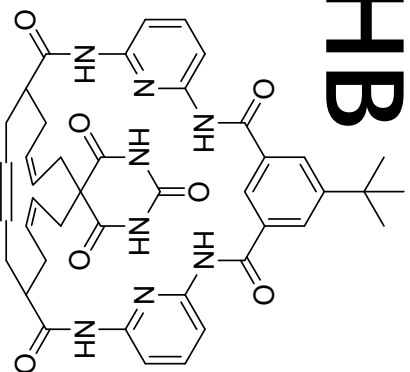


# cm-HHH

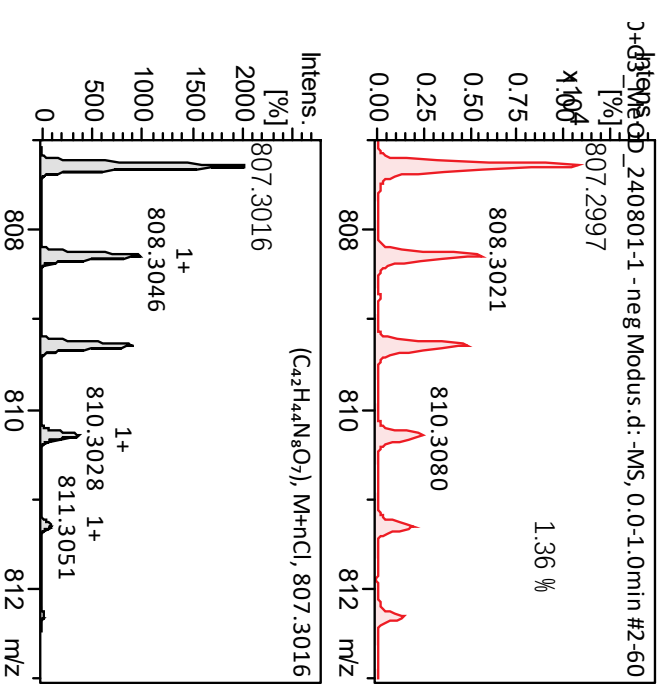
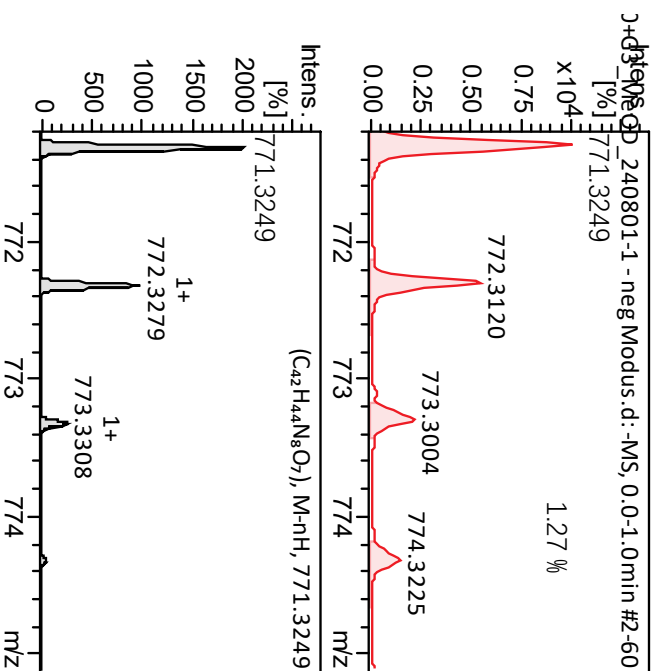


Chemical Formula: (C<sub>34</sub>H<sub>36</sub>N<sub>6</sub>O<sub>4</sub>)<sub>3</sub>  
Molecular Weight: 592.70\*3=1778.07

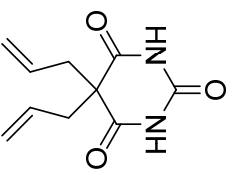




Molecular Weight: 772.86

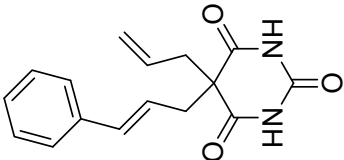
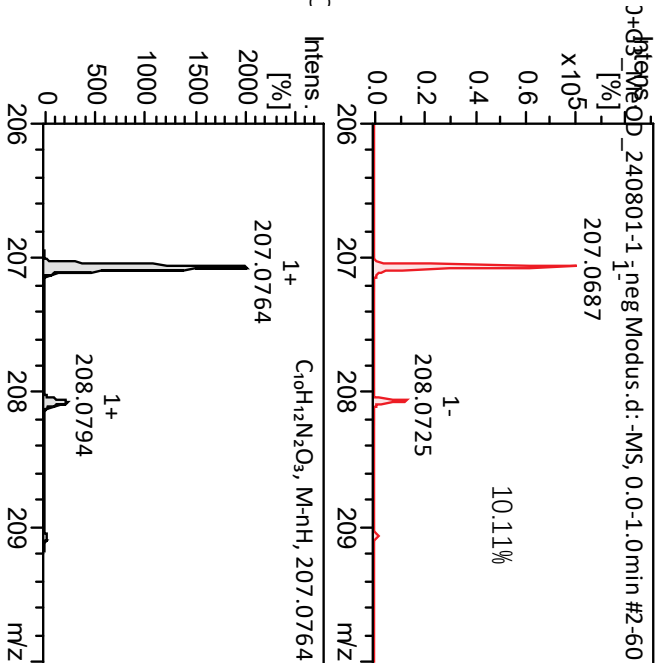


# Intermediates and Starting Materials



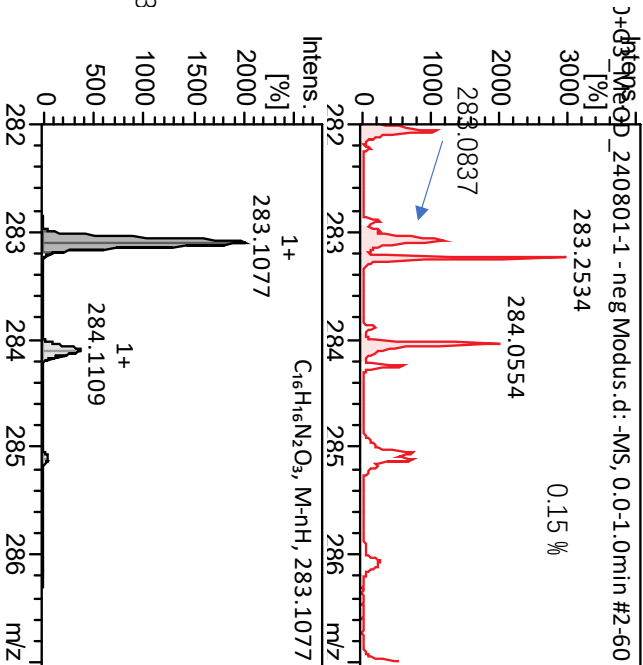
Chemical Formula: C<sub>10</sub>H<sub>12</sub>N<sub>2</sub>C  
Exact Mass: 208.08

Ba



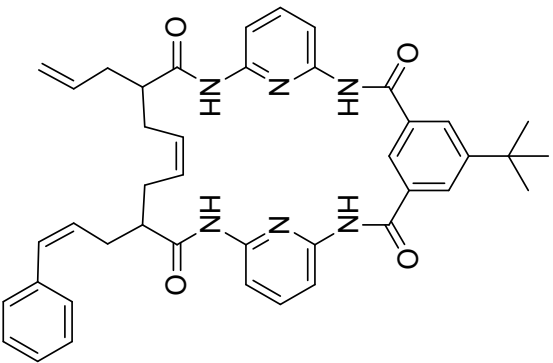
Chemical Formula: C<sub>16</sub>H<sub>16</sub>N<sub>2</sub>O<sub>3</sub>  
Exact Mass: 284.1161

Int-B1



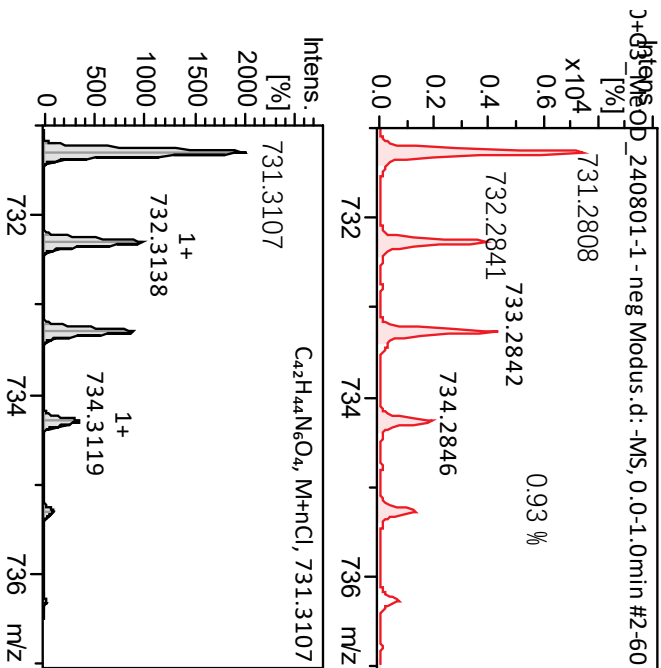
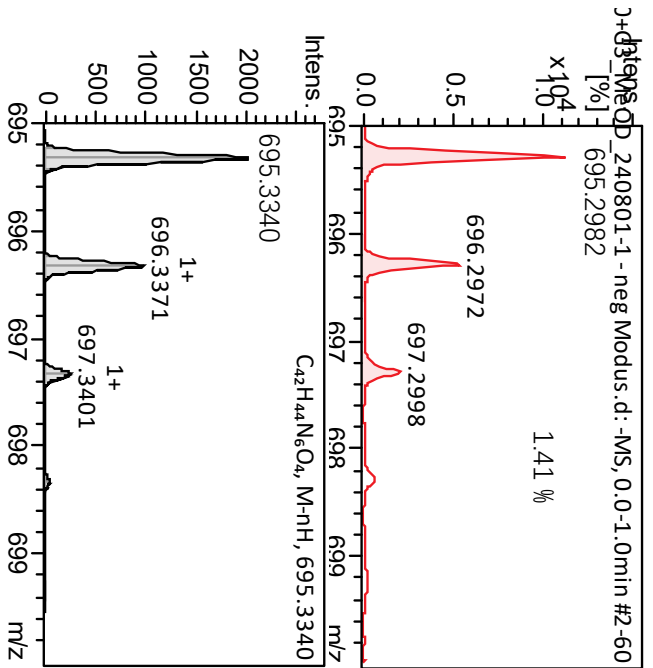


Intermediates and Starting Materials



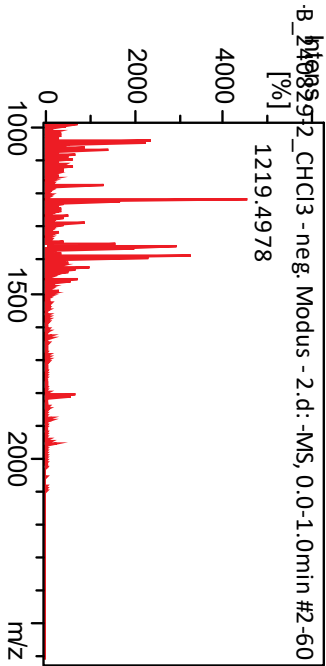
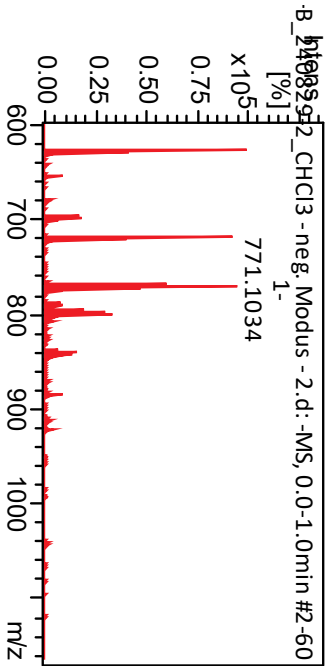
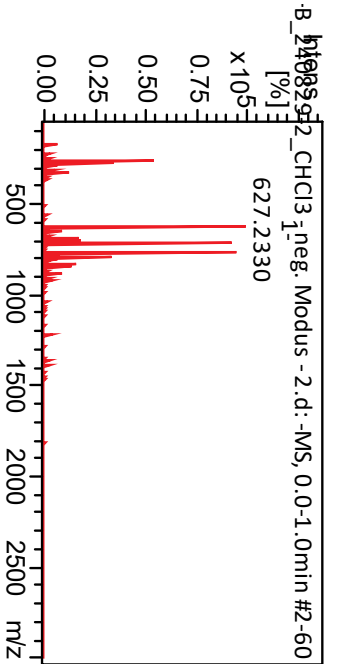
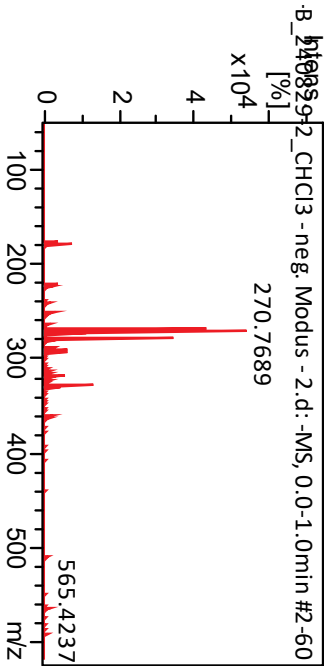
Chemical Formula:  $C_{42}H_{44}N_6O_4$   
Exact Mass: 696.34

Int-H1

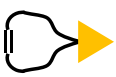


ESI MS spectrum for products from Entry 5

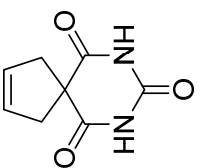
Selected range



# cm-B

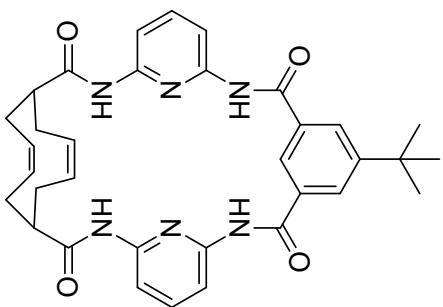
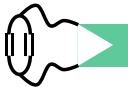


Chemical Formula: C<sub>8</sub>H<sub>8</sub>N<sub>2</sub>O<sub>3</sub>  
Molecular Weight: 180.16

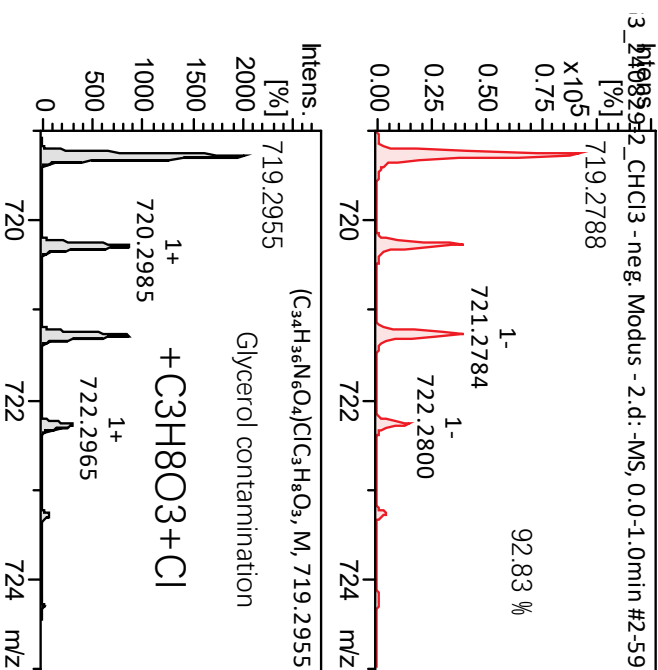
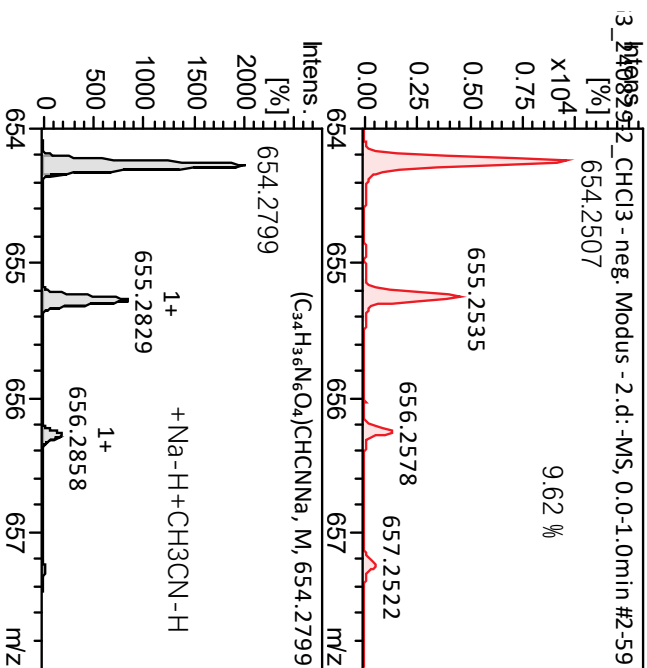
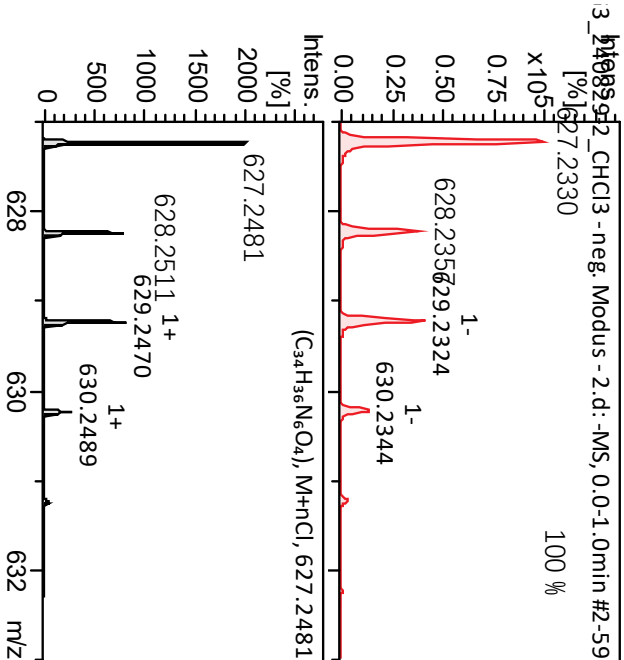


N a

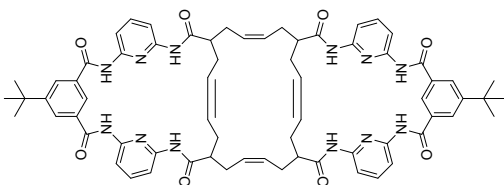
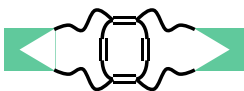
# cm-H



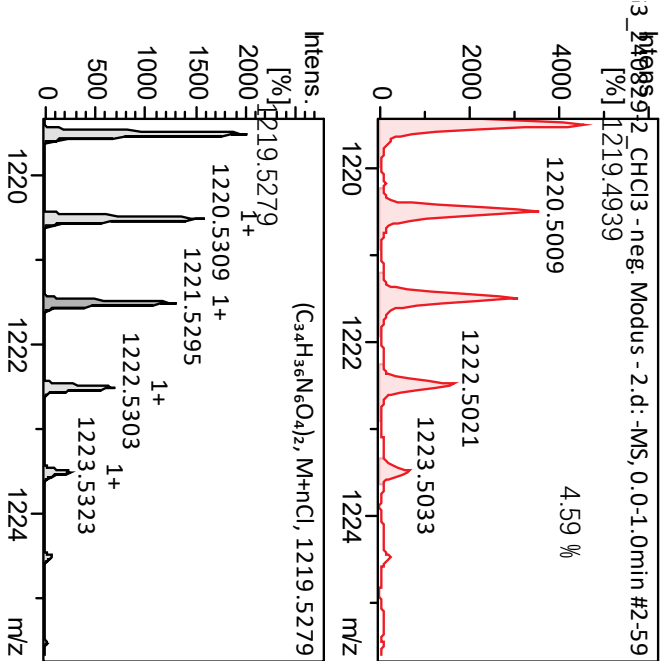
Chemical Formula: C<sub>34</sub>H<sub>36</sub>N<sub>6</sub>O<sub>4</sub>  
Molecular Weight: 592.70



# cm-HH

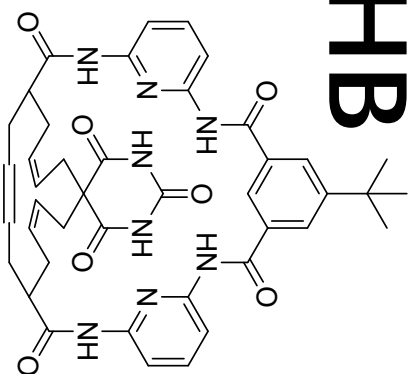
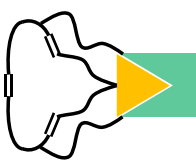


Chemical Formula: C<sub>68</sub>H<sub>72</sub>N<sub>12</sub>O<sub>8</sub>  
Molecular Weight: 1185.40

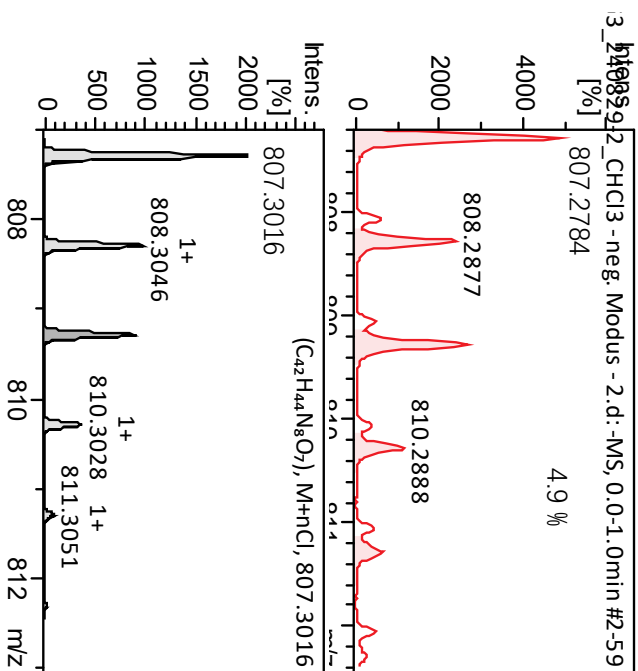




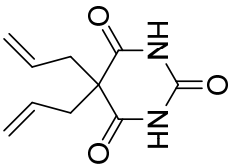
# cm-HB



Chemical Formula: C<sub>42</sub>H<sub>44</sub>N<sub>8</sub>O<sub>7</sub>  
Molecular Weight: 772.86



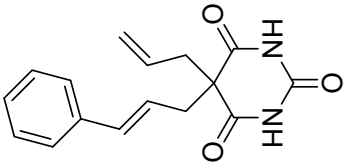
Intermediates and Starting Materials



Chemical Formula: C<sub>10</sub>H<sub>12</sub>N<sub>2</sub>O<sub>3</sub>  
Exact Mass: 208.08

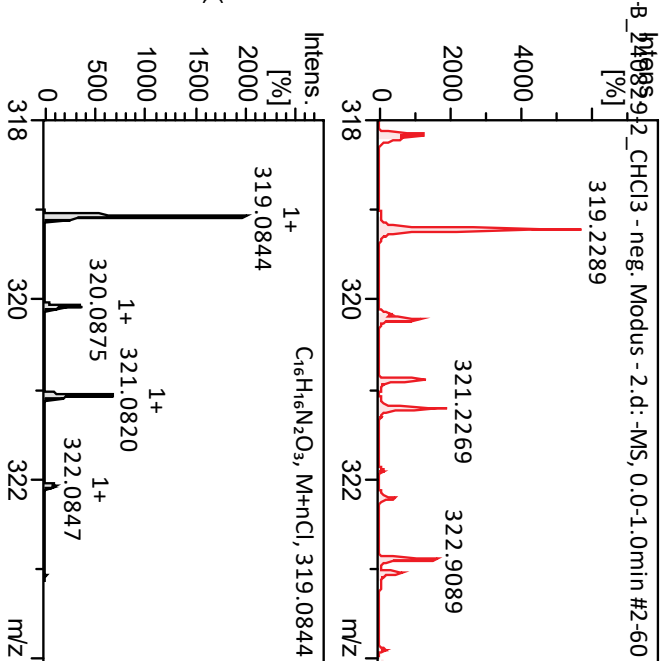
N a

Ba



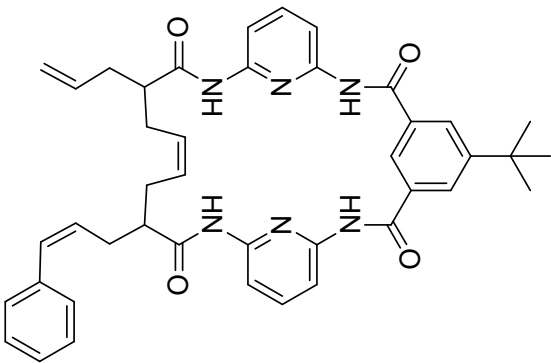
Chemical Formula: C<sub>16</sub>H<sub>16</sub>N<sub>2</sub>O<sub>3</sub>  
Exact Mass: 284.1161

Int-B1



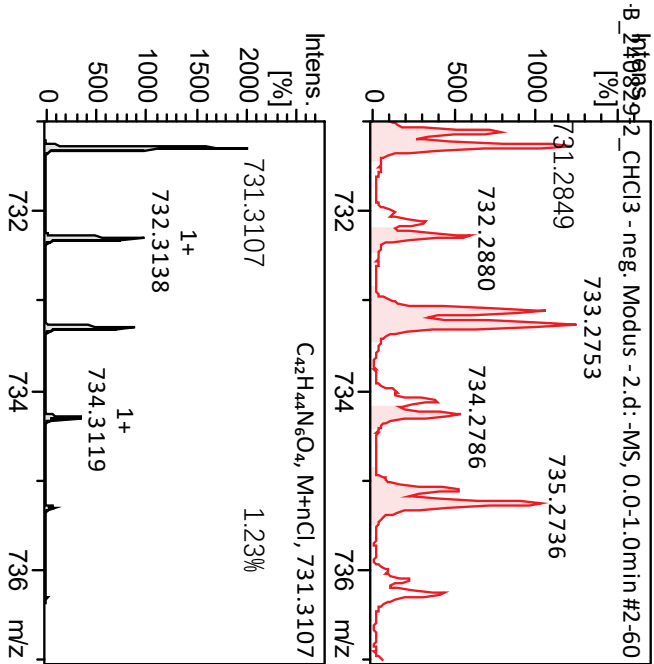


Intermediates and Starting Materials



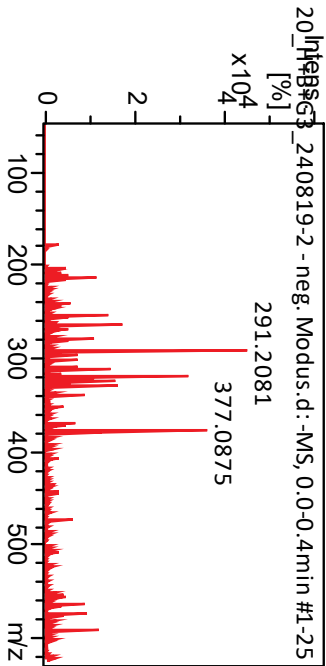
Chemical Formula:  $C_{42}H_{44}N_6O_4$   
Exact Mass: 696.34

Int-H1

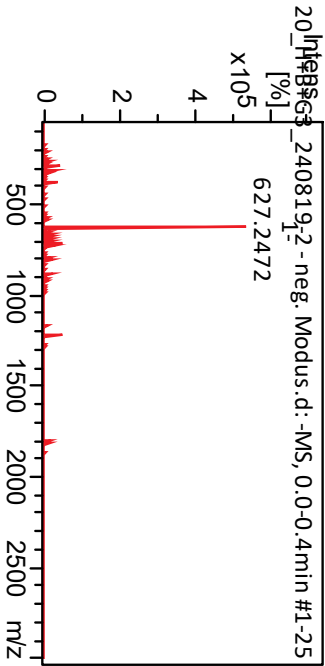


ESI MS spectrum for products from Entry 6

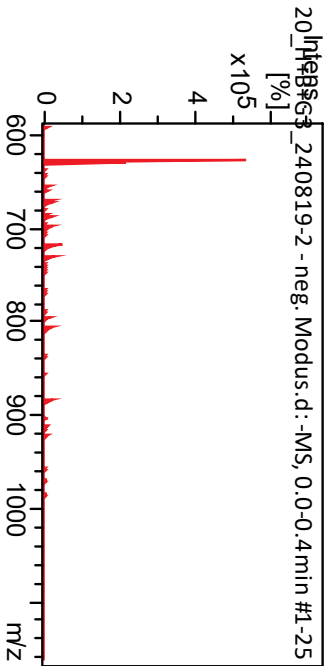
Selected range



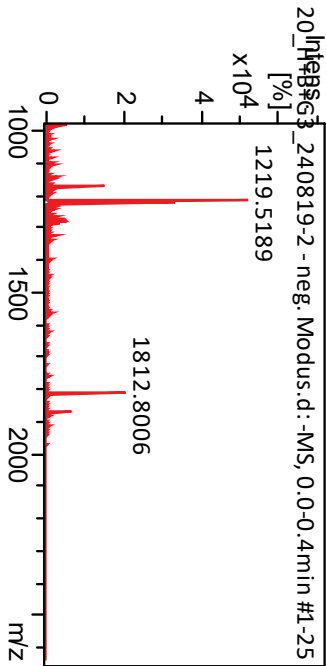
All range



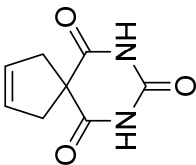
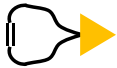
Selected range



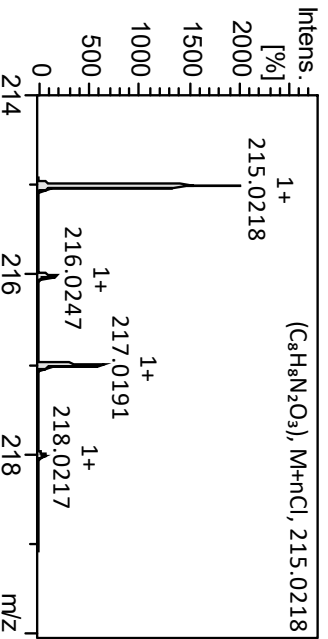
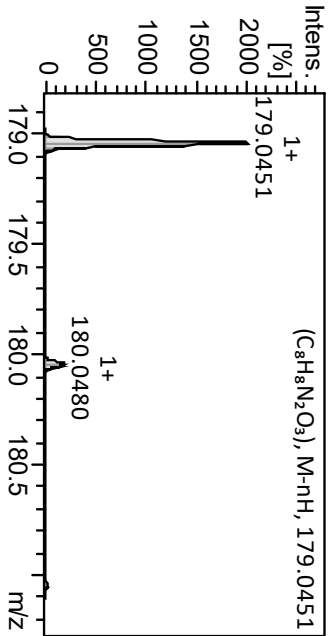
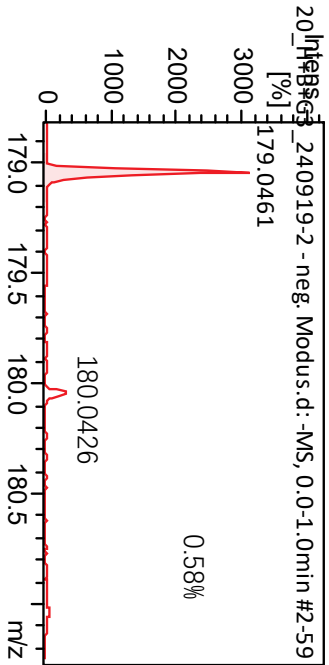
All range



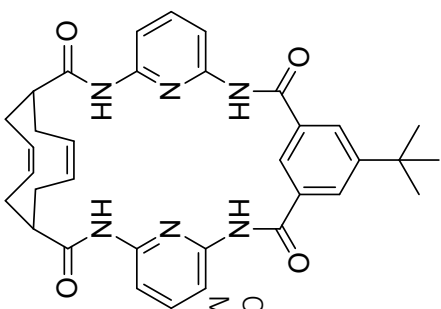
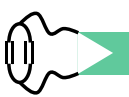
# cm-B



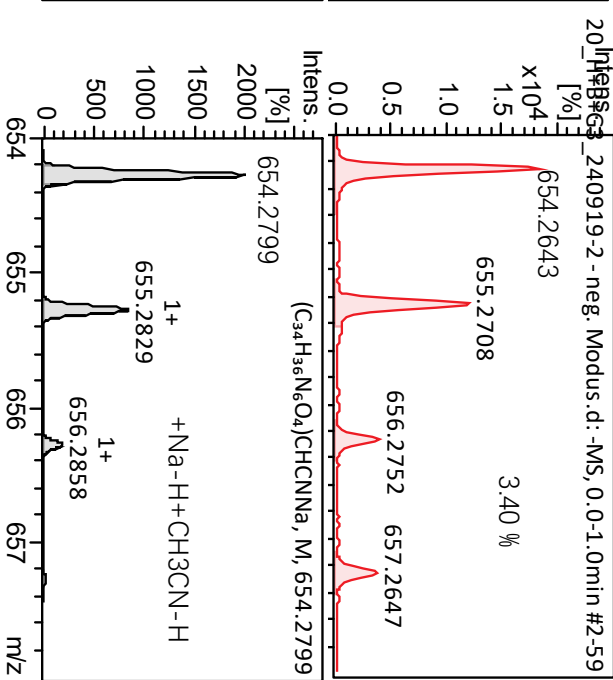
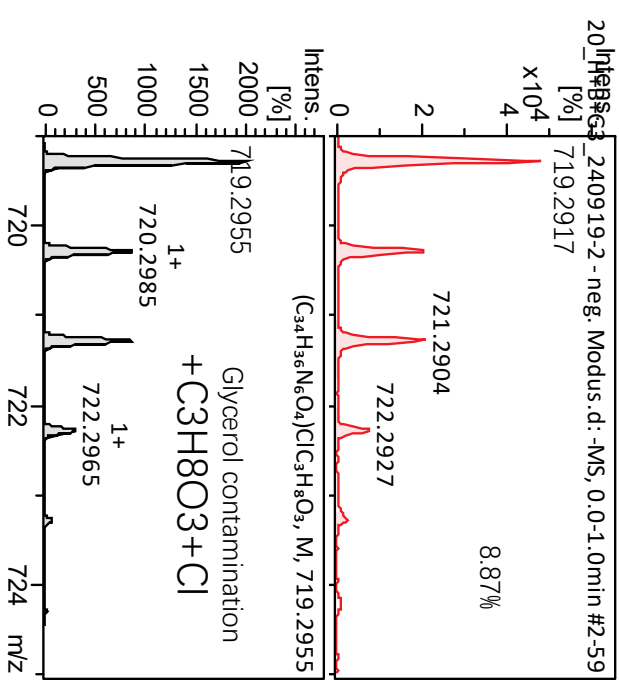
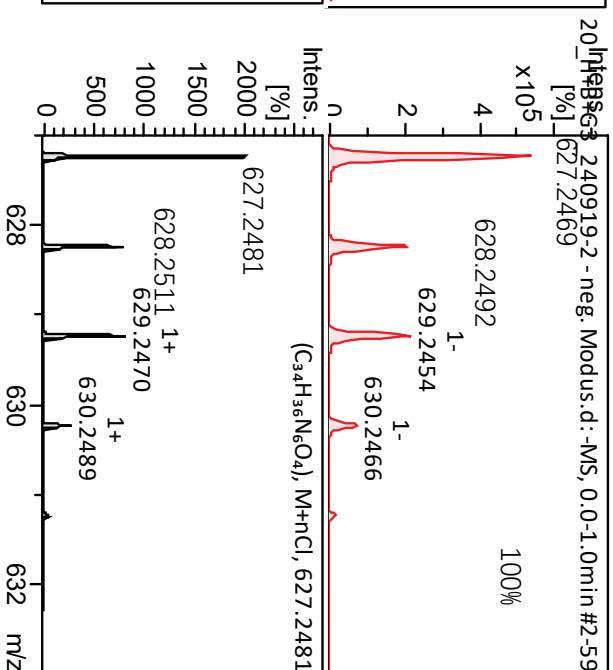
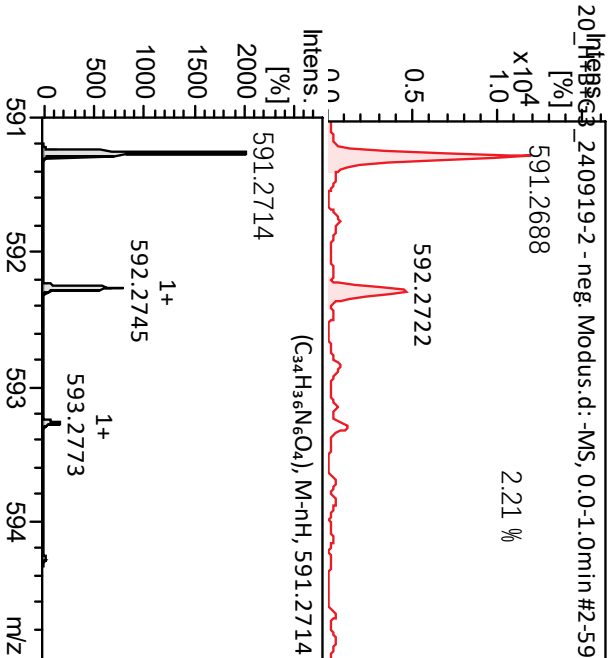
Chemical Formula: C<sub>8</sub>H<sub>8</sub>N<sub>2</sub>O<sub>3</sub>  
Molecular Weight: 180.16



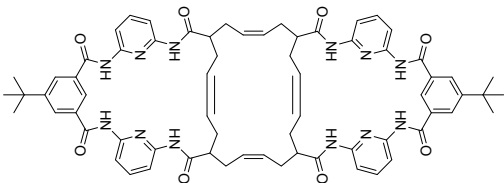
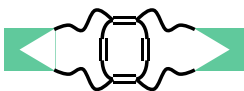
# cm-H



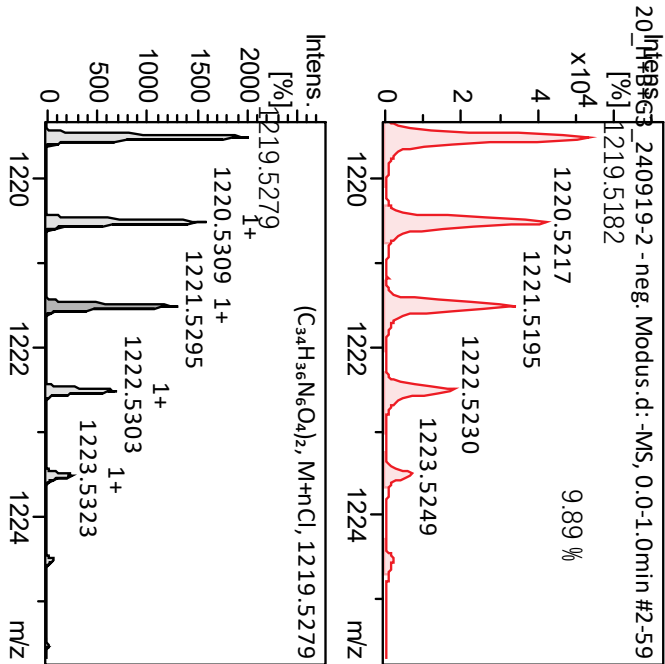
Chemical Formula: C<sub>34</sub>H<sub>36</sub>N<sub>6</sub>O<sub>4</sub>  
Molecular Weight: 592.70



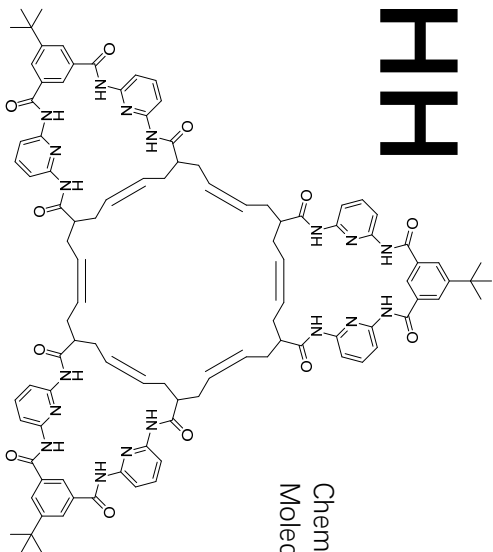
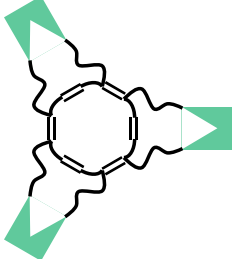
# cm-HH



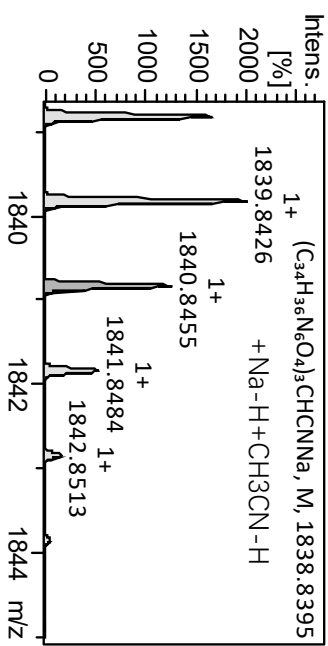
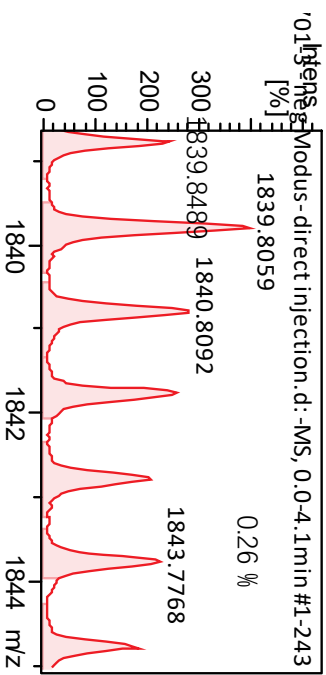
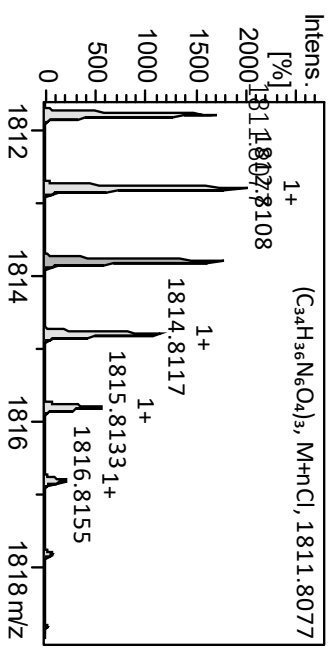
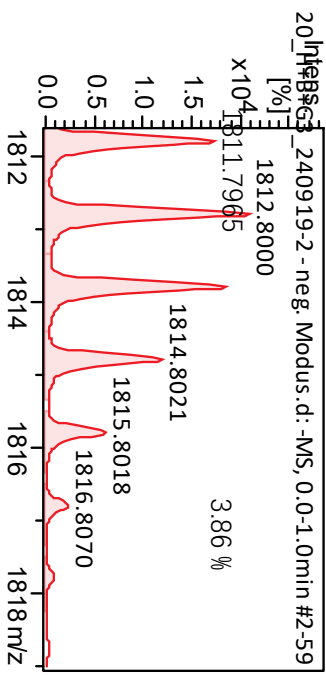
Chemical Formula: C<sub>68</sub>H<sub>72</sub>N<sub>12</sub>O<sub>8</sub>  
Molecular Weight: 1185.40

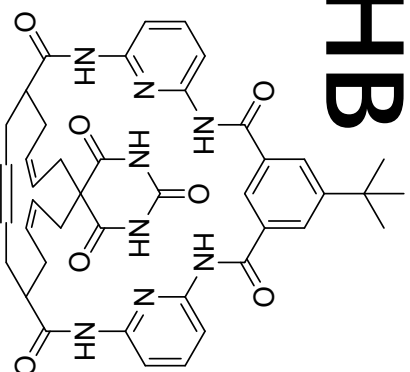


# cm-HHH

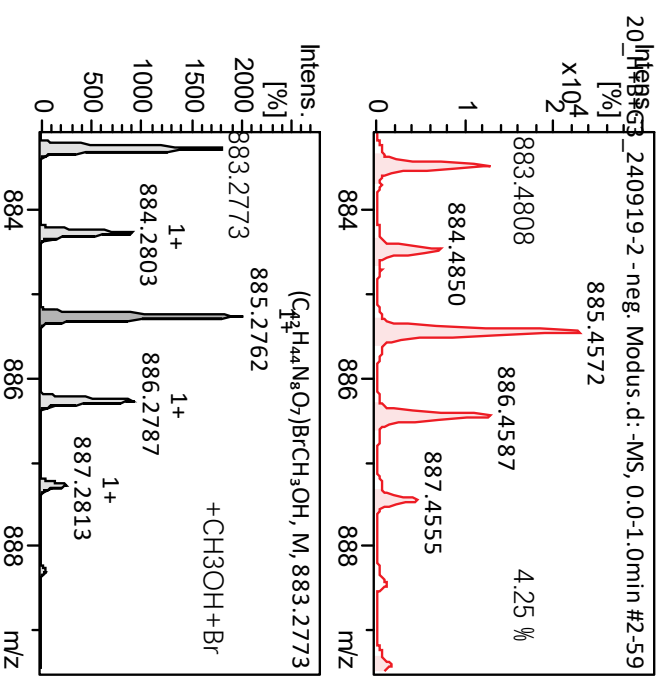
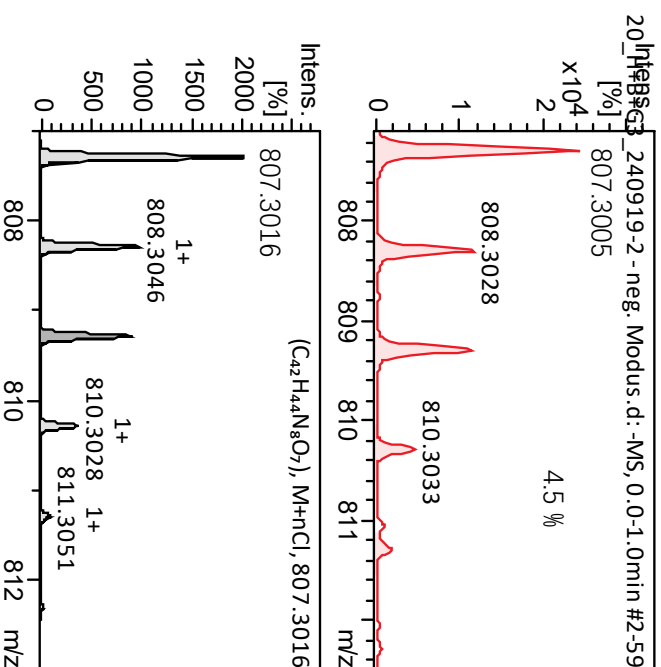
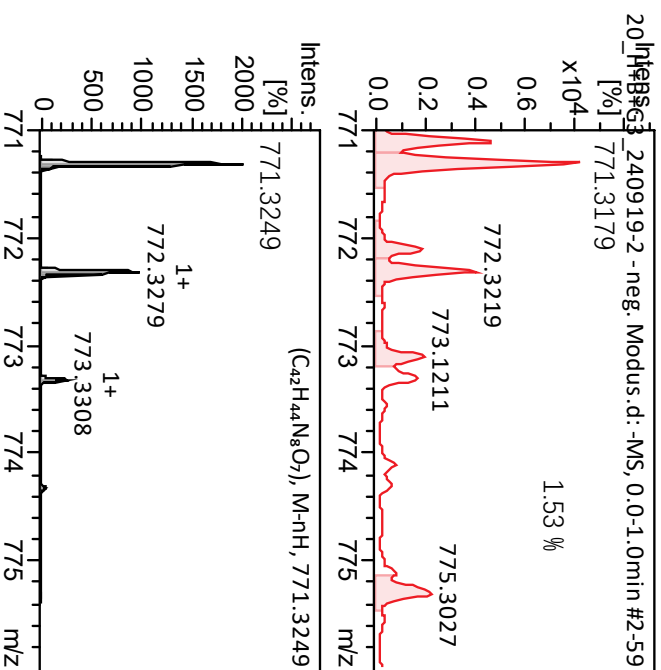


Chemical Formula: (C<sub>34</sub>H<sub>36</sub>N<sub>6</sub>O<sub>4</sub>)<sub>3</sub>  
Molecular Weight: 592.70\*3=1778.07

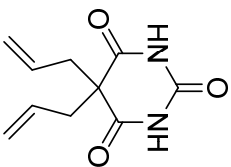




Chemical Formula: C<sub>42</sub>H<sub>44</sub>N<sub>8</sub>O<sub>7</sub>  
Molecular Weight: 772.86



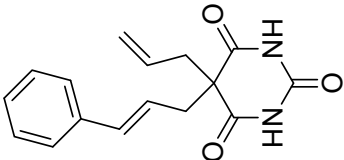
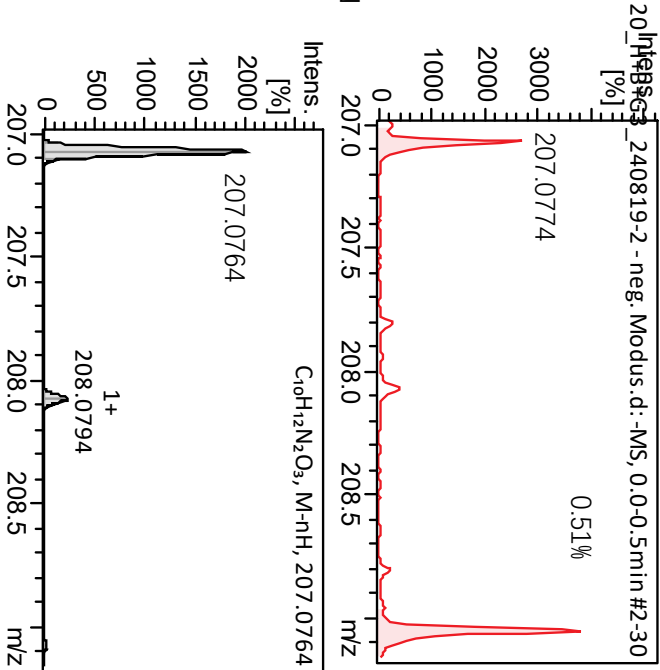
# Intermediates and Starting Materials



Chemical Formula: C<sub>10</sub>H<sub>12</sub>N<sub>2</sub>

Exact Mass: 208.08

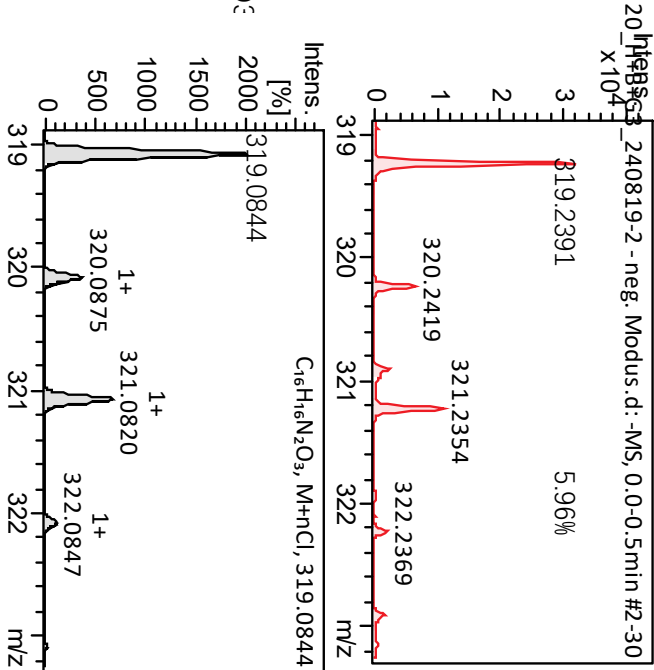
Ba



Chemical Formula: C<sub>16</sub>H<sub>16</sub>N<sub>2</sub>O<sub>3</sub>

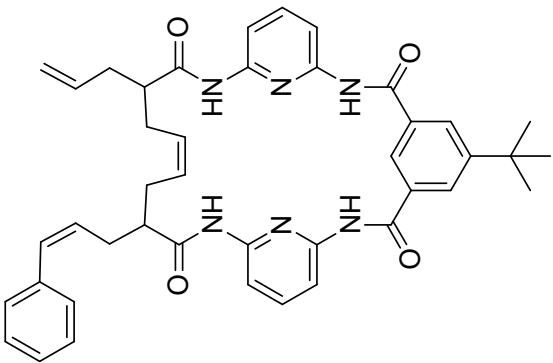
Exact Mass: 284.1161

Int-B1



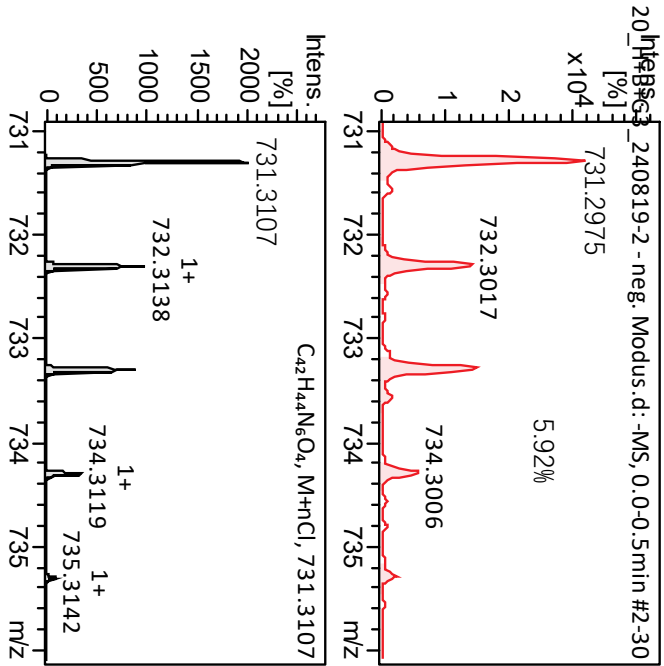


Intermediates and Starting Materials



Chemical Formula: C<sub>42</sub>H<sub>44</sub>N<sub>6</sub>O<sub>4</sub>  
Exact Mass: 696.34

Int-H1



# Curriculum Vitae

## Chenming Li

Birth Date: xx.xx.xxxx  
Nationality: Chinese  
Place of Birth: China  
Adress: xxxx xxxx xxxx  
E-mail: xxxx xxxx xxxx  
Tel.: xxxx xxxx xxxx



## Education

- Doctorate: Dr. rer. nat. – Macromolecular Chemistry 06.2020-12.2024  
- Martin Luther University Halle-Wittenberg, Halle (Saale), Germany
- Master: Msc. – Polymer Materials Science 09.2017-05.2020  
- Martin Luther University Halle-Wittenberg, Halle (Saale), Germany
- Bachelor: BEng. – Polymer Materials and Engineering 09.2013-06.2017  
- South-Central Minzu University, Wuhan, China
- Senior High School 09.2010-06.2013  
- Kaifeng High School, Kaifeng, China

## Research

Synthesis, characterization, and application of hydrogen-bonded polymers, ionic liquids, and polymeric ionic liquids; synthesis of polymers via controllable methods: RAFT, ATRP, NMP, LCCP, LAP; hydrogen bonds in polymers; (thio-)barbiturate chemistry; sulfur chemistry

## Skills

- Polymer Chemistry (GPC, Rheology, Tensile, DSC, TGA, MALDI MS, DLS, BDS)
- Organic Synthesis (NMR, UV-Vis, FT-IR, MS, HPLC, Glovebox, MW reactor)
- Scientific Writing & Publishing
- Academic Presentation
- Project/Research Management
- Onboarding & Teaching (supervising Master/HiWi students)
- Program: MS Office, MestReNova, ChemDraw, Origin, eLabFTW

## Conferences

- International Symposium on Macrocyclic and Supramolecular Chemistry  
Hangzhou, China, May 2024, *Oral presentation*
- 8th International Conference on Self-Healing Materials ICSHM  
Milan, Italy, June 2022, *Oral presentation*
- Bordeaux Polymer Conference BPC  
Bordeaux, France, June 2022, *Oral presentation*

## Experience

- Lyondell Basell, Frankfurt, Germany 05.2023  
- Visiting R&D department, PP production line, and polymer engineering line
- Fraunhofer-PAZ, Schkopau, Germany 04.2018  
- Visiting pilot plant, upscaling lab, and polymer engineering lab

## Language

Chinese: Native

English: IELTS 6.5

Deutsch: B1

## Publication List

1. Comparing C2=O and C2=S Barbiturates: Different Hydrogen-Bonding Patterns of Thiobarbiturates in Solution and the Solid State

Chenming Li, Philipp Hilgeroth, Nazmul Hasan, Dieter Ströhl, Jörg Kressler, and Wolfgang H. Binder\*

*Int. J. Mol. Sci.* **2021**, 22(23), 12679;

<https://doi.org/10.3390/ijms222312679>

2. Synthesis and Characterization of Quadrupolar-Hydrogen-Bonded Polymeric Ionic Liquids for Potential Self-Healing Electrolytes

Chenming Li, Rajesh Bhandary, Anja Marinow, Dmitrii Ivanov, Mengxue Du, René Androsch, and Wolfgang H. Binder\*

*Polymers* **2022**, 14(19), 4090

<https://doi.org/10.3390/polym14194090>

3. Stability of Quadruple Hydrogen Bonds in an Ionic Liquid Environment

Chenming Li, Rajesh Bhandary, Anja Marinow, Stephanie Bachmann, Ann-Christin Pöppler, and Wolfgang H. Binder\*

*Macromol. Rapid Commun.* **2024**, 45, 2300464

<https://doi.org/10.1002/marc.202300464>

4. Proximity Effects and Aggregation of Hamilton-Receptor Barbiturate Host-Guest Complexes Probed by Cross-Metathesis and ESI MS Analysis

Chenming Li, Pascal Mai, Niclas Festag, Anja Marinow, and Wolfgang H. Binder\*

*Chem. Eur. J.* **2024**, e202403939

<https://doi.org/10.1002/chem.202403939>

5. Catalyst-Free, Mechanically Robust, and Ion-Conductive Vitrimers for Self-Healing Ionogel Electrolytes

Xiaozhuang Zhou, Chenming Li, Rajesh Bhandary, Zviadi Katcharava, Fanfan Du, René Androsch, Anja Marinow, and Wolfgang H. Binder\*

*ACS Appl. Eng. Mater.* **2023**, 1, 1997–2003

<https://doi.org/10.1021/acsaenm.3c00286>

# Eigenständigkeitserklärung

Hiermit erkläre ich an Eides statt, dass ich die vorliegende Arbeit selbstständig und ohne fremde Hilfe verfasst habe. Andere als die angegebenen Quellen und Hilfsmittel wurden nicht benutzt und die den benutzten Werken wörtlich oder inhaltlich entnommenen Stellen wurden als solche kenntlich gemacht.

Außerdem erkläre ich, die vorliegende Dissertation an keiner anderen wissenschaftlichen Einrichtung zur Erlangung eines akademischen Grades eingereicht zu haben.

Halle (Saale), den

---

Chenming Li